STUDIES IN PHOTOCHEMICAL SMOG CHEMISTRY:

I. ATMOSPHERIC CHEMISTRY OF TOLUENE

II. ANALYSIS OF CHEMICAL REACTION MECHANISMS FOR PHOTOCHEMICAL SMOG

Thesis by

Joseph Anthony Leone

In Partial Fulfillment of the Requirements

for the Degree of

Doctor of Philosophy

California Institute of Technology

Pasadena, California

1985

(submitted August 27, 1984)

ACKNOWLEDGMENT

This thesis has truly been a team effort, and there are many members of the team that I would like to acknowledge for their special contributions. I could not have made it to first base without the guidance of my "manager" John Seinfeld. Quite simply, he is a true "all star." The numerous ideas and suggestions of my "coaches," Daniel Grosjean, Rick Flagan, and Glen Cass were essential when I was about to "strike out" on my own. My job was made a great deal easier by the outstanding play of my "teammates," especially Dale Warren, Greg McRae, and Toby Shafer. I am indebted to my "groundskeeper" Elton Daily for constructing much of my equipment, and to my "scorekeeper" Lenore Kerner for keeping track of all my "errors" while typing the manuscripts that make up this thesis. There is not enough space to thank all of the "fans" who made my stay at Caltech some of the most enjoyable years of my life. Special thanks go to Barry Bentley, Russ Bone, Gary Whatley, Rohit Khanna, Tony Geller, and especially to my "tenth player," Chris Chow. I could have never made it to "home plate" without the dedication and support of my wife Dee, and my parents. Finally, I acknowledge the financial support of the "owners," the National Science Foundation, the United States Environmental Protection Agency, the California Air Resources Board, and the California Institute of Technology.

ABSTRACT

This study focuses on two related topics in the gas phase organic chemistry of importance in urban air pollution. Part I describes an experimental and modeling effort aimed at developing a new explicit reaction mechanism for the atmospheric photooxidation of toluene. This mechanism is tested using experimental data from both indoor and outdoor smog chamber facilities. The predictions of the new reaction mechanism are found to be in good agreement with both sets of experimental data. Additional simulations performed with the new mechanism are used to investigate various mechanistic paths, and to gain insight into areas where our understanding is not complete. The outdoor experimental facility, which was built to provide the second set of experimental data, consists of a 65 cubic meter teflon smog chamber together with full instrumentation capable of measuring ozone, nitrogen dioxide, nitric oxide, peroxyacetyl nitrate (PAN), carbon monoxide, relative humidity, temperature, aerosol size distributions, and of course toluene and its photooxidation products.

In Part II, we present a theoretical analysis of lumped chemical reaction mechanisms for photochemical smog. Included is a description of a new counter species analysis technique which can be used to analyze any complex chemical reaction mechanism. When applied to mechanisms for photochemical smog, this analysis is shown capable of providing answers to previously inaccessible questions such as the relative contributions of individual organics to photochemical ozone formation. The counter species analysis is applied to six existing mechanisms for photochemical smog to determine why they predict substantially different degrees of emission controls to achieve the same desired air quality under identical conditions. For each mechanism critical areas are identified that when altered bring the predictions of the various mechanisms

into much closer agreement. Finally, a new lumped mechanism for photochemical smog is developed and tested against experimental data from two smog chamber facilities. Advantages of this mechanism relative to the existing lumped mechanisms are discussed.

TABLE OF CONTENTS

CHAPTER 1

Introduction

INTRODUCTION

In order to better understand and control air pollution in urban areas, one needs to be able to predict how changes in emission levels of pollutants will affect ambient air quality. Currently, this is achieved through the use of mathematical models termed urban airshed simulation models. An important component of these airshed models is a description of atmospheric organic chemistry. This description usually takes the form of a simplified or "lumped" reaction mechanism in which the detailed chemistry of hundreds of different organics has been greatly simplified. Unfortunately, the development of a lumped reaction mechanism that accurately describes atmospheric organic chemistry, and, at the same time, is computationally tractable, is a difficult undertaking.

Since these lumped mechanisms for photochemical smog represent simplifications of the detailed atmospheric chemistry, the logical starting points for the formulation of a lumped mechanism are the detailed, explicit reaction mechanisms for the most important atmospheric organics. While accurate explicit reaction mechanisms exist for representative alkanes and alkenes, our understanding of aromatic hydrocarbon photooxidation is poor at best. The goal of Part I of this study was to develop an accurate reaction mechanism describing the atmospheric photooxidation of toluene, one of the most important atmospheric aromatics.

The formulation and testing of this new toluene photooxidation mechanism is described in Chapter 2. The experiments used to evaluate the performance of this mechanism were carried out at the University of California at Riverside. In order to evaluate the performance of this mechanism under a different set of conditions, we built our own smog chamber facility and carried out a new series of experiments. The results of simulating this new series of experiments are

presented in Chapter 3, along with a detailed description of the experimental facility.

In Part II of this study we change our focus from explicit mechanisms to the analysis of lumped reaction mechanisms for photochemical smog. Chapter 4 contains a detailed description of six mechanisms that have been developed to describe photochemical smog chemistry. Included in Chapter 4 are analyses of the treatments of the basic chemistry, of photolysis reactions, and of organic lumping in both initial conditions and rate constants.

The six mechanisms described in Chapter 4 are all based on the same body of kinetic and mechanistic data, and each has been evaluated against experimental data from several different smog chamber facilities. The differences among these mechanisms would not be of any concern if each mechanism gave similar predictions over a range of atmospheric conditions. However, several recent investigations have shown that different mechanisms predict substantially different degrees of emission controls to achieve the same desired air quality under identical conditions (1-3). Analyzing the behavior of these reaction mechanisms is a demanding task because of the large number of species and reactions each contains, and because of the interwoven nature of the free radical chain reactions characterizing each mechanism. In Chapter 5 we present the details of a counter species analysis technique which can be used to analyze any complex chemical reaction mechanism. Examples are given to illustrate how this analysis can be used to assess the differences among the available photochemical smog mechanisms.

In Chapter 6, we present a detailed counter species analysis of the six reaction mechanisms described in Chapter 4. Based on the results of this analysis, specific aspects of each mechanism are identified that are responsible for the discrepancies with other mechanisms and with an explicit mechanism

based on the latest understanding of atmospheric chemistry. When these critical areas are modified, the predictions of the lumped mechanisms are shown to be in much closer agreement.

Based on what we have learned from our analysis of the six existing lumped mechanisms, we present in Chapter 7 the formulation of a new lumped mechanism for photochemical smog. This new mechanism is extensively tested against data from two smog chamber facilities. Advantages of this new mechanism relative to the existing mechanisms are discussed.

REFERENCES

Carter, W.P.L., Winer, A.M. and Pitts, J.N., Jr. (1982) "Effect of Kinetic Mechanisms and Hydrocarbon Composition on Oxidant-Precursor Relationships Predicted by the EKMA Isopleth Technique," Atmospheric Environment, **16**, 113-120.

Jeffries, H.E., Sexton, K.G. and Salmi, C.N. (1981), Effects of Chemistry and Meteorology on Ozone Control Calculations Using Simple Trajectory Models and the EKMA Procedure, Final Report to the U.S. Environmental Protection Agency Under Contract Number 68-02-3523, School of Public Health, University of North Carolina, Chapel Hill, North Carolina, 373 pp.

Whitten, G.Z. (1981) Comments at U.S. Environmental Protection Agency Workshop on the Empirical Kinetic Modeling Approach, December 15-16, Research Triangle Park, North Carolina.

I. ATMOSPHERIC CHEMISTRY OF TOLUENE

CHAPTER 2

Updated Chemical Mechanism for Atmospheric Photooxidation of Toluene

Published in the

International Journal of Chemical Kinetics, **16**, 159 (1984).

Updated Chemical Mechanism for Atmospheric Photooxidation of Toluene

JOSEPH A. LEONE and JOHN H. SEINFELD
Department of Chemical Engineering, California Institute of Technology, Pasadena, California 91125

Abstract

A new reaction mechanism describing the atmospheric photochemical oxidation of toluene is formulated and tested against environmental chamber data from the University of California, Riverside, Statewide Air Pollution Research Center (SAPRC). On simulations of toluene–NO_x and toluene–benzaldehyde–NO_x irradiations, the average predicted O_3 and PAN maxima are within 3% of the experimental values. Simulations performed with the new mechanism are used to investigate various mechanistic paths, and to gain insight into areas where our understanding is not complete. Specific areas that are investigated include benzaldehyde photolysis, organic nitrate formation, alternate ring fragmentation pathways, and conjugated γ-dicarbonyl condensation to the aerosol phase.

Introduction

Aromatic hydrocarbons represent a significant fraction of the reactive organics present in polluted atmospheres. For example, in Los Angeles, approximately 25% of the nonmethane hydrocarbons are aromatic compounds [1,2]. Of this 25%, approximately one-third is toluene, and another one-third consists of the xylene isomers [2]. Since most aromatics react at significant rates in urban atmospheres, they represent important precursors of photochemical oxidant and organic aerosols. In the past few years, several experimental programs have yielded data that have enabled the formulation and evaluation of aromatic reaction mechanisms. Because of its ambient abundance and reactivity, toluene has been the most widely studied atmospheric aromatic compound.

There currently exist three chemical reaction mechanisms for toluene photooxidation [3–5], but new developments, including very recent experimental data concerning (1) α-dicarbonyl photochemistry and (2) the fate of the initial toluene–OH adduct, have sufficiently altered our understanding of toluene photooxidation chemistry to suggest the need for the development of an updated reaction mechanism. In this

International Journal of Chemical Kinetics, Vol. 16, 159–193 (1984)
 CCC 0538-8066/84/020159-35$04.00

paper we present a detailed chemical mechanism describing the atmospheric photooxidation of toluene, and evaluate this mechanism with smog chamber data. In evaluating the performance of the mechanism, we have not attempted to improve agreement with the experimental data by varying parameters. Each rate constant has been assigned its recommended value and is not varied. Similarly, those chamber-dependent effects that are included are determined by the conditions of the experiment being simulated. After presenting the results of the smog chamber simulations, we explore in some detail the sensitivity of the mechanism to the important uncertain features of toluene chemistry.

Chemical Reaction Mechanism and Chamber Effects

The toluene photooxidation mechanism developed here is given in the Appendix, Table AI. Most of the inorganic rate constants are taken from the most recent NASA and CODATA evaluations [6,7]. The majority of the aromatic rate constants are taken from the recent review of Atkinson and Lloyd [8]. The initial conditions and selected physical parameters for each experiment are given in Table AII.

The experimental data used in this study were obtained from the indoor evacuable chamber facility at SAPRC. These data were obtained under conditions of constant temperature, light intensity, and spectral distribution. The only chamber effects included in the simulations presented here involve (1) heterogeneous nitric acid formation [reaction (25)], (2) NO_x off-gassing [reaction (104)], (3) the wall loss of ozone [reaction (103)], (4) chamber dilution, and (5) chamber radical sources. Table I contains the necessary information regarding the first four effects, and the chamber radical source question is discussed below.

A major issue of controversy in previous attempts at simulating aromatic hydrocarbon photooxidation concerned the use of chamber

TABLE I. Chamber-dependent parameters for simulations of experiments in SAPRC evacuable chamber.

Process	Reaction Number (Table A.1)	Rate Constant
$O_3 \rightarrow$ Wall	103	1.65×10^{-3} min^{-1}
Wall $\rightarrow$ NO	104	1.0×10^{-4} ppm min^{-1}
$N_2O_5 + H_2O \xrightarrow{\text{wall}} 2HNO_3$	25	4.4×10^{-6} ppm^{-1} min^{-1}
dilution*	-	$(2.6\text{-}3.4) \times 10^{-4}$ min^{-1}

* The rate constant for dilution D is defined by $dc_i/dt = -Dc_i$, where c_i is the concentration of species i.

derived radical sources. Atkinson et al. [4] included a significant wall source of OH radicals, while Hendry et al. [3] assumed a combination of initial HONO and a wall source of $HO_2\cdot$. In contrast, Killus and Whitten [5] have included only small amounts of initial HONO as radical inputs in their simulations. Since the above studies were completed, Carter et al. [9] have reported a thorough investigation of chamber-derived radical sources using four environmental chambers at SAPRC. Their investigation presents strong evidence that chamber radical sources were present in all of the chambers studied. The data from the SAPRC evacuable chamber were fairly well fit by an OH wall source for RH $\geq$ 50% equal to $k_1[(0.39 \pm 0.04) + (1.37 \pm 0.12)[NO_2]]$ ppb/min [9]. Since all of the experiments that we are attempting to simulate were performed in the evacuable chamber at $\approx$50% relative humidity, we chose to use this expression (without the uncertainties) in considering all of the SAPRC experiments [see reactions (105) and (106)]. The Carter et al. [9] study also reported that some HONO was probably present at the beginning of irradiation, and that the amount needed to give the best fit to the experimental data was a function of the initial NO_2/NO concentration ratio. For this reason, we also include initial HONO in our simulations. However, because there does not appear to be a good correlation between the initial conditions and the amount of initial HONO required to give the best data fit in the Carter et al. [9] study, we have assumed 7 ppb of initial HONO for each of the experiments simulated here. This is a typical amount, and small variations around it have very little effect on the simulations.

Simulations of Toluene Photooxidation Experiments

The results of our simulations are summarized in Table II and shown in Figures 1–11. The maximum oxidant yields were predicted very well, with the average O_3 maximum being 2% high and the average PAN maximum 3% high. The predicted O_3 peak came an average of 11% later than experimentally observed. NO_2 peak heights were consistently overpredicted, being an average of 10% high; but the time of the NO_2 peak was predicted very accurately. The NO/NO_2 crossover times were also well predicted, as shown in Table II.

The results of this study are compared with those of previous toluene simulations in Table III. We note that the present study leads to much more accurate predictions of both maximum oxidant levels and the time of the NO_2 peak. The predicted NO_2 maxima are in error by about the same amount as previous studies, as are the predicted times of the O_3 peak.

Figure 1 shows the effect of varying the percentage of the initial toluene–OH reaction proceeding by the abstraction pathway for SAPRC

TABLE II. Predicted O_3, NO_2, and PAN maxima and times of occurrence of maxima and NO/NO_2 crossover times for SAPRC chamber experiments.

		Experiment Number								
		EC-265	EC-266	EC-269	EC-271	EC-273	EC-327	EC-337	EC-339	EC-340
$[O_3]_{max}$(ppb)	measured	393	403	298*	296	215	376*	325	225*	344*
	predicted	396	429	305	290	211	383	334	207	341
Time of $[O_3]_{max}$ (min)	measured	210	215	360*	90	80	360*	255	360*	330*
	predicted	230	250	360	115	110	360	280	360	330
$[NO_2]_{max}$(ppb)	measured	300	300	260	140	64	260	260	240	250
	predicted	325	338	294	154	77	284	284	250	270
Time of $[NO_2]_{max}$ (min)	measured	90	90	140	~30	~30	135	105	195	120
	predicted	90	85	140	~35	~30	125	105	190	120
$[PAN]_{max}$(ppb)	measured	69	75	50	53	31	41	47	24	42
	predicted	72	84	41	47	29	53	51	22	48
NO/NO_2 Crossover (min)	measured	40	50	70	~15	~15	65	60	110	50
	predicted	40	45	70	~15	~15	60	55	110	50

* Value at the end of the experiment.

experiment EC-266. Although the system reactivity increases as the percentage of abstraction is decreased, the observed changes in the simulation are small.

The effect of assuming radical or nonradical products from the photolysis of benzaldehyde is illustrated in Figure 2. The data are from toluene–benzaldehyde–NO_x irradiations EC-337 and EC-339. It is readily apparent that the data are consistent with the assumption of nonradical benzaldehyde photolysis products.

Figure 3 shows the effect on predicted concentration–time profiles of varying the ratio of cresol formation to ring opening (k_{65}/k_{67}) from the initial toluene–OH adduct. Experimental data are from SAPRC experiment EC-337. With each of the experiments simulated here, the best results are obtained with $k_{65}/k_{67} \approx 0.2$, in excellent agreement with the recent study of Atkinson et al. [10].

The effect of organic nitrate formation on predicted concentration–time profiles for toluene–NO_x experiment EC-271 is shown in Figure 4. The radical scavenging effect of nitrate formation leads to a system with a much lower reactivity than the experimental data indicate. Thus we conclude that these unobserved nitrates are probably not formed to any appreciable extent in aromatic hydrocarbon–NO_x photooxidation.

Figure 5 shows the effect on mechanism predictions of assuming alternative ring fragmentation reactions for experiment EC-340. Only mechanisms assuming fragmentation of the cyclyzed toluene–OH–O_2 adducts to form 100% methyl glyoxal and 2-butene-1,4-dial (as opposed to some percentage of glyoxal and 2-pentene-1,4-dial) allow the data to be simulated.

ATMOSPHERIC PHOTOOXIDATION OF TOLUENE

TABLE III. Comparison of predicted and observed properties of SAPRC toluene experiments by four toluene mechanisms.

SAPRC Experiment No.	Mechanism	O_3 max. (ppb) [% error]	O_3 max. (min) [% error]	NO_2 max. (ppb) [% error]	NO_2 max. (min) [% error]	PAN max (ppb) [% error]
EC-265	Hendry et al. [3]	600 [54]	310 [41]	330 [10]	90 [0]	N.C.[1]
	Atkinson et al. [4]	450 [15]	190 [-9]	298 [0]	45 [-50]	90 [30]
	Killus & Whitten [5]	451 [-15]	160 [-24]	268 [-11]	95 [5]	87 [26]
	Current Study	396 [<1]	230 [9]	325 [8]	90 [0]	72 [4]
EC-266	Hendry et al. [3]	600 [50]	310 [41]	330 [10]	90 [0]	N.C.
	Atkinson et al. [4]	465 [15]	200 [-7]	315 [5]	60 [-33]	95 [27]
	Killus & Whitten [5]	465 [15]	155 [-28]	338 [13]	90 [0]	103 [37]
	Current Study	429 [6]	250 [16]	338 [13]	85 [-6]	84 [12]
EC-269	Hendry et al. [3]	300 [0]	360 [-]	290 [11]	160 [14]	N.C.
	Atkinson et al. [4]	388 [30]	360 [-]	277 [6]	90 [-36]	48 [-4]
	Killus & Whitten [5]	388 [30]	330 [-8]	300 [15]	175 [25]	60 [20]
	Current Study	305 [2]	360 [-]	294 [13]	140 [0]	41 [-18]
EC-271	Hendry et al. [3]	400 [33]	150 [67]	144 [2]	50 [67]	N.C.
	Atkinson et al. [4]	292 [-1]	75 [-17]	140 [0]	~30 [0]	61 [15]
	Killus & Whitten [5]	352 [19]	70 [-22]	154 [10]	45 [50]	68 [28]
	Current Study	290 [-2]	115 [28]	154 [10]	~35 [15]	47 [-11]
EC-273	Hendry et al. [3]	250 [14]	110 [37]	70 [9]	~35 [15]	N.C.
	Atkinson et al. [4]	198 [-8]	85 [+6]	70 [9]	~30 [0]	34 [10]
	Killus & Whitten [5]	245 [14]	70 [-12]	78 [22]	~35 [15]	40 [29]
	Current Study	211 [-2]	110 [37]	77 [20]	~30 [0]	29 [-6]
EC-327	Hendry et al. [3]	390 [3]	360 [-]	270 [4]	140 [4]	N.C.
	Atkinson et al. [4]	421 [12]	340 [-6]	270 [4]	90 [-33]	53 [29]
	Killus & Whitten [5]	411 [9]	300 [-17]	288 [11]	155 [15]	61 [33]
	Current Study	383 [2]	360 [-]	284 [9]	125 [-7]	53 [29]
EC-337	Hendry et al. [3]	580 [81]	360 [41]	290 [11]	115 [9]	N.C.
	Atkinson et al. [4]	415 [28]	280 [10]	271 [4]	90 [-24]	64 [36]
	Killus & Whitten [5]	360 [11]	210 [-18]	276 [6]	110 [5]	54 [15]
	Current Study	334 [3]	280 [10]	284 [9]	105 [0]	51 [8]
EC-339	Hendry et al. [3]	380 [73]	360 [-]	290 [21]	150 [-23]	N.C.
	Atkinson et al. [4]	269 [20]	360 [-]	245 [2]	135 [-31]	24 [0]
	Killus & Whitten [5]	268 [20]	360 [-]	249 [4]	170 [-13]	24 [0]
	Current Study	207 [8]	360 [-]	250 [4]	190 [-3]	22 [-8]
EC-340	Hendry et al. [3]	400 [16]	360 [-]	260 [4]	135 [12]	N.C.
	Atkinson et al. [4]	421 [22]	330 [-]	257 [3]	90 [-25]	51 [21]
	Killus & Whitten [5]	395 [15]	315 [-4]	271 [8]	155 [29]	56 [33]
	Current Study	341 [<1]	330 [-]	270 [8]	120 [0]	48 [14]
Average Error %	Hendry et al. [3]	[+36]	[25]	[+9]	[+11]	N.C.
	Atkinson et al. [4]	[+15]	[-3]	[+4]	[-26]	[+18]
	Killus & Whitten [5]	[+16]	[-15]	[+9]	[+15]	[+25]
	Current Study	[+2]	[+11]	[+10]	[<1]	[+3]

[1] N.C.—Not calculated.

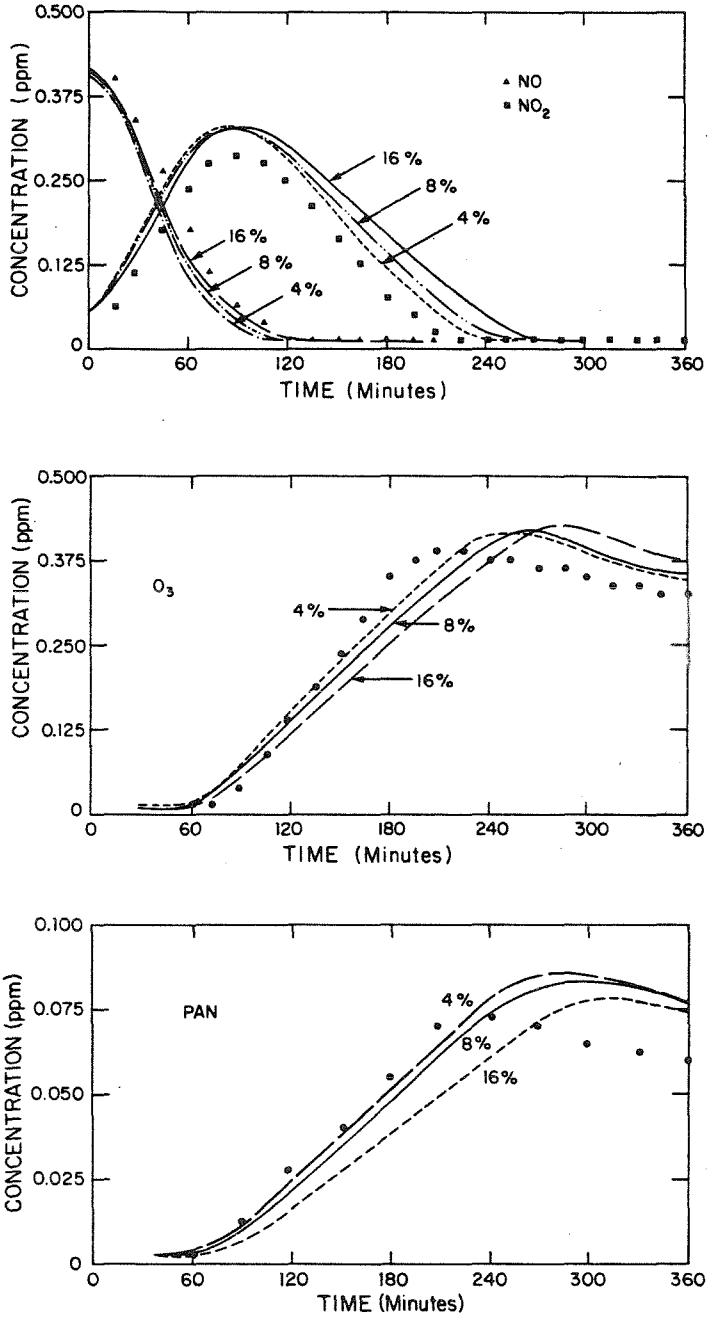

Figure 1. Observed and calculated concentration–time profiles for toluene–NO_x experiment EC-266. Effect of varying the percentage of the abstraction pathway.

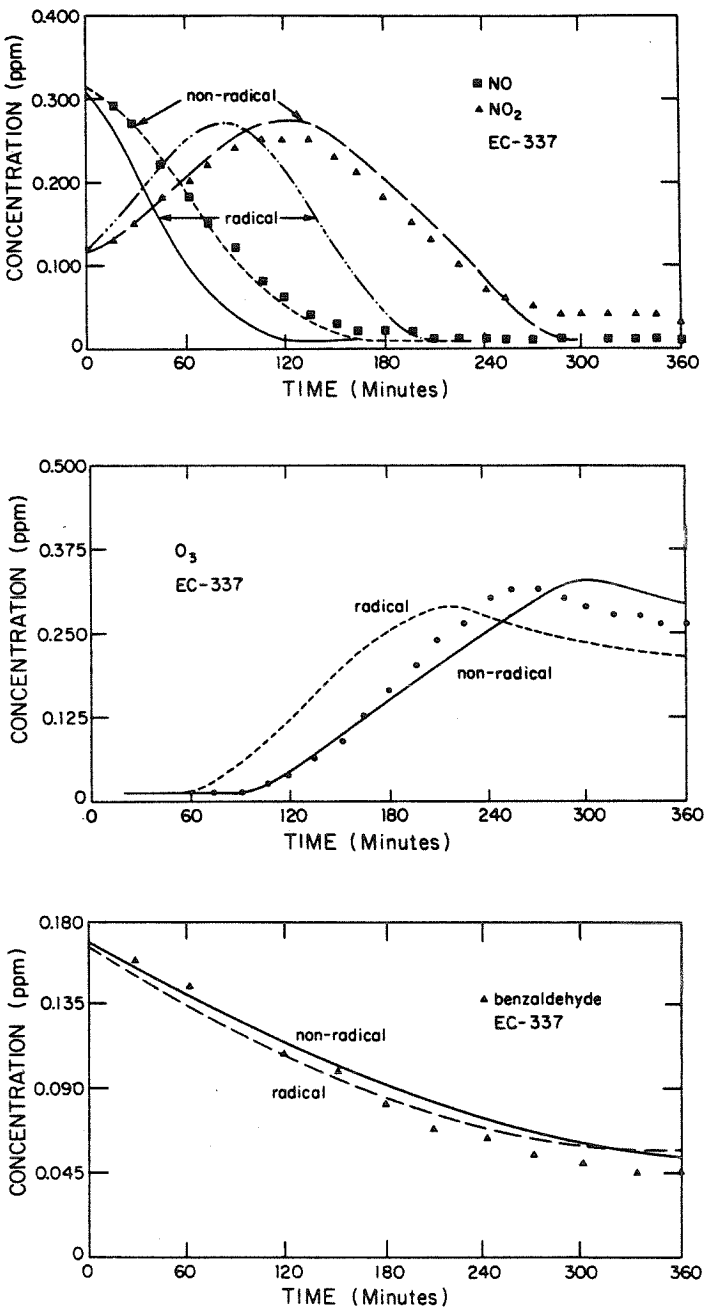

Figure 2. Observed and calculated concentration–time profiles for toluene–benzaldehyde–NO_x experiments EC-337 and EC-339. Effect of assuming different benzaldehyde photolysis products.

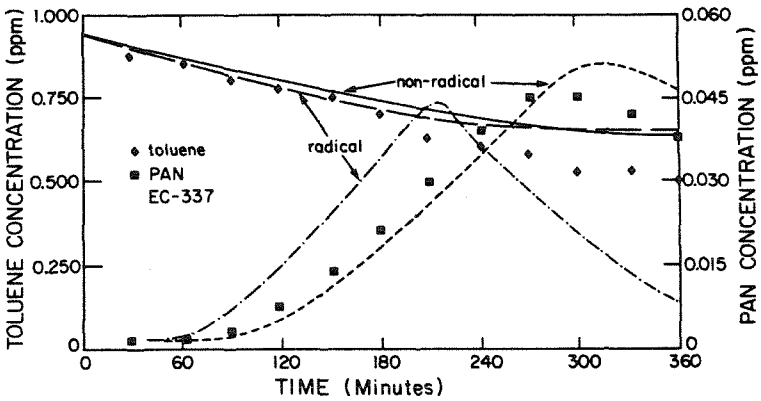

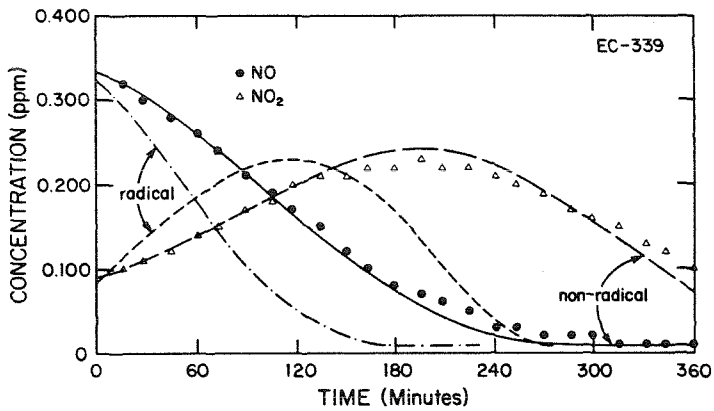

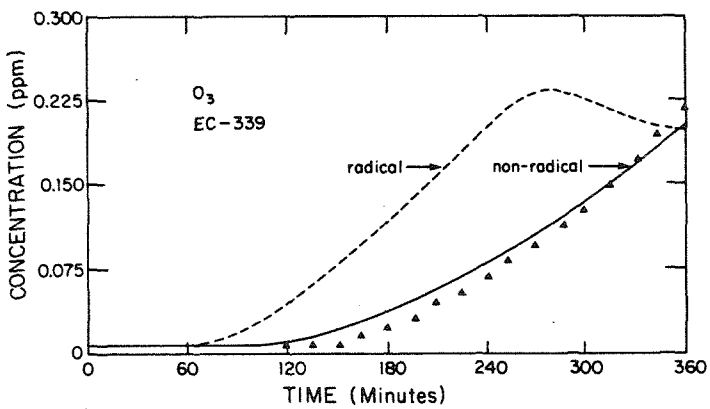

Figure 2. *(continued from the previous page)*

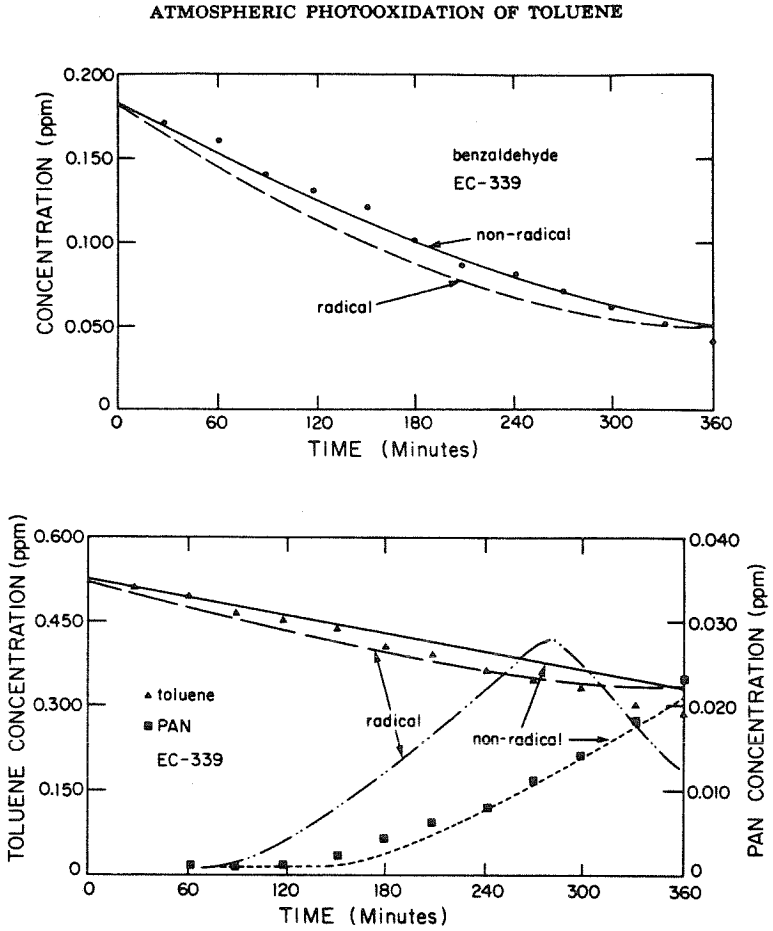

Figure 2. (*continued from the previous page*)

The results of assuming that various percentages of the conjugated γ-dicarbonyls condense to the aerosol phase and do not further react, are illustrated in Figure 6. In general, assuming some condensation brings the reactivity of the mechanism in closer agreement with the experimental data. However, at the same time the O_3 and PAN maxima are overpredicted. Thus the experimental data do not allow us to choose between mechanisms assuming different amounts of condensation.

Figures 7–9 compare the results of simulations with experimental data from toluene–NO_x experiments EC-269, EC-273, and EC-327, respectively. Figures 10 and 11 show the results of simulations for *o*-cresol–NO_x experiment EC-281 and *p*-cresol–NO_x experiment EC-290. Although the agreement between the predicted and observed concentration–time profiles is not as good for the cresol–NO_x experiments

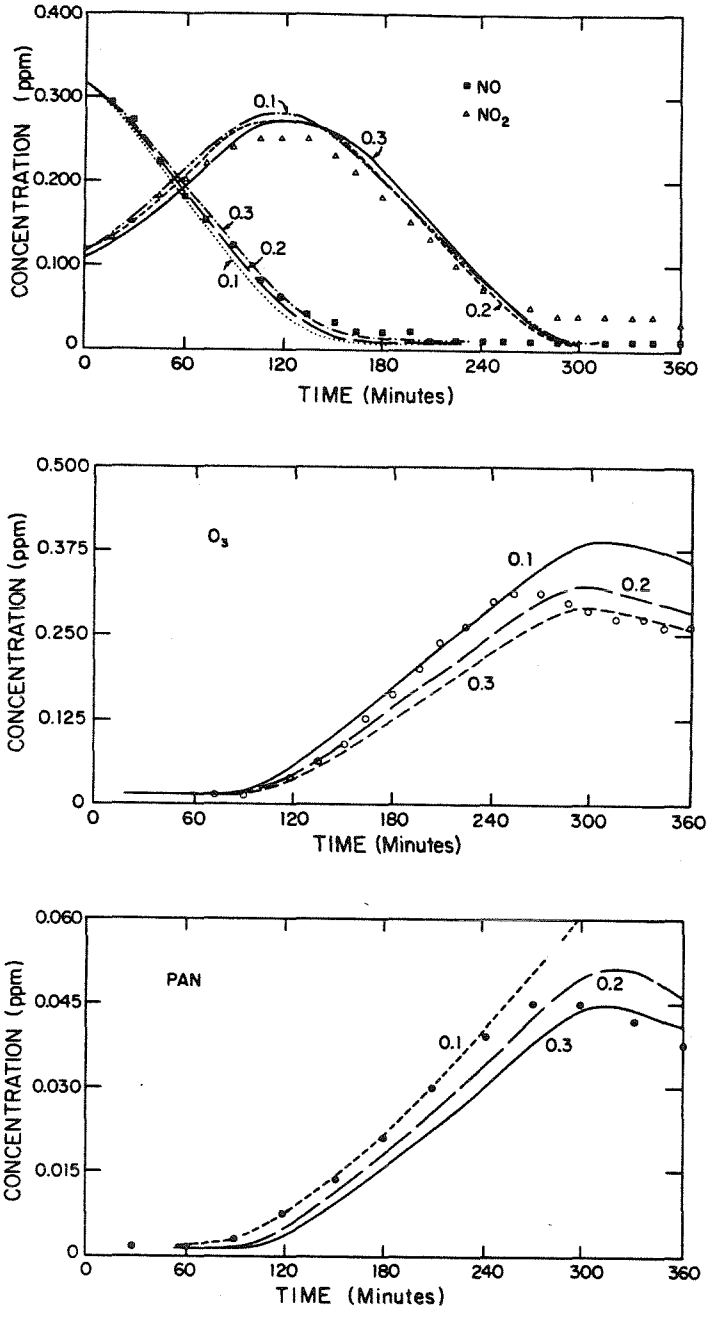

Figure 3. Observed and calculated concentration–time profiles for toluene–NO_x experiment EC-337. Effect of assuming varying ratios of cresol formation to ring opening (k_{a6}/k_{a7}).

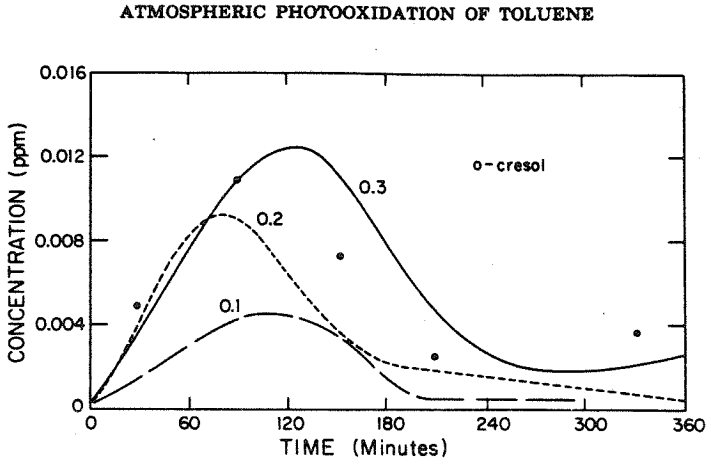

Figure 3. (*continued*)

as for those for toluene, the mechanism predictions lie fairly close to the experimental data.

Discussion

Toluene Photooxidation Chemistry. The only important removal process for aromatic hydrocarbons in the atmosphere is reaction with OH [3,4,11]. Toluene reacts with OH by two pathways, addition and H-atom abstraction,

(48)[1] 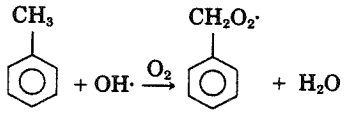

(64) 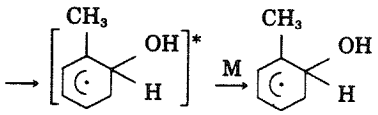

with $k_{48} + k_{64} = 9.4 \times 10^{-3}$ ppm^{-1} · min^{-1} at ~300 K [8]. Addition at the ortho position predominates [3,4], so we consider only that avenue here. The percentage of the overall reaction proceeding by abstraction has been estimated at 16% by Perry et al. [12], as 15% by Hendry et al. [13] and Atkinson et al. [4], as 4% by Tully et al. [14], and as 8% by Atkinson et al. [10]. All of the recent toluene photooxidation mechanisms have assumed 15% abstraction [3–5].

[1] Reaction numbers correspond to those found in Table AI.

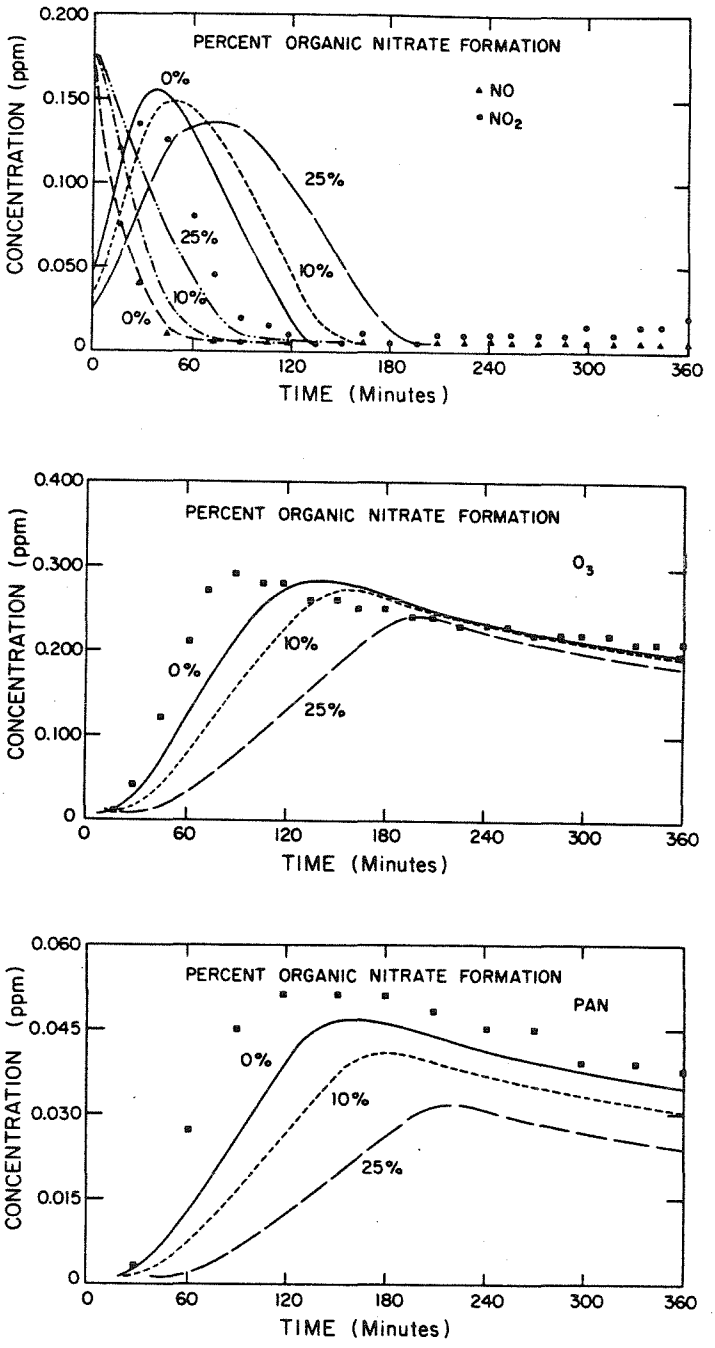

Figure 4. Observed and calculated concentration–time profiles for toluene–NO_x experiment EC-271. Effect of assuming organic nitrate formation.

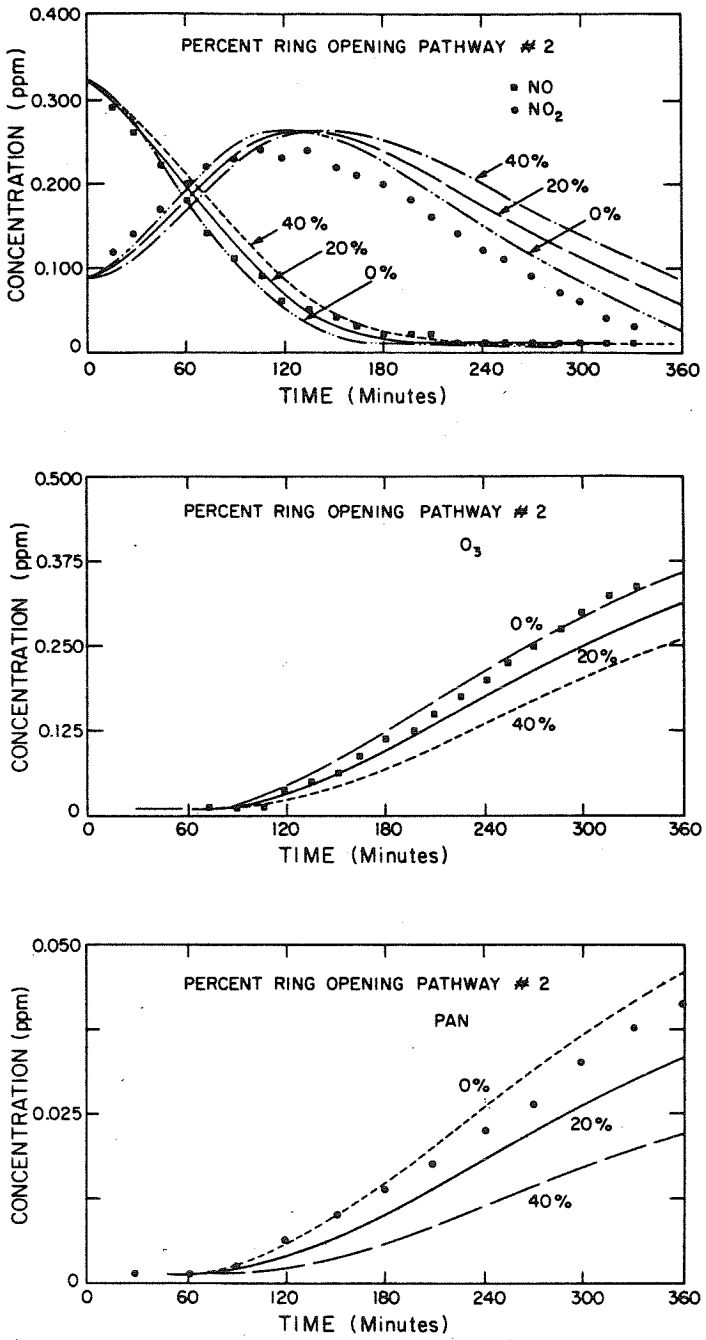

Figure 5. Observed and calculated concentration–time profiles for toluene–NO_x experiment EC-340. Effect of assuming different ring opening pathways.

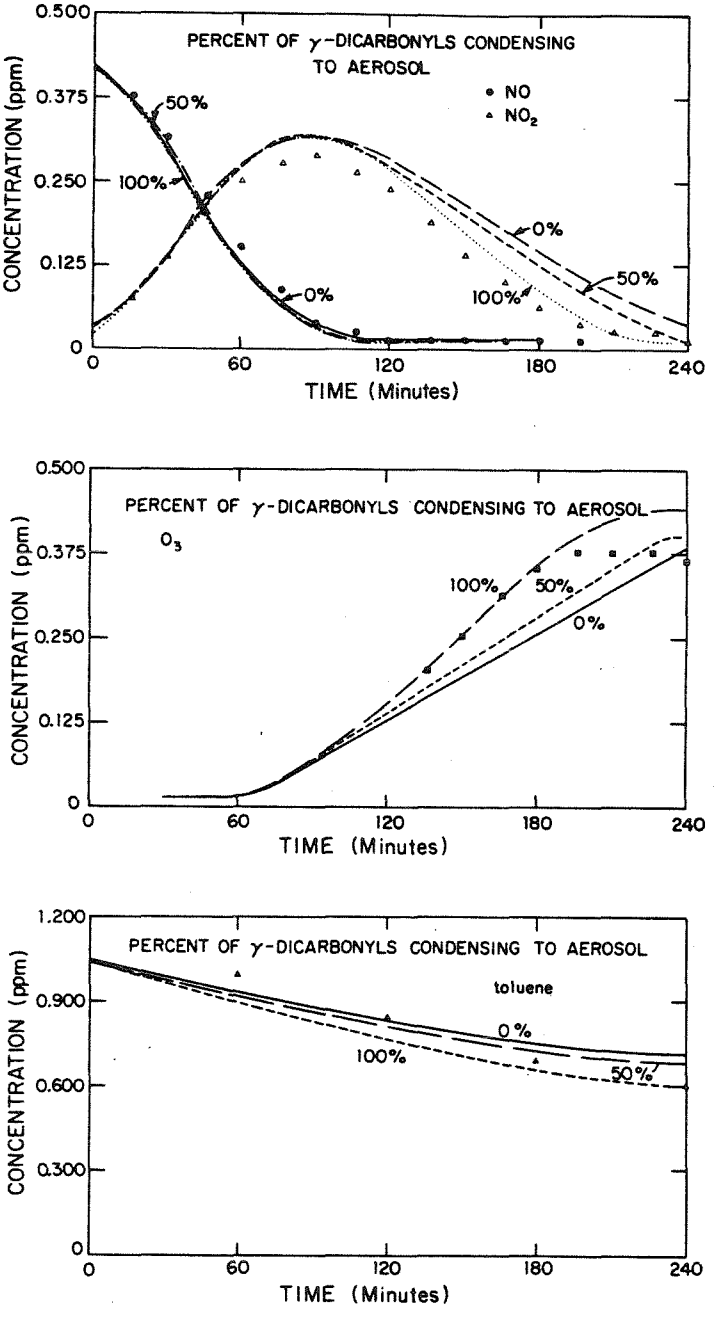

Figure 6. Observed and calculated concentration–time profiles for toluene–NO_x experiment EC-265. Effect of assuming some condensation of the conjugated γ-dicarbonyls.

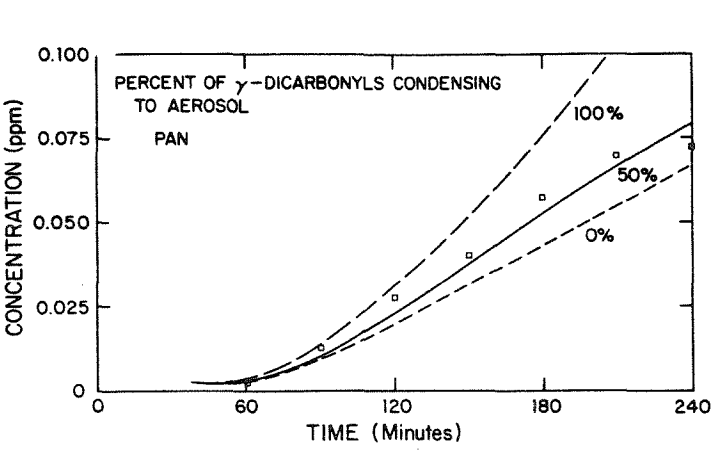

Figure 6. *(continued from the previous page)*

However, it now appears that 8% is a more accurate value [8]. Thus for our studies we have used:

$$k_{48} = 7.5 \times 10^2 \text{ ppm}^{-1} \cdot \text{min}^{-1}$$

$$k_{64} = 8.7 \times 10^3 \text{ ppm}^{-1} \cdot \text{min}^{-1}$$

Increasing the percentage of the reaction proceeding via OH addition leads to a more reactive system since the ring opening portion of the addition pathway leads to a large fraction of the NO to NO_2 conversions. Figure 1 shows the effect on model predictions of varying the fraction abstraction between 4 and 16%. Although the data in Figure 1 are

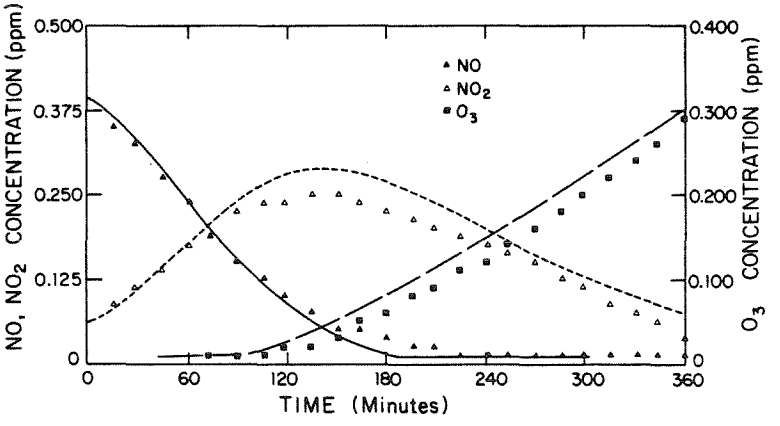

Figure 7. Observed and calculated concentration–time profiles for toluene–NO_x experiment EC-269.

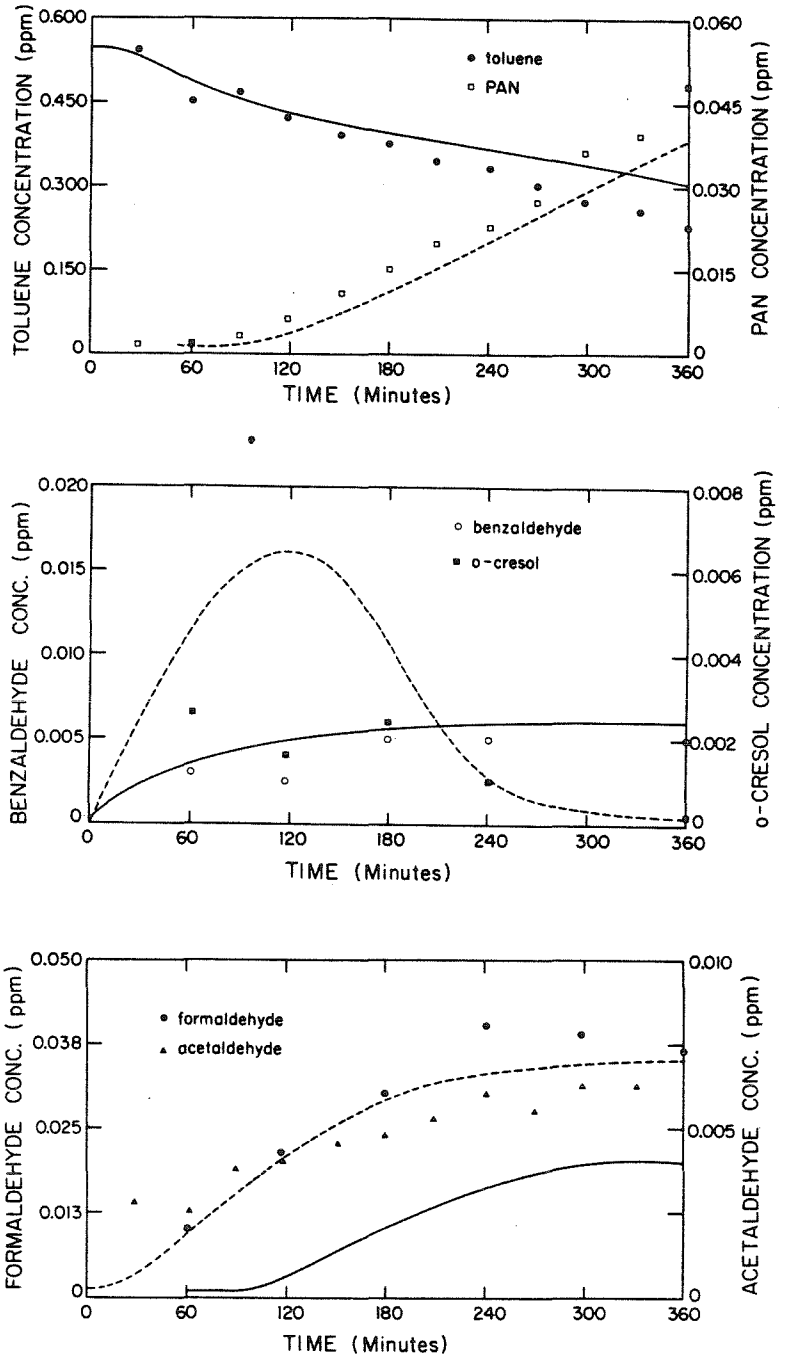

Figure 7. *(continued from the previous page)*

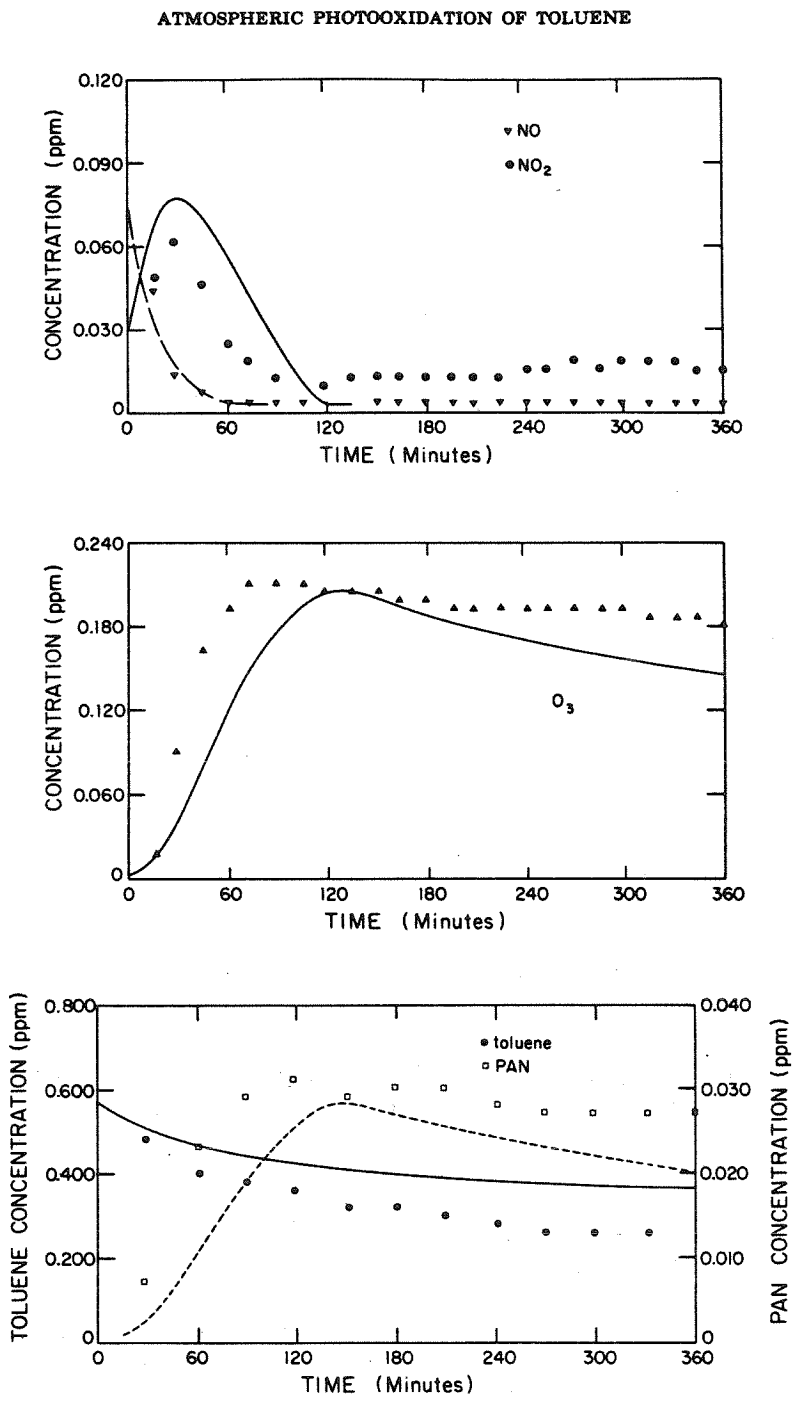

Figure 8. Observed and calculated concentration–time profiles for toluene–NO_x experiment EC-273.

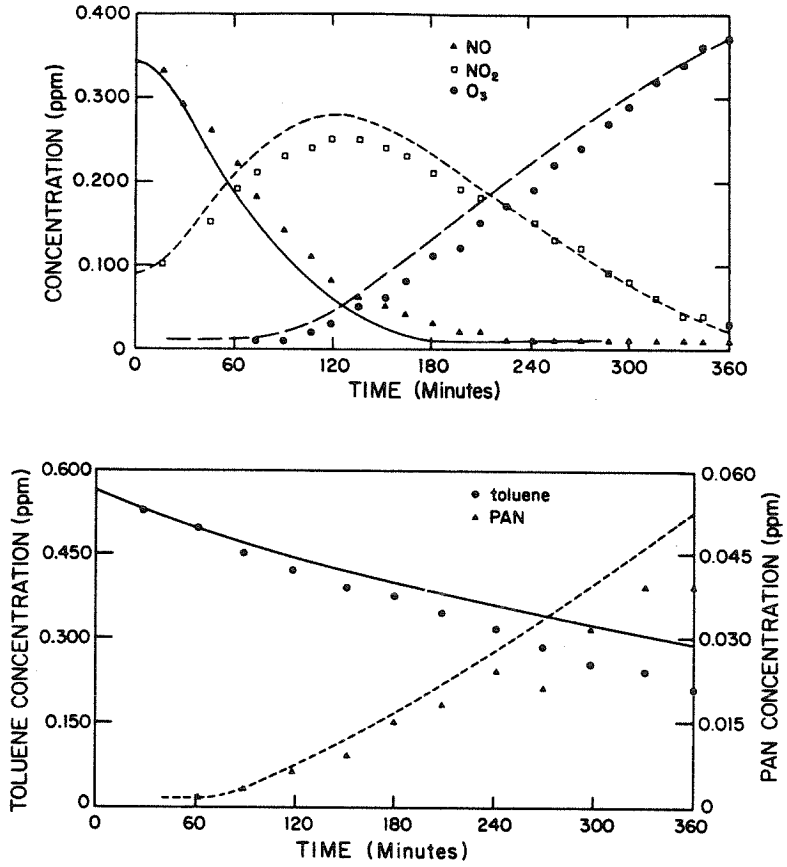

Figure 9. Observed and calculated concentration–time profiles for toluene–NO_x experiment EC-327.

from SAPRC experiment EC-266, very similar results are obtained with data from the other experiments considered here. We see that although the system reactivity does increase as the percentage of OH addition increases, the differences between the simulations are small, and it is not possible to select a best-fit value of the abstraction fraction. At the same time, we see that the predictive ability of our mechanism is not affected by the uncertainty in the rate constant ratio k_{48}/k_{64}.

Abstraction Pathway. The toluene–OH abstraction pathway, which is summarized in Figure 12, proceeds through the formation of benzaldehyde and benzyl nitrate. The specifics of this pathway have been discussed previously [3,4,8] and are therefore not reiterated here. The major uncertainty in the abstraction mechanism concerns benzaldehyde photolysis.

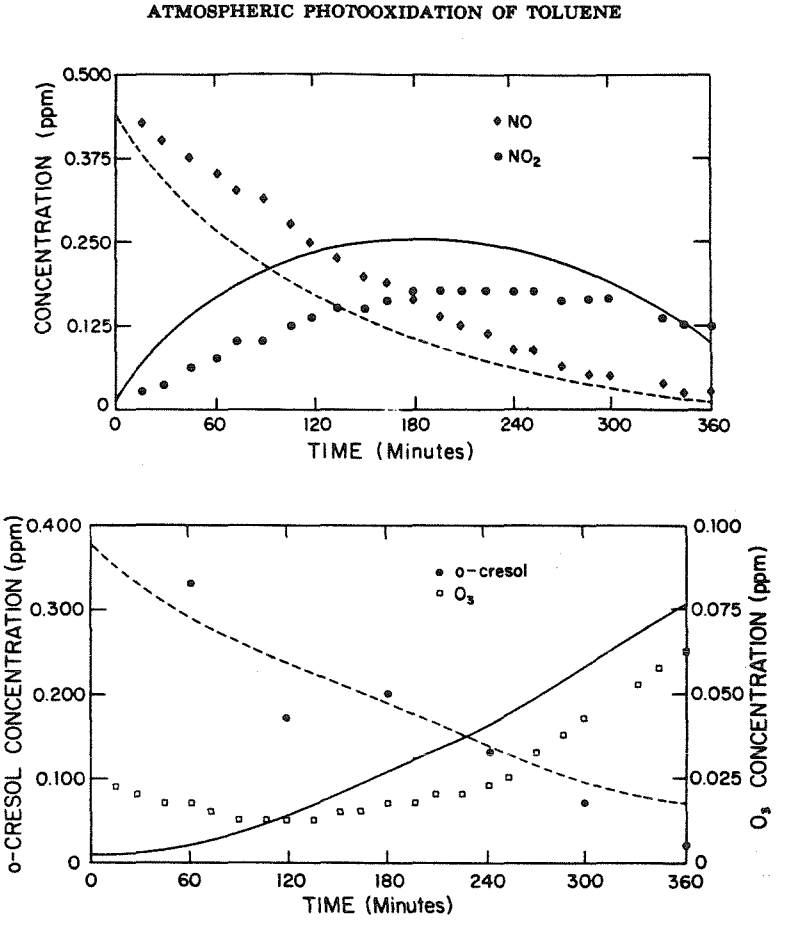

Figure 10. Observed and calculated concentration–time profiles for *o*-cresol–NO_x experiment EC-281.

Both Atkinson et al. [4] and Killus and Whitten [5] have found that in order to simulate the observed decay of benzaldehyde in toluene–benzaldehyde–NO_x irradiations, it is necessary to include a first-order decay (photolysis) of benzaldehyde. Additional evidence of relatively rapid benzaldehyde photolysis was found in the Carter et al. [9] study of chamber-dependent radical sources. The uncertainty surrounding benzaldehyde chemistry is centered on the photolysis products. Atkinson et al. [4] found that their mechanism could simulate toluene photooxidation data only if it is assumed that nonradical products are formed, while Killus and Whitten [5] concluded that benzaldehyde photolysis must produce radical products. Additional evidence supporting the hypothesis of nonradical products is found in the Carter et al. [9] study, where the addition of benzaldehyde to irradiated NO_2–air mixtures produced measured reductions in OH radical concentrations that

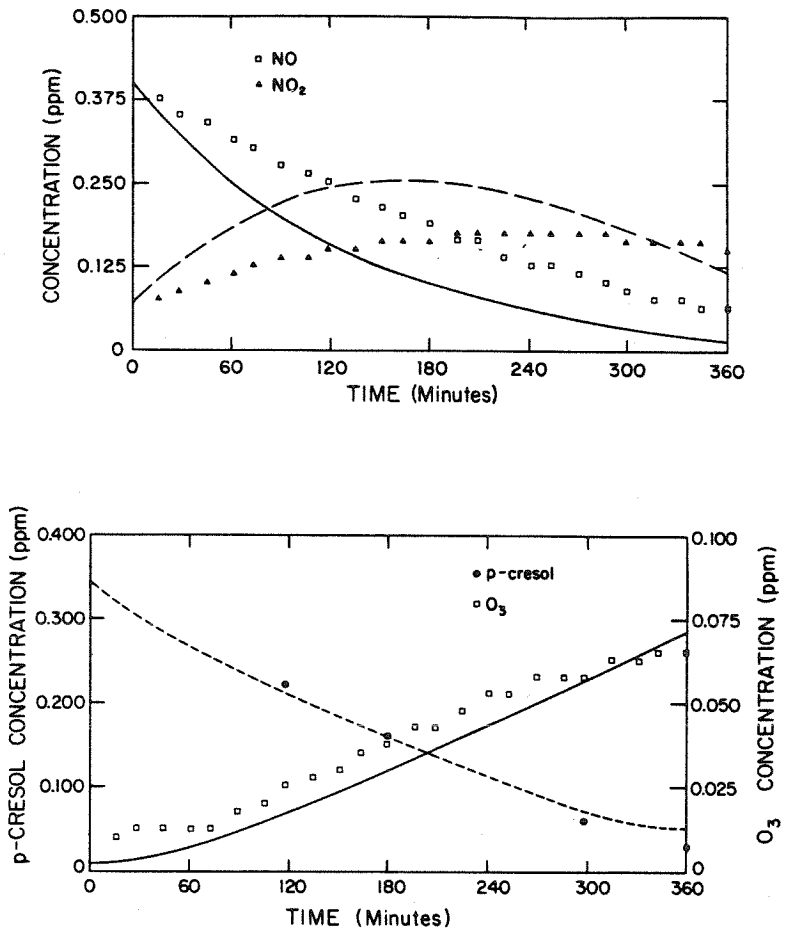

Figure 11. Observed and calculated concentration–time profiles for *p*-cresol–NO_x experiment EC-290.

agreed with the predictions of mechanisms assuming no radical production from benzaldehyde.

Figure 2 shows the effect of varying the benzaldehyde photolysis products on the predictions of the toluene mechanism presented here. The data are from toluene–benzaldehyde–NO_x experiments EC-337 and EC-339. Clearly, all of the experimental data are more consistent with the assumption of nonradical products. The deviation between experiment and theory observed when radical products are assumed is much greater than the discrepancies found in any of the seven SAPRC toluene experiments simulated in this study. These results

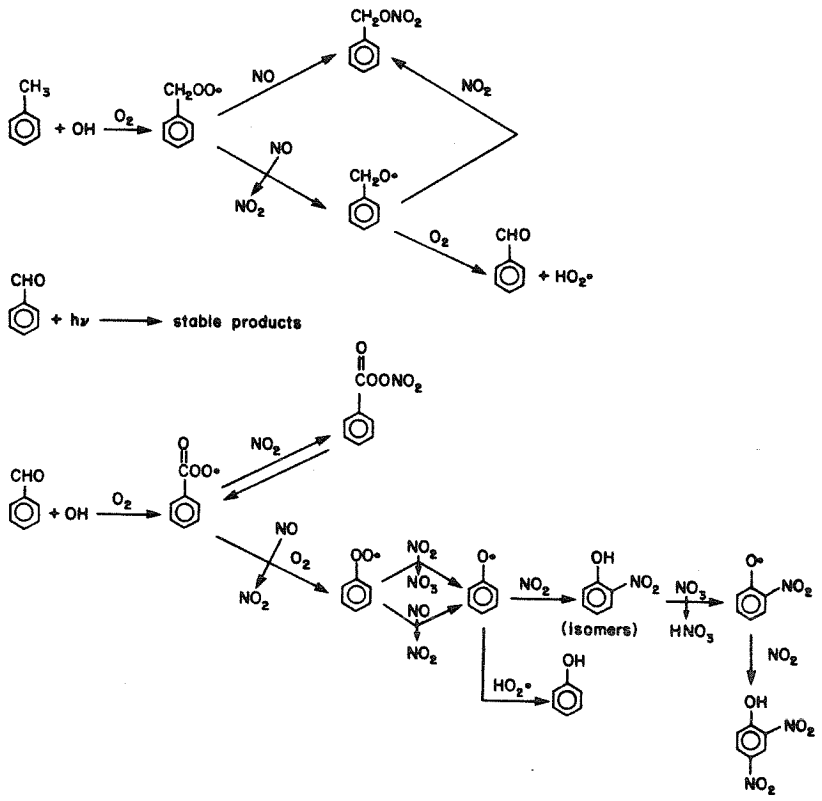

Figure 12. Toluene–OH abstraction pathway reaction mechanism.

represent a convincing argument for the hypothesis of nonradical benzaldehyde photolysis products.

Since benzaldehyde photolysis apparently does not result in radical formation, benzene and CO appear to be the most likely products [3,4]. However, the benzene yields in experiments at SAPRC were less than 1% of the benzaldehyde calculated to be consumed by photolysis [4]. Thus at the present time, the products of benzaldehyde photolysis represent an important piece of unknown information in the toluene mechanism, although this uncertainty does not inhibit the predictive ability of our toluene mechanism.

Addition Pathway. The toluene–OH addition pathway reaction mechanism is summarized in Figure 13. Of the 92% of the overall reaction that proceeds via addition, Kenley et al. [15] report the following distribution by location of addition: 81% *ortho*, 14% *para*, and 5% *meta*. The thermalized adduct produced in reaction (64) can react with either O_2 or NO_2,

(65) 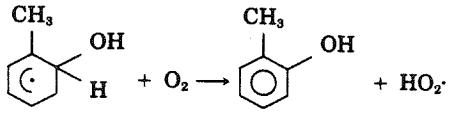

(67) 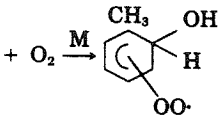

(66) 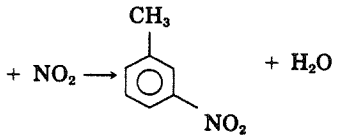

with [8]

$$k_{65} = 10 \text{ ppm}^{-1} \cdot \text{min}^{-1} \qquad \text{at } \sim 300 \text{ K}$$

and

$$\frac{k_{65}}{k_{66}} = (4.4 \pm 0.5) \times 10^3$$

Because of a possible pressure effect, there is a great deal of uncertainty surrounding the k_{66}/k_{65} ratio, but in any event, reaction (66) is only a minor pathway. A much more important parameter is the rate constant ratio k_{65}/k_{67}. Both the Atkinson et al. [4] and the Killus and Whitten [5] studies assumed that *o*-cresol is formed 25% of the time ($k_{65}/k_{67} \approx 0.34$). However, in the very recent product yield study of Atkinson et al. [10], a yield of 13% *o*-cresol was observed. If we make use of the isomeric cresol distribution of Kenley et al. [15], we arrive at ~17% cresol formation, or

$$\frac{k_{65}}{k_{67}} \approx 0.2$$

This leads to an effective k_{67} at 298 K of

$$k_{67} = 50 \text{ ppm}^{-1} \cdot \text{min}^{-1}$$

Figure 3 shows the effect on mechanism predictions of varying the ratio k_{65}/k_{67}. With the experiments simulated in this study, the mechanism shown in Table AI gives results that fit the data best when $k_{65}/k_{67} \approx 0.2$, in excellent agreement with the recent Atkinson et al. [10] study. As expected, the predicted concentration–time profiles are a fairly strong function of this ratio, since toluene ring opening produces the potent photoinitiator methyl glyoxal, while *o*-cresol ring opening does not.

The toluene–OH–O_2 adduct produced in reaction (67) reacts with O_2 and NO, and then, following ring fragmentation, leads to α-dicarbonyl

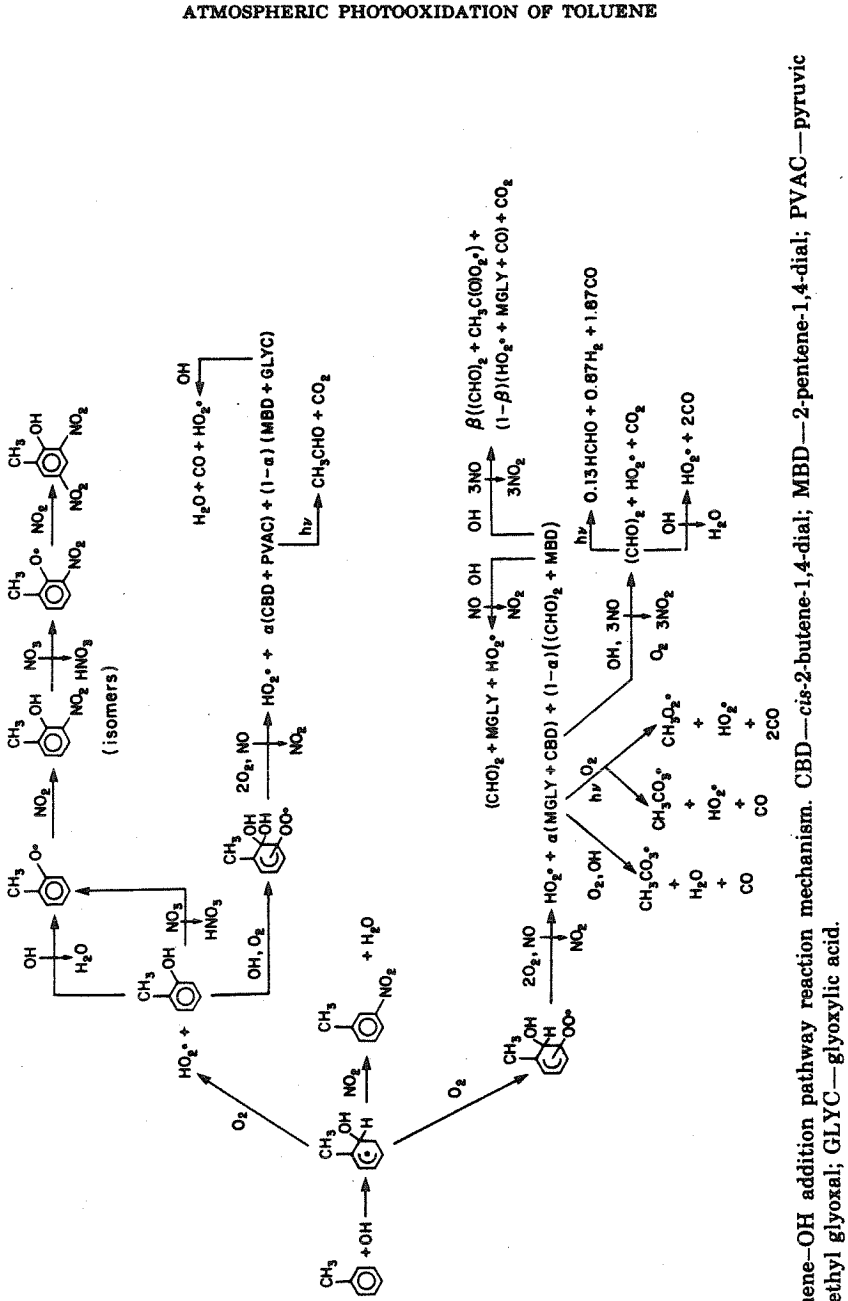

Figure 13. Toluene–OH addition pathway reaction mechanism. CBD—*cis*-2-butene-1,4-dial; MBD—2-pentene-1,4-dial; PVAC—pyruvic acid; MGLY—methyl glyoxal; GLYC—glyoxylic acid.

and conjugated γ-dicarbonyl products,

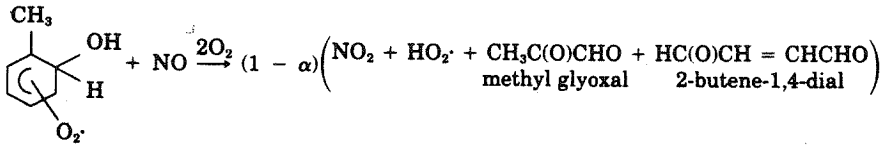

(68)

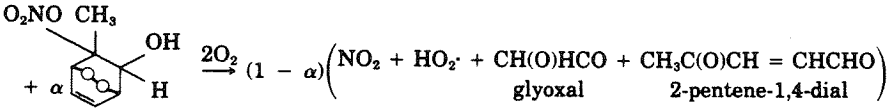

(isomers)

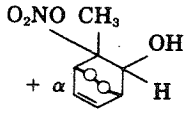

(isomers)

(69)

The specific mechanisms of the above reactions have been discussed in detail elsewhere [4,8]. Two aspects of the ring opening sequence that are not completely understood are (1) the fraction α of organic nitrate formation, and (2) the relative abundance of the possible decomposition pathways [i.e., the relative rates of reactions (68) and (69)]. The results of examining these two issues using the mechanism in the Appendix are now discussed.

In an attempt to improve the fit of calculated to observed O_3 yields in toluene–NO_x irradiations, Atkinson et al. [4] assumed that about 25% of the reaction of NO with the various bicyclic peroxy radicals postulated to be formed in reactions (68) and (69) result in the formation of an organic nitrate. However, since it is now clear that the mechanism presented in Atkinson et al. [4] employed too large a rate of photolysis of methyl glyoxal (to be discussed shortly), we expect a priori that a mechanism using a more appropriate methyl glyoxal photolysis rate would not supply enough radicals to compensate for the large radical sink that this nitrate formation represents.

Figure 4 shows the effect of assuming various percentages of organic nitrate formation on the performance of the mechanism in Table AI. Including any amount of nitrate formation significantly reduces the reactivity of the system and degrades the performance of the mechanism in each of the experiments simulated in this study. Alkyl nitrate yields observed from reactions of simple aliphatic hydrocarbon peroxy radicals with NO probably cannot serve as a useful basis for *a priori* estimates for analogous reactions in aromatic systems, since the presence of electron-withdrawing peroxy groups on bicyclic peroxy radicals or the aromaticity of the benzyl peroxy radicals may significantly affect the energetics of the system. Furthermore, even if the aliphatic RO_2–NO

system can serve as a basis for such estimates, it should be noted that the peroxy radicals formed in the aromatic system are much "tighter" than those formed from the *n*-alkane, which would imply lower alkyl nitrate yields. Thus on the basis of current information, we estimate that the formation of bicyclic peroxy organic nitrates is probably not important in aromatic systems. If such nitrates are indeed formed, their atmospheric fate may, in fact, be condensation into the aerosol phase. Thus the gas phase chemistry of such species can probably be safely neglected.

In the simulation study of Atkinson et al. [4] the experimental data could be fit to similar degrees of accuracy by assuming that either reaction (68) dominates reaction (69), or that both reactions are important. In another simulation study, Killus and Whitten [5] assumed that reaction (68) occurs exclusively. Nojima et al. [16] irradiated toluene–NO_x and *m*-xylene–NO_x mixtures at high concentrations and found methyl glyoxal as the major dicarbonyl product. Figure 5 shows the effect of changing the ratio k_{68}/k_{70} in the mechanism. It can be seen that the data are consistent with exclusive formation of methylglyoxal and 2-butene-1,4-dial via reaction (68). When glyoxal (which does not photolyze to radicals) and 2-pentene-1,4-dial are assumed to be formed at significant rates from reaction (69), the system reactivity is much too slow. This reduction in reactivity was counteracted in the Atkinson et al. [4] study by what we know to be an overestimated rate of methyl glyoxal photolysis (~8 times the currently recommended value).

It should be emphasized that our conclusions regarding organic nitrate formation and the importance of reaction (68) are dependent on the assumption that both the measured methyl glyoxal photolysis rate of Plum et al. [17] and the chamber radical source term are accurate. An increase in either of these, or any other change which would increase radical concentrations, might require a reevaluation of these conclusions.

o-Cresol Chemistry

The atmospheric fate of the cresols is discussed in detail elsewhere [3,4,8] and is therefore not discussed here.

α-Dicarbonyl Chemistry

The two α-dicarbonyls produced in the toluene–NO_x system are glyoxal (CH(O)CHO) and methyl glyoxal ($CH_3C(O)CHO$). Both species react with OH and photolyze under simulated atmospheric conditions, but it is the photolysis of methyl glyoxal that has the greatest effect on the behavior of the system. Plum et al. [17] recently measured the photolysis rates of glyoxal, methyl glyoxal, and biacetyl, and measured

the OH rate constants of glyoxal and methyl glyoxal. The measured methyl glyoxal photolysis rate is a factor of ~8 lower than that used in the Atkinson et al. [4] study, and more than a factor of 2 lower than that used by Killus and Whitten [5]. The importance of methyl glyoxal photolysis is shown in Figure 14.

Although our current mechanism makes use of the Plum et al. [17] photolysis rates for both glyoxal and methyl glyoxal, that study provided very little information regarding the photolysis products. However, these investigators did observe an ~13% yield of HCHO in the photolysis of glyoxal, indicating that the process

$$HC(O)CHO + h\nu \rightarrow HCHO + CO$$

is occurring. Most of the reaction is probably occurring via [18]

$$HC(O)CHO + h\nu \rightarrow 2CO + H_2$$

Thus in our mechanism we represent glyoxal photolysis by

$$\text{(47)} \quad HC(O)CHO + h\nu \rightarrow 0.13HCHO + 1.87CO + 0.87H_2$$

The formation of peroxyacetylnitrate (PAN) and the high rate of radical initiation found in toluene–NO_x irradiations indicate that methyl glyoxal photolysis, at least partially, produces peroxyacetyl and HO_2 radicals via

$$\text{(44a)} \quad CH_3C(O)CHO + h\nu \rightarrow CH_3\dot{C}O + H\dot{C}O \xrightarrow[fast]{2O_2} CH_3CO_3\cdot + CO + HO_2\cdot$$

$$\text{(44b)} \quad \rightarrow CH_3C(O)\dot{C}O + H\cdot \xrightarrow[fast]{} CH_3\dot{C}O + CO + H\cdot \xrightarrow[fast]{2O_2} CH_3CO_3\cdot + HO_2\cdot + CO$$

However, methyl glyoxal photolysis may also proceed via

$$\text{(45)} \quad CH_3C(O)CHO + h\nu \rightarrow C_3H\cdot + HC(O)\dot{C}O \xrightarrow[fast]{2O_2} CH_3O_2\cdot + HO_2\cdot + 2CO$$

Atkinson et al. [4] assumed that 100% of methyl glyoxal photolysis proceeds via reactions (44a) or (44b), while Killus and Whitten [5] found that PAN yields were better fit with their mechanism by assuming 35% of the photolysis proceeds via reaction (45). We find that the data are best fit by assuming ~30% of the photolysis proceeds via reaction (45). However, this percentage changes somewhat as the ratio of *o*-cresol formation to ring opening (k_{65}/k_{67}) is varied within its uncertainty limits. Thus further experimental evidence is needed to de-

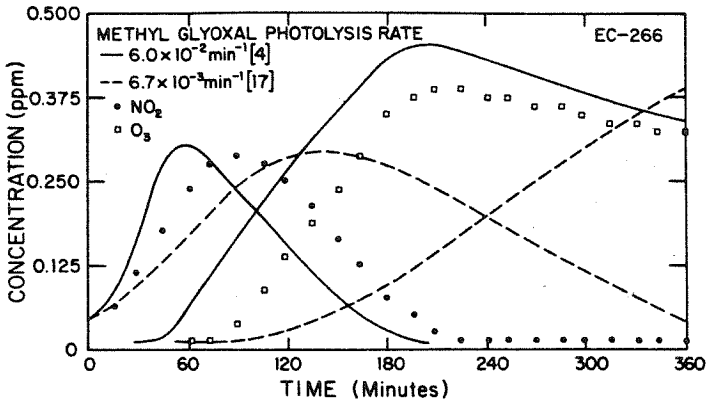

Figure 14. Results of changing the methyl glyoxal photolysis rate in the Atkinson et al. [4] toluene mechanism from its stated value to the recently measured Plum et al. [17] value.

termine unambiguously the relative importance of reactions (44) and (45).

Conjugated α-Dicarbonyl Chemistry

The chemistry of the conjugated α-dicarbonyls formed from toluene–NO_x photooxidation is discussed in detail elsewhere [4,8]. It has generally been assumed that these species are sufficiently volatile to remain in the gas phase long enough to undergo homogeneous reaction. This may, in fact, not be the case since bifunctional compounds such as these are generally much less volatile than monofunctional compounds. Gas-to-particle conversion of these species could partially account for the poor carbon balances obtained in product studies of aromatic photooxidation, as well as for the observed aerosol formation in such systems. If this is the case, their formation may have no impact on subsequent gas phase chemistry.

We have performed a number of simulations where we have attempted to represent the condensation of conjugated γ-dicarbonyls by simply reducing the rate constant for their initial reaction with OH. Some typical results of these calculations are shown in Figure 6. We see that when some aerosol formation is assumed, the reactivity of the simulated system is closer to the experimental results. However, the oxidant levels tend to be overpredicted. We can obtain better agreement between the experimental and simulated PAN profiles by lowering the ratio k_{44}/k_{45}, but this leads to even greater O_3 offsets. Thus we are unable to determine unambiguously if conjugated γ-dicarbonyl condensation is important.

Conclusions

The chemical mechanism for toluene photooxidation which is developed here contains the latest available kinetic and mechanistic data, and has been extensively tested against smog chamber data. This new mechanism gives good agreement between the predicted and observed concentration–time profiles for all the major species in both toluene–NO_x and toluene–benzaldehyde–NO_x experiments performed with a variety of initial conditions. The agreement between theoretically predicted and experimentally observed oxidant yields is especially good.

The new mechanism has been used to gain insight into areas of toluene photooxidation which are not completely understood. At present the major uncertainties in the mechanism center around the methylglyoxal and benzaldehyde photolysis products, the exact ring fragmentation pathways, and the aerosol formation ability of some of the oxidation products. Although further experimental information on any of these items would be very useful and should be given a high priority, we feel that the mechanism presented here can be used confidently in its current form, and can also serve as a useful starting point toward the development of accurate lumped mechanisms for modeling gas phase aromatic hydrocarbon photooxidation.

Appendix

TABLE AI. Toluene reaction mechanism.

Reaction[1]	Rate Constant[2]	Activation Energy (K)	Reference	Note
Inorganic Reactions:				
1) $NO_2 + h\nu \rightarrow NO + O(^3P)$	*	-	-	1
2) $O(^3P) + O_2 \rightarrow O_3$	2.6×10^1	-5.1×10^2	6,7	-
3) $O_3 + NO \rightarrow NO_2 + O_2$	2.7×10^1	1.5×10^3	6,7	-
4) $O(^3P) + NO_2 \rightarrow NO + O_2$	1.4×10^4	-	6,7	-
5) $O_3 + NO_2 \rightarrow NO_3 + O_2$	4.7×10^{-2}	2.45×10^3	6,7	-
6) $NO_3 + NO \rightarrow 2NO_2$	3.0×10^4	-	6,7	-
7) $HO_2 + NO_2 \rightarrow HO_2NO_2$	1.6×10^3	-	8	-
8) $NO_2 + OH \rightarrow HNO_3$	1.6×10^4	-	6,7	-
9) $O_3 + OH \rightarrow HO_2 + O_2$	9.9×10^1	9.7×10^2	6,7	-
10) $O_3 + HO_2 \rightarrow OH + 2O_2$	3.0×10^0	5.8×10^2	6,7	-
11) $HO_2NO_2 \rightarrow HO_2 + NO_2$	5.1×10^0	1.042×10^4	8	-

(continued)

ATMOSPHERIC PHOTOOXIDATION OF TOLUENE

TABLE AI. *(Continued)*

Reaction	Rate Constant	Activation Energy (K)	Reference	Note
12) $HO_2 + NO \rightarrow NO_2 + OH$	1.2×10^4	-2.4×10^2	6,7	-
13) $HO_2 + HO_2 \rightarrow H_2O + O_2$	3.9×10^3	-1.2×10^3	6,7	-
14) $HO_2 + HO_2 + H_2O \rightarrow H_2O_2 + O_2 + H_2O$	2.2×10^{-1}	-5.8×10^3	8	-
15) $O_3 + h\nu \rightarrow O(^3P) + O_2$	1.4×10^{-2}	-	4	-
16) $O_3 + h\nu \rightarrow O(^1D) + O_2$	5.9×10^{-4}	-	4	-
17) $O(^1D) + O_2 \rightarrow O(^3P) + O_2$	4.3×10^4	-	6	-
18) $O(^1D) + H_2O \rightarrow 2OH$	3.2×10^5	-	6	-
19) $NO + OH \rightarrow HONO$	9.7×10^3	-	8	-
20) $HONO + h\nu \rightarrow NO + OH$	6.6×10^{-2}	-	4	-
21) $NO + NO + O_2 \rightarrow 2NO_2$	7.2×10^{-10}	-5.3×10^2	8	-
22) $NO_3 + NO_2 \rightarrow NO + NO_2 + O_2$	5.9×10^{-1}	1.23×10^3	8	-
23) $NO_3 + NO_2 \rightarrow N_2O_5$	1.6×10^3	-	6,7	-
24) $N_2O_5 \rightarrow NO_2 + NO_3$	3.1×10^0	1.108×10^4	7	-
25) $N_2O_5 + H_2O \rightarrow 2HNO_3$	4.4×10^{-6}	-	4	-
26) $H_2O_2 + OH \rightarrow HO_2 + H_2O$	2.5×10^3	-	6,7	-
27) $H_2O_2 + h\nu \rightarrow 2OH$	2.8×10^{-4}	-	4	-
28) $CO + OH \xrightarrow{O_2} HO_2 + CO_2$	4.0×10^2	-	6,7	-
29) $NO_3 + h\nu \rightarrow 0.3NO + 0.7NO_2 + 0.7O(^3P)$	6.1×10^0	-	-	2
Aldehyde Reactions and PAN Formation:				
30) $CH_3CHO + h\nu \xrightarrow{2O_2} CH_3O_2\cdot + HO_2 + CO$	*	-	-	3
31) $CH_3CHO + OH \xrightarrow{O_2} CH_3C(O)O_2\cdot + H_2O$	2.4×10^4	-2.6×10^2	7	-
32) $CH_3O_2\cdot + NO \rightarrow NO_2 + CH_3O\cdot$	1.1×10^4	-	6,7	-
33) $CH_3O\cdot + O_2 \rightarrow HCHO + HO_2\cdot$	2.1×10^0	1.35×10^3	6,7	-
34) $CH_3O\cdot + NO_2 \rightarrow CH_3ONO_2$	2.2×10^4	-	8	-
35) $CH_3O_2\cdot + HO_2 \rightarrow CH_3OOH + O_2$	9.2×10^3	-1.3×10^3	6,7	-
36) $CH_3C(O)O_2\cdot + NO \xrightarrow{2O_2} NO_2 + CH_3O_2\cdot + CO_2$	1.1×10^4	-	8	-
37) $CH_3C(O)O_2\cdot + NO_2 \rightarrow PAN$	6.9×10^3	-	8	-
38) $CH_3C(O)O_2\cdot + HO_2 \rightarrow CH_3C(O)O_2H + O_2$	4.4×10^3	-	8	-
39) $PAN \rightarrow CH_3C(O)O_2\cdot + NO_2$	2.2×10^{-2}	1.354×10^4	8	-

(continued)

TABLE AI. (*Continued*)

Reaction	Rate Constant	Activation Energy (K)	Reference	Note
40) $HCHO + h\nu \rightarrow H_2 + CO$	*	-	-	3
41) $HCHO + h\nu \xrightarrow{2O_2} 2HO_2 + CO$	*	-	-	3
42) $HCHO + OH \xrightarrow{O_2} HO_2 + CO + H_2O$	1.6×10^4	-	7	-
α-Dicarbonyl Chemistry:				
43) $CH_3C(O)CHO + OH \xrightarrow{O_2} CH_3C(O)O_2\cdot + CO + H_2O$	2.5×10^4	-	17	-
44) $CH_3C(O)CHO + h\nu \xrightarrow{2O_2} CH_3C(O)O_2\cdot + + HO_2 + CO$	*	-	17	4
45) $CH_3C(O)CHO + h\nu \xrightarrow{2O_2} CH_3O_2\cdot + HO_2 + 2CO$	*	-	17	-
46) $(CHO)_2 + OH \xrightarrow{O_2} HO_2 + 2CO + H_2O$	1.7×10^4	-	17	-
47) $(CHO)_2 + h\nu \rightarrow 0.13HCHO + 0.87H_2 + 1.87CO$	*	-	17	4
Toluene Abstraction Pathway:				
48) $C_6H_5\text{-}CH_3 + OH \xrightarrow{O_2} C_6H_5\text{-}CH_2O_2\cdot + H_2O$	7.5×10^2	-	8	-
49) $C_6H_5\text{-}CH_2O_2\cdot + NO \rightarrow NO_2 + C_6H_5\text{-}CH_2O\cdot$	9.0×10^3	-	8	-
50) $C_6H_5\text{-}CH_2O_2\cdot + NO \rightarrow C_6H_5\text{-}CH_2ONO_2$	1.0×10^3	-	8	-
51) $C_6H_5\text{-}CH_2O\cdot + O_2 \rightarrow C_6H_5\text{-}CHO + HO_2$	1.0×10^1	6.9×10^2	8	-
52) $C_6H_5\text{-}CH_2O\cdot + NO_2 \rightarrow C_6H_5\text{-}CH_2ONO_2$	1.9×10^4	-	8	-
53) $C_6H_5\text{-}CHO + h\nu \rightarrow$ stable products	1.6×10^{-3}	-	-	5
54) $C_6H_5\text{-}CHO + OH \xrightarrow{O_2} C_6H_5\text{-}C(O)O_2\cdot + H_2O$	1.9×10^4	-	8	-
55) $C_6H_5\text{-}C(O)O_2\cdot + NO \xrightarrow{O_2} NO_2 + C_6H_5\text{-}O_2\cdot + CO_2$	1.0×10^4	-	8	-
56) $C_6H_5\text{-}C(O)O_2\cdot + NO_2 \rightarrow C_6H_5\text{-}C(O)O_2NO_2$	6.9×10^3	-	8	-
57) $C_6H_5\text{-}C(O)O_2NO_2 \rightarrow C_6H_5\text{-}C(O)O_2\cdot + NO_2$	9.6×10^{-3}	1.304×10^4	8	-
58) $C_6H_5\text{-}O_2\cdot + NO \rightarrow NO_2 + C_6H_5\text{-}O\cdot$	9.0×10^3	-	8	-
59) $C_6H_5\text{-}O_2\cdot + NO_2 \rightarrow NO_3 + C_6H_5\text{-}O\cdot$	1.0×10^4	-	8	-
60) $C_6H_5\text{-}O\cdot + NO_2 \rightarrow$ 	2.2×10^4	-	8	-
61) 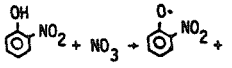	3.0×10^3	-	19	6

(continued)

ATMOSPHERIC PHOTOOXIDATION OF TOLUENE

TABLE AI. (*Continued*)

	Reaction	Rate Constant	Activation Energy (K)	Reference	Note
62)	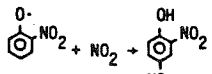	2.2×10^4	-	-	7
63)	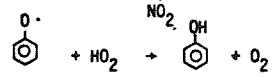	7.4×10^3	-	8	-
	Toluene Addition Pathway:				
64)	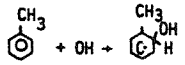	8.7×10^3	-	8	-
65)	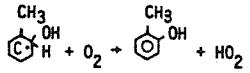	1.0×10^1	6.9×10^2	8	-
66)	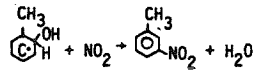	4.4×10^4	-	8	-
67)	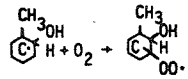	4.9×10^1	-	8	-
68)	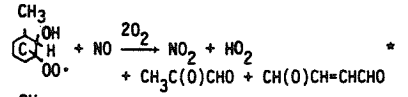	*	-	8	8
69)	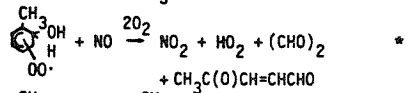	*	-	8	8
70)	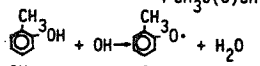	4.9×10^3	9.0×10^2	8	-
71)	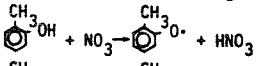	1.5×10^4	-	8	-
72)	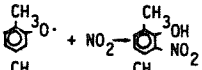	2.2×10^4	-	8	-
73)	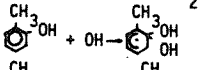	5.6×10^4	-	8	-
74)	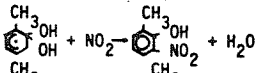	4.4×10^4	-	8	-
75)	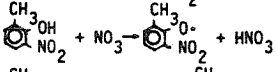	1.5×10^4	-	19	9
76)	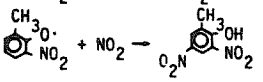	2.2×10^4	-	-	7
77)	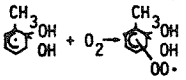	4.9×10^1	-	8	-

(continued)

TABLE AI. *(Continued)*

	Reaction	Rate Constant	Activation Energy (K)		Reference	Note
	Toluene addition path (continued)					
78)	+ NO $\xrightarrow{2O_2}$ $NO_2 + HO_2$ + CH(O)CH=CHCHO + $CH_3C(O)COOH$	*	-		8	8
79)	+ NO $\xrightarrow{2O_2}$ NO_2 + HO_2 + $CH_3C(O)CH=CHCHO$ + CH(O)COOH	*	-		8	8
80)	$CH(O)COOH + OH \rightarrow HO_2 + H_2O + CO$	4.7×10^{4}	-		8	-
81)	$CH_3C(O)COOH + h\nu \rightarrow CH_3CHO + CO_2$	5.0×10^{-3}	-		5	-
	Conjugated γ-dicarbonyl chemistry					
82)	$HC(O)CH=CHCHO + OH \xrightarrow{O_2} HC(O)CH=CHC(O)O_2\cdot + H_2O$	4.4×10^{4}	-		8	-
83)	$HC(O)CH=CHC(O)O_2\cdot + NO \xrightarrow{O_2} NO_2 + CO_2 + HC(O)CH=CHO_2\cdot$	1.0×10^{4}	-		8	-
84)	$HC(O)CH=CHO_2\cdot + NO \xrightarrow{O_2} NO_2 + HC(O)CH(O_2\cdot)CHO$	1.0×10^{4}	-		8	-
85)	$HC(O)CH(O_2\cdot)CHO + NO \rightarrow HC(O)CH(ONO_2)CHO$	4.0×10^{2}	-		8	-
86)	$HC(O)CH=CHC(O)O_2\cdot + NO_2 \rightarrow HC(O)CH=CHCO_3NO_2$	6.9×10^{3}	-		8	-
87)	$HC(O)CH=CHCO_3NO_2 \rightarrow HC(O)CH=CHC(O)O_2\cdot + NO_2$	2.2×10^{-2}	-		8	-
88)	$HC(O)CH(O_2\cdot)CHO + NO \xrightarrow{O_2} (CHO)_2 + HO_2 + NO_2 + CO$	1.0×10^{4}	-		8	-
89)	$HC(O)CH=CHO_2\cdot + NO \rightarrow HC(O)CH=CHONO_2$	4.0×10^{2}	-		8	-
90)	$HC(O)CH=CHO_2\cdot + NO_2 \xrightarrow{O_2} HC(O)CH(O_2\cdot)CHO + NO_3$	1.0×10^{4}	-		8	-
91)	$CH_3C(O)CH=CHCHO + OH \xrightarrow{O_2} H_2O + CH_3C(O)CH=CHC(O)O_2\cdot$	2.2×10^{4}	-		8	10
92)	$CH_3C(O)CH=CHCHO + OH \xrightarrow{O_2} CH_3C(O)CH(OH)C(O_2\cdot)HCHO$	7.4×10^{3}	-		8	10
93)	$CH_3C(O)CH(OH)C(O_2\cdot)HCHO + NO \xrightarrow{O_2} NO_2 + HO_2 + CH_3C(O)CHO + (CHO)_2$	1.0×10^{4}	-		8	10
94)	$CH_3C(O)CH=CHC(O)O_2\cdot + NO \xrightarrow{O_2} NO_2 + CO_2 + CH_3C(O)CH=CHO_2\cdot$	1.0×10^{4}	-		8	10
95)	$CH_3C(O)CH=CHO_2\cdot + NO \xrightarrow{O_2} NO_2 + CH_3C(O)CH(O_2\cdot)CHO$	1.0×10^{4}	-		8	10
96)	$CH_3C(O)CH(O_2\cdot)CHO + NO \rightarrow CH_3C(O)CH(ONO_2)CHO$	8.0×10^{6}	-		8	10
97)	$CH_3C(O)CH=CHC(O)O_2\cdot + NO \rightarrow CH_3C(O)CH=CHCO_3NO_2$	6.9×10^{3}	-		8	10
98)	$CH_3C(O)CH=CHCO_3NO_2 \rightarrow CH_3C(O)CH=CHC(O)O_2\cdot + NO_2$	2.2×10^{-2}	-		8	10
99)	$CH_3C(O)CH(O_2\cdot)CHO + NO \xrightarrow{O_2} NO_2 + CH_3C(O)O_2\cdot + (CHO)_2$	5.0×10^{3}	-		8	10
100)	$CH_3C(O)CH(O_2\cdot)CHO + NO \xrightarrow{O_2} NO_2 + HO_2 + CH_3C(O)CHO + CO$	5.0×10^{3}	-		8	10
101)	$CH_3C(O)CH=CHO_2\cdot + NO \rightarrow CH_3C(O)CH=CHONO_2$	8.0×10^{2}	-		8	10
102)	$CH_3C(O)CH=CHO_2\cdot + NO_2 \xrightarrow{O_2} NO_3 + CH_3C(O)CH(O_2\cdot)CHO$	1.0×10^{4}	-		8	10

(continued)

TABLE AI. (*Continued*)

Reaction	Rate Constant	Activation Energy(K)	Reference	Note
Chamber dependent reactions:				
103) O_3 → wall	1.65×10^{-3}	-	4	11
104) wall → NO	1.0×10^{-4}	-	4	11
105) wall → OH	*	-	9	12
106) NO_2 → OH	*	-	9	12

* See note below.

[1] Only one isomer is shown, even when many isomers are possible.

[2] ppm min units.

Notes to Table AI

1—See Table AII.

2—Atkinson et al. [4] use

$$NO_3 + h\nu \rightarrow NO_2 + O(^3P) \qquad k = 4.4\ \text{min}^{-1}$$
$$NO_3 + h\nu \rightarrow NO + O_2 \qquad k = 1.7\ \text{min}^{-1}$$

We combine these two steps to give

$$NO_3 + h\nu \rightarrow 0.3NO + 0.7NO_2 + 0.7O(^3P) \qquad k_{29} = 6.1 \times 10^0\ \text{min}^{-1}$$

3—The rate constants used in our mechanism are based on Demerjian et al. [20],

$$k_{30} = 8.4 \times 10^{-4} k_1$$
$$k_{40} = 3.4 \times 10^{-3} k_1$$
$$k_{41} = 3.5 \times 10^{-3} k_1$$

Horowitz and Calvert [21] have suggested lower values for all of these rate constants. However, only insignificant changes in the model predictions result when the Horowitz and Calvert values [21] are used in our mechanism.

4—From Plum et al. [17],

$$k_{44} + k_{45} = 0.019 k_1$$
$$k_{47} = 0.008 k_1$$

We find that the PAN data are best simulated by assuming $k_{44}/(k_{44} + k_{45}) \approx 0.7$.

5—k_{53} was chosen to give the best fit of benzaldehyde profiles in toluene–benzaldehyde–NO_x runs EC-337 and EC-339.

6—k_{61} is assumed to be about the same as the rate constant for the phenol + NO_3 reaction [19].

7—k_{62} is assumed to be of the same order as the rate constant for another RO· + NO_2 reactions.

8—From Atkinson and Lloyd [8],

$$k_{68} + k_{69} = k_{78} + k_{79} = 1.0 \times 10^4\ \text{ppm}^{-1} \cdot \text{min}^{-1}$$

See text for a discussion of the effects of varying $k_{68}/(k_{68} + k_{69})$ and $k_{78}/(k_{78} + k_{79})$.

9—k_{75} is assumed to be of the same order as the rate constant for the *o*-cresol + NO_3 abstraction reaction.

10—These reactions are only needed if k_{68} or k_{78} is not equal to zero. Since we find the best results are obtained with $k_{68} = k_{78} = 0$, no 2-pentene-1,4-dial is produced. Thus reactions (91)–(102) can be ignored.

11—Chamber-dependent.

12—From Carter et al. [9] we arrive at

$$k_{105} = 0.39 k_1$$
$$k_{106} = 1.37 k_1$$

TABLE AII. Initial conditions and important physical parameters for SAPRC experiments.

Experiment	Initial Concentration (ppb) Toluene	NO	NO_2	Benzaldehyde	HCHO	CO	HONO[1]	Average RH (%)	k_1 (min^{-1})	Average Temperature (K)
EC-265	1070	435	48	-	1	-	7	54	0.35	303
EC-266	1196	432	59	-	1	330	7	47	0.35	303
EC-269	566	398	74	1	3	~200	7	46	0.35	303
EC-271	1146	186	29	-	4	~600	7	49	0.36	303
EC-273	587	96	14	-	2	326	7	49	0.35	304
EC-281	394[2]	458	20	-	-	825	7	48	0.35	303
EC-290	364[3]	413	67	-	-	251	7	52	0.39	303
EC-327	573	357	96	-	13	*	7	*	0.40	303
EC-337	959	322	124	172	172	*	7	66	0.39	303
EC-339	536	341	102	187	2	*	7	64	0.39	303
EC-340	537	333	96	2	5	2593	7	63	0.40	303

[1] Assumed in this study.
[2] *o*-Cresol experiment, no toluene present.
[3] *p*-Cresol experiment, no toluene present.
* Not reported.

Acknowledgments

This research was supported by the State of California Air Resources Board under agreement A2-042-32 and National Science Foundation under Grant ATM-8208625. We wish to acknowledge W. P. L. Carter for helpful discussions.

Bibliography

[1] A. P. Altshuller, W. A. Lonnemon, F. D. Sutterfield, and S. L. Kopczynski, *Environ. Sci. Technol.*, **5**, 1009 (1971).
[2] W. A. Lonneman, S. L. Kopczynski, P. E. Darley, and F. D. Sutterfield, *Environ. Sci Technol.*, **8**, 229 (1974).
[3] D. G. Hendry, A. C. Baldwin, and D. M. Golden, "Computer Modeling of Simulated Photochemical Smog," EPA-600/3-80-029, Feb. 1980.
[4] R. Atkinson, W. P. L. Carter, K. R. Darnall, A. M. Winer, and J. N. Pitts, Jr., *Int. J. Chem. Kinet.*, **12**, 779 (1980).
[5] J. P. Killus and G. Z. Whitten, *Atmos. Environ.*, **16**, 1973 (1982).
[6] W. B. Demore, R. T. Watson, D. M. Golden, R. F. Hampson, M. Kurylo, C. J. Howard, M. J. Molina, and A. R. Ravishankara, "Chemical Kinetics and Photochemical Data for Use in Stratosphere Modeling," Jet Propulsion Lab. Rep. 82-57, July 15, 1982.
[7] D. L. Baulch, R. A. Cox, P. J. Crutzen, R. F. Hampson, Jr., J. A. Kerr, J. Troe, and R. T. Watson, *J. Phys. Chem. Ref. Data*, **11**, 327 (1982).
[8] R. Atkinson and A. C. Lloyd, *J. Phys. Chem. Ref. Data*, to be published (1983).
[9] W. P. L. Carter, R. Atkinson, A. M. Winer, and J. N. Pitts, Jr., *Int. J. Chem. Kinet.*, **14**, 1071 (1982).

[10] R. Atkinson, W. P. L. Carter, and A. M. Winer, *J. Phys. Chem.*, **87**, 1605 (1983).
[11] R. Atkinson, K. R. Darnall, A. C. Lloyd, A. M. Winer, and J. N. Pitts, Jr., *Adv. Photochem.*, **11**, 375 (1979).
[12] R. A. Perry, R. Atkinson, and J. N. Pitts, Jr., *J. Phys. Chem.*, **81**, 296 (1977).
[13] D. G. Hendry, R. A. Kenley, J. E. Davenport, and B. Y. Lan, "Reactions of Oxy Radicals in the Atmosphere," EPA-600/3-79-020, 1979.
[14] F. P. Tully, A. R. Ravishankara, R. L. Thompson, J. M. Nicovich, R. C. Shah, N. M. Kreutter, and P. H. Wine, *J. Phys. Chem.*, **85**, 2262 (1981).
[15] R. A. Kenley, J. E. Davenport, and D. G. Hendry, *J. Phys. Chem.*, **82**, 1095 (1978).
[16] K. Nojima, K. Fukaya, S. Fukai, and S. Kanno, *Chemosphere*, **5**, 247 (1974).
[17] C. N. Plum, E. Sanhueza, R. Atkinson, W. P. L. Carter, and J. N. Pitts, Jr., "OH Radical Rate Constants and Photolysis Rates of α-Dicarbonyls," *Environ. Sci. Technol.*, **17**, 479 (1983).
[18] Y. Osamura, H. F. Schaefer III, M. Dupuis, and W. A. Lester, Jr., *J. Chem. Phys.*, **75**, 5228 (1981).
[19] W. P. L. Carter, A. M. Winer, and J. N. Pitts, Jr., *Environ. Sci. Technol.*, **15**, 829 (1981).
[20] K. L. Demerjian, K. L. Schere, and J. T. Peterson, *Adv. Environ. Sci. Technol.*, **10**, 369 (1980).
[21] A. Horowitz and J. G. Calvert, *J. Phys. Chem.*, **86**, 3105 (1982).

Received April 12, 1983
Accepted June 22, 1983

CHAPTER 3

An Outdoor Smog Chamber and Modeling Study of Toluene-NO_x Photooxidation

Accepted for Publication in the

International Journal of Chemical Kinetics

AN OUTDOOR SMOG CHAMBER AND MODELING STUDY OF TOLUENE-NO_x PHOTOOXIDATION

Joseph A. Leone, Richard C. Flagan, Daniel Grosjean and John H. Seinfeld
Department of Chemical Engineering
California Institute of Technology
Pasadena, California 91125

ABSTRACT

An experimental investigation of the gas-phase photooxidation of toluene-NO_x-air mixtures at part-per-million concentrations has been carried out in a 65 m^3, outdoor smog chamber to assess our understanding of the atmospheric chemistry of toluene. In addition, six CO-NO_x-air irradiations were conducted to characterize the chamber with regard to any wall radical sources. Measured parameters in the toluene-NO_x experiments included O_3, NO, NO_2, HNO_3, peroxyacetyl nitrate (PAN), CO, toluene, benzaldehyde, o-cresol, m-nitrotoluene, peroxybenzoyl nitrate (PBZN), temperature, relative humidity, aerosol size distributions, and particulate organic carbon. Predictions of the reaction mechanism of Leone and Seinfeld [7] are found to be in good agreement with the data under a variety of initial conditions. Additional simulations are used to investigate various mechanistic pathways in areas where our understanding of toluene chemistry is still incomplete.

INTRODUCTION

There currently exists a need for accurate chemical reaction mechanisms describing the atmospheric photooxidation of aromatic hydrocarbons, since aromatics represent a substantial portion of the reactive hydrocarbons present in the urban atmosphere [1-3], and since they are important precursors of both ozone and organic aerosols.

Toluene accounts for about one-third of the atmospheric aromatics [3], and has been the most widely studied aromatic compound with respect to its atmospheric chemistry. There have been four previous attempts to develop reaction mechanisms describing the photooxidation of toluene [4-7]. In the most recent of these studies, Leone and Seinfeld [7] developed a reaction mechanism that describes very well the features of toluene-NO_x photooxidations performed in the indoor evacuable chamber at the University of California Riverside Statewide Air Pollution Research Center (SAPRC) [5]. The SAPRC chamber has been a prime facility for generating data for evaluating photochemical reaction mechanisms. However, it has been shown that reactions carried out in this chamber are influenced by a significant source of free radicals from the chamber walls [8]. For this reason, it is useful to continue to evaluate our understanding of toluene chemistry with data taken from another smog chamber. In this work we present the results of such an evaluation using experimental data from a recently constructed outdoor smog chamber facility that has been carefully characterized with regard to all of the important chamber parameters, including wall radical sources.

In the next section we present a detailed description of our experimental facility. Next, we discuss the results of six CO-NO_x-air irradiations which were performed in order to characterize the wall radical source in our outdoor chamber. The results of six toluene-NO_x irradiations are then

presented and compared with the predictions of the toluene reaction mechanism developed in Leone and Seinfeld [7]. The effects of assuming alternative mechanistic pathways on the predictions of this mechanism are discussed, along with the implications of some recent experimental data concerning yields from the toluene-OH reaction.

DESCRIPTION OF THE OUTDOOR CHAMBER FACILITY

Experiments were performed in a flexible outdoor smog chamber constructed by heat-sealing together 10 panels of 2 mil thick Teflon film measuring four feet by 26 feet each. Mylar tape was placed over the heat-sealed edges as reinforcement. The chamber volume, as measured by the injection of known amounts of NO and/or NO_2, was 65 m^3, resulting in a surface-to-volume ratio of 1.5 m^{-1}. Negligible changes in the size of the chamber were noticeable 6-7 hour after inflation, indicating the absence of any significant leaks. The chamber and associated laboratory facility are located on the rooftop of a three-story building on the Caltech campus. The bottom of the chamber was supported about two feet above the rooftop to allow for the circulation of air beneath the chamber. A dark tarpaulin was placed on the rooftop immediately below the chamber to help minimize the amount of UV radiation being reflected off the roof. More than adequate mixing of the chamber contents was provided by the wind acting on the flexible walls of the chamber.

Figure 1 shows a schematic representation of the outdoor chamber facility. The majority of the instrumentation is housed in a laboratory adjacent to the chamber. Sampling from the chamber is made via Teflon tubing that extends approximately two feet into the chamber through all Teflon ports.

Filling of the chamber with purified air is initiated automatically at approximately 1:00 AM (PST) on the days of experiments. Purified air is

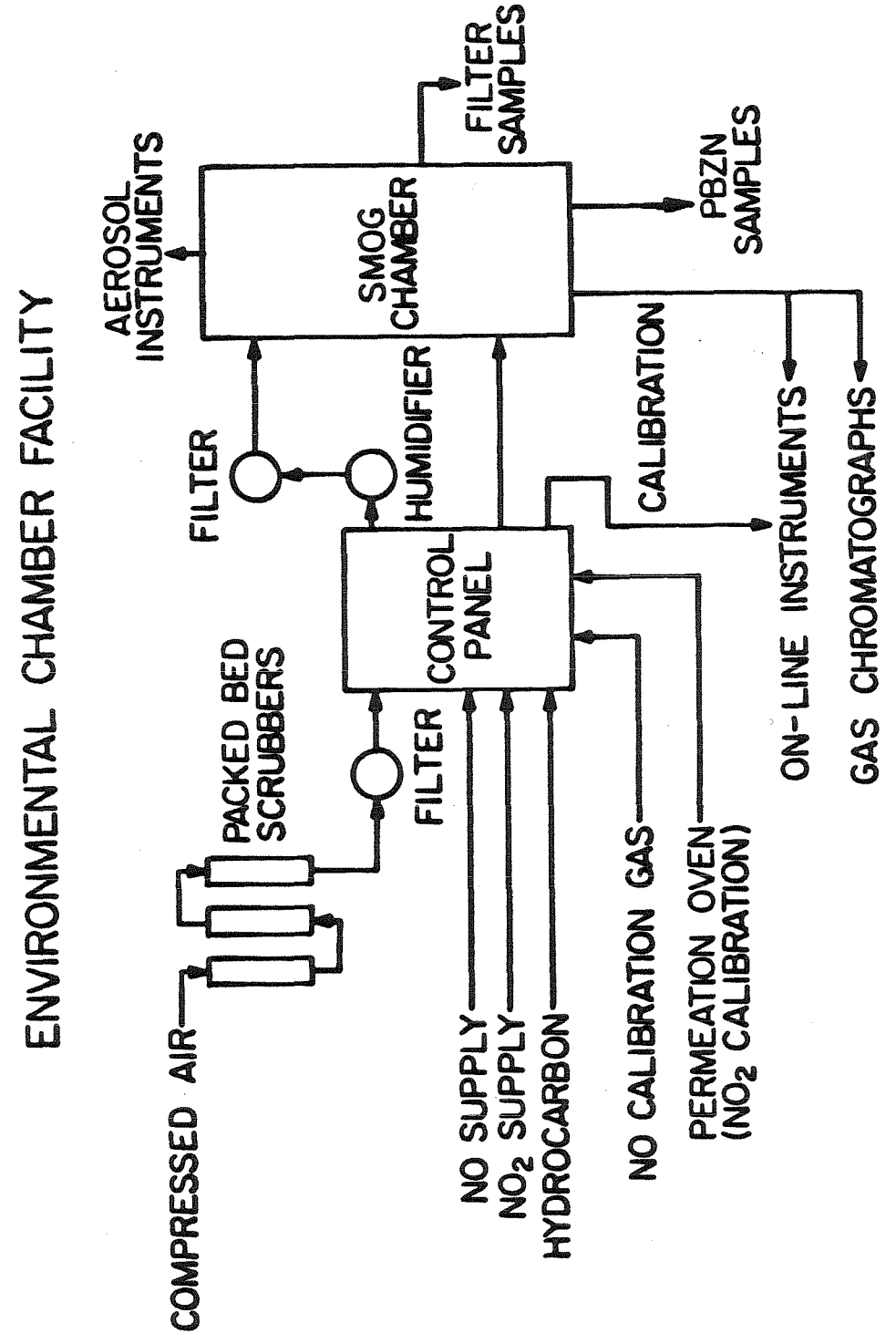

Figure 1. Schematic representation of the outdoor environmental chamber facility.

obtained by passing laboratory compressed air through three consecutive packed beds containing, in order, purafil [9], drierite and 13X molecular sieves, and activated carbon. Each of the beds is three inches in diameter, with the first two being 18 in. long, and the activated carbon bed 36 in. long. The resulting air routinely contained less than 15 ppb total NO_x, and only trace amounts of background organics. This dry, purified air was humidified to about 65 percent relative humidity (RH) at about 23°C before entering the chamber. When the chamber reached ∿3/4 of its final volume, the reactants were introduced. NO and NO_2 were added first from certified cylinders containing 600 ppb of each gas in ultra pure nitrogen (Scott-Marin Inc.). Toluene was injected by syringe into a 250 ml bulb, and then expanded into the chamber. The reactants were allowed to mix while the filling of the chamber continued to completion (between 30 min. and one hr). During the entire filling process, a dark cover was maintained over the chamber in order to prevent the intrusion of any solar radiation.

The parameters measured on-line during these experiments included O_3, NO, NO_2, NO_x, HNO_3, CO, chamber temperature, sample line temperature, sample line relative humidity, and aerosol size distribution. The signals from all of the on-line instruments were sent directly to a PDP-11/03 mini-computer for data acquisition and processing. The course of the experiment could be followed in real time by plotting the concentration-time profiles of any of these parameters on a terminal located in the laboratory. Two gas chromatographs (GC) were used to measure the concentrations of the important organic species. A Hewlett-Packard model 5830A GC equipped with dual flame ionization detectors was used to measure toluene, o-cresol, benzaldehyde, and m-nitrotoluene. The column used was either (1) a 6 ft. x 1/8 in. stainless steel column packed with 60/80 mesh Tenax GC, temperature programmed from

403 to 523K at 10K/min, or (2) a 6 ft X 1/8 in. Teflon lined stainless steel column packed with one percent SP-1240DA on 100/120 mesh Supelcoport, temperature programmed from 333 to 443K at 10K/min. In either case, a 300cc sample of the chamber contents was collected by pumping it through a cold trap (sample loop packed with glass beads) kept at -78°C by a mixture of dry ice and acetone. When pumping was complete, the dry ice/acetone mixture was replaced by a dewar of hot water, and the concentrated sample transferred by the carrier gas to the column. With this procedure, concentrations of the organics were measured every 15 to 20 minutes. Peroxyacetyl nitrate (PAN) was measured on a Varian 1440 gas chromatograph equipped with an electron capture detector using an 18 in. X 1/8 in. Teflon column of 10 percent Carbowax 400 on 60/80 mesh Chromosorb G at 303K. A 15 minute cam-timer, a pneumatic solenoid valve and an all Teflon 8-port sampling valve were used to automate the sampling and analysis.

Off-line measurements included peroxybenzoyl nitrate (PBZN) and particulate organic carbon. PBZN was sampled using impingers containing 10 ml of 5×10^{-3}N aqueous potassium hydroxide, and was measured as benzoic acid using ion chromatography with ultraviolet detection [10]. Quartz filters were used to collect aerosol samples at the conclusion of each experiment. These filters were analyzed for total organic carbon using a Dohrmann model DC-50 carbon analyzer [11,12]. All of the on-line instruments were connected to a common glass manifold, while the two gas chromatographs sampled via a separate line. A third port was used for the aerosol instruments, impinger samples, and filter samples. Table 1 summarizes the instruments employed, the corresponding calibration methods, and the estimated uncertainty in each measurement.

Table 1. Summary of Measured Parameters and Analytical Methods

Parameter/ Species	Instrument/Method	Calibration	Estimated Uncertainty %
I) Port No. 1: On-Line Instruments			
NO	Thermo Electron Model 14D/E	Gas Cylinder (Scott-Marin Inc.)	±10
NO_2	Thermo Electron Model 14D/E'	Permeation Tube	±15
HNO_3	Thermo Electron Model 14D/E with Nylon Filter'		
O_3	Dasibi Model 1008-PC	California Air Resources Board	±5
CO	Beckman Model 6800 GC	Gas Cylinder (Scott-Marin Inc.)	±10
Chamber Temp.	YSI Model 43 Thermistor	Precision Thermometer	small
Sample Temp.	YSI Model 43 Thermistor	Precision Thermometer	small
Relative Humidity	Hygrometrix Model 8501	Factory Calibration	<5
II) Port No. 2: Gas Chromatographs			
Gas Phase Organics	Hewlett-Packard Model 5830A with Dual FID Detectors	Gas Cylinders (Scott-Marin Inc.) and Authentic Samples (Aldrich)	±15
PAN	Varian Model 1440 with ECD detector	Irradiation of acetaldehyde-chlorine-NO_2 mixtures [36]	±15
III) Port No. 3: Impinger, Filter, and Aerosol Samples			
Peroxybenzoyl Nitrate (PBZN)	Ion Chromatography	Benzoic Acid Standards [10]	±15
Total Carbon	Dohrmann Model DC-50	Potassium hydrogen phthalate [11,12]	large[2]
Aerosol Size Distribution	Thermo Systems Inc. Model 3030 Electrical Aerosol Analyzer.	Factory	N.A.,[3]
	Royco Model 226 Laser Optical Particle Counter	Polystyrene Latex Spheres	N.A.[3]

[1]
[2]Corrected for PAN interference
[3]Due to losses to the chamber walls
[4]In this work, the aerosol instruments were used only to detect the formation of aerosols. Thus, any uncertainties in the size distribution measurements are not important.

All of the experiments reported here were performed in October and November of 1983. After each experiment, the chamber was emptied and then flushed with purified air. Next, the chamber was filled with purified air and "baked-out" in sunlight for an entire day. Finally, the chamber was flushed once again with purified air before being used for another experiment. Using this procedure, we encountered no problems in reproducing experimental results.

A number of control experiments and pollutant stability studies were carried out in order to characterize the chamber with regard to the dark and light stability of NO, NO_2, and O_3, and the off-gassing of CO and hydrocarbons. The ozone loss rate in purified air was about 2%/hr in sunlight, while the NO_x loss rate in sunlight was very small, about 0.2%/hr. Sunlight irradiations of purified air showed net ozone formation rates of about 2 ppb/hr.

CHARACTERIZATION OF THE CHAMBER RADICAL SOURCE

The presence of chamber-specific free radical wall sources has posed major problems in attempts at modeling hydrocarbon-NO_x photooxidations carried out in smog chambers. These radical sources have been treated differently by different investigators. For example, in previous studies with aromatics, Atkinson et al. [5] included a significant wall source of OH radicals, while Killus and Whitten [6] assumed only small amounts of initial HONO as radical inputs. Hendry et al. [4] assumed a combination of initial HONO and a wall source of HO_2 radicals in their work. Since the above three studies were completed, Carter et al. [8] and Sakamaki et al. [13] have performed detailed experimental studies of smog chamber radical sources. Carter et al. [8] examined four different chambers; however, the major portion of their effort dealt with the SAPRC evacuable chamber. They concluded that both a constant

radical source and the presence of initial HONO are necessary in order to account for the reactivities observed in the evacuable chamber. The constant source of radicals was represented as follows (for RH $\gtrsim$ 50 percent):

(1) Radical Source = $k_1\{0.39 + 1.37[NO_2]\}$ ppb/min

where k_1 is the NO_2 photolysis rate. The study of Sakamaki et al. [13] focused on the dark formation of HONO in a chamber similar in design to the evacuable chamber at SAPRC. These investigators found that HONO, and smaller amounts of NO, were formed in the dark from NO_2 and H_2O, and that the formation rates were first-order with respect to both NO_2 and H_2O. Two reactions are used to represent this source of HONO [13]:

(2) $NO_2 + H_2O \xrightarrow{\text{wall}} HONO$ $\qquad k_2 = 1.01\times10^{-8}$ ppm^{-1} min^{-1}

(3) $NO_2 \xrightarrow{\text{wall}} HONO$ $\qquad k_3 = 3.90\times10^{-5}$ min^{-1} .

The studies of Carter et al. [8] and Sakamaki et al. [13] present convincing evidence for the existence in two indoor, evacuable smog chambers of both a continuous radical source and initial HONO. It is therefore necessary to characterize our outdoor chamber with regard to possible wall radical sources before attempting to evaluate any of the experimental data. The nitrous acid formed in reactions 2 and 3 undergoes photolysis to OH radicals via,

(4) $HONO + h\nu \rightarrow OH + NO$.

If we lump the water vapor concentration in with the rate constant k_2 (since the water vapor concentration was nearly the same in each of our experiments), reactions 2 and 3 can be written:

(5) $NO_2 \xrightarrow{\text{wall}} HONO$

where the rate constant k_5 is chamber-dependent.

In order to evaluate the importance of reaction 5 in our chamber, we performed six sunlight irradiations of CO-NO_x mixtures in purified air with [CO] ≈ 50 ppm. These experiments were based on a suggestion by Killus and Whitten [14]. Since the chemistry of the CO-NO_x system is well understood, one can determine k_5 by simply finding the value of k_5 that gives the closest agreement between predicted and observed NO and NO_2 concentration-time profiles. Based on our six experiments, we determined a value of $k_5 = (5.0 \pm 1.2) \times 10^{-4}$ min^{-1}, where the stated uncertainties are estimated *maximum* uncertainties. We note here that the concentration of formaldehyde (HCHO) was measured at the beginning of three of the six CO-NO_x-air irradiations, and found to be about 2 ppb. Since formaldehyde photolysis is an important radical source, we included 2 ppb of initial HCHO in each of our simulations.

The concentration-time profiles of OH in these CO-NO_x-air irradiations can be estimated as follows. In the presence of large amounts of CO, OH radicals are converted to HO_2 radicals via:

$$\text{(6)} \qquad OH + CO \xrightarrow{O_2} HO_2 + CO_2 \ .$$

The HO_2 produced rapidly converts NO to NO_2 via:

$$\text{(7)} \qquad HO_2 + NO \rightarrow NO_2 + OH \ .$$

If we assume that the continuous source of radicals is due to the off-gassing of HONO (as suggested by the work of Sakamaki et al. [13]) and that HONO and HO_2 are in steady state, we can write

$$\text{(8)} \qquad \frac{d[NO]}{dt} \approx k_5[NO_2] - k_6[OH][CO] \ .$$

Rearranging equation (8) gives:

$$[OH] \approx \frac{k_5[NO_2] - d[NO]/dt}{k_6[CO]} \quad . \tag{9}$$

Using this expression and the experimentally observed NO decay rates, we can estimate the experimental OH concentration-time profiles. Representative OH concentrations determined in this way are shown in Figure 2, for experiment COR22. Also shown in Figure 2 are the predicted OH concentration profiles obtained by using, (A) only the homogeneous gas phase chemistry, (B) gas phase chemistry plus initial HONO, (C) gas phase chemistry plus reaction 5, and (D) gas phase chemistry with both reaction 5 and initial HONO. The amounts of initial HONO used in these simulations were calculated as

$$[HONO]_o = k_5[NO_2]_o x\ t_{mixing} \tag{10}$$

where t_{mixing} is the time between the injection of NO_2 and the start of the experiment (typically 30 - 60 min), and $k_5 = 5x10^{-4}$ min^{-1}. The results shown in Figure 2 are similar to those presented by Carter et al. [8], and demonstrate that both a continuous radical source and a small amount of initial HONO are needed to predict the OH concentrations observed in these basic experiments.

It is interesting to compare the radical flux predicted by reaction 5 with that predicted by the Carter et al. [8] expression (equation 1) and the Sakamaki et al. [13] expressions (reactions 2 and 3). Since equation (1) has a constant term in addition to the NO_2-dependent term, the results of this comparison will depend on the initial conditions of the simulation. With this in mind, Table 2 shows the total chamber dependent radical flux obtained by using these three expressions after four hours of simulation. The initial conditions for these simulations are those of our six CO-NO_x-air

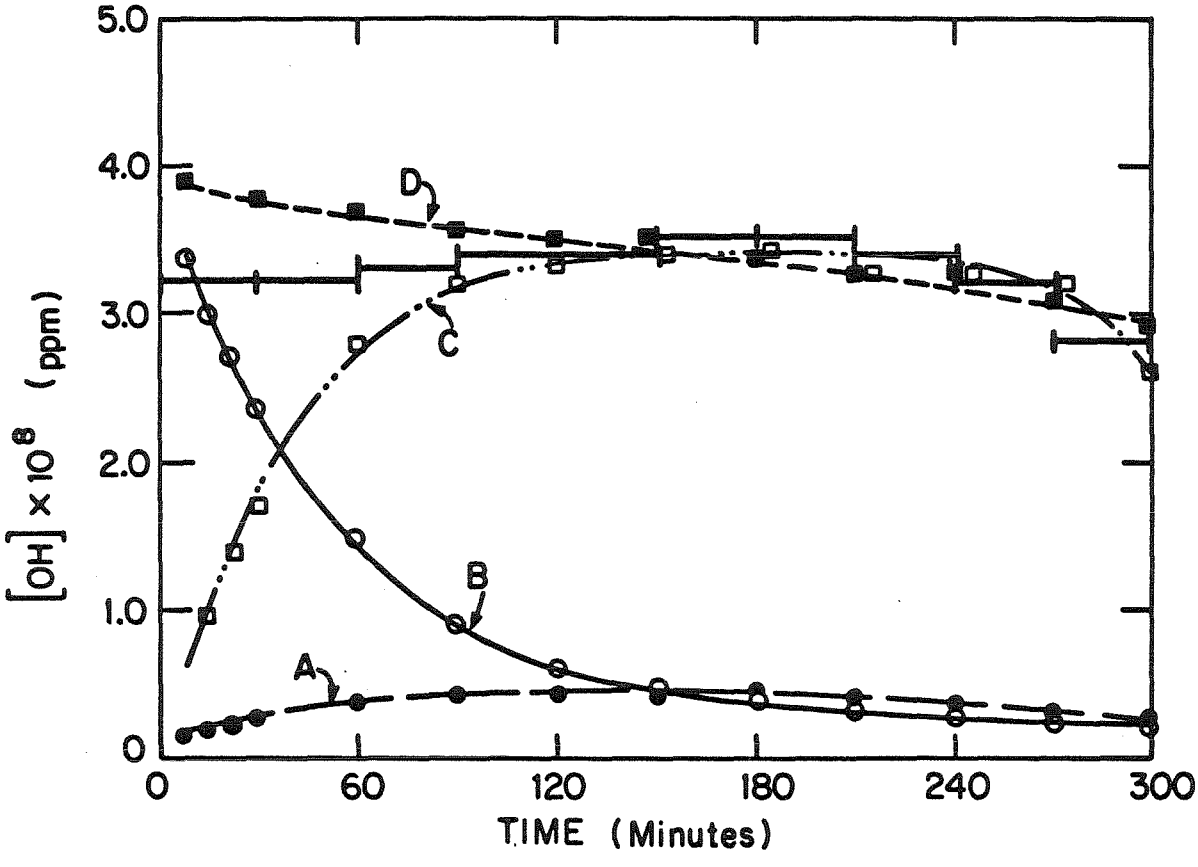

Figure 2. Hydroxyl radical concentration-time profile in CO-NO_x experiment COR22. Experimental data (calculated from equation 9), ⊢⊣ ; curve A-model predictions using gas-phase chemistry; curve B-model predictions with $[HONO]_o$ = 2.7 ppb; curve C-model predictions with k_4 = 5x10^{-4} min^{-1}; curve D-model predictions with $[HONO]_o$ = 2.7 ppb and k_4 = 5x10^{-4} min^{-1}.

Table 2. Comparison of chamber radical flux magnitudes predicted by reaction (5) with $k_5 = 5.0 \times 10^{-4}$ min^{-1}, expression (1) (SAPRC), and reactions 2 and 3 (Sakamaki et al. [13]).

Experiment Number	Initial Conditions (ppm) CO	NO	NO_2	Total OH Flux after 4 hr. (ppb) Carter et al [8]	Sakamaki et al.[13]	Present Study	Radical-Flux Present Study as Percent of: Carter et al.[8]	Sakamaki et al.[13]
COR21	54.7	0.376	0.060	68.7	6.4	15.3	22%	239%
COR22	54.4	0.370	0.077	70.9	8.6	18.6	26%	216%
COR23	58.3	0.192	0.033	57.9	6.3	13.2	23%	209%
COR24	49.4	0.380	0.245	81.3	16.6	37.1	45%	223%
COR25	46.7	0.196	0.206	72.6	14.0	29.4	40%	210%
COR26	58.9	0.380	0.075	70.7	8.7	18.5	26%	213%

irradiations. One can see that the total chamber radical flux in our outdoor chamber varies between 22 and 45 percent of the flux predicted for the SAPRC chamber under identical initial conditions, and is about twice as large as the radical flux found in the Sakamaki et al. [13] chamber. However, because of the high initial NO_2 concentrations, the results for experiments COR24 and COR25 are probably not representative of a typical hydrocarbon-NO_x photooxidation. In these experiments, our expression for the radical source term (reaction 2) will lead to a relatively larger flux of radicals (as compared to equation 1), because the entire radical source is dependent on the concentration of NO_2. Thus, experiments COR21-23 are probably more representative of a toluene-NO_x irradiation. We therefore conclude that the flux of chamber dependent radicals in our outdoor chamber is probably about 20 to 25 percent of the radical flux observed in the SAPRC chamber. It is somewhat surprising that the wall radical flux in our large outdoor chamber is larger than that observed in the smaller chamber of Sakamaki et al. [13]. However, since these two chambers differ greatly in design, chamber size may not be that important.

Based on the above analysis, we represent the chamber-dependent radical source in our toluene-NO_x mechanism by reaction 5, with $k_5 = 5.0 \times 10^{-4}$ min^{-1}. Also included in each simulation is an amount of initial HONO, as calculated by equation (10). Note that the value of k_5 is assumed to be identical in each simulation, and therefore is not an adjustable parameter. We also reiterate that the uncertainty limits stated for k_5 above are maximum estimated uncertainties. Later in this paper we present results showing that k_5 can be varied outside of this uncertainty range, with only minor influence on the predictions of our mechanism. This information, together with the high

degree of reproducibility observed in our CO-NO_x-air irradiations, leads us to conclude that the results of this study will not be influenced by uncharacterized chamber effects.

CHEMICAL REACTION MECHANISM AND EXPERIMENTAL PARAMETERS

The toluene photooxidation mechanism being evaluated in this work is shown in the Appendix, Table A.1. The details regarding the formulation of this mechanism can be found in Leone and Seinfeld [7], and are therefore not discussed here. The vast majority of the rate constants used in this mechanism are taken from three sources [15-17]. The only chamber-dependent reactions included in this mechanism are reaction 25 (heterogeneous nitric acid formation), reaction 103 (O_3 wall loss), and reaction 104 (chamber radical source).

In performing the numerical simulations, necessary inputs for the chemical mechanism are the initial concentrations of the reactants, the temperature, and the NO_2 photolysis rate profile. The initial conditions for each experiment are shown in Table 3, together with the average chamber temperatures. The NO_2 photolysis rate (k_1) profiles were not measured, but were calculated assuming clear sky conditions, as a function of latitude, longitude, date, and time of day [18]. These calculated k_1's may not be absolutely applicable to each of our experiments because of cloud and aerosol scattering, reflection from nearby surfaces, or attenuation by the chamber walls. Most of our experiments were performed on days of relatively light smog in Pasadena in order to minimize light scattering by atmospheric aerosols. All but one of the experiments were performed under clear sky conditions, so cloud scattering was probably unimportant. Attenuation by the chamber walls can be neglected since several investigators have shown that new Teflon film

Table 3. Initial conditions and average temperatures for toluene-NO_x irradiations

Experiment	TOLR22	TOLR23	TOLR24	TOLR25	TOLR26	TOLR27
Irradiation time (hr)	6	5.5	5.75	6	6.5	4.5
Initial concentrations (ppm)						
NO	0.455	0.371	0.198	0.400	0.397	0.108
NO_2	0.050	0.153	0.025	0.065	0.120	0.039
toluene	1.28	0.57	1.19	1.46	0.77	0.82
H_2O	25,200	22,400	23,000	22,700	22,000	21,200
CO	2.16	3.31	3.49	3.51	3.03	5.33
HCHO[1]	0.002	0.002	0.002	0.002	0.002	0.002
Avg. temperature (K)	310	308	315	310	311	311

[1]Based on measurements with our purified air, 2 ppb of initial formaldehyde was included in each of the simulations.

transmits ≥95 percent of the ultraviolet light [19,20]. Finally, as noted previously, reflection from the rooftop was kept to a minimum by placing a dark tarpaulin underneath the chamber. Nevertheless, measurements with a pyroheliometer indicated that, after about 12:00 noon (PDT), reflection from surfaces near the chamber increased the flux of total solar radiation reaching the chamber by about 10 percent.

All of the simulations presented here (except TOLR23) make use of the theoretically predicted k_1 values before 12:00 noon (PDT), and of these same k_1's increased by 10 percent after 12:00 noon (PDT). Based on the above discussion, we expect that these values should have an uncertainty of less than ±15 percent. There were periods of light cloudiness during experiment TOLR23, and the k_1 values during these periods were arbitrarily reduced by 30 percent to take this into account. Thus, whereas the k_1 profile was specified based on the date and time of day, some adjustments were necessary to account for the influences of atmospheric conditions and reflection from surfaces near the chamber.

SIMULATIONS OF TOLUENE PHOTOOXIDATION EXPERIMENTS

The results of our simulations are summarized in Table 4 and Figures 3-8. Table 4 indicates that the maximum O_3 and PAN yields were predicted very well, with the average O_3 maximum being less than six percent overpredicted. The NO_2 maxima were consistently overpredicted, but the time of the NO_2 peak was predicted very accurately. Figures 3-7 present the predicted and observed concentration-time profiles for most of the six toluene-NO_x irradiations. In general, the agreement between experiment and theory is good for both the major and minor product species. Carbon recovery

Table 4. Predicted and observed O_3, NO_2, and PAN maxima, and times of occurrence of maxima for toluene-NO_x irradiations.

		Experiment Number					
		TOLR22	TOLR23	TOLR24	TOLR25	TOLR26	TOLR27
$[O_3]_{max}$ (ppb)	measured	579	101	395	542	474	283
	(predicted)	(582)	(119)	(370)	(545)	(540)	(303)
time of $[O_3]_{max}$ (min)	measured	195	>330	130	180	>390	120
	(predicted)	(240)	(350)	(140)	(205)	(>390)	(140)
$[PAN]_{max}$ (ppb)	measured	69	8	19	55	40	20
	(predicted)	(71)	(10)	(25)	(69)	(46)	(24)
time of $[PAN]_{max}$ (min)	measured	240	>330	120	210	>390	130
	(predicted)	(195)	(>330)	(145)	(210)	(>390)	(135)
$[NO_2]_{max}$ (ppb)	measured	420	408	180	385	400	125
	(predicted)	(365)	(351)	(175)	(348)	(355)	(112)
time of $[NO_2]_{max}$ (min)	measured	115	230	60	105	180	45
	(predicted)	(115)	(225)	(70)	(95)	(165)	(50)

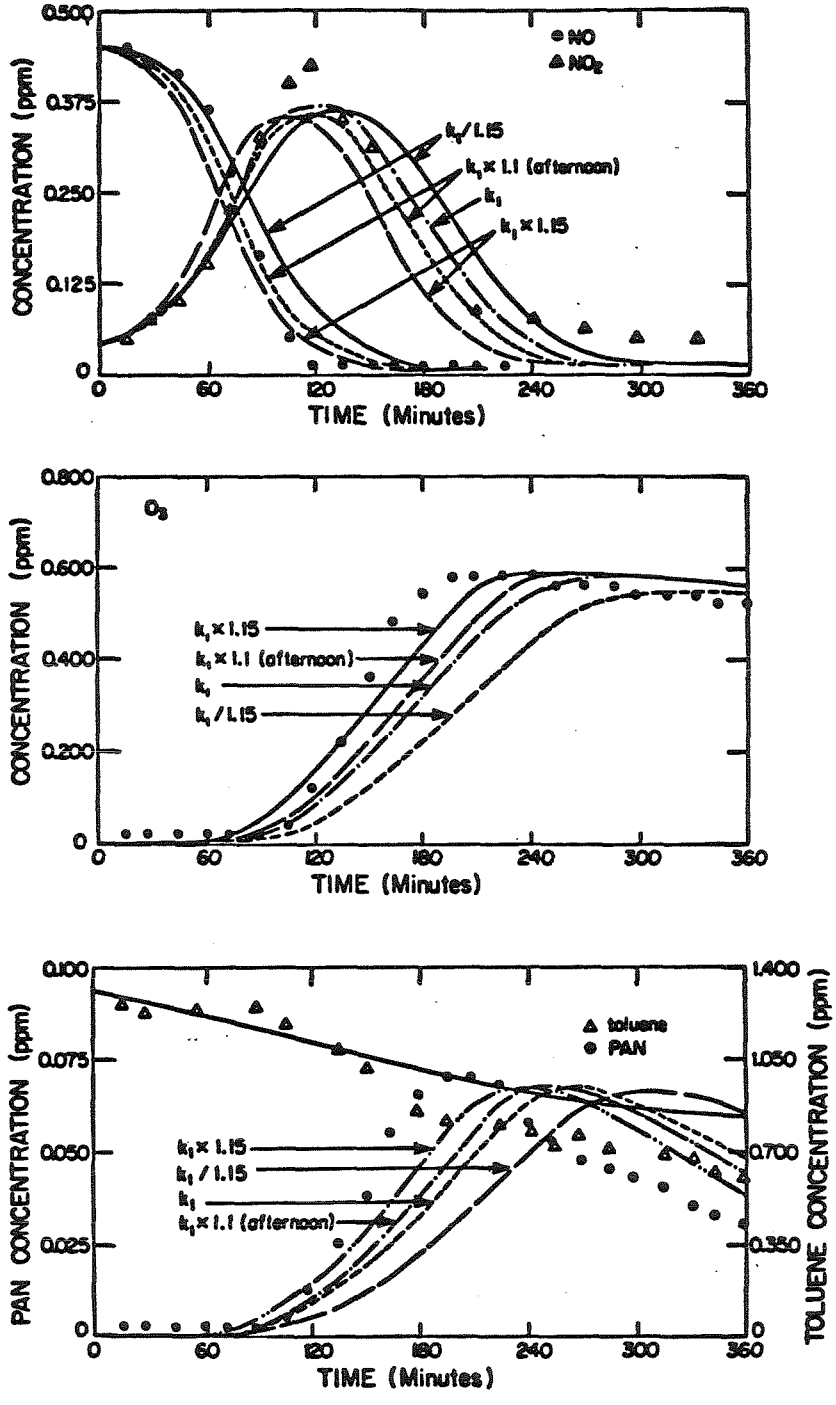

Figure 3. Observed and predicted concentration-time profiles for toluene-NO_x experiment TOLR22. Effect of varying the NO_2 photolysis rate profile. When multiple curves are not shown, only very minor effects on the predicted concentration-time profiles are observed.

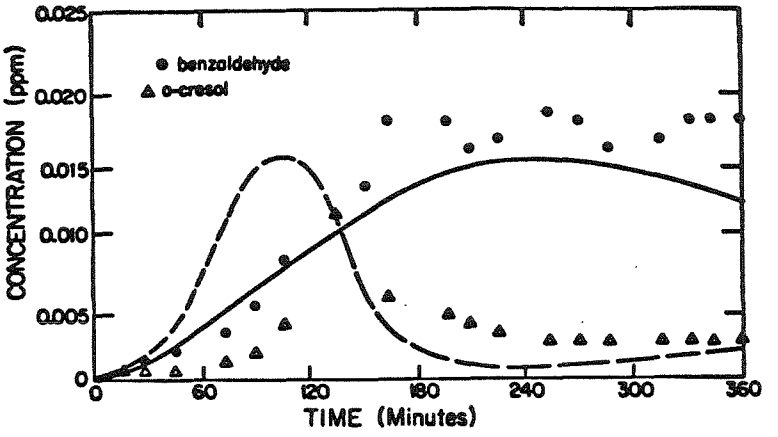

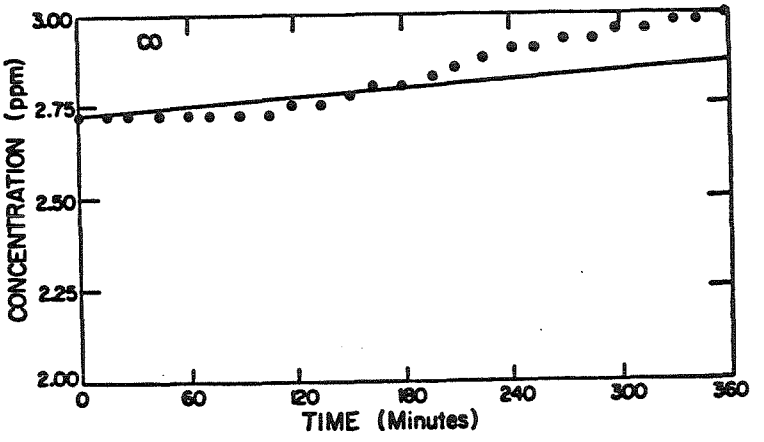

Figure 3. (continued) Observed and predicted concentration-time profiles for toluene-NO_x experiment TOLR22. Effect of varying the NO_2 photolysis rate profile. When multiple curves are not shown, only very minor effects on the predicted concentration-time profiles are observed.

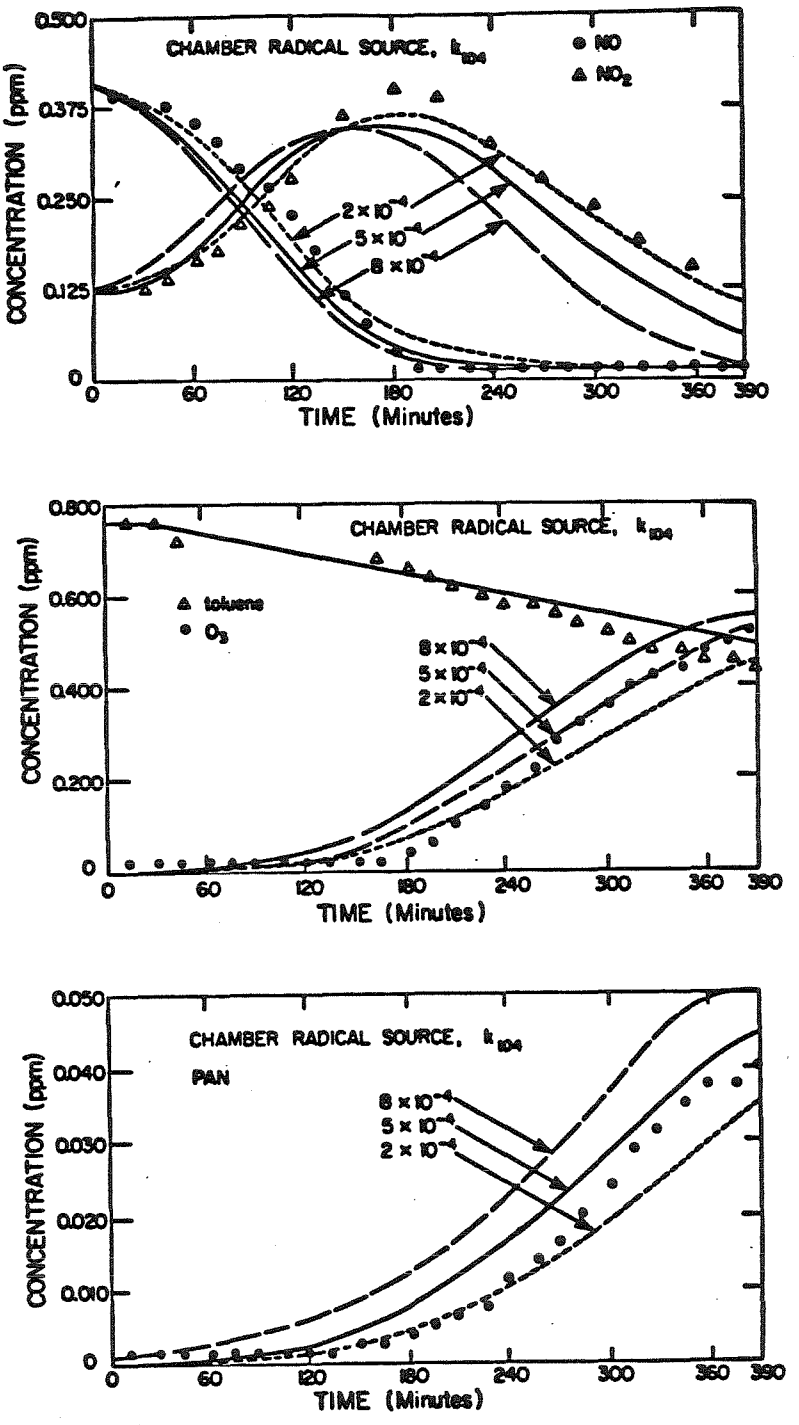

Figure 4. Observed and predicted concentration-time profiles for toluene-NO_x experiment TOLR26. Effect of changing the magnitude of the chamber radical source. When multiple curves are not shown, only very minor effects on the predicted concentration-time profiles are observed.

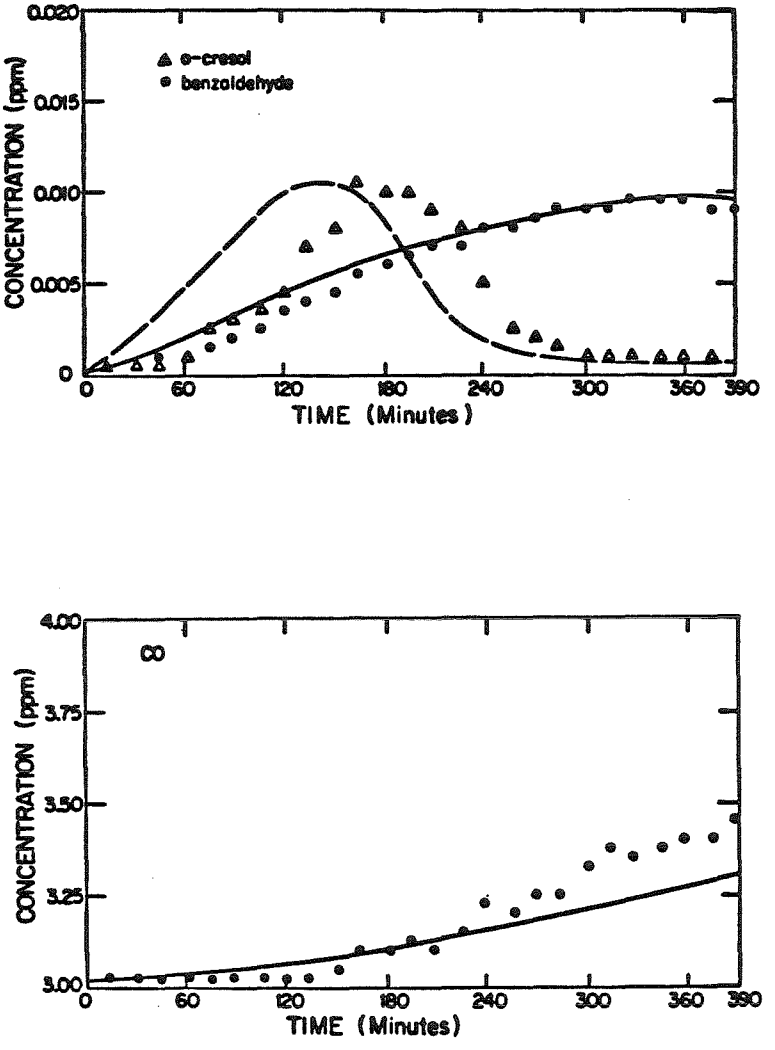

Figure 4. (continued) Observed and predicted concentration-time profiles for toluene-NO_x experiment TOLR26. Effect of changing the magnitude of the chamber radical source. When multiple curves are not shown, only very minor effects on the predicted concentration-time profiles are observed.

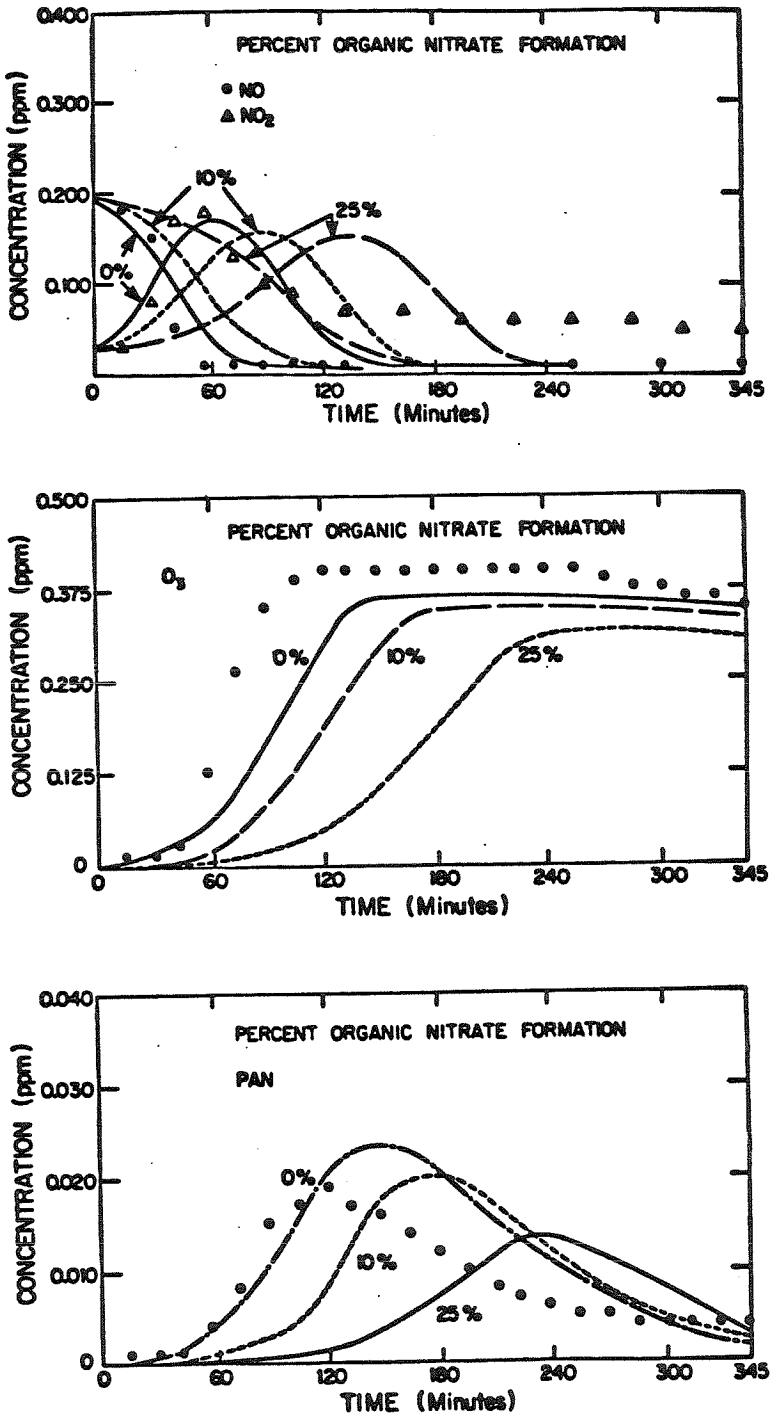

Figure 5. Observed and predicted concentration-time profiles for toluene-NO_x experiment TOLR24. Effect of assuming different amounts of bicyclic peroxy organic nitrate formation. When multiple curves are not shown, only very minor effects on the predicted concentration-time profiles are observed.

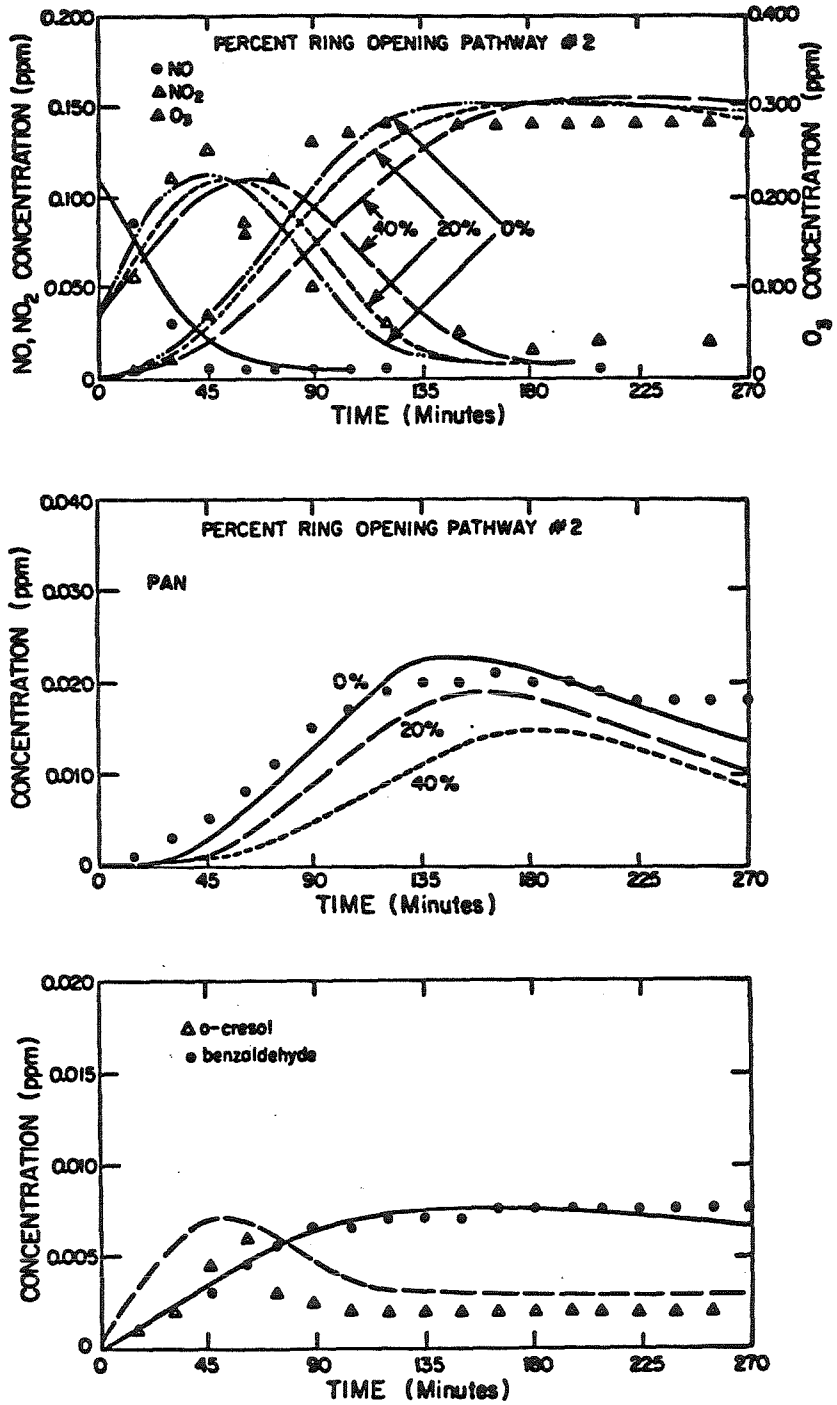

Figure 6. Observed and predicted concentration-time profiles for toluene-NO_x experiment TOLR27. Effect of assuming different ring opening pathways. When multiple curves are not shown, only very minor effects on the predicted concentration-time profiles are observed.

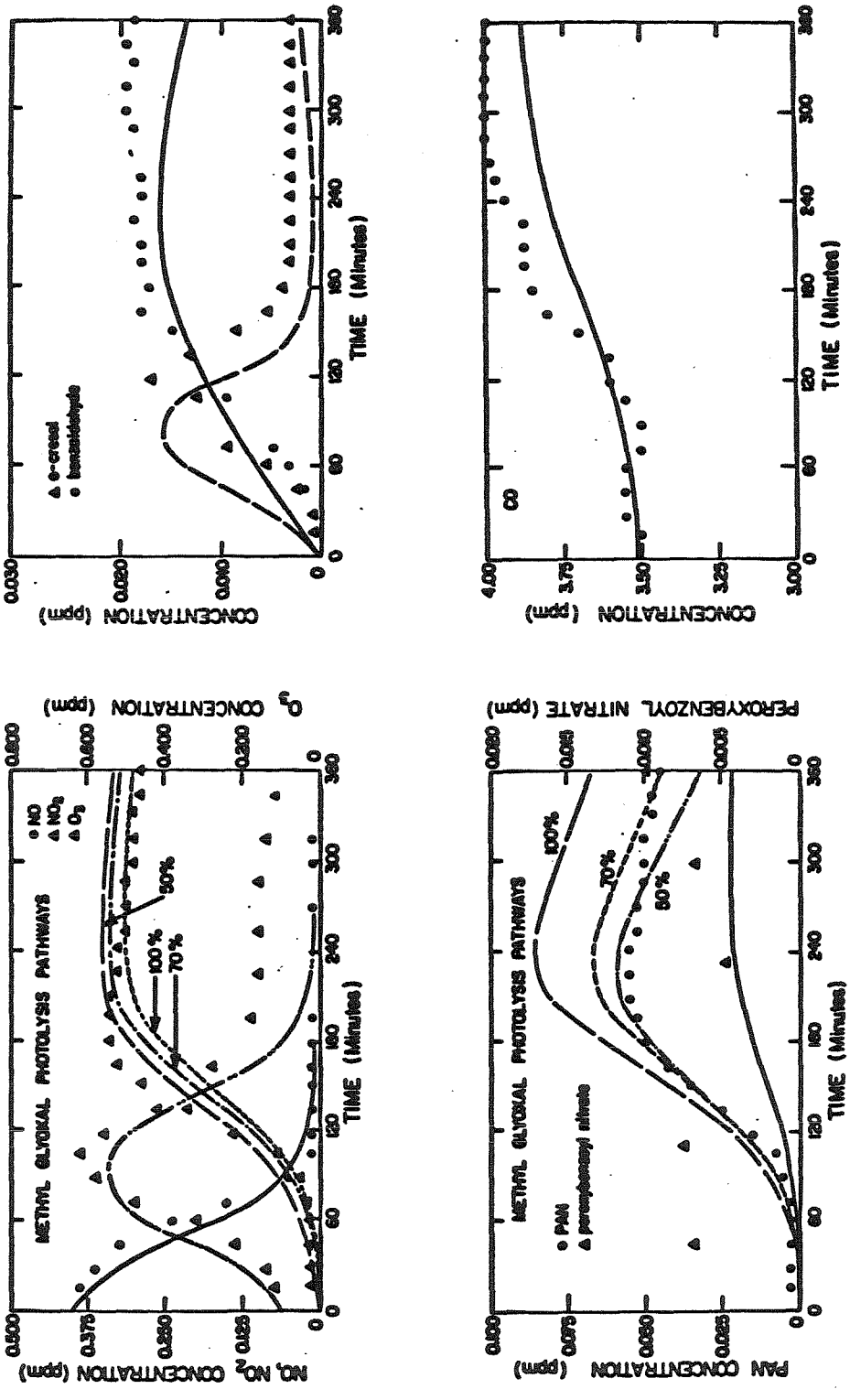

Figure 7. Observed and predicted concentration-time profiles for toluene-NO_x experiment TOLR25. Effect of varying the methyl glyoxal photolysis pathways. The percentages shown are the percent of photolysis leading to $CH_3\dot{C}O$ and $H\dot{C}O$ radicals. When multiple curves are not shown, only very minor effects on the predicted concentration-time profiles are observed.

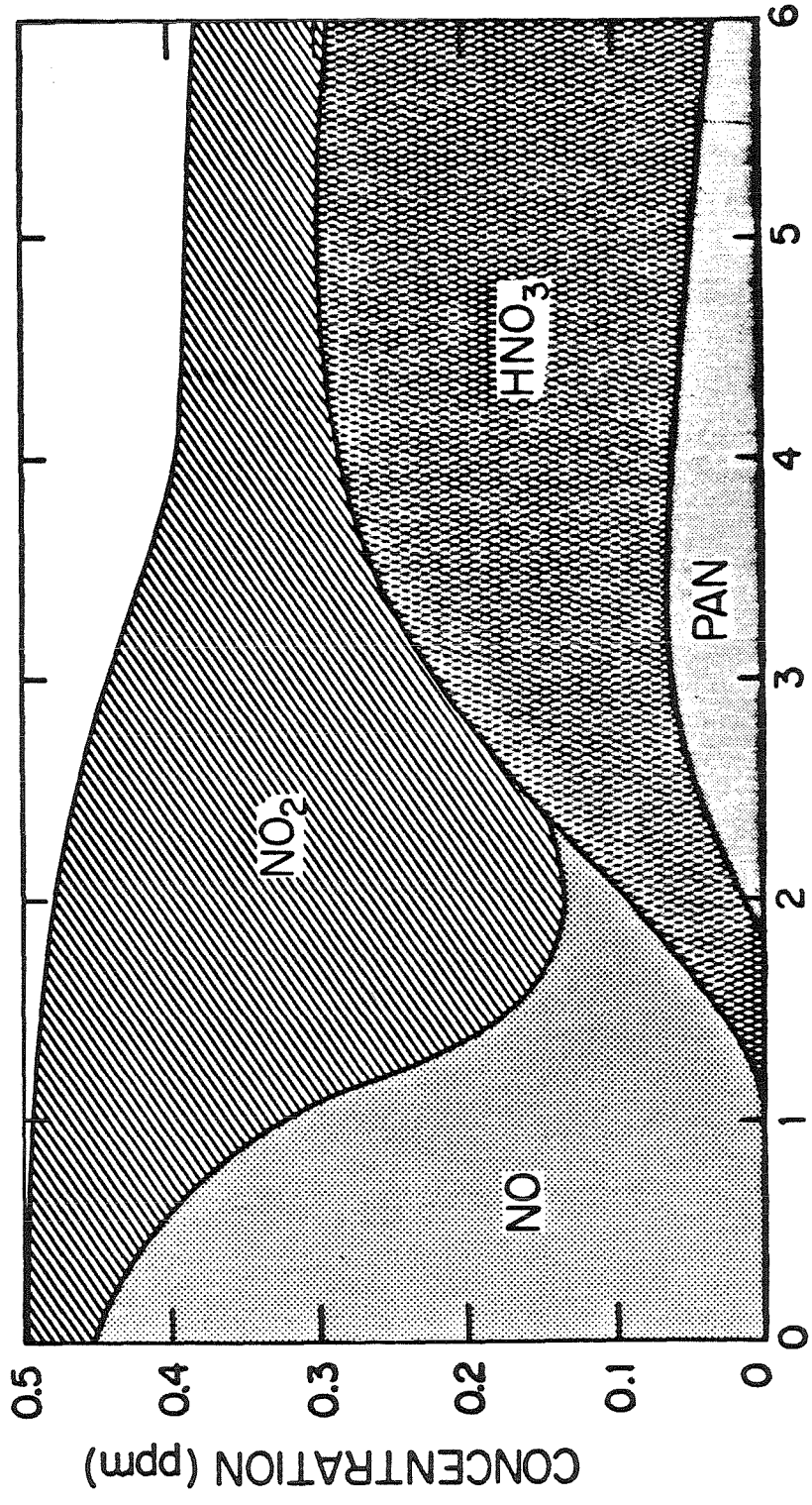

Figure 8. Concentration-time profiles of nitrogen compounds for experiment TOLR22.

in these experiments was about 25-30 percent, with 2-6 percent of the initially present carbon observed in the aerosol phase at the end of the runs. These aerosol yields are consistent with those of Schwartz [32,33] and of Grosjean et al. [34], but are much lower than the aerosol yields reported by O'Brien et al. [35] who used much smaller vessels.

Effect of NO_2 Photolysis Rate and Chamber Radical Source

Two of the most important parameters that enter into the simulations via the chemical reaction mechanism are the NO_2 photolysis rate profile and the magnitude of the chamber radical source. It is important that the effects of any uncertainties in these parameters not influence the predictions of the chemical mechanism to the degree that the conclusions drawn from comparing experiment and theory are influenced by these uncertainties. In Figure 3, the effects of varying the NO_2 photolysis rate (k_1) by ±15 percent (the estimated maximum uncertainty) are presented using experimental data from TOLR22. Similar results are obtained with data from the other experiments. The reactivity of the system clearly increases with the rate of NO_2 photolysis; however, the changes in reactivity are not large enough that the agreement between theory and experiment is significantly altered. Since 15 percent is the estimated maximum uncertainty in our estimates of k_1, we conclude that the absence of measured NO_2 photolysis rates should not influence the conclusions of this study.

The result of varying the magnitude of the chamber radical source is illustrated in Figure 4. Experimental data are from run TOLR26, but once again very similar results are found with each of the experiments. In the simulations shown, the wall radical flux has been varied by more than twice its estimated uncertainty. One can see that this large change in the magnitude of the wall radical flux has a noticeable, but not overwhelming, effect on the agreement between experiment and simulation. Variations in the magnitude of the wall radical flux within the uncertainty limits should therefore produce only small changes in mechanism predictions. Thus, we conclude that these uncertainties can also be safely ignored.

Toluene-OH Reaction Mechanism

The toluene-OH reaction proceeds via two pathways, OH addition to the aromatic ring and H-atom abstraction from the methyl group [5,17,21],

(64)[1] 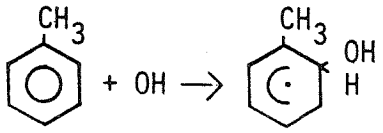

(48) 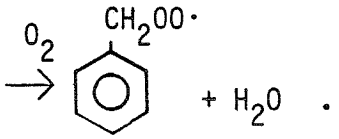 .

The abstraction pathway is only about eight percent of the overall reaction [22], and its mechanism is fairly well understood. Of the ∿92 percent of the reaction proceeding via OH addition, about 80 percent occurs at the ortho position [17,23], so we consider only that avenue here.

The toluene-OH adduct produced in reaction 64 can react with O_2 or NO_2,

(65) 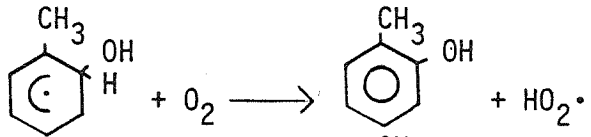

(67) 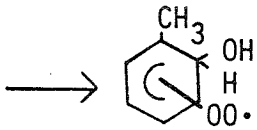

(66) 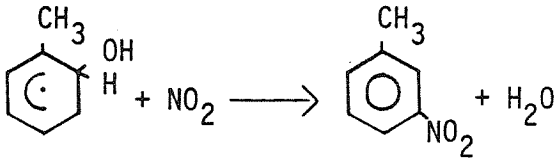

with k_{65} = 10 ppm^{-1} min^{-1} at 300K [17]. Reaction 66 must be a minor pathway, since only very small amounts of m-nitrotoluene were observed in our experiments as well as in those of Atkinson et al. [5]. Atkinson et al. [5] and

[1]Reaction numbers correspond to those found in Table A.1.

Killus and Whitten [6] assume that cresol formation represents about 25 percent of the reaction with O_2, i.e., $k_{65}/k_{67} \sim 0.33$. However, the recent study of Atkinson et al. [22] indicates that the cresol yield is about 17 percent, i.e., $k_{65}/k_{67} \sim 0.2$. With the six outdoor irradiations being analyzed here, we find the best agreement between theory and observation is indeed obtained with $k_{65}/k_{67} \sim 0.2$. Moreover, this same conclusion was reached in our previous study of toluene photooxidation [7] using data from the evacuable chamber at SAPRC.

The major uncertainty in the toluene reaction mechanism involves the fate of the toluene-OH-O_2 adduct formed in reaction 67. The currently accepted reaction sequence involves adduct cyclization followed by reaction with O_2 and NO:

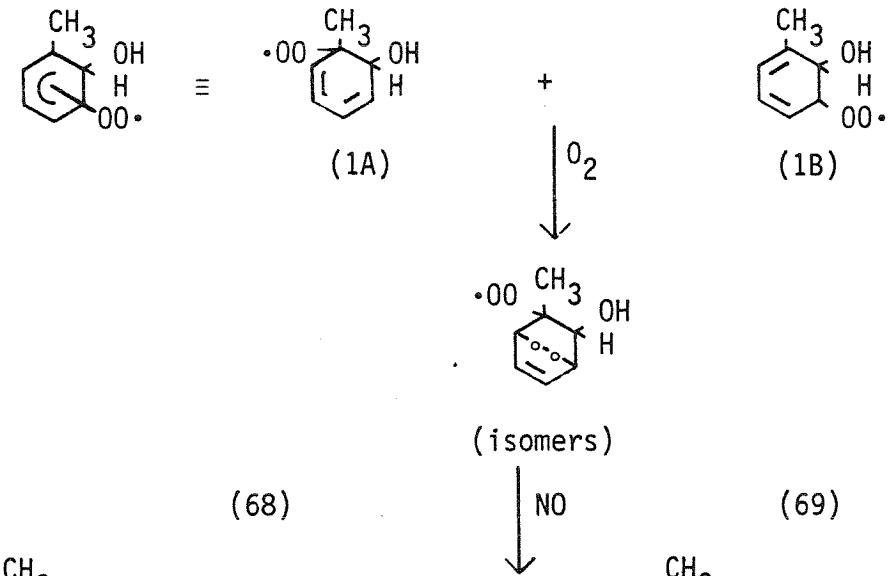

$HO_2\cdot$ + CH(O)CH=CHCHO + $CH_3C(O)CHO$)
2-butene-1,4-dial methyl glyoxal

$HO_2\cdot$ + $CH_3C(O)CH=CHCHO$ + $(CHO)_2$)
4-oxo-2-pentenal glyoxal .

In our previous study of toluene photooxidation [7], we found that the SAPRC data were consistent only with mechanisms assuming negligible amounts of bicyclic peroxy organic nitrate formation, i.e., $\alpha = 0$. A number of simulations have been performed to see if this conclusion is consistent with the data from the present study. Some typical results are shown in Figure 5, using experimental data from TOLR24. As with the data from SAPRC, assuming any significant amount of bicyclic peroxy organic nitrate formation reduces the reactivity of the system to the point that the experimental data are no longer successfully simulated.

The relative occurrence of reactions 68 and 69, and reactions 78 and 79, was also investigated in our previous study. The data from SAPRC could be successfully simulated only if ring opening was assumed to occur exclusively via reactions 68 and 78. Figure 6 illustrates the effect on predicted concentration-time profiles of varying the relative amounts of the two ring opening pathways with experimental data from run TOLR27. Once again, we see that only ring opening via reactions 68 and 78 allows the data to be successfully simulated. Thus, in both the experiments reported here, and those carried out at SAPRC, assuming any significant amount of bicyclic peroxy organic nitrate formation, or ring opening to glyoxal and 4-oxo-2-pentenal (reactions 69 and 79), leads to a predicted system reactivity that is much slower than is experimentally observed. For this reason, all of the simulations presented here (except those in Figure 6) were obtained with $k_{69} = k_{79} = 0$.

The results in Figure 6 illustrate that ring opening to methyl glyoxal and 2-butene-1,4-dial (reaction 68) leads to a much more reactive system than does ring opening to glyoxal and 4-oxo-2-pentenal. This is because the photolysis of methyl glyoxal is assumed to be a major source of radicals in the toluene-NO_x system. Although the rate of methyl glyoxal photolysis has recently been measured [24,25], the photolysis products are still undetermined [24-26]. The formation of significant amounts of peroxyacetylnitrate (PAN)

indicates that methyl glyoxal photolysis leads, at least partially, to the production of peroxyacetyl and HO_2 radicals via:

(44a) $CH_3C(O)CHO + h\nu \rightarrow CH_3\dot{C}O + H\dot{C}O \xrightarrow[fast]{2O_2} CH_3CO_3\cdot + HO_2\cdot + CO$

(44b) $\rightarrow CH_3C(O)\dot{C}O + H\cdot \xrightarrow[fast]{O_2} CH_3\dot{C}(O) + CO + HO_2\cdot$

$\downarrow O_2$

$CH_3CO_3\cdot$

However, methyl glyoxal photolysis may also proceed via

(45) $CH_3C(O)CHO + h\nu \rightarrow CH_3\cdot + HC(O)\dot{C}O \xrightarrow[fast]{2O_2} CH_3O_2\cdot + HO_2\cdot + 2CO$

The effect of varying the relative importance of reactions 44 and 45 on the agreement between predicted and observed PAN concentration-time profiles has been studied with each of the six toluene-NO_x experiments. Some typical results are shown in Figure 7 using data from experiment TOLR25. The results of this analysis indicate that between ∿50 and 80 percent of methyl glyoxal photolysis proceeds via reaction 44. Unfortunately, the experimental data do not allow a more precise determination of the relative abundance of these two pathways. However, this result is consistent with our earlier study of SAPRC data [7], where the best agreement with the experimental data was obtained by assuming that reaction 44 occurs about 70 percent of the time.

Since the mechanism shown in the Appendix closely simulates the data from both the SAPRC evacuable chamber and our outdoor chamber, one might conclude that it represents a fairly accurate description of the actual toluene photooxidation process. However, Tuazon et al. [27] have recently reported yields of methyl glyoxal from toluene that are much smaller than those predicted by our mechanism or, for that matter, by any of the existing toluene

mechanisms [4-6]. Specifically, Tuazon et al. [27] observed methyl glyoxal and glyoxal yields from toluene of about 10 and 17 percent, respectively. By contrast, the mechanism in Table A.1 yields methyl glyoxal 72 percent of the time (8 percent abstraction and 20 percent cresol formation), and gives glyoxal only from the reaction of 2-butene-1,4-dial. If the yields reported by Tuazon et al [27] are correct, only about 55 percent of the toluene reaction pathways are accounted for (8 percent abstraction, 20 percent cresol formation, 10 percent methyl glyoxal, and 17 percent glyoxal).

It is useful to compare the predictions of the current toluene mechanism with a mechanism that incorporates the Tuazon et al. [27] α-dicarbonyl yields. To do so, one must postulate reaction pathways for the remaining 45 percent of the toluene reaction. One possible pathway involves unimolecular decomposition of the toluene-OH-O_2 adduct to yield unsaturated dicarbonyl products, i.e.,

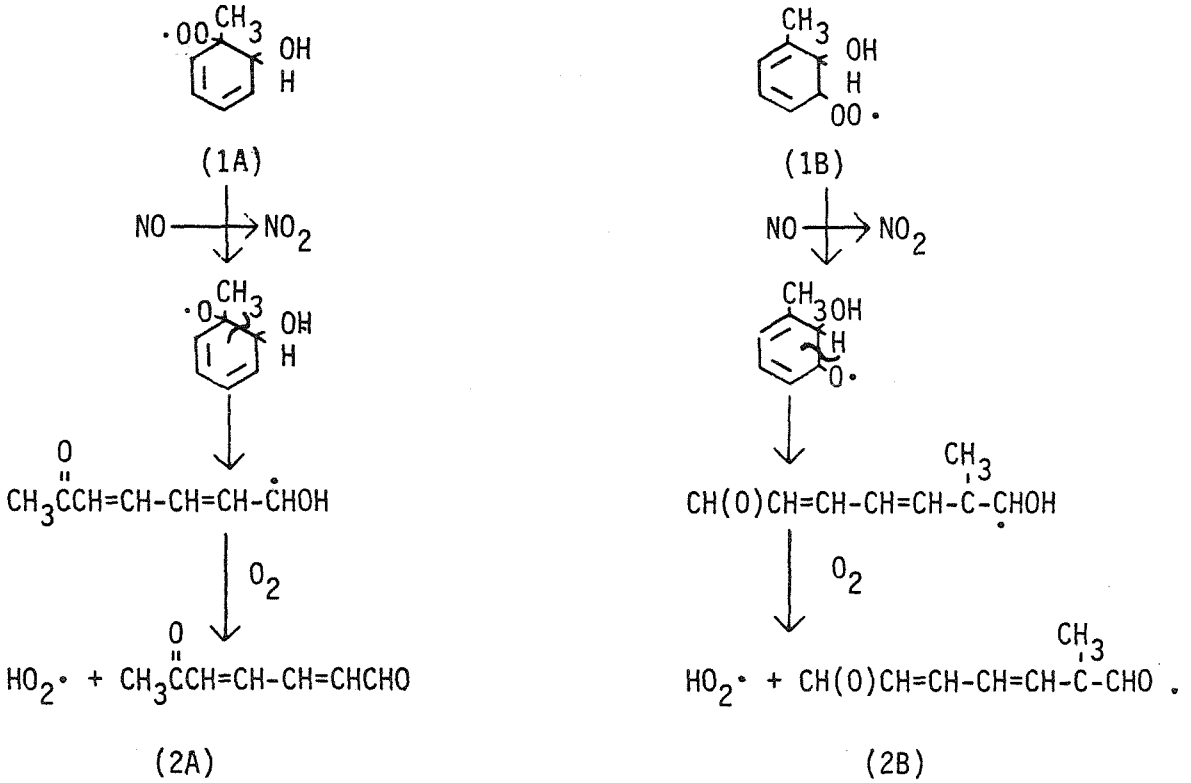

One of these C7 dicarbonyls, compound 2A, has recently been observed by Dumdei and O'Brien [28] in the aerosol phase products of toluene-NO_x photooxidations. These C7 dicarbonyls are expected to react with OH via both addition and abstraction, giving rise to α- and conjugated-γ-dicarbonyl products as shown in Table A.2 of the Appendix.

By adding the reactions listed in Table A.2 to our toluene mechanism and changing the yields of the α-dicarbonyls, we can examine the effects of assuming the α-dicarbonyl yields reported by Tuazon et al. [27]. Some typical results are shown in Figure 9. One can see that the overall system reactivity predicted with these changes is much slower than is experimentally observed, an observation that is not surprising, since the yield of methyl glyoxal has been reduced by a factor of about 7. Counter species analysis [29] shows that about 39 percent of the total amount of NO to NO_2 conversions predicted by the mechanism in Table A.1 are attributable to methyl glyoxal. The OH reactions of the C7 dicarbonyls proceed much too slowly to compensate for the radical production that is lost by reducing the yield of methyl glyoxal.

The above discussion is not intended to argue that the α-dicarbonyl yields reported by Tuazon et al. [27] cannot be correct. It does, however, imply that if these new yields are correct, there must be a powerful source of radicals in toluene photooxidation that has not yet been identified. One possible radical source is the photolysis of the C7 dicarbonyls. A possible sequence for the photolysis of these species is also shown in Table A.2. However, it can be shown that these species must photolyze nearly as rapidly as methyl glyoxal ($\sim 0.019 \times k_1$) in order to predict the observed system reactivity. If all of the conjugated dicarbonyls (C4, C5, and C7) are allowed to photolyze,

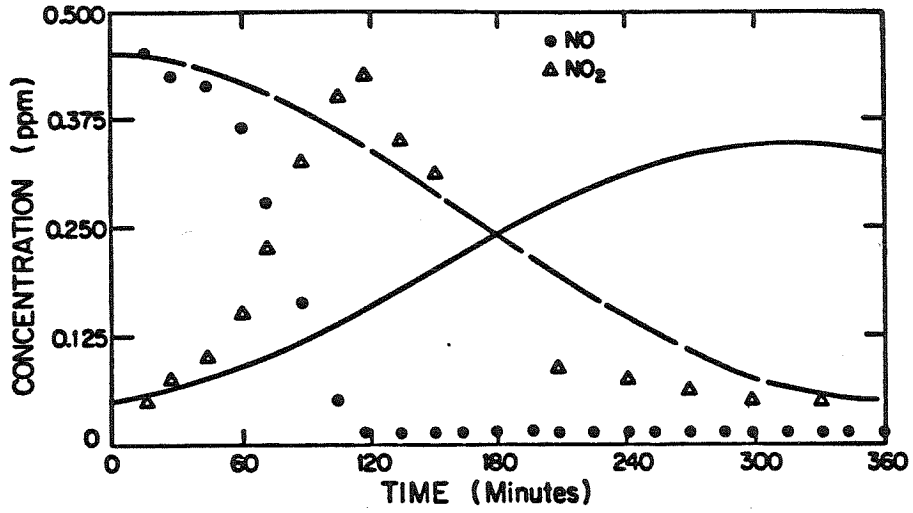

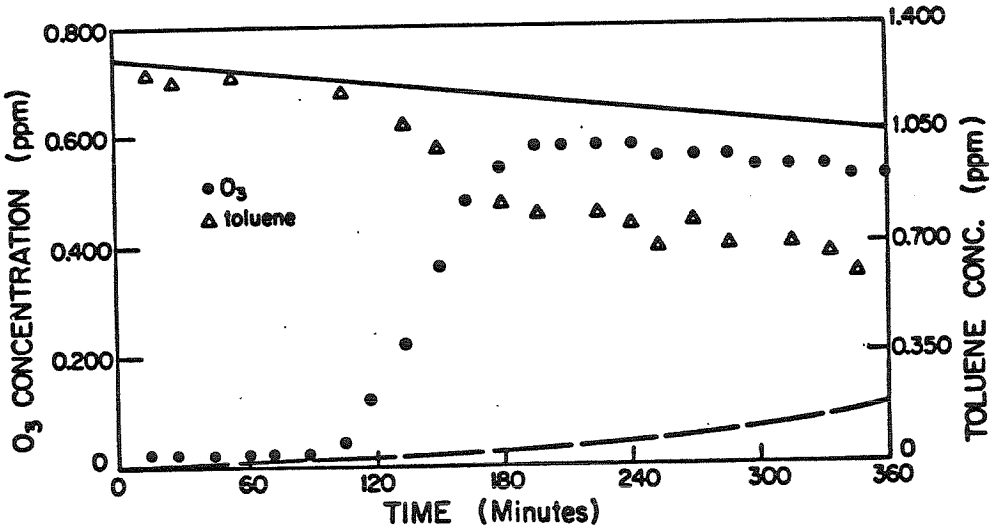

Figure 9. Predicted concentration-time profiles obtained with a reaction mechanism employing the α-dicarbonyl yields of Tuazon et al. [27]. Experimental data are from run TOLR22.

the photolysis rate needed to predict the observed OH concentrations is about that of glyoxal (0.008 x k_1). Although photolysis rates for these species have not been measured, they are currently thought to be very slow under atmospheric conditions [17]. It appears that the only way to resolve this contradiction is by carrying out more detailed product yield studies of toluene-NO_x photooxidations.

Nitrogen Balances

Figure 8 illustrates a nitrogen balance for experiment TOLR22. This is representative of the nitrogen balances obtained with each of the six toluene-NO_x experiments. The largest nitrogen "deficit" occurs at the end of the runs, where about 20 percent of the initial nitrogen is unaccounted for. A notable feature of these nitrogen balances is the large amount of nitric acid (HNO_3) that is present in the gas phase. Although we expect to form a large amount of nitric acid (both homogeneously and heterogeneously on the chamber walls), previous investigators have found that most of the HNO_3 either remains on the chamber walls, or is lost to the walls during the run [30,31]. The large amount of gas phase HNO_3 observed in our experiments is probably attributable to the relatively high temperature of our chamber walls. Whereas previous studies were carried out at or near 298K, the temperature inside our chamber in the afternoon was always above 310K, and sometimes as high as 322K.

CONCLUSIONS

The toluene-NO_x reaction mechanism developed and tested by Leone and Seinfeld [7] gives good agreement with experimental data from a new outdoor environmental chamber facility under a variety of initial conditions. Even though the mechanism developed in Leone and Seinfeld [7] has now been evaluated successfully against experimental data from two environmental chamber facilities, there is concern because this mechanism is not consistent with some very recent experimental findings concerning dicarbonyl yields. However, no reasonable sequence could be established that makes use of these new data, and, at the same time, gives reasonable predictions of the observed concentration-time profiles in toluene-NO_x irradiations. Thus, it is clear that additional experimental work is needed, especially with respect to the nature and yields of the carbonyl products and their subsequent reactions under atmospheric conditions. Until experimental information on the above topics is available, the toluene-NO_x photooxidation mechanism shown in Table A.1 should provide a useful starting point from which to derive lumped treatments of atmospheric aromatic chemistry for use in urban airshed simulation models.

ACKNOWLEDGMENTS

This work was supported by National Science Foundation Grant ATM-8208625. The authors wish to gratefully acknowledge the assistance of Toby Shafer and Dale Warren in performing the chamber experiments. Helpful discussions with Dr. W. P. L. Carter are also acknowledged.

Bibliography

[1] D. Grosjean, and K. Fung, J. Air Pollut. Control Assoc., 34, 537 (1984).

[2] F. M. Black, L. E. High, and J. M. Lang, J. Air Pollut. Control Assoc., 30, 1216 (1980).

[3] W. A. Lonneman, S. L. Kopczynski, P. E. Darley, and F. D. Sutterfield, Environ. Sci. and Tech. 8, 229 (1974).

[4] D. G. Hendry, A. C. Baldwin, and D. M. Golden, "Computer Modeling of Simulated Photochemical Smog," EPA-600/3-80-029, February 1980.

[5] R. Atkinson, W. P. L. Carter, K. R. Darnall, A. M. Winer, and J. N. Pitts, Jr., Int. J. Chem. Kinet. 12, 779 (1980).

[6] J. P. Killus and G. Z. Whitten, Atmos. Environ. 16, 1973 (1982).

[7] J. A. Leone and J. H. Seinfeld, Int. J. Chem. Kinet., 16, 159 (1984).

[8] W. P. L. Carter, R. Atkinson, A. M. Winer, and J. N. Pitts, Jr., Int. J. Chem. Kinet. 14, 1071 (1982).

[9] Purafil Inc., Chamblee, Georgia.

[10] D. Grosjean and K. Fung, "Atmospheric Measurements of Peroxybenzoyl Nitrate," Pacific Conference on Chemistry and Spectroscopy, Pasadena, CA, Oct. 26-28, 1983.

[11] D. Grosjean, Sci. Total Environ., 32, 133 (1984).

[12] P. K. Mueller, K. Fung, S. L. Heisler, D. Grosjean, and G. M. Hidy, "Atmospheric Particulate Carbon Observations in Urban and Rural Areas of the United States," in Particulate Carbon: Atmospheric Life Cycle, G. T. Wolff and R. L. Klimich, ed., Plenum Press, N.Y. pp. 343-370.

[13] F. Sakamaki, S. Hatakeyama, and H. Akimoto, Int. J. Chem. Kinet., 15, 1013 (1983).

[14] J. P. Killus and G. Z. Whitten, private communication to W. P. L. Carter, Dec. 1981, cited in reference [8].

[15] W. B. Demore, R. T. Watson, D. M. Golden, R. F. Hampson, M. Kurylo, C. J. Howard, M. J. Molina, and A. R. Ravishankara, "Chemical Kinetics and Photochemical Data for Use in Stratospheric Modeling," Jet Propulsion Laboratory Report 82-57, July 15, 1982.

[16] D. L. Baulch, R. A. Cox, P. J. Crutzen, R. F. Hampson, Jr., J. A. Kerr, J. Troe, and R. T. Watson, J. Phys. Chem. Ref. Data 11, 327 (1982).

[17] R. Atkinson and A. C. Lloyd, "Evaluation of Kinetic and Mechanistic Data for Modeling of Photochemical Smog," J. Phys. Chem. Ref. Data, to be published, 1984.

[18] K. L. Demerjian, K. L. Schere, and J. T. Peterson, Adv. Environ. Sci. Technol., 15, 829 (1981).

[19] N. A. Kelly, Environ. Sci. Technol., 16, 763 (1982).

[20] D. Grosjean, Atmos. Environ., 17, 2379 (1983).

[21] R. Atkinson, K. R. Darnall, A. C. Lloyd, A. M. Winer, and J. N. Pitts, Jr., Adv. Photochem., 11, 375 (1979).

[22] R. Atkinson, W. P. L. Carter, and A. M. Winer, J. Phys. Chem., 87, 1605 (1983).

[23] R. A. Henley, J. E. Davenport, and D. G. Hendry, J. Phys. Chem., 82, 1095 (1978).

[24] C. N. Plum, E. Sanheuza, R. Atkinson, W. P. L. Carter, and J. N. Pitts, Jr., Environ. Sci. Technol., 17, 479 (1983).

[25] A. C. Besemer, Atmos. Environ., 16, 1599 (1982).

[26] A. C. Besemer, Atmos. Environ., 17, 1598 (1983).

[27] E. C. Tuazon, R. Atkinson, H. MacLeod, H. W. Biermann, A. M. Winer, W. P. L. Carter, and J. N. Pitts, Jr., "Yields of Glyoxal and Methyl Glyoxal from the NO_x-Air Photooxidations of Toluene and m- and p-Xylene," Environ. Sci. Tech., to be published, 1984.

[28] B. E. Dumdei and R. J. O'Brien, "The Products of Toluene's Degradation Under Simulated Atmospheric Conditions," Amer. Chem. Soc., Div. Environ. Chem., Preprints, St. Louis, MO, April, 1984.

[29] J. A. Leone and J. H. Seinfeld, Environ. Sci. Technol., 18, 280 (1984).

[30] W. P. L. Carter, private communication to J. A. Leone, April, 1984.

[31] D. Grosjean, "Atmospheric Reactions of Ortho Cresol: Gas Phase Aerosol Products," Atmos. Environ., to be published, 1984.

[32] W. D. Schwartz, "Chemical Characterization of Model Aerosols," EPA-650/3-74-011, 1974.

[33] W. D. Schwartz, G. D. Mendenhall, P. W. Jones, C. J. Riggle, A. P. Graffeo, and D. F. Miller, "Chemical Characterization of Model Aerosols," EPA-600/3-76-085, 1976.

[34] D. Grosjean, K. Van Cauwenberghe, D. R. Fitz, and J. N. Pitts, Jr., Photooxidation Products of Toluene-NO_x Mixtures under Simulated Atmospheric Conditions. ACS Div. Environ. Chem. Preprints, 18, No. 1, 354-356, 1978.

[35] R. J. O'Brien, P. J. Green, N. L. Nguyen, R. A. Doty, and B. E. Dumdei, Environ. Sci. Technol., 17, 183 (1983).

[36] D. Grosjean, K. Fung, J. Collins, J. Harrison and E. Breitung, Anal. Chem., 56, 569 (1984).

[37] A. Horowitz and J. G. Calvert, J. Phys. Chem., 86, 3105 (1982).

[38] W. P. L. Carter, A. M. Winer, and J. N. Pitts, Jr., Environ. Sci. Technol., 15, 829 (1981).

APPENDIX

Table A.1. Toluene Reaction Mechanism

Reaction[1]	Rate Constant[2]	Activation Energy (K)	Reference	Note
Inorganic Reactions:				
1) $NO_2 + h\nu \rightarrow NO + O(^3P)$	*	-	-	1
2) $O(^3P) + O_2 \rightarrow O_3$	2.6×10^1	-5.1×10^2	15,16	-
3) $O_3 + NO \rightarrow NO_2 + O_2$	2.7×10^1	1.5×10^3	15,16	-
4) $O(^3P) + NO_2 \rightarrow NO + O_2$	1.4×10^4	-	15,16	-
5) $O_3 + NO_2 \rightarrow NO_3 + O_2$	4.7×10^{-2}	2.45×10^3	15,16	-
6) $NO_3 + NO \rightarrow 2NO_2$	3.0×10^4	-	15,16	-
7) $HO_2 + NO_2 \rightarrow HO_2NO_2$	1.6×10^3	-	17	-
8) $NO_2 + OH \rightarrow HNO_3$	1.6×10^4	-	15,16	-
9) $O_3 + OH \rightarrow HO_2 + O_2$	9.9×10^1	9.7×10^2	15,16	-
10) $O_3 + HO_2 \rightarrow OH + 2O_2$	3.0×10^0	5.8×10^2	15,16	-
11) $HO_2NO_2 \rightarrow HO_2 + NO_2$	5.1×10^0	1.042×10^4	17	-
12) $HO_2 + NO \rightarrow NO_2 + OH$	1.2×10^4	-2.4×10^2	15,16	-
13) $HO_2 + HO_2 \rightarrow H_2O_2 + O_2$	3.9×10^3	-1.2×10^3	15,16	-
14) $HO_2 + HO_2 + H_2O \rightarrow H_2O_2 + O_2 + H_2O$	2.2×10^{-1}	-5.8×10^3	17	-
15) $O_3 + h\nu \rightarrow O(^3P) + O_2$	1.4×10^{-2}	-	5	-
16) $O_3 + h\nu \rightarrow O(^1D) + O_2$	5.9×10^{-4}	-	5	-
17) $O(^1D) + O_2 \rightarrow O(^3P) + O_2$	4.3×10^4	-	15	-
18) $O(^1D) + H_2O \rightarrow 2OH$	3.2×10^5	-	15	-
19) $NO + OH \rightarrow HONO$	9.7×10^3	-	17	-
20) $HONO + h\nu \rightarrow NO + OH$	6.6×10^{-2}	-	5	-
21) $NO + NO + O_2 \rightarrow 2NO_2$	7.2×10^{-10}	-5.3×10^2	17	-
22) $NO_3 + NO_2 \rightarrow NO + NO_2 + O_2$	5.9×10^{-1}	1.23×10^3	17	-

Table A.1 (continued)

Reaction	Rate Constant	Activation Energy (K)	Reference	Note
23) $NO_3 + NO_2 \rightarrow N_2O_5$	1.6×10^3	-	15,16	-
24) $N_2O_5 \rightarrow NO_2 + NO_3$	3.1×10^0	1.108×10^4	16	-
25) $N_2O_5 + H_2O \rightarrow 2HNO_3$	4.4×10^{-6}	-	5	-
26) $H_2O_2 + OH \rightarrow HO_2 + H_2O$	2.5×10^3	-	15,16	-
27) $H_2O_2 + h\nu \rightarrow 2OH$	2.8×10^{-4}	-	5	-
28) $CO + OH \xrightarrow{O_2} HO_2 + CO_2$	4.0×10^2	-	15,16	-
29) $NO_3 + h\nu \rightarrow 0.3NO + 0.7NO_2 + 0.70(^3P)$	6.1×10^0	-	7	-
Aldehyde Reactions and PAN Formation:				
30) $CH_3CHO + h\nu \xrightarrow{2O_2} CH_3O_2\cdot + HO_2 + CO$	*	-	-	2
31) $CH_3CHO + OH \xrightarrow{O_2} CH_3C(O)O_2\cdot + H_2O$	2.4×10^4	-2.6×10^2	16	-
32) $CH_3O_2\cdot + NO \rightarrow NO_2 + CH_3O\cdot$	1.1×10^4	-	15,16	-
33) $CH_3O\cdot + O_2 \rightarrow HCHO + HO_2\cdot$	2.1×10^0	1.35×10^3	15,16	-
34) $CH_3O\cdot + NO_2 \rightarrow CH_3ONO_2$	2.2×10^4	-	17	-
35) $CH_3O_2\cdot + HO_2 \rightarrow CH_3OOH + O_2$	9.2×10^3	-1.3×10^3	15,16	-
36) $CH_3C(O)O_2\cdot + NO \xrightarrow{O_2} NO_2 + CH_3O_2\cdot + CO_2$	1.1×10^4	-	17	-
37) $CH_3C(O)O_2\cdot + NO_2 \rightarrow PAN$	6.9×10^3	-	17	-
38) $CH_3C(O)O_2\cdot + HO_2 \rightarrow CH_3C(O)O_2H + O_2$	4.4×10^3	-	17	-
39) $PAN \rightarrow CH_3C(O)O_2\cdot + NO_2$	2.2×10^{-2}	1.354×10^4	17	-
40) $HCHO + h\nu \rightarrow H_2 + CO$	*	-	-	2
41) $HCHO + h\nu \xrightarrow{2O_2} 2HO_2 + CO$	*	-	-	2

Table A.1 (continued)

Reaction	Rate Constant	Activation Energy (K)	Reference	Note
42) $HCHO + OH \xrightarrow{O_2} HO_2 + CO + H_2O$	1.6×10^4	-	16	-
α-Dicarbonyl Chemistry:				
43) $CH_3C(O)CHO + OH \xrightarrow{O_2} CH_3C(O)O_2\cdot + CO + H_2O$	2.5×10^4	-	24	-
44) $CH_3C(O)CHO + h\nu \xrightarrow{2O_2} CH_3C(O)O_2\cdot + + HO_2 + CO$	*	-	24	3
45) $CH_3C(O)CHO + h\nu \xrightarrow{2O_2} CH_3O_2\cdot + HO_2 + 2CO$	*	-	24	3
46) $(CHO)_2 + OH \xrightarrow{O_2} HO_2 + 2CO + H_2O$	1.7×10^4	-	24	-
47) $(CHO)_2 + h\nu \rightarrow 0.13HCHO + 0.87H_2 + 1.87CO$	*	-	24	3
Toluene Abstraction Pathway:				
48) $C_6H_5\text{-}CH_3 + OH \xrightarrow{O_2} C_6H_5\text{-}CH_2O_2\cdot + H_2O$	7.5×10^2	-	17	-
49) $C_6H_5\text{-}CH_2O_2\cdot + NO \rightarrow NO_2 + C_6H_5\text{-}CH_2O\cdot$	9.0×10^3	-	17	-
50) $C_6H_5\text{-}CH_2O_2\cdot + NO \rightarrow C_6H_5\text{-}CH_2ONO_2$	1.0×10^3	-	17	-
51) $C_6H_5\text{-}CH_2O\cdot + O_2 \rightarrow C_6H_5\text{-}CHO + HO_2$	1.0×10^1	6.9×10^2	17	-
52) $C_6H_5\text{-}CH_2O\cdot + NO_2 \rightarrow C_6H_5\text{-}CH_2ONO_2$	1.9×10^4	-	17	-
53) $C_6H_5\text{-}CHO + h\nu \rightarrow$ stable products	1.6×10^{-3}	-		4
54) $C_6H_5\text{-}CHO + OH \xrightarrow{O_2} C_6H_5\text{-}C(O)O_2\cdot + H_2O$	1.9×10^4	-	17	-
55) $C_6H_5\text{-}C(O)O_2\cdot + NO \xrightarrow{O_2} NO_2 + C_6H_5\text{-}O_2\cdot + CO_2$	1.0×10^4	-	17	-

Table A.1 (continued)

Reaction	Rate Constant	Activation Energy (K)	Reference	Note
56) $C_6H_5\text{-}C(O)O_2\cdot + NO_2 \rightarrow C_6H_5\text{-}C(O)O_2NO_2$	6.9×10^3	-	17	-
57) $C_6H_5\text{-}C(O)O_2NO_2 \rightarrow C_6H_5\text{-}C(O)O_2\cdot + NO_2$	9.6×10^{-3}	1.304×10^4	17	-
58) $C_6H_5\text{-}O_2\cdot + NO \rightarrow NO_2 + C_6H_5\text{-}O\cdot$	9.0×10^3	-	17	-
59) $C_6H_5\text{-}O_2\cdot + NO_2 \rightarrow NO_3 + C_6H_5\text{-}O\cdot$	1.0×10^4	-	17	-
60) $C_6H_5\text{-}O\cdot + NO_2 \rightarrow$ 	2.2×10^4	-	17	-
61) 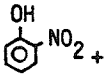 $+ NO_3 \rightarrow$ 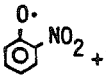 $+ HNO_3$	3.0×10^3	-	38	5
62) 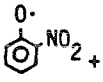 $+ NO_2 \rightarrow$ 	2.2×10^4	-	-	6
63) 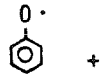 $+ HO_2 \rightarrow$ 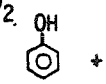 $+ O_2$	7.4×10^3	-	17	-
Toluene Addition Pathway:				
64) 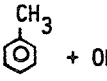 $+ OH \rightarrow$ 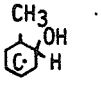	8.7×10^3	-	17	-
65)  $+ O_2 \rightarrow$ 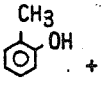 $+ HO_2$	1.0×10^1	6.9×10^2	17	-
66)  $+ NO_2 \rightarrow$ 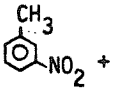 $+ H_2O$	4.4×10^4	-	17	-
67) 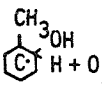 $+ O_2 \rightarrow$ 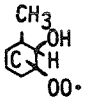	4.9×10^1	-	17	-
68) 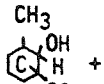 $+ NO \xrightarrow{2O_2} NO_2 + HO_2$ $+ CH_3C(O)CHO + CH(O)CH{=}CHCHO$	1.0×10^4	-	17	7

Table A.1 (continued)

Reaction	Rate Constant	Activation Energy (K)	Reference	Note
Toluene addition path (continued)				
69) 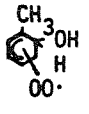 + NO $\xrightarrow{2O_2}$ $NO_2 + HO_2 + (CHO)_2$ + $CH_3C(O)CH=CHCHO$	0	-	17	7
70) 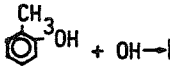 + $OH \rightarrow$  + H_2O	4.9×10^3	9.0×10^2	17	-
71) 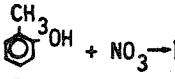 + $NO_3 \rightarrow$  + HNO_3	1.5×10^4	-	17	-
72) 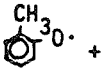 + $NO_2 \rightarrow$ 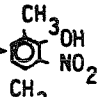	2.2×10^4	-	17	-
73) 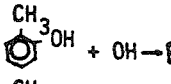 + $OH \rightarrow$ 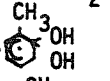	5.6×10^4	-	17	-
74) 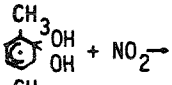 + $NO_2 \rightarrow$ 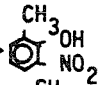 + H_2O	4.4×10^4	-	17	-
75) 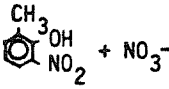 + $NO_3 \rightarrow$ 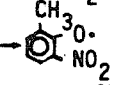 + HNO_3	1.5×10^4	-	38	8
76) 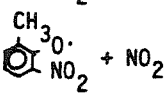 + $NO_2 \rightarrow$ 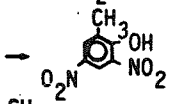	2.2×10^4	-	-	6
77) 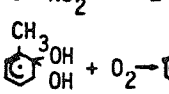 + $O_2 \rightarrow$ 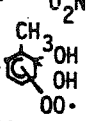	4.9×10^1	-	17	-
78)  + NO $\xrightarrow{2O_2}$ $NO_2 + HO_2$ + $CH(O)CH=CHCHO$ + $CH_3C(O)COOH$	1.0×10^4	-	17	7
79)  + NO $\xrightarrow{2O_2}$ $NO_2 + HO_2$ + $CH_3C(O)CH=CHCHO$ + $CH(O)COOH$	0	-	17	7

Table A.1 (continued)

	Reaction	Rate Constant	Activation Energy(K)	Reference	Note
80)	$CH(O)COOH + OH \xrightarrow{O_2} HO_2 + H_2O + CO + CO_2$	4.7×10^{4}	-	17	-
81)	$CH_3C(O)COOH + h\nu \rightarrow CH_3CHO + CO_2$	5.0×10^{-3}	-	6	-
	Conjugated γ-dicarbonyl chemistry				
82)	$HC(O)CH=CHCHO + OH \xrightarrow{O_2} HC(O)CH=CHC(O)O_2\cdot + H_2O$	4.4×10^{4}	-	17	-
83)	$HC(O)CH=CHC(O)O_2\cdot+NO \xrightarrow{O_2} NO_2+CO_2+HC(O)CH=CHO_2\cdot$	1.0×10^{4}	-	17	-
84)	$HC(O)CH=CHO_2\cdot+NO \xrightarrow{O_2} NO_2+HC(O)CH(O_2\cdot)CHO$	1.0×10^{4}	-	17	-
85)	$HC(O)CH(O_2\cdot)CHO+NO \rightarrow HC(O)CH(ONO_2)CHO$	4.0×10^{2}	-	17	-
86)	$HC(O)CH=CHC(O)O_2\cdot+NO_2 \rightarrow HC(O)CH=CHCO_3NO_2$	6.9×10^{3}	-	17	-
87)	$HC(O)CH=CHCO_3NO_2 \rightarrow HC(O)CH=CHC(O)O_2\cdot+NO_2$	2.2×10^{-2}	-	17	-
88)	$HC(O)CH(O_2\cdot)CHO+NO \xrightarrow{O_2} (CHO)_2+HO_2+NO_2+CO$	1.0×10^{4}	-	17	-
89)	$HC(O)CH=CHO_2\cdot+NO \rightarrow HC(O)CH=CHONO_2$	4.0×10^{2}	-	17	-
90)	$HC(O)CH=CHO_2\cdot+NO_2 \xrightarrow{O_2} HC(O)CH(O_2\cdot)CHO+NO_3$	1.0×10^{4}	-	17	-
91)	$CH_3C(O)CH=CHCHO + OH \xrightarrow{O_2} H_2O+CH_3C(O)CH=CHC(O)O_2\cdot$	2.2×10^{4}	-	17	9
92)	$CH_3C(O)CH=CHCHO+OH \xrightarrow{O_2} CH_3C(O)CH(OH)C(O_2\cdot)HCHO$	7.4×10^{3}	-	17	9
93)	$CH_3C(O)CH(OH)C(O_2\cdot)HCHO+NO \xrightarrow{O_2} NO_2+HO_2 + CH_3C(O)CHO+(CHO)_2$	1.0×10^{4}	-	17	9
94)	$CH_3C(O)CH=CHC(O)O_2\cdot+NO \xrightarrow{O_2} NO_2+CO_2 + CH_3C(O)CH=CHO_2\cdot$	1.0×10^{4}	-	17	9
95)	$CH_3C(O)CH=CHO_2\cdot+NO \xrightarrow{O_2} NO_2+CH_3C(O)CH(O_2\cdot)CHO$	1.0×10^{4}	-	17	9
96)	$CH_3C(O)CH(O_2\cdot)CHO+NO \rightarrow CH_3C(O)CH(ONO_2)CHO$	8.0×10^{6}	-	17	9
97)	$CH_3C(O)CH=CHC(O)O_2\cdot+NO \rightarrow CH_3C(O)CH=CHCO_3NO_2$	6.9×10^{3}	-	17	9
98)	$CH_3C(O)CH=CHCO_3NO_2 \rightarrow CH_3C(O)CH=CHC(O)O_2\cdot+NO_2$	2.2×10^{-2}	-	17	9
99)	$CH_3C(O)CH(O_2\cdot)CHO+NO \xrightarrow{O_2} NO_2+CH_3C(O)O_2\cdot+(CHO)_2$	5.0×10^{3}	-	17	9

Table A.1 (continued)

Reaction	Rate Constant	Activation Energy(K)	Reference	Note
Conjugated γ-dicarbonyl chemistry (continued)				
100) $CH_3C(O)CH(O_2\cdot)CHO+NO \xrightarrow{O_2} NO_2+HO_2+CH_3C(O)CHO+CO$	5.0×10^{3}	-	17	9
101) $CH_3C(O)CH=CHO_2\cdot+NO \rightarrow CH_3C(O)CH=CHONO_2$	8.0×10^{2}	-	17	9
102) $CH_3C(O)CH=CHO_2\cdot+NO_2 \xrightarrow{O_2} NO_3+CH_3C(O)CH(O_2\cdot)CHO$	1.0×10^{4}	-	17	9
Chamber dependent reactions:				
103) $O_3 \rightarrow$ wall	1.65×10^{-3}	-	-	10
104) $NO_2 \rightarrow HONO$	5.0×10^{-4}	-	-	10,11

*See note

[1]Only one isomer is shown, even when many isomers are possible.

[2]ppm-min units

Notes: See next page.

Notes:

(1) Estimated theoretically [18], see text for discussion.

(2) The rate constants used in our mechanism are based on Demerjian et al. [18],

$$k_{30} = 8.4\times10^{-4} k_1$$
$$k_{40} = 3.4\times10^{-3} k_1$$
$$k_{41} = 3.5\times10^{-3} k_1$$

Horowitz and Calvert [37] have suggested lower values for all of these rate constants. However, only insignificant changes in the model predictions result when the Horowitz and Calvert values are used in our mechanism.

(3) From Plum et al. [24],

$$k_{44} + k_{45} = 0.019 k_1$$
$$k_{47} = 0.008 k_1$$

We find the PAN data are best simulated by assuming $k_{44}/(k_{44}+k_{45}) \approx 0.7$

(4) k_{53} was chosen to give the best fit of benzaldehyde profiles in SAPRC toluene-benzaldehyde-NO_x runs EC-337 and EC-339, see [7].

(5) k_{61} is assumed to be about the same as the rate constant for the phenol + NO_3 reaction [38].

(6) k_{62} is assumed to be of the same order as the rate constant for other RO· + NO_2 reactions.

(7) From Atkinson and Lloyd [17]

$$k_{68} + k_{69} = k_{78} + k_{79} = 1.0\times10^{4}\ \text{ppm}^{-1}\ \text{min}^{-1}$$

See text for a discussion of the effects of varying $k_{68}/(k_{68}+k_{69})$ and $k_{78}/(k_{78}+k_{79})$.

(8) k_{75} is assumed to be of the same order as the rate constant for the o-cresol + NO_3 reaction abstraction reaction.

(9) These reactions are only needed if k_{69} or k_{79} is not equal to zero. Since we find the best results are obtained with $k_{69} = k_{79} = 0$, no 4-oxo-2-pentenal is produced. Thus, reactions 91-102 can be ignored.

(10) Chamber-dependent.

(11) See text.

Table A.2. Possible reaction pathways for C7 conjugated dicarbonyls[1]

A) OH abstraction

1) Species (2A):

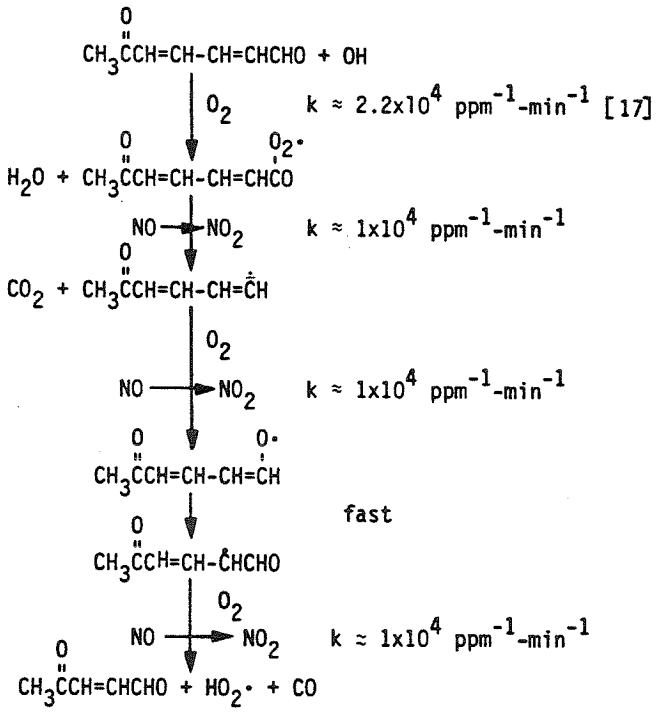

2) Species (2b):

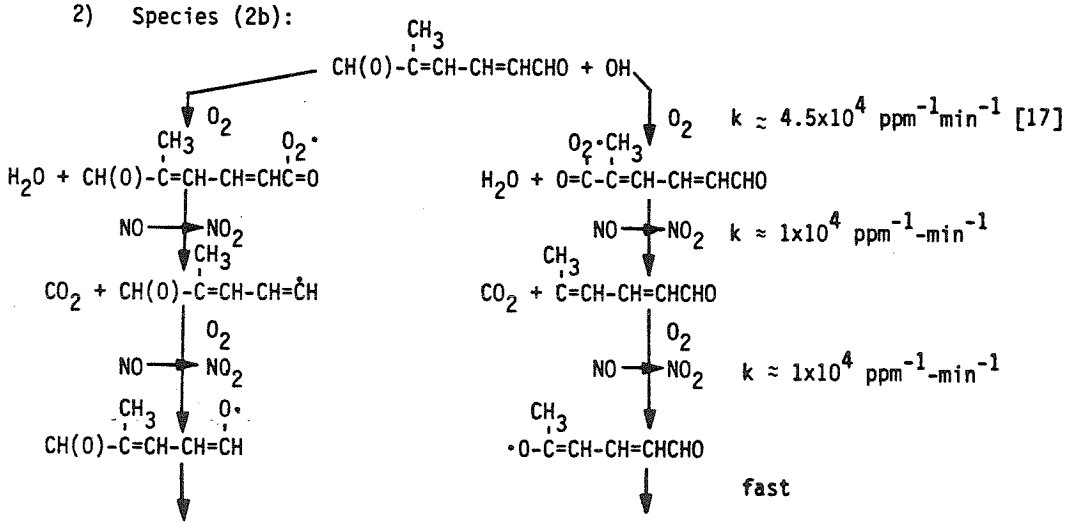

Table A.2. Possible reaction pathways for C7 conjugated dicarbonyls[1] (continued)

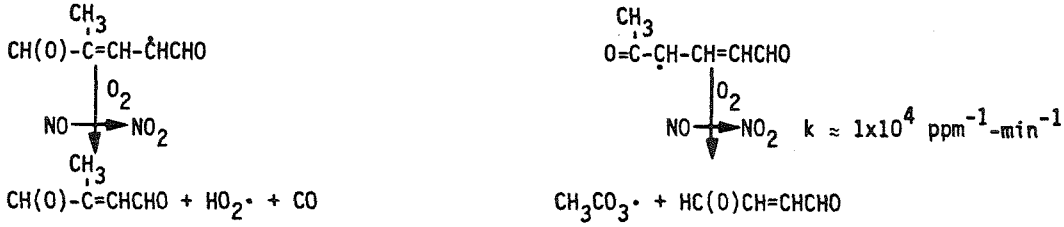

B) OH addition, $k_{add} \approx 7.4 \times 10^3$ $ppm^{-1}\text{-}min^{-1}$ [17]

1) Species (2A):

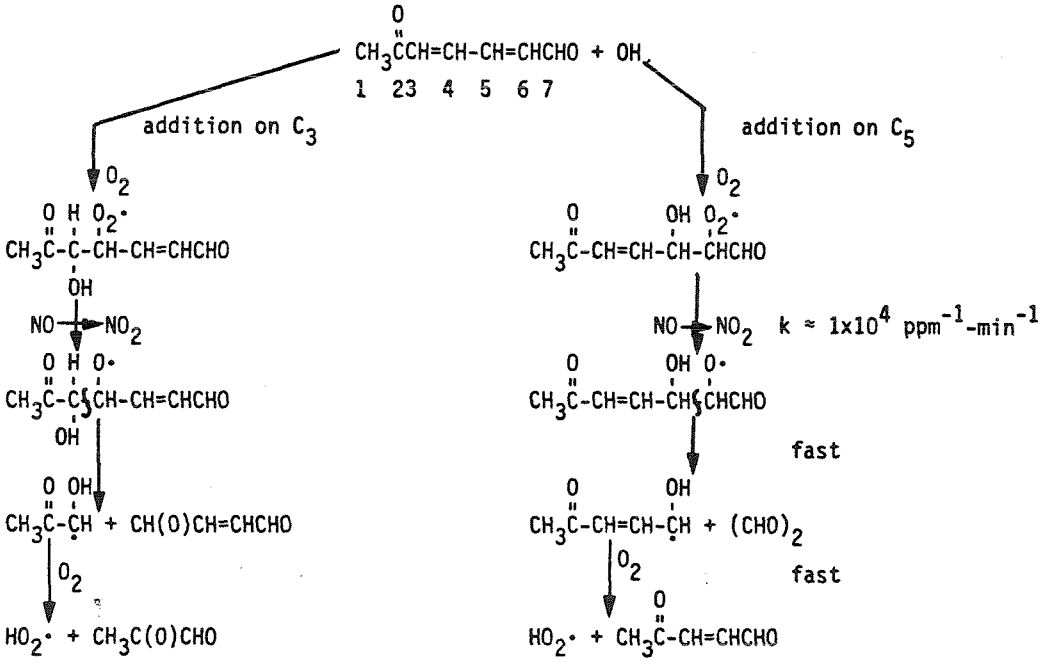

Note: addition on C_4 gives the same products

Note: addition on C_6 gives the same products

Table A.2. Possible reaction pathways for C7 conjugated dicarbonyls[1] (continued)

2) Species (2B):

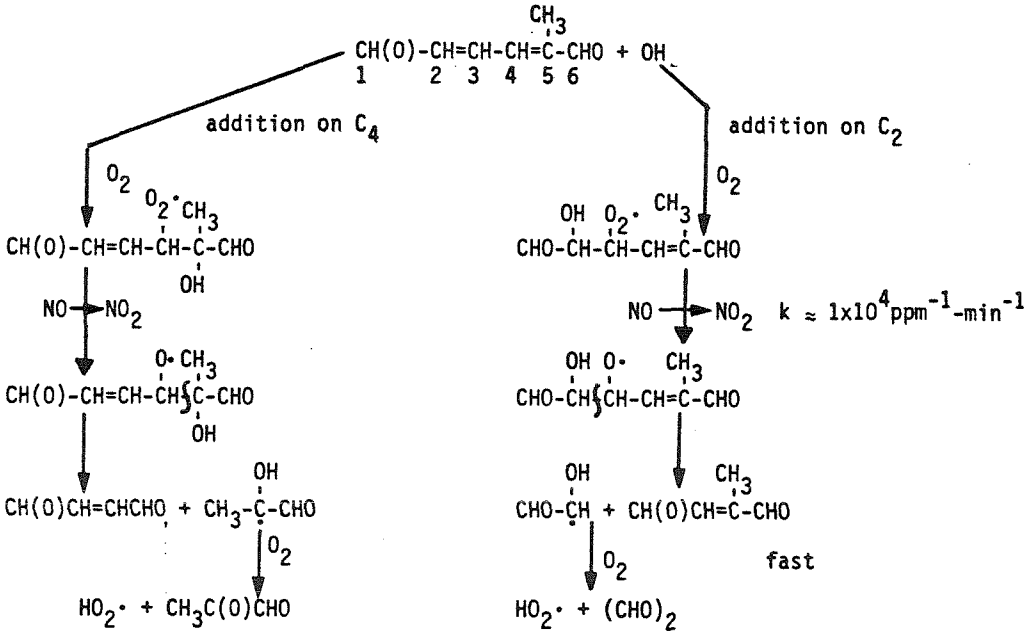

Note: addition on C_5 gives the same products

Note: addition on C_3 gives the same products

C) Photolysis

1) Species (2A):

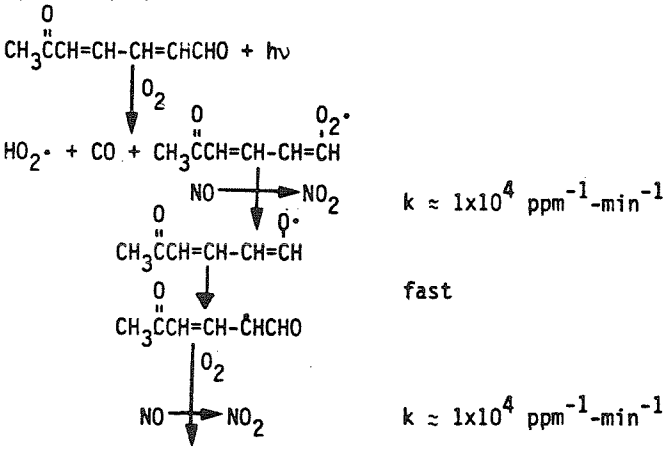

Table A.2. Possible reaction pathways for C7 conjugated dicarbonyls[1] (continued

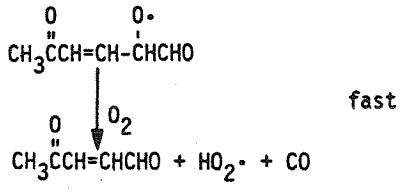

2) Species (2B):

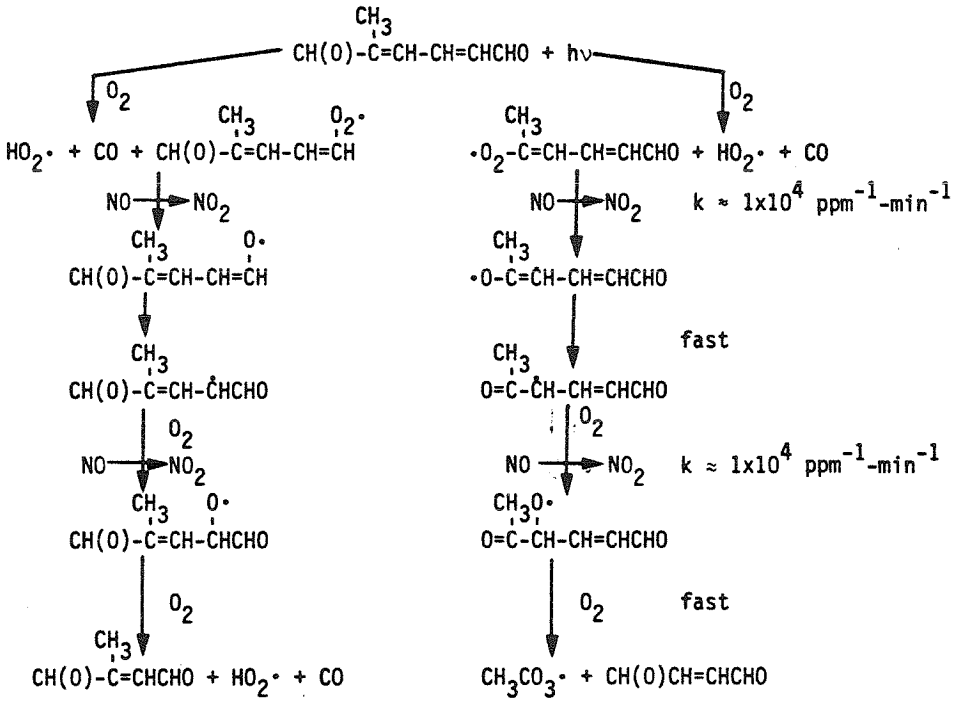

[1]Reactions of the α- and conjugated-γ-dicarbonyls which are produced from the C7 dicarbonyls are shown in Table A.1.

II. ANALYSIS OF CHEMICAL REACTION MECHANISMS FOR PHOTOCHEMICAL SMOG

CHAPTER 4

Evaluation of Chemical Reaction Mechanisms for Photochemical Smog. Part 1: Mechanism Descriptions and Documentation

EVALUATION OF CHEMICAL REACTION MECHANISMS FOR PHOTOCHEMICAL SMOG

PART I. MECHANISM DESCRIPTIONS AND DOCUMENTATION

by

Gregory J. McRae
Joseph A. Leone
John H. Seinfeld

California Institute of Technology
Pasadena, California 91125

Cooperative Agreement 810184

Project Officer

Marcia C. Dodge

Gas Kinetics and Photochemistry Branch
Environmental Sciences Research Laboratories
Research Triangle Park, North Carolina 27711

ENVIRONMENTAL SCIENCES RESEARCH LABORATORY
OFFICE OF RESEARCH AND DEVELOPMENT
U.S. ENVIRONMENTAL PROTECTION AGENCY
RESEARCH TRIANGLE PARK, NORTH CAROLINA 27711

ABSTRACT

Over the past ten years or so a great deal of effort has been devoted to developing chemical reaction mechanisms for photochemical air pollution. Because the actual number of atmospheric organic species is too large for the detailed chemistry of each to be included in a mechanism, it has been necessary to reduce the number of organic species to a manageable set by a process referred to as lumping. The manner in which this lumping has been carried out constitutes one of the major differences among existing mechanisms. It has recently been demonstrated that different chemical mechanisms predict different degrees of hydrocarbon and NO_x control to achieve the same level of ozone reduction under identical conditions. Because of the necessity of using reaction mechanisms for photochemical smog in determining air pollution control strategies, these results point to a serious need to analyze the fundamental behavior of such mechanisms and to understand the key elements of their behavior. Such an analysis is the subject of this two part report. The current volume, Part I, contains a detailed description of six mechanisms that have been developed to describe photochemical smog chemistry, including analyses of the treatments of the basic chemistry, of photolysis reactions and organic lumping in initial conditions and rate constants. It is found that the mechanisms differ in virtually all aspects. Part II is devoted to a detailed analysis of the behavior of each of the mechanisms.

TABLE OF CONTENTS

LIST OF FIGURES

LIST OF TABLES

LIST OF TABLES (Continued)

LIST OF TABLES (Continued)

ACKNOWLEDGEMENT

We wish to acknowledge the assistance of: Alan C. Lloyd, Fred Lurmann, Marcia Dodge, Kenneth Demerjian, Kenneth Schere, Gary Whitten, Jim Killus and Joyce Penner for providing computer codes and documentation of their mechanisms. Thanks are also due to Richard Kee of SANDIA Laboratories for supplying a copy of the kinetics solution program CHEMKIN. Appreciation is extended to William P.L. Carter for his assistance.

CHAPTER 1

INTRODUCTION

Over the past ten years or so, a great deal of effort has been devoted to developing chemical reaction mechanisms for photochemical air pollution, and, as a result, several mechanisms exist at the present time. Since the atmosphere contains literally scores of hydrocarbon species, it is virtually impossible to write a reaction mechanism that includes the detailed chemistry of each hydrocarbon species present. Although each mechanism is based, more or less, on the same body of experimental kinetic data, the manner of treatment of the hydrocarbon chemistry varies among them. Because the actual number of hydrocarbon species is, as we have noted, too large for the detailed chemistry of each to be included in a mechanism, it has been necessary to reduce the number of hydrocarbon species to a manageable set by a process referred to as lumping. The manner in which this lumping has been carried out constitutes one of the major differences among existing mechanisms.

The differences among the several existing reaction mechanisms would not be of concern if their predictions were in essential agreement over the range of conditions of interest for atmospheric predictions. It has recently been demonstrated, however, that different mechanisms predict rather different degrees of hydrocarbon and NO_x control to achieve the same level of ozone reduction under identical conditions (Jeffries et al., 1981; Whitten, 1981; Carter et

al., 1982). Because of the necessity of using reaction mechanisms for photochemical smog in determining air pollution control strategies, these results point to a serious need to analyze the fundamental nature of such mechanisms and to understand the key elements of their behavior. Such an analysis is the subject of this work.

Figure 1 depicts the ways in which hydrocarbon lumping has been approached in photochemical smog mechanisms. In the surrogate species approach, typified by the mechanism of Dodge (1977), the entire atmospheric mixture is represented by a small number of surrogate hydrocarbon species. In the mechanism of Dodge (1977), propene and n-butane, together with small quantities of formaldehyde and acetaldehyde, represent the entire atmospheric mix.

The other lumping approaches are indicated in Figure 1. Lumped molecule approaches refer to those in which the atmospheric hydrocarbons are lumped into identifiable molecular species. For example, in the surrogate species lumped molecule approach, certain hydrocarbons serve as surrogate species for an entire group of actual species. For example, n-butane can be used to represent all atmospheric alkanes, and the alkane portion of the full mechanism then consists of the detailed explicit chemistry of n-butane. Thus, a mixture of many alkanes is represented by a comparable concentration of n-butane. A mechanism based on this approach is that of Atkinson et al. (1982). We should point out that the mechanism of Dodge (1977), referred to above, is, in essence, also a surrogate species mechanism; however, the n-butane and propene are not necessarily identified with

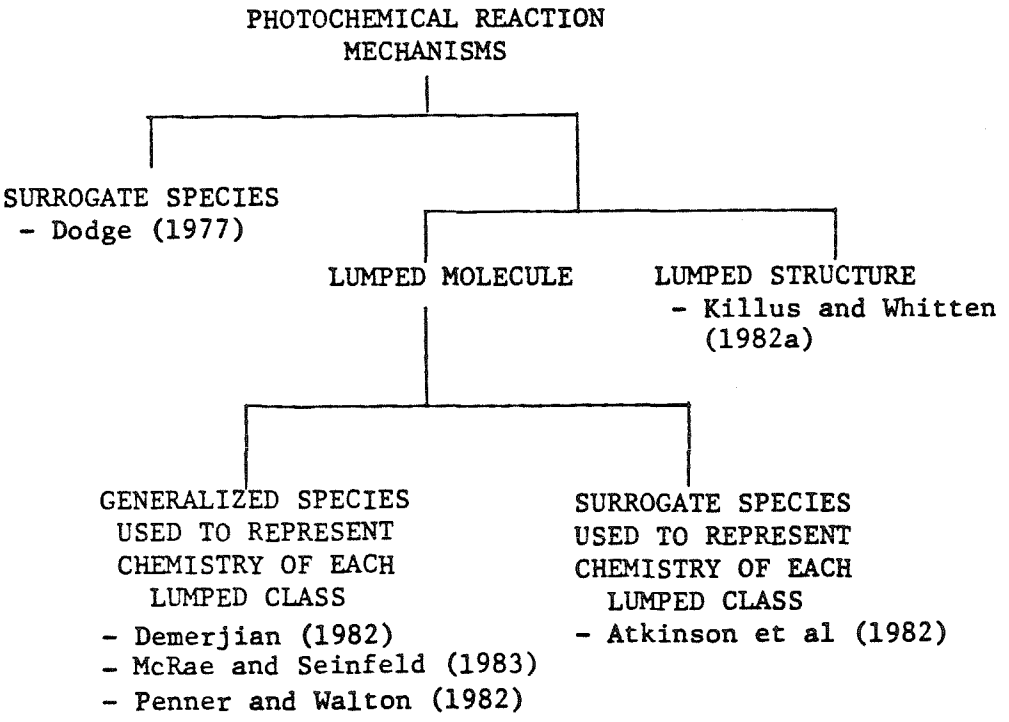

FIGURE 1

Classification of Photochemical Reaction Mechanisms Used in Evaluation

alkane and alkane species, respectively. Rather, propene and n-butane represent the entire atmospheric mix, where only the total concentration of non-methane hydrocarbons in parts per million by carbon is matched to the initial concentrations of propene and n-butane.

The other type of lumped molecule approach is that of generalized species lumping, in which an entire group of compounds is represented by a generalized species the chemistry of which reflects the common features of that of the whole group. For example, alkanes could be represented by a species called ALKANE, whose rate constants and reaction mechanisms are, in some manner, an average of those of all alkanes. Mechanisms in this class include those of McRae and Seinfeld (1983), Demerjian (1982), and Penner and Walton (1982).

Finally, in the lumped structure approach, lumped species represent various classes of structural units, such as, single-bonded carbon atoms, double-bonded carbon atoms, and carbonyl carbon atoms. An initial mixture of organics is therefore apportioned by bond type rather than by molecule type to obtain the lumped species. The one mechanism of this type is that of Killus and Whitten (1982a). The Killus and Whitten mechanism, referred to as the Carbon Bond mechanism, treats the reactions of five different types of carbon atoms: 1-alkene carbon atoms except ethene, ethene, single bonded carbon atoms, reactive aromatic rings, carbonyl carbon atoms including carbon atoms from internal olefins.

It is important to point out that any reaction mechanism for the atmospheric chemistry of photochemical smog must involve some aspect of hydrocarbon lumping. It is sometimes mistakenly assumed that lumping is not involved in a surrogate mechanism, since a surrogate mechanism consists of the explicit chemistry of the surrogate species. Although the mechanism itself contains only explicit chemical steps, not involving any generalized species, the representation of an atmospheric mixture requires that many species not explicitly included in the mechanism be apportioned to the surrogate species. It is, in fact, the way in which species are apportioned that really constitutes the differences among mechanisms, although mechanisms do differ in the values of rate constants used and in the importance of mechanistic steps where the available experimental information is open to interpretation.

As noted earlier, it has been found that several available photochemical reaction mechanisms do not predict the same ozone levels for the same initial quantities of reactive hydrocarbons and NO_x. Analyzing the behavior of each mechanism is not a straightforward undertaking because of the length of the mechanism (usually between 50 and 100 reactions) and because of the intricate nature of the free radical reaction chains involved. Consequently, it is desirable to employ a technique that enables one to track the complex species flows in a mechanism. Such a method has been developed by Leone and Seinfeld (1983b) and is employed in Part II of this work.

The particular mechanisms chosen for initial testing in this study are shown in Figure 1 and Table 1. Several different criteria were used to select representative mechanisms, including: the availability of supporting documentation and the degree of testing against smog chamber experiments. One additional requirement was that each mechanism had to have been implemented in an air quality model and used in emissions control calculations. With this background the following material was requested from each investigator responsible for the development of the reaction mechanism: (1) All the available open and report literature references that describe the scientific basis and testing of the reaction mechanism; (2) A computer listing of the reactions, species names and a duplication of a test case. This latter information was requested to ensure that the mechanism has been implemented in the manner intended by the developer. A summary of the mechanism characteristics, documentation sources and bases for validation is shown in Table 1. The validation bases of the Atkinson et al. (1982), Killus and Whitten (1982a) and Penner and Walton (1982) mechanisms are experiments conducted at the University of California, Riverside, whereas the Demerjian (1982) and Dodge (1977) mechanisms were evaluated on Bureau of Mines smog chamber data. The Killus and Whitten (1982a) mechanism has also been tested against outdoor smog chamber data from the University of North Carolina. Chapter 2 contains summaries of the mechanisms.

Chapter 3 contains a discussion of the basis of the lumping approaches of the five lumped mechanisms: Atkinson et al. (1982),

TABLE 1

Photochemical Reaction Mechanisms Considered for Evaluation - Their Characteristics and Their Validation Base

REACTION MECHANISM	TYPE[a]	NUMBER OF REACTIONS/ SPECIES	NUMBER OF ORGANIC CLASSES[b]	VALIDATION BASIS EXPERIMENT NUMBERS[c]	VALIDATION BASIS TYPE OF EXPERIMENT
Atkinson et al. (1979, 1982)[c]	LM	81/52	14	EC-178	n-butane/NO_x
Carter et al. (1979) Lurmann (1982, 1983)				EC-143	ethene/NO_x
				EC-146	tr-2-butene/NO_x
				EC-216	propene/NO_x
				EC-340	toluene/NO_x
				EC-344	m-xylene/NO_x
				EC-161	4 alkenes/NO_x
				EC-237,EC-242,EC-246	7 hydrocarbons/NO_x
				AGC-119,AGC-133,AGC-134 AGC-135,AGC-138,AGC-150 AGC-156	surrogate (multi-hydrocarbon)/NO_x
				AP-28,AP-30,AP-35,AP-37	hydrocarbon/NO_x/SO_2
Demerjian (1982) Schere (1983)	LM	45/30	4		40 Bureau of Mines smog chamber experiments with dilute auto exhaust and added NO_x. Several UCR aromatic hydrocarbon/NO_x experiments
Dodge (1977) Durbin et al. (1975)	S	76/39	4		17 Bureau of Mines smog chamber experiments with dilute auto exhaust and added NO_x

Table 1 (continued)

REACTION MECHANISM	TYPE[a]	NUMBER OF REACTIONS/ SPECIES	NUMBER OF ORGANIC CLASSES[b]	VALIDATION BASIS EXPERIMENT NUMBERS[c]	VALIDATION BASIS TYPE OF EXPERIMENT
Killus and Whitten (1982a) Whitten et al. (1980a,b)	LS	79/41	5	EC-231,EC-232,EC-233, EC-237,EC-238,EC-242, EC-243,EC-245,EC-246, EC-247	7 hydrocarbon/NO_x experiments at SAPRC
				—	2 day urban hydrocarbon mix at UNC
Falls and Seinfeld (1978)[d] Falls et al. (1979) McRae et al. (1982) McRae and Seinfeld (1983)	LM	52/32	6	EC-237	7 hydrocarbon/NO_x
				SUR-119J,SUR-121J, SUR-126J,SUR-132J, SUR-133J,SUR-134J	surrogate atmospheric mix
Gelinas and Skewes-Cox (1975) MacCracken and Sauter (1975)	LM	59/22	4	—	several individual hydrocarbon/NO_x experiments
Penner and Walton (1982)				EC-231,EC-232,EC-233, EC-237,EC-238,EC-241, EC-242,EC-243,EC-245	7 hydrocarbon/NO_x

Footnotes for Table 1

(a) The mechanism type refers to: LM - Lumped molecule, S - Surrogate and LS - Lumped structure.

(b) Number of reactive organic groupings for which either emissions or initial conditions must be specified in practical applications.

(c) A list of references is provided for each reaction mechanism documenting the evolution, if any, of the mechanism. The mechanism presented here corresponds to that in the most recent reference cited.

(d) This mechanism was developed by Falls and Seinfeld (1978), with updated rate constants presented by McRae and Seinfeld (1983).

(e) The experiment numbers refer to the following laboratories:

EC, SUR	Statewide Air Pollution Research Center (SAPRC) of the University of California, Riverside
UNC	University of North Carolina

referred to as ALW, Demerjian (1982), Killus and Whitten (1982), referred to as KW, McRae and Seinfeld (1983), referred to as MS, and Penner and Walton (1982), referred to as PW. Our discussion of the chemistry of photochemical smog is based almost exclusively on the extensive review of Atkinson and Lloyd (1983). Thus, unless otherwise noted, the source of statements concerning individual chemical steps and rate constants in Chapter 3 is that review.

We then examine the specification of photolysis rates (Chapter 4) and initial conditions (Chapter 5) in each of the mechanisms. Chapter 6 contains a summary of the key findings of Part I. Part II of this report is devoted to a detailed evaluation of the characteristics of each of the mechanisms.

CHAPTER 2

DOCUMENTATION AND INITIAL TESTING OF REACTION MECHANISMS

2.1 The Reaction Mechanisms

We now present the detailed mechanisms to be considered in this study. Two tables are used to document each reaction set, the first of which contains the list of elementary reactions. Photolysis steps are denoted by expressions containing the symbol HV; i.e.,

$$X_j + HV \text{ --> } \quad .$$

The second table contains the species names and a set of initial conditions, corresponding to a particular test case. Note that only upper-case characters are used to define the species names. They can be directly read by the computer program used to solve the kinetics. Certain species are held at constant concentration during any one experiment; they include water (H2O), molecular oxygen (O2) and M. Each reaction rate constant has been coded with a key that identifies one of four different ways of specifying the rate data.

KEY	RATE CONSTANT FORMAT
1	$k = A * TEMP^B * EXP(- C/T)$
2	Rate constant specified externally, this form is usually only used for photolysis steps.
3	Rate constant expressed as a proportion of another rate constant so that $K = A * K(B)$ where B identifies the reaction number.
4	For some reactions the rates can be expressed in terms of a zenith angle scaling of another basic rate constant. For example, the ozone photolysis rate could be defined as a zenith angle scaling of the NO_2 rate so that $k(O_3+H_2O+hv) = D(Z) * K(NO_2+hv)$.

The units used to specify the rate constants, initial conditions and species concentrations are based on the ppm-min system. In some cases the reaction rate constants have been derived from literature values that have been reported in terms of cm-molecule-sec units. The formulae used for converting first-, second- and third-order rate constants are:

$$k(min^{-1}) = 60.0\ k(sec) \tag{2.1}$$

$$k(ppm^{-1}\text{-}min^{-1}) = 4.40\times10^{17}(P/T)\ \ k(cm^3\text{-}molecule^{-1}\text{-}sec^{-1}) \tag{2.2}$$

$$k(ppm^{-2}\text{-}min^{-1}) = 3.23\times10^{33}(P/T)^2\ k(cm^6\text{-}molecule^{-2}\text{-}sec^{-1}) \tag{2.3}$$

where P is the pressure in atmospheres and T the temperature in ^oK. The presence of temperature in the denominators of (2.2) and (2.3) can be treated, in the reaction coding, by including the appropriate exponent B in the rate constant. Given this background it is now

possible to present the mechanisms considered for detailed evaluation; they are shown in Tables 2 - 13.

A cursory examination of the tables reveals several features of reaction product stoichiometry that deserve further explanation: the presence of non-integer stoichiometric coefficients, negative coefficients for some of the species and individual reactions that appear to violate mass conservation. All of these arise as a result of the need to minimize both the number of species and reactions. There are several ways in which non integer coefficients can arise. For example in the Atkinson et al. (1982) mechanism the photodissociation of nitrogen trioxide is treated as the single step

$$NO_3 + h\nu \xrightarrow{19} 0.3\ NO + 0.7\ NO_2 + 0.7\ O_3 \ .$$

The composite reaction is the result of combining the two elementary reaction steps

$$NO_3 + h\nu \xrightarrow{a} NO + O_2$$

$$\xrightarrow{b} NO_2 + O(^3P) \ .$$

By assuming that the production of molecular oxygen in step a can be ignored and that $O(^3P)$ reacts very rapidly through the reaction $O(^3P) + O_2 + M \longrightarrow O_3 + M$ to form ozone, the two pathways can be combined into a single reaction of the form

TABLE 2

Definition of the Atkinson et al. (1982) Reaction Mechanism[a]

REACTION[b]	NUMBER	RATE CONSTANT[c] A	B	C	KEY
NO2 + HV —> NO + O3	(01)	0.35	0	0.	2
NO + O3 —> NO2 + O2	(02)	1.0E+6	-1	1450.	1
O3 + H2O + HV —> 2 OH + O2	(03)	0.	1	0.	4
OH + NO —> HONO	(04)	8.7E+8	-2	0.	1
OH + NO2 —> HNO3	(05)	1.5E+9	-2	0.	1
HONO + HV —> OH + NO	(06)	.17	1	0.	3
NO2 + NO —> OH + NO2	(07)	3.7E+6	-1	0.	1
NO2 + NO2 —> HNO4	(08)	1.5E+8	-2	0.	1
HNO4 —> HO2 + NO2	(09)	7.8E+15	0	10420.	1
HO2 + HO2 —> H2O2 + O2	(10)	3.4E+4	-1	-1100.	1
HO2 + HO2 + H2O —> H2O2 + O2	(11)	5.8E-5	-2	-5800.	1
H2O2 + HV —> 2 OH	(12)	7.1E-4	1	0.	3
OH + CO —> HO2	(13)	1.3E+5	-1	0.	1
NO2 + O3 —> NO3	(14)	5.3E+4	-1	2450.	1
NO + NO3 —> 2 NO2	(15)	8.4E+6	-1	0.	1
NO2 + NO3 —> N2O5	(16)	3.1E+7	-1	1100.	1
N2O5 —> NO2 + NO3	(17)	3.5E+18	0	12280.	1
N2O5 + H2O —> 2 HNO3	(18)	1.33E-3	-1	0.	1
NO3 + HV —> 0.3 NO + 0.7 NO2 + 0.7 O3	(19)	15.5	1	0.	3
OH + O3 —> HO2	(20)	7.0E+5	-1	940.	1
HO2 + O3 —> OH	(21)	4.8E+3	-1	580.	1
HCHO + HV —> 2 HO2 + CO	(22)	0.	1	0.	4
HCHO + HV —> CO + H2	(23)	0.	1	0.	4
OH + HCHO —> HO2 + CO	(24)	4.4E+6	-1	0.	1
ALD2 + HV —> MPOX + HO2 + CO	(25)	0.	1	0.	4
OH + ALD2 —> ACOX	(26)	3.0E+6	-1	-250.	1
ACOX + NO2 —> PAN	(26)	2.1E+6	-1	0.	1
PAN —> ACOX + NO2	(28)	1.2E+18	0	13543.	1
ACOX + NO —> NO2 + MPOX	(29)	3.1E+6	-1	0.	1
MPOX + NO —> HCHO + HO2 + NO2	(30)	3.1E+6	-1	0.	1
OH + PRPA —> PO2	(31)	6.6E+6	-1	680.	1
PO2 + NO —> HO2 + NO2 + ACET	(32)	3.1E+6	-1	0.	1
OH + ALKA —> AO2	(33)	6.6E+6	-1	400.	1
AO2 + NO —> 1.7 NO2 + 0.9 HO2 + 0.15 HCHO + 0.3 ALD2 + 0.1 RCHO + 0.30 ACET + 0.45 MEK + 0.8 NO	(34)	3.1E+6	-1	0.	1
OH + RCHO —> RCO3	(35)	9.2E+6	-1	0.	1
RCO3 + NO2 —> PPN	(36)	2.1E+6	-1	0.	1
PPN —> RCO3 + NO2	(37)	1.2E+18	0	13543.	1
RCO3 + NO —> ETO2 + NO2	(38)	3.1E+6	-1	0.	1
ETO2 + NO —> ALD2 + HO2 + NO2	(39)	3.1E+6	-1	0.	1
RCHO + HV —> ETO2 + CO + HO2	(40)	8.4E-4	1	0.	3
OH + MEK —> XO2	(41)	4.4E+6	-1	330.	1

TABLE 2 (Continued)

REACTION[b]	NUMBER	RATE CONSTANT[c] A	B	C	KEY
XO2 + NO —> NO2 + ALD2 + ACOX	(42)	3.1E+6	-1	0.	1
MEK + HV —> ACOX + ETO2	(43)	1.7E-3	1	0.	3
ACET + HV —> ACOX + MPOX	(44)	1.7E-4	1	0.	3
OH + ETHE —> NO2 + HO2 + 2.0 HCHO - 1.0 NO	(45)	9.7E+5	-1	-380.	1
OH + PRPE —> NO2 + HO2 + 1.0 HCHO + 1.0 ALD2 - 1.0 NO	(46)	1.8E+6	-1	-540.	1
OH + BUTE —> 0.9 NO2 + 0.9 HO2 + 1.8 ALD2 - 1.0 NO	(47)	5.0E+6	-1	-540.	1
O3 + ETHE —> HCHO + 0.4 CHO2 + 0.4 CO + 0.12 HO2	(48)	4.2E+3	-1	2560.	1
O3 + PRPE —> 0.5 HCHO + 0.5 ALD2 + 0.2 CHO2 + 0.2 CD + 0.3 CO + 0.2 HO2 + 0.1 OH + 0.2 MPOX	(49)	3.1E+3	-1	1900.	1
O3 + BUTE —> ALD2 + 0.40 CD + 0.3 HO2 + 0.2 OH + 0.45 MPOX + 0.2 CO	(50)	3.3E+3	-1	1050.	1
CHO2 + NO —> HCHO + NO2	(51)	3.1E+6	-1	0.	1
CHO2 + NO2 —> HCHO + NO3	(52)	3.1E+5	-1	0.	1
CHO2 + H2O —> PROD	(53)	1.5E+0	-1	0.	1
CD + NO —> ALD2 + NO2	(54)	3.1E+6	-1	0.	1
CD + NO2 —> ALD2 + NO3	(55)	3.1E+5	-1	0.	1
CD + H2O —> PROD	(56)	1.5E+0	-1	0.	1
OH + BENZ —> 0.25 CRES + 0.25 HO2 + 0.75 ADD	(57)	5.3E+5	-1	0.	1
OH + TOLU —> 0.15 ARO2 + 0.20 CRES + 0.65 ADD + 0.20 HO2	(58)	2.7E+6	-1	0.	1
OH + XYEN —> 0.25 CRES + 0.25 HO2 + 0.75 ADD	(59)	7.9E+6	-1	0.	1
ADD + NO —> 0.75 NO2 + 0.75 HO2 + 0.75 DIAL + B01*GLY + B02*MGLY	(60)	3.1E+6	-1	0.	1
OH + DIAL —> EL	(61)	1.3E+7	-1	0.	1
EL + NO2 —> ENO2	(62)	2.1E+6	-1	0.	1
ENO2 —> EL + NO2	(63)	1.2E+18	0	13543.	1
EL + NO —> 3 NO2 - 2 NO + B03*HO2+B03*GLY + B04*ACOX + B04*MGLY + B03*CO	(64)	3.1E+6	-1	0.	1
OH + GLY —> HO2 + CO	(65)	8.8E+6	-1	0.	1
GLY + HV —> HCHO + CO	(66)	1.E-10	1	0.	3
OH + MGLY —> ACOX + CO	(67)	6.6E+6	-1	0.	1
MGLY + HV —> ACOX + HO2 + CO	(68)	0.15	1	0.	3
OH + CRES —> ADD2	(69)	1.9E+7	-1	0.	1
ADD2 + NO —> 0.75 NO2 + 0.75 HO2 + 0.75 DIAL	(70)	3.1E+6	-1	0.	1
NO3 + CRES —> HNO3 + PHEN	(71)	6.6E+6	-1	0.	1
PHEN + NO2 —> PRODN	(72)	6.6E+6	-1	0.	1
ARO2 + NO —> 0.75 NO2 + 0.75 HO2 + 0.75 ACHO	(73)	3.1E+6	-1	0.	1
ACHO + HV —> PROD	(74)	4.5E-3	1	0.	3
ACHO + OH —> ARC3	(75)	5.7E+6	-1	0.	1
ARC3 + NO2 —> PBZN	(76)	2.1E+6	-1	0.	1

TABLE 2 (Continued)

REACTION[b]	NUMBER	RATE CONSTANT[c] A	B	C	KEY
PBZN —> ARC3 + HO2	(77)	1.0E+17	0	13025.	1
ARC3 + HO —> PHO2 + HO2	(78)	3.1E+6	-1	0.	1
PHO2 + HO —> PHEN + HO2	(79)	3.1E+6	-1	0.	1
:					
: Wall source terms for OH production and O3 loss					
:					
CONE —> OH	(80)	4.0E-4	0	0.	1
O3 —> WALL	(81)	1.7E-3	0	0.	1

Footnotes for Table 2

(a) Mechanism documentation: Atkinson et al.(1979, 1982), Carter et al.(1979) A computer tape containing the reaction mechanism was obtained from F. Lurmann, Environmental Research and Technology, Inc., Westlake Villiage, California, on 8 July 1982.

(b) In two reactions (60,64) the product stoichiometry varies as a function concentration. The functional forms for the coefficients BO1, BO2, BO3 and BO4 are given by:

$$BO1 = 0.75*(K(57)*BENZ + 0.1*K(59)*XYEN) / (K(57)*BENZ + K(58)*TOLU + K(59)*XYEN)$$

$$BO3 = (K(57)*BENZ + K(58)*TOLU + 0.5*K(59)*XYEN)/ (K(57)*BENZ + K(58)*TOLU + K(59)*XYEN)$$

$$BO2 = 0.75 - BO1$$

$$BO4 = 1.0 - BO3$$

In these expressions, BENZ, TOLU and XYEN are the species concentrations and K(57), K(58) and K(59) are rate constants.

(c) Reaction rate constants are of the form $k = A * TEMP^B * \exp(-C/TEMP)$ with units in terms of the ppm-min system. The scaling coefficients for the photolysis reactions 3, 22, 23 and 25 are given in the accompaning table.

SCALING FACTORS D(Z) FOR PHOTOLYSIS RATES RELATIVE TO NO_2

Zenith Angle - Z°	03 O3+H2O+hv —>	22 HCHO+hv —>	23 HCHO+hv —>	25 ALD2+hv —>
0	4.20E-8	0.0035	0.0034	8.4E-4
10	4.10E-8	0.0035	0.0034	8.3E-4
20	3.80E-8	0.0034	0.0034	8.0E-4
30	3.30E-8	0.0033	0.0033	7.4E-4
40	2.60E-8	0.0033	0.0032	6.7E-4
50	1.90E-8	0.0028	0.0030	5.6E-4
60	1.20E-8	0.0024	0.0028	4.4E-4
70	6.20E-9	0.0019	0.0025	3.1E-4
78	3.00E-9	0.0016	0.0022	2.1E-4
84	1.30E-9	0.0014	0.0022	1.3E-4

TABLE 3

Species Used in the Atkinson et al. (1982) Reaction Mechanism

NUMBER	CODE	I.C.[a]	SPECIES NAME
1	ACET		Acetone
2	ACHO		Benzaldehyde
3	ACOX		CH_3CO_3
4	ADD		OH-Aromatic-O_2 adducts
5	ADD2		OH-Aromatic-O_2 adducts
6	ALD2		Acetaldehyde
7	ALKA	1.488	>C3 alkanes
8	AO2		Alkyl peroxy radical
9	ARO2		Aromatic peroxy radical
10	ARC3		Peroxy benzoyl
11	BENZ		Benzene
12	BUTE	0.050	>C3 alkenes
13	CD		CH_3CHOO
14	CHO2		CH_2O_2
15	CO		Carbon monoxide
15	CONE	1.0	Wall source term for OH
17	CRES		Cresol
18	DIAL		Conjugated gamma dicarbonyls
19	EL		Radical formed from DIAL
20	ENO2		PAN analog from -dicarbonyls
21	ETHE	0.875	Ethylene
22	ETO2		$C_2H_5O_2$
23	GLY		Glyoxal
24	HCHO		Formaldehyde
25	HNO3		Nitric acid
26	HNO4		Pernitric acid
27	HONO		Nitrous acid
28	HO2		Hydroperoxyl radical
29	H2O	23480.0	Water vapor
30	H2O2		Hydrogen peroxide
31	MEK		Methylethylketone
32	MGLY		Methylglyoxal
33	MPOX		Methyl peroxy radical (CH_3O_2)
34	NO	0.377	Nitric oxide
35	NO2	0.106	Nitrogen dioxide
36	NO3		Nitrogen trioxide
37	N2O5		Nitrogen pentoxide
38	OH		Hydroxyl radical
39	O3	0.0001	Ozone
40	PAN		Peroxyacetyl nitrate
41	PBZN		Peroxy Benzoyl nitrate
42	PHEN		Phenoxy Radical
43	PHO2		$C_6H_5O_2$ Radical
44	PO2		Propoxy Radical

TABLE 3 (Continued)

NUMBER	CODE	I.C.[a]	SPECIES NAME
45	PPN		Higher PANS
46	PRPA		Propane
47	PRPE	0.100	Propylene
48	RCHO		C3-C5 aldehydes
49	RCO3		Acylperoxy
50	TOLU	0.086	Toluene
51	XO2		Peroxy radical
52	XYEN	0.091	>C7 aromatics

Footnotes for Table 3

(a) The initial conditions correspond to smog chamber experiment number EC-237 carried out at the University of California Riverside. The additional information needed to specify the experiment is given by

Dilution Rate = 0.0003 min^{-1}
Chamber Temperature = 302.0 ^{o}K

TABLE 4

Definition of the Demerjian (1982) Reaction Mechanism[a]

REACTION	NUMBER	RATE CONSTANT[b] A	B	C	KEY
NO2 + HV —> NO + O	(01)	0.35E+0	0	0.	2
O2 + O + M —> O3 + M	(02)	3.90E-6	0	-510.	1
O3 + NO —> NO2 + O2	(03)	3.40E+3	0	1450.	1
O3 + NO2 —> NO3 + O2	(04)	1.77E+2	0	2450.	1
O3 + HV —> O1D + O2	(05)	6.57E-4	0	0.	2
O1D + M —> O + M	(06)	6.68E+4	0	0.	1
O1D + H2O —> 2 OH	(07)	4.14E+5	0	0.	1
NO3 + NO —> 2 NO2	(08)	2.96E+4	0	0.	1
NO3 + NO2 —> N2O5	(09)	1.36E+16	-4.6	0.	1
N2O5 —> NO3 + NO2	(10)	1.30E+16	0	9700.	1
N2O5 + H2O —> 2 HNO3	(11)	1.92E-5	0	0.	1
HONO + HV —> HO + NO	(12)	6.10E-2	0	0.	2
HO + CO —> HO2 + CO2	(13)	4.10E+2	0	0.	1
HO2 + NO2 —> HONO + O2	(14)	4.40E+0	0	0.	1
HO2 + NO —> HO + NO2	(15)	6.36E+3	0	-200.	1
HO2 + NO2 + M —> HO4N + M	(16)	2.63E-3	0	0.	1
HO4N —> HO2 + NO2	(17)	5.21E+15	0	10420.	1
HO + HONO —> NO2 + H2O	(18)	9.75E+3	0	0.	1
HO + NO2 + M —> HNO3 + M	(19)	1.54E-2	0	0.	1
HO + NO + M —> HONO + M	(20)	7.39E-3	0	0.	1
HO + HNO3 —> H2O + NO3	(21)	1.26E+2	0	0.	1
HO2 + O3 —> HO + 2 O2	(22)	2.07E+1	0	600.	1
HO + O3 —> HO2 + O2	(23)	2.81E+3	0	1000.	1
HO2 + HO2 —> H2O2 + O2	(24)	3.40E+3	0	0.	1
H2O2 + HV —> 2 HO	(25)	2.64E-4	0	0.	2
HC1 + O —> RO2 + HC3 + HO2	(26)	5.10E+3	0	0.	1
HC1 + O3 —> RO2 + HC3 + HO2	(27)	1.40E-2	0	0.	1
HC1 + HO —> RO2 + HC3	(28)	3.10E+4	0	0.	1
HC2 + HO —> RO2	(29)	5.00E+3	0	0.	1
HC3 + HV —> 0.5 RO2 + 1.5 HO2 + CO	(30)	1.02E-3	0	0.	2
HC3 + HO —> 0.3 R1O2 + 0.7 HO2 + 0.7 CO	(31)	1.35E+4	0	0.	1
RO2 + NO —> RO + NO2	(32)	1.10E+4	0	0.	1
RO + O2 —> HC3 + HO2	(33)	7.39E+2	0	2000.	1
R1O2 + NO2 —> PAN	(34)	2.07E+3	0	0.	1
PAN —> R1O2 + NO2	(35)	4.77E+16	0	12516.	1
RO + NO2 —> RNO3	(36)	1.00E+2	0	0.	1
RO2 + O3 —> RO + 2 O2	(37)	2.00E+0	0	0.	1
R1O2 + NO —> RO2 + NO2	(38)	4.00E+3	0	0.	1
HC4 + HO —> R2O2 + 2 HC3 + CO	(39)	2.30E+4	0	0.	1
R2O2 + NO —> R2O + NO2	(40)	1.10E+4	0	0.	1
R2O + O2 —> HC3 + NO2 + 2 CO	(41)	8.87E-1	0	0.	1
R2O2 + O3 —> R2O + 2 O2	(42)	2.00E+0	0	0.	1
R1O2 + O3 —> RO2 + 2 O2	(43)	2.00E+0	0	0.	1
HC3 + HV —> CO	(44)	1.11E-3	0	0.	2
HC1 + O3 —> COOH + HC3	(45)	1.50E-3	0	0.	1

Footnotes for Table 4

(a) Mechanism Documentation: Demerjian (1982) and Schere (1983)
A computer tape containing the reaction mechanism was obtained from K. Schere, U.S. Environmental Protection Agency, Research Triangle Park, North Carolina, on 16 June 1982.

(b) Reaction rate constants are of the form $k = A * TEMP^B * \exp(-C/TEMP)$ with units in terms of the ppm-min system

TABLE 5

Species Used in the Demerjian (1982) Reaction Mechanism

NUMBER	CODE	I.C.[a]	SPECIES NAME
1	CO	2.0	Carbon monoxide
2	COOH		Criegee intermediate
3	CO2	320.0	Carbon dioxide
4	HC1	0.038	Olefins including C2H4
5	HC2	0.0459	Alkanes (excluding methane)
6	HC3	0.0230	Aldehydes
7	HC4	0.0237	Aromatics
8	HNO3		Nitric acid
9	HO		Hydroxyl radical
10	HO4N		Pernitric acid
11	HONO	0.006	Nitrous acid
12	HO2		Hydroperoxyl radical
13	H2O	20000.0	Water vapor
14	H2O2	0.000001	Hydrogen peroxide
15	M	1.0E+06	Third body for deactivation
16	NO	0.225	Nitric oxide
17	NO2	0.040	Nitrogen dioxide
18	NO3		Nitrogen trioxide (nitrate radical)
19	N2O5		Nitrogen pentoxide
20	O		Atomic oxygen
21	O1D		Singlet D oxygen
22	O2	2.1E+05	Molecular oxygen
23	O3		Ozone
24	PAN		Peroxacetylnitrate
25	RNO3		Alkyl nitrate
26	RO		Alkoxyl radical
27	RO2		Alkylperoxy radical
28	R1O2		Peroxyacyl radical
29	R2O		Alkoxy radical
30	R2O2		Peroxy radical

Footnotes for Table 5

(a) The initial conditions correspond to smog chamber experiment number 4LUMP-HC carried out by the Bureau of Mines. The additional data needed to characterize the experimental conditions are:

Dilution Rate = 0.000383 min^{-1}
Chamber Temperature = 306.5 ^{o}K

TABLE 6

Definition of the Dodge (1977) Reaction Mechanism[a]

REACTION	NUMBER	RATE CONSTANT[b] A	B	C	KEY
NO2 + HV —> NO + O	(1)	0.35	0	0.	2
O + O2 + M —> O3 + M	(2)	2.0E-5	0	0.	1
NO + O3 —> NO2	(3)	25.0	0	0.	1
O3 + NO2 —> NO3	(4)	0.045	0	0.	1
O + NO2 —> NO	(5)	1.3E+4	0	0.	1
NO + NO3 —> 2 NO2	(6)	1.3E+4	0	0.	1
NO3 + NO2 —> N2O5	(7)	5.6E+3	0	0.	1
N2O5 —> NO2 + NO3	(8)	22.0	0	0.	1
H2O + N2O5 —> 2 WHNO3	(9)	2.5E-6	0	0.	1
NO2 + NO + H2O —> 2 HONO	(10)	1.0E-9	0	0.	1
HONO + HONO —> NO + NO2	(11)	1.0E-3	0	0.	1
HONO + HV —> OH + NO	(12)	6.3E-3	0	0.	2
NO2 + OH —> HNO3	(13)	8.0E+3	0	0.	1
NO + OH —> HONO	(14)	3.0E+3	0	0.	1
NO + HO2 —> NO2 + OH	(15)	1.2E+3	0	0.	1
HO2 + HO2 —> HOOH + O2	(16)	8.4E+3	0	0.	1
HOOH + HV —> 2 OH	(17)	8.4E-4	0	0.	2
O3 + HV —> O1D	(18)	9.5E-4	0	0.	2
O3 + HV —> O	(19)	1.9E-2	0	0.	2
O1D + M —> O + M	(20)	8.7E+4	0	0.	1
O1D + H2O —> 2 OH	(21)	5.1E+5	0	0.	1
O3 + OH —> HO2 + O2	(22)	84.0	0	0.	1
HO2 + O3 —> OH	(23)	2.4	0	0.	1
OH + PROP —> ADD	(24)	2.5E+4	0	0.	1
NO + ADD —> X + NO2	(25)	1.0E+3	0	0.	1
ADD + ADD —> 2 X	(26)	1.2E+4	0	0.	1
MEO2 + ADD —> X + MEO	(27)	1.0E+3	0	0.	1
C2O2 + ADD —> X + C2O	(28)	1.0E+3	0	0.	1
C3O2 + ADD —> X + C3O	(29)	1.0E+3	0	0.	1
X —> HCHO + ALD2 + HO2	(30)	1.0E+5	0	0.	1
O3 + PROP —> OH + HO2 + ALD2	(31)	8.0E-3	0	0.	1
O3 + PROP —> OH + C2O3 + HCHO	(32)	8.0E-3	0	0.	1
OH + BUT —> SCO2	(33)	1.8E+3	0	0.	1
OH + BUT —> C4O2	(34)	1.8E+3	0	0.	1
C4O2 + NO —> NO2 + C4O	(35)	1.8E+3	0	0.	1
SCO2 + NO —> NO2 + SCO	(36)	1.8E+3	0	0.	1
C3O2 + NO —> NO2 + C3O	(37)	1.8E+3	0	0.	1
C2O2 + NO —> NO2 + C2O	(38)	1.8E+3	0	0.	1
MEO2 + NO —> NO2 + MEO	(39)	1.8E+3	0	0.	1
C4O —> HCHO + C3O2	(40)	7.5E+4	0	0.	1
SCO —> ALD2 + C2O2	(41)	1.0E+5	0	0.	1
C3O —> HCHO + C2O2	(42)	8.0E+3	0	0.	1

TABLE 6 (Continued)

REACTION	NUMBER	RATE CONSTANT[b] A	B	C	KEY
C2O —> HCHO + MEO2	(43)	4.0E+3	0	0.	1
C4O + O2 —> ALD4 + HO2	(44)	0.7	0	0.	1
SCO + O2 —> MEK + HO2	(45)	1.4	0	0.	1
C3O + O2 —> ALD3 + HO2	(46)	0.5	0	0.	1
C2O + O2 —> ALD2 + HO2	(47)	0.4	0	0.	1
MEO + O2 —> HCHO + HO2	(48)	0.4	0	0.	1
HCHO + HV —> PROD	(49)	3.0E-3	0	0.	2
HCHO + HV —> 2 HO2	(50)	1.0E-3	0	0.	2
OH + HCHO —> HO2 + CO	(51)	1.5E+4	0	0.	1
ALD2 + HV —> PROD	(52)	4.2E-6	0	0.	2
ALD2 + HV —> MEO2 + HO2	(53)	9.8E-4	0	0.	2
OH + ALD2 —> C2O3	(54)	1.5E+4	0	0.	1
ALD3 + HV —> PROD	(55)	6.0E-5	0	0.	1
ALD3 + HV —> C2O2 + HO2	(56)	2.5E-3	0	0.	1
OH + ALD3 —> C3O3	(57)	4.5E+4	0	0.	1
ALD4 + HV —> PROD	(58)	6.0E-5	0	0.	1
ALD4 + HV —> C3O2 + HO2	(59)	1.9E-3	0	0.	1
OH + ALD4 —> C4O3	(60)	4.5E+4	0	0.	1
C4O2 + ADD —> X + C4O	(61)	1.0E+3	0	0.	1
SCO2 + ADD —> X + SCO	(62)	1.0E+3	0	0.	1
NO + C4O3 —> C3O2 + NO2	(63)	8.0E+2	0	0.	1
NO + C3O3 —> C2O3 + NO2	(64)	8.0E+2	0	0.	1
NO + C2O3 —> MEO2 + NO2	(65)	8.0E+2	0	0.	1
NO2 + C4O3 —> PAN	(66)	1.0E+2	0	0.	1
NO2 + C3O3 —> PAN	(67)	1.0E+2	0	0.	1
NO2 + C2O3 —> PAN	(68)	1.0E+2	0	0.	1
HO2 + C4O2 —> PROD	(69)	4.0E+3	0	0.	1
HO2 + C3O2 —> PROD	(70)	4.0E+3	0	0.	1
HO2 + SCO2 —> PROD	(71)	4.0E+3	0	0.	1
HO2 + C2O2 —> PROD	(72)	4.0E+3	0	0.	1
HO2 + MEO2 —> PROD	(73)	4.0E+3	0	0.	1
HO2 + C4O3 —> PROD	(74)	4.0E+3	0	0.	1
HO2 + C3O3 —> PROD	(75)	4.0E+3	0	0.	1
HO2 + C2O3 —> PROD	(76)	4.0E+3	0	0.	1

Footnotes for Table 6

(a) Mechanism Documentation: Dodge (1977) and Durbin et al. (1975) The actual coding for the reactions and the rate constants were derived from the computer program: OZIPP - Isopleth Plotting Program obtained from H.L. Jeffries on 20 November 1982.

(b) Reaction rate constants are of the form $k = A * TEMP^B * \exp(-C/TEMP)$ with units in terms of the ppm-min system

TABLE 7

Species Used in the Dodge (1977) Reaction Mechanism

NUMBER	CODE	I.C.[a]	SPECIES NAME
1	ADD		$CH_3CH(OH)CH_2OO$
2	ALD2	0.012	CH_3CHO
3	ALD3		CH_3CH_2CHO
4	ALD4		$CH_3CH_2CH_2CHO$
5	BUT	0.1238	n-Butane ($n\text{-}C_4H_{10}$)
6	C2O		CH_3CH_2O
7	C2O2		$CH_3CH_2O_2$
8	C2O3		$CH_3C(O)O_2$
9	C3O		$CH_3CH_2CH_2O$
10	C3O2		$CH_3CH_2CH_2O_2$
11	C3O3		$CH_3CH_2C(O)O_2$
12	C4O		$CH_3CH_2CH_2CH_2O$
13	C4O2		$CH_3CH_2CH_2CH_2O_2$
14	C4O3		$CH_3CH_2CH_2C(O)O_2$
15	HCHO	0.018	Formaldehyde
16	HNO3		Nitric acid
17	HONO	0.006	Nitrous acid
18	HO2		Hydroperoxyl radical
19	H2O	20000	Water vapor
20	HOOH		Hydrogen peroxide
21	M	1.0E+06	Third body
22	MEK		Methyl ethyl ketone
23	MEO		Methoxy radical
24	MEO2		Methyl peroxy radical
25	NO	0.225	Nitric oxide
26	NO2	0.040	Nitrogen dioxide
27	NO3		Nitrogen trioxide (nitrate radical)
28	N2O5		Nitrogen pentoxide
29	O		Atomic oxygen $O(^3P)$
30	OH		Hydroxyl radical
31	O1D		Singlet D oxygen
32	O2	2.1E+05	Molecular oxygen
33	O3		Ozone
34	PAN		Peroxyacetyl nitrate
35	PROP	0.055	Propylene
36	SCO		$CH_3CH(O)CH_2CH_3$
37	SCO2		$CH_3CH(O_2)CH_2CH_3$
38	PROD		Stable products
39	X		$CH_3CH(OH)CH_2O$

Footnotes for Table 7

(a) Same conditions as Table 5.

TABLE 8

Definition of the Killus and Whitten (1982a) Reaction Mechanism[a]

REACTION	NUMBER	RATE CONSTANT[b] A	B	C	KEY
NO2 + HV —> NO + O	(1)	0.30	0	0.	2
O —> O3	(2)	4.40E+6	0	0.	1
NO + O3 —> NO2 + O2	(3)	3.45E+3	0	1450.	1
NO2 + O3 —> NO3 + O2	(4)	1.79E+2	0	2450.	1
NO2 + O —> NO + O2	(5)	1.34E+4	0	0.	1
O3 + OH —> HO2 + O2	(6)	2.87E+1	0	1000.	1
O3 + HO2 —> OH + 2 O2	(7)	4.01E+2	0	1525.	1
OH + NO2 —> HNO3	(8)	1.60E+4	0	0.	1
OH + CO —> HO2	(9)	4.40E+2	0	0.	1
NO + NO —> 2 NO2	(10)	1.50E-4	0	0.	1
NO + NO3 —> 2 NO2	(11)	2.80E+4	0	0.	1
NO3 + NO2 + H2O —> 2 HNO3	(12)	5.56E-19	0	-10600.	1
NO + HO2 —> NO2 + OH	(13)	1.20E+4	0	0.	1
HO2 + HO2 —> H2O2 + O2	(14)	1.50E+4	0	0.	1
X + PAR —>	(15)	1.00E+5	0	0.	1
OH + PAR —> MEO2 + H2O	(16)	8.51E+3	0	560.	1
O + OLE —> MEO2 + ACO3 + X	(17)	8.04E+3	0	325.	1
O + OLE —> CARB + PAR	(18)	8.04E+3	0	325.	1
OH + OLE —> RAO2	(19)	6.04E+3	0	-540.	1
O3 + OLE —> CARB + CRIG	(20)	4.70	0	1900.	1
O3 + OLE —> CARB + MCRG + X	(21)	4.70	0	1900.	1
O + ETH —> MEO2 + HO2 + CO	(22)	8.79E+3	0	800.	1
O + ETH —> CARB + PAR	(23)	8.79E+3	0	800.	1
OH + ETH —> RBO2	(24)	3.33E+3	0	-382.	1
O3 + ETH —> CARB + CRIG	(25)	1.29E+1	0	2560.	1
NO + ACO3 —> NO2 + MEO2 + CO2	(26)	1.04E+4	0	0.	1
NO + RBO2 —> NO2 + 2 CARB + HO2	(27)	1.20E+4	0	0.	1
NO + RAO2 —> NO2 + 2 CARB + HO2	(28)	1.20E+4	0	0.	1
NO + MEO2 —> NO2 + CARB + MEO2 + X	(29)	3.80E+3	0	0.	1
NO + MEO2 —> NO2 + CARB + HO2	(30)	7.70E+3	0	0.	1
NO + MEO2 —> NRAT	(31)	5.00E+2	0	0.	1
O3 + RBO2 —> 2 CARB + HO2 + O2	(32)	5.00	0	0.	1
O3 + RAO2 —> 2 CARB + HO2 + O2	(33)	2.00E+2	0	0.	1
OH + CARB —> CRO2 + X	(34)	5.00E+2	0	0.	1
OH + CARB —> HO2 + CO	(35)	7.00E+3	0	0.	1
OH + CARB —> ACO3 + X	(36)	6.00E+3	0	0.	1
CARB + HV —> CO + H2	(37)	1.90E-4	0	0.	2
CARB + HV —> 1.333 HO2 + CO + 0.667 MEO2 + 0.667 X	(38)	3.80E-4	0	0.	2
ACO3 + NO2 —> PAN	(39)	7.00E+3	0	0.	1
PAN —> ACO3 + HO2	(40)	1.04E+18	0	13500.	1
ACO3 + HO2 —> PRD1	(41)	1.50E+4	0	0.	1
MEO2 + HO2 —> PRD2	(42)	9,00E+3	0	0.	1
NO + CRIG —> HO2 + CARB	(43)	1.20E+4	0	0.	1

TABLE 8 (Continued)

REACTION									NUMBER	RATE CONSTANT A	B	C	KEY
NO2	+ CRIG	—>	NO3	+ CARB					(44)	8.00E+3	0	0.	1
CARB	+ CRIG	—>	OZD						(45)	2.00E+3	0	0.	1
NO	+ MCRG	—>	NO2	+ CARB					(46)	1.20E+4	0	0.	1
NO2	+ MCRG	—>	NO3	+ CARB	+ PAR				(47)	8.00E+3	0	0.	1
CARB	+ MCRG	—>	OZD						(48)	2.00E+3	0	0.	1
	CRIG	—>	CO	+ H2O					(49)	6.70E+2	0	0.	1
	CRIG	—>	PRD3						(50)	2.40E+2	0	0.	1
	CRIG	—>	2 HO2	+ CO2					(51)	9.00E+1	0	0.	1
	MCRG	—>	PRD4						(52)	1.50E+2	0	0.	1
	MCRG	—>	MEO2	+ OH	+ CO				(53)	3.40E+2	0	0.	1
	MCRG	—>	MEO2	+ HO2	+ CO2				(54)	4.25E+2	0	0.	1
	MCRG	—>	2 HO2	+ CARB	+ CO				(55)	8.50E+1	0	0.	1
ARO	+ OH	—>	RARO	+ H2O					(56)	5.99E+4	0	600.	1
ARO	+ OH	—>	OPEN	+ HO2					(57)	5.55E+4	0	400.	1
RARO	+ NO	—>	NO2	+ PHEN	+ HO2				(58)	4.00E+3	0	0.	1
OPEN	+ NO	—>	NO2	+ DCRB	+ X	+ APRC			(59)	6.00E+3	0	0.	1
APRC		—>	DCRB	+ CARB	+ CO	+ X			(60)	1.00E+4	0	0.	1
APRC		—>	2 CARB	+ 2 CO					(61)	1.00E+4	0	0.	1
PHEN	+ NO3	—>	PHO	+ HNO3					(62)	5.00E+3	0	0.	1
PHO	+ NO2	—>	NPHN						(63)	4.00E+3	0	0.	1
PHO	+ HO2	—>	PHEN						(64)	5.00E+4	0	0.	1
OPEN	+ O3	—>	DCRB	+ APRC	+ X				(65)	4.00E+1	0	0.	1
PHEN	+ OH	—>	HO2	+ APRC	+ PAR	+ CARB			(66)	3.00E+4	0	0.	1
DCRB	+ HV	—>	HO2	+ 0.5 AC03	+								
			1.5 CO	+ 0.5 MEO2					(67)	1.35E-2	0	0.	2
PHEN	+ OH	—>	PHO						(68)	1.00E+4	0	0.	1
CRO2	+ NO	—>	NO2	+ CARB	+ AC03	+ X			(69)	1.20E+4	0	0.	1
DCRB	+ OH	—>	AC03	+ CO					(70)	7.00E+3	0	0.	1
HONO	+ HV	—>	OH	+ NO					(71)	1.80E-1	0	0.	2
NO	+ OH	—>	HONO						(72)	9.77E+3	0	0.	1
03	+ HV	—>	O1D						(73)	1.00E-4	0	0.	2
O1D		—>	O						(74)	4.44E+10	0	0.	1
O1D	+ H2O	—>	2 OH						(75)	3.40E+5	0	0.	1

TABLE 8 (Continued)

REACTION	NUMBER	RATE CONSTANT[b] A	B	C	KEY
:					
: Wall loss term for ozone, NO2, NO3, N2O5					
:					
O3 —> WALL	(76)	1.60E-3	0	0.	1
NO2 + NO3 + H2O —> 2 WNO3	(77)	1.70E-3	0	0.	1
:					
: Wall source term for NOx					
:					
—> NO	(78)	1.00E-4	0	0.	1
:					
: Water production					
:					
H2O —>	(79)	-6.93E-4	0	0.	1

Footnotes for Table 8

(a) Mechanism documentation: Killus and Whitten (1982a) and Whitten et al. (1980a,b). The reaction mechanism was coded from Table 3 of Killus and Whitten (1982a) with the photolysis rates and wall terms obtained from a computer listing supplied by J.P. Killus on 25 August 1982. Reactions 26, 48, 54, 60, 69 and 70 have been corrected to maintain the overall carbon balance.

(b) Reaction rate constants are of the form $k = A * TEMP^B * \exp(-C/TEMP)$ with units in terms of the ppm-min system.

TABLE 9

Species Used in the Killus and Whitten (1982a) Reaction Mechanism

NUMBER	CODE[a]	I.C.[b]	SPECIES NAME
1	ACO3 (2)		Peroxyacyl radical (Two-carbon surrogate for RCO3)
2	APRC (4)		Conjugated gamma-dicarbonyls
3	ARO (6)	0.229	Reactive aromatic rings
4	CO (1)	1.63	Carbon monoxide
5	CO2 (1)		Carbon dioxide
6	CRIG (1)		Criegee intermediate
7	CRO2 (2)		Peroxy radical
8	DCRB (3)		Highly photolytic alpha-dicarbonyl compounds including methyl glyoxal and biacetyl
9	ETH (2)	1.051	Slow double bonds that are almost exclusively ethylene
10	CARB (1)	0.130	Carbonyl compounds such as aldehydes and ketones
11	HNO3		Nitric acid
12	HONO	0.006	Nitrous acid
13	HO2		Hydroperoxy radical
14	H2		Hydrogen
15	H2O	17000.0	Water vapor
16	H2O2		Hydrogen peroxide
17	MCRG (2)		Criegee intermediate
18	MEO2 (1)		Peroxy radical (one-carbon surrogate for RO2)
19	NO	0.44	Nitric oxide
20	NO2	0.052	Nitrogen dioxide
21	NO3		Nitrogen trioxide (nitrate radical)
22	NPHN (6)		Nitrophenol
23	NRAT (1)		Nitrate
24	OLE (2)	0.108	Relatively reactive double-bonded carbon molecules
25	O		Atomic oxygen O(3P)
26	OH		Hydroxyl radical
27	OPEN (6)		Bicyclic peroxy radical
28	O1D		Atomic oxygen O(1D)
29	O2	209000.0	Molecular oxygen
30	O3		Ozone
31	OZD (2)		Ozonide
32	OZON (1)		Ozonide
33	PAN (2)		Peroxyacetyl nitrate
34	PAR (1)	9.365	Single-bonded carbon atoms whose principal constituents are paraffinic carbon molecules
35	PHEN (6)		Phenol

TABLE 9 (Continued)

NUMBER	CODE[a]	I.C.[b]	SPECIES NAME
35	PHO (6)		C_6H_5O Radical
36	RAO2 (2)		Peroxy radical
37	RARO (6)		Peroxy radical
38	RBO2 (2)		Peroxy radical
39	WNO3		Wall loss of NO_x species
40	X	(-1)	Species introduced to maintain Carbon balance

Footnotes for Table 9

(a) The values in brackets are the species carbon numbers.

(b) The initial conditions correspond to smog chamber experiment number EC231 carried out at the University of California Riverside. The additional data needed to characterize the experimental conditions are:

Dilution Rate = 0.000693 min^{-1}
Chamber Temperature = 303.0 ^oK

TABLE 10

Definition of the McRae and Seinfeld (1983) Reaction Mechanism[a]

REACTION[b]	NUMBER	RATE CONSTANT[c] A	B	C	KEY
NO2 + HV —> NO + O3P	(1)	0.30	0	0.	2
O3P + O2 + M —> O3 + M	(2)	0.346	-2	-510.	1
O3 + NO —> NO2 + O2	(3)	9.24E+05	-1	1450.	1
NO2 + O3P —> NO + O2	(4)	3.99E+06	-1	0.	1
NO + O3P —> NO2	(5)	1.67E+05	-1	-584.	1
NO2 + O3P —> NO3	(6)	1.07E+06	-1	0.	1
O3 + NO2 —> NO3 + O2	(7)	5.19E+04	-1	2450.	1
NO3 + NO —> 2NO2	(8)	8.05E+06	-1	0.	1
NO + OH —> HONO	(9)	5.07E+06	-1	0.	1
HONO + HV —> OH + NO	(10)	0.0548	0	0.	2
HO2 + NO2 —> HONO + O2	(11)	1.73E+01	-1	-1006.	1
HONO + OH —> NO2 + H2O	(12)	2.91E+06	-1	0.	1
NO2 + HO2 —> HO2NO2	(13)	1.73E+04	-1	-1006.	1
HO2NO2 —> HO2 + NO2	(14)	1.80E+15	0	9950.	1
HO2 + NO —> NO2 + OH	(15)	3.58E+06	-1	0.	1
RO2 + NO —> NO2 + RO	(16)	3.58E+06	-1	0.	1
RCO3 + NO —> NO2 + RO2 + CO2	(17)	1.13E+06	-1	0.	1
NO2 + OH —> HONO2	(18)	4.53E+06	-1	0.	1
CO + OH —> HO2 + CO2	(19)	1.31E+05	-1	0.	1
O3 + HV —> O3P + O2	(20)	0.0214	0	0.	2
HCHO + HV —> 2 HO2 + CO	(21)	0.00113	0	0.	2
HCHO + HV —> H2 + CO	(22)	0.00242	0	0.	2
HCHO + OH —> HO2 + H2O + CO	(23)	4.14E+06	-1	0.	1
RCHO + HV —> RO2 + HO2 + CO	(24)	0.00096	0	0.	2
RCHO + OH —> RCO3	(25)	2.57E+04	0	0.	1
C2H4 + OH —> RO2	(26)	1.16E+04	0	0.	1
C2H4 + O3P —> RO2 + HO2	(27)	1.22E+03	0	0.	1
OLE + OH —> RO2	(28)	5.85E+04	0	0.	1
OLE + O3P —> RO2 + RCO3	(29)	9.93E+03	0	0.	1
OLE + O3 —> A01*RCHO + A02*HCHO + A03*HO2 + A04*RO2 + A05*OH + A06*RO	(30)	0.056	0	0.	1
ALK + OH —> RO2	(31)	6.06+03	0	0.	1
ALK + O3P —> RO2 + OH	(32)	99.8	0	0.	1
ARO + OH —> RO2 + RCHO	(33)	2.21E+04	0	0.	1
RO —> B01*HO2 + B02*HCHO + B03*RCHO + B04*RO2	(34)	2.0E+05	0	0.	1
RONO + HV —> NO + RO	(35)	0.066	0	0.	2
RO + NO —> RONO	(36)	4.38E+06	-1	0.	1
RO + NO2 —> RONO2	(37)	2.19E+06	-1	0.	1
RO + NO2 —> RCHO + HONO	(38)	6.39E+02	0	0.	1
NO2 + RO2 —> RO2NO2	(39)	1.64E+06	-1	0.	1
NO2 + RO2 —> RCHO + HONO2	(40)	1.64E+03	-1	0.	1
RO2NO2 —> NO2 + RO2	(41)	1.80E+15	0	9950.	1

TABLE 10 (Continued)

REACTION[b]	NUMBER	RATE CONSTANT[c] A	B	C	KEY
RCO3 + NO2 —> PAN	(42)	6.17E+05	-1	0.	1
PAN —> RCO3 + NO2	(43)	4.77E+16	0	12516.	1
NO2 + NO3 —> N2O5	(44)	2.20E+06	-1	0.	1
N2O5 —> NO2 + NO3	(45)	3.44E+016	0	10600.	1
H2O + N2O5 —> 2 HONO2	(46)	4.47E-03	-1	0.	1
O3 + OH —> HO2 + O2	(47)	6.62E+05	-1	1000.	1
O3 + HO2 —> OH + 2 O2	(48)	4.85E+03	-1	580.	1
O3 —> WALL	(49)	0.0023	0	0.	1
HO2 + HO2 —> H2O2 + O2	(50)	8.28E+03	0	0.	1
H2O2 + HV —> 2 OH	(51)	7.69E-04	0	0.	2
RO2 + RO2 —> 2 RO	(52)	2.04E+04	-1	-223.	1

Footnotes for Table 10

(a) Mechanism documentation: Falls and Seinfeld (1978) Falls et al. (1979), McRae et al. (1982) and McRae and Seinfeld (1983) (15 November 1982).

(b) In two reactions (30,34) the product stoichiometry varies as a function concentration. The functional forms for the coefficients A01 - A06 and B01-B04 are given by:

A01 = 0.5 A02 = 0.5 A03 = 0.304
A04 = 0.306 A05 = 0.136 A06 = 0.034

and

B01 = 1.0 B02 = 0.5 B03 = 0.5
B04 = (1-B01) = 0.0

(c) Reaction rate constants are of the form $k = A * TEMP^b * \exp(-C/TEMP)$ with units in terms of the ppm-min system.

(d) $k_{37}/(k_{37} + k_{38}) = 0.92$ for CH_3, $k_{38} = 0.087\ k_{37}$

(e) Rate constants for reactions 39 and 40 are based on the assumption that $k_{16}/(k_{39} + k_{40}) = 2.2$.

(f) Rate constant for reaction 18 determined from

$$1.477\times10^{15}\times10^{-(11.6T/(17.4+T))}\sqrt{280/T}$$

(g) Rate constant for reaction 50 determined from

$$k_{50} = \frac{3.4\times10^{4}}{T}\exp(1100/T) + \frac{5.8\times10^{-5}}{T^2}\exp(5800/T)[H_2O]$$

at 298 °K, $[H_2O = 20000$ ppm$]$ $k_{50} = 8.28\times10^{3}$

TABLE 11

Species Used in the McRae and Seinfeld (1983) Reaction Mechanism[a]

NUMBER	CODE	I.C.[b]	SPECIES NAME
1	ALK	1.488	Alkanes (excluding CH4)
2	ARO	0.177	Aromatics
3	CO		Carbon monoxide
4	CO2		Carbon dioxide
5	ETH	0.875	Ethylene (C2H4)
6	HCHO		Formaldehyde
7	HNO2	0.01	Nitrous acid
8	HNO3		Nitric acid
9	HNO4		Pernitric acid
10	HO2		Hydroperoxyl radical
11	H2		Hydrogen
12	H2O	15500.	Water vapor
13	H2O2		Hydrogen peroxide
14	M	1000000.	Third body for collisional deactivation
15	NO	0.377	Nitric oxide
16	NO2	0.106	Nitrogen dioxide
17	NO3		Nitrogen trioxide
18	N2O5		Dinitrogen pentoxide
19	OLE	0.150	Olefins excluding ethylene
20	O		Atomic oxygen (O(3P))
21	OH		Hydroxyl radical
22	O2	210000.	Molecular oxygen
23	O3		Ozone
24	PAN		Peroxacetylnitrate
25	RCHO	0.0012	Higher aldehydes
26	RCO3		Peroxyacyl radical
27	RO		Alkoxyl radical
28	RONO		Alkyl nitrite
29	RNO4		Peroxyalkyl nitrate
30	RO2		Alkylperoxy radical
31	RNO3		Alkyl nitrate
32	WALL		Wall loss term

Footnotes for Table 11

(a) Mechanism documentation: McRae et al.(1982), Falls et al.(1979), Falls and Seinfeld (1978) and McRae and Seinfeld (1983).

(b) The initial conditions correspond to smog chamber experiment number EC - 237 carried out at the University of California Riverside. The additional data needed to characterize the to characterize the experimental conditions are:

Dilution Rate = 0.0003 min^{-1}
Chamber Temperature = 302.0 ^{o}K

TABLE 12

Definition of the Penner and Walton (1982) Reaction Mechanism[a]

REACTION	NUMBER	RATE CONSTANT[b] A	B	C	KEY
:					
: Inorganic reactions (R1 - R23)					
:					
O + O2 + M —> O3 + M	(01)	3.90E-6	0	-510.	1
O3 + NO —> NO2 + O2	(02)	1.01E+6	-1	1450.	1
O + NO —> NO2	(03)	1.59E+7	-1.5	0.	1
O + NO2 —> NO + O2	(04)	4.09E+6	-1	0.	1
O + NO2 —> NO3	(05)	2.05E+8	-2	0.	1
O3 + NO2 —> NO3 + O2	(06)	5.28E+4	-1	2450.	1
NO3 + NO2 —> N2O5	(07)	6.05E+4	-0.7	0.	1
N2O5 —> NO2 + NO3	(08)	2.16E+18	-0.7	11180.	1
NO3 + NO —> 2 NO2	(09)	8.80E+6	-1	0.	1
N2O5 + H2O —> 2 HNO3[c]	(10)	1.32E-3	-1	0.	1
HO + NO2 —> HNO3	(11)	8.67E+7	-1.5	0.	1
HO + NO —> HNO2	(12)	4.99E+7	-1.5	0.	1
HO + CO —> HO2	(13)	1.19E+5	-1	0.	1
HO2 + NO —> HO + NO2	(14)	1.54E+6	-1	-250.	1
HNO2 + HO —> NO2	(26)	2.90E+6	-1	0.	1
HO2 + HO2 —> H2O2 + O2	(27)	3.70E+4	-1	-1250.	1
HO + HO2 —> H2O + O2	(36)	3.52E+7	-1	0.	1
HO + H2O2 —> HO2	(72)	7.04E+5	-1	0.	1
HO + HNO4 —> H2O + NO2 + O2	(93)	1.76E+6	-1	0.	1
HNO4 —> HO2 + NO2	(84)	3.00E+16	0	10720.	1
HO2 + NO2 —> HNO4	(34)	6.23E+15	-5	0.	1
HO + O3 —> HO2	(48)	7.04E+5	-1	940.	1
HO2 + O3 —> HO	(49)	4.84E+3	-1	580.	1
:					
: Reactions of HC1 (Alkenes, isoprene and mono-terpenes)					
:					
HC1 + HO —> RO2 + HC4	(17)	1.76E+7	-1	120.	1
HC1 + O3 —> HO2 + HC4	(16)	1.54E+3	-1	1900.	1
HC1 + O3 —> HC4	(47)	1.54E+3	-1	1900.	1
HC1 + O —> RO2 + RCO3	(15)	4.40E+6	-1	360.	1
HC1 + NO3 —> RO2 + RNO3	(40)	4.40E+5	-1	1400.	1
:					
: Reactions of HC2 (Alkanes)					
:					
HC2 + HO —> RO2 + H2O	(19)	2.20E+7	-1	900.	1
HC2 + O —> RO2 + HO	(18)	7.04E+6	-1	2000.	1
:					
: Reactions of HC4 (Aldehydes and Ketones)					
:					
HC4 + HO —> RCO3 + H2O	(20)	3.52E+6	-1	0.	1
HC4 + HO —> CO + HO2 + H2O	(37)	3.43E+6	-1	150.	1
HC4 + NO3 —> RCO3 + HNO3	(35)	1.32E+3	-1	200.	1

TABLE 12 (Continued)

REACTION	NUMBER	RATE CONSTANT[b] A	B	C	KEY
:					
: Reactions of HC3 (Aromatics)					
:					
HC3 + HO —> BRO2OHHH	(86)	1.76E+6	-1	0.	1
HC3 + HO —> HO2	(87)	1.06E+6	-1	0.	1
HO + BRO2OHHH —> HO2 + MGLY + NO2	(88)	8.80E+7	-1	0.	1
HO + MGLY —> H2O + RCO3 + CO	(91)	7.04E+6	-1	0.	1
:					
: Reactions of Organic Radicals					
:					
RCO3 + HO2 —> RO2H	(41)	2.64E+6	-1	0.	1
RCO3 + NO —> RO2 + NO2	(22)	1.13E+6	-1	0.	1
RCO3 + NO2 —> PAN	(23)	5.98E+5	-1	0.	1
PAN —> NO2 + RCO3	(43)	4.74E+16	0	12516.	1
RO2 + NO —> RO + NO2	(21)	3.08E+6	-1	0.	1
HO2 + RO2 —> RO2H + O2	(28)	1.19E+6	-1	0.	1
RO2 + RO2 —> 2 RO + O2	(29)	1.76E+5	-1	0.	1
RO2 + O3 —> RO + O2	(38)	4.84E+3	-1	580.	1
RO + O2 —> HO2 + HC4	(24)	2.20E+5	-1	2000.	1
RO + NO2 —> RNO3	(25)	4.40E+6	-1	0.	1
:					
: These terms are the Photolysis reaction steps (J1 - J12)					
:					
NO2 + HV —> NO + O	(51)	0.30	0	0.	2
O3 + HV —> O + O2	(58)	1.62E-2	0	0.	2
O3 + HV —> O2 + 2 HO	(59)	1.37E-4	0	0.	2
HNO2 + HV —> HO + NO	(52)	6.60E-2	0	0.	2
H2O2 + HV —> 2 HO	(53)	3.72E-4	0	0.	2
NO3 + HV —> NO2 + O	(57)	5.70	0	0.	2
NO3 + HV —> NO + O2	(83)	0.72	0	0.	2
N2O5 + HV —> 2 NO2 + O	(60)	9.96E-7	0	0.	2
HC4 + HV —> CO	(42)	4.80E-4	0	0.	2
HC4 + HV —> CO + 2 NO2	(50)	3.90E-4	0	0.	2
HC4 + HV —> RO2 + HO2 + CO	(54)	3.90E-4	0	0.	2
MGLY + HV —> RCO3 + HO2 + CO	(90)	1.38E-2	0	0.	2
:					
: Wall loss terms					
:					
O3 —> WALL	(62)	1.68E-03	0	0.	1
H2O2 —> WALL	(71)	4.20E-03	0	0.	1

Footnotes for Table 12

(a) Mechanism Documentation: Gelinas et al. (1974), Luther and Gelinas (1976), Gelinas and Skewes-Cox (1975), MacCracken and Sauter eds. (1975) and Penner and Walton (1982). A computer tape containing the reaction mechanism was obtained from J. Penner, Lawrence Livermore National Laboratory, Livermore, California, on 2 July 1982. There are a number of differences between the mechanism described in Penner and Walton (1982) and Table 12. Several reaction steps have been included to account for wall effects in smog chamber experiments.

(b) Reaction rate constants are of the form $k = A * TEMP^B * \exp(-C/TEMP)$ with units in terms of the ppm-min system. Note that the values used in this table have been converted from the cgs system reported in Penner and Walton (1982).

(c) HNO_3, RNO_2, RNO_3, RO_2H, Wall, H_2O, M, and O_2 are not calculated in the PW mechanism.

TABLE 13

Species Used in the Penner and Walton (1982) Reaction Mechanism

NUMBER	CODE	I.C.[a]	SPECIES NAME
1	BRO2OHHH		Oxygenated aromatic radical
2	CO	2.50	Carbon monoxide
3	HC1	1.29	Alkenes, isoprene and mono-terpenes
4	HC2	0.78	Alkanes
5	HC3	1.91	Aromatics
6	HC4	0.0143	Aldehydes and ketones
7	HNO2		Nitrous acid
8	HNO3		Nitric acid
9	HNO4		Peroxy nitric acid
10	HO		Hydroxyl radical
11	HO2		Hydroperoxyl radical
12	H2O	21219.	Water vapor
13	H2O2		Hydrogen peroxide
14	M	1000000.	Third body for deactivation
15	MGLY		Methylglyoxal
16	NO	0.744	Nitric Oxide
17	NO2	0.260	Nitrogen Dioxide
18	NO3		Nitrogen trioxide (nitrate radical)
19	N2O5		Dinitrogen pentoxide
20	O		Atomic oxygen
21	O2	210162.	Molecular oxygen
22	O3		Ozone
23	PAN		Peroxactyl nitrate
24	RCO3		Peroxyacyl radical
25	RNO2		Alkyl nitrite
26	RNO3		Alkyl nitrate
27	RO		Alkoxyl radical
28	RO2		Alkylperoxy radical
29	RO2H		Peroxide
30	WALL		Loss term

(a) The initial conditions correspond to smog chamber experiment number EC245 carried out at the University of California Riverside. The additional data needed to characterize the experimental conditions are:

Dilution Rate = 0.0003 min^{-1}
Chamber Temperature = 302.6 ^{o}K

$$NO_3 + h\nu \xrightarrow{k_a + k_b} \frac{k_a}{k_a + k_b} NO + \frac{k_b}{k_a + k_b} NO_2 + \frac{k_b}{k_a + k_b} O_3 \ .$$

Under typical atmospheric conditions both of the simplifying assumptions are reasonable. The final form used by Atkinson et al. (1982) is based on measurements that give $k_a/(k_a + k_b) \cong 0.3$ and $k_b/(k_a + k_b) \cong 0.7$. The procedure for combining reactions can be used in reverse to eliminate non-integer stoichiometric coefficients.

In many cases species can be eliminated from the reaction set if their characteristic reaction times are very short. In some cases this can lead to apparent violations of mass conservation. Consider the first reaction in the Atkinson et al. (1982) mechanism

$$NO_2 + h\nu \xrightarrow{1} NO + O_3 .$$

As in the previous example this reaction is the result of combining two elementary reaction steps

$$NO_2 + h\nu \longrightarrow NO + O(^3P)$$
$$O(^3P) + O_2 + M \longrightarrow O_3 + M \ .$$

Since the second step is very fast, the two reactions can be written as

$$NO_2 + h\nu \longrightarrow NO + O(^3P) \xrightarrow{+ O_2 + M} O_3$$

to give the composite form used in the mechanism. The use of this

simplification has reduced the number of reactions and species. In some cases, however, the elimination of fast intermediates can lead to the appearance of negative stoichiometric coefficients. To illustrate this point consider the reactions

$$CO + OH \xrightarrow[(O_2)]{1} CO_2 + HO_2$$

and

$$HO_2 + NO \xrightarrow{2} NO_2 + O_2 .$$

If the second reaction is considerably faster that the first, then HO_2 can be eliminated to give the equivalent step with one negative stoichiometric coefficient

$$CO + OH \longrightarrow CO_2 + NO_2 - NO + O_2 .$$

This approach is used in the Atkinson et al. (1982) mechanism to treat NO to NO_2 conversions by the intermediate radicals that are generated as a result of OH attack on organics.

2.2 Numerical Solution of the Chemical Kinetics

There are many computer programs available for the routine solution of chemical kinetics. Operationally these programs accept a description of the reaction mechanism and then use numerical solution techniques to calculate the species concentration dynamics. In this study extensive use has been made of the CHEMKIN package developed by Kee et al. (1980). There were several reasons for selecting this particular approach. Perhaps the most important was that CHEMKIN provided a very general framework for manipulating and solving complex

reaction mechanisms. By using the concept of a chemical compiler (Edelson; 1975, 1976, 1981) it is possible to algebraically manipulate the governing differential equations. This capability simplifies the implementation of sensitivity analysis procedures such as the FAST method (Koda et al. 1979; McRae et al. 1982) or the direct techniques of Kramer et al. (1981, 1982). In addition to CHEMKIN, we have made extensive use of the program CHEMK developed by Whitten and Hogo (1980). For further details about these and other analysis programs the reader is referred to McRae (1983).

2.3 Implementation and Initial Mechanism Testing

Before subjecting any mechanism to a detailed evaluation it is important to ensure that the reaction scheme has been implemented in the manner intended by each investigator. Four basic tests were carried out: duplication of the sample calculations supplied by each investigator, a check on mass conservation properties, modeling of a particular smog chamber experiment and finally the preparation of a standard isopleth. Full details of each test have been compiled in a form suitable for distribution to the investigators who have submitted mechanisms for evaluation. In the interests of space the results of these tests are not presented here.

Most of the mechanisms considered in this study were supplied with a test problem. The first step in verifying that the mechanism had been implemented correctly was to reproduce the results of the test problem. Given the initial conditions and the reaction stoichiometry shown in Tables 2-13, each mechanism was used to predict the

concentration time histories. In all cases the sample problems were reproduced to within acceptable accuracy.

CHAPTER 3

DISCUSSION OF THE CHEMICAL FORMULATION OF THE MECHANISMS

3.1 Carbonyl Chemistry and Lumping

The treatment of carbonyl chemistry in each of the lumped mechanisms is summarized in Table 14. For reference, the photooxidation mechanisms of formaldehyde, acetaldehyde, and propionaldehyde and of acetone and methyl ethyl ketone are given in Figures 2 and 3, respectively.

In the ALW mechanism, aldehydes are represented by HCHO, CH_3CHO and RCHO, where the reactions of RCHO are those of propionaldehyde. Thus the first three aldehydes serve as surrogates for all aldehydes; specifically propionaldehyde serves as a surrogate for itself and all higher aldehydes. Acetone and methyl ethyl ketone are treated explicitly. The only acetone reaction included is photolysis, whereas both photolysis and OH-reaction are included for methyl ethyl ketone. The methyl ethyl ketone-OH reaction is assumed to proceed totally by the path resulting from internal carbon atom OH attack. Because of the relative slowness of the OH reaction, this assumption is not expected to be a source of error.

The photolysis products in the Demerjian mechanism are consistent with the assumption that the generalized aldehyde species HC3 consists of a 50/50 mixture of formaldehyde and higher aldehydes, whereas the products of the HC3-OH reaction reflect an assumed distribution of 70 percent formaldehyde and 30 percent higher aldehydes. In the PW

TABLE 14

Representation of Carbonyl Chemistry by Lumped Mechanisms

MECHANISM	REACTIONS[a]	COMMENTS
Atkinson et al. (1982) (ALW)	See Table 2	Explicit chemistry of HCHO, CH_3CHO, CH_3CH_2CHO, $CH_3C(O)CH_3$ and $CH_3CH_2C(O)CH_3$
Demerjian (1982)	HC3 + hν ⟶ 0.5 RO_2 + 1.5 HO_2 + CO	Generalized aldehyde species HC3
	HC3 + OH ⟶ 0.3 RIO_2 + 0.7 HO_2 + 0.7 CO	
McRae and Seinfeld (1983)(MS)	HCHO explicit	Aldehydes divided into HCHO and higher aldehyde RCHO with CH_3CHO rate constants
	RCHO + hν ⟶ RO_2 + HO_2 + CO	
	RCHO + OH ⟶ RCO_3	
Killus and Whitten (1982) (KW)	CARB + hν ⟶ H_2 + CO	See text
	⟶ (1+a)HO_2 + (1-a)MEO_2 + CO - (1-a)PAR	
	CARB + OH ⟶ HO_2 + CO_2 + H_2O (52%)	
	⟶ ACO_3 + H_2O - PAR (44%)	
	⟶ CRO_2 - PAR (4%)	
Penner and Walton (1982) (PW)	HC4 + hν ⟶ CO (38%)	Generalized aldehyde species HC4
	⟶ CO + 2HO_2 (31%)	
	⟶ RO_2 + HO_2 + CO (31%)	
	HC4 + OH ⟶ RCO_3 + H_2O (63%)	
	⟶ CO + HO_2 + H_2O (37%)	

Footnotes for Table 14:

[a] When we write reactions from these mechanisms we will use the species nomenclature employed by the mechanism developers. Thus, even though each of these three mechanisms employs the generalized species, RO_2, this species has a specific definition in each mechanism. In all cases, RO_2 is a peroxy radical, although its reactions are somewhat different in each of the three mechanisms.

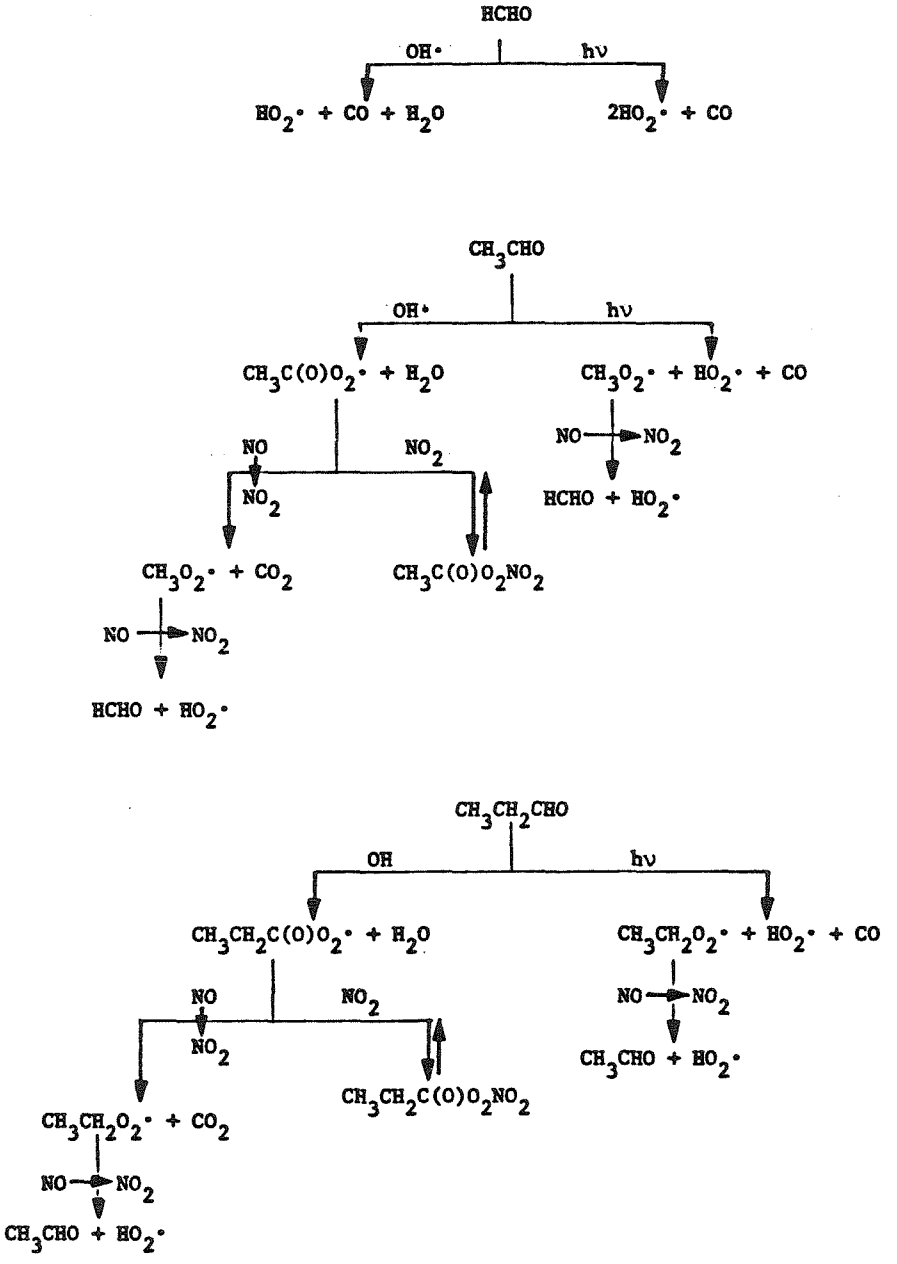

Figure 2. Formaldehyde, Acetaldehyde and Propionaldehyde Photooxidation Mechanisms

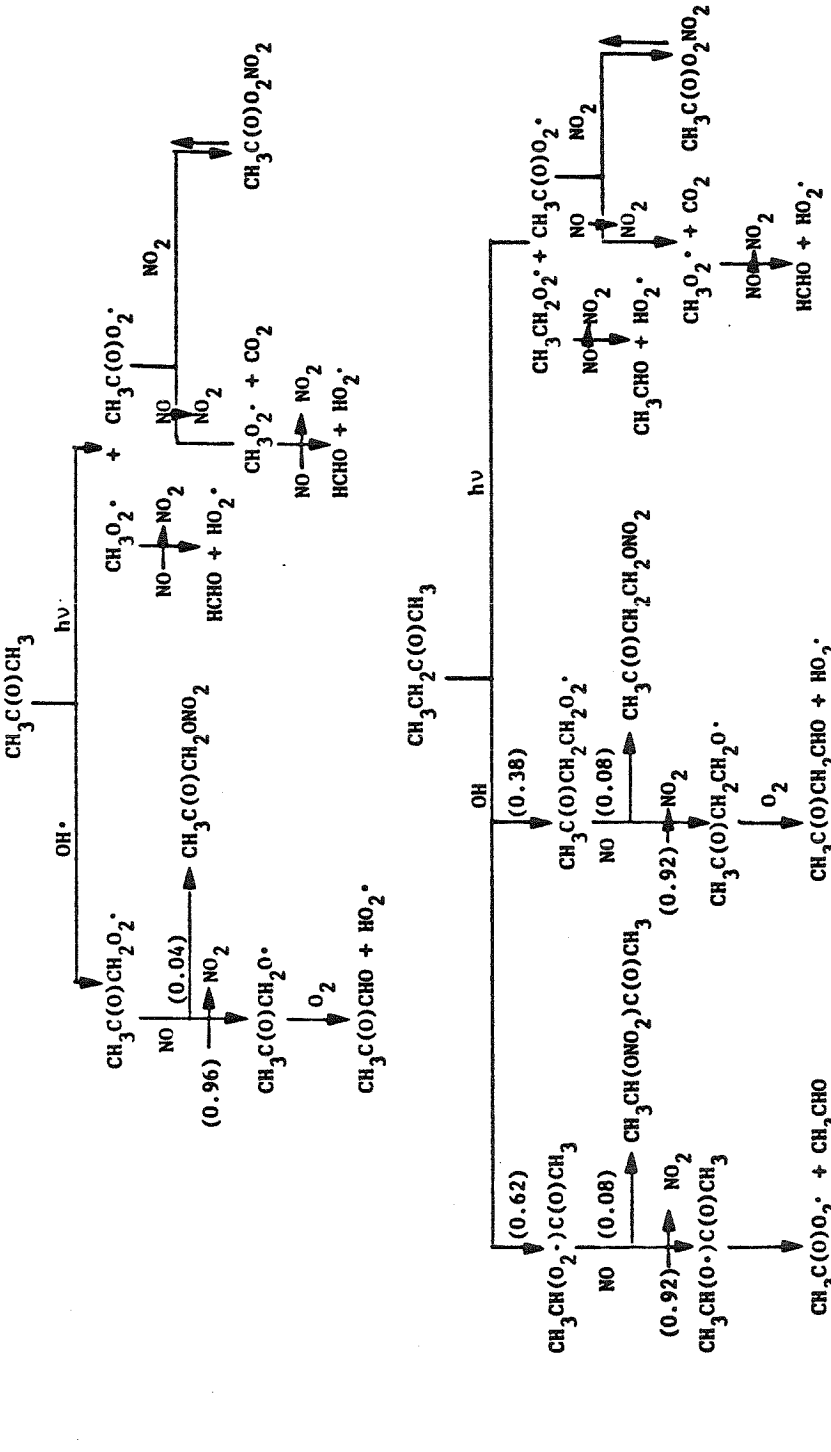

Figure 3. Acetone and Methyl Ethyl Ketone Photooxidation Mechanisms

mechanism, the lumped group HC4 is treated as 0.5 HCHO and 0.5 CH_3CHO. Thus, the three photolysis steps of HC4 are assigned rates equal to one-half those for HCHO and CH_3CHO. The KW mechanism requires some development to understand how its carbonyl chemistry was arrived at, and thus we now discuss that mechanism.

The KW mechanism, referred to as the Carbon Bond mechanism, represents carbonyl species as a combination of the two lumped species, CARB and PAR, where [CARB] is the total concentration of carbonyl groups and [PAR] is the sum of the number of carbon atoms in each alkane group,

$$[PAR] = \sum_i n_i[RH_i] + \sum_i m_i [CX_i]$$

where n_i is the number of carbon atoms in alkane RH_i and m_i is the number of paraffinic carbon atoms in other types of molecules, CX_i, e.g., carbonyl compounds. For a four aldehyde system, for example,

$$[CARB] = [HCHO] + [CH_3CHO] + [CH_3CH_2CHO] + [CH_3CH_2CH_2CHO]$$

$$[PAR] = [CH_3CHO] + 2[CH_3CH_2CHO] + 3[CH_3CH_2CH_2CHO] .$$

To develop the treatment of aldehyde chemistry in the KW mechanism, let us consider first the photolysis of formaldehyde and acetaldehyde,

$$HCHO + h\nu \xrightarrow{1} H_2 + CO$$

$$\xrightarrow{2} 2HO_2^{\cdot} + CO$$

$$CH_3CHO + h\nu \xrightarrow{3} CH_3O_2^{\cdot} + HO_2^{\cdot} + CO\,.$$

If [CARB] = [HCHO] + [CH_3CHO], then the decay of [CARB] due to photolysis is described by

$$-\frac{d[CARB]}{dt} = k_1[HCHO] + k_2[HCHO] + k_3[CH_3CHO]\,. \qquad (3.1)$$

Letting a = [HCHO]/[CARB], this relation becomes

$$-\frac{d[CARB]}{dt} = ak_1[CARB] + \{ak_2 + (1-a)k_3\}[CARB]\,. \qquad (3.2)$$

Based on (3.2), the photolysis of CARB can be expressed as three parallel reactions,*

---

* Consider the two parallel first-order reactions

$$A \xrightarrow{k_1} B$$

$$A \xrightarrow{k_2} C\,.$$

Then

$$\frac{d[A]}{dt} = -(k_1 + k_2)[A]$$

$$\frac{d[B]}{dt} = k_1[A] \text{ and } \frac{d[C]}{dt} = k_2[A]$$

$$\text{CARB} + h\nu \xrightarrow{ak_1} H_2 + CO$$

$$\xrightarrow{ak_2} 2HO_2\cdot + CO$$

$$\xrightarrow{(1-a)k_3} CH_3O_2\cdot + HO_2\cdot + CO \ .$$

Actually it is desired to represent these three reactions as two, an inert product path (reaction 1) and a radical producing path (reactions

---

We can express the two parallel reactions as a single reaction

$$A \xrightarrow{k_1+k_2} a_1B + a_2C \ ,$$

that has the overall first-order rate constant k_1+k_2. The rate of formation of B is given by a_1 times the rate of the reaction,

$$\frac{d[B]}{dt} = a_1(k_1 + k_2)[A] \ .$$

Likewise,

$$\frac{d[C]}{dt} = a_2(k_1 + k_2)[A] \ .$$

For these rates to equal those of the original parallel reactions,

$$a_1 = \frac{k_1}{k_1 + k_2} \qquad a_2 = \frac{k_2}{k_1 + k_2} \ .$$

Thus, a_1 is just the fraction of the overall rate constant, $k_1 + k_2$, for reaction 1, and likewise for a_2. In other words, if A decays with a total rate $k_1 + k_2$, the fraction of that rate ascribable to reaction 1 is the fraction of products that is B. In this manner, parallel reactions can be combined into a single overall reaction.

2 and 3). Writing the second and third reactions as a single reaction, we obtain the radical-producing path as

$$\text{CARB} + h\nu \xrightarrow{ak_2+(1-a)k_3} \frac{ak_2}{ak_2+(1-a)k_3}\{2HO_2 + CO\} + \frac{(1-a)k_3}{ak_2+(1-a)k_3}\{CH_3O_2 + HO_2 + CO\} .$$

In the KW mechanism the rate constants k_1, k_2 and k_3 are related by $k_1 = k_2 = 2k_3 = k_f$. With this relation among the three rate constants, the correct representation of the two CARB photolysis steps is

$$\text{CARB} + h\nu \xrightarrow{ak_f} H_2 + CO$$

$$\xrightarrow{\frac{a+1}{2}k_f} \frac{3a+1}{a+1} HO_2 + \frac{1-a}{a+1} CH_3O_2 + CO .$$

However, in the KW mechanism the second reaction is written as

$$\text{CARB} + h\nu \xrightarrow{\frac{a+1}{2}k_f} (1+a)HO_2 + (1-a)CH_3O_2 + CO .$$

In this form the rate constants and stoichiometric coefficients are inconsistent.

As we will see shortly, instead of CH_3O_2, the KW mechanism uses the generalized species MEO_2 that contains one carbon atom. Thus, the CARB photolysis reactions are written as (the second reaction is incorrect in its stoichiometric coefficents as noted above),

$$\text{CARB} + h\nu \xrightarrow{ak_f} H_2 + CO$$

$$\xrightarrow{\frac{a+1}{2}k_f} (1+a)HO_2 + (1-a)MEO_2 + CO - (1-a)PAR.$$

The (1-a)PAR term must be subtracted to transfer the needed carbon atom for MEO_2 from the PAR pool to the MEO_2 pool.* In the KW mechanism, the parameter a actually represents ([HCHO] + [KETONES])/[CARB]. This definition does not change the stoichiometric coefficient error noted above, however. The general CARB-OH reaction can be developed from HCHO and CH_3CHO:

$$HCHO + OH \xrightarrow{ak} HO_2 + CO + H_2O$$

$$CH_3CHO + OH \xrightarrow{(1-a)k} CH_3C(O)O_2 + H_2O$$

$$\underset{(1)}{\text{CARB}} + OH \xrightarrow{k} a\underset{(1)}{HO_2} + a\underset{(1)}{CO} + (1-a)\underset{(2)}{ACO_3} - (1-a)\underset{(1)}{PAR} + H_2O$$

where the number in parenthesis below a species indicates the number of carbon atoms in the species. This reaction can be written as (ACO_3 is the KW designation for $CH_3C(O)O_2$.)

---

* The transfer can also be effected by replacing -(1-a)PAR with (1-a)X, followed by the rapid reaction X + PAR ⟶ . This device is what is actually employed in the KW mechanism.

$$\text{CARB} + \text{OH} \xrightarrow{ak} \text{HO}_2 + \text{CO} + \text{H}_2\text{O}$$

$$\xrightarrow{(1-a)k} \text{ACO}_3 + \text{H}_2\text{O} - \text{PAR}$$

where k is an average rate constant for all carbonyl-OH reactions.

If the group CARB includes ketones in addition to aldehydes, the following reaction is added

$$\underset{(1)}{\text{CARB}} + \text{OH} \xrightarrow{a_k k} \underset{(2)}{\text{CRO}_2} - \underset{(1)}{\text{PAR}}$$

where CRO_2 denotes the peroxy radical formed from OH attack on a ketone. The composite mechanism can now be written in the form, where we include the rate constants to show the assumed split among the three steps,

$\text{CARB} + \text{OH} \xrightarrow{a_f k}$	$\text{HO}_2 + \text{CO}_2 + \text{H}_2\text{O}$	$7000\ \text{ppm}^{-1}\ \text{min}^{-1}$
$\xrightarrow{(1-a_f-a_k)}$	$\text{ACO}_3 + \text{H}_2\text{O} - \text{PAR}$	6000 "
$\xrightarrow{a_k k}$	$\text{CRO}_3 - \text{PAR}$	500 " .

In the KW mechanism ketone chemistry is represented through the OH reaction of the fraction of CARB assumed to be ketones. While accomplishing an economy of species, the lumping of aldehydes and ketones together in the CARB species neglects differences in the photolysis rates and OH mechanisms of the two classes of compounds. The ketone-OH reaction generally proceeds by attack on a hydrogen atom adjacent to the carbonyl group, followed by elimination of an aldehyde

and an acylperoxy radical, including an NO/NO_2 conversion. The competitive rates of photolysis and OH attack are different between aldehydes and ketones. The attempt to represent this difference is reflected by the percentage of CARB-OH reactions that proceed to give CRO_2. This split is fixed in the KW mechanism and thus does not reflect the actual distribution of aldehydes and ketones comprising CARB in a particular application.

Let us summarize the results of this section. By considering the treatment of carbonyl chemistry in each of the five mechaniss, we have provided examples of the lumping approaches delineated in Figure 1. In the surrogate species lumped molecule approach of the ALW mechanism, the representation of carbonyl chemistry is exact through propionaldehyde and methyl ethyl ketone, and higher aldehydes and ketones are represented by a comparable concentration of propionaldehyde and methyl ethyl ketone. The three generalized species lumped molecule mechanisms require one to partition all aldehydes into one or two lumped classes.

All carbonyl compounds are represented by the single species CARB in the KW mechanism, the concentration of which is equal to that of all $-C=O$ groups.

We can compare the ALW and KW aldehyde reactions. If we let a be the formaldehyde fraction of total aldehydes, then the ALW aldehyde reaction can be written as

$$CARB + h\nu \longrightarrow [2a + 3(1-a)]NO_2 - [2a + 3(1-a)]NO + 2OH + (1-a)HCHO + CO$$

whereas the KW step is

$$CARB + h\nu \longrightarrow 2.9NO_2 - 2.94NO + 1.96OH + 0.94CARB + CO + 0.04NRAT - 0.67PAR .$$

The aldehyde-OH steps are:

$$ALW: \quad CARB + OH \longrightarrow aNO_2 - aNO + aOH + aCO + (1-a)CH_3C(O)O_2 + H_2O$$

$$KW: \quad CARB + OH \longrightarrow 0.6NO_2 - 0.6NO + 0.56OH + 0.52CO + 0.44ACO_3 + 0.96H_2O + 0.04Dicarbonyl .$$

A value of $a \tilde{=} 0.1$ in the ALW mechanism produces comparable stoichiometries in the carbonyl photolysis steps of the two mechanisms, whereas a value of $a \tilde{=} 0.6$ is needed for the two carbonyl-OH steps to correspond.

3.2 Alkane Photooxidation Chemistry

We now consider the atmospheric chemistry of alkanes. Since OH reaction is the only significant alkane oxidation process in the atmosphere, we consider only that reaction here. The general features of

the alkane-OH reaction are, first, OH abstraction of a hydrogen atom from a terminal or internal carbon atom, followed by rapid addition of O_2 to form a peroxyalkyl radical, the principal fate of which is reaction with NO to give either NO_2 and an alkoxy radical or an alkyl nitrate. The key issues in alkane photooxidation chemistry are 1) the relative proportions of alkoxy radical and NO_2 formation versus alkyl nitrate formation in the peroxyalkyl-NO reaction, and 2) the fate of the alkoxy radical produced in the peroxyalkyl-NO reaction.

To elucidate the representation of alkane chemistry in the lumped mechanisms we will consider the explicit chemistry of propane, n-butane, and 2,3-dimethylbutane. The propane-OH photooxidation mechanism is:

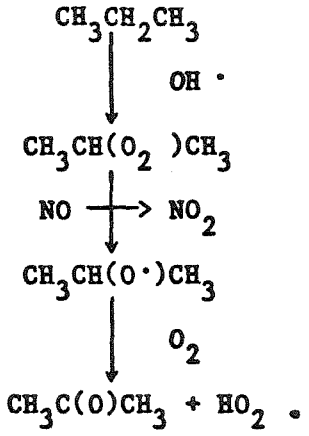

Internal H-atom abstraction predominates, and alkyl nitrate formation does not occur in the $CH_3CH(O_2^{\cdot})CH_3$-NO reaction. The overall reaction can be written as:

$$C_3H_8 + OH^{\cdot} \longrightarrow NO_2 - NO + CH_3C(O)CH_3 + HO_2^{\cdot} \quad .$$

The n-butane-OH reaction leads to the mechanism given in Figure 4. Definitive data concerning the relative importance of the two paths of reaction of the sec-butoxy radical, $CH_3CH_2CH(O^{\cdot})CH_3$, are not currently available, and Atkinson and Lloyd (1983) do not recommend a firm value for the ratio of the rate constants of these two reactions. Consequently, the split is indicated by the fraction b in the n-butane mechanism.

Finally, we consider the photooxidation of 2,3-dimethylbutane, as given in Figure 5.

We now consider the representation of alkane chemistry by the lumped mechanisms as given in Table 15. The propane, n-butane and 2,3-dimethylbutane photooxidation mechanisms provide a benchmark to evaluate the lumped alkane steps.

SURROGATE SPECIES LUMPED MOLECULE MECHANISM (ALW)

The ALW mechanism represents alkane chemistry through the explicit chemistries of propane, n-butane, and $\geq C_4$ alkanes. The n-butane reaction given in Table 15 can be derived as follows. The first step is written as

$$\text{n-butane} + OH \longrightarrow AO_2$$

where AO_2 consists of 0.85 of 2-butyl peroxy and 0.15 of 1-butyl peroxy. Based on the splits in the n-butane mechanism above, the reaction of AO_2 and NO is written as (assuming b = 0.38),

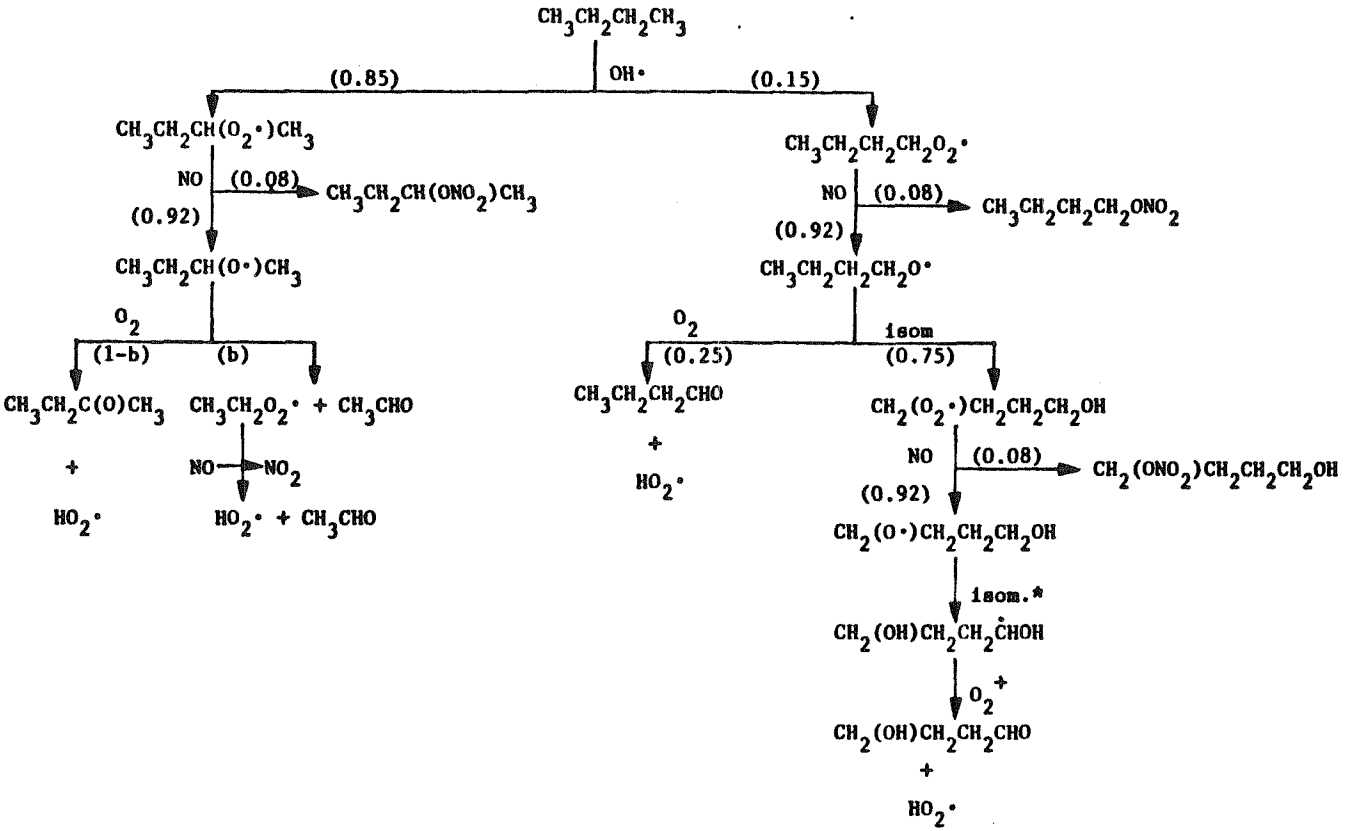

Figure 4. n-Butane Photooxidation Mechanism

*This isomerization is estimated to be a factor of five faster than the first isomerization of the $CH_3CH_2CH_2CH_2O$ radical, so that competition with O_2 reaction is not considered at this step.

+The predominant fate of α-hydroxy radicals is reaction with O_2. For example

$$\cdot CH_2OH + O_2 \rightarrow HCHO + HO_2\cdot$$

$$CH_3\dot{C}HOH + O_2 \rightarrow CH_3CHO + HO_2\cdot .$$

In the n-butane mechanism, the α-hydroxy radical, $CH_2(OH)CH_2CH_2\dot{C}HOH$, reacts rapidly with O_2 to form 4-hydroxy-butanal, $CH_2(OH)CH_2CH_2CHO$.

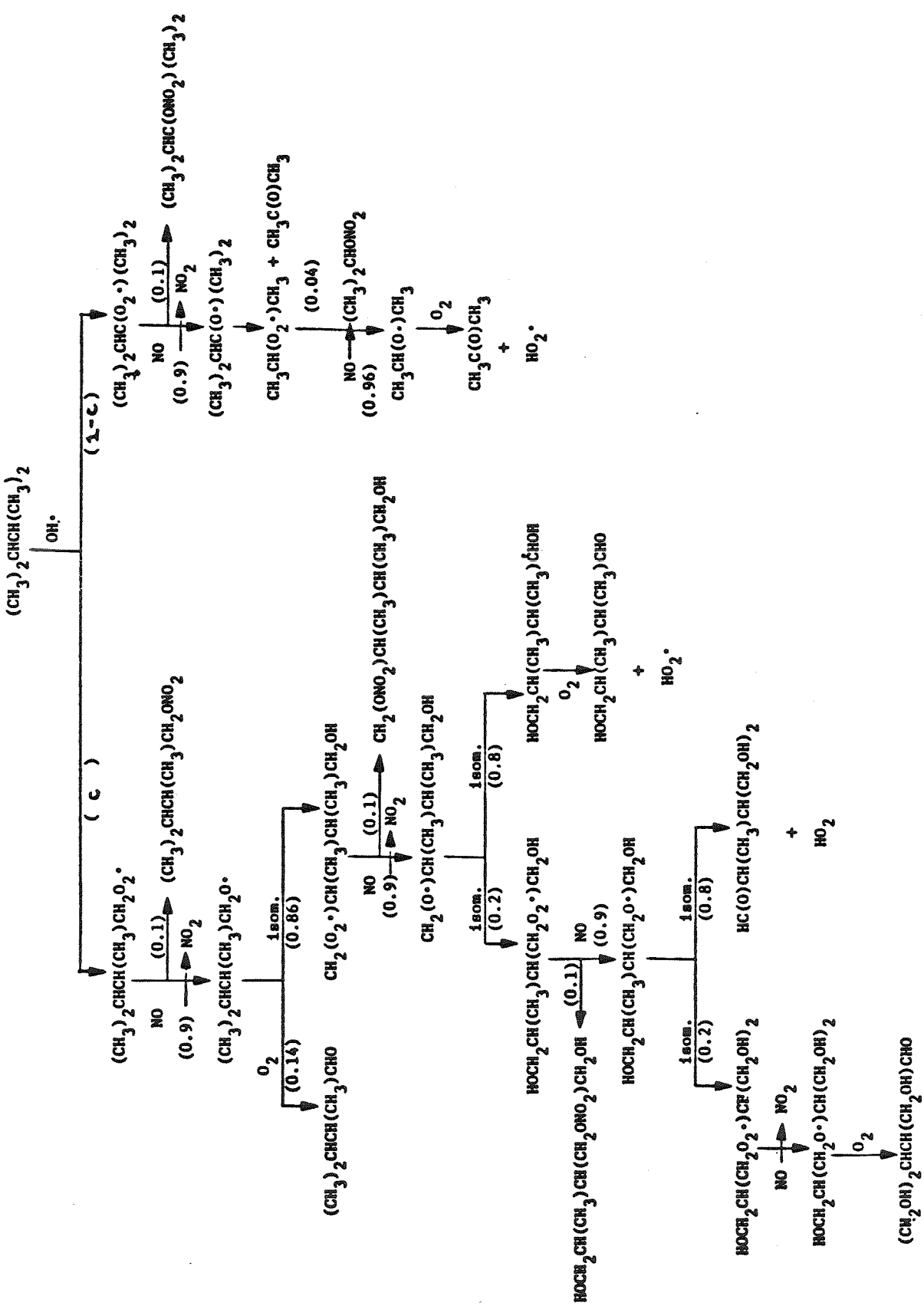

Figure 5. 2,3-Dimethyl butane Photooxidation Mechanism

TABLE 15

Representation of Alkane Chemistry by Lumped Mechanisms

MECHANISM	REACTIONS	COMMENTS
Atkinson et al. (1982) (ALW)	$C_3H_8 + OH \longrightarrow NO_2 - NO + CH_3C(O)CH_3 + HO_2$ n-butane + $OH \longrightarrow AO_2$ $AO_2 + NO \longrightarrow 1.28\ NO_2 - 0.39\ NO + 0.88\ HO_2 + 0.58\ CH_3CHO + 0.12\ RCHO + 0.47\ CH_3C(O)C_2H_5 + 0.11\ AONO_2$ C_4 alkanes + $OH \longrightarrow BO_2$ $BO_2 + NO \longrightarrow 1.7\ NO_2 - 0.8\ NO + 0.9\ HO_2 + 0.15\ HCHO + 0.3\ CH_3CHO + 0.1\ RCHO + 0.3\ CH_3C(O)CH_3 + 0.45\ CH_3C(O)C_2H_5 + 0.11\ AONO_2$	Propane, n-butane and $\geq C_4$ alkanes
Demerjian (1982)	$HC2 + OH \longrightarrow RO_2$ $RO_2 + NO \longrightarrow NO_2 + RO$ $RO + O_2 \longrightarrow HC3 + HO_2$	Generalized alkane species HC2, peroxyalkyl radical RO_2, and alkoxy radical RO
McRae and Seinfeld (1983) (MS)	$ALK + OH \longrightarrow RO_2$ $RO_2 + NO \longrightarrow NO_2 + RO$ $RO \longrightarrow b_1HO_2 + b_2HCHO + b_3RCHO + b_4RO_2$	Generalized alkane species ALK peroxy radical RO_2, and alkoxy radical RO
Killus and Whitten (1982) (KW)	$PAR + OH \longrightarrow MEO_2 + H_2O$ $MEO_2 + NO \longrightarrow NO_2 + CARB + HO_2$ (64%) $\longrightarrow NO_2 + CARB + MEO_2 - PAR$ (32%) $\longrightarrow NRAT$ (4%)	PAR represents single-bonded carbon atoms
Penner and Walton (1982) (PW)	$HC2 + OH \longrightarrow RO_2 + H_2O$ $RO_2 + NO \longrightarrow NO_2 + RO$ $RO + O_2 \longrightarrow HC4 + HO_2$	Generalized alkane species HC2, peroxyalky radical RO_2, and alkoxy radical RO

$$AO_2 + NO \longrightarrow 1.28\ NO_2 - 0.39\ NO + 0.88\ HO_2 + 0.58\ CH_3CHO + 0.12\ RCHO + 0.47\ CH_3C(O)C_2H_5 + 0.11\ AONO_2$$

with a similar approach to deriving the $\geq C_4$-alkane-OH reaction.

3.2.1 Generalized Species Lumped Molecule Mechanisms

The generalized alkane-OH reactions of the Demerjian, MS and PW mechanisms given in Table 15 are self-explanatory except for the generalized alkoxy radical reaction in the MS mechanism. We defer discussion of that step until we consider alkene chemistry since the generalized alkoxy radical in the MS mechanism arises from both alkane and alkene reactions.

3.2.2 Carbon Bond Mechanism (KW)

Let us now consider the KW mechanism and the carbon bond lumping approach to alkane-OH chemistry. The first step is

$$\underset{(1)}{OH} + \underset{(1)}{PAR} \longrightarrow \underset{(1)}{MEO_2} + H_2O\ .$$

Because alkane carbon atoms are represented by the single species PAR, it is necessary to assign a rate constant for this reaction that is, in some sense, an average OH-rate constant for all reactions represented by the single PAR-OH reaction. Based on alkane-OH rate constants and on the composition of typical atmospheric mixtures, KW chose a rate constant of 1300 $ppm^{-1}\ min^{-1}$, slightly less than the value for a secondary carbon atom.

By considering the n-butane-OH mechanism and letting $[AO_2]$ = $[CH_3CH_2CH(O_2^{\cdot})CH_3]$ + $[CH_3CH_2CH_2CH_2O_2^{\cdot}]$, the AO_2-NO reaction can be expressed in Carbon Bond nomenclature as

$$\begin{aligned} AO_2 + NO &\longrightarrow NO_2 + CARB + HO_2 \\ &\longrightarrow NO_2 + MEO_2 \\ &\longrightarrow NO_2 + CARB + MEO_2 - PAR \\ &\longrightarrow NRAT \ . \end{aligned}$$

Because the general peroxyalkyl radical MEO_2 arises from aldehydes, aromatics, etc. in addition to alkanes, the above reactions with MEO_2 replacing AO_2 are too specific to the alkane system to represent the general MEO_2-NO reaction. The general MEO_2-NO reaction adopted in the KW mechanism, together with the rate constants used, is

$$\begin{aligned} MEO_2 + NO &\longrightarrow NO_2 + CARB + HO_2 && 7700\ ppm^{-1}\ min^{-1} \\ &\longrightarrow NO_2 + CARB + MEO_2 - PAR && 3800\ ppm^{-1}\ min^{-1} \\ &\longrightarrow NRAT && 500\ ppm^{-1}\ min^{-1}. \end{aligned}$$

If the total MEO_2-NO rate constant $k = 12000\ ppm^{-1}\ min^{-1}$ is apportioned according to

$$\begin{aligned} \theta\nu k &= 7700 \\ (1-\theta)\nu k &= 3800 \\ (1-\nu)k &= 500 \end{aligned}$$

where ν is the fraction of MEO_2-NO reactions that leads to NO_2, i.e., 0.96, then θ can be interpreted in terms of the following cycle

$$\xrightarrow{OH} MEO_2 \longrightarrow \theta HO_2 + (1-\theta)MEO_2 \ .$$

Thus, the total number T of MEO_2 molecules produced from one molecule of MEO_2 is

$$T = \sum_{n=1}^{\infty} (1-\theta)^{n-1} = \frac{1}{\theta} .$$

In the KW mechanism, the values of the rate constants used imply that $\theta = 0.67$ or $T = 1.5$.

The ALW n-butane-OH reaction may be written as

$$\text{n-butane} + OH \longrightarrow 1.28\ NO_2 - 1.39\ NO + 0.88\ HO_2 + 0.58 \underbrace{CH_3CHO + 0.12\ RCHO}_{1.17\ RCHO} + 0.47\ MEK .$$

Whereas the comparable step in the KW mechanism is

$$PAR + OH \longrightarrow 1.41\ NO_2 - 1.47\ NO + 0.94\ HO_2 + 1.41\ CARB .$$

Thus, the KW mechanism is slightly more reactive than the ALW mechanism in terms of this step.

3.3 Alkene Photooxidation Chemistry

3.3.1 Alkene-O and Alkene-OH Reactions

Alkene-O and alkene-OH reactions in the lumped mechanisms are given in Tables 16 and 17, respectively. For comparison, the detailed chemistry of ethene, propene, and trans-2-butene is given in Figures 6 and 7. Since alkene-O atom reactions are not of major importance in photochemical smog, their omission is not expected to be a source of error.

TABLE 16

Alkene-O Reactions in the Lumped Mechanisms

MECHANISM	REACTIONS	COMMENTS
Atkinson et al. (1982) (ALW)		Not included
Demerjian (1982)	HC1 + O $\longrightarrow$ RO_2 + HC3 + HO_2	
Killus and Whitten (1982a) (KW)	OLE + O $\longrightarrow$ MEO_2 + ACO_3 + X	
	$\longrightarrow$ CARB + PAR	
	ETH + O $\longrightarrow$ MEO_2 + HO_2 + CO	
	$\longrightarrow$ CARB + PAR	
McRae and Seinfeld (1983) (MS)	C_2H_4 + O $\longrightarrow$ RO_2 + HO_2	
	OLE + O $\longrightarrow$ RO_2 + RCO_3	
Penner and Walton (1982) (PW)	HC1 + O $\longrightarrow$ RO_2 + RCO_3	
	HC2 + O $\longrightarrow$ RO_2 + OH	

TABLE 17

Alkene-OH Reactions in the Lumped Mechanisms

MECHANISM	REACTION	COMMENTS
Atkinson et al. (1982) (ALW)	$C_2H_4 + OH \longrightarrow NO_2 - NO + 2HCHO + HO_2$	Ethene, propene, and trans-2-butene
	$C_3H_6 + OH \longrightarrow NO_2 - NO + CH_3CHO + HCHO + HO_2$	
	$C_4H_8 + OH \longrightarrow 0.9\ NO_2 - NO + 1.8\ CH_3CHO + 0.9\ HO_2 + 0.1\ RONO_2$	
Demerjian (1982)	$HC1 + OH \longrightarrow RO_2 + HC3$	Generalized alkene species HC1
	$RO_2 + NO \longrightarrow RO + NO_2$	
	$RO + O_2 \longrightarrow HC3 + HO_2$	
McRae and Seinfeld (1983) (MS)	$OLE + OH \longrightarrow RO_2$	Generalized alkene species OLE
	$RO_2 + NO \longrightarrow RO + NO_2$	
	$RO \longrightarrow b_1HO_2 + (1-b_1)RO_2 + b_2HCHO + b_3RCHO$	$b_1 = b_2 = 0.5$, $b_3 = 0.5$
Killus and Whitten (1982) (KW)	$ETH + OH \longrightarrow RBO_2$	
	$RBO_2 + NO \longrightarrow NO_2 + 2CARB + HO_2$	
	$OLE + OH \longrightarrow RAO_2$	
	$RAO_2 + NO \longrightarrow NO_2 + 2CARB + HO_2$	
Penner and Walton (1982) (PW)	$HC1 + OH \longrightarrow RO_2 + HC4$	
	$RO_2 + NO \longrightarrow RO + NO_2$	
	$RO + O_2 \longrightarrow HC4 + HO_2$	

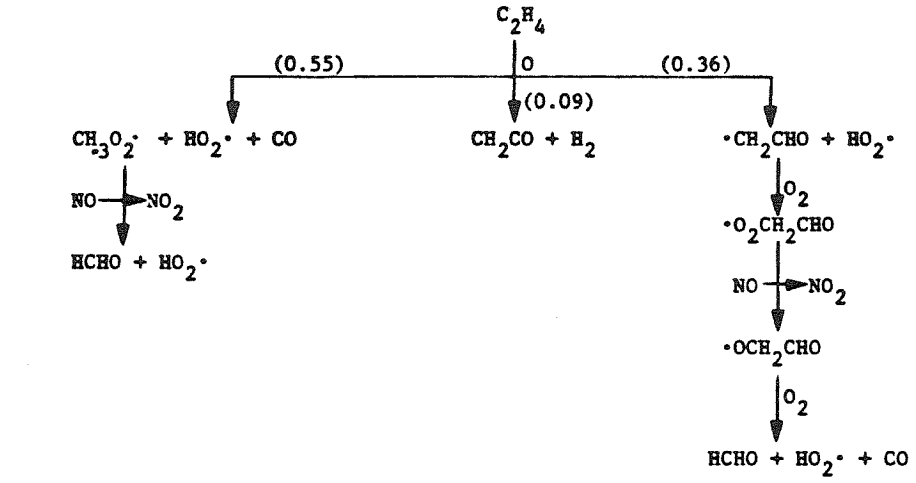

Net: $C_2H_4 + O \rightarrow 0.55(NO_2 - NO + HCHO + 2HO_2\cdot + CO)$
$+ 0.36(NO_2 - NO + HCHO + 2HO_2\cdot + CO)$
$+ 0.09(CH_2CO + H_2)$

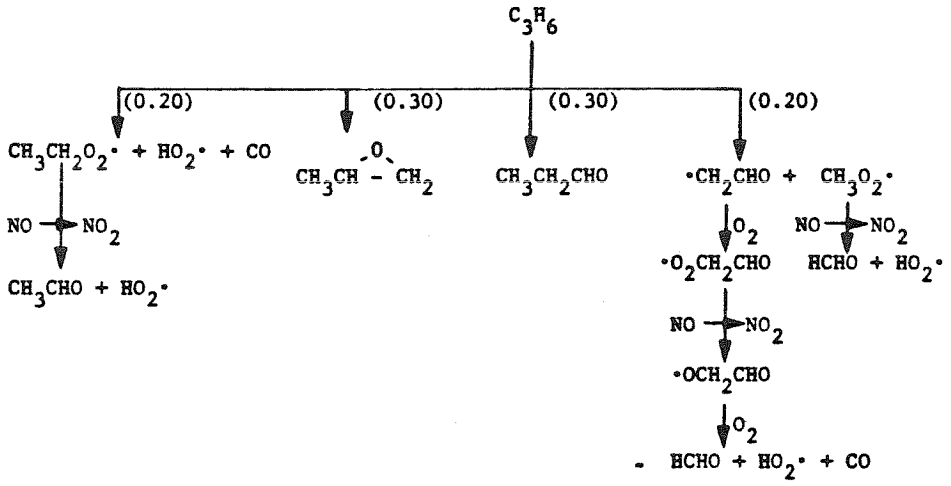

Net: $C_3H_6 + O \rightarrow 0.3\ CH_3CH\text{-}O\text{-}CH_2 + 0.3\ CH_3CH_2CHO$
$+ 0.2(2NO_2 - 2NO + 2HCHO + 2HO_2\cdot + CO)$
$+ 0.2(NO_2 - NO + CH_3CHO + 2HO_2\cdot + CO)$

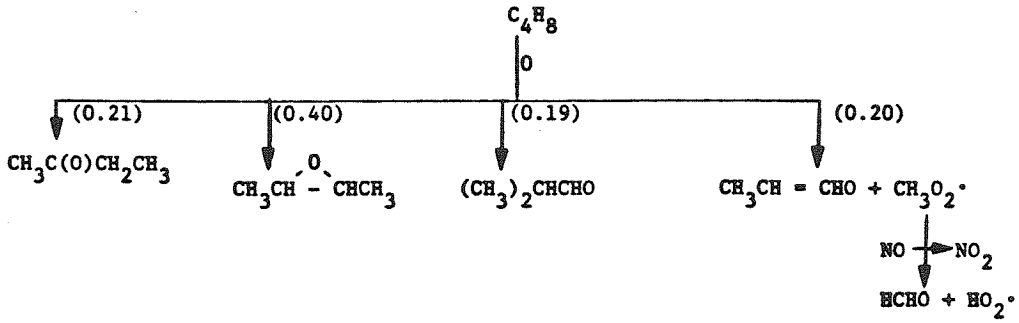

Figure 6. Ethene, Propene, Trans-2-Butene-O Reaction Mechanisms

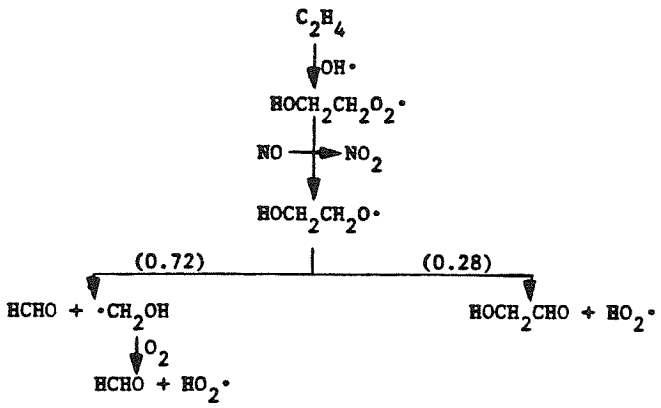

Net: $C_2H_4 + OH\cdot \rightarrow NO_2 - NO + 1.44\ HCHO + 0.28\ HOCH_2CHO + HO_2\cdot$

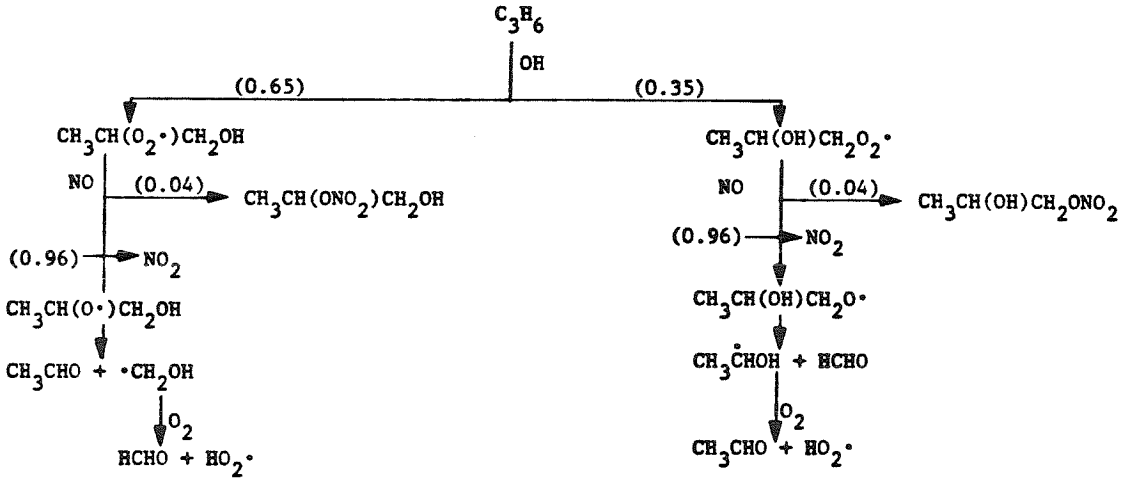

Net: $C_3H_6 + OH\cdot \rightarrow 0.96\ NO_2 - NO + 0.96\ (CH_3CHO + HCHO + HO_2\cdot)$

$+ 0.04(0.65\ CH_3CH(ONO_2)CH_2OH + 0.35\ CH_3CH(OH)CH_2ONO_2)$

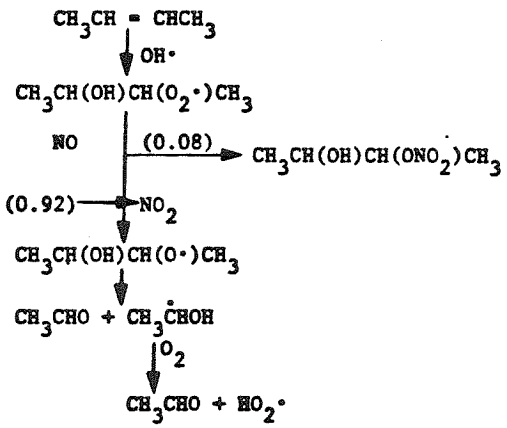

Net: $CH_3CH = CHCH_3 + OH\cdot \rightarrow 0.92\ NO_2 - NO + 0.92\ (2CH_3CHO + HO_2\cdot)$

$+ 0.08\ CH_3CH(OH)CH(ONO_2)CH_3$

Figure 7. Ethene, Propene, and Trans-2-Butene-OH Reaction Mechanisms

Table 17 presents the generalized alkene-OH reactions in the mechanisms. Ethene, propene, and trans-2-butene are treated explicitly in the ALW mechanism. The error incurred by omitting the glycol aldehyde production path in the ethene-OH reaction is not significant since it is implicitly replaced by two formaldehyde molecules. Likewise, the omission of the four percent nitrate forming path in the propene-OH reaction is not expected to be a noticeable source of error. To assess the lumped reaction steps in Table 17, let us review the reactions of several of the alkoxy radicals, as done in Table 18. Most of the alkoxy radical reactions lead to HO_2; thus, HO_2 is a product in each of the RO reactions in each of the three generalized species mechanisms. The Demerjian and PW mechanisms lump all aldehydes into the species HC3 and HC4, respectively, so no distinction need be made between formaldehyde and higher aldehydes in these two mechanisms. Since in the MS mechanism formaldehyde and higher aldehydes are segmented, it is necessary to specify the split of aldehyde products, and values of $b_2 = 0.5$ and $b_3 = 0.5$ have been used. We note that the extra aldehyde produced in the alkene-OH reaction is not included in the MS mechanism as in the other two generalized species mechanisms. Although alkoxy radicals are not treated explicitly in the ALW and KW mechanisms, their assumed chemistry is implicit in the products of the peroxy radical-NO reaction. In the KW mechanism, for example, the implied alkoxy radical chemistry is

$$MEO \longrightarrow CARB + 0.67\ HO_2 + 0.33\ MEO_2$$

$$RBO \longrightarrow 2CARB + HO_2$$

TABLE 18

Alkoxy and Hydroxy Alkoxy Radical Reactions Interpreted According to RO $\longrightarrow$ $b_1HO_2^{\cdot} + (1-b_1)RO_2^{\cdot} + b_2HCHO + b_3RCHO$

HYDROCARBON SOURCE	RADICAL	b_1	b_2	b_3
Acetaldehyde	$CH_3O^{\cdot}$	1	1	0
Propane	$CH_3CH(O^{\cdot})CH_3$	1	0	1
n-Butane	$CH_3CH_2CH(O^{\cdot})CH_3$	0.62	0	1
	$CH_3CH_2CH_2CH_2O^{\cdot}$	0.25	0	0.25
2,3-Dimethyl butane	$(CH_3)_2CHCH(CH_3)CH_2O^{\cdot}$	0.14	0	0.14
	$(CH_3)_2CHC(O^{\cdot})(CH_3)_2$	0	0	1
Ethene	$HOCH_2CH_2O^{\cdot}$	1	1.44	0.28
Propene	$CH_3CH(O^{\cdot})CH_2OH$	1	1	1
	$CH_3CH(OH)CH_2O^{\cdot}$	1	1	1
trans-2-Butene	$CH_3CH(OH)CH(O^{\cdot})CH_3$	1	0	2

$$RAO \longrightarrow 2CARB + HO_2 .$$

Because the reaction product split from MEO includes 0.33 MEO_2, all else being equal, the KW mechanism can be expected to predict somewhat more reactivity than the other mechanisms that assume 100 percent HO_2 as product.

3.3.2 Alkene-O_3 Reactions

It is now reasonably well established that the initial step in the alkene-O_3 reaction is the formation of a molozonide that rapidly decomposes to a carbonyl and an energy-rich biradical, called the Criegee intermediate,

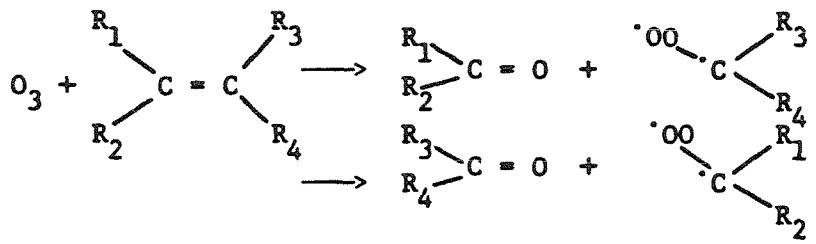

where a 50-50 split between the two paths is usually assumed. The major problem in describing the O_3-alkene reaction lies in establishing the subsequent chemistry of the Criegee intermediate.

The initial O_3 reaction steps for ethene, propene, 1-butene and trans-2-butene are

$$CH_2 = CH_2 + O_3 \longrightarrow HCHO + H_2COO$$

$$CH_3CH = CH_2 + O_3 \longrightarrow HCHO + CH_3CHOO$$

$$\longrightarrow CH_3CHO + H_2COO$$

$$CH_2 = CHCH_2CH_3 + O_3 \longrightarrow HCHO + CH_3CH_2CHOO$$

$$\longrightarrow CH_3CH_2CHO + H_2COO$$

$$CH_3CH = CHCH_3 + O_3 \longrightarrow CH_3CHO + CH_3CHOO .$$

The dynamics of the Criegee intermediate can be analyzed from the general mechanism:

$$\text{ALKENE} + O_3 \xrightarrow{1} \text{CARBONYL} + \text{CRIG*}$$

$$\text{CRIG*} \xrightarrow{2} \text{PRODUCTS}$$

$$\text{CRIG*} + \text{M} \xrightarrow{3} \text{CRIG} + \text{M}$$

$$\text{CRIG} \xrightarrow{4} \text{PRODUCTS}$$

$$\text{CRIG} + X_i \xrightarrow{5i} \text{PRODUCTS}$$

where CRIG* denotes an energetic form of the Criegee intermediate. If we assume that CRIG* is in a pseudo-steady state, then

$$[\text{CRIG*}]_{ss} = \frac{k_1[\text{ALKENE}][O_3]}{k_2 + k_3[\text{M}]} .$$

Thus, the kinetics of the stabilized Criegee intermediate CRIG are given by

$$\frac{d[\text{CRIG}]}{dt} = \frac{k_1[\text{ALKENE}][O_3]}{1 + \dfrac{k_2}{k_3[\text{M}]}} - \{k_4 + \sum_i k_{5i}[X_i]\}\,[\text{CRIG}]$$

and if CRIG is in a pseudo-steady state,

$$[\text{CRIG}]_{ss} = \frac{k_1[\text{ALKENE}][O_3]}{\{1 + \dfrac{k_2}{k_3[\text{M}]}\}\quad\{k_4 + \sum_i k_{5i}[X_i]\}} .$$

The mechanism above includes two decomposition steps, 2 and 4. If

decomposition occurs, it probably does so via reaction 2, so we can assume that $k_4 = 0$. The ratio $k_3[M]/(k_2 + k_3[M])$ is the fraction of the energetic intermediates that are stabilized.

In their review of the chemistry of H_2COO, Atkinson and Lloyd (1983) recommend the following fate of H_2COO,

$$H_2COO^* + M \longrightarrow H_2COO + M \qquad (0.40)$$

$$\longrightarrow CO_2 + H_2 \qquad (0.12)$$

$$\longrightarrow CO + H_2O \qquad (0.42)$$

$$\xrightarrow{2O_2} CO_2 + 2HO_2 \qquad (0.06) .$$

The thermalized H_2COO biradicals are then available for bimolecular reactions with CO, HCHO, CH_3CHO and SO_2. The ethene-O_3 reaction can then be written as

$$C_2H_4 + O_3 \longrightarrow HCHO + 0.40\ H_2COO + 0.18\ CO_2 + 0.42\ CO + 0.12\ H_2 + 0.42\ H_2O + 0.12\ HO_2 .$$

For the chemistry of the CH_3CHOO biradical, Atkinson and Lloyd (1983) recommend

$$CH_3CHOO^* + M \longrightarrow CH_3CHOO + M \qquad (0.40)$$

$$\longrightarrow CH_4 + CO_2 \qquad (0.12)$$

$$\xrightarrow{O_2} CH_3O_2^{\cdot} + CO + OH^{\cdot} \qquad (0.192)$$

$$\xrightarrow{2O_2} CH_3O_2^{\cdot} + CO_2 + HO_2^{\cdot} \qquad (0.192)$$

$$\xrightarrow{O_2} HO_2^{\cdot} + CO + CH_3O^{\cdot} \qquad (0.048)$$

$$\xrightarrow[2O_2]{} HO_2^{\cdot} + CO_2 + CH_3O_2^{\cdot} \qquad (0.048)$$

leading to

$$CH_3CHOO^* \longrightarrow 0.40\ CH_3CHOO + 0.12\ CH_4 + 0.36\ CO_2 + 0.24\ CO + 0.29\ HO_2^{\cdot} + 0.19\ OH^{\cdot} + 0.05\ CH_3O^{\cdot} + 0.43\ CH_3O_2^{\cdot}$$

and thus

$$C_3H_6 + O_3 \longrightarrow 0.5\ HCHO + 0.5\ CH_3CHO + 0.5\ H_2COO^* + 0.5\ CH_3CHOO^*$$

followed by the above reactions of H_2COO^* and CH_3CHOO^*.

We note that the radical yields from the ethene-O_3 and propene-O_3 reactions are 0.12 $HO_2^{\cdot}$ radicals per ethene molecule reacted and 0.205 $HO_2^{\cdot}$ + 0.095 $OH^{\cdot}$ + 0.025 $CH_3O^{\cdot}$ + 0.215 $C_3O_2^{\cdot}$ per propene molecule reacted.

Finally, for trans-2-butene, we have

$$CH_3CH = CHCH_3 + O_3 \longrightarrow CH_3CHO + CH_3CHOO^*$$

followed by the above reactions of CH_3CHOO^*.

The thermalized Criegee intermediates are then available to react with other molecules in the system,

$$RCHOO + NO \longrightarrow NO_2 + RCHO$$
$$+ NO_2 \longrightarrow NO_3 + RCHO$$
$$+ SO_2 \longrightarrow SO_3 + RCHO$$
$$+ H_2O \longrightarrow RCOOH + H_2O$$

Consider now the propene-O_3 reaction:

$$CH_3CH = CH_2 + O_3 \quad \begin{matrix} HCHO + CH_3CHOO^* & (50\%) \\ CH_3CHO + H_2COO^* & (50\%) \end{matrix} .$$

The 50-50 split is assumed in virtually all current reaction mechanisms. Niki et al. (1977) studied the dynamics of CH_3CHOO^*, and found 18 percent stabilization, whereas a value of 40 percent is assumed in the ALW mechanism. We can express the fate of CH_3CHOO^* as

$$CH_3CHOO^* \longrightarrow c_2\ CH_3CHOO + (1-c_2)\{e_1(CH_3O_2^{\cdot}+CO+OH^{\cdot}) + e_2(CH_3O_2^{\cdot}+CO_2+HO_2^{\cdot}) + e_3(HCHO+2HO_2^{\cdot}+CO) + (1-e_1-e_2-e_3)(CH_4+CO_2)\}$$

where c_2 is the fraction of stabilization of CH_3CHOO^*. The product distribution splits assumed in the mechanisms we have been studying are given in Table 19. We see that the values of e_1, e_2 and e_3 used in the ALW and KW mechanisms are:

	e_1	e_2	e_3
ALW	0.33	0.33	0.05
KW	0.34	0.425	0.05 .

We note that the Criegee intermediate decomposition in the KW mechanism, which occurs at an overall rate of 10^3 min^{-1}, in the proportions shown in Table 19, is competitive with its reaction with NO and NO_2. Because decomposition is competitive with reaction, the fraction of stabilization depends on the concentrations of the species with

TABLE 19

Alkene-O_3 Reactions in the Lumped Mechanisms

MECHANISM	REACTIONS
Atkinson et al. (1982) (ALW)	PROPENE + O_3 $\longrightarrow$ 0.5 HCHO + 0.5 CH_3CHO + 0.2 H_2COO + 0.2 CH_3CHOO + 0.3 CO + 0.2 HO_2 + 0.1 OH + 0.2 CH_3O_2
	BUTENE + O_3 $\longrightarrow$ CH_3CHO + 0.4 CH_3CHOO + 0.2 CO + 0.2 OH + 0.3 HO_2 + 0.45 CH_3O_2
Demerjian (1982)	HC1 + O_3 $\longrightarrow$ HC_3 + RO_2 + HO_2
McRae and Seinfeld (1982) (MS)	OLE + O_3 $\longrightarrow$ 0.5 RCHO + 0.5 HCHO + 0.304 HO_2 + 0.306 RO_2 + 0.136 OH + 0.034 RO
Killus and Whitten (1982) (KW)	ETH + O_3 $\longrightarrow$ CARB + CRIG
	CRIG $\longrightarrow$ H_2O + CO (67%)
	$\longrightarrow$ stable products (24%)
	$\longrightarrow$ $2HO_2$ + CO (9%)
	CRIG + NO $\longrightarrow$ NO_2 + CARB
	CRIG + NO_2 $\longrightarrow$ NO_3 + CARB
Penner and Walton (1982) (PW)	HC1 + O_3 $\longrightarrow$ HC4 + 0.5 HO_2

which CRIG reacts. Using the rate constants of the mechanism, that fraction is given by

$$f = \frac{1.2\times10^4\,[NO] + 8\times10^3\,[NO]}{10^3 + 1.2\times10^4\,[NO] + 8\times10^3\,[NO_2]} .$$

For example, if $[NO] = [NO_2] = 0.1$ ppm, $f = 0.67$, whereas if $[NO] = [NO_2] = 0.01$ ppm, $f = 0.167$. The KW mechanism involves a similar treatment of the OLE-O_3 reaction.

We see that the ALW mechanism is based on the general Criegee mechanism given earlier with $k_4 = 0$; i.e., a certain fraction of the energetic Criegee intermediates is assumed to decompose immediately into stable products, the remainder being then available to react with other species in the system. The fraction stabilized is assumed to be 0.4 for both H_2COO and CH_3CHOO; in the latter case, this fraction is high when compared to the single available experimental value of 0.18. In the KW mechanism, on the other hand, 100 percent stabilization is assumed to occur immediately, and thus $k_2 = 0$. The stabilized Criegee intermediate then may either decompose into stable products or react with other species in the system. The rate constant for decomposition is fixed at 1000 min^{-1}, so that, as shown above, the amount of Criegee intermediate actually decomposing depends on the concentration of other species. Although the available experimental data concerning the fate of Criegee intermediate tend to support the idea that the energetic intermediate first either decomposes or is stabilized, the quantity of such data is insufficient to draw a definite conclusion concerning

which approach to representing Criegee intermediate chemistry is, in fact, the more justifiable.

Of the alkene-O_3 reactions in the three generalized species mechanisms, assuming equal rate constants, the Demerjian mechanism is most "reactive," predicting two peroxy radical products, in addition to the aldehyde product specified in all mechanisms, whereas the PW mechanism is least "reactive" with only 0.5 peroxy radicals formed per alkene-O_3 reaction. The MS mechanism lies intermediate between the other two in reactivity with about 0.78 radicals formed per O_3 attack. In the MS mechanism, 80 percent of the Criegee intermediate is assumed to decompose, the other 20 percent going to non-radical products. The assumptions leading to the radical products in the Demerjian and PW mechanisms have not been discussed in their mechanism descriptions. We recall that in the ALW mechanism, 60 percent of the Criegee intermediate is assumed to decompose, with the remaining 40 percent reacting as a peroxy radical, whereas, in the KW mechanism, about 85 percent of the intermediate is assumed to decompose although that decomposition is competitive with other reactions.

In summary, we note that each of the five lumped mechanisms treats the alkene-O_3 reaction somewhat differently, leading to different "reactivities" of the steps. From the distribution of radical products one can obtain a qualitative indication of the relative order of reactivity of the alkene-O_3 reaction steps, although different assumptions concerning the reaction paths of the Criegee intermediate

make it difficult to make precise comparisons without detailed computations.

3.4 Aromatic Photooxidation Chemistry

The only important atmospheric oxidation pathway for aromatic hydrocarbons is reaction with OH. Current understanding concerning aromatic photooxidation chemistry has been summarized by Atkinson and Lloyd (1983).

3.4.1 Toluene-OH Reaction

The toluene-OH reaction proceeds by both abstraction and addition pathways. Figure 8 shows the toluene-OH abstraction mechanism including benzaldehyde chemistry, and Figure 9 presents a summary of a proposed toluene-OH addition mechanism.

3.4.2 m-Xylene-OH Reaction

m-Xylene chemistry is similar to toluene chemistry, with approximately 96 percent of the initial OH attack proceeding via addition. A summary of the addition pathway is shown in Figure 10.

3.4.3 Treatment of Aromatic Photooxidation by the ALW Mechanism

The ALW mechanism treats benzene chemistry explicitly, uses toluene to represent monoalkylbenzenes, and uses a lumped average xylene to represent di- and tri-alkylbenzenes.

It has been found experimentally that the fraction of the initial OH reaction proceeding by abstraction has the following approximate values:

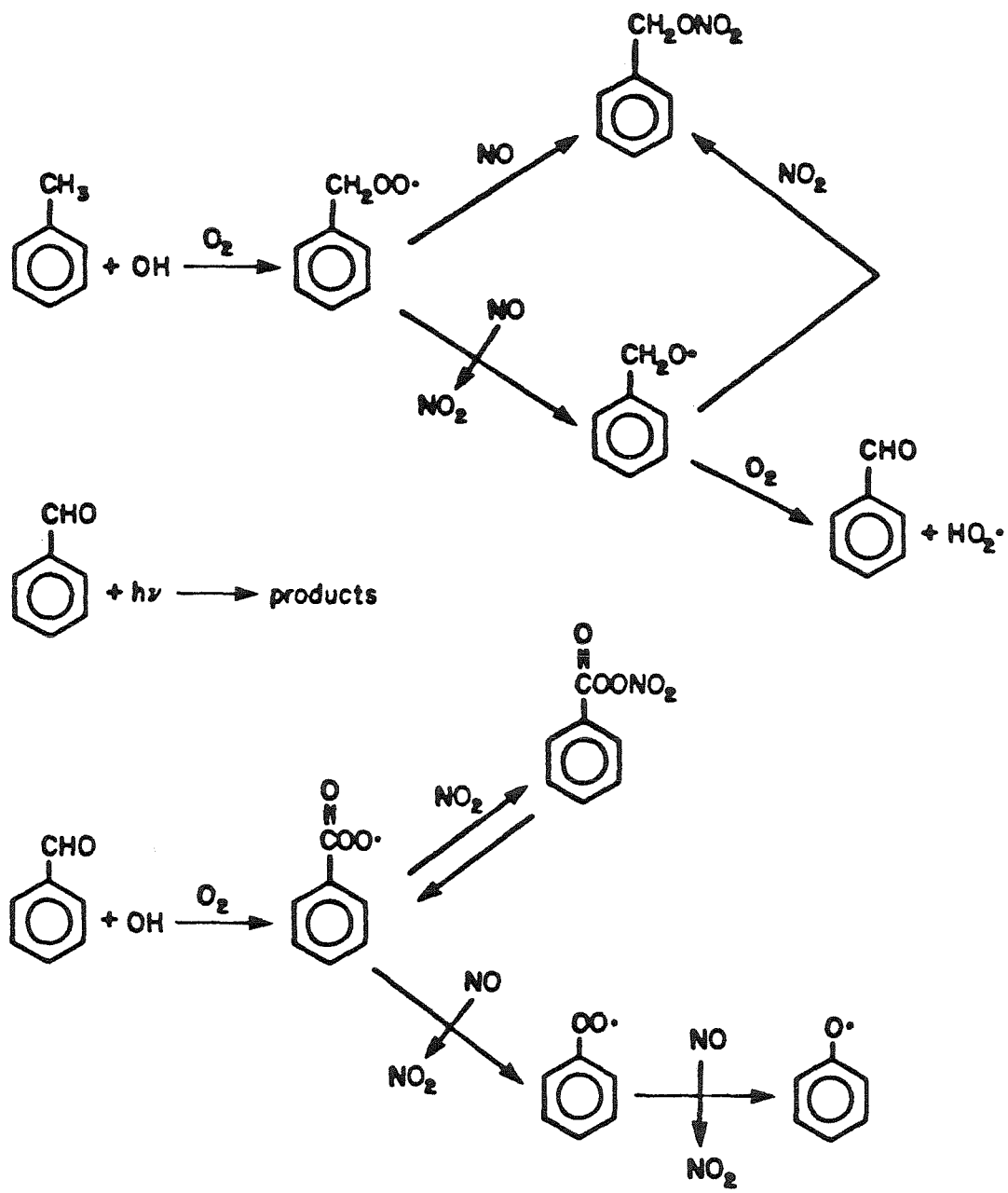

Figure 8. Toluene-OH abstraction pathway reaction mechanism

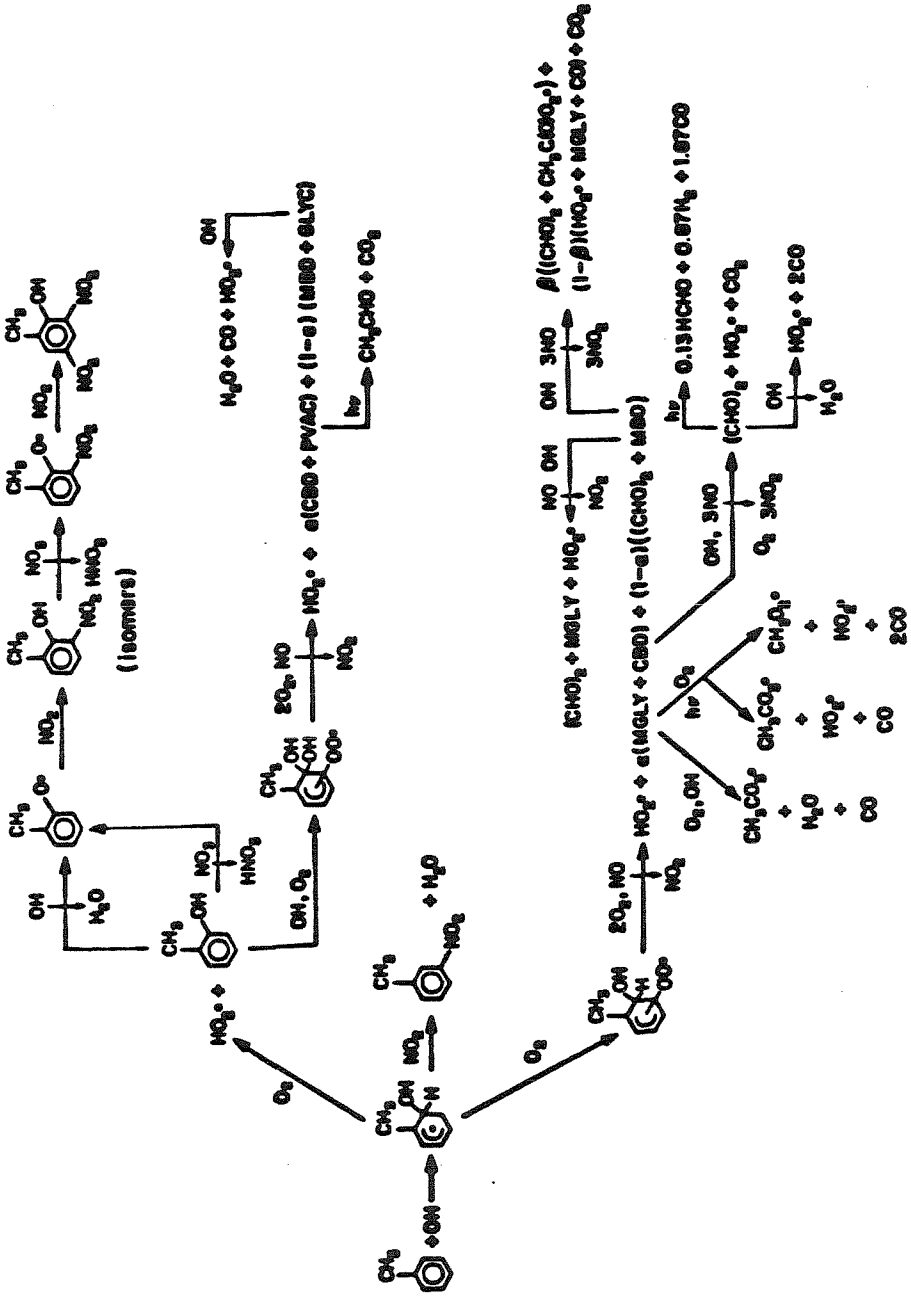

Figure 9. Proposed Toluene-OH addition pathway reaction mechanism (MGLY = methyl glyoxal, CBD = cis-2-butene-1,4-dial, MBD = 2-pentene-1,4-dial, PVAC = pyruvic acid)

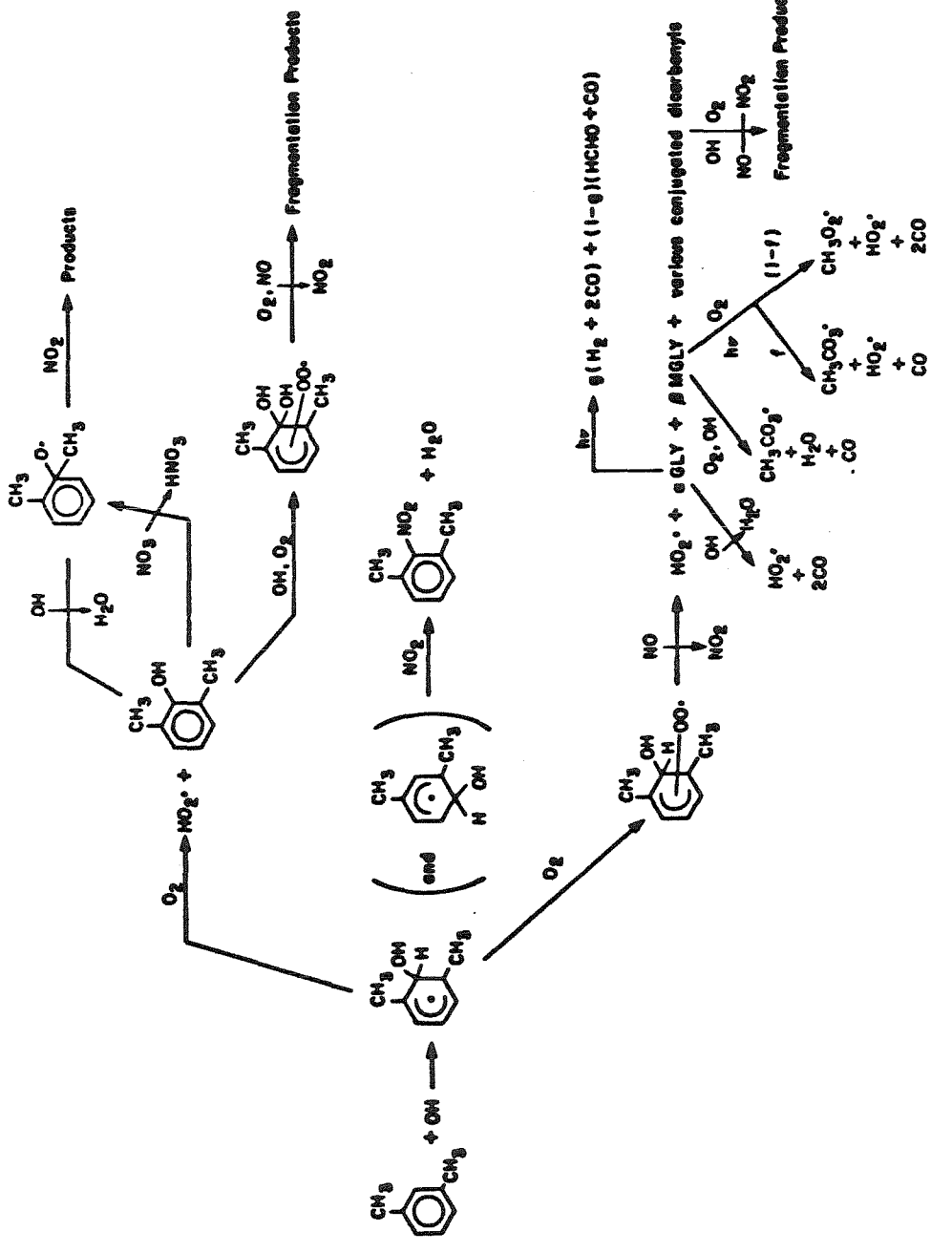

Figure 10. m-Xylene-OH addition pathway reaction mechanism
GLY = glyoxal
MGLY = methylglyoxal

0.1 for toluene

< 0.05 for benzene

0.2 for o-xylene

0.04 for m-xylene

0.07 for p-xylene .

In the ALW mechanism, the abstraction fraction is 0.15 for toluene, but 0 for benzene and xylene. ALW also assume no m-nitrotoluene formation and 25 percent cresol formation, and therefore 75 percent adduct formation. No distinction is made between benzene, toluene and xylene with regard to cresol formation. Thus, although benzene yields phenol and the xylenes form dimethyl phenol, the mechanism represents these species by o-cresol.

The initial step can therefore be written as

$$TOL + OH \xrightarrow{58} 0.15\ ARO_2 + 0.85[0.25(HO_2 + CRES) + 0.75\ ADD]$$

or, simplifying,

$$TOL + OH \xrightarrow{58} 0.15\ ARO_2 + 0.2(HO_2 + CRES) + 0.65\ ADD\ .$$

For benzene and the di- and tri-alkylbenzenes, the ALW mechanism employs

$$BEN + OH \xrightarrow{57} 0.25(CRES + HO_2) + 0.75\ ADD$$

$$XYL + OH \xrightarrow{59} 0.25(CRES + HO_2) + 0.75\ ADD\ .$$

In all three of the above reactions, the toluene-OH-O_2 adduct is represented by the single species ADD. Differences in the adducts

formed from toluene, benzene and xylene are incorporated into the reactions of the ADD species.

In the abstraction pathway it is assumed that 25 percent of the aromatic peroxy radicals add NO to form nitrates. (Recent evidence suggests that this percentage is probably substantially lower (Leone and Seinfeld, 1983a)). Thus, the ALW mechanism includes the reaction

$$ARO_2 + NO \xrightarrow{70} 0.75(NO_2 + HO_2 + BENA).$$

Benzaldehyde photolysis is represented as

$$BENA + h\nu \xrightarrow{74} \text{Products}$$

where non-radical products are assumed.

In the addition pathway, the adduct-NO reaction is represented by

$$ADD + NO \xrightarrow{60} 0.75(NO_2 + HO_2 + \underset{\text{cis-2-butene-1,4 dial}}{HC(O)CH=CHCHO} + g_1\underset{\text{glyoxal}}{(CHO)_2} + (1-g_1)\underset{\text{methyl glyoxal}}{CH_3C(O)CHO})$$

where the factor 0.75 arises from assuming that 25 percent of the adducts form nitrates that do not react further. The fraction g_1 is used to account for the different forms of the adducts formed from benzene, toluene, and xylene. It has been proposed that the dicarbonyls are produced as follows:

toluene $\longrightarrow$ methyl glyoxal (MGLY) + cis-2-butene-1,4-dial (DIAL)

benzene $\longrightarrow$ glyoxal (GLY) + DIAL

xylene $\longrightarrow$ 0.1 GLY + 0.9 MGLY + dicarbonyls similar to cis-2-butene-1,4-dial (DIAL).

Thus, the ALW mechanism employs

$$g_1 = \frac{k_2[BEN] + 0.1k_3[XYL]}{k_1[TOL] + k_2[BEN] + k_3[XYL]} .$$

The ALW mechanism uses o-cresol to represent the chemistry of all phenolic species (phenol, cresols, and dimethyl phenols). The reactions employed are

$$CRES + OH \xrightarrow{69} ADD2 \quad (OH \text{ addition})$$

$$ADD2 + NO \xrightarrow{70} 0.75 \quad (NO_2 + HO_2 + \text{cis-2-butene-1,4-dial})$$

$$CRES + NO_3 \xrightarrow{71} HNO_3 + PHO \quad (H\text{-atom abstraction})$$

where PHO represents the various oxy radicals, and 25 percent nitrate formation is assumed in reaction 70.

The ALW mechanism treats methyl glyoxal photolysis and the methyl glyoxal-OH reaction explicitly,

$$MGLY + h\nu \xrightarrow{68} ACO_3 + HO_2 + CO$$

$$MGLY + OH \xrightarrow{67} ACO_3 + CO .$$

The glyoxal reactions are represented by

$$GLY + OH \xrightarrow{65} HO_2 + 2CO$$

$$GLY + h\nu \xrightarrow{66} HCHO + CO .$$

The chemistry of the conjugated-γ-dicarbonyls is represented by

$$\text{DIAL} + \text{OH} \xrightarrow[O_2]{61} \text{EL}$$

$$\text{EL} + \text{NO} \underset{63}{\overset{62}{\rightleftharpoons}} \text{ELNO}_2$$

$$\text{EL} + \text{NO} \xrightarrow{64} 3\text{NO}_2 - 2\text{NO} + g_3(\text{HO}_2 + \text{GLY} + \text{CO}) + (1-g_3)(\text{ACO}_3 + \text{MGLY}).$$

The rationale behind this reaction sequence is as follows:

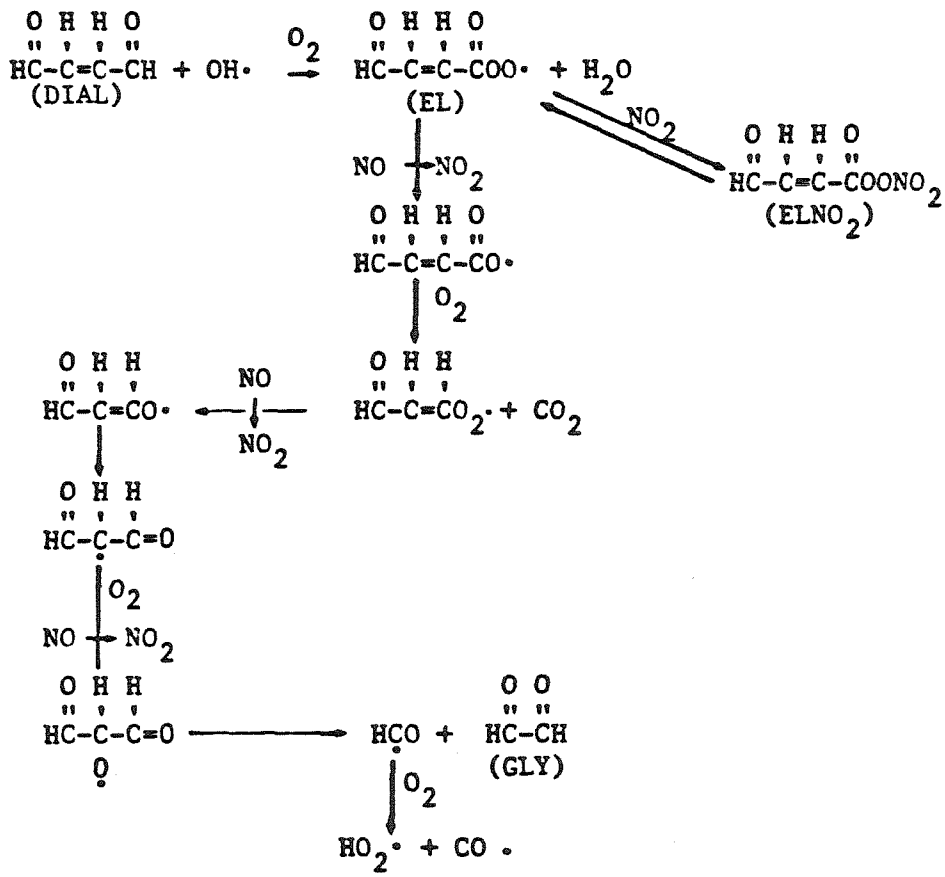

The predicted product yields from the three aromatic classes considered are:

$$\text{benzene} \longrightarrow \dot{H}CO + GLY$$

$$\text{toluene} \longrightarrow \dot{H}CO + GLY$$

$$\text{xylene} \longrightarrow \dot{H}CO + GLY,\ CH_3\dot{C}O + GLY,\ \text{and}\ \dot{H}CO + MGLY.$$

The estimated average composition of products from a lumped xylene species is

$$0.45\ ACO_3 + 0.65\ GLY + 0.55\ (HO_2 + CO) + 0.35\ MGLY$$

based on which the ALW mechanism assumes a product distribution of $0.5(ACO_3 + GLY + HO_2 + CO + MGLY)$. Consequently, g_3 is given by

$$g_3 = \frac{k_1[TOL] + k_2[BEN] + 0.5k_3[XYL]}{k_1[TOL] + k_2[BEN] + k_3[XYL]}.$$

3.4.4 Treatment of Aromatic Photooxidation by the KW Mechanism

The basic lumped aromatic unit in the KW mechanism is the species ARO which contains six carbon atoms and represents the benzene ring. For example, then, toluene = 1 ARO + 1 PAR, and xylene = 1 ARO + 2 PAR.

The initial reactions in the KW mechanism are

$$\underset{(6)}{ARO} + OH \xrightarrow[O_2]{57} HO_2 + \underset{(6)}{OPEN}$$

$$\xrightarrow[O_2]{56} \underset{(6)}{RARO} + H_2O$$

$$\underset{(6)}{RARO} + NO \xrightarrow[O_2]{58} NO_2 + \underset{(6)}{PHEN} + HO_2.$$

There is no aromatic-OH abstraction reaction shown here because the abstraction pathway is lumped with the single bonded carbon portion of this mechanism. In other words,

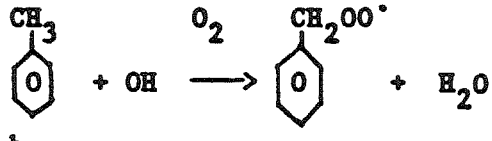

is represented by

$$PAR + OH \longrightarrow MEO_2 + H_2O \,.$$

Based on the rate constants used for the above steps, the percent of the addition pathway leading to ring cleavage is 65 percent. As in the ALW mechanism, m-nitrotoluene formation is not included.

There are two ring opening reactions employed in the KW mechanism,

$$\underset{(6)}{OPEN} + NO \xrightarrow{59} NO_2 + \underset{(3)}{DCRB} + \underset{(4)}{APRC} - \underset{(1)}{PAR}$$

$$\underset{(6)}{OPEN} + O_3 \xrightarrow{65} \underset{(3)}{DCRB} + \underset{(4)}{APRC} - \underset{(1)}{PAR}$$

where DCRB is a lumped species representing methyl glyoxal and biacetyl, and APRC represents the aromatic carbon portion that remains after the dicarbonyls are subtracted from the aromatic ring.

Reactions of the phenolic compounds are represented by

$$\underset{(6)}{PHEN} + OH \xrightarrow{68} \underset{(6)}{PHO} + H_2O \quad \text{(H-atom abstraction by OH)}$$

$$\underset{(6)}{\text{PHEN}} + NO_3 \longrightarrow \underset{(6)}{\text{PHO}} + HNO_3 \quad \text{(H-atom abstraction by } NO_3\text{)}$$

$$\underset{(6)}{\text{PHEN}} + OH \longrightarrow HO_2^{\cdot} + \underset{(4)}{\text{APRC}} + \underset{(1)}{\text{CARB}} + \underset{(1)}{\text{PAR}} \quad \text{(OH addition and ring opening)}$$

where PHO represents various oxy radicals.

The chemistry of methyl glyoxal and biacetyl is represented by the two reactions

$$\underset{(3)}{\text{DCRB}} + h\nu \xrightarrow{67} 0.5\ (\underset{(2)}{ACO_3} + \underset{(1)}{MEO_2}) + HO_2^{\cdot} + 1.5\ \underset{(1)}{CO}$$

$$\text{DCRB} + OH \xrightarrow{70} \underset{(2)}{ACO_3} + \underset{(1)}{CO}\ .$$

Glyoxal is represented as I CARB + 1 CO, based on the similarity between the glyoxal-OH reaction and the formaldehyde-OH reaction:

$$GLY + OH \longrightarrow HO_2 + 2CO$$

$$HCHO + OH \longrightarrow HO_2 + CO + H_2O\ .$$

The relation GLY = CARB + CO is then evident when reactions a and b are compared.

The chemistry of APRC is represented in the KW mechanism by the two reactions,

$$\underset{(4)}{\text{APRC}} \xrightarrow[O_2]{61} \underset{(1)}{\text{2CARB}} + \underset{(1)}{\text{2CO}}$$

$$\xrightarrow[O_2]{60} \underset{(3)}{\text{DCRB}} + \underset{(1)}{\text{CARB}} + \underset{(1)}{\text{CO}} - \underset{(1)}{\text{PAR}} .$$

3.4.5 Evaluation of the Aromatic Hydrocarbon Reactions in the Generalized Species Mechanisms

The Demerjian, MS and PW lumped mechanisms employ simple reaction schemes to describe the photooxidation of aromatic hydrocarbons. The success of these short reaction schemes depends on how well they simulate the radical formation processes occurring in aromatic systems, because it is the formation of radicals which brings about the conversion of NO to NO_2.

The MS mechanism relies on a single reaction step to describe the chemistry of aromatic compounds

$$\text{ARO} + \text{OH} \longrightarrow \text{RO}_2 + \text{RCHO} .$$

Because only one step is included, it must account for both the decay of the initial aromatic species and the formation of radicals. To perform both of these functions accurately, and in one step, is difficult. For example, in the aromatic portion of the ALW mechanism one or another radical species is formed at 20 different points.

The Demerjian mechanism includes three steps to describe atmospheric aromatic chemistry.

$$HC_4 + OH \longrightarrow R2O2 + 2HC3 + CO$$

$$R2O2 + NO \longrightarrow NO_2 + R2O$$

$$R2O + O_2 \longrightarrow HC3 + HO_2 + 2CO$$

where HC4 represents aromatics, HC3 aldehydes, R2O2 is a peroxy radical, and R2O is an alkoxy radical. The main difference between this mechanism and the MS mechanism is that the peroxy and alkoxy radicals formed from the aromatic hydrocarbons (R2O2 and R2O) are distinguished from those formed in the alkane and alkene portion of the mechanism.

PW use four steps in the aromatic portion of their mechanism,

$$HC3 + OH \longrightarrow BRO2OHHH$$

$$\longrightarrow HO_2$$

$$BRO2OHHH + NO \longrightarrow NO_2 + HO_2 + MGLY$$

$$MGLY + OH \longrightarrow H_2O + RCO_3 + CO$$

where BRO2OHHH represents the aromatic radical which undergoes ring scission, MGLY represents methylglyoxal, and RCO_3 the peroxyacyl radical. The advantages of this reaction scheme relative to the earlier two are that it accounts for both the cresol formation and ring opening pathways of the addition reaction and it includes the formation of the important α-dicarbonyl, methyl glyoxal.

It is clear that the aromatic portions of the Demerjian, MS and PW mechanisms require an updating to reflect information that has become available since their original formulation. Moreover, it

appears that such abbreviated aromatic mechanisms as currently exist in these three mechanisms are inconsistent with the level of detail accorded to the other aspects of the overall photochemistry, especially in light of the relative importance of aromatic compounds in the total atmospheric hydrocarbon mix.

CHAPTER 4

SPECIFICATION OF PHOTOLYSIS RATE CONSTANTS

One of the most important processes that influences the species concentration dynamics observed in the atmosphere or in smog chambers is the dissociation of photochemically active reactants. This chapter presents a comparison of approaches used in specifying the photolysis rate constants in the mechanisms. The objective of this work is to summarize, in one convenient location, all the documentation needed to reproduce the values used in the six mechanisms introduced in Chapter 2.

4.1 Methods for the Determination of Photolysis Rate Constants

In most photochemical mechanisms the photodissociation reactions are typically represented by steps of the form

$$X_i + h\nu \xrightarrow{k_i} \text{Products}$$

where X_i, denotes species i, and k_i the associated rate constant.* As shown in Table 20 there are substantial differences both in terms of the number of species and photolysis steps used in each of the mechanisms. In addition these disparities are compounded by significant variations in the magnitude of the rate constants.

---

* When discussing photolysis reactions, we will use the notation k_i to denote the rate constant for photolysis of species i. Ordinarily k_i refers to reaction number i.

TABLE 20

Summary of Photolysis Reaction Steps From Mechanism Survey

PHOTOLYSIS STEP[a]	REACTION MECHANISM[b] 1	2	3	4	5	6
$NO_2 + hv \longrightarrow NO + O(^3P)$	*	*	*	*	*	*
$HONO + hv \longrightarrow OH + NO$	*	*	*	*	*	*
$H_2O_2 + hv \longrightarrow 2OH$	*	*	*		*	*
$NO_3 + hv \longrightarrow NO_2 + O(^3P)$	*					*
$\longrightarrow NO + O_2$	*					*
$N_2O_5 + hv \longrightarrow 2NO_2 + O$						*
$O_3 + hv \longrightarrow O_2 + O(^3P)$	*		*		*	*
$\longrightarrow O(^1D) + O_2(^1g)$		*	*	*		*
$HCHO + hv \longrightarrow CO + H_2$	*	*	*		*	
$\longrightarrow HCO + H$	*				*	
$CH_3CHO + hv \longrightarrow CH_4 + CO$	*		*			
$\longrightarrow HCO + CH_3$	*		*			
$RCHO + hv \longrightarrow CO + a_1HO_2 + a_2RO_2$	*	*	*		*	*
$CARB + hv \longrightarrow b_1HO_2 + b_2MEO_2 + b_3CO + b_4X$				*		
$DCRB + hv \longrightarrow c_1HO_2 + c_2MEO_2 + c_3ACO_2 + c_4CO + X$				*		
$(CHO)_2 + hv \longrightarrow HCHO + CO$	*					
$CH_3COCH_3 + hv \longrightarrow CH_3CO_3 + C_2H_5O_2$	*					
$CH_3COCHO + hv \longrightarrow HO_2 + RCO_3 + CO$	*					*
$CH_3COC_2H_5 + hv \longrightarrow CH_3CO_3 + C_2H_5O_2$	*					
$RONO + hv \longrightarrow NO + RO$					*	

Footnotes for Table 20

(a) Only the initial products of the photolysis steps are shown in the above Table. Many of the mechanisms combine elementary reaction steps and eliminate product species that have very short lives.

Footnotes for Table 20 (Continued)

(b) Reaction Mechanisms

1	Atkinson et al. (1982)	-	Table 22
2	Demerjian (1982)	-	Table 23
3	Dodge (1977)	-	Table 25
4	Killus and Whitten (1982a)	-	Table 27
5	McRae and Seinfeld (1983)	-	Table 28
6	Penner and Walton (1982)	-	Table 29

How closely the kinetics of the photodissociation step can reproduce the concentration dynamics of X_i is closely tied to the accuracy with which the rate constant k_i can be specified. Depending on the particular application, one of two basic methods is usually used to establish the photolysis rates. The most direct way is to measure rates with chemical actinometers. In this approach the species of interest is isolated and allowed to photolyze under controlled conditions in either a flow or batch reactor. From a knowledge of the initial concentration, the exposure time and the resulting product distribution the photolysis rate can be calculated for the particular radiation conditions.

In smog chamber studies the NO_2 photolysis is often determined by using a quartz flow reactor in which a continuous stream of NO_2 is photolyzed in a co-flowing stream of nitrogen (Pitts et al. 1976). By monitoring the NO concentration level in the effluent it is possible to determine the NO_2 photolysis rate. Chemical actinometers have also been used to determine NO_2 photolysis rates under atmospheric conditions (Zafonte et al., 1977 and Stedman et al., 1977). These experiments have usually only been carried out for limited time periods, fortunately, these investigators correlated their results against concurrent measurements of the solar radiation in the ultraviolet (uv) portion of the spectrum. Radiometric data were obtained with Eppley ultraviolet pyranometers that have a full bandwidth sensitivity of 295-385 nm, a wavelength interval relevant to many photochemical reactions. Provided that the spectral distribution of the radiation remains

constant, the results of the correlations provide a direct means of determining the NO_2 photolysis rate from a knowledge of solar radiation measurements. A similar methodology has been employed by Pitts et al. (1976) to report smog chamber photolysis rates. While chemical actinometry offers the most direct means for determining rate constants, the technique has unfortunately only been applied to determine the photolysis rates of a few species, principally NO_2 and HCHO.

In smog chambers as well as in atmospheric applications photolysis rates are needed for a much larger number of species. The method that is usually applied in these circumstances is to calculate the rates from a knowledge of the spectral distribution of the photolyzing radiation and the properties of the molecule itself. If the concentration of the species X_i is low enough that it does not significantly affect the transfer of radiation, then photolytic rate constant k_i can be calculated from

$$k_i = \sum_{\lambda = 290\ nm}^{800\ nm} \sigma_i \phi_i\ I \qquad (4.1)$$

where $\sigma_i(\lambda)$ (cm^2) is the molecular absorption cross section for species i, $\phi_i(\lambda)$ is the quantum yield, and I is the actinic irradiance (photons cm^{-2}-s^{-1}), the radiometric energy incident on single molecules and, as conventionally defined, applies to ultraviolet wavelengths. In addition to wavelength, σ_i and ϕ_i depend on temperature. The actinic irradiance is typically obtained from either mathematical models of atmospheric radiative transfer or direct monochrometer measurements of the spectral distribution. Demerjian et al. (1980), for example, have

published the data needed to evaluate (4.1) for a range of species likely to be encountered in atmospheric modeling applications.

4.2 Specification of the Actinic Irradiance

Since the wavelength-dependent absorption cross sections and quantum yields are fixed, the variation of the species photolysis rate constant in space and time depends primarily on the variation of actinic flux. This parameter is very difficult to estimate from customary solar radiation measurements, in particular, those made with broad band 180^{o} pyroheliometers. As a result most photolysis rate constants are based on theoretical calculations of the solar flux in the spectral band of interest.

Compared to the total solar spectrum, the wavelength interval of interest in photochemical modeling applications is quite small ($290 \leq \lambda \leq 800$ nm), since solar radiation of wavelengths less than 290 nm does not reach the troposphere. The upper limit for the summation in (4.1) is set either by the reduction in species cross section or quantum yield as a function of increasing wavelength.

Many previous modeling studies have employed the photolysis rate tabulations of Leighton (1961). His results were based on a radiative transfer calculation which, by necessity, employed many simplifying assumptions. The availability of more sophisticated radiative transfer models and more recent measurements of the upper atmospheric properties has led to considerable refinement in the calculation of solar fluxes. Penner and Walton (1982) used the model of Luther and Gelinas (1976) as

a basis for determining ultraviolet fluxes. In the Atkinson et al. (1982), Demerjian (1982), Killus and Whitten (1982a) and McRae and Seinfeld (1983) mechanisms the actinic irradiance is based on Demerjian et al. (1980). The results reported by Demerjian et al. (1980) are based on the calculations by Peterson (1976) using the computer program developed by Braslau and Dave (1973ab), which includes aerosol scattering and absorption, Rayleigh scattering, and ozone absorption. The atmospheric state assumed in the model corresponds to annual average U.S. urban conditions, corresponding to a cloud-free atmosphere over a typical urban environment. The actinic irradiance, at a particular time and elevation, is usually specified as a function of the solar zenith angle Z. For example, the zenith angle variation of the NO_2 photolysis rate, calculated using the methodology of Demerjian et al. (1980), is shown in Table 21.

4.3 Scaling of Photolysis Rates in Atmospheric Applications

Most theoretical calculations of the photolysis rate constants assume "clear sky" conditions. Besides its diurnal variation, the actinic flux is sensitive to changes in surface albedo, amount of O_3 in the air column, cloudiness, surface elevation, atmospheric aerosol concentrations, and altitude above the surface (Peterson et al., 1977). In most cases the photolysis rates used in photochemical mechanisms have been calculated using ground level actinic irradiance data. Within the lowest 5-10 km of the atmosphere the actinic flux increases with elevation which in turn leads to higher photolysis rates. The results of Demerjian et al. (1980) and Peterson et al. (1977), for NO_2

TABLE 21

Nitrogen Dioxide Photolysis Rate as a Function of Zenith Angle

ZENITH ANGLE (Z^{o})	PHOTOLYSIS RATE (min^{-1})	RATE RELATIVE TO $Z=0^{o}$
0	0.533	1.000
10	0.529	0.992
20	0.515	0.966
30	0.493	0.925
40	0.457	0.857
50	0.403	0.756
60	0.329	0.617
70	0.214	0.402
78	0.105	0.197
86	0.023	0.043
90	0.000	0.000

Source: Demerjian et al. (1980)

and HCHO show a significant increase with height. For example, at an elevation of 0.98 km the photolysis rate for these species, at a zenith angle of 0^{o}, is approximately 20% higher than the corresponding ground level value. This suggests that the photolysis rates need to be adjusted if the region being studied is at a high elevation.

One additional problem that is encountered in practical applications is how to modify the calculated results when there is a perturbation to the basic atmospheric state employed in the radiative transfer calculations. Increased aerosol loadings or the presence of clouds would require scaling of the photodissociation rates. For example, Penner and Walton (1982) adjust their photolysis rates to account for the presence of clouds or aerosols in the surface layer. When only broad-band measurements of solar radiation are available, the correction of the calculated values can be based on the ratio of pyranometer observations to the theoretical clear-sky transmission. One important point to note is that scalings based on total solar fluxes may not provide a good representation of the variation in the ultraviolet (uv) flux density. The reason for this is that the total solar fluxes are not strongly influenced by cloud and aerosols. On the other hand, the ultraviolet fluxes are markedly attenuated by any increase in scattering. Despite these caveats a crude estimate of the NO_2 photolysis rate constant can be developed by scaling the calculated value of k_1 against the measured total solar radiation flux TSR. By combining routine monitoring data, collected in Los Angeles, with the theoretical results of Demerjian et al. (1980) for the same location, the relationship between

the photolysis rate and the total flux is given by

$$k_1 \ (min^{-1}) = 0.4 \ TSR \ (cal\text{-}cm^{-2}\text{-}min^{-1}) \ . \qquad (4.2)$$

In situations where ultraviolet pyranometer data are available, another approach is possible. As described previously, Zafonte et al. (1977) and Stedman et al. (1977) plotted their NO_2 photodissociation rates against measurements of solar radiation in the ultraviolet portion of the spectrum. Their results provide a direct means for scaling calculated photolysis rates. The scale factor applied to the theoretical estimates is simply the ratio of the measured and calculated actinic irradiances. Schere and Demerjian (1977) used ultraviolet measurements and the calculated clear solar fluxes to scale the rate constants, with the ultraviolet scaled photolysis rates closely matching the results obtained using a chemical actinometer.

Photochemical smog production depends on ultraviolet radiation differently at the short (300-330 nm) wavelength region than at the long (360-400 nm) wavelength part of the ultraviolet. The smog production rate is more sensitive to the shorter wavelengths (Winer et al., 1979). Although NO_2 photolysis has been the measure of smog potential, measurements using UV-B filters which characterize only the shorter wavelengths would be useful. This part of the spectrum (239-330 nm) characterizes aldehyde photolysis to which smog production is sensitive.

4.4 Specification of Mechanism Photolysis Rate Constants

In atmospheric modeling applications the photolysis rates are usually established by evaluating the summation (4.1) for each of the species of interest. One of the first applications of this method was the pioneering work of Leighton (1961). More recently, Gelinas et al. (1974), Schere and Demerjian (1977) and Demerjian et al. (1980) have developed computer programs that enable the direct calculation of the photolysis rates given the actinic irradiance, quantum yields and absorption cross sections. While the availability of these algorithms considerably reduces the computational burden, there has, unfortunately, been no attempt at standardization of the necessary input information. The objective of this section is to document the procedures and literature sources used in developing the rate constants for each of the mechanisms.

In the current version of the Atkinson et al. (1982) mechanism, the species absorption cross sections and quantum yield data are based on the results from the review of Atkinson and Lloyd (1983). The actinic irradiance data of Demerjian et al. (1980) were used by Lurmann (1982) to calculate the photolysis rates shown in Table 22. Each rate has been scaled relative to the NO_2 value to facilitate comparisons of these rates among different reaction mechanisms. Since the NO_2 rates used in the Atkinson et al. (1982) mechanism are identical to those of Demerjian et al. (1980), the absolute magnitude of the NO_2 photolysis rate, as a function of the zenith angle, can be obtained from Table 21. Diurnal variations in the photolysis rates of most species can be

TABLE 22

Photolysis Reaction Steps in the Atkinson et al. (1982) Photochemical Reaction Mechanism[a]

REACTION NUMBER	PHOTODISSOCIATION STEP[(b)]	PHOTOLYSIS RATE RELATIVE TO NO_2[(c)]
1	$NO_2 + h\nu \longrightarrow NO + O(^3P)$	1.0
3	$O_3 + h\nu \longrightarrow 2OH$	4.20×10^{-8}
6	$HONO + h\nu \longrightarrow OH + NO$	1.70×10^{-1}
11	$H_2O_2 + h\nu \longrightarrow 2OH$	7.10×10^{-4}
18	$NO_3 + h\nu \longrightarrow 0.3NO + 0.7NO_2 + 0.7O_3$	1.55×10^{1}
21	$HCHO + h\nu \longrightarrow 2HO_2 + CO$	3.50×10^{-3}
22	$HCHO + h\nu \longrightarrow CO + H_2$	3.40×10^{-3}
24	$CH_3CHO + h\nu \longrightarrow CH_3O_2 + HO_2 + CO$	8.40×10^{-4}
39	$RCHO + h\nu \longrightarrow C_2H_5O_2 + CO + HO_2$	8.40×10^{-4}
42	$MEK + h\nu \longrightarrow CH_3CO_3 + C_2H_5O_2$	1.70×10^{-3}
43	$CH_3COCH_3 + h\nu \longrightarrow CH_3CO_3 + CH_3O_2$	1.70×10^{-4}
67	$(CHO)_2 + h\nu \longrightarrow HCHO + CO$	1.00×10^{-10}
69	$CH_3COCHO + h\nu \longrightarrow CH_3CO_3 + HO_2 + CO$	1.50×10^{-1}
75	$ARCHO + h\nu \longrightarrow$ Products	4.50×10^{-3}

Footnotes for Table 22

(a) Mechanism documentation: Atkinson et al.(1979,1982), Carter et al.(1979) The particular values selected for the species absorption cross sections and quantum yields are described in Atkinson and Lloyd (1983).

(b) RCHO - Higher aldehydes $\geq C_3$
MEK - Methyl ethyl ketone ($CH_3COC_2H_5$)
ARCHO - Benzaldehyde
Products - Non reactive reaction products
$(CHO)_2$ - Glyoxal

Footnotes for Table 22 (Continued)

(c) The photolysis rates have been scaled relative to the NO_2 value; however, for the species O_3, HCHO and CH_3CHO the scaling is a function of the zenith angle. Table 23 gives the scale parameters for these species.

determined by applying the scale factors to the corresponding NO_2 rate. For the species O_3, HCHO and CH_3CHO, the scaling, as shown in Table 23, is a function of the zenith angle.

Killus and Whitten (1982a) and McRae and Seinfeld (1983) primarily base their mechanism photolysis rates on the work of Demerjian et al. (1980). Since this is perhaps the most widely used procedure for calculating the diurnal variations in photolysis rates it is useful to describe the underlying basis of the method. Demerjian et al. (1980) carried out an extensive literature survey and collected the data needed to calculate the photolysis rates for the following eleven reactions of interest in atmospheric modeling applications.

$$NO_2 + h\nu \longrightarrow NO + O(^3P)$$

$$HONO + h\nu \longrightarrow NO + OH$$

$$HNO_3 + h\nu \longrightarrow OH + NO_2$$

$$O_3 + h\nu \longrightarrow O_2 + O(^3P)$$

$$O_3 + h\nu \longrightarrow O_2 + O(^1D)$$

$$O_3 + h\nu \longrightarrow O + O_2$$

$$HCHO + h\nu \longrightarrow 2HO_2 + CO$$

$$HCHO + h\nu \longrightarrow H_2 + CO$$

$$H_2O_2 + h\nu \longrightarrow 2OH$$

$$CH_3CHO + h\nu \longrightarrow CH_3 + HO_2 + CO$$

$$CH_3CHO + h\nu \longrightarrow CH_4 + CO$$

For each species and reaction pathway they tabulated the absorption cross sections and quantum yields in 10 nm wavelength increments over the range 290 to 800 nm. The actinic flux used by Demerjian et al.

TABLE 23

Photolysis Scaling Ratios Relative to NO_2 Rate for the Atkinson et al. (1982) Photochemical Reaction Mechanism[a]

ZENITH ANGLE (°)	PHOTOLYSIS SCALING RATIOS RELATIVE TO NO_2			
	$O_3+H_2O+hv->$	$HCHO+hv -> H_2$	$HCHO+hv -> H^\cdot$	$CH_3CHO+hv->HCO^\cdot$
0	4.20×10^{-8}	3.5×10^{-3}	3.4×10^{-3}	8.4×10^{-4}
10	4.10×10^{-8}	3.5×10^{-3}	3.4×10^{-3}	8.3×10^{-4}
20	3.80×10^{-8}	3.4×10^{-3}	3.4×10^{-3}	8.0×10^{-4}
30	3.30×10^{-8}	3.3×10^{-3}	3.3×10^{-3}	7.4×10^{-4}
40	2.60×10^{-8}	3.3×10^{-3}	3.2×10^{-3}	6.7×10^{-4}
50	1.90×10^{-8}	2.8×10^{-3}	3.0×10^{-3}	5.6×10^{-4}
60	1.20×10^{-8}	2.4×10^{-3}	2.8×10^{-3}	4.4×10^{-4}
70	6.20×10^{-9}	1.9×10^{-3}	2.5×10^{-3}	3.1×10^{-4}
78	3.00×10^{-9}	1.6×10^{-3}	2.2×10^{-3}	2.1×10^{-4}
84	1.30×10^{-9}	1.4×10^{-3}	2.2×10^{-3}	1.3×10^{-4}

Footnotes for Table 23

(a) The scaling ratios are based on modifications, by Lurmann (1982), of the zenith angle variations in photolysis photolysis rates presented in Demerjian et al. (1980). Given an NO_2 photolysis rate and the corresponding zenith angle this table can be used to establish the O_3, HCHO and CH_3CHO rates.

(1980) was obtained by solving a modified form of the numerical model developed by Braslau and Dave (1973ab). This information together with the species data was then used to determine the photolysis rates as a function of zenith angle and elevation above the surface.

The photolysis reaction steps in the Killus and Whitten (1982a), McRae and Seinfeld (1983), Demerjian (1982), and Dodge (1977) mechanisms are given in Tables 24 -27.

At the time of the publication of Demerjian et al. (1980) there were substantial uncertainties associated with the quantum yields of acetaldehyde (CH_3CHO) and to a certain extent those of formaldehyde (HCHO). The most recent acetaldehyde rates, which are based on the recent quantum yield determinations of Horowitz and Calvert (1982), are a factor of two lower than the old values. In some cases, particularly for nitrous acid (HONO), hydrogen peroxide H_2O_2, and the aldehydes there are almost factors of three difference between older and newer rates. The current versions of the Killus and Whitten (1982a) and McRae and Seinfeld (1983) mechanisms, shown in Tables 26-28, have not been modified to reflect the most recent determinations of the acetaldehyde quantum yields.

Penner and Walton (1982) employ an approach similar to Demerjian et al. (1980), see Table 28, and base their species data on: NO_2-Hudson and Reed (1979), O_3-Hudson and Reed (1979), H_2O_2-Molina et al. (1977), NO_3-Magnotta and Johnston (1980), N_2O_5-Hudson and Reed (1979), HCHO-Bass et al. (1980), with quantum yields of Moortgat et al. (1980),

TABLE 24

Photolysis Reaction Steps in the Killus and Whitten (1982a) Photochemical Reaction Mechanism[a]

REACTION NUMBER	PHOTODISSOCIATION STEP[b]	PHOTOLYSIS RATE RELATIVE TO NO_2[c]
1	$NO_2 + hv \longrightarrow NO + O(^3P)$	1.0
37	$CARB + hv \longrightarrow CO + H_2$	1.00×10^{-3}
38	$CARB + hv \xrightarrow{O_2} 2/3(2HO_2 + CO) + 1/3(2MEO_2 + CO + 2X)$	2.00×10^{-3}
67	$DCRB + hv \xrightarrow{O_2} 1/2(HO_2 + ACO_3 + CO) + 1/2(MEO_2 + HO_2 + CO)$	4.00×10^{-2}
71[d]	$HONO + hv \longrightarrow OH + NO$	1.80×10^{-1}
73	$O_3 + hv \longrightarrow O(^1D)$	1.00×10^{-3}

Footnotes for Table 24

(a) Mechanism documentation: Killus and Whitten (1982ab) and Whitten et al. (1980ab). There is little or no documentation of the sources used to establish the photolysis rate constants. In published applications of the mechanism, the rates appear to have been adjusted to match the experimental conditions.

(b) CARB - Denotes carbonyl compounds such as aldehydes and ketones
DCRB - Highly photolytic alpha-dicarbonyl compounds
MEO_2 - Surrogate for alkylperoxyl radical
X - Compound introduced to maintain carbon balance

(c) The scaling ratios reported above are based on Table 3 of Killus and Whitten (1982a). The diurnal variations in photolysis rates, of most species, are based on the NO_2 value. The carbonyl (CARB) rates are determined from Demerjian et al.(1980) HCHO values using the formulae $k_{37} = 1/2\ k(HCHO+hv \rightarrow CO+H_2)$ and $k_{38} = 2/3\ k(HCHO+hv \rightarrow HCO+H)$ (Killus, 1982a). Using Demerjian et al.(1980) $k_{37}/k_1 = K_{38}/k_1 = 2.8 \times 10^{-3}$.

TABLE 25

Photolysis Reaction Steps in the McRae and Seinfeld (1983) Photochemical Reaction Mechanism[a]

REACTION NUMBER	PHOTODISSOCIATION STEP[b]	PHOTOLYSIS RATE RELATIVE TO NO_2[c]
1	$NO_2 + h\nu \longrightarrow NO + O(^3P)$	1.00
10	$HONO + h\nu \longrightarrow OH + NO$	1.9×10^{-1}
20	$O_3 + h\nu \longrightarrow O(^3P) + O_2$	6.46×10^{-2}
21	$HCHO + h\nu \longrightarrow 2HO_2 + CO$	5.59×10^{-3}
22	$HCHO + h\nu \longrightarrow H_2 + CO$	9.31×10^{-3}
25	$RCHO + h\nu \longrightarrow RO_2 + HO_2 + CO$	5.12×10^{-3}
35[d]	$RONO + h\nu \longrightarrow NO + RO$	2.20×10^{-1}
51	$H_2O_2 + h\nu \longrightarrow 2OH$	3.17×10^{-3}

Footnotes for Table 25

(a) Mechanism documentation: Falls and Seinfeld (1978), Falls et al. (1979), McRae et al. (1982ab) and McRae and Seinfeld (1983). The quantum yield and absorption cross sections used to calculate the photolysis rates are based on Schere and Demerjian (1977) and Demerjian et al. (1980).

(b) RCHO - Higher aldehydes
RONO - Alkyl nitrite
RO - Alkoxyl radical
RO_2 - Alkylperoxy radical

(c) The rates have been scaled relative to the NO_2 photolysis step corresponding to a zenith angle $z=0^\circ$. Diurnal variations are specified using the procedures described in either McRae et al. (1982b) or Demerjian et al. (1980).

(d) The RONO rate has been set to be 0.22 of the value for NO_2.

TABLE 26

Photolysis Reaction Steps in the Demerjian (1982) Photochemical Reaction Mechanism[a]

REACTION NUMBER	PHOTODISSOCIATION STEP[b]	PHOTOLYSIS RATE RELATIVE TO NO_2[c]
1	$NO_2 + hv \longrightarrow NO + O(^3P)$	1.0
5	$O_3 + hv \longrightarrow O(^1D) + O_2$	5.13×10^{-3}
12	$HONO + hv \longrightarrow OH + NO$	1.80×10^{-1}
25	$H_2O_2 + hv \longrightarrow 2OH$	1.01×10^{-3}
30	$HC_3 + hv \longrightarrow 0.5RO_2 + 1.5HO_2 + CO$	2.34×10^{-3}
44	$HC_3 + hv \longrightarrow CO$	2.81×10^{-3}

Footnotes for Table 26

(a) Mechanism documentation: Demerjian (1982) and Schere (1983). The absorption cross sections and quantum yields for the species NO_2, O_3, HONO and H_2O_2 are based on the tabulations given in Demerjian et al. (1980). The photolysis rate constants for the aldehyde class (HC3) are based on a series of correction formulae developed by Schere (1983) to account for more recent quantum yield data obtained by Horowitz and Calvert (1982). The corrections are given by

$$HC3 + hv \xrightarrow{30} k_{30} = 0.75\, k(A) + 0.25\, k(C)$$

$$HC3 + hv \xrightarrow{44} k_{44} = 0.75\, k(B)$$

where

$k(A) = 0.714\, k(HCHO + hv \longrightarrow H + HCO)$
$k(B) = 0.676\, k(HCHO + hv \longrightarrow H_2 + CO)$
$K(C) = 0.444\, k(CH_3CHO + hv \longrightarrow CH_3 + HCO)$ (Lower Limit)

The values for k(HCHO) and $k(CH_3CHO)$ are from Demerjian et al. (1980).

(b) HC_3 - Aldehydes
RO_2 - alkylperoxy radical

(c) The photolysis rates have been scaled relative to the NO_2 value at a fixed zenith angle of $z=0^o$.

TABLE 27

Photolysis Reaction Steps in the Dodge (1977) Photochemical Reaction Mechanism[a]

REACTION NUMBER	PHOTODISSOCIATION STEP[b]	PHOTOLYSIS RATE RELATIVE TO NO_2[c]
1	$NO_2 + h\nu \longrightarrow NO + O(^3P)$	1.0
12	$HONO + h\nu \longrightarrow OH + NO$	5.62×10^{-2}
17	$H_2O_2 + h\nu \longrightarrow 2OH$	2.82×10^{-3}
18	$O_3 + h\nu \longrightarrow O(^1D)$	7.28×10^{-3}
19	$O_3 + h\nu \longrightarrow O(^3P)$	5.72×10^{-2}
49	$HCHO + h\nu \longrightarrow$ Products	9.68×10^{-3}
50	$HCHO + h\nu \longrightarrow 2HO_2$	3.70×10^{-3}
52	$ALD2 + h\nu \longrightarrow$ Products	1.56×10^{-5}
53	$ALD2 + h\nu \longrightarrow MEO_2 + HO_2$	7.35×10^{-4}

Footnotes for Table 27

(a) Mechanism Documentation: Dodge (1977). The absorption cross-section and quantum yield data used to develop the photolysis rates for this mechanism are based on the compilations of Schere and Demerjian (1977). The following photolysis reaction steps have fixed rate constants.

55	ALD3 + hv ⟶ Products	6.0×10^{-5}	min^{-1}
56	ALD3 + hv ⟶ C2O2 + HO2	2.5×10^{-3}	min^{-1}
58	ALD4 + hv ⟶ Products	6.0×10^{-5}	min^{-1}
59	ALD4 + hv ⟶ C3O2 + HO2	1.9×10^{-3}	min^{-1}

(b) C2O2 - $CH_3CH_2O_2$
C3O2 - $CH_3CH_2CH_2O_2$
ALD2 - CH_3CHO
ALD3 - CH_3CH_2CHO
ALD4 - $CH_3CH_2CH_2CHO$

(c) The photolysis rates have been scaled relative to the NO_2 value at a fixed zenith angle of $z=0^o$.

TABLE 28

Photolysis Reaction Steps in the Penner and Walton (1982) Photochemical Reaction Mechanism[a]

REACTION NUMBER	PHOTODISSOCIATION STEP[b]	PHOTOLYSIS RATE RELATIVE TO NO_2[c]
J1	$NO_2 + h\nu \longrightarrow NO + O(^3P)$	1.0
J2	$O_3 + h\nu \longrightarrow O(^3P) + O_2$	5.19×10^{-2}
J3[d]	$O_3 + h\nu \longrightarrow O_2 + 2OH$	4.77×10^{-2}
J4	$HONO + h\nu \longrightarrow OH + NO$	2.26×10^{-1}
J5	$H_2O_2 + h\nu \longrightarrow 2OH$	1.41×10^{-3}
J6	$NO_3 + h\nu \longrightarrow NO_2 + O(^3P)$	1.56×10^{1}
J7	$NO_3 + h\nu \longrightarrow NO + O_2$	1.9
J8	$N_2O_5 + h\nu \longrightarrow NO_2 + NO_2 + O$	4.64×10^{-6}
J9[e]	$HC_4 + h\nu \longrightarrow CO + H_2$	1.72×10^{-3}
J10	$HC_4 + h\nu \longrightarrow CO + 2HO_2$	1.56×10^{-3}
J11[f]	$HC_4 + h\nu \longrightarrow CO + RO_2 + HO_2$	1.56×10^{-3}
J12[g]	$M\text{-}GLY + h\nu \longrightarrow HO_2 + RCO_3 + CO$	5.05×10^{-2}

Footnotes for Table 28

(a) Mechanism documentation: Gelinas and Skewes-Cox (1975), MacCracken and Sauter eds. (1975), Penner and Walton (1982).
The absorption cross-section and quantum yield data used to calculate the photolysis rate are based on the values reported in the survey of Hudson and Reed (1979). The actinic irradiance values have been calculated using the model described in Luther and Gelinas (1976) using an assumption of "clear" sky conditions. This results in higher NO_2 values than Demerjian et al. (1980). For example, the NO_2 rate corresponding to a zenith angle $Z=0^o$ is 0.694 min^{-1}. In atmospheric modeling applications this rate must be corrected for the presence of clouds and aerosols. In the application of the mechanism, the clear sky rate is multiplied by a cloud factor that usually ranges from 0.6 to 0.9. As such, it then describes photolysis in the middle of the one-layer model, e.g., about 200 m in San Francisco at mid-day.

Footnotes for Table 28 (Continued)

(b) HC_4 - Aldehydes and ketones
M-GLY - Methylglyoxal (CH_3COCHO)
RO_2 - Alkylperoxy radical
RCO_3 - Peroxyacyl radical

(c) The rates have been scaled relative to the NO_2 photolysis step at a zenith angle $Z=0^o$. The variation of the photolysis rates for other zenith angles is given in Table 30.

(d) This value is multiplied by $\frac{[H_2O]}{[M]} \times \frac{2.3 \times 10^{-10}}{3.05 \times 10^{-11}}$.

(e) The photolysis rates J9 and J10 for aldehydes and ketones (HC4) are equal to one-half of the values for HCHO shown in Table 29.

(f) The photolysis rate J11 is assumed to be 1/2 of the rate for the step HCHO + hv —> HCO + H$^\cdot$.

(g) The methylgloyxal photolysis rate has been set to be 0.045 $k(NO_2)$ on the basis of Darnall et al. (1979).

CH_3COCHO-5% of NO_2 rate and the actinic fluxes from Gelinas et al. (1974) and Luther and Gelinas (1976). Table 29 presents the zenith angle dependence of the photolysis rates used by Penner and Walton (1982).

A comparison of the photolysis rates used in each of the mechanisms is shown in Table 30. We note that, even for common reactions, there are major differences in the rates. For further details about currently accepted values for σ_i and ϕ_i the reader is referred to the extensive evaluated reviews of Hudson and Reed (1979), Baulch et al. (1980,1982), WMO (1981), DeMore et al. (1982) and Atkinson and Lloyd (1983).

4.5 Uncertainty Estimates for the Photolysis Rates

There are two basic sources of uncertainty that arise during the calculation of photolysis rates needed for atmospheric modeling applications. One, which is common to all species and reaction mechanisms, is the specification of the actinic irradiance. Most of the mechanisms considered in this study establish the actinic flux from numerical solutions of mathematical models that describe the radiative transfer processes in the atmosphere. Many assumptions need to be made in order to specify the input data for these models, including the surface albedo and the the vertical distribution of aerosols and gases in the upper atmospheres. Depending on the choice of input data, this choice can lead to a $\pm$ 20% difference in the calculated fluxes. Similar levels of uncertainty are involved if the photolysis rates are based on ambient measurements of the ultraviolet flux.

TABLE 29

Calculated Ground Level Values of the Photolysis Rate Constants of Key Species as a Function of the Solar Zenith Angle for the Penner and Walton (1982) Photochemical Reaction Mechanism[a]

ZENITH ANGLE	PHOTOLYSIS RATE CONSTANTS (min^{-1})[b]							
	NO_2	HCHO->H	HCHO->H_2	HONO	H_2O_2	CH_3CHO	O_3->$O(^3P)$	O_3->$O(^1D)$
0	0.694	2.16×10^{-3}	2.38×10^{-3}	0.157	9.82×10^{-4}	2.16×10^{-3}	3.60×10^{-2}	3.67×10^{-3}
10	0.687	2.14×10^{-3}	2.36×10^{-3}	0.155	9.70×10^{-4}	2.12×10^{-3}	3.58×10^{-2}	3.54×10^{-3}
20	0.665	1.98×10^{-3}	2.24×10^{-3}	0.151	9.18×10^{-4}	1.98×10^{-3}	3.50×10^{-2}	2.53×10^{-3}
30	0.625	1.76×10^{-3}	2.04×10^{-3}	0.140	8.22×10^{-4}	1.76×10^{-3}	3.32×10^{-2}	2.52×10^{-3}
40	0.567	1.46×10^{-3}	1.78×10^{-3}	0.127	7.08×10^{-4}	1.46×10^{-3}	3.10×10^{-2}	1.80×10^{-3}
50	0.493	1.11×10^{-3}	1.45×10^{-3}	0.110	5.64×10^{-4}	1.11×10^{-3}	2.84×10^{-2}	1.09×10^{-3}
60	0.395	7.20×10^{-4}	1.05×10^{-3}	0.087	3.98×10^{-4}	7.20×10^{-4}	2.49×10^{-2}	4.92×10^{-4}
70	0.270	3.48×10^{-4}	6.02×10^{-4}	0.057	2.22×10^{-4}	3.58×10^{-4}	2.04×10^{-2}	1.26×10^{-4}
78	0.143	1.23×10^{-4}	2.62×10^{-4}	0.029	9.40×10^{-5}	1.23×10^{-4}	1.56×10^{-2}	2.45×10^{-5}
86	0.033	1.86×10^{-5}	5.48×10^{-5}	0.007	1.84×10^{-5}	1.86×10^{-5}	6.06×10^{-3}	3.42×10^{-6}
90	0.0	0.0	0.0	0.0	0.0	0.0	0.0	0.0

Footnotes for Table 29

(a) Material in this table has been derived from Penner and Walton (1982).

(b) The photolysis rates for NO_3 and Methylgloyxal are expressed as a fraction of the NO_2 rate as shown in Table 28.

TABLE 30

Comparison of Key Photolysis Steps Used In Different Photochemical Reaction Mechanisms

PHOTOLYSIS STEP	PHOTOLYSIS RATE RELATIVE TO NO_2 (a)					
	1	2	3	4	5	6
NO_2 Normalized Photolysis Rates (b)						
NO_2 + hv ⟶ NO + $O(^3P)$	1.0	1.0	1.0	1.0	1.0	1.0
HONO + hv ⟶ OH + NO	0.17	0.18	0.056	0.18	0.19	0.23
HCHO + hv ⟶ CO + H_2	0.0034	0.0038	0.0097	0.001	0.0093	0.0034
⟶ HCO$^\cdot$ + H$^\cdot$	0.0035	0.0030	0.0037	0.002	0.0056	0.00312
CH_3CHO+hv ⟶ HCO$^\cdot$ + CH3$^\cdot$	0.0008	0.00036	0.0007	--	--	--
RCHO + hv ⟶ CO + a_1HO_2 + a_2RO_2	0.0008	0.0023	0.0025	--	0.0051	--

Footnotes for Table 30

(a) Reaction Mechanisms

1 Atkinson et al. (1982)
2 Demerjian (1982)
3 Dodge (1977)
4 Killus and Whitten (1982a)
5 McRae and Seinfeld (1983)
6 Penner and Walton (1982)

(b) The photolysis rates used by each mechanism have been normalized against the peak NO_2 values.

While the spectral distribution and intensity of the incident radiation are common to all the species, the efficiency with which light is absorbed depends on the properties of the molecule itself. Uncertainties associated with measurements of the species absorption cross sections and quantum yields are the second major source of inaccuracy in the calculation of photolysis rates. Meaningful error assignment is a difficult problem partly because the measurement uncertainties tend to be random in nature. Table 31 gives the estimated reliability factors for some of the more important photochemical reactions. These factors represent the assessments by DeMore et al. (1982), Plum et al. (1983), Atkinson and Lloyd (1983) and WMO (1981) of the combined uncertainty in cross sections and quantum yields. The tabulated values indicate, for example, that the product $\sigma\phi$ for NO_2, over the wavelength band of interest, is uncertain to within one standard deviation by a factor of ± 1.2. By combining this information with the errors involved in setting the actinic irradiance it is possible to set bounds for systematic sensitivity studies of the effects of photolytic processes on mechanism performance.

TABLE 31

Uncertainty Estimates for Photolysis Steps

PHOTOLYSIS STEP[a]	UNCERTAINTY ESTIMATE[b]
$NO_2 + h\nu \longrightarrow NO + O(^3P)$	1.2
$HONO + h\nu \longrightarrow OH + NO$	1.4
$H_2O_2 + h\nu \longrightarrow 2OH$	1.4
$NO_3 + h\nu \longrightarrow NO_2 + O(^3P)$	2.0
$\longrightarrow NO + O_2$	1.2
$N_2O_5 + h\nu \longrightarrow 2NO_2 + O$	2.0
$O_3 + h\nu \longrightarrow O_2 + O(^3P)$	1.1
$\longrightarrow O(^1D) + O_2(^1g)$	1.4
$HCHO + h\nu \longrightarrow CO + H_2$	1.4
$\longrightarrow HCO + H$	2.0
$CH_3CHO + h\nu \longrightarrow CH_4 + CO$	2.0
$\longrightarrow HCO + CH_3$	2.0
$RCHO + h\nu \longrightarrow CO + a_1HO2 + a_2RO2$	2.0
$GLY + h\nu \longrightarrow HCHO + CO$	2.0
$M\text{-}GLY + h\nu \longrightarrow HO_2 + RCO_3 + CO$	2.0
$MEK + h\nu \longrightarrow CH_3CO_3 + C_2H_5O_2$	2.0

Footnotes for Table 31

(a) Mechanism steps as defined in Table 20

(b) Based on Atkinson and Lloyd (1983), WMO (1981) and DeMore et al. (1982)

CHAPTER 5

SPECIFICATION OF INITIAL CONDITIONS AND REACTION RATE CONSTANTS FOR LUMPED ORGANIC REACTIONS

Each mechanism considered in this study employs a different method for partitioning individual organics into the appropriate lumped classes. The primary purpose of this chapter is to document these procedures and the methods used to establish initial conditions and lumped rate constants. Two basic questions are addressed. The first, is given a set of detailed hydrocarbon measurements, how should the individual species be allocated to the lumped classes. A more difficult problem, and one that is frequently encountered in practice, is how to establish initial concentrations for the lumped classes when only total or non-methane hydrocarbon measurements are available.

5.1 Species Assignment to Lumped Hydrocarbon Classes

As noted previously in Chapter 1, the six reaction schemes considered in this study use one of three basic approaches to hydrocarbon lumping. With the exception of those mechanisms employing surrogate species most of the other lumping schemes utilize an organic classification scheme that is based on either the molecule type or carbon bond structure. A summary of these approaches is presented in Table 32. Formal definitions of the compositions of the lumped classes used in each mechanism are presented in Tables 33-38.

Table 39 shows how the initial concentrations in smog chamber experiment SUR-119J are classified for the five mechanisms. This particular chamber run was carried out at the University of California, Riverside (Pitts et al. 1976) and was simulated in this study to test the

TABLE 32

Number of Organic Classes and Lumping Procedures
Used in the Reaction Mechanism Survey

	REACTION MECHANISM DOCUMENTATION	NUMBER OF REACTIVE ORGANIC GROUPINGS[a]	APPROACH TO ORGANIC LUMPING
1	Atkinson et al. (1979,1982) Carter et al. (1979) Lurmann (1982,1983)	14	Grouping by molecule type with surrogate species for particular classes
2	Demerjian (1982) Schere (1983)	4	Grouping by molecule type
3	Dodge (1977) Durbin et al. (1975)	4	Chemistry represented by a surrogate mixture of propene and butane
4	Killus and Whitten (1982a,b) Whitten et al. (1980a,b)	5	Species grouping on the basis of bond structure
5	McRae and Seinfeld (1983) McRae et al. (1982) Falls et al. (1979) Falls and Seinfeld (1978)	6	Grouping by molecule type
6	Penner and Walton (1982) MacCracken and Sauter (1975) Gelinas and Skewes-Cox (1975)	4	Grouping by molecule type

Footnotes for Table 32

(a) The detailed class definitions are contained in the following

1 Atkinson et al. (1982) - Table 33
2 Demerjian (1982) - Table 34
3 Dodge (1977) - Table 35
4 Killus and Whitten (1982) - Table 36
5 McRae and Seinfeld (1983) - Table 37
6 Penner and Walton (1982) - Table 38

TABLE 33

Definition of Organic Classes in the Atkinson et al. (1982) Photochemical Reaction Mechanism[a]

ORGANIC CLASS	DEFINITION OF THE ORGANIC CLASS	COMPUTER CODE[b]
Alkanes	Propane (excluding CH_4 and C_2H_6)	PRPA
	Alkanes with carbon number $\geq$ 4	ALKA
Alkenes	Ethylene	ETHE
	Propene is the surrogate species for the 1-alkenes	PRPE
	Trans-2-butene is the surrogate species for the internal alkenes	BUTE
Aromatics	Benzene	BENZ
	Toluene is the surrogate species for the monoalkylbenzenes	TOLU
	Xylene is the surrogate species for the di- and tri-alkylbenzenes	XYEN
Carbonyls	Formaldehyde	HCHO
	Acetaldehyde	ALD2
	Benzaldehyde	ACHO
	Propionaldehyde is the surrogate species for the higher aldehydes	RCHO
	Acetone	ACET
	Methylethylketone is the surrogate for higher ketones	MEK
Unreactive		UR

Footnotes for Table 33:

(a) Mechanism documentation: Atkinson et al.(1979,1982), Carter et al.(1979).

(b) The computer codes correspond to those used in Chapter 1.

TABLE 34

Definition of Organic Classes in the Demerjian (1982) Photochemical Reaction Mechanism[a]

ORGANIC CLASS	DEFINITION OF THE ORGANIC CLASS	COMPUTER CODE[b]
Alkenes	All alkenes including ethylene	HC1
Alkanes	All alkanes other than methane	HC2
Aldehydes	All aldehyde species	HC3
Aromatics	All aromatic species	HC4
Unreactive		UR

Footnotes for Table 34:

(a) Mechanism documentation: Demerjian (1982), Schere (1983)

(b) The computer codes correspond to those used in Chapter 1.

TABLE 35

Definition of Organic Classes in the Dodge (1977) Photochemical Reaction Mechanism[a]

ORGANIC CLASS	DEFINITION OF THE ORGANIC CLASS	COMPUTER CODE[b]
Alkenes	Propylene	PROP
Alkanes	Butane	BUT
Aldehydes	Formaldehyde	HCHO
	Acetaldehyde (CH_3CHO)	ALD2
Unreactive		UR

Footnotes for Table 35:

(a) Mechanism Documentation: Dodge (1977)

(b) The computer codes correspond to those used in Chapter 1.

TABLE 36

Definition of Organic Classes in the Killus and Whitten (1982a) Photochemical Reaction Mechanism[a]

ORGANIC CLASS	DEFINITION OF THE ORGANIC CLASS	CARBON NUMBER	COMPUTER CODE[b]
Olefins	1-alkene carbon atoms except ethene	2	OLE
	Ethene	2	ETH
Paraffins	Single-bonded carbon atoms	1	PAR
Aromatics	Reactive aromatic rings	6	ARO
Carbonyls	Carbonyl carbon atoms plus the carbon atoms from internal olefins	1	CARB
Unreactive		-	UR

Footnotes for Table 36:

(a) Mechanism documentation: Killus and Whitten (1982a)
Whitten et al. (1980a,b)

(b) The computer codes correspond to those used in Chapter 1.

TABLE 37

Definition of Organic Classes in the McRae and Seinfeld (1983) Photochemical Reaction Mechanism[a]

ORGANIC CLASS	DEFINITION OF THE ORGANIC CLASS	COMPUTER CODE[b]
Aldehydes	Formaldehyde	HCHO
	Higher aldehydes	RCHO
Aromatics	All aromatics	ARO
Alkenes	Ethene	C2H4
	All olefins except ethene	OLE
Alkanes	All alkanes except methane	ALK
Unreactive		UR

Footnotes for Table 37:

(a) Mechanism documentation: Falls and Seinfeld (1978), Falls et al. (1979) McRae et al. (1982), McRae and Seinfeld (1982)

(b) The computer codes correspond to those used in Chapter 1.

TABLE 38

Definition of Organic Classes in the Penner and Walton (1982) Photochemical Reaction Mechanism[a]

ORGANIC CLASS	DEFINITION OF THE ORGANIC CLASS	COMPUTER CODE[b]
Alkenes	Includes all alkenes, isoprene and mono-terpenes. The reaction rate constants are based on propylene.	HC1
Alkanes	Includes all alkanes except methane. The reaction rate constants are based on n-butane.	HC2
Aromatics	Includes all aromatics. The reaction rate constants are based on toluene.	HC3
Carbonyls	Includes all aldehydes and ketones. The rate constants are based on a a 50%-50% mixture of HCHO and CH_3CHO.	HC4
Unreactive		UR

Footnotes for Table 38:

(a) Mechanism documentation: Gelinas and Skewes-Cox (1975)
MacCracken and Sauter eds. (1975)
Penner and Walton (1982)

(b) The computer codes correspond to those used in Chapter 1.

TABLE 39

Classification of Organic Species into Lumped Classes[a] for the Smog Chamber Experiment SUR-119J

SPECIES	CONCENTRATION ppbV	CONCENTRATION ppbC	SPECIES ASSIGNMENT FOR EACH MECHANISM[b] 1	2	4	5	6
Methane (CH_4)	2740.0	2740.0	UR	UR	1UR	UR	UR
Acetylene (C_2H_2)	46.4	92.8	UR	UR	1UR	UR	UR
Ethane (C_2H_6)	76.8	153.6	UR	HC2	2UR	ALK	HC2
Propane (C_3H_8)	17.0	51.0	PRPA	HC2	1.5PAR+1.5UR	ALK	HC2
Acetone (CH_3COCH_3)	35.2	105.6	ACET	UR	2PAR+1CARB	UR	HC4
Isobutane (C_4H_{10})	0.2	0.8	ALKA	HC2	4PAR	ALK	HC2
n-Butane	166	664	ALKA	HC2	4PAR	ALK	HC2
2,3-Dimethyl Butane (C_4H_8-$(CH_3)_2$)	97.6	585.6	ALKA	HC2	6PAR	ALK	HC2
Ethene (C_2H_4)	43.2	86.4	ETHE	HC1	1ETH	C2H4	HC1
Propene (C_3H_6)	10.6	31.8	PRPE	HC1	1OLE+1PAR	OLE	HC1
Trans-2-Butene (C_4H_8)	0.7	2.8	BUTE	HC1	2PAR+2CARB	OLE	HC1
Cis-2-Butene (C_4H_8)	13.0	52.0	BUTE	HC1	2PAR+2CARB	OLE	HC1
2-methyl-2-Butene (C_4H_7-CH_3)	14.8	74.0	BUTE	HC1	3PAR+2CARB	OLE	HC1
Benzene (C_6H_6)	1.6	9.6	BENZ	HC4	6UR	ARO	HC3
Toluene (C_6H_5-CH_3)	16.8	117.6	TOLU	HC4	1PAR+1ARO	ARO	HC3
Ethyl Benzene (C_6H_5-C_2H_5)	6.4	51.2	TOLU	HC4	2PAR+1ARO	ARO	HC3
Meta-xylene (C_6H_4-$(CH_3)_2$)	42.4	339.2	XYEN	HC4	2PAR+1ARO	ARO	HC3
Isopropyl Benzene (C_6H_5-C_3H_7)	0.4	3.6	TOLU	HC4	3PAR+1ARO	ARO	HC3
n-Propyl Benzene ((C_6H_4-C_3H_7)$_n$)	0.1	0.9	TOLU	HC4	3PAR+1ARO	ARO	HC3
Meta-Ethyl Toluene (C_6H_4-CH_3-C_2H_5)	1.0	9.0	XYEN	HC4	3PAR+1ARO	ARO	HC3
1,2,3 Trimethyl Benzene (C_6H_3-$(CH_3)_3$)	1.6	14.4	XYEN	HC4	3PAR+1ARO	ARO	HC3

TABLE 39 (Continued)

SPECIES	CONCENTRATION ppbV	CONCENTRATION ppbC	SPECIES ASSIGNMENT FOR EACH MECHANISM 1	2	4	5	6
Formaldehyde (HCHO)	38.0	38.0	HCHO	HC3	1CARB	HCHO	HC4
Acetaldehyde (CH_3CHO)	20.0	40.0	ALD2	HC3	1PAR+1CARB	RCHO	HC4
Propionaldehyde (C_2H_5CHO)	3.2	9.6	RCHO	HC3	2PAR+1CARB	RCHO	HC4
Nitric Oxide (NO)	301.0						
Nitrogen Dioxide (NO_2)	41.0						
Nitrous Acid (HONO)	12.0						
Carbon Monoxide (CO)	7450.0						
Water (H_2O) (ppm)	15500.0						
Oxygen (O_2) (ppm)	210,000.0						
M (ppm)	1,000,000.0						
TOTALS FOR MIXTURE							
Nitrogen oxides (ppbV)	354.0						
THC (ppbV)	3393.0						
THC (ppbC)	5274.0						

Footnotes for Table 39:

(a) The initial conditions correspond to smog chamber experiment SUR-119J carried out at the University of California Riverside. The additional data needed to characterize the experimental conditions are (Pitts et al. 1976):

Dilution Rate = 3.5×10^{-4} min^{-1}
Chamber temperature = 303.5 - 306.1 °K
Relative humidity = 58.5 - 53.0 %
Photolysis Rate k_1 = 0.31 min^{-1}.

(b) Some "unreactive" species are included in Penner and Walton (1982) but with low reactivity coefficients. For example, the reactivity of methane relative to HC2 is 3.6×10^{-3}.

various mechanisms.

The first step in the assignment process for any mechanism is to classify each species into its appropriate lumped class. For example, 1,2,3-trimethylbenzene is an aromatic compound and is assigned to the following lumped classes.

Mechanism	Class Assignment
Atkinson et al. (1982)	XYEN
Demerjian (1983)	HC4
Killus and Whitten (1982a)	3 PAR + 1 ARO
McRae and Seinfeld (1983)	ARO
Penner and Walton (1982)	HC3

The process is repeated for each species to calculate the molar concentration of each lumped class. The results of these calculations together with the determinations of the average carbon numbers for smog chamber experiment SUR-119J are shown in Table 40.

In the mechanism of Killus and Whitten (1982a) the molecular bond is used as a basic unit rather than the molecule itself. To illustrate how the initial apportionment is carried out, consider the two compounds, propene and cis-2-butene, shown in Figure 11. On the basis of the above class definitions propene, is equivalent to 1 PAR + 1 OLE and cis-2-butene is composed of 2 PAR and 1 OLE. While this assignment process is straightforward, there are some important exceptions to it. In Figure 11 cis-2-butene is shown to be equivalent to 2 PAR + 1 OLE; however, Killus and Whitten (1982a) recommend that the molecule be split into 2 PAR and 2 CARB. The reason for this is that internal alkenes react more rapidly than do terminal alkenes such as propene. In order to eliminate intermediate species that have very short lifetimes, Killus

TABLE 40

Summary of the Concentrations in Each Lumped Class
for the Smog Chamber Experiment SUR-119J

	CODE	ppbV	ppbC	C#
Atkinson et al. (1982)				
1	PRPA	17.00	51.00	3.00
2	ALKA	263.80	1250.40	4.74
3	ETHE	43.20	86.40	2.00
4	PRPE	10.60	31.80	3.00
5	BUTE	28.50	128.80	4.52
6	BENZ	1.60	9.60	6.00
7	TOLU	23.70	173.30	7.31
8	XYEN	45.00	362.60	8.06
9	HCHO	38.00	38.00	1.00
10	ALD2	20.00	40.00	2.00
12	RCHO	3.20	9.60	3.00
13	ACET	35.20	105.60	3.00
15	UR	2863.20	2986.40	1.04
Demerjian (1982)				
1	HC1	82.30	247.00	3.00
2	HC2	357.60	1455.00	4.07
3	HC3	61.20	87.60	1.43
4	HC4	70.30	545.50	7.76
5	UR	2821.60	2938.40	1.04
Killus and Whitten (1982a)				
1	OLE	10.60	21.20	2.00
2	PAR	1578.80	1578.80	1.00
3	ARO	68.70	412.20	6.00
4	CARB	153.40	153.40	1.00
5	ETH	43.20	86.40	2.00
6	UR	2975.10	3021.50	1.02

TABLE 40 (Continued)

	CODE	ppbV	ppbC	C#
McRae and Seinfeld (1983)				
1	HCHO	38.00	38.00	1.00
2	RCHO	23.20	49.60	2.14
3	ARO	70.30	545.50	7.76
4	C2H4	43.20	86.40	2.00
5	OLE	39.10	160.60	4.11
6	ALK	357.60	1455.00	4.07
7	UR	2821.60	2938.40	1.04
Penner and Walton (1982)				
1	HC1	82.30	247.00	3.00
2	HC2	357.60	1455.00	4.07
3	HC3	70.30	545.50	7.76
4	HC4	96.40	193.20	2.00
5	UR	2786.40	2832.80	1.02

Propylene (Propene) 1 OLE + 1 PAR

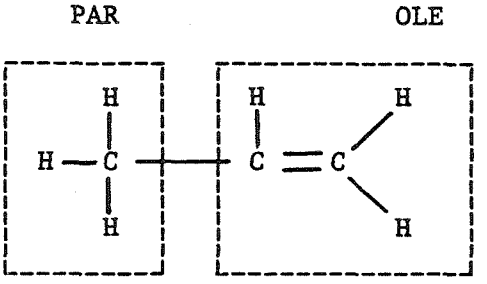

(a)

Cis-2-Butene 1 OLE + 2 PAR

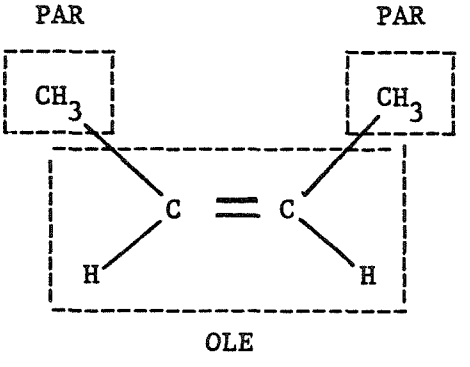

(b)

FIGURE 11

Classification of (a) Propylene and
(b) Cis-2-Butene into the Carbon-Bond Categories

and Whitten treat internal alkenes as if they had already reacted. Thus, cis-2-butene is classified as being equivalent to 2 PAR + 2 CARB. In passing it is interesting to note that the use of this approximation ignores one NO to NO_2 conversion by the peroxy radical formed from the initial OH attack (See Figure 7).* Cycloparaffins are another case where the simple carbon bond class definitions are insufficient. For these compounds, Killus and Whitten (1982a) assume that at some point in the reaction scheme the ring structure must break, yielding two reactive sites instead of one. To account for this property a CARB group is added to the split for the paraffin group. For example, cyclopentane (C_5H_{10}) is decomposed into 4 PAR + 1 CARB. Killus and Whitten have classified over 200 compounds into their carbon bond classes providing guidance as to how an individual organic should be apportioned.

5.2 Calculation of Lumped Reaction Rate Constants

Once the methodology for assigning individual species to each lumped organic class has been defined, then the only remaining information needed to specify the reaction kinetics is the corresponding lumped rate constants.

Five basic methods for specifying the needed rate constants have been developed:

---

* The loss of an NO to NO_2 conversion is approximately compensated by the elimination of the ozone loss to the ozone-alkene reaction that would have occurred in the mechanism if the alkene were not treated as having already reacted.

(1) the use of surrogate species rate constants (Dodge, 1977)

(2) the use of surrogate species rate constants for particular lumped classes (Atkinson et al., 1982)

(3) the use of mole-weighted lumped rate constants based on initial concentrations (Demerjian, 1982; McRae and Seinfeld, 1983)

(4) the use of reactivity-weighted lumped rate constants (Penner and Walton, 1982)

(5) the use of fixed rate constant values based on the reactions of particular carbon bond types (Killus and Whitten, 1982a)

When the mixture chemistry is represented by a set of surrogate species that have known rate constants, e.g., Dodge (1977) and Atkinson et al. (1982), the lumping problem is embodied in that of determining the proper initial conditions for the surrogate species. As an illustration of the effect of the selection of species to be used as surrogates for specifying lumped rate constants, consider the reactions of the hydroxyl radical and those alkene species that comprise the internal alkene class (BUTE) used in the Atkinson et al. (1982) mechanism. For the reactions of cis-2-butene and trans-2-butene the arithmetic average rate constant for the BUTE + OH $\longrightarrow$ reaction is 9.14×10^4, whereas the surrogate rate constant, which for Atkinson et al. (1982) is based on trans-2-butene, is 10.3×10^4. Thus, the use of this surrogate rate constant may lead to an overestimate of the reaction rate for the lumped class depending on the distribution of species comprising that class. Note that, in the surrogate species approach, the surrogate rate constant does not reflect the initial conditions of the mixture. For example, in smog chamber experiment SUR-119J, the species distribution of the cis-2-butene (13.0 ppb) and trans-2-butene (0.7 ppb) that comprise the lumped class is not reflected in the rate constant value.

One way of accounting for the differences in composition and chemical reactivity of the species comprising each lumped class is to use a weighting scheme for lumped rate constants based on the initial molar concentrations of the species. This formulation, which is used by Demerjian (1982) and McRae and Seinfeld (1983), provides a simple way of incorporating the contribution of individual species to the reactivity of the mixture as a whole. In particular, it ensures that the lumped rate constant is not dominated by those species that may have large rate constants but only small initial concentrations. As an illustration of this point, the mole-weighted OH rate constant, corresponding to the conditions of experiment SUR-119J, is 8.09×10^4 ppm^{-1}-min^{-1}. This value reflects the fact that the most of the initial mixture is composed of cis-2-butene. Practical applications of the mole-weighting scheme are considerably simplified because of the availability of extensive literature compilations of basic species rate constant data, e.g., Hampson and Garvin (1978), Atkinson et al. (1979), Baulch et al. (1980, 1982), DeMore et al. (1982), and Atkinson and Lloyd (1983). A shortcoming of this approach is that, as the mixture reacts, the molar distribution changes, and this change is not reflected in the rate constants which were set based on the initial concentrations.

Penner and Walton (1982) determine the lumped rate constants so that the lumped reaction rate matches the rate based on the individual species in each class.

In the carbon-bond mechanism the carbon bond, rather than the molecule itself, is used as the basic unit in each reaction step. It

is assumed that: (1) the reactions of each carbon atom (or double bond) are independent of the reactions elsewhere in the molecule and (2) carbon atoms with similar bonding react at similar rates (Whitten et al. 1980). Greiner (1970), for example, has shown that the total rate of H-atom abstraction by OH attack on an alkane molecule can be predicted from a knowledge of the molecule structure defined in terms of the number of primary, secondary or tertiary carbon atoms. Using this idea Whitten et al. (1980b)established a suggested, or default, value for the rate constant for the reaction between the singly bonded alkane group PAR and the hydroxyl radical. The default value of 1300 $ppmC^{-1}$-min^{-1}, expressed on a per carbon atom basis, is within 35% of the OH rates of alkanes that are likely to be encountered in atmospheric modeling applications.

Documentation of the carbon bond mechanism (Killus and Whitten, 1982a) indicates that the use of default carbon bond rate constants can provide quite accurate simulations of several urban mixes. Nevertheless, Killus and Whitten have provided potential users of the mechanism documentation (Whitten et al., 1980b)for modifying the carbon bond rate constants for special cases outside the range of urban mixes considered. In such cases, the weighted RMS average is recommended for the actual molecules to be simulated. For example, the current default rate constant for aromatics chemistry is based on a 50/50 mix of toluene and m-xylene; if the potential simulation involves exclusively xylenes, then the OH-rate constant should be increased to the weighted RMS value and the secondary chemistry should be modified to reflect the

known differences between mono (toluene) and the more substituted benzenes.

One of the advantages of the carbon bond approach is that the use of default values for each carbon-bond category reduces the range of rate constants that must be averaged in forming condensed reaction steps. Consider specifying the OH + PAR rate constant for the smog chamber experiment EC-231. The alkanes, n-butane (4 PAR) and 2,3-dimethylbutane (6 PAR) have OH rate constants of approximately 3,828 and 8,380 ppm^{-1}-min^{-1} (Atkinson et al. 1979). If these rates are grouped by the numbers of single-bonded carbon atoms these rates become 957 and 1396 $ppmC^{-1}$-min^{-1}. Even though the rate constant range has been reduced the net reaction rate of the two species is unchanged. While the per carbon atom default rate constant is lower than than the equivalent mole-weighted rate, the concentrations of the species comprising the lumped class are much higher because they are expressed on a carbon basis. As a result the combination of a reduced rate constant and higher initial conditions leads to no change in the range of the rates contributing to the PAR kinetics.

5.3 Atmospheric Modeling Applications

Over the past decade there have been significant improvements in the knowledge of the chemistry of polluted atmospheres. From a practical point of view the usefulness of these advances has, to a certain extent, been negated by the lack of similar developments in the collection and analysis of air quality and emissions data. For example, at present the only data on ambient hydrocarbon levels, that are available

on a routine basis, are measurements of total, and in some cases, non-methane hydrocarbons. Given this highly aggregated information it can be expected that the process of establishing the appropriate initial conditions, for atmospheric modeling applications, can lead to a great deal of uncertainty.

Before discussing the different approaches that can be used to set the initial conditions in atmospheric applications it is useful to describe some of the limitations imposed by the use of routine monitoring data. Stephens and Hellrich (1980) discuss some of the errors involved in trying to establish just the non-methane (NMHC) fraction from the total hydrocarbon data collected by air pollution control agencies. If the flame ionization detectors are not accurately calibrated for both methane and THC it is possible to generate negative NMHC values! This is just one illustration; for further details about experimental techniques and the effects of interferences the reader is referred to Leinster et al. (1977), Lamb et al. (1980) and Simoneit and Mazurek (1981). We now describe some of the methods that can be used to set initial conditions when only highly aggregated data are available.

Despite the inherent limitations of the routine monitoring data there are, nevertheless, several methods that can be used to estimate the needed composition information. One of the most commonly employed techniques is to apportion the ambient hydrocarbon measurements into the appropriate lumped classes by using splitting factors derived from detailed gas chromatographic studies. For example, the published

results of Altshuller et al. (1963,1971), Calvert (1976), Jettes and Burghardt (1972), Kopczynski et al. (1972,1975), Lonneman et al. (1974,1978), Neligan (1962), Pitts et al. (1976) and Stephens and Burleson (1969) serve as an information base for establishing typical hydrocarbon levels in urban areas. Detailed reviews of these and other measurement programs can be found in; Gradel (1978), Killus and Whitten (1982a), Leinster et al. (1977), Lamb et al. (1980) and Simoneit and Mazurek (1981). Table 41 presents a typical composition profile for Los Angeles that was derived by combining the measurements made by Calvert (1976) with carbonyl data from Pitts et al. (1976). Given such a profile the splitting factors for each mechanism can be calculated by applying the procedures described in Section 5.1.

Once the splitting factors have been developed they then provide a means for allocating ambient measurements of either total or non-methane hydrocarbons to the appropriate lumped class used by each mechanism. A summary of the results from one set of calculations is shown in Table 42. While the above procedures are quite simple to use, some uncertanties can arise in atmospheric modeling applications. Such factors as the location of the area, the availability of gas chromatograph measurements and the judgement of the investigator can influence the selection of a "typical" composition profile. Some indication of the effect of these differences can be seen in Table 43 where the urban splitting factors, recommended by the developer of each reaction mechanism, have been compared with splitting factors based on Table 42. The differences are particularly high for those lumped classes that

TABLE 41

Classification of Hydrocarbon Species into Lumped Classes
for a Typical Urban Composition Profile

	HYDROCARBON SPECIES	ppbV	SPECIES ASSIGNMENT FOR EACH MECHANISM[a]					
			1	2	4		5	6[b]
1	1-heptene	4.4	PRPE	HC1	1 OLE	+ 5 PAR	OLE	HC1
2	1-hexene	1.7	PRPE	HC1	1 OLE	+ 4 PAR	OLE	HC1
3	1-pentene	4.0	PRPE	HC1	1 OLE	+ 3 PAR	OLE	HC1
4	2.2.4-trimethylpentane	2.5	ALKA	HC2	8 PAR		ALK	HC2
5	2.2.3-trimethylbutane	7.7	ALKA	HC2	7 PAR		ALK	HC2
6	2.2.5-trimethylhexane	1.0	ALKA	HC2	9 PAR		ALK	HC2
7	2.3.3-trimethylpentane	1.9	ALKA	HC2	8 PAR		ALK	HC2
8	2.2-dimethyl-1-butene	0.8	PRPE	HC1	4 PAR	+ 2 CARB	OLE	HC1
9	2-methyl pentane	11.0	ALKA	HC2	6 PAR		ALK	HC2
10	2-methyl-2-butene	0.8	BUTE	HC1	3 PAR	+ 2 CARB	OLE	HC1
11	2-methylhexane	6.9	ALKA	HC2	7 PAR		ALK	HC2
12	3-methyl pentane	10.0	ALKA	HC2	6 PAR		ALK	HC2
13	3-methyl hexane	6.3	ALKA	HC2	7 PAR		ALK	HC2
14	Acetaldehyde	20.0	ALD2	HC3	1 PAR	+ 1 CARB	RCHO	HC4
15	Acetylene	38.0	UR	UR	1 UR		UR	UR
16	Benzene	8.2	BENZ	HC4	6 UR		ARO	HC3
17	1-butene	1.5	PRPE	HC1	1 OLE	+ 2 PAR	OLE	HC1
18	Cyclohexene	10.7	BUTE	HC1	4 PAR	+ 2 CARB	OLE	HC1
19	Cyclopentane	2.6	ALKA	HC2	4 PAR	+ 1 CARB	ALK	HC2
20	Ethane	49.0	UR	HC2	2 UR		ALK	HC2
21	Ethylbenzene	4.1	TOLU	HC4	2 PAR	+ 1 ARO	ARO	HC3
22	Ethylene	43.0	ETHE	HC1	1 ETH		C2H4	HC1
23	Formaldehyde	38.8	HCHO	HC3	1 CARB		HCHO	HC4
24	Heptane	4.3	ALKA	HC2	7 PAR		ALK	HC2
25	Hexane	10.0	ALKA	HC2	6 PAR		ALK	HC2
26	Iso-butane	12.0	ALKA	HC2	4 PAR		ALK	HC2
27	Iso-pentane	44.3	ALKA	HC2	5 PAR		ALK	HC2
28	Isobutylene	3.0	PRPE	HC1	1 OLE	+ 2 PAR	OLE	HC1
29	Methane	2010.0	UR	UR	1 UR		UR	UR
30	Methylcyclohexane	3.7	ALKA	HC2	6 PAR	+ 1 CARB	ALK	HC2
31	Methylcyclohexene	4.7	BUTE	HC1	5 PAR	+ 2 CARB	OLE	HC1
32	Nonane	1.3	ALKA	HC2	9 PAR		ALK	HC2
33	Octane	2.1	ALKA	HC2	8 PAR		ALK	HC2
34	Propane	37.0	PRPA	HC2	1.5 PAR	+1.5 UR	ALK	HC2
35	Proprionaldehyde	6.4	RCHO	HC3	2 PAR	+ 1 CARB	RCHO	HC4
36	Propylene	8.7	PRPE	HC1	1 OLE	+ 1 PAR	OLE	HC1
37	Sec-butylbenzene	5.0	TOLU	HC4	4 PAR	+ 1 ARO	ARO	HC3

TABLE 41 (Continued)

Classification of Hydrocarbon Species into Lumped Classes
for a Typical Urban Composition Profile

	HYDROCARBON SPECIES	ppbV	SPECIES ASSIGNMENT FOR EACH MECHANISM[a] 1	2	4			5	6
38	Toluene	20.0	TOLU	HC4	1 PAR	+ 1 ARO		ARO	HC3
39	Undecane	1.0	ALKA	HC2	11 PAR			ALK	HC2
40	n-butane	37.0	ALKA	HC2	4 PAR			ALK	HC2
41	n-decane	1.1	ALKA	HC2	10 PAR			ALK	HC2
42	n-dodecane	3.0	ALKA	HC2	12 PAR			ALK	HC2
43	n-pentane	16.2	ALKA	HC2	5 PAR			ALK	HC2
44	n-propylbenzene	1.0	TOLU	HC4	3 PAR	+ 1 ARO		ARO	HC3
45	o-xylene	6.0	XYEN	HC4	2 PAR	+ 1 ARO		ARO	HC3
46	p-xylene	14.0	XYEN	HC4	2 PAR	+ 1 ARO		ARO	HC3
	Totals	2526.7							

Footnotes for Table 41

(a) The codes used for each reaction mechanism are defined in the following tables

1 Atkinson et al. (1982)
2 Demerjian (1982)
4 Killus and Whitten (1982a)
5 McRae and Seinfeld (1983)
6 Penner and Walton (1982)

(b) The Penner and Walton (1982) mechanism uses reactivity weighting when individual hydrocarbons are grouped into the lumped classes. For example, 1 ppm of ethene is represented as 0.5 ppm of HC1 in order to account for the lower reactivity of ethene relative to propene. Thus, for the PW mechanism the lumped classes shown in this table represent only the class into which each hydrocarbon is grouped.

TABLE 42

Summary of the Concentrations in Each Lumped Class
for a Typical Urban Composition Profile

	CODE	ppbV	ppbC	C#	THC SPLIT	RHC SPLIT
Atkinson et al. (1982)						
1	PRPA	37.00	111.00	3.00	0.0089	0.0187
2	ALKA	185.90	1030.50	5.54	0.0447	0.0940
3	ETHE	43.00	86.00	2.00	0.0103	0.0217
4	PRPE	24.10	109.90	4.56	0.0058	0.0122
5	BUTE	16.20	101.10	6.24	0.0039	0.0082
6	BENZ	8.20	49.20	6.00	0.0020	0.0041
7	TOLU	30.10	231.80	7.70	0.0072	0.0152
8	XYEN	20.00	160.00	8.00	0.0048	0.0101
9	HCHO	38.80	38.80	1.00	0.0093	0.0196
10	ALD2	20.00	40.00	2.00	0.0048	0.0101
12	RCHO	6.40	19.20	3.00	0.0015	0.0032
15	UR	2097.00	2184.00	1.04	0.5039	1.0604
Demerjian (1982)						
1	HC1	83.30	297.00	3.57	0.0200	0.0401
2	HC2	271.90	1239.50	4.56	0.0653	0.1310
3	HC3	65.20	98.00	1.50	0.0157	0.0314
4	HC4	58.30	441.00	7.56	0.0140	0.0281
5	UR	2048.00	2086.00	1.02	0.4921	0.9868
Killus and Whitten (1982b)						
1	OLE	23.30	46.60	2.00	0.0056	0.0124
2	PAR	1334.10	1334.10	1.00	0.3206	0.7124
3	ARO	50.10	300.60	6.00	0.0120	0.0268
4	CARB	105.50	105.50	1.00	0.0254	0.0563
5	ETH	43.00	86.00	2.00	0.0103	0.0230
6	UR	2250.70	2288.70	1.00	0.5408	1.2018
McRae and Seinfeld (1983)						
1	HCHO	38.80	38.80	1.00	0.0093	0.0187
2	RCHO	26.40	59.20	2.24	0.0063	0.0127
3	ARO	58.30	441.00	7.56	0.0140	0.0281
4	C2H4	43.00	86.00	2.00	0.0103	0.0207
5	OLE	40.30	211.00	5.24	0.0097	0.0194
6	ALK	271.90	1239.50	4.56	0.0653	0.1310
7	UR	2048.00	2086.00	1.02	0.4921	0.9868

TABLE 42 (Continued)

	CODE	ppbV	ppbC	C#	THC SPLIT	RHC SPLIT
Penner and Walton (1982)						
1	HC1	83.30	297.00	3.57	0.0200	0.0401
2	HC2	271.90	1239.50	4.56	0.0653	0.1310
3	HC3	58.30	441.00	7.56	0.0140	0.0281
4	HC4	65.20	98.00	1.50	0.0157	0.0314
5	UR	2048.00	2086.00	1.02	0.4921	0.9868

TABLE 43

Comparison of Splitting Factors for Different Reaction Mechanisms

MECHANISM	MEASUREMENTS[a]	APPROACH TO SPECIES ALLOCATION[b]
Atkinson et al. (1982)	----	No splitting factors have been developed because in all applications of this mechanism detailed measurements have been available to specify the initial conditions for each of the lumped classes.
Demerjian (1982)	NMHC	Splitting factors have been generated by Schere (1983) for apportioning non-methane hydrocarbon measurements made in St Louis.

HC Class	St Louis	Profile Table 3.12	
HC1	0.0657	0.0401	(0.61)
HC2	0.0786	0.1310	(1.67)
HC3	0.0810	0.0314	(0.39)
HC4	0.0248	0.0281	(1.13)

Dodge (1977) — NMHC

There is no direct means for allocating hydrocarbon measurements to the surrogate species used in this mechanism. The default composition of the mixture used in EKMA is 25% propene and 75% n-butane (on a carbon basis). Formaldehyde and acetaldehyde are assumed to be present at 2% and 3% of the initial hydrocarbon level.

HC Class	Default Split
PROP	0.0833
BUT	0.1875
HCHO	0.0200
ALD2	0.0150

Killus & Whitten (1982a) — RHC

The default values used below are based on the recommendations given in Table 17 of Killus and Whitten (1982a) for typical urban hydrocarbon mixtures.

HC Class	Recommended	Profile Table 42	
OLE	0.0150	0.0124	(0.82)
PAR	0.6500	0.7124	(1.10)
ARO	0.0367	0.0268	(0.73)
CARB	0.0500	0.0563	(1.13)
ETH	0.0250	0.0230	(0.92)

TABLE 43 (Continued)

MECHANISM	MEASUREMENTS[a]	APPROACH TO SPECIES ALLOCATION[b]
McRae and Seinfeld (1983)	THC	These splitting factors have been developed to partition total hydrocarbon measurements for conditions occurring during 1974 in Los Angeles. The coefficients were compiled from McRae and Seinfeld (1983)

HC Class	Los Angeles	Profile Table 42	
HCHO	0.0118	0.0093	(0.79)
RCHO	0.0043	0.0063	(1.46)
ARO	0.0075	0.0140	(1.87)
C2H4	0.0247	0.0103	(0.42)
OLE	0.0110	0.0097	(0.88)
ALK	0.0419	0.0653	(1.56)

Penner and Walton (1982)	NMHC	The default values used for splitting ambient measurements of non-methane hydrocarbons for San Francisco are based on Penner and Walton (1982).[c]

HC Class	San Francisco	Profile Table 42	
HC1	0.025	0.0401	(1.60)
HC2	0.1625	0.1310	(0.81)
HC3	0.050	0.0281	(0.56)
HC4	0.0075	0.0314	(4.19)

Footnotes for Table 43

(a) The codes used to identify measurements expressed on a carbon basis are:

NMHC - Non-methane hydrocarbons
RHC - Reactive hydrocarbons
THC - Total hydrocarbons

Note that the U.S. Environmental Protection Agency has an additional class defined as Non-reactive Organic Gases (NROG) that contains those species not considered to be ozone precursors. The compounds are: methane, ethane, methylene chloride, methyl chloroform, trifluoromethane, trichlorotrifluoroethane, trichlorofluoromethane, chlorodifluoromethane, dichlorodifluoromethane, dichlorotetrafluoroethane and chloropentafluoroethane. Further details are contained in 42 FR 48941 - July 8.

(b) The numbers in brackets ( ) are the ratio of the splitting factors derived from Table 42 and the procedures recommended for partitioning ambient measurements.

(c) Shown for comparison only. In actual implementation, reactivity weighting factors are used.

involve carbonyl compounds. There is a great need for additional field measurements of these compounds.

The carbon bond concentrations for ETH, OLE, ARO and CARB are exactly comparable to molecular concentrations in the atmosphere. To compare PAR requires an extremely detailed knowledge of all species, but PAR can be used along with the carbon numbers of the carbon bond species to compare the THC or RHC values in ppmC units. For example, the THC splits for the Atkinson et al. (1982) mechanism can be compared with the carbon bond splits using Table 42 as follows:

THC Splits

Carbon Bond Species	KW	ALW	ALW Species
ETH	0.0103	0.0103	ETHE
ARO	0.0120	0.0120	TOLU + XYEN
OLE	0.0056	0.0058	PRPE
CARB	0.0254	0.0234	HCHO + ALD2 + RCHO + 2x BUTE

The minor differences in OLE and CARB occur because 2,2-dimethyl-1-butene and the cycloparaffins reactivities were interpreted differently. Whitten (private communication, 1983) has analyzed some of the original data from which Calvert (1976) generated the data presented in Table 41 and has found that 2,2-dimethyl-1-butene should be 2,3-dimethyl-1-butene and that compound 18 of Table 41 should probably be cyclohexane rather than cyclohexene.

Another approach to the development of splitting factors for ambient air quality data is to assume that ambient hydrocarbon compositions are similar to emissions. Bucon et al. (1978) and Trijonis and

TABLE 44

Hydrocarbon Splitting Factors for McRae and Seinfeld (1983) Mechanism Based on Los Angeles Emissions Inventory for 1974[a]

SPECIES[b]	KG/SEC	MW	MOLES/SEC	C#	MOLES/SEC OF CARBON	CARBON FRACTION	RHC SPLIT
HCHO	0.18	30.0	6.00	1.00	6.00	0.0060	0.0060
RCHO	0.25	63.1	3.96	3.36	13.30	0.0133	0.0040
ARO	2.03	100.2	20.26	7.56	153.17	0.1528	0.0202
C2H4	0.82	28.0	29.29	2.00	58.58	0.0584	0.0292
OLE	1.98	67.4	29.38	4.83	141.25	0.1409	0.0292
ALK	9.04	83.5	108.26	5.82	630.07	0.6286	0.1080
Totals	14.30		197.15		1002.37		

Footnotes for Table 44

(a) The emissions inventory is based on McRae and Seinfeld (1983).

(b) Emissions of terpenes have not been included.

Arledge (1975) have compiled detailed composition profiles for many of the source classes that are likely to be encountered in atmospheric modeling applications. Given estimates of reactive hydrocarbon emissions from each source class these profiles can be used to develop a chemically resolved inventory. In much the same manner as above, the detailed emissions inventory can be used to develop splitting factors. Usually these factors should only be applied to reactive hydrocarbon measurements because of the uncertainties associated with estimating total emissions in an urban airshed (McRae and Seinfeld, 1983). A typical example of the application of this technique is presented in Table 44. There is almost a factor of three difference between the carbonyl splitting factors based on air quality data and those derived from the emissions inventory. Without further emissions and air quality data it will be difficult to account accurately for these discrepancies.

In summary, if chemically resolved modeling approaches are to be used in urban environments, both the emissions inventory data and the ambient hydrocarbon measurements need to be improved to the point where they have the same chemical resolution as the requirements of the particular photochemical mechanism. Unless this is carried out, the large uncertainties in specifying initial conditions may negate any improvements in air quality predictions that may arise as a result of the use of more sophisticated chemical mechanisms.

5.4 Conclusions

In this chapter the primary goal has been to present a comparison of the way in which the initial conditions and rate constants for

lumped hydrocarbon steps are treated in each of the reaction mechanisms. If a detailed hydrocarbon profile is available, the procedures to be followed for specifying the initial conditions and rate constants for the lumped classes are relatively straightforward. On the other hand, if the only measurements are total or reactive hydrocarbons, the problem of establishing the initial conditions is considerably more difficult and leads to substantial uncertainities. The use of organic lumping schemes imposes a requirement that both the organic emission inventory and ambient monitoring data have the same resolution as the chemical mechanism. There is a critical need for comprehensive studies of both the composition and amount of organics emitted into urban environments. Particular attention needs to be given to carbonyl compounds. Without this information the uncertanties in specifying the input data can overwhelm the improvements in air quality predictions that might arise from the use of a more refined mechanism.

CHAPTER 6

CONCLUSIONS

This report has presented a detailed description of six lumped reaction mechanisms for photochemical smog:

Atkinson et al. (1982)

Demerjian (1982)

Dodge (1977)

Killus and Whitten (1982a)

McRae and Seinfeld (1983)

Penner and Walton (1982)

The description includes a discussion of the basic assumptions in each mechanism's treatment of the fundamental chemistry, photolysis reactions, and organic lumping via initial conditions and organic rate constants. In general, it is found that the mechanisms differ in virtually all aspects, and, without detailed, quantitative, numerical comparisons, it is difficult to predict simply from inspection how each mechanism will perform in a particular application. Nevertheless, if one removes those mechanism aspects included only to account for smog chamber-dependent radical sources, such as a wall source of OH radicals or initial HONO, it is possible to rank the mechanisms according to overall "reactivity." We find on the basis of our analysis that such a ranking is:

Killus and Whitten (1982a)
Demerjian (1982)
McRae and Seinfeld (1983)
} most reactive

Atkinson et al. (1982)
Penner and Walton (1982) } less reactive

The Dodge (1977) mechanism cannot be ranked in this scale because the split between propene and n-butane is fixed.

Our object is to be able to tell specifically what aspects of each mechanism are key to its performance, as measured by its "reactivity." To do so requires the detailed, quantitative, numerical comparisons referred to above. Such comparisons are the subject of Part II.

REFERENCES

Altshuller, A.P. and Bellar, T.A. (1963), "Gas Chromatographic Analysis of Hydrocarbons in the Los Angeles Atmosphere," J. Air Pollution Control Association, 13, 81-87.

Altshuller, A.P., Lonneman, W.A., Sutterfield, F.D. and Kopczynski, S.L. (1971), "Hydrocarbon Composition of the Atmosphere of the Los Angeles Basin," Environmental Science and Technlogy, 5, 1009-1016.

Atkinson, R. and Lloyd, A.C. (1983), "Evaluation of Kinetic and Mechanistic Data for Modeling of Photochemical Smog," J. Phys. Chem. Ref. Data (in press).

Atkinson, R., Darnall, K.R., Lloyd, A.C., Winer, A.M. and Pitts, J.N. Jr. (1979), "Kinetics and Mechanisms of the Reaction of the Hydroxyl Radical with Organic Compounds in the Gas Phase," Advances in Photochemistry, 11, 375-488.

Atkinson, R., Lloyd, A.C. and Winges, L. (1982), "An Updated Chemical Mechanism for Hydrocarbons/NO_x/SO_2 Photooxidations Suitable for Inclusion in Atmospheric Simulation Models," Atmospheric Environment, 16, 1341-1355.

Bass, A.M., Glasgow, L.C., Miller, C., Jesson, J.P. and Filkin, D.L. (1980), "Temperature Dependent Absorption Cross Sections for Formaldehyde (CH_2O): The Effect of Formaldehyde on Stratospheric Chlorine Chemistry," Planetary and Space Science, 28, 675-679.

Baulch, D.L., Cox, R.A., Hampson, R.F., Kerr, J.A., Troe, J. and Watson, R.T. (1980), "Evaluated Kinetic and Photochemical Data for Atmospheric Chemistry," J. Physical and Chemical Reference Data, 9, 295-471.

Baulch, D.L., Cox, R.A., Crutzen, P.J., Hampson, R.F., Kerr, J.A., Troe, J. and Watson, R.T. (1982), "Evaluated Kinetic and Photochemical Data for Atmospheric Chemistry: Supplement 1. CODATA Task Group on Chemical Kinetics," J. Physical and Chemical Reference Data, 11, 327-496.

Braslau, N. and Dave, J.V. (1973a), "Effect of Aerosols on the Transfer of Solar Energy through Realistic Model Atmospheres, Part I: Non-Absorbing Aerosols," J. Applied Meteorology, 12, 601-615.

Braslau, N. and Dave, J.V. (1973b), "Effect of Aerosols on the Transfer of Solar Energy through Model Atmospheres, Part II: Partly - Absorbing Aerosols," J. Applied Meteorology, 12, 616-619.

Bucon, H.W., Malko, J.F. and Taback, H.J. (1978), Volatile Organic Compound (VOC) Species Data Manual, U.S. Environmental Protection Agency Report No. EPA-450/3-78-119.

Calvert, J.G. (1976), "Hydrocarbon Involvement in Photochemical Smog Formation in Los Angeles Atmosphere," Environmental Science and Technology, 10 256-262.

Carter, W.P.L., Lloyd, A.C., Sprung, J.L. and Pitts, J.N. Jr. (1979) "Computer Modeling of Smog Chamber Data: Progress in Validation of a Detailed Mechanism for the Photooxidation of Propane and n-Butane in Photochemical Smog," Int. J. Chemical Kinetics, XI, 45-101.

Carter, W.P.L., Winer, A.M. and Pitts, J.N., Jr. (1982) "Effect of Kinetic Mechanisms and Hydrocarbon Composition on Oxidant-Precursor Relationships Predicted by the EKMA Isopleth Technique," Atmospheric Environment, 16, 113-120.

Darnall, K.R., Atkinson, R. and Pitts, J.N. (1979), "Observation of Biacetyl from the Reaction of OH Radicals with o-Xylene: Evidence for Ring Clevage," J. Physical Chemistry, 83, 1943-1946.

Demerjian, K.L., Schere, K.L. and Peterson, J.T. (1980), "Theoretical Estimates of Actinic (Spherically Integrated) Flux and Photolytic Rate Constants of Atmospheric Species in the Lower Troposphere," Advances in Environmental Science and Technology, 10, 369-459.

Demerjian, K.L. (1982), Personal Communication.

DeMore, W.B., Watson, R.T., Howard, C.J., Golden, D.M., Molina, M.J., Hampson, R.F., Kurylo, M. and Ravishankara, A.R. (1982), Chemical Kinetics and Photochemical Data for Use in Stratospheric Modeling, Jet Propulsion Laboratory Publication 82-57, California Institute of Technology, Pasadena, California.

Dodge, M.C. (1977), "Combined Use of Modeling Techniques and Smog Chamber Data to Derive Ozone--Precursor Relationships," U.S. Environmental Protection Agency Report, EPA-600/3-77-001a, 881-889.

Durbin, P.A., Hecht, T.A. and Whitten, G.Z. (1975), "Mathematical Modeling of Simulated Photochemical Smog," U.S. Environmental Protection Agency Report, EPA-650/4-75-026.

Edelson, D. (1975), "The New Look in Chemical Kinetics," J. Chemical Education, 52, 642-644.

Edelson, D. (1976), "A Simulation Language and Compiler to Aid Computer Solution of Chemical Kinetic Problems," Computers and Chemistry, 1, 29-33.

Edelson, D. (1981), "Computer Simulation in Chemical Kinetics," Science, 214, 981-986.

Falls, A.H. and Seinfeld, J.H. (1978), "Continued Development of a Kinetic Mechanism for Photochemical Smog," Environmental Science and Technology, 12, 1398-1406.

Falls, A.H., McRae, G.J. and Seinfeld, J.H. (1979), "Sensitivity and Uncertainty of Reaction Mechanisms for Photochemical Air Pollution," Int. J. Chemical Kinetics, 11, 1137-1162.

Gelinas, R.J., Dickerson, R.P. and Grant, K.E. (1974), Solar Flux and Photodissociation Calculations for LLL Atmospheric Physics Programs, Lawrence Livermore Laboratory Report UCRL-74944 Rev. 1, Lawrence Livermore National Laboratory, University of California, Livermore, California.

Gelinas, R.J. and Skewes-Cox, P.D. (1975), "Tropospheric-Photochemical Mechanisms," J. Physical Chemistry, 81, 2468-2479.

Gradel, T.E. (1978), Chemical Compounds in the Atmosphere, Academic Press, New York.

Greiner, N.R. (1970), "Hydroxyl Radical Kinetics by Kinetic Spectroscopy VI. Reactions with Alkanes in the Range 300-500 ^{o}K," J. Chemical Physics, 53, 1070-1076.

Hampson, R.F. and Garvin, D. (1978), "Reaction Rate and Photochemical Data for Atmospheric Chemistry - 1977," U.S. Department of Commerce National Bureau of Standards Special Publication 513, 111 pp.

Hindmarsh, A.C. (1980), "LSODE and LSODI, Two New Initial Value Ordinary Differential Equation Solvers," ACM-Signum Newsletter, 15, 10-11.

Horowitz, A. and Calvert, J.G. (1982), "Wavelength Dependence of the Primary Processes in Acetaldehyde Photolysis," J. Physical Chemistry, 86, 3105-3114.

Hudson, R.D. and Reed. E.I. eds. (1979), The Stratosphere: Present and Future, NASA Reference Publication No. 1049.

Jeffries, H.E., Sexton, K.G. and Salmi, C.N. (1981), Effects of Chemistry and Meteorology on Ozone Control Calculations Using Simple Trajectory Models and the EKMA Procedure, Final Report to the U.S. Environmental Protection Agency Under Contract No.68-02-3523, School of Public Health, University of North Carolina, Chapel Hill, North Carolina, 373 pp.

Jettes, R. and Burghardt, E. (1972), "Automatic Gas Chromatographic Measurement of C_1-C_5 Hydrocarbons in Air," Atmospheric Environment, 6, 793-805.

Kee, R.J., Miller, J.A. and Jefferson, T.H. (1980), CHEMKIN: A General Purpose, Problem-Independent, Transportable, FORTRAN Chemical Kinetics Code Package, Sandia Laboratories Report No. SAND80-8003, Albuquerque, New Mexico, 204 pp.

Killus, J.P. (1982a), Personal Communication - 26 August 1982

Killus, J.P. (1982b), Computer Output - 23 August 1982

Killus, J.P. and Whitten, G.Z. (1982a), A New Carbon-Bond Mechanism for Air Quality Modeling, U.S. Environmental Protection Agency Report No. EPA-600/3-82-041.

Killus, J.P. and Whitten, G.Z. (1982b), "A Mechanism Describing the Photochemical Oxidation of Toluene in Smog," Atmospheric Environment, 16, 1973-1988.

Kopczynski, S.L., Kuntz, R.L. and Bufalini, J.J. (1975), "Reactivities of Complex Hydrocarbon Mixtures," Environmental Science and Technology, 9, 648-653.

Kopczynski, S.L., Lonneman, W.A., Sutterfield, F.D. and Darley, P.E. (1972), "Photochemistry of Atmospheric Samples in Los Angeles," Environmental Science and Technology, 6, 342-347.

Kramer, M.A., Kee, R.J. and Rabitz, H. (1982), CHEMSEN: A Computer Code for Sensitivity Analysis of Elementary Chemical Reaction Models, Sandia Laboratories Report No. SAND82-8230, Albuquerque, New Mexico, 23 pp.

Kramer, M.A., Calo, J.M. and Rabitz, H. (1981), "An Improved Computational Method for Sensitivity Analysis: Green's Function Method with 'AIM'," Applied Mathematical Modelling, 5, 432-441.

Koda, M., McRae, G.J. and Seinfeld, J.H. (1979), "Automatic Sensitivity Analysis of Reaction Mechanisms," Int. J. Chemical Kinetics, 11, 427-444.

Lamb, S.I., Petrowski, C., Kaplan, I.R. and Simoneit, B.R.T. (1980), "Organic Compounds in Urban Atmospheres: A Review of Distribution Collection and Analysis," J. Air Pollution Control Association, 30, 1098-1115.

Leighton, P.A. (1961), Photochemistry of Air Pollution, Academic Press, New York, 300 pp.

Leinster, P., Perry, R. and Young, R.J. (1977), "Detection and Measurement of Volatile Hydrocarbons at Ambient Concentrations in the Atmosphere," Talanta, 24, 205-213.

Leone, J.A. and Seinfeld, J.H. (1983) "Analysis of the Characteristics of Complex Chemical Reaction Mechanisms - Application to Photochemical Smog Chemistry " (submitted for publication).

Lonneman, W.A., Seila, R.L. and Bufalini, J.J. (1978), "Ambient Air Hydrocarbon Concentrations in Florida," Environmental Science and Technology, 12, 459-463.

Lonneman, W.A., Kopczynski, S.L., Darley, P.E. and Sutterfield, F. (1974), "Hydrocarbon composition of Urban Air Pollution," Environmental Science and Technology, 8, 229-236.

Lurmann, F. (1982), "Personal Communication - Computer Listing."

Lurmann, F. (1983), "Personal Communication - HC Speciation."

Luther, F.M. and Gelinas, R.J. (1976), "Effects of Molecular Multiple Scattering and Surface Albedo on Atmospheric Photodissociation Rates," J. Geophysical Research, 81, 1125-1132.

MacCracken, M.C. and Sauter, G.C. eds. (1975), "Development of an Air Pollution Model for the San Francisco Bay Area," Final Report to the National Science Foundation, Lawrence Livermore Report UCRL-51920, 1169 pp.

Magnotta, F. and Johnston, H.S. (1980), "Photodissociation Quantum Yields for the NO_3 Free Radical," Geophysical Research Letters, 7, 769-772.

McRae, G.J. (1983), Computer Programs for the Solution and Analysis of Chemical Systems: User Manual, Environmental Quality Laboratory, California Institute of Technology, Pasadena, California (in preparation).

McRae, G.J., Goodin, W.R. and Seinfeld, J.H. (1982), "Development of a Second-Generation Mathematical Model for Urban Air Pollution I. Model Formulation," Atmospheric Environment, 16, 679-696.

McRae, G.J. and Seinfeld, J.H. (1983), "Development of a Second-Generation Mathematical Model for Urban Pollution II: Model Performance Evaluation," Atmospheric Environment, 17, 501-523.

McRae, G.J., Tilden, J.W. and Seinfeld, J.H. (1982), "Global Sensitivity Analysis - A Computational Implementation of the Fourier Amplitude Sensitivity Test (FAST)," Computers and Chemical Engineering, 6, 15-25.

Molina, L.T., Schinke, S.D. and Molina, M.J. (1977), "Ultraviolet Absorption Spectrum of Hydrogen Peroxide Vapor," Geophysics Research Letters, 4, 580-582.

Moortgat, G.K., Klippel, W., Mobius, K.H., Seiler, W., and Warneck, P. (1980) Laboratory Measurements of Photolytic Parameters for Formaldehyde, Federal Aviation Administration Report No. FAA-EE-80-47, U.S. Department of Transportation, Office of Environment and Energy, Washington, D.C.

Neligan, R.E. (1962), "Hydrocarbons in the Los Angeles Atmosphere," Archives of Environmental Health, 5, 581-591.

Niki, H., Maker, P.D., Savage, C.M. and Breitenbach, L.P. (1977) "Fourier Transform IR Spectroscopic Observation of Propylene Ozonide in the Gas-Phase Reaction of Ozone-Cis-2-Butene-Formaledhyde," Chem. Phys. Letters, 46, 327-330.

Penner, J.E. and Walton, J.J. (1982) Air Quality Model Update, Lawrence Livermore Laboratory Report UCID - 19300, Lawrence Livermore National Laboratory, University of California, Livermore, California, 55 pp.

Peterson, J.T. (1976), "Calculated Actinic Fluxes (290-700 nm) for Air Pollution Photochemistry Application," U.S. Environmental Protection Agency Report EPA-600/4-76-025, 63 pp.

Peterson, J.T., Demerjian, K.L. and Schere, K.L. (1977), "Actinic Solar Flux and Photolytic Rate Constants in the Troposphere," Proc. International Conference on Photochemical Oxidant and its Control, Vol II, Raleigh, North Carolina, Sept. 12-17, 1976, NTIS PB-264 233, 763-773.

Pitts, J.N, Winer, A.M., Darnall, K.R. et al. (1976), Chemical Consequences of Air Quality Standards and of Control Implementation Programs: Roles of Hydrocarbons, Oxides of Nitrogen, and Aged Smog in the Production of Photochemical Oxidant, Final Report to the California Air Resources Board under Contract Number 4-212, Statewide Air Pollution Research Center, University of California Riverside, California, 444 pp.

Plum, C.N., Sanhueza, E., Atkinson, R., Carter, W.P.L. and Pitts, J.N. (1983), "OH Radical Rate Constants and Photolysis Rates of Alpha-Dicarbonyls," Environmental Science and Technology (in press).

Schere, K.L. (1983), "Personal Comunication - Letter dated 14 January."

Schere, K.L. and Demerjian, K.L. (1977), "Calculation of Selected Photolytic Rate Constants Over A Diurnal Range," U.S. Environmental Protection Agency, Report EPA-600/4-77-015, 71 pp.

Simoneit, B.R.T. and Mazurek, M.A. (1981), "Air Pollution: The Organic Components," CRC Critical Reviews in Environmental Control, 11(3), 219-276.

Stedman, D.H., Harvey, R.B. and Dickerson, R.R. (1977), "Measurement of Photons Indicated in Photochemical Oxidant Formation," Proc. International Conference on Photochemical Oxidant and its Control, Vol II, Raleigh, North Carolina, NTIS PB-264 233, 753-762.

Stephens, E.R. and Hellrich, O.P. (1980), "Chromatographic Monitoring of Hydrocarbons in Ambient Air," Environmental Science and Technology, 14, 836-838.

Stephens, E.R. and Burleson, F.R. (1969), "Distribution of Light Hydrocarbons in Ambient Air," J. Air Pollution Control Association, 19, 929-936.

Trijonis, J.C. and Arledge, K.W. (1975), Utility of Reactivity Criteria in Organic Emissions Control Strategies for Los Angeles, TRW Corporation, Final report to the U.S. Environmental Protection Agency under Contract No. 68-02-1735, Los Angeles, California.

Whitten, G.Z., and Hogo, H. (1978), User's Manual for Kinetics Model and Ozone Isopleth Plotting Package, U.S. Environmental Protection Agency Report No. EPA-600/8-78-014a, prepared by Systems Application Inc., San Rafael, California, 35 pp.

Whitten, G.Z., and Hogo, H. (1980), Modeling of Simulated Photochemical Smog with Kinetic Mechanisms: Volume 2 CHEMK - A Computer Modeling Scheme for Chemical Kinetics, U.S. Environmental Protection Agency Report No. EPA-600/3-80-028b, prepared by Systems Application Inc., San Rafael, California, 113 pp.

Whitten, G.Z., Hogo, H. and Killus, J.P. (1980a), "The Carbon-Bond Mechanism: A Condensed Kinetic Mechanism for Photochemical Smog," Environmental Science and Technology, 14, 690-700.

Whitten, G.Z., Hogo, H. and Killus, J.P. (1980b), Modeling of Simulated Photochemical Smog with Kinetic Mechanisms: Volume 1, U.S. Environmental Protection Agency Report No. EPA-600/3-80-028a, prepared by Systems Applications Inc., San Rafael, California, 362 pp.

Whitten, G.Z. (1981) Comments at U.S. Environmental Protection Agency Workshop on the Empirical Kinetic Modeling Approach, December 15-16, Research Triangle Park, NC.

Winer, A.M., Brauer, G.M., Carter, W.P.L., Darnall, K.R. and Pitts, J.N., Jr. (1979) "Effects of Ultraviolet Spectral Distribution on the Photochemistry of Simulated Polluted Atmospheres," Atmospheric Environment, 13, 989-998.

WMO (1981), The Stratosphere 1981 Theory and Field Measurements, World Meteorological Organization Global Ozone Research and Monitoring Project Report No. 11, World Meteorological Organization, Geneva, Switzerland.

Zafonte, L., Rieger, P.L. and Holmes, J.R., (1977), "Nitrogen Dioxide Photolysis in the Los Angeles Atmosphere," Environmental Science and Technology, II, 483-487.

CHAPTER 5

Analysis of the Characteristics of Complex Chemical Reaction Mechanisms: Application to Photochemical Smog Chemistry

Published in

Environmental Science and Technology, **18**, 280 (1984).

Reprinted from ENVIRONMENTAL SCIENCE & TECHNOLOGY, Vol. 18, Page 280, April, 1984

Analysis of the Characteristics of Complex Chemical Reaction Mechanisms: Application to Photochemical Smog Chemistry

Joseph A. Leone and John H. Seinfeld*

Department of Chemical Engineering, California Institute of Technology, Pasadena, California 91125

■ To elucidate the features of complex chemical reaction mechanisms, we develop an analysis based on the use of so-called "counter species", fictitious products added to the reactions in the mechanism that allow one to determine the relative contributions of individual reactions to the overall behavior of the mechanism. The method is developed by considering a mechanism for the atmospheric photooxidation of the three simplest aldehydes and is then applied, in a full-scale simulation, to analyze the behavior of a complex chemical reaction mechanism for photochemical smog. The method is shown capable of providing answers to previously inaccessible questions such as the relative contributions of individual hydrocarbons to photochemical ozone formation. Application of the counter species concept to analyze complex environmental reaction mechanisms is straightforward and can be readily implemented in the standard routines in widespread use for solving sets of chemical reaction rate equations.

Introduction

A number of important systems in environmental chemistry are characterized by lengthy and complex chemical reaction mechanisms. In such complex mechanisms it is not generally possible to determine the relative contributions of individual reactions or of certain reaction subnetworks to the overall behavior of the mechanism. Sensitivity analysis, in which the responses of the concentrations to perturbations in parameters (such as rate constants) are computed, is one technique to ascertain the relative importance of individual reactions on predicted behavior (*1–3*).

As a means of elucidating the features of a chemical reaction mechanism, we introduce here a simple technique based on the use of species, which we term counter species. The counter species do not represent actual chemical entities; rather they are purely mathematical quantities that allow us to track flows in a mechanism. In the past, counter species have been used to keep track of the integrated reaction rate for a given chemical reaction (*12–14*). In this paper, we greatly expand the use of this idea as a part of an analysis technique that allows one to examine the inner workings of complex mechanisms, answering questions that were previously inaccessible. The technique is very simple to use and can be implemented readily in the standard computer routines used for solving sets of chemical rate equations.

Because the counter species idea is a simple one, we devote most of this paper to illustrations of its use. In particular, mechanisms describing the chemistry of photochemical smog are notably complex (*4–8*), and consequently, we will develop the counter species method through its application to two reaction mechanisms arising in the description of photochemical smog.

Concept of Counter Species

In this section we introduce the counter species concept using an abbreviated mechanism for photochemical smog.

Photooxidation of the Three Simplest Aldehydes. Let us consider one of the simplest atmospheric reaction mechanisms—the photooxidation of the three aldehydes, formaldehyde, acetaldehyde, and propionaldehyde, in the presence of NO and NO_2. For the purpose of illustrating the technique, assume that we wish to limit the number of species appearing in our mechanism by lumping propionaldehyde together with acetaldehyde. A typical reaction mechanism for this situation might contain the following reactions:

$$NO_2 + h\nu \xrightarrow[O_2]{} NO + O_3 \quad (1)$$

$$NO + O_3 \rightarrow NO_2 + O_2 \quad (2)$$

$$HO_2\cdot + NO \rightarrow NO_2 + OH\cdot \quad (3)$$

$$HCHO + h\nu \xrightarrow[2O_2]{} 2HO_2\cdot + CO \quad (4)$$

$$HCHO + h\nu \rightarrow H_2 + CO \quad (5)$$

$$HCHO + OH\cdot \xrightarrow[O_2]{} HO_2\cdot + CO + H_2O \quad (6)$$

$$CH_3CHO + h\nu \xrightarrow[2O_2]{} CH_3O_2\cdot + HO_2\cdot + CO \quad (7)$$

$$CH_3CHO + OH\cdot \xrightarrow[O_2]{} CH_3C(O)O_2\cdot + H_2O \quad (8)$$

$$CH_3C(O)O_2\cdot + NO \xrightarrow[O_2]{} NO_2 + CH_3O_2\cdot + CO_2 \quad (9)$$

$$CH_3C(O)O_2\cdot + NO_2 \rightarrow CH_3C(O)O_2NO_2(PAN) \quad (10)$$

$$PAN \rightarrow CH_3C(O)O_2\cdot + NO_2 \quad (11)$$

$$CH_3O_2\cdot + NO \rightarrow CH_3O\cdot + NO_2 \quad (12)$$

$$CH_3O\cdot + O_2 \rightarrow HCHO + HO_2\cdot \quad (13)$$

$$NO_2 + OH\cdot \rightarrow HNO_3 \quad (14)$$

In the atmosphere these aldehydes react to produce HO_2, CH_3O_2, and $CH_3C(O)O_2$ radicals that can convert NO to NO_2 and thus cause $[NO_2]/[NO]$, and consequently O_3, to increase. Ozone formation will continue as long as aldehydes and NO_x are both present. NO_x is consumed via reactions 10 and 14, so ultimate O_3 yields are limited by NO_x availability as well as by how fast the aldehydes lead to O_3 formation through the conversion of NO to NO_2.

In analyzing mechanisms for photochemical smog, the key features which need to be examined concern (1) the relative importance of the various radical initiation and termination steps and (2) the conversion of NO to NO_2, which ultimately leads to the accumulation of O_3. For example, in the reaction mechanism shown above, NO to NO_2 conversions occur via reactions 3, 9, and 12. We seek to know the number of these NO to NO_2 conversions attributable to formaldehyde, acetaldehyde, and propionaldehyde and, within each of these, the number due to

 0013-936X/84/0918-0280$01.50/0

Table I. Initial Conditions and Photolysis Rates for the Three Aldehyde/NO_x Simulation[a]

initial reactant concn, ppb	photolysis rates, $(min)^{-1}$
$[NO]_0$, 600	$k_1 = 0.35$
$[NO_2]_0$, 80	$k_4 = 8.6 \times 10^{-4}$
$[HCHO]_0$, 100	$k_5 = 8.2 \times 10^{-4}$
$[CH_3CHO]_0$, 50	$k_7 = 1.3 \times 10^{-4}$
$[CH_3CH_2CHO]_0$, 7	

[a] Temperature = 298 K; pressure = 1 atm.

photolysis and OH reaction. In order to obtain this information, we first rewrite the mechanism as the following:

$$NO_2 + h\nu \xrightarrow[O_2]{} NO + O_3 \quad (1)$$

$$NO + O_3 \rightarrow NO_2 + O_2 \quad (2)$$

$$HO_2\cdot + NO \rightarrow NO_2 + OH\cdot + C3 \quad (3)$$

$$HCHO + h\nu \xrightarrow[2O_2]{} 2HO_2\cdot + CO + C4 \quad (4)$$

$$HCHO + h\nu \rightarrow H_2 + CO \quad (5)$$

$$HCHO + OH\cdot \xrightarrow[O_2]{} HO_2\cdot + CO + H_2O + C6 \quad (6)$$

$$CH_3CHO(a) + h\nu \xrightarrow[2O_2]{} CH_3O_2\cdot + HO_2\cdot + CO + C7 \quad (7)$$

$$CH_3CHO(a) + OH\cdot \xrightarrow[O_2]{} CH_3C(O)O_2\cdot + H_2O + C8 \quad (8)$$

$$CH_3C(O)O_2\cdot + NO \xrightarrow[O_2]{} NO_2 + CH_3O_2\cdot + CO_2 + C9 \quad (9)$$

$$CH_3C(O)O_2\cdot + NO_2 \rightarrow CH_3C(O)O_2NO_2(PAN) \quad (10)$$

$$PAN \rightarrow CH_3C(O)O_2\cdot + NO_2 \quad (11)$$

$$CH_3O_2\cdot + NO \rightarrow CH_3O\cdot + NO_2 + C12 \quad (12)$$

$$CH_3O\cdot + O_2 \rightarrow HCHO + HO_2\cdot + C13 \quad (13)$$

$$NO_2 + OH\cdot \rightarrow HNO_3 + C14 \quad (14)$$

$$HCHI + h\nu \xrightarrow[2O_2]{} 2HO_2\cdot + CO + C15 \quad (15)$$

$$HCHI + h\nu \rightarrow H_2 + CO \quad (16)$$

$$HCHI + OH\cdot \xrightarrow[O_2]{} HO_2\cdot + CO + H_2O + C17 \quad (17)$$

$$CH_3CHO(b) + h\nu \xrightarrow[2O_2]{} CH_3O_2\cdot + HO_2\cdot + CO + C18 \quad (18)$$

$$CH_3CHO(b) + OH\cdot \xrightarrow[O_2]{} CH_3C(O)O_2\cdot + H_2O + C19 \quad (19)$$

Three changes have been made from the original mechanism. First, for reasons that will be made clear shortly, reactions 15, 16, and 17 have been added to the mechanism. For now, we note that whenever a species that is present initially is also formed as a product in the reaction mechanism, we represent this species by two separate species. Thus, we now have photolysis and OH reactions for both HCHO (formaldehyde formed as a product) and HCHI (initially present formaldehyde). If there were initially 30 ppb of formaldehyde present, we would specify 30 ppb as the initial concentration of HCHI.

The second change from the original mechanism is the addition of reactions 18 and 19. Because we wish to distinguish the NO to NO_2 conversions due to the initial acetaldehyde from those due to the initial propionaldehyde, we include reactions for both CH_3CHO(a) (acetaldehyde) and CH_3CHO(b) (propionaldehyde). If there were initially 20 ppb of acetaldehyde and 5 ppb of propionaldehyde, we would specify 20 ppb of CH_3CHO(a) and 5 ppb of CH_3CHO(b) as initial conditions.

The third change from the original mechanism is the addition of fictitious products, C*i*, to some of the reactions. These products are produced only in one reaction and are not consumed. For instance, one "molecule" of C9 is formed for each molecule of NO converted to NO_2 by reaction 9. Since C*i* counts the number of times reaction *i* has occurred, we call C*i* a counter species, and we term the analysis using the C*i* a counter species analysis.

The next step in the counter species analysis is to determine the fraction of the molecules of any product species S that has led to NO to NO_2 conversions up until any time *t*:

F_s = (number of NO/NO_2 conversions due to produced species S, up to time *t*)/(number of molecules of S formed up to time *t*)

Using this definition and the mechanism shown above, we find that

$$F_{HO_2} = \frac{C3}{2C4 + C6 + C7 + C13 + 2C15 + C17 + C18}$$

$$F_{HCHO} = \frac{F_{HO_2}(2C4 + C6)}{C13}$$

$$F_{CH_3O} = \frac{C13(F_{HO_2} + F_{HCHO})}{C12}$$

$$F_{CH_3O_2} = \frac{C12(1 + F_{CH_3O})}{C7 + C9 + C18}$$

$$F_{CH_3C(O)O_2} = \frac{C9(1 + F_{CH_3O_2})}{C8 + C19}$$

The reason for dividing formaldehyde into two species, HCHI (representing the initially present formaldehyde) and HCHO (representing formaldehyde produced by reaction 13), can now be explained fully. We need to form F_{HCHO}, which represents the fraction of all *produced* formaldehyde molecules that lead to NO to NO_2 conversions. By definition, this fraction does not involve any of the initially present HCHO. Thus, we must separate the two types of formaldehyde in order to properly calculate the relation F_{HCHO}. The desired quantities are then expressed in terms of the fractional relations:

number of NO to NO_2 conversions measured as a concentration due to

photolysis of initial formaldehyde = $2C15F_{HO_2}$

photolysis of initial acetaldehyde = $C7(F_{CH_3O_2} + F_{HO_2})$

photolysis of initial propionaldehyde = $C18(F_{CH_3O_2} + F_{HO_2})$

OH reaction of initial formaldehyde = $C17F_{HO_2}$

Table II. Counter Species Results Calculated after 6 h of Irradiation for the Three Aldehyde/NO_x Simulation

(A) Fractional Relation Results

species (S)	fractional value (F_S)
$HO_2\cdot$	1.00
HCHO	0.43
$CH_3O\cdot$	1.43
$CH_3O_2\cdot$	2.43
$CH_3C(O)O_2\cdot$	3.39

(B) Integrated Rates

reaction	amount of NO to NO_2 conversions attributable to each reaction, ppb	amount of radicals produced via each reaction, ppb	amount of radicals scavenged via each reaction, ppb	amount of NO_x sinks attributable to each reaction, ppbN
formaldehyde photolysis	38	44.7		
formaldehyde + OH	25			
acetaldehyde photolysis	6	3.3		
acetaldehyde + OH	71			
propionaldehyde photolysis	0.5	0.3		
propionaldehyde + OH	5.7			
PAN formation			0.3	0.3
HNO_3 formation			48	48

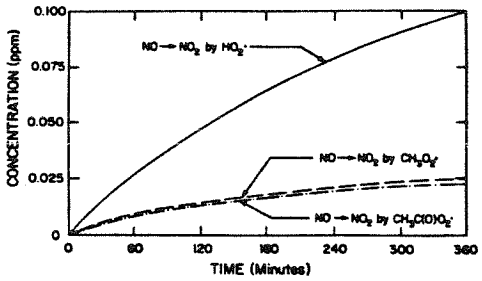

Figure 1. Counter species results for the three aldehyde/NO_x simulation. Number of NO to NO_2 conversions due to hydroperoxyl ($HO_2\cdot$), methylperoxy ($CH_3O_2\cdot$), and peroxyacetyl ($CH_3C(O)O_2\cdot$) radicals.

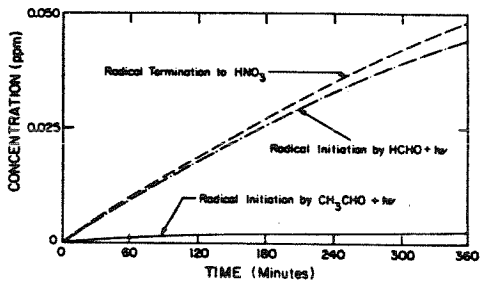

Figure 2. Counter species results for the three aldehyde/NO_x simulation. Number of radical initiation and radical termination steps for the most important radical-producing and radical-scavenging reactions.

$$\text{OH reaction of initial acetaldehyde} = C8F_{CH_3C(O)O_2}$$

$$\text{OH reaction of initial propionaldehyde} = C19F_{CH_3C(O)O_2}$$

If desired, we can gain additional information from the counter species analysis. For example

NO to NO_2 conversions due to

$$\text{photolysis of produced HCHO} = 2C4F_{HO_2}$$

$$\text{OH reaction of produced HCHO} = C6F_{HO_2}$$

radical initiation due to the photolysis of

$$\text{formaldehyde} = 2C15 + 2C4$$

$$\text{acetaldehyde} = 2C7$$

$$\text{propionaldehyde} = 2C18$$

radical termination to

$$\text{PAN} = [\text{PAN}]$$

$$HNO_3 = [HNO_3]$$

It is of interest to calculate these quantities for a given set of initial conditions and photolysis rates. These are shown in Table I. The initial NO_x and aldehyde concentrations are approximately twice the typical values found in early morning Los Angeles air. The counter species results are given in Table II and shown in Figures 1–3. We see that the CH_3CHO + OH reaction accounts for most of the NO to NO_2 conversion, while the photolysis of acetaldehyde and propionaldehyde give rise only to a small percentage of the NO oxidations. Figure 1 shows that most of the NO to NO_2 conversions involve the HO_2 radical via reaction 3. The results shown in Figure 2 in-

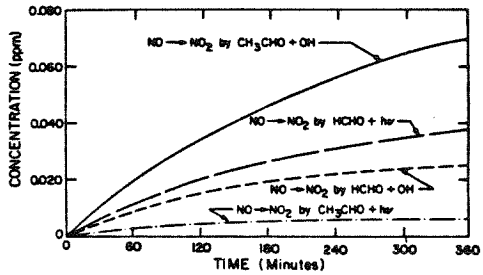

Figure 3. Counter species results for the three aldehyde/NO_x simulation. Number of NO to NO_2 conversions due to the photolysis and OH reactions of formaldehyde and acetaldehyde.

Table III. Initial Conditions for the Hydrocarbon/NO_x Simulation

species	initial concn, ppb	lumped classification in the Atkinson et al. mechanism (7)	initial condition, ppb
propane	17.0	propane	17.0 propane
acetone	35.2	acetone	35.2 acetone
isobutane	0.2	alkane	0.2 alkane
n-butane	166	alkane	166 alkane
2,3-dimethylbutane	97.6	alkane	97.6 alkane
ethene	43.2	ethene	43.2 ethene
propene	10.6	propene	10.6 propene
trans-2-butene	0.7	butene	0.7 butene
cis-2-butene	13.0	butene	13.0 butene
2-methyl-2-butene	14.8	butene	14.8 butene
benzene	1.6	benzene	1.6 benzene
toluene	16.8	toluene	16.8 toluene
ethylbenzene	6.4	toluene	6.4 toluene
m-xylene	42.4	xylene	42.4 xylene
isopropylbenzene	0.4	toluene	0.4 toluene
n-propylbenzene	0.1	toluene	0.1 toluene
m-ethyltoluene	1.0	xylene	1.0 xylene
1,2,3-trimethylbenzene	1.6	xylene	1.6 xylene
formaldehyde	38.0	formaldehyde	38.0 HCHO
acetaldehyde	20.0	acetaldehyde	20.0 CH_3CHO
propionaldehyde	3.2	RCHO	3.2 RCHO
NO	301.0		
NO_2	41.0		
HONO	12.0		
CO	7 450		
H_2O, ppm	15 500		
O_2, ppm	210 000		
M, ppm	1 000 000		
	Totals for the Lumped Classes		
propane	17.0		
alkane	263.8		
acetone	35.2		
ethene	43.2		
propene	10.6		
butene	28.5		
benzene	1.6		
toluene	23.7		
xylene	45.0		
HCHO	38.0		
CH_3CHO	20.0		
RCHO	3.2		

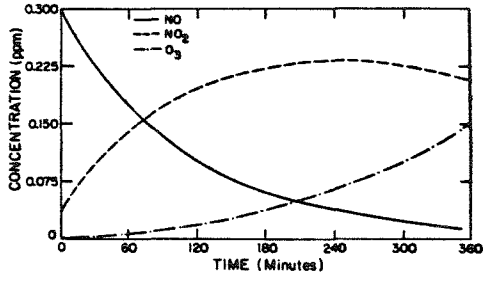

Figure 4. NO, NO_2, and O_3 concentration–time profiles obtained by using the hydrocarbon/NO_x photooxidation mechanism of Atkinson et al. with initial conditions shown in Table IV.

dicate that the only important radical initiation step is formaldehyde photolysis and that the only significant radical termination process and NO_x sink are nitric acid formation.

With simple mechanisms such as the three aldehyde mechanisms shown above, there is an alternate way of using counter species to obtain the desired information. By applying the pseudo-steady-state approximation to the HO_2, CH_3O_2, and CH_3O radicals, we can write a compact mechanism in which these fast-reacting species are eliminated. With these "condensed" mechanisms the number of NO to NO_2 conversions due to each reaction pathway is given by the counters themselves. No fractional relationships are needed.

Unfortunately, all of the useful chemical reaction mechanisms describing photochemical smog are much more complicated than the simple aldehyde mechanism presented above. With these mechanisms, it becomes extremely difficult to eliminate the fast-reacting species using the pseudo-steady-state approximation. Nevertheless, the counter species analysis provides an effective means to examine the properties of these complex mechanisms. Such an analysis is presented in the next section.

Application of Counter Species To Analyze a Complex Atmospheric Reaction Mechanism

A number of chemical reaction mechanisms have been proposed as suitable for inclusion in urban airshed simulation models (*7–10*). Each of these mechanisms uses some form of hydrocarbon "lumping" in order to reduce the number of species and reactions to a reasonable number. Typical of these is the mechanism proposed by Atkinson et al. (7), which we analyze in this section. This mechanism uses the lumped molecule approach, in which one or more reactants of similar structure and reactivity are grouped into a single class. For example, this mechanism represents

Table IV. Counter Species Relations and Results for the Number of NO to NO_2 Conversions Attributable to Various Radicals, Inorganic Compounds, and Organics Appearing in the Hydrocarbon/NO_x Photooxidation Mechanism of Atkinson et al. (7)

(A) NO Oxidation by Radical Species

species	NO to NO_2 conversions: counter species expressions[a]	ppb	%
$HO_2\cdot$	C7	279	58.9
$AO_2\cdot$	1.7C33	59.3	12.6
$CH_3O_2\cdot$	C29	35.6	7.5
hydroxyalkylperoxy radicals[b]	C44 + C45 + 0.9C46	34.1	7.2
$CH_3C(O)O_2\cdot$	C28	27.7	5.8
ADD	0.75C61	14.5	3.1
EL	3C65	11.3	2.4
$C_2H_4O_2\cdot$	C38	3.2	0.7
$CH_2\dot{C}HO\dot{O}$	C54	3.1	0.7
ADD2	0.75C71	1.6	0.3
$RCO_3\cdot$	C37	1.4	0.3
$PO_2\cdot$	C31	0.9	0.2
$XO_2\cdot$	C41	0.9	0.1
$\dot{C}H_2\dot{O}_2$	C50	0.6	0.1
$ARO_2\cdot$	0.75C74	0.5	0.1
$ARO_3\cdot$	C79	~0	0
$PHO_2\cdot$	C80	~0	0
total		473.7[d]	100

(B) NO Oxidation by Inorganic Compounds

species	counter species expression	NO to NO_2 conversions, ppb
O_3	C2	25070
NO_3	C14	220

(C) NO Oxidations by Different Reaction Pathways

reaction pathway[c]	NO to NO_2 conversions: counter species expression	ppb	%
HCHO + OH	$C23F_{HO_2\cdot}$	9.3	2.0
HCHO + $h\nu$	$2C21F_{HO_2\cdot}$	14.8	3.1
CH_3CHO + OH	$C25F_{CH_3C(O)O_2\cdot}$	17.8	3.8
CH_3CHO + $h\nu$	$C24(F_{HO_2\cdot} + F_{CH_3O_2\cdot})$	2.3	0.5
RCHO + OH	$C34F_{RCO_3\cdot}$	2.7	0.6
RCHO + $h\nu$	$C39(F_{HO_2\cdot} + F_{C_2H_5O_2\cdot})$	0.5	0.1
total aldehyde		47.4	10.1
propane + OH	$C30F_{PO_2\cdot}$	1.9	0.4
ALK + OH	$C32F_{AO_2\cdot}$	115.2	24.3
total alkanes		117.1	24.7
ethene + OH	$C44(1 + F_{HO_2\cdot} + 2F_{HCHO})$	30.5	6.4
propene + OH	$C45(1 + F_{HO_2\cdot} + F_{CH_3CHO} + F_{HCHO})$	18.6	3.9
butene + OH	$0.9C46(1 + F_{HO_2\cdot} + 2F_{CH_3CHO})$	59.8	12.7
total alkene + OH		108.9	23.0
ethene + O_3	$C47(0.12F_{HO_2\cdot} + 0.4F_{\dot{C}H_2\dot{O}_2} + F_{HCHO})$	1.9	0.4
propene + O_3	$C48[0.5(F_{HCHO} + F_{CH_3CHO}) + 0.2(F_{\dot{C}H_2\dot{O}_2} + F_{CH_3\dot{C}HO_2} + F_{HO_2} + F_{CH_3O_2\cdot})]$	3.2	0.7
butene + O_3	$C49(F_{CH_3CHO} + 0.4F_{CH_3\dot{C}HO_2} + 0.3F_{HO_2\cdot} + 0.45F_{CH_3O_2\cdot})$	25.4	5.3
total alkene + O_3		30.5	6.4
total alkene		139.4	29.4
benzene + OH	$0.25C58(F_{cresol} + F_{HO_2\cdot}.3F_{ADD})$	0.9	0.2
toluene + OH abstraction	$0.75C74(1 + F_{HO_2\cdot}) + C79 + C80$	1.2	0.2
toluene + OH addition	$0.20C59(F_{cresol} + F_{HO_2\cdot} + 3.25F_{ADD})$	14.0	2.9
xylene + OH	$0.25C60(F_{cresol} + F_{HO_2\cdot} + 3F_{ADD})$	73.9	15.6
total aromatic		90.0	18.8
$CH_3C(O)CH_3$ + $h\nu$	$C43(F_{CH_3C(O)O_2\cdot} + F_{CH_3O_2\cdot})$	2.9	0.6
OH + CO	$C12F_{HO_2}$	80.6	17.0
		474.4[d]	100
miscellaneous			
toluene ring opening	$0.65C59F_{ADD}$	12.4	2.6
cresol ring opening	$C70F_{ADD2}$	5.2	1.1
conjugated γ-dicarbonyl (DIAL) reactions	$C62F_{EL}$	20.9	4.4
glyoxal ($(CHO)_2$) reactions	$C66F_{HO_2\cdot} + C67F_{HCHO}$	0.6	0.1

Table IV (*Continued*)

reaction pathway[c]	NO to NO_x conversions: counter species expression	ppb	%
methylglyoxal ($CH_3C(O)CHO$) photolysis	$C69(F_{CH_3C(O)O_2\cdot} + F_{HO_2\cdot})$	27.8	5.9
methylglyoxal + OH	$C68F_{CH_3C(O)O_2\cdot}$	4.4	0.9
MEK + $h\nu$	$C42(F_{C_2H_5O_2\cdot} + F_{CH_3C(O)O_2\cdot})$	7.4	1.6
MEK + OH	$C40F_{XO_2}$	3.4	0.7

[a] The C*i* in these expressions are fictitious products added to each of the reactions in the Atkinson et al. (7) mechanism. For example, C7 is listed as a product in reaction 7. [b] These radicals are formed in the OH-alkene reactions (reactions 44-66). [c] In cases where a species is both present initially and formed as a product, the numbers and expressions shown above refer only to the initially present amount. For example, the 14.8 ppb of NO to NO_x conversions shown under formaldehyde photolysis is due to the photolysis of initially present formaldehyde. [d] Obviously, the total amount of NO to NO_x conversions shown in parts A and C of this table must agree if the counter species analysis has been performed correctly.

the alkenes in the following manner. Ethene is treated separately because it reacts with OH and O_3 at significantly slower rates than other alkenes. The terminal alkenes are lumped into one group whose chemistry is represented by that of propene. In the same fashion, the chemistry of *trans*-2-butene is used to represent that of all internally bonded alkenes. This type of approach is used with each of the hydrocarbon groups, resulting in a mechanism that contains 81 reactions and 52 species.

A detailed description and derivation of the Atkinson et al. mechanism can be found in the original paper (7) and is therefore not presented here. The only differences between the mechanism used in this study and that originally presented by Atkinson et al. (7) are (1) the three chamber-dependent reactions and the SO_2 reaction are not included here, (2) some photolysis rates have been changed to reflect experimental data that have been acquired since the original mechanism was published, and (3) counter species have been added to many of the reactions. The initial conditions chosen for this study correspond to those used in smog chamber experiment SUR-119J, performed at the University of California, Riverside (*11*), the detailed composition of which is shown in Table III, together with the corresponding initial conditions to be used with the Atkinson et al. (7) mechanism. The concentration–time profiles of NO, NO_2, and O_3, obtained by using this slightly modified Atkinson et al. mechanism, with the above-mentioned initial conditions, are given in Figure 4.

The counter species analysis of this mechanism proceeds in the same manner as was shown earlier with the simple aldehyde mechanism. We first formulate the F_s, which represents the fraction of species S that have led to NO to NO_2 conversions up until any specified time. Next, we formulate expressions for the number of NO to NO_2 conversions due to various species and reaction pathways. Table IV shows these relationships, together with their resulting values after 6 h of the simulation. Listed in section A of Table IV is the number of NO to NO_2 conversions attributable to the various radicals appearing in this system. We see that a majority of the NO oxidations are caused by HO_2 radicals and that most of the remaining NO to NO_2 conversions are due to alkylperoxy (AO_2), methylperoxy (CH_3O_2), hydroxyalkylperoxy (R-OH-O_2), and peroxyacetyl ($CH_3C(O)O_2$) radicals. For comparison, section B of Table IV shows the number of NO oxidations due to the inorganic reactions. Section C of Table IV presents the most useful counter species results, from which we can draw many conclusions. For example, we see that the di- and trialkylbenzenes, represented in this mechanism by xylene, account for 82% of the NO to NO_2 conversions due to the aromatic hydrocarbons. Of the 19% of the total NO oxidations that are due to the aromatics, 6% are due to methylglyoxal photolysis alone. We also conclude that alkene–OH reactions lead to significantly more NO to NO_2 conversions than alkene–O_3 reactions. In addition, notice that the percent of NO to NO_2 conversions due to the alkane plus OH reaction (24.7%) is about the same as the percent conversion due to alkene–OH reactions (23.0%). This is an interesting result since alkanes are generally viewed as less important than alkenes or aromatics. Also notice that the amount of NO converted to NO_2 due to the alkanes is completely dominated by the $n \geq 4$ alkanes (butane in the Atkinson et al. mechanism). This leads us to conclude that, for most urban applications, treating propane as unreactive will not cause any noticeable change in the predictive ability of lumped mechanisms. One last point which we note here is that the ketones and higher aldehydes ($n > 2$) lead to only a small number of NO to NO_2 conversions.

The second type of information that we desire, and which the counter species analysis provides, concerns radical initiation and termination and NO_x sinks. These results are presented in Table V. We see that for the test case considered here, formaldehyde photolysis is the most important radical source. The photolysis of O_3 and methylglyoxal is also important, as is the reaction of O_3 with the internally bonded alkenes (butene). The most important radical and NO_x sink are nitric acid formation via reaction 5. Peroxyacetyl nitrate (PAN) formation represents the only remaining NO_x and radical sink of any significance. The most important radical sources and sinks for the first 6 h of the simulation are shown in Figure 5.

Conclusions

The counter species analysis developed here enables one to assess quantitatively the importance of individual reactions and reaction subnetworks to the overall behavior of a complex chemical mechanism. The method is conceptually simple and is easy to implement with any mechanism. By applying the counter species analysis to a complex chemical mechanism describing photochemical smog, we are able to determine the relative importance of individual hydrocarbons and reaction steps to ozone formation, radical initiation and termination, and NO_x removal.

The counter species analysis has applications in any problem where complex chemical reaction mechanisms arise. Applications relevant to the field of atmospheric hydrocarbon chemistry include the following:

(1) The first application is evaluating the performance of "lumped" reaction mechanisms by applying the counter species analysis to both the lumped and explicit mechanisms. One could then quantitatively evaluate how well

Table V. Radical Source, Radical Sink, and NO_x Removal Results from the Counter Species Analysis of the Hydrocarbon/NO_x Photooxidation Simulation

reaction(s)	counter species expression	integrated rates: radical sources, ppb	integrated rates: radical sinks, ppb	integrated rates: NO_x sinks, ppb
HCHO + $h\nu$	2C21	33.5		
O_3 + $h\nu$	2C3	24.8		
$CH_3C(O)CHO$ + $h\nu$	2C69	18.0		
O_3 + butene	1.35C49	12.5		
HONO + $h\nu$	C6–C4	11.7		
CH_3CHO + $h\nu$	2C24	5.2		
cresol + NO_3	C72	4.1		
MEK + $h\nu$	2C42	3.0		
O_3 + propene	0.9C48	1.6		
$CH_3C(O)CH_3$ + $h\nu$	2C43	1.5		
O_3 + ethene	0.52C47	1.0		
RCHO + $h\nu$	2C39	0.5		
HNO_3 formation	C5		76.1	76.1
PAN formation			17.2	17.2
aromatic nitrate formation	0.25(C61 + C71)		5.4	5.4
nitrophenol formation	C73		4.1	4.1
$CH_3\dot{C}HO_2$ reactions	C54 + C55 + C57		4.0	
alkyl nitrate formation	0.1C33		3.5	3.5
LNO_2 formation			2.9	2.9
alkyl nitrate from OH + butene	0.1C46		1.9	1.9
$\dot{C}H_2\dot{O}_2$ reactions	C50 + C51 + C53		1.1	
PPN formation			0.8	0.8
benzyl nitrate formation	0.25C74		0.2	0.2
HO_2NO_2 formation			0.2	0.2
PBZN formation			~0	~0
H_2O_2 formation	C10		~0	~0
HNO_3 formation	C17 + C72			8.6
N_2O_5 formation				0.4
		117.4	117.4	121.3

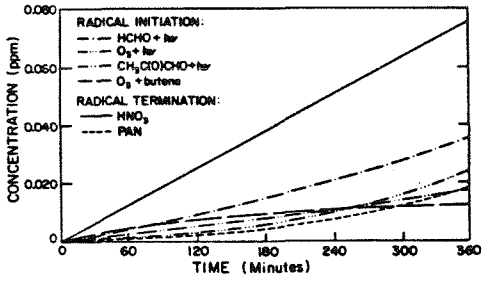

Figure 5. Counter species results for the hydrocarbon/NO_x simulation. Number of radical initiation and radical termination steps for the most important radical-producing and radical-scavenging reactions.

each reaction in the lumped mechanism represents the actual chemistry as depicted in the explicit mechanism.

(2) The second application is comparing two or more mechanisms that describe the same system. For example, different lumped reaction mechanisms can be compared to see exactly how the corresponding lumped classes in each mechanism compare with regard to O_3 formation, radical production, etc.

(3) The third application is obtaining a better understanding of how hydrocarbons should be grouped into classes in lumped mechanisms. In addition, the analysis will help one to choose which hydrocarbons, or lumped classes, can be eliminated without significantly affecting mechanism predictions.

(4) The fourth application is evaluating the importance of individual reaction steps and reaction pathways toward oxidant formation, radical initiation and termination, and NO_x sinks, as was illustrated for the Atkinson et al. (7) mechanism in this paper.

Registry No. O_3, 10028-15-6; HCHO, 50-00-0; CH_3CHO, 75-07-0; CH_3CH_2CHO, 123-38-6; NO, 10102-43-9; NO_2, 10102-44-0.

Literature Cited

(1) Falls, A. H.; McRae, G. J.; Seinfeld, J. H. *Int. J. Chem. Kinet.* **1979**, *11*, 1137–1162.
(2) McRae, G. J.; Tilden, J. W.; Seinfeld, J. H. *Comput. Chem. Eng.* **1982**, *6*, 15–25.
(3) Koda, M.; McRae, G. J.; Seinfeld, J. H. *Int. J. Chem. Kinet.* **1979**, *11*, 427–444.
(4) Atkinson, R.; Darnall, K. R.; Lloyd, A. C.; Winer, A. M.; Pitts, J. N., Jr. *Adv. Photochem.* **1979**, *11*, 375–487.
(5) Whitten, G. Z.; Killus, J. P.; Hogo, H. "Modeling of Simulated Photochemical Smog with Kinetic Mechanisms"; U.S. Environmental Protection Agency: 1980; EPA-600/3-80-028a, pp 1–348.
(6) Hendry, D. G.; Baldwin, A. C.; Golden, D. M. "Computer Modeling of Simulated Photochemical Smog"; U.S. Environmental Protection Agency: 1980; EPA-600/3-80-029, pp 1–207.
(7) Atkinson, R.; Lloyd, A. C.; Winges, L. *Atmos. Environ.* **1982**, *16*, 1341–1355.
(8) Killus, J. P.; Whitten, G. Z. "A New Carbon-Bond Mechanism for Air Quality Modeling", final report to the U.S. Environmental Protection Agency under Contract 68-02-3281, 1982, pp 1–107.
(9) Dodge, M. C. "Combined Use of Modeling Techniques and Smog Chamber Data to Derive Ozone-Precursor Relationships"; U.S. Environmental Protection Agency: 1977; EPA-600/3-77-001a, pp 881–889.
(10) Falls, A. H.; Seinfeld, J. H. *Environ. Sci. Technol.* **1978**, *12*, 1398–1406.

(11) Pitts, J. N.; Winer, A. M.; Darnall, K. R. "Chemical Consequences of Air Quality Standards and of Control Implementation Programs: Roles of Hydrocarbons, Oxides of Nitrogen, and Aged Smog in the Production of Photochemical Oxidant", final report to the California Air Resources Board under Contract 4-212, 1976, pp 1–444.
(12) Graedel, T. E. *J. Phys. Chem.* **1977**, *81*, 2372–2374.
(13) Jeffries, H. E., personal communication.
(14) Whitten, G. Z., personal communication.

Received for review May 2, 1983. Accepted October 3, 1983. This work was supported by the State of California Air Resources Board Agreement A2-042-32.

CHAPTER 6

Evaluation of Chemical Reaction Mechanisms for Photochemical Smog. Part 2: Quantitative Evaluation of the Mechanisms

EVALUATION OF CHEMICAL REACTION MECHANISMS FOR PHOTOCHEMICAL SMOG

PART II. QUANTITATIVE EVALUATION OF THE MECHANISMS

by

Joseph A. Leone
and
John H. Seinfeld

California Institute of Technology
Pasadena, California 91125

Cooperative Agreement 810184

Project Officer

Marcia C. Dodge

Gas Kinetics and Photochemistry Branch
Environmental Sciences Research Laboratories
Research Triangle Park, North Carolina 27711

ENVIRONMENTAL SCIENCES RESEARCH LABORATORY
OFFICE OF RESEARCH AND DEVELOPMENT
U.S. ENVIRONMENTAL PROTECTION AGENCY
RESEARCH TRIANGLE PARK, NORTH CAROLINA 27711

ABSTRACT

The six chemical reaction mechanisms for photochemical smog described in Part I are analyzed to determine why, under identical conditions, they predict different maximum ozone concentrations. To perform the analysis, a counter species analysis technique is used to determine the contributions of individual reactions or sets of reactions to the overall behavior of a chemical reaction mechanism. Using this technique, we can obtain answers to previously inaccessible questions such as the relative contributions of individual organic species to photochemical ozone formation. Based on the results of the analysis we have identified specific aspects of each mechanism that are responsible for the discrepancies with other mechanisms and with a master mechanism based on the latest understanding of atmospheric chemistry. For each mechanism critical areas are identified that when altered bring the predictions of the various mechanisms into much closer agreement. Thus, we have been able to identify why the predictions of the mechanisms are different, and have recommended research efforts that are needed to eliminate many of the discrepancies.

TABLE OF CONTENTS

FIGURE CAPTIONS

LIST OF TABLES

ACKNOWLEDGEMENT

We wish to acknowledge the assistance of: Alan C. Lloyd, Fred Lurmann, Marcia Dodge, Kenneth Demerjian, Kenneth Schere, Gary Whitten, Jim Killus and Joyce Penner for providing computer codes and documentation of their mechanisms. Appreciation is extended to Gregory J. McRae for his assistance.

CHAPTER 1

INTRODUCTION

In determining emission control levels, one must be able to predict how changes in emission levels will affect ambient air quality. An important component of such an approach is a description of atmospheric organic chemistry. Unfortunately, the development of a chemical reaction mechanism that accurately describes atmospheric chemistry and, at the same time, is computationally tractable, is a difficult undertaking. Since typical urban atmospheres contain hundreds of different organic species, it is not feasible to write a mechanism that includes each individual species. Thus, these reaction mechanisms must maintain a balance between the level of chemical detail and, for numerical reasons, the number of species and reaction pathways.

Currently, several chemical reaction mechanisms exist that describe the organic chemistry of the urban atmosphere and that attempt to maintain a balance between chemical detail and mechanism length (McRae et al., 1983). These mechanisms are all based on the same body of experimental rate constant data, and each mechanism has been evaluated against data from various smog chamber facilities. In each mechanism, the detailed atmospheric chemistry has been greatly simplified by a process referred to as lumping (McRae et al., 1983). However, because this simplification, or lumping process, has been carried out in different ways, no two mechanisms are the same. The differences among mechanisms would not be of any concern if each of the mechanisms gave similar predictions over a range of atmospheric conditions. However, several recent investigations have shown that different mechanisms predict substantially different degrees of emission controls to achieve the same desired air quality under identical conditions (Jeffries et al., 1981;

Whitten, 1981; Carter et al., 1982a). Since tremendous expenses are involved in implementing hydrocarbon and NO_x emission controls predicted by such mechanisms, there is an urgent need to understand the fundamental reasons for these discrepancies.

Analyzing the behavior of these atmospheric reaction mechanisms is a demanding task because of the large number of species and reactions that each contains, and because of the interwoven nature of the free radical chain reactions characterizing each mechanism. We make use of a method termed counter species analysis that enables one to account for the influence of individual reactions or reaction networks on the predictions of a mechanism. Using this technique one can assess the differences among the available photochemical smog mechanisms and, where appropriate, point out areas where improvements in our understanding of atmospheric chemistry are needed.

This report represents the second part of a three-part study of lumped reaction mechanisms for photochemical smog. Part I (McRae et al., 1983) contains information concerning the various approaches to lumping, and about how the particular mechanisms chosen for this study were selected. Also included in Part I is a detailed description of each lumped mechanism.

Part II of our study contains the quantitative analysis of the six lumped mechanisms selected for study. In the next chapter we describe "counter species analysis" and the "master" mechanism, both of which play an important role in our comparison of the lumped mechanisms. Also included in Chapter 2 is a summary of the initial conditions and NO_2 photolysis rate profile used in our tests. The bulk of this report is contained in Chapter 3, which presents and discusses all the major results for each of the mechanisms. Chapter 4 summarizes the key findings of this study.

In Part III we will extend the analysis contained in Part II to conditions approximating the real atmosphere. The emission control requirements predicted by the various mechanisms will be examined. In Part III we will also consider the effects of atmospheric hydrocarbon makeup, continous dilution, and the presence of background pollutant concentrations.

CHAPTER 2

METHOD OF ANALYSIS

2.1 Introduction

In this three-part study we want to determine why the various photochemical smog mechanisms predict different emission control requirements to reach the same desired air quality (specifically, the same maximum ozone concentration). The goal of Part II of this study is to understand why these mechanisms, under identical conditions, predict that substantially different levels of O_3 will be reached. In order to answer this question, we would like to determine how much of the total O_3 production can be attributed to each of the initially present organic species in each mechanism. With this information, we could determine the relative contributions of individual organics (or reactions, reaction pathways, etc.) to overall behavior of each mechanism.

Unfortunately, because of the interwoven nature of the free radical chemistry, there is no direct way of calculating the relative amounts of O_3 that each organic species is responsible for producing in a mechanism. We can, however, using a method described below, keep track of the number of NO to NO_2 conversions that arise as a result of the presence of each organic species. The amount of O_3 attributable to a given organic species is well established to be directly proportional to the amount of NO oxidation affected by the species.

The technique we use to determine the number of NO to NO_2 conversions attributable to individual species is called *counter species analysis*. The idea of counter species has been used previously by several investigators (Calvert et al. 1978; Graedel 1977; Whitten, 1983), and the technique used here is described in detail elsewhere (Leone and Seinfeld, 1983a). However, for completeness, we include in the next section an example illustrating its use.

2.2 Counter Species Analysis

Let us consider one of the simplest atmospheric reaction mechanisms - the photooxidation of the three aldehydes, formaldehyde, acetaldehyde, and propionaldehyde, in the presence of NO and NO_2. For the purpose of illustrating the technique, assume that we wish to limit the number of species appearing in our mechanism by lumping propionaldehyde together with acetaldehyde. A typical reaction mechanism for this situation might contain the following reactions:

$$NO_2 + h\nu \xrightarrow[O_2]{1} NO + O_3$$

$$NO + O_3 \xrightarrow{2} NO_2 + O_2$$

$$HO_2\cdot + NO \xrightarrow{3} NO_2 + OH\cdot$$

$$HCHO + h\nu \xrightarrow[2O_2]{4} 2HO_2\cdot + CO$$

$$HCHO + h\nu \xrightarrow{5} H_2 + CO$$

$$HCHO + OH\cdot \xrightarrow[O_2]{6} HO_2\cdot + CO + H_2O$$

$$CH_3CHO + h\nu \xrightarrow[2O_2]{7} CH_3O_2\cdot + HO_2\cdot + CO$$

$$CH_3CHO + OH\cdot \xrightarrow[O_2]{8} CH_3C(O)O_2\cdot + H_2O$$

$$CH_3C(O)O_2\cdot + NO \xrightarrow[O_2]{9} NO_2 + CH_3O_2\cdot + CO_2$$

$$CH_3C(O)O_2\cdot + NO_2 \xrightarrow{10} CH_3C(O)O_2NO_2(PAN)$$

$$PAN \xrightarrow{11} CH_3C(O)O_2\cdot + NO_2$$

$$CH_3O_2\cdot + NO \xrightarrow{12} CH_3O\cdot + NO_2$$

$$CH_3O\cdot + O_2 \rightarrow HCHO + HO_2\cdot$$

$$NO_2 + OH\cdot \xrightarrow{14} HNO_3 .$$

In the atmosphere these aldehydes react to produce HO_2, CH_3O_2, and $CH_3C(O)O_2$ radicals that can convert NO to NO_2, and thus cause $[NO_2]/[NO]$, and consequently O_3, to increase. Ozone formation will continue as long as aldehydes and NO_x are both present. NO_x is consumed via reactions 10 and 14, so ultimate O_3 yields are limited by NO_x availability as well as by how fast the aldehydes lead to O_3 formation through the conversion of NO to NO_2. In the reaction mechanism shown above, NO to NO_2 conversions occur via reactions 3, 9, and 12. We seek to know the number of these NO to NO_2 conversions attributable to formaldehyde, acetaldehyde, and propionaldehyde, and, within each of these, the number due to photolysis and OH reaction. In order to obtain this information, we first rewrite the mechanism as:

$$NO_2 + h\nu \xrightarrow[O_2]{1} NO + O_3$$

$$NO + O_3 \xrightarrow{2} NO_2 + O_2$$

$$HO_2\cdot + NO \xrightarrow{3} NO_2 + OH\cdot + C3$$

$$HCHO + h\nu \xrightarrow{4} 2HO_2\cdot + CO + C4$$

$$HCHO + h\nu \xrightarrow[2O_2]{5} H_2 + CO$$

$$HCHO + OH\cdot \xrightarrow{6} HO_2\cdot + CO + H_2O + C6$$

$$CH_3CHO(a) + h\nu \xrightarrow[2O_2]{7} CH_3O_2\cdot + HO_2\cdot + CO + C7$$

$$CH_3CHO(a) + OH\cdot \xrightarrow[O_2]{8} CH_3C(O)O_2\cdot + H_2O + C8$$

$$CH_3C(O)O_2\cdot + NO \xrightarrow[O_2]{9} NO_2 + CH_3O_2\cdot + CO_2 + C9$$

$$CH_3C(O)O_2\cdot + NO_2 \xrightarrow{10} CH_3C(O)O_2NO_2(PAN)$$

$$PAN \xrightarrow{11} CH_3C(O)O_2\cdot + NO_2$$

$$CH_3O_2\cdot + NO \xrightarrow{12} CH_3O\cdot + NO_2 + C12$$

$$CH_3O\cdot + O_2 \xrightarrow{13} HCHO + HO_2\cdot + C13$$

$$NO_2 + OH\cdot \xrightarrow{14} HNO_3$$

$$HCHI + h\nu \xrightarrow[2O_2]{15} 2HO_2\cdot + CO + C15$$

$$HCHI + h\nu \xrightarrow{16} H_2 + CO$$

$$HCHI + OH\cdot \xrightarrow[O_2]{17} HO_2\cdot + CO + H_2O + C17$$

$$CH_3CHO(b) + h\nu \xrightarrow[2O_2]{18} CH_3O_2\cdot + HO_2\cdot + CO + C18$$

$$CH_3CHO(b) + OH\cdot \xrightarrow[O_2]{19} CH_3C(O)O_2\cdot + H_2O + C19.$$

Three changes have been made from the original mechanism. First, for reasons that will be made clear shortly, reactions 15, 16, and 17 have been added to the mechanism. For now, we note that whenever a species that is present initially is also formed as a product in the reaction mechanism, we represent this species by two separate species. Thus, we now have photolysis and OH reactions for both HCHO (formaldehyde formed as a product) and HCHI (initially present formaldehyde). If there were initially 30 ppb of formaldehyde present, we would specify 30 ppb as the initial concentration of HCHI.

The second change from the original mechanism is the addition of reactions 18 and 19. Because we wish to distinguish the NO to NO_2 conversions due to the initial acetaldehyde from those due to the initial propionaldehyde, we include reactions for both $CH_3CHO(a)$ (acetaldehyde) and $CH_3CHO(b)$ (propionaldehyde). If there were initially 20 ppb of acetaldehyde and 5 ppb of propionaldehyde, we would specify 20 ppb of $CH_3CHO(a)$ and 5 ppb of $CH_3CHO(b)$ as initial conditions.

The third change from the original mechanism is the addition of fictitious products, Ci, to some of the reactions. These products are produced only in one reaction and are not consumed. For instance, one "molecule" of C9 is formed for each molecule of NO converted to NO_2 by reaction 9. Since Ci counts the number of times reaction i has occurred, Ci is called a counter species, and the analysis using the Ci is termed a counter species analysis.

The next step in the counter species analysis is to determine the fraction of the molecules of any product species S that have led to NO to NO_2 conversions up until any time t,

$$F_S = \frac{\text{Number of NO/NO}_2 \text{ conversions due to produced species S, up to time t}}{\text{Number of molecules of S formed up to time t}} .$$

Using this definition and the mechanism shown above, we find that:

$$F_{HO_2} = \frac{C3}{2C4+C6+C7+C13+2C15+C17+C18}$$

$$F_{HCHO} = \frac{(2C4+C6)F_{HO_2}}{C13}$$

$$F_{CH_3O} = \frac{C13(F_{HO_2}+F_{HCHO})}{C12}$$

$$F_{CH_3O_2} = \frac{C12(1+F_{CH_3O})}{C7+C9+C18}$$

$$F_{CH_3C(O)O_2} = \frac{C9(1+F_{CH_3O_2})}{C8+C19} \quad .$$

The desired quantities are then expressed in terms of these fractional relations.

Number of NO to NO_2 conversions due to:

photolysis of initial formaldehyde = $2C15\ F_{HO_2}$

photolysis of initial acetaldehyde = $C7(F_{CH_3O_2} + F_{HO_2})$

photolysis of initial propionaldehyde = $C18(F_{CH_3O_2} + F_{HO_2})$

OH reaction of initial formaldehyde = $C17\ F_{HO_2}$

OH reaction of initial acetaldehyde = $C8\ F_{CH_3C(O)O_2}$

OH reaction of initial propionaldehyde = $C19\ F_{CH_3C(O)O_2}$.

If desired, we can gain additional information from the counter species analysis. For example,

NO to NO_2 conversions due to:

photolysis of produced HCHO = $2C4\ F_{HO_2}$

OH reaction of produced HCHO = $C6\ F_{HO_2}$

radical initiation due to the photolysis of:

initial formaldehyde = 2C15

acetaldehyde = 2C7

propionaldehyde = 2C18

radical termination to:

PAN = [PAN]

$HNO_3 = [HNO_3]$.

The reason for dividing formaldehyde into two species, HCHI(representing the initially present formaldehyde) and HCHO (representing formaldehyde produced by reaction 13), can now be fully explained. We need to form F_{HCHO}, which represents the fraction of all *produced* formaldehyde molecules that lead to NO to NO_2 conversions. By definition this fraction does not involve any of the initially present HCHO. Thus, we must separate the two types of formaldehyde in order to properly calculate the relation F_{HCHO}.

The mechanisms to be evaluated shortly are considerably more complicated than the simple aldehyde mechanism described above. However, no matter how complex the mechanism, the counter species analysis proceeds exactly as illustrated above, even though the expressions are more complicated. As a means of ensuring the accuracy of the analysis, we can count the actual number of NO to NO_2 conversions, and compare this to the total obtained via the counter species analysis. For instance, in our simple example above, the actual number of NO to NO_2 conversions that have occurred up to any time is given by C3+C9+C12. This same result must be obtained when we total the NO oxidations attributed to the three aldehydes (calculated from the relations on page 9). All of the results given in Chapter 3 have been confirmed in this way.

In summary, the counter species analysis enables one to assess quantitatively the importance of individual reactions and reaction sub-networks to the overall behavior of a complex mechanism. By using the counter species analysis on the six lumped mechanisms considered in this study, we can compare individual portions of these mechanisms to each other. These individual comparisons are then used to determine the reasons for the observed differences in overall behavior.

2.3 Master Mechanism

Each of the lumped mechanisms represents an attempt to simplify the detailed chemistry of the atmospheric organic/NO_x system. The lumped mechanisms are, it is important to stress, derived from known detailed, explicit chemistry and are not simply empirical curve fits of data. For this reason, it is appropriate to compare the structure and behavior of each mechanism to a fully explicit, detailed mechanism containing as many of the important organic species as possible. In doing so, we can assess the degree to which each of the lumped mechanisms represents the explicit chemistry of the organic constituents that are included in the lumped classes in the mechanisms.

Table 1 gives the initial composition of smog chamber experiment SUR-119J performed at the Statewide Air Pollution Research Center (SAPRC), University of California at Riverside (Pitts et al., 1976). The individual species concentrations for this experiment were chosen to represent the 6-9 AM ambient pollutant burden in the Los Angeles atmosphere. If we exclude the first three hydrocarbons (methane, acetylene, and ethane) because of their low reactivity, we see that the remainder of the list is dominated by the presence of about 10-12 organic species. A great deal of kinetic and mechanistic data dealing with the atmospheric chemistry of these species has been obtained over the past decade or so. These data have been analyzed and summarized by Atkinson and Lloyd (1984). Thus, with this information, we feel that a realistic, explicit reaction mechanism can be formulated for the key species in Table 1. We call this the "master mechanism."

2.4 Details of the Master Mechanism

A listing of the master mechanism is given in Table A.1 of the Appendix. The primary organics whose explicit chemistry is contained in the

TABLE 1

Composition of Smog Chamber Experiment SUR-119J
(Pitts et al., 1976)

SPECIES	CONCENTRATION ppbV	ppbC
Methane (CH_4)	2740.0	2740.0
Acetylene (C_2H_2)	46.4	92.8
Ethane (C_2H_6)	76.8	153.6
Propane (C_3H_8)	17.0	51.0
Acetone (CH_3COCH_3)	35.2	105.6
Isobutane (C_4H_{10})	0.2	0.8
n-butane	166.0	664.0
2,3-Dimethyl Butane (C_4H_8-$(CH_3)_2$)	97.6	585.6
Ethene (C_2H_4)	43.2	86.4
Propene (C_2H_4)	10.6	31.8
Trans-2-Butene (C_4H_8)	0.7	2.8
Cis-2-Butene (C_4H_8)	13.0	52.0
2-methyl Butene-2 (C_4H_7-CH_3)	14.8	74.0
Benzene (C_6H_6)	1.6	9.6
Toluene (C_6H_5-CH_3)	16.8	117.6
Ethyl Benzene (C_6H_5-C_2H_5)	6.4	51.2
Meta-xylene (C_6H_4-$(CH_3)_2$)	42.4	339.2
Isopropyl Benzene (C_6H_5-C_3H_7)	0.4	3.6
n-Propyl Benzene ((C_6H_4-C_3H_7)$_n$)	0.1	0.9
Meta-Ethyl Toluene (C_6H_4-CH_3-C_2H_5)	1.0	9.0
1,2,3 Trimethyl Benzene (C_6H_3-$(CH_3)_3$)	1.6	14.4

Table 1 (Continued)

SPECIES	CONCENTRATION ppbV	ppbC
Formaldehyde (HCHO)	38.0	38.0
Acetaldehyde (CH_3CHO)	20.0	40.0
Propionaldehyde (C_2H_5CHO)	3.2	9.6
Nitric Oxide (NO)	301.0	
Nitrogen Dioxide (NO_2)	41.0	
Nitrous Acid (HONO)	12.0	
Carbon Monoxide (CO)	7450.0	
Water (H_2O) (ppm)	15500.0	
Oxygen (O_2) (ppm)	210,000.0	
M (ppm)	1,000,000.0	
TOTALS FOR MIXTURE		
Nitrogen oxides (ppbV)	354.0	
THC (ppbV)	3393.0	
THC (ppbC)	5274.0	

master mechanism are:

propane	alkanes	toluene	aromatics
n-butane		m-xylene	
2,3-dimethylbutane			
ethene	alkenes	formaldehyde	aldehydes and ketones
propene		acetaldehyde	
trans-2-butene		propionaldehyde	
		acetone	

These species were chosen from the list of compounds contained in experiment SUR-119J. The reasoning behind this choice was as follows. Propene was selected because it is treated explicitly in some of the lumped mechanisms. Acetone is included because it is present at significant concentrations and is also formed from alkane photooxidation. Of the four alkanes included in SUR-119J, we include the chemistry of propane, n-butane, and 2,3-dimethylbutane in the master mechanism. Isobutane is ignored because of its low concentration. Three alkenes are included in the master mechanism, ethene, propene, and 2-butene (included as trans-2-butene). We have chosen to ignore 2-methyl-2-butene. Two aromatic hydrocarbons are included, toluene and m-xylene. These are the two most abundant, and best understood atmospheric aromatics. Benzene is not important because of its low concentration and reactivity. The remainder of the aromatics are present in small amounts, and is therefore ignored.

Excluding methane, acetylene, and ethane, 529.8 ppbv of initial organics are present in SUR-119J. Of these, 503.7 ppbv or 95 percent is represented by the 12 organics included in the master mechanism. Thus, to the extent that the mixture studied in experiment SUR-119J is representative, we

feel that the master mechanism provides a reasonable description of the chemistry occurring in typical urban atmospheres.

The reactions and rate constants comprising the master mechanism were taken almost exclusively from three sources. The inorganic reactions were compiled using the recent reviews of Baulch et al. (1982), Demore et al. (1982), and Atkinson and Lloyd (1984). The vast majority of the organic reactions was taken from the review of Atkinson and Lloyd (1984).

2.5 Verification of the Master Mechanism

The evaluation of mechanisms with smog chamber data is not the object of this report. In fact, it is our feeling that with the current controversy regarding the magnitude of chamber radical sources (see section 2.6), it is difficult to consider any mechanism validated simply because it can simulate chamber data. However, because the master mechanism plays an important role in this study, we feel it is useful to include the results of simulating a series of experiments performed in the evacuable chamber at SAPRC.

The particular experiments simulated here are EC-231, EC-232, EC-233, EC-237, EC-238, EC-241, EC-242, EC-243, EC-245, EC-246, and SUR-119J. The series of "EC" experiments are hydrocarbon-NO_x experiments in which both the initial hydrocarbon distribution and the $[RHC]_o/[NO_x]_o$ are varied. The initial conditions for experiment SUR-119J are shown in Table 1. The chamber-dependent reactions added to the master mechanism to adopt it for modeling chamber experiments are (Carter et al., 1982b):

O_3 wall loss: $k = 1.65 \times 10^{-3}$ min^{-1}

NO wall source: $k = 1.0 \times 10^{-4}$ min^{-1}

OH radical source: $k = k_{NO_2}(0.39 + 1.37[NO_2])$ ppb-min^{-1}

heterogeneous HNO_3 formation $k = 4.4 \times 10^{-6}$ ppm^{-1} - min^{-1} .

It is important to note at this point that the evaluation of the master mechanism is the only place in this report where chamber effects are included in the simulations.

The results of simulating most of the above experiments with the master mechanism are shown in the Appendix (Figures A1-A9). In nearly every case the agreement among experiment and mechanism predictions is excellent. One should keep in mind that the master mechanism contains no adjustable parameters. Similarly, the chamber-dependent terms are held constant and not varied as the initial conditions of the experiments change.

2.6 Chamber Effects

The question of smog chamber radical sources has proven to be one of the most perplexing problems in the study of photochemical smog chemistry. Because our concern in the present study is with atmospheric application of the mechanisms, and not with the modeling of smog chamber experiments, we do not consider chamber effects here (except in the evaluation of the master mechanism in section 2.5). Consequently, all of the results shown in Chapter 3 are obtained with mechanisms that contained no chamber dependent reactions.

The Carter et al. (1982b) study of chamber-dependent radical sources provides strong evidence that chamber radical sources exist in the evacuable chamber at SAPRC. However, there is still considerable controversy over the magnitude of these radical sources. In fact, the magnitude of the radical source term varies substantially between the mechanisms considered in this study. Since each mechanism in its original form can simulate experimental data, it is obvious that the predicted reactivity will differ between the mechanisms once the chamber radical source terms are removed. This result is also evident from the analysis presented in Chapter 3. The point we wish

to make here is that this disagreement in predicted reactivity will continue to exist until the chamber radical source issue is understood, and agreed upon by all investigators.

2.7 Initial Reactant Conditions

The performance of lumped mechanisms is, because of their very nature, sensitive to the initially assumed organic species distributions. Ideally, one would like to test each mechanism using a wide variety of initial hydrocarbon distributions and $[RHC]/[NO_x]$ ratios. To keep the results presented to a manageable level, we have chosen to compare the mechanisms using three related sets of initial conditions, hereafter denoted initial condition sets 1, 2, and 3. Initial condition set 1, which is loosely based on smog chamber experiment SUR-119J, is given in Table 2. These conditions were chosen to represent the early morning pollutant levels found in a typical urban atmo phere. Initial condition set 2 is obtained from set 1 by doubling the initial loadings of all hydrocarbons and halving the initial NO and NO_2 concentrations. This modification changes the $[RHC]_o/[NO_x]_o$ ratio from 7.14 to 28.6. Initial condition set 3 has $[RHC]_o/[NO_x]_o = 1.79$, which is obtained by doubling the NO and NO_2 loadings while halving the hydrocarbon concentrations from set 1. The three sets of initial conditions thus span a range of initial $[RHC]_o/[NO_x]_o$ ratios, which is acknowledged to be one of the key parameters influencing O_3 formation.

2.8 NO_2 Photolysis Rate Profile

Each of our simulations is carried out for a total of seven hours. The NO_2 photolysis rate profile used over this time period is shown in Table 3. This profile corresponds approximately to the NO_2 photolysis profile from 8 AM to 3 PM on a clear September day in Los Angeles.

TABLE 2

Initial Conditions and Other Important Parameters for Test Cases 1, 2, and 3

SPECIES	CONCENTRATION (ppbV) CASE 1	CASE 2	CASE 3
NO	300	150	600
NO_2	50	25	100
Propane	20	40	10
n-Butane	190	380	95
2,3-Dimethylbutane	110	220	55
Ethene	50	100	25
Propene	15	30	7.5
tr-2-butene	30	60	15
Toluene	20	40	10
m-Xylene	50	100	25
Formaldehyde	45	90	22.5
Acetaldehyde	25	50	12.5
Propionaldehyde	5	10	2.5
Acetone	35	70	17.5
CO	7450	7450	7450
H_2O	15,500	15,500	15,500
HONO	12	12	12

Table 2 (Continued)

ADDITIONAL PARAMETERS:

Temperature (K)	298	298	298
Pressure (atm)	1.0	1.0	1.0
Dilution	0	0	0
$[RHC]_o/[NO_x]_o$ (ppmC/ppm)	7.14	28.6	1.79

TABLE 3

NO_2 Photolysis Rate Profile Used in Each of the Test Cases

TIME (MINUTES)	NO_2 PHOTOLYSIS RATE (min^{-1})
0	0.30
60	0.39
120	0.44
180	0.46
240	0.47
300	0.46
360	0.41
420	0.34

CHAPTER 3

RESULTS AND DISCUSSION

3.1 Introduction

In this chapter we present and discuss the detailed analysis of the relative behavior of the six lumped mechanisms under consideration. We first present the complete results in both tabular and graphical form, and then consider each mechanism individually. These individual discussions are divided into two parts. First, a very brief discussion of the mechanism itself is presented, primarily to note any changes from the listings included in Part I. Second, the counter species results for NO to NO_2 conversions are compared to those for both the master mechanism and the other lumped mechanisms. In the final section of this chapter we re-examine the predictions of each mechanism after they have been modified to reflect the results of the analysis.

3.2 Counter Species Results

The counter species results obtained using initial condition sets 1, 2, and 3 are presented in Tables 4, 5, and 6, respectively. The amount of NO to NO_2 conversions attributable to the various reaction pathways is listed for each of the seven mechanisms in this study. The results obtained with initial condition sets 1 and 3 correspond to an analysis time of 360 minutes, i.e., the end of a six-hour simulation. With initial condition set 2 each mechanism predicted the time of the O_3 peak to be less than 150 minutes. For this reason an analysis time of 150 minutes was chosen with this set of conditions. These same results are presented graphically in Figures 1-3. In addition, Figures 4, 5, and 6 present the results in a different form. There,

the percentage of the total NO to NO_2 conversions due to each of four organic classes is shown.

Note that each of the initially present organic species contributes to the total amount of NO to NO_2 conversions predicted by each mechanism. For example, even though the Dodge mechanism does not include aromatic hydrocarbons, the initially present toluene and m-xylene are represented as 75 percent butane and 25 percent propene. Thus, these initially present aromatics do lead to NO to NO_2 conversions.

TABLE 4

Counter Species Results Obtained with Initial Condition Set 1
($[RHC]_o/[NO_x]_o$ = 7.14)

The Amount of NO to NO_2 Conversions Attributable to Various Species and Reaction Pathways is Shown.
The Time of Analysis is After 360 Minutes of Simulation.

	NO TO NO_2 CONVERSIONS (ppb)[a]						
	Master	Killus & Whitten	Atkinson & Lloyd	Penner & Walton	Demerjian	McRae & Seinfeld	Dodge
I) AROMATICS							
Toluene abstraction	1	4	1	} 22	} 68	} 72	} 48
Toluene addition	14	82	17				
m-Xylene + OH	170	228	128	195	171	181	138
Methyl glyoxal + hv	73	143[b]	62	90	—	—	—
Methyl glyoxal + OH	11	4[b]	2	—	—	—	—
Glyoxal	1	—	1	—	—	—	—
Benzaldehyde	0	—	0	—	—	—	—
o-Cresol	1	} 14	} 6	—	—	—	—
Dimethyl phenols	9			—	—	—	—
cis-2-butene-1,4-dial	4	} 93	} 30	—	—	—	—
4-oxo-2-pentenal	18			—	—	—	—
Other γ-dicarbonyls	25			—	—	—	—
Pyruvic acid	1	—	NI	—	—	—	—
TOTAL AROMATIC	185	314	146	217	239	253	186
II) ALKANES							
Propane + OH	3	7	3	6	15	16	} 21
Propane + $O(^3P)$	NI	NI	NI	NI	NI	0	
Butane + $O(^3P)$	0	NI	NI	0	NI	1	} 263
Butane + OH	68	168	112	88	142	154	
2,3-Dimethylbutane + $O(^3P)$	1	NI	NI	0	NI	0	} 228
2,3-Dimethylbutane + OH	85	146	65	124	82	89	
TOTAL ALKANE	157	321	180	218	239	260	512

Table 4 (Continued)

	NO TO NO_2 CONVERSIONS (ppb)[a]						
	Master	Killus & Whitten	Atkinson & Lloyd	Penner & Walton	Demerjian	McRae & Seinfeld	Dodge
III) ALKENES							
Ethene + OH	47	81	48	41	105	70	} 35
Ethene + $O(^3P)$	NI	1	NI	1	3	1	
Ethene + O_3	4	13	6	5	74	NI	
Propene + OH	36	39	31	38	31	33	} 16
Propene + $O(^3P)$	NI	0	NI	1	1	1	
Propene + O_3	5	9	9	5	22	10	
Butene + OH	66	} 81	69	206	63	66	} 41
Butene + $O(^3P)$	NI		NI	4	2	2	
Butene + O_3	23		28	25	45	19	
Ethene + NO_3	NI	NI	NI	0	NI	NI	NI
Propene + NO_3	NI	NI	NI	0	NI	NI	NI
Butene + NO_3	NI	NI	NI	1	NI	NI	NI
CH_2OO	3	9	4	—	—	—	—
CH_3CHOO	7	4	8	—	—	—	—
TOTAL ALKENE	181	221	191	327	346	202	92
IV) ALDEHYDES AND KETONES							
Initial HCHO	32	51	35	42	43	33	44
Initial CH_3CHO	23	34	28	34	24	53	50
Initial CH_3CH_2CHO	8	8	7	8	5	11	5
Initial $CH_3C(O)CH_3$ + OH	2	} 55	NI	0	26	—	} 36
Initial $CH_3C(O)CH_3$ + hv	3		4[d]	0	NI	—	
Initial HCHO + NO_3	NI	NI	NI	0	NI	NI	NI
Initial CH_3CHO + NO_3	NI	NI	NI	0	NI	NI	NI
Initial CH_3CH_2CHO + NO_3	NI	NI	NI	0	NI	NI	NI
Initial $CH_3C(O)CH_3$ + NO_3	NI	NI	NI	0	NI	NI	NI
Created HCHO	43	} 360[c]	58	} 282[e]	} 384[f]	88	128
Created CH_3CHO	61		73				130
Created CH_3CH_2CHO	1		5[d]				37
Created $CH_3CH_2CH_2CHO$	3					} 345[g]	59
Created $CH_3C(O)CH_3$ + OH	2		NI				—
Created $CH_3C(O)CH_3$ + hv	3		1				—
Created MEK + OH	1		15				—
Created MEK + hv	8		6				—
TOTAL ALDEHYDE	68	148	74	84	98	97	135

GRAND TOTAL	591	1007	591	846	922	812	925
ACTUAL NUMBER OF NO/NO_2 CONVERSIONS[h]	597	1005	587	847	923	813	927

Footnotes for Table 4:

a NI stands for not included
b The number shown is for the lumped group DCRB
c The number shown is for the lumped group CARB
d Number of conversions due to created RCHO species
e Number of conversions due to created HC4 species
f Number of conversions due to created HC3 species
g Number of conversions due to created RCHO species
h This is the actual number of NO to NO_2 conversions which have taken place. The grand total predicted by the counter species analysis should approximately equal this number.

TABLE 5

Counter Species Results Obtained with Initial Condition Set 2
($[RHC]_o/[NO_x]_o$ = 28.6)

The Amount of NO to NO_2 Conversions Attributable to Various Species and Reaction Pathways is Shown.
The Time of Analysis is After 150 Minutes of Simulation.

	NO TO NO_2 CONVERSIONS (ppb)[a]						
	Master	Killus & Whitten	Atkinson & Lloyd	Penner & Walton	Demerjian	McRae & Seinfeld	Dodge
I) AROMATICS							
Toluene abstraction	1	3	2	} 19	} 66	} 64	} 37
Toluene addition	15	65	15				
m-Xylene + OH	159	178	125	169	165	160	105
Methyl glyoxal + hv	47	104[b]	48	87	—	—	—
Methyl glyoxal + OH	7	2[b]	1	—	—	—	—
Glyoxal	1	—	0	—	—	—	—
Benzaldehyde	0	—	0	—	—	—	—
o-Cresol	0	7	3	—	—	—	—
Dimethyl phenols	5			—	—	—	—
cis-2-butene-1.4-dial	1	} 81	} 10	—	—	—	—
4-oxo-2-pentenal	10			—	—	—	—
Other γ-dicarbonyls	11			—	—	—	—
Pyruvic acid	0	—	NI	—	—	—	—
TOTAL AROMATIC	175	246	142	188	231	224	142
II) ALKANES							
Propane + OH	4	5	4	5	14	14	} 16
Propane + $O(^3P)$	NI	NI	NI	0	NI	0	
Butane + $O(^3P)$	0	NI	NI	0	NI	0	} 200
Butane + OH	77	117	129	72	128	137	
2,3-Dimethylbutane + $O(^3P)$	0	NI	NI	0	NI	0	} 174
2,3-Dimethylbutane + OH	116	101	74	102	74	79	
TOTAL ALKANE	197	223	207	179	216	230	390

Table 5 (Continued)

	NO TO NO_2 CONVERSIONS (ppb)[a]						
	Master	Killus & Whitten	Atkinson & Lloyd	Penner & Walton	Demerjian	McRae & Seinfeld	Dodge
III) ALKENES							
Ethene + OH	58	61	57	43	122	66	
Ethene + $O(^3P)$	NI	0	NI	0	1	0	26
Ethene + O_3	5	6	5	7	126	NI	
Propene + OH	42	34	37	40	37	41	
Propene + $O(^3P)$	NI	0	NI	0	0	0	12
Propene + O_3	8	11	10	6	38	18	
Butene + OH	71		72	215	73	81	
Butene + $O(^3P)$	NI	63	NI	1	1	1	32
Butene + O_3	48		48	34	76	36	
Ethene + NO_3	NI	NI	NI	0	NI	NI	NI
Propene + NO_3	NI	NI	NI	0	NI	NI	NI
Butene + NO_3	NI	NI	NI	3	NI	NI	NI
CH_2OO	3	5	3	—	—	—	—
CH_3CHOO	10	6	10	—	—	—	—
TOTAL ALKENE	232	175	229	349	474	243	70
IV) ALDEHYDES AND KETONES							
Initial HCHO	39	41	41	34	40	45	46
Initial CH_3CHO	12	26	16	29	22	39	36
Initial CH_3CH_2CHO	5	6	5	7	4	8	4
Initial $CH_3C(O)CH_3$ + OH	2	42	NI[d]	0	24	—	28
Initial $CH_3C(O)CH_3$ + hv	2		2[d]	0	NI	—	
Initial HCHO + NO_3	NI	NI	NI	0	NI	NI	NI
Initial CH_3CHO + NO_3	NI	NI	NI	0	NI	NI	NI
Initial CH_3CH_2CHO + NO_3	NI	NI	NI	0	NI	NI	NI
Initial $CH_3C(O)CH_3$ + NO_3	NI	NI	NI	0	NI	NI	NI
Created HCHO	28		37			66	65
Created CH_3CHO	27		34				51
Created CH_3CH_2CHO	0		2[d]				11
Created $CH_3CH_2CH_2CHO$	1				259		34
Created $CH_3C(O)CH_3$ + OH	1	122[c]	NI	135[e]	259[f]	155[g]	—
Created $CH_3C(O)CH_3$ + hv	1		0				—
Created MEK + OH	0		3				—
Created MEK + hv	3		5				—
TOTAL ALDEHYDE	60	115	64	70	90	92	114

GRAND TOTAL	664	759	642	786	1011	789	716
ACTUAL NUMBER OF NO/NO_2 CONVERSIONS[h]	668	759	637	787	1010	789	715

Footnotes for Table 5:

a NI stands for not included
b The number shown is for the lumped group DCRB
c The number shown is for the lumped group CARB
d Number of conversions due to created RCHO species
e Number of conversions due to created HC4 species
f Number of conversions due to created HC3 species
g Number of conversions due to created RCHO species
h This is the actual number of NO to NO_2 conversions which have taken place. The grand total predicted by the counter species analysis should approximately equal this number.

TABLE 6

Counter Species Results Obtained with Initial Condition Set 3
($[RHC]_o/[NO_x]_o$ = 1.79)

The Amount of NO to NO_2 Conversions Attributable to Various Species and Reaction Pathways is Shown.
The Results are Calculated at a Simulation Time of 360 Minutes.

	NO TO NO_2 CONVERSIONS (ppb)[a]						
	Master	Killus & Whitten	Atkinson & Lloyd	Penner & Walton	Demerjian	McRae & Seinfeld	Dodge
I) AROMATICS							
Toluene abstraction	0	1	0	} 5	} 17	} 26	} 18
Toluene addition	4	36	7				
m-Xylene + OH	65	96	61	48	42	69	51
Methyl glyoxal + hv	35	71[b]	35	31	—	—	—
Methyl glyoxal + OH	4	2[b]	1	—	—	—	—
Glyoxal	0	—	0	—	—	—	—
Benzaldehyde	0	—	0	—	—	—	—
o-Cresol	0	} 10	} 4	—	—	—	—
Dimethyl phenols	4			—	—	—	—
cis-2-butene-1,4-dial	1	} 44	} 17	—	—	—	—
4-oxo-2-pentenal	6			—	—	—	—
Other γ-dicarbonyls	10			—	—	—	—
Pyruvic acid	1	—	NI	—	—	—	—
TOTAL AROMATIC	69	133	68	53	59	95	69
II) ALKANES							
Propane + OH	1	2	1	1	3	5	} 8
Propane + $O(^3P)$	NI	NI	NI	0	NI	0	
Butane + $O(^3P)$	0	NI	NI	0	NI	0	} 96
Butane + OH	18	46	34	13	26	45	
2,3-Dimethylbutane + $O(^3P)$	0	NI	NI	0	NI	0	} 88
2,3-Dimethylbutane + OH	23	40	19	18	15	26	
TOTAL ALKANE	41	88	54	32	44	76	187

Table 6 (Continued)

	NO TO NO_2 CONVERSIONS (ppb)[a]						
	Master	Killus & Whitten	Atkinson & Lloyd	Penner & Walton	Demerjian	McRae & Seinfeld	Dodge
III) ALKENES							
Ethene + OH_3	12	26	14	12	45	21	
Ethene + $O(^3P)$	NI	1	NI	1	5	1	13
Ethene + O_3	0	1	0	0	13	NI	
Propene + OH_3	10	18	12	11	14	19	
Propene + $O(^3P)$	NI	1	NI	1	1	3	6
Propene + O_3	1	1	1	0	4	3	
Butene + OH_3	34		37	58	27	37	
Butene + $O(^3P)$	NI	47	NI	5	3	5	15
Butene + O_3	8		10	1	8	6	
Ethene + NO_3	NI	NI	NI	0	NI	NI	NI
Propene + NO_3	NI	NI	NI	0	NI	NI	NI
Butene + NO_3	NI	NI	NI	0	NI	NI	NI
CH_2OO	0	1	0	—	—	—	—
CH_3CHOO	2	0	3	—	—	—	—
TOTAL ALKENE	65	95	74	89	120	96	34
IV) ALDEHYDES AND KETONES							
Initial HCHO	14	32	16	21	21	15	20
Initial CH_3CHO	13	20	16	18	11	39	31
Initial CH_3CH_2CHO	4	4	5	4	2	8	2
Initial $CH_3C(O)CH_3$ + OH	1	29	NI[d]	0	5	—	13
Initial $CH_3C(O)CH_3$ + hv	2		3[d]	0	NI	—	
Initial HCHO + NO_3	NI	NI	NI	0	NI	NI	NI
Initial CH_3CHO + NO_3	NI	NI	NI	0	NI	NI	NI
Initial CH_3CH_2CHO + NO_3	NI	NI	NI	0	NI	NI	NI
Initial $CH_3C(O)CH_3$ + NO_3	NI	NI	NI	0	NI	NI	NI
Created HCHO	13		20			31	40
Created CH_3CHO	23		31				56
Created CH_3CH_2CHO	0		2[d]				24
Created $CH_3CH_2CH_2CHO$	1	146[c]		51[e]	93[f]	162[g]	31
Created $CH_3C(O)CH_3$ + OH	0		NI				—
Created $CH_3C(O)CH_3$ + hv	1		1				—
Created MEK + OH	0		1				—
Created MEK + hv	3		6				—

TOTAL ALDEHYDE	34	85	40	43	39	62	66
GRAND TOTAL	209	401	236	217	262	329	356
ACTUAL NUMBER OF NO/NO_2 CONVERSIONS[h]	214	398	236	217	260	330	355

Footnotes for Table 6:

a NI stands for not included
b The number shown is for the lumped group DCRB
c The number shown is for the lumped group CARB
d Number of conversions due to created RCHO species
e Number of conversions due to created HC4 species
f Number of conversions due to created HC3 species
g Number of conversions due to created RCHO species
h This is the actual number of NO to NO_2 conversions which have taken place. The grand total predicted by the counter species analysis should approximately equal this number.

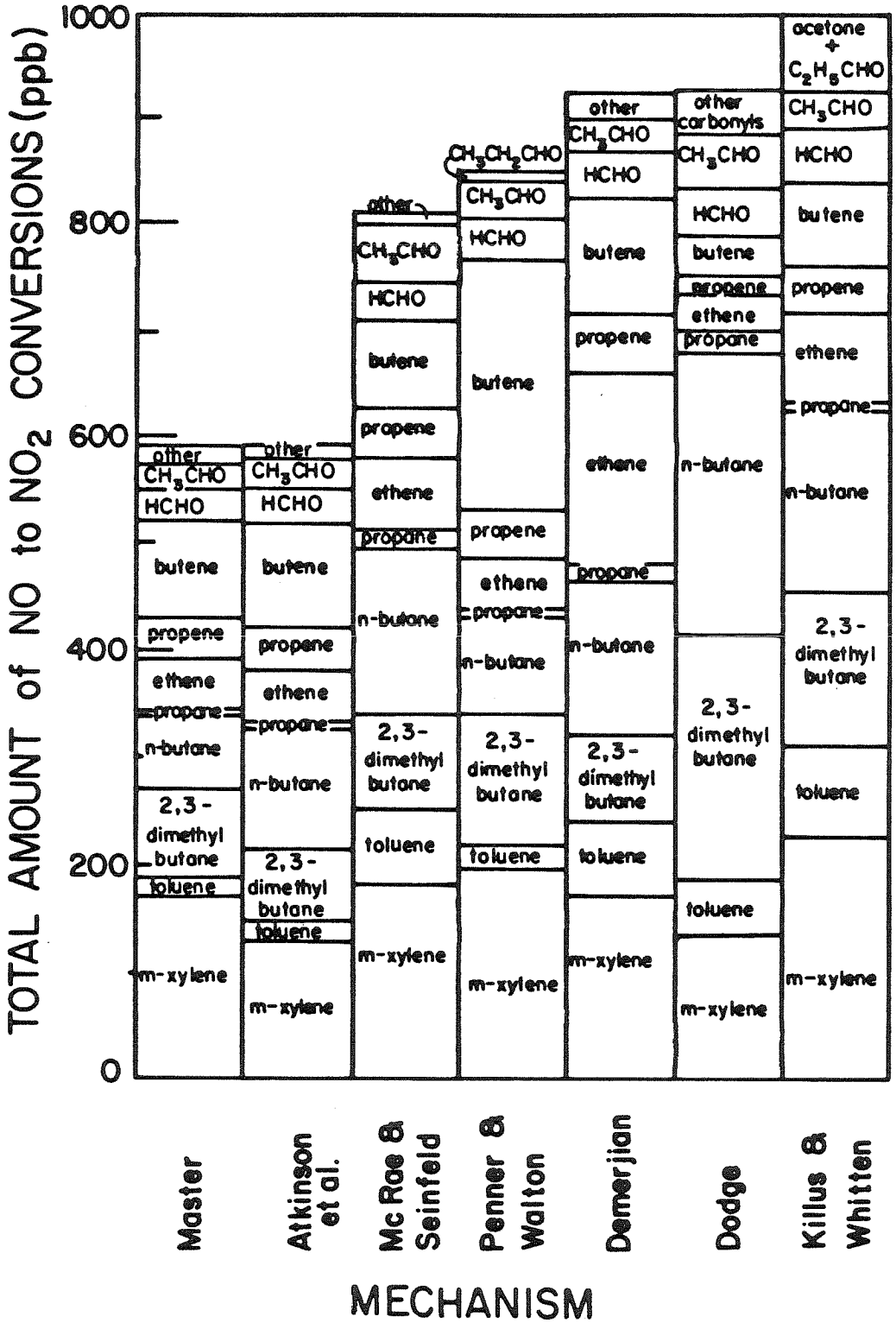

Figure 1. Counter Species Results Obtained Using Initial Condition Set 1. Amount of NO to NO_2 Conversions Attributable to Each of the Initially Present Organics.

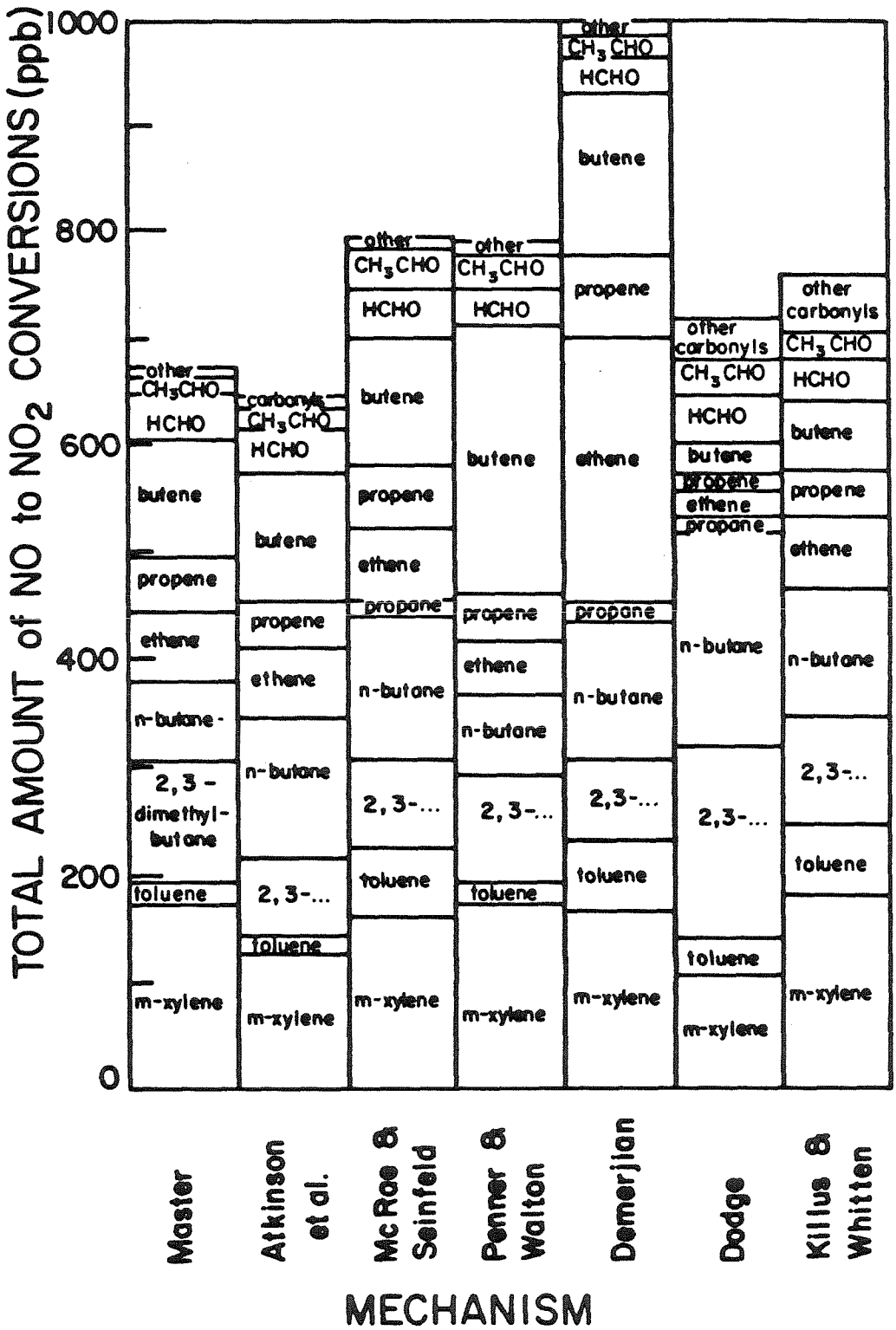

Figure 2. Counter Species Results Obtained Using Initial Condition Set 2. Amount of NO to NO_2 Conversions Attributable to Each of the Initially Present Organics.

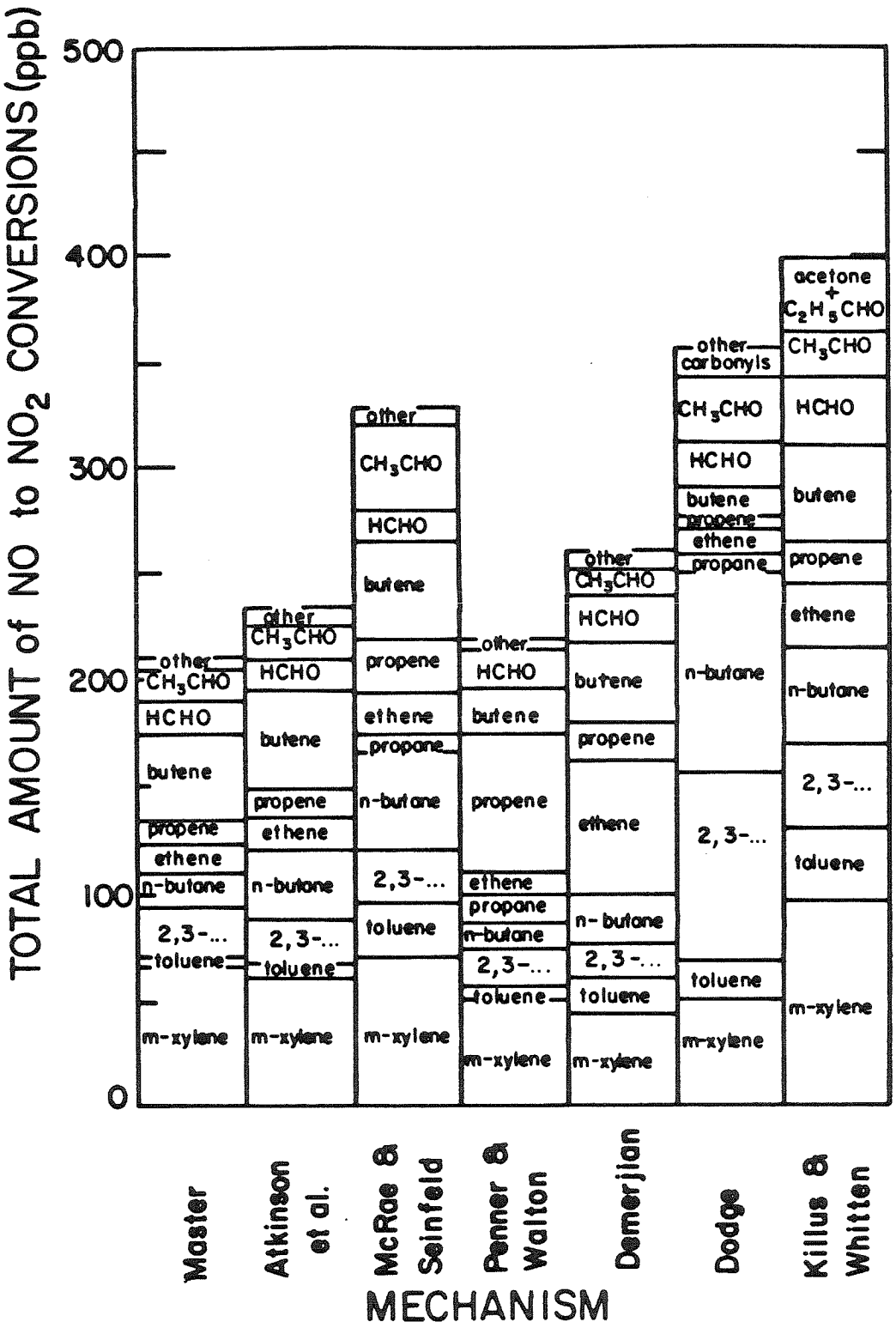

Figure 3. Counter Species Results Obtained Using Initial Condition Set 3. Amount of NO to NO_2 Conversions Attributable to Each of the Initially Present Organics.

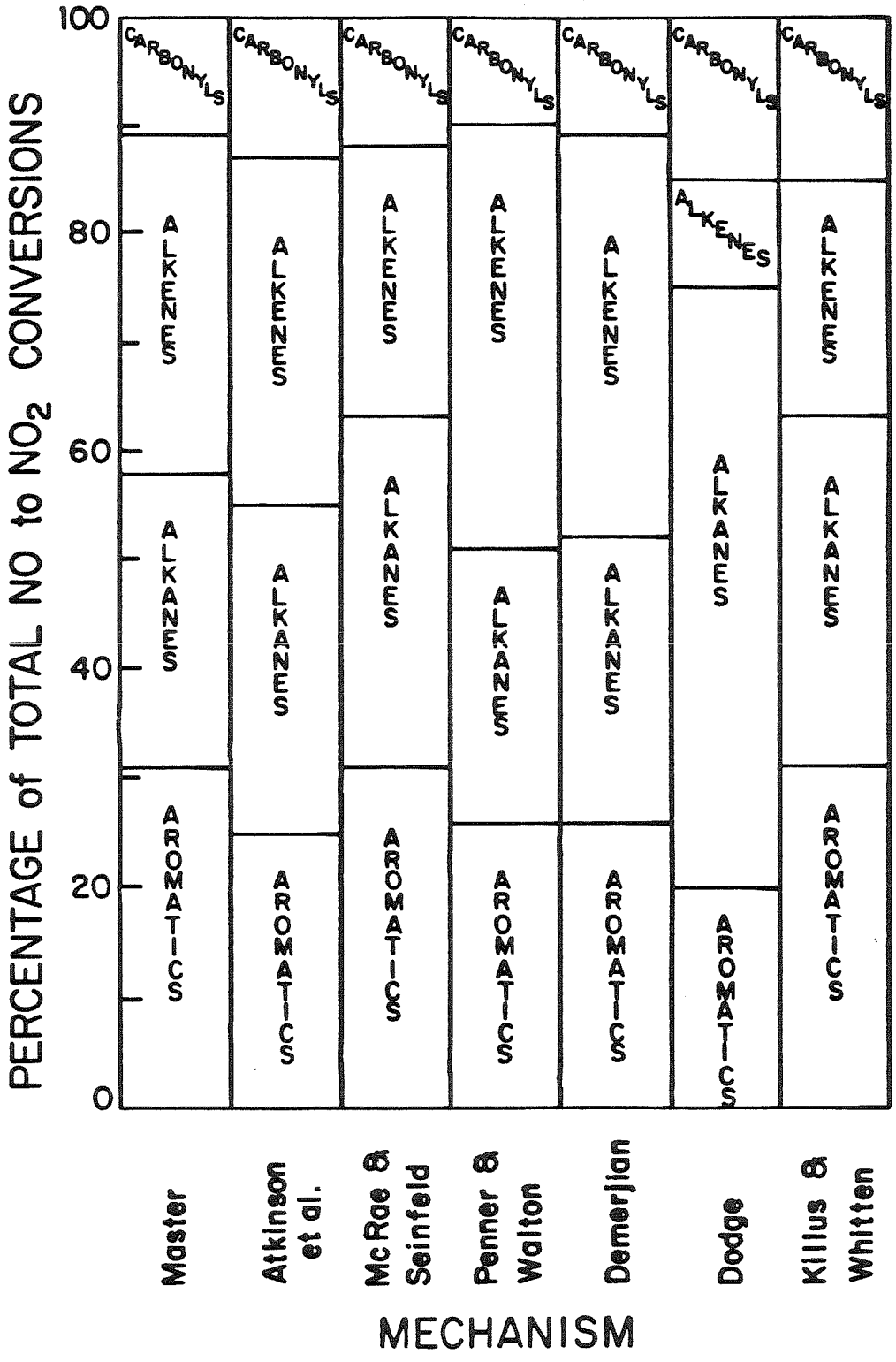

Figure 4. Percent of the Total NO to NO_2 Conversions Due to Each Class of Organic for the Simulation Using Initial Condition Set 1.

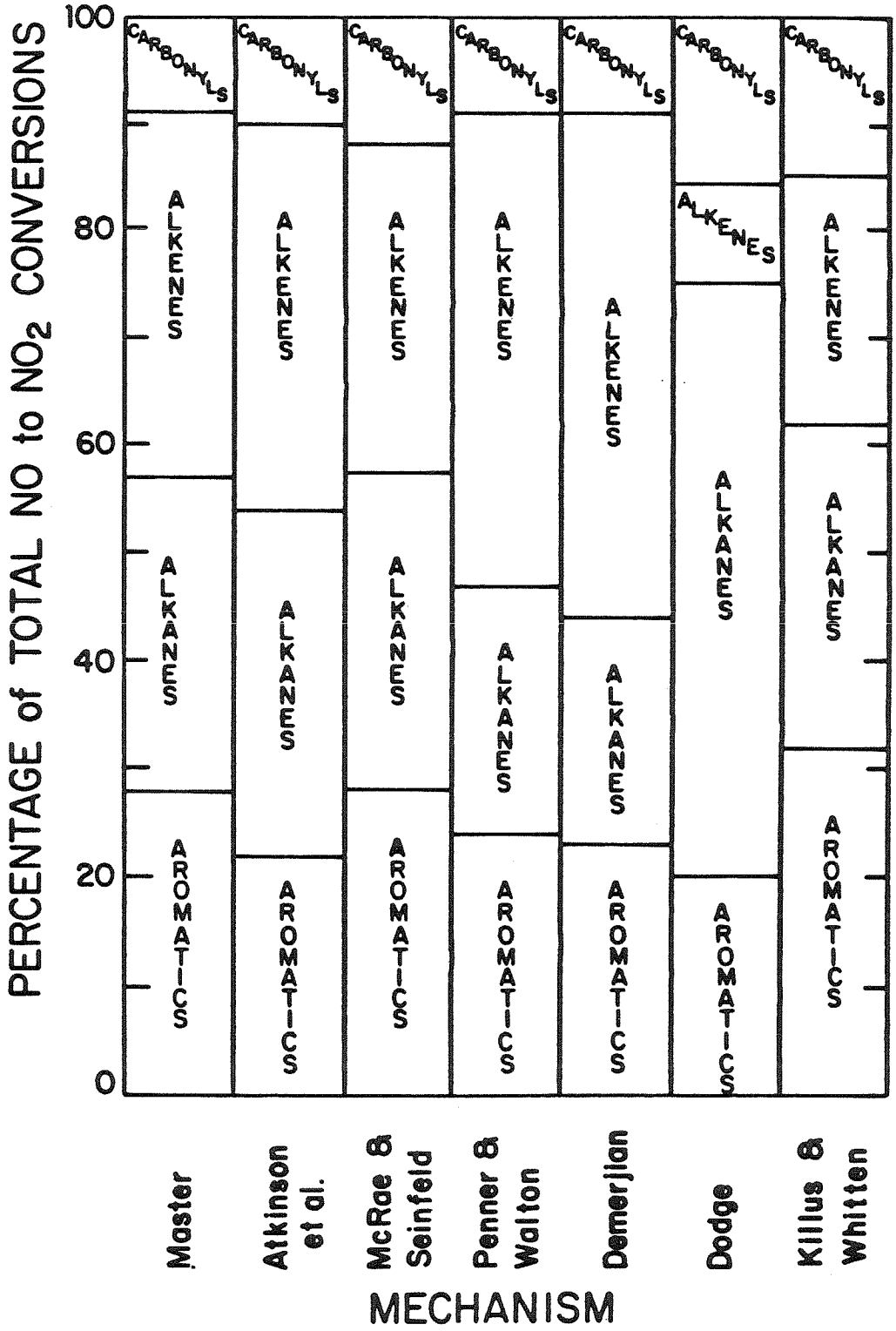

Figure 5. Percent of the Total NO to NO_2 Conversions Due to Each Class of Organic for the Simulation Using Initial Condition Set 2.

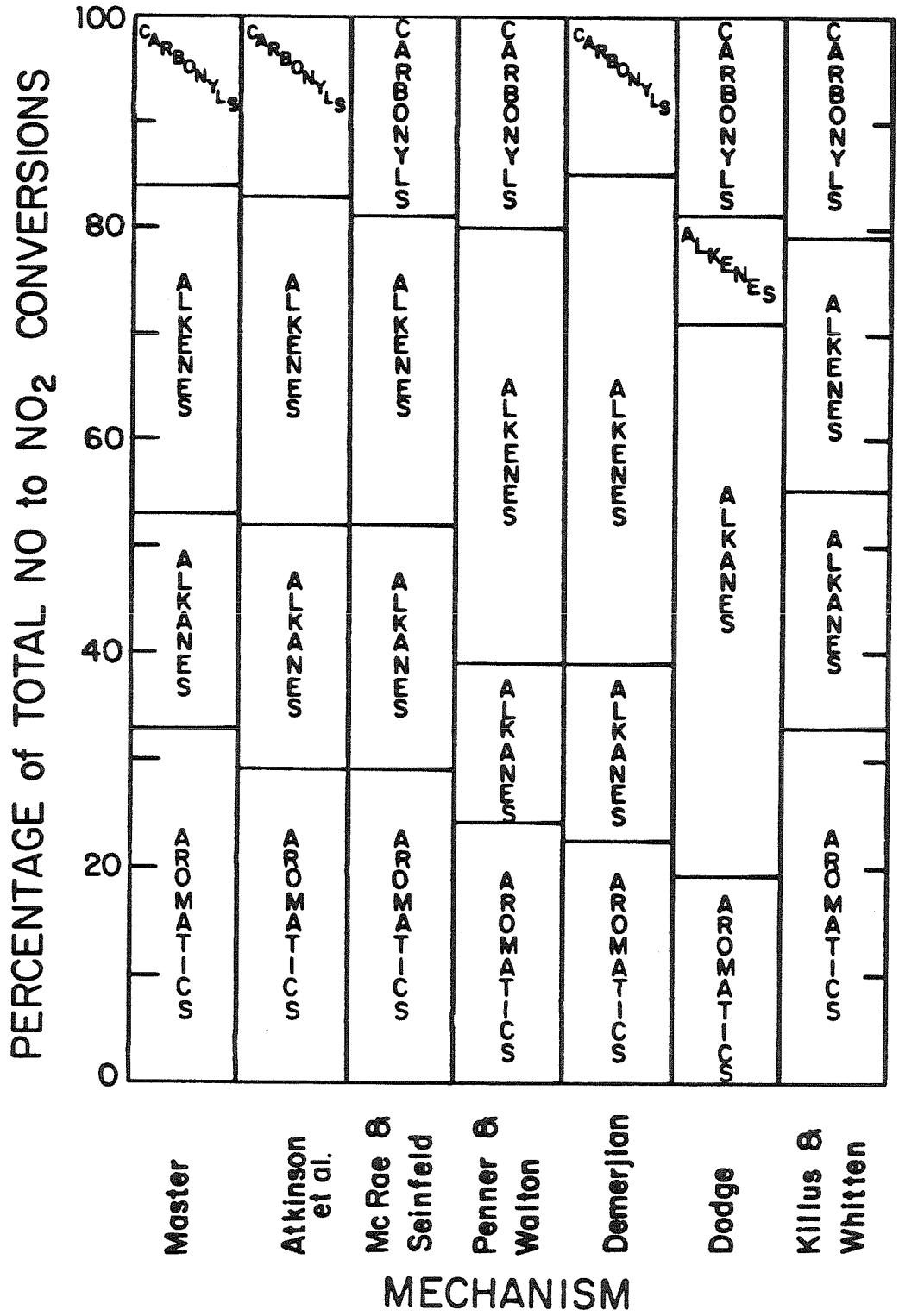

Figure 6. Percent of the Total NO to NO_2 Conversions Due to Each Class of Organic for the Simulation Using Initial Condition Set 3.

Although we will shortly discuss these results in detail for each mechanism, a few of the salient features are noted here. First, note that, except for the Atkinson et al. (1982) mechanism (which bears the closest resemblance to the master mechanism) each of the lumped mechanisms consistently predicts more NO to NO_2 conversions than does the master mechanism. Also, note the differences in the bar graph patterns found between Figures 1, 2, and 3. For instance, in Figure 2 ($[RHC]_o/[NO_x]_o$ = 28.6, high O_3) the Demerjian (1982) mechanism predicts many more NO to NO_2 conversions than does the Killus and Whitten (1982) mechanism. However, in Figure 3 ($[RHC]_o/[NO_x]_o$ = 1.79, low O_3) the opposite is true. Examination of Figures 4 to 6 shows that the percentage of the total NO to NO_2 conversions attributable to each class of organic varies substantially between the mechanisms.

3.3 NO to NO_2 Conversions vs. O_3 Yield

Before we discuss the counter species results in detail, it is interesting to examine, for each mechanism, the relationship between the total number of NO to NO_2 conversions and the maximum predicted O_3 concentration. Although the amount of O_3 for which a given reaction is responsible is proportional to the number of NO to NO_2 conversions attributable to that reaction, the overall yield of O_3 depends not only on the number of NO molecules converted to NO_2, but also on the NO and NO_2 removal mechanisms. Thus, if two mechanisms predict a similar number of NO to NO_2 conversions but have vastly different NO_x removal mechanisms, they will not agree on the resulting O_3 concentrations. By and large, the differences among the NO_x removal steps in the lumped mechanisms are not substantial. The one exception is the Dodge (1977) mechanism. For example, the PAN reactions in the Dodge (1977) mechanism differ significantly from the corresponding reactions in

the other lumped mechanisms. We might therefore expect that the relationship between $[O_3]$ and the number of NO to NO_2 conversions in the Dodge (1977) mechanism will be somewhat different from those in the other lumped mechanisms.

Figures 7, 8, and 9 depict the relationship between the number of NO to NO_2 conversions and the maximum O_3 concentration for each lumped mechanism. We see that for the most part, as we proceed horizontally across the various mechanisms, the O_3 concentrations (shaded) follow the pattern of the NO to NO_2 conversions (unshaded). As we noted, the exception is the Dodge (1977) mechanism, which predicts a much smaller O_3 concentration per NO to NO_2 conversion than the others. This difference must be taken into account in our subsequent discussions concerning the Dodge (1977) mechanism.

3.4 The Atkinson et al. (1982) Mechanism

3.4.1 Description of the Mechanism:

The Atkinson et al. (1982) mechanism as used in this study appears in Table A2 of the Appendix. The only differences between the mechanism used here and that shown in Table 22 of Part I of this report (McRae et al. 1983), are the following:

(1) The chamber-dependent reactions have been removed (reactions 18, 80, and 81 of Table 22, Part I).

(2) The rate constant used for reaction 59 is the value recommended by Atkinson et al. (1982) for m-xylene ($k_{59} = 1.05 \times 10^{7} T^{-1}$), not the value for a lumped xylene ($k = 7.9 \times 10^{6} T^{-1}$).

(3) Since there is no benzene present in our initial hydrocarbon mix, and we have only m-xylene (no other isomers), the expression for BO1

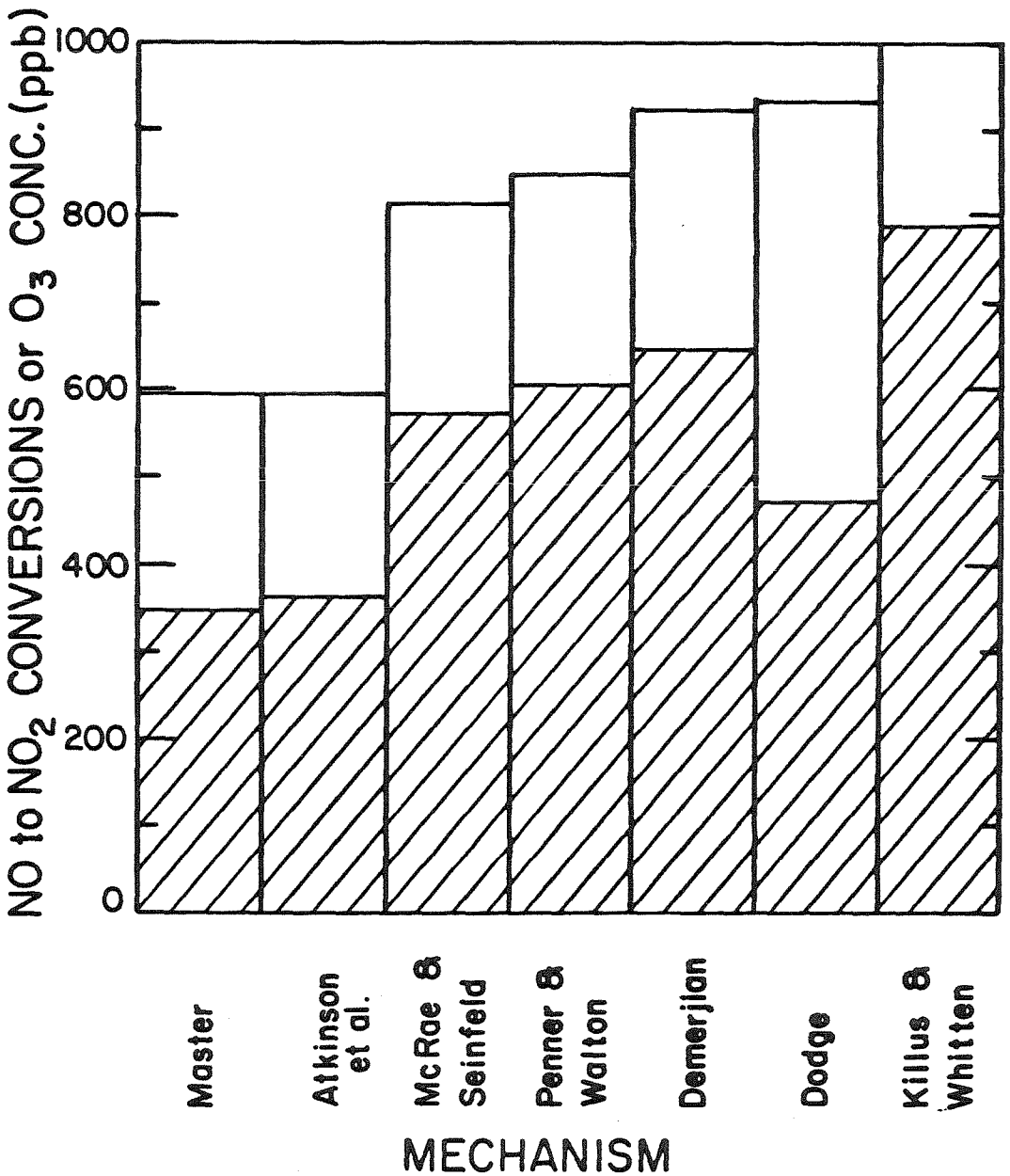

Figure 7. O_3 Yield (shaded) vs. Total Amount of NO to NO_2 Conversions (unshaded) for Each Mechanism Obtained with Initial Condition Set 1 ($[RHC]_o/[NO_x]_o$ = 7.14).

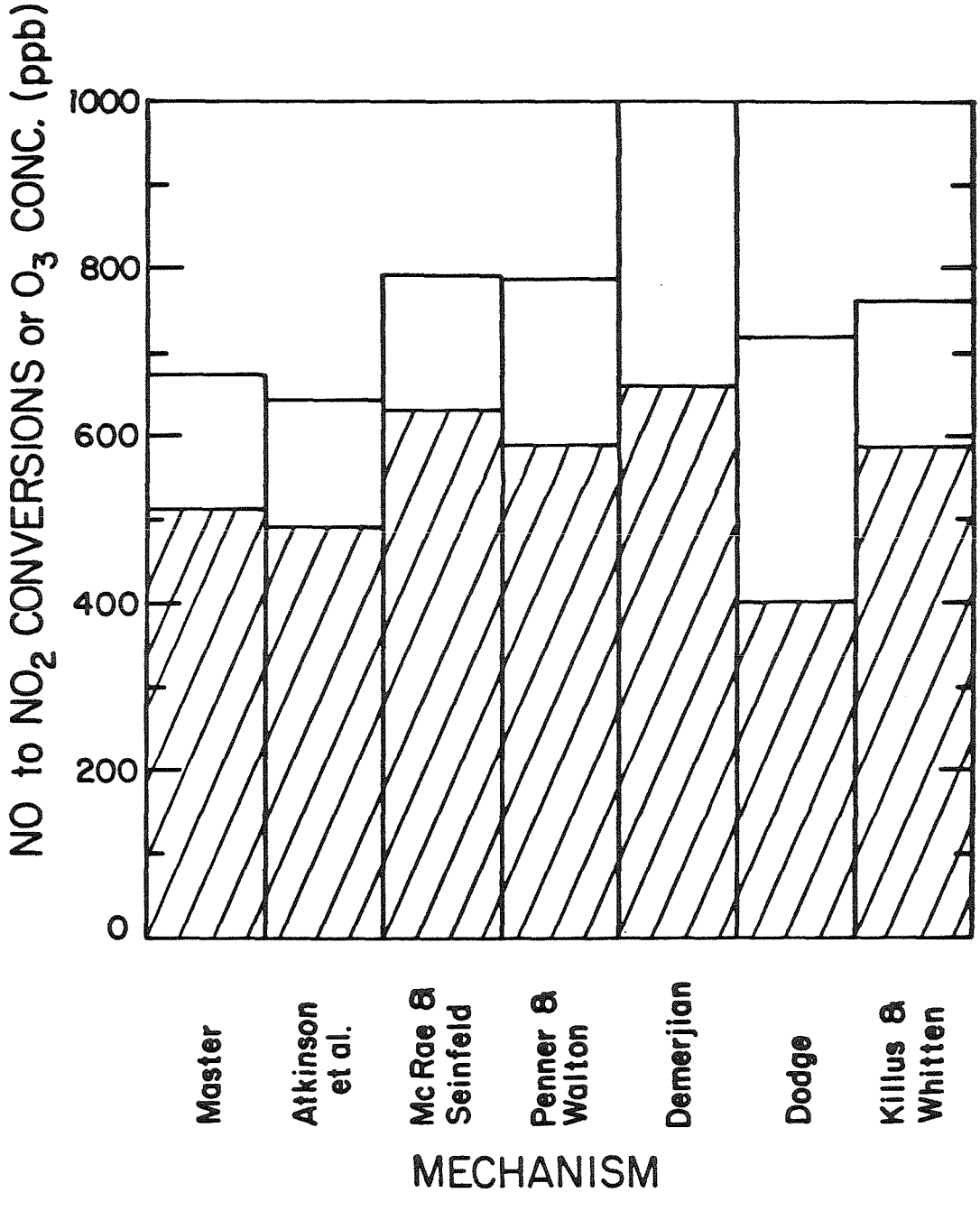

Figure 8. O_3 Yield (shaded) vs. Total Amount of NO to NO_2 Conversions (unshaded) for Each Mechanism Obtained with Initial Condition Set 2 ($[RHC]_o/[NO_x]_o$ = 28.6)

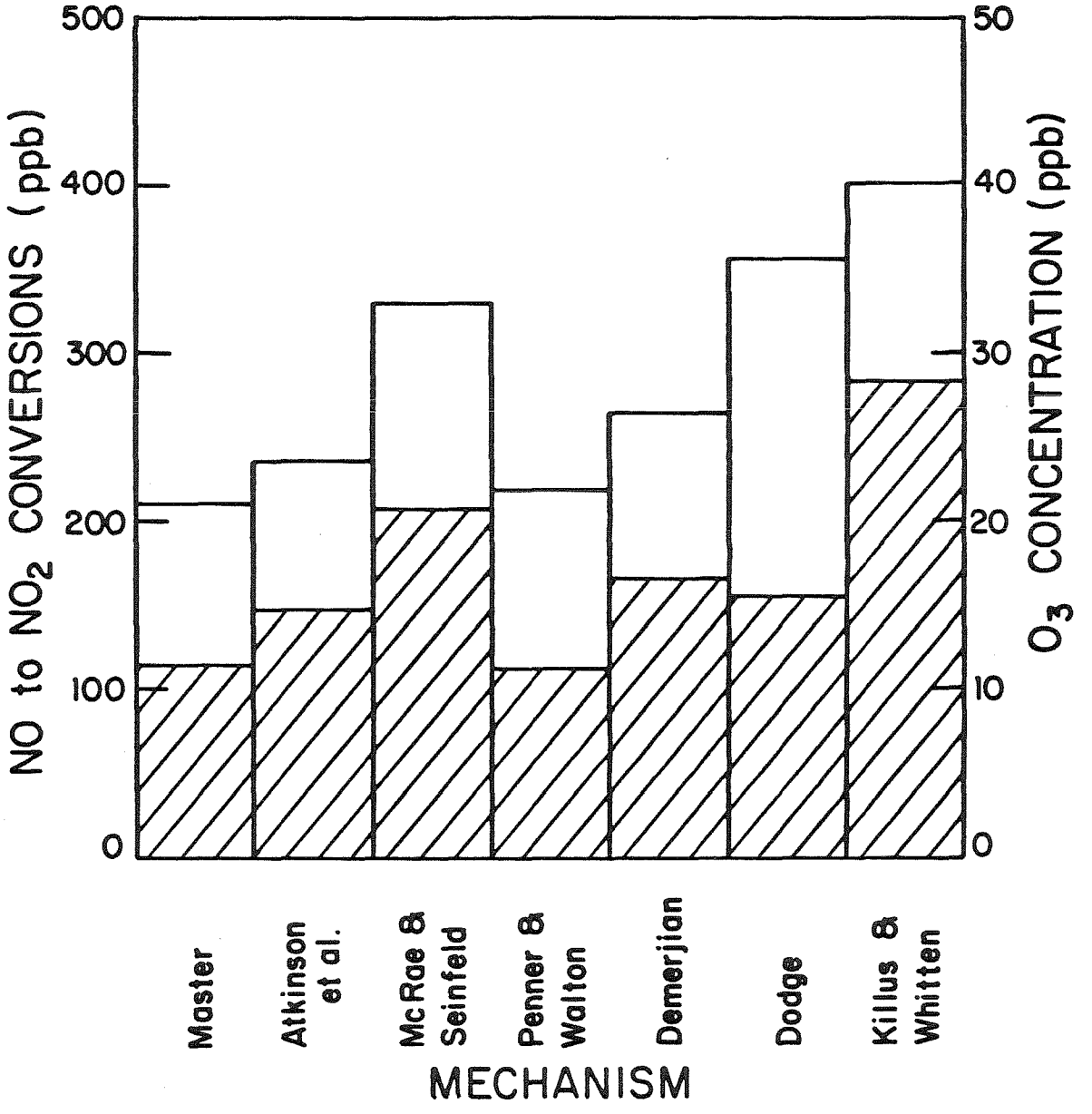

Figure 9 . O_3 Yield (shaded) vs. Total Amount of NO to NO_2 Conversions (unshaded) for Each Mechanism Obtained with Initial Condition Set 3 ($[RHC]_o/[NO_x]_o$ = 1.79).

given on page 15 of Part I becomes

$$B01 = \frac{0.75\ k_{57}[\text{benzene}]}{k_{57}[\text{benzene}]+k_{58}[\text{toluene}]+k_{59}[\text{m-xylene}]} = 0$$

$$B02 = 0.75 - B01 = 0.75.$$

(4) The variable stoichiometric coefficients appearing in reaction 64 were held constant throughout the course of our simulations. The value for B03 was chosen by first setting B03 = 0.55, its value at the beginning of the simulation. Next, a simulation was performed using $[B03]_i = 0.55$, during which the actual values of B03 were calculated at constant time intervals. Using these values, an average B03 was then calculated and the simulations repeated using this average value. Although this is an approximation, we feel that using an average value for B03 has only a minor effect on the reported results. For instance, the average value for B03 in the simulation with initial condition set 1 was 0.58, as compared with the initial value of 0.55.

PHOTOLYSIS RATES: The photolysis rates for reactions 3, 31, 22, and 24 were obtained by averaging over a zenith angle ranging from 30° to 60°. This was done because the NO_2 photolysis profile used in our simulations approximately represents a zenith angle distribution of 30°-60°. The data needed to calculate these averages were obtained from Table 23 of Part I. Rates for the remaining photolysis reactions were taken directly from Table 22 of Part I.

3.4.2 NO to NO_2 Conversion Results

As can be seen from Tables 4-6, the Atkinson et al. (1982) mechanism consistently predicts fewer overall NO to NO_2 conversions than the other lumped mechanisms. Notice also that the Atkinson et al. (1982)

results are very similar to those found by using the master mechanism. This is true for each of the three $[RHC]_o/[NO_x]_o$ ratios and is not unexpected since this mechanism bears the closest resemblance to the master mechanism. In particular, the numbers of NO to NO_2 conversions due to the alkanes, alkenes, and carbonyl compounds in this mechanism are very close to the values obtained with the master mechanism. The majority of the discrepancy between the two mechanisms involves the aromatic hydrocarbons. It can be seen from Tables 4-6 that the Atkinson et al (1982) mechanism consistently predicts fewer NO to NO_2 conversions due to the initial m-xylene than the master mechanism. The reasons for this discrepancy are:

(1) The Atkinson et al. (1982) mechanism assumes that 25 percent of the aromatic-OH-O_2 adducts react with NO to yield stable (?) nitrates. Based on the work of Atkinson et al. (1980) with toluene and the cresols, this 25 percent aromatic nitrate formation was the prevailing opinion at the time when this lumped mechanism was formulated. More recent investigations have led us to conclude that this nitrate formation probably does not occur to any significant extent (Leone and Seinfeld, 1983b). Thus, since the master mechanism does not include any nitrate formation, all of the aromatic-OH-O_2 adducts lead to ring opening, and therefore give rise to more NO to NO_2 conversions. When the assumed 25 percent nitrate formation is removed from the Atkinson et al. (1982) mechanism, the number of NO to NO_2 conversions attributed to m-xylene (using initial condition set 1) increases from 128 ppb to 172 ppb, much closer to the 170 ppb predicted by the master mechanism.

(2) By necessity, the representation of the chemistry of the conjugated-γ-dicarbonyls in the Atkinson et al. (1982) mechanism is considerably simplified relative to that in the explicit mechanism. In the course of condensing this chemistry a number of NO to NO_2 conversions are not accounted for. However, since the detailed chemistry of these compounds is not well understood, changes in the current version of the Atkinson et al. (1982) mechanism in this aspect of the chemistry can not really be justified at this time.

(3) At the time the Atkinson et al. (1982) mechanism was formulated, the photolysis rate of methyl glyoxal was estimated to be, approximately, $k_{MGLY} \approx 0.15\ k_{NO_2}$. Recently, experimental data have indicated that the earlier estimates were about eight times too large (Plum et al., 1983), i.e., $k_{MGLY} \approx 0.019\ k_{NO_2}$. Since methyl glyoxal is an efficient source of radicals, this would indicate that the Atkinson et al. (1982) mechanism actually over estimates the number of NO to NO_2 conversions attributable to methyl glyoxal. However, there is another difference between the methyl glyoxal chemistry contained in these two mechanisms. The Atkinson et al. (1982) mechanism assumes that the only methyl glyoxal photolysis pathway leads to $CH_3C(O)O_2\cdot$ and $HO_2\cdot$ radicals, while the master mechanism, based on Leone and Seinfeld (1983b),

contains two photolysis pathways,

$$CH_3C(O)CHO + h\nu \xrightarrow{O_2} CH_3C(O)O_2\cdot + HO_2\cdot + CO \qquad (65\%)$$

$$\xrightarrow{O_2} CH_3O_2\cdot + HO_2\cdot + 2CO \qquad (35\%)$$

with their approximate percentages of occurrence indicated. Because a fraction of the peroxyacetyl radicals ($CH_3C(O)O_2\cdot$) leads to PAN, they do not effect as many NO to NO_2 conversions as do methoxy radicals ($CH_3O_2\cdot$). As an example, at a simulation time of 360 minutes using initial condition set 1, the fractions of these species leading to NO to NO_2 conversions are,

$$F_{CH_3O_2} = 2.52$$

$$F_{CH_3C(O)O_2} = 1.77$$

This difference somewhat counteracts the overestimated rate of methyl glyoxal photolysis.

The formaldehyde and acetaldehyde photolysis rates used in the Atkinson et al. (1982) mechanism are also out of date. Horowitz and Calvert (1982) have recently measured quantum yields for acetaldehyde, and have proposed updated values for formaldehyde photolysis. These latest recommendations lead to significantly different rates for the aldehyde photolysis steps. For example, when these updated aldehyde photolysis rates are substituted into the Atkinson et al. (1982) mechanism the amount of NO to NO_2 oxidations attributable to these aldehydes is reduced by about 10 percent. This results in even closer agreement with the master mechanism.

3.4.3 Possible Modifications to the Atkinson et al. (1982) Mechanism

Based on our analysis we would recommend that the following modifications for the Atkinson et al. mechanism be considered:

(1) The 25 percent nitrate formation from the aromatic-OH-O_2 adduct reaction with NO be removed.

(2) The photolysis rate of methyl glyoxal be updated to the currently accepted value.

(3) The photolysis rates of formaldehyde and acetaldehyde be updated to reflect the quantum yields of Horowitz and Calvert (1982).

The results in Tables 5-7 support the view expressed by Atkinson et al. that a number of species can be eliminated from this mechanism without significantly affecting its ozone predictions. Our results show that eliminating propane, acetone, the two Criegee intermediates, glyoxal, and benzaldehyde and its oxidation products ($ARCO_3$, PBZN, and PHO_2) will have an almost imperceptible effect on the simulations. Additional species, such as benzene, can be eliminated with only very minor effects. This will bring the size of the mechanism more in line with those used in complex transport models. It should be noted, however, that small differences in ozone predictions can sometimes lead to relatively large differences in emission control estimates.

3.5 The Killus and Whitten (1982) Mechanism

3.5.1 Description of the Mechanism

The Killus and Whitten mechanism as used in this study, is shown in Table A.4 of the Appendix. The only change from the mechanism as listed in Table 8 of Part I is that the four chamber dependent reactions (reactions 76-79) have been removed.

PHOTOLYSIS RATES: The photolysis rates relative to NO_2 for each photolysis step (reactions 37, 38, 67, 71, and 73) were taken from Table 24 of Part I.

3.5.2 NO to NO_2 Conversion Results

Examination of Tables 4 to 6 shows that the Killus and Whitten mechanism (also known as the Carbon Bond Mechanism) always predicts more NO to NO_2 conversions than does the master mechanism. In most cases, the Killus and Whitten mechanism also predicts more NO to NO_2 conversions than do the other lumped mechanisms considered in this study. The counter species results also show that the greater "reactivity" of the Killus and Whitten mechanism is present in each of the organic classes. In our attempt to pinpoint the reasons for these differences, we first examine the treatment of aromatic hydrocarbon photooxidation in the Killus and Whitten mechanism.

The aromatic portion of the Killus and Whitten mechanism reflects much of what has been learned over the past five years regarding the photooxidation of aromatic hydrocarbons. However, one reason for the discrepancy between the predictions of this mechanism and those of the master mechanism is the new photolysis rate of methyl glyoxal. In the Killus and Whitten mechanism, methyl glyoxal and biacetyl are lumped together into the group DCRB. The photolysis rate assigned to DCRB is that of biacetyl, $k_{DCRB} = 0.04\ k_{NO_2}$. This rate is about twice as large as the recently measured value for methyl glyoxal, $k_{MGLY} = 0.019\ k_{NO_2}$.

Only methyl glyoxal is formed from the aromatic hydrocarbons appearing in initial condition sets 1-3. Thus, to investigate the effect of the photolysis rate of DCRB, we first modify the Killus and Whitten mechanism by reducing the photolysis rate of DCRB from $0.04\ k_{NO_2}$ to $0.019\ k_{NO_2}$. This change reduces the total number of NO to NO_2 conversions, in case 1, from 1007 ppb to 949 ppb.

Even after updating the DCRB photolysis rate, the aromatic portion of the Killus and Whitten mechanism still predicts significantly more NO to NO_2 conversions than does the master mechanism. Killus and Whitten use the species APRC to represent the remainder of the aromatic-OH-O_2 adduct after an α-dicarbonyl has been subtracted. In the master mechanism this species is assumed to be a stable conjugated-γ-dicarbonyl, such as cis-2-butene-1,4-dial, which can undergo reaction with OH radicals. In the Killus and Whitten mechanism, however, APRC is assumed to be a free radical intermediate that falls apart to yield two α-dicarbonyls:

$$\text{APRC} \rightarrow \text{DCRB} + \text{GLY} + \text{X}$$

$$\text{APRC} \rightarrow 2\text{GLY},$$

where DCRB is a methyl-substituted dicarbonyl, GLY is glyoxal, and X is a fictitious species used to maintain carbon-mass balance. Killus and Whitten then make the further assumption that the oxidation of GLY is similar to the oxidation of HCHO (represented as CARB in their mechanism) except that GLY produces an extra molecule of CO. Killus and Whitten, therefore, assume that GLY is equivalent to CARB + CO and the reactions of APRC then become:

$$\text{APRC} \xrightarrow{60} \text{DCRB} + \text{CARB} + \text{CO} + \text{X} \qquad k_{60} = 1\text{x}10^4 \text{ min}^{-1}$$

$$\text{APRC} \xrightarrow{61} 2\text{CARB} + 2\text{CO} \qquad k_{61} = 1\text{x}10^4 \text{ min}^{-1}.$$

The authors state that experiments containing equal amounts of toluene and xylene are best modeled by assigning equal rates for the above pathways. We find that representing APRC as a free radical rather than as a stable conjugated-γ-dicarbonyl leads to a substantially more reactive system. Examination of Tables 4 to 6 shows that the number of NO to NO_2 conversions due to the APRC species in the Killus and Whitten mechanism is very high as

compared to the number due to the conjugated-γ-dicarbonyls in the master mechanism. For example, in case 1, these species account for 93 ppb of NO to NO_2 conversions in the Killus and Whitten mechanism, while the master mechanism attributes only 47 ppb of conversions to these compounds.

If we modify the Killus and Whitten mechanism and treat APRC as a conjugated-γ-dicarbonyl instead of a free radical, the predictions of this mechanism are in much better agreement with those of the master mechanism. For instance, Atkinson et al. (1982) have condensed the chemistry of APRC into the four reaction steps shown below:

$$\text{APRC} + \text{OH} \xrightarrow{61} \text{EL} \qquad k_{61} = 4.4\times10^{4}\ \text{ppm}^{-1}\text{-min}^{-1}$$

$$\text{EL} + \text{NO}_2 \xrightarrow{62} \text{LNO}_2 \qquad k_{62} = 7.1\times10^{3}\ \text{ppm}^{-1}\text{-min}^{-1}$$

$$\text{LNO}_2 \xrightarrow{63} \text{EL} + \text{NO}_2 \qquad k_{63} = 2.2\times10^{-2}\ \text{min}^{-1}$$

$$\text{EL} + \text{NO} \xrightarrow{64} 3\text{NO}_2 - 2\text{NO} + \alpha_3\text{HO}_2\cdot + \alpha_3(\text{CHO})_2 + \alpha_4\ \text{CH}_3\text{CO}_3\cdot + \alpha_4\text{CH}_3\text{C(O)CHO} + \alpha_3\text{CO} \qquad k_{64} = 1.04\times10^{4}\ \text{ppm}^{-1}\text{-min}^{-1}$$

For the initial conditions used in our study, $\alpha_3 \approx \alpha_4 \approx 0.5$. Also, since the Killus and Whitten mechanism represents glyoxal ($(CHO)_2$) as GLY = HCHO + CO, reaction 64 shown above becomes, in carbon-bond form,

$$\text{EL} + \text{NO} \xrightarrow{64} 3\text{NO}_2 - 2\text{NO} + 0.5\ \text{HO}_2\cdot + 0.5\ \text{HCHO} + \text{CO} + 0.5\ \text{AC03} + 0.5\ \text{DCRB}\ .$$

Substituting this reaction sequence for APRC into the Killus and Whitten mechanism, along with the updated DCRB photolysis rate, leads to the results shown in Table 7. By making these two changes, the overall reactivity of the system decreases appreciably, in that the total number of

TABLE 7

Counter Species Results for the Original and Modified Versions of the Killus and Whitten (1982) Mechanism Using Initial Condition Set 1 ($[RHC]_o/[NO_x]_o$ = 7.14)

The Modifications Involved in These Results Deal with the DCRB Photolysis Rate, and the Reactions of the Lumped Group APRC.

ORGANIC CLASS	NO TO NO_2 CONVERSIONS (ppb) MASTER MECHANISM	ORIGINAL KILLUS AND WHITTEN	MODIFIED KILLUS AND WHITTEN
Aromatics	185	314	222
Alkanes	157	321	257
Alkenes	181	224	208
Aldehydes and Ketones	68	148	147
TOTAL	591	1007	834

NO to NO_2 conversions has been reduced from 1007 ppb to 834 ppb, which is substantially closer to the 591 ppb predicted by the master mechanism. Although these changes primarily affect the aromatic hydrocarbon results, better agreement also results with the alkane and alkene portions.

One caveat should be made before we end our discussion of the Killus and Whitten treatment of aromatics chemistry. We are not suggesting that the Atkinson et al. treatment of the aromatic-OH-O_2 adduct be used in the Killus and Whitten mechanism. The fate of this adduct is unknown. It may react to form an α-dicarbonyl and a conjugated-γ-dicarbonyl as suggested by Atkinson et al., or it may cleave to form three α-dicarbonyls as suggested by Killus and Whitten. Thus, attempting to modify the chemistry of aromatics in the Killus and Whitten mechanism may not be justifiable. What is needed at this time is a better understanding of the atmospheric fate of aromatic hydrocarbons.

Even after the above two changes are made, the Killus and Whitten mechanism still predicts considerably more NO to NO_2 conversions than does the master mechanism. Examining the counter species results shown in Tables 4 to 7 shows that the carbonyl compounds in the Killus and Whitten mechanism are ascribed many more conversions than in the master mechanism. There are a number of possible explanations for this behavior:

(1) The Killus and Whitten mechanism contains an inconsistency in the product stoichiometry for the radical producing photolysis pathway from the carbonyls (McRae et al., 1983). Without going into details, the Killus and Whitten mechanism uses the following expression for this reaction:

$$\text{CARB} + h\nu \xrightarrow{\frac{a+1}{2} k_f} (1+a)\ HO_2\cdot + (1-a)MEO_2 + CO$$

where

$$a = \frac{[\text{HCHO}]+[\text{ketones}]}{[\text{total carbonyls}]}$$

k_f = photolysis rate of formaldehyde to molecular products.

As derived in Part I, this expression should read:

$$\text{CARB} = + h\nu \xrightarrow{\frac{a+1}{2} k_f} \frac{3a+1}{a+1} HO_2\cdot + \frac{1-a}{1+a} MEO_2 + CO \quad .$$

(2) In each of the mechanism listings sent to us by Killus and Whitten, the product stoichiometry for reaction 37 indicated that the parameter "a" (defined above) was assigned a value of 0.33, independent of the initial conditions. Apparently then, 0.33 is the default value for this parameter. However, if we calculate this parameter based on the initial conditions of our study, we find that a $\approx$ 0.75. Making this adjustment may be important in applying the Killus and Whitten mechanism to the conditions of our study.

(3) In formulating the carbonyl photolysis reaction mechanisms appearing in the Carbon Bond Mechanism, Killus and Whitten assumed that the two formaldehyde photolysis pathways proceed at equal rates, and that acetaldehyde photolyzes at about one-half of this rate. In other words, Killus and Whitten assume:

$$HCHO + h\nu \xrightarrow{k_a} H_2 + CO \qquad (a)$$

$$HCHO + h\nu \xrightarrow[O_2]{k_b} 2HO_2\cdot + CO \qquad (b)$$

$$CH_3CHO + h\nu \xrightarrow[O_2]{k_c} CH_3O_2\cdot + HO_2 + CO \qquad (c)$$

$$k_a = k_b = k_f$$

$$k_c = \frac{k_f}{2} \quad .$$

If we take the recent recommendations of Horowitz and Calvert (1982), and average these over a zenith angle range of 30° - 60°, we obtain the following approximate rates,

$$k_a \approx 3.3\text{x}10^{-3}\ k_{NO_2}$$

$$k_b \approx 2.3\text{x}10^{-3}\ k_{NO_2}$$

$$k_c \approx 3\text{x}10^{-4}\ k_{NO_2} \quad .$$

Thus, a more accurate description of carbonyl photolysis in the Killus and Whitten mechanism might be obtained by choosing,

$$k_a = k_f = 3.3\text{x}10^{-3}\ \text{min}^{-1}$$

$$k_b = \frac{2}{3}\ k_f$$

$$k_c = \frac{1}{10}\ k_f \quad .$$

(4) The Killus and Whitten mechanism treats acetone as part paraffin and part carbonyl, i.e.,

acetone = 2PAR + 1CARB .

Since acetone leads to very few NO to NO_2 conversions, we would suggest treating it as being unreactive, or as 3PAR.

We now examine the effect on the Killus and Whitten mechanism of adopting each of the above modifications. In each of the tests described below, the Killus and Whitten mechanism has been modified to include our first two suggestions concerning the DCRB photolysis rate and the reactions of APRC.

Correcting the Killus and Whitten treatment of CARB photolysis changes the radical producing pathway from,

$$\text{CARB} + h\nu \xrightarrow{0.67k_f} 1.33\ HO_2\cdot + 0.67\ MEO_2 + CO + 0.67X$$

to

$$\text{CARB} + h\nu \xrightarrow{0.67k_f} 1.5\ HO_2\cdot + 0.5\ MEO_2 + CO + 0.5X \quad .$$

Making this change in the Killus and Whitten mechanism reduces the total number of NO to NO_2 conversions by about 30 ppb, from 834 ppb to 802 ppb. Thus, at least for a = 0.33, this change has only a minor effect.

If we change the parameter "a" from its default value of 0.33 to its value at the beginning of our simulations, 0.75, the carbonyl photolysis pathways change from

$$\text{CARB} + h\nu \xrightarrow{0.33k_f} H_2 + CO$$

$$\xrightarrow{0.67k_f} 1.5\ HO_2\cdot + 0.5\ MEO_2 + CO + 0.5X$$

to

$$\text{CARB} + h\nu \xrightarrow{0.75k_f} H_2 + CO$$

$$\xrightarrow{0.875k_f} 1.86\ HO_2\cdot + 0.14\ MEO_2 + CO + 0.14X \quad .$$

The stoichiometric coefficients shown above are calculated using the corrected expression shown on page 53. Modifying the Killus and Whitten mechanism in this manner actually increases the number of NO to NO_2 conversions from 802 ppb to 847 ppb. This change does not reflect a problem with the Killus and Whitten (1982) mechanism, but merely represents the adaptation of the mechanism to the conditions of our study.

Choosing $k_a = \frac{3}{2} k_b = 10k_c$ and assuming a = 0.75 results in,

$$\text{CARB} + h\nu \xrightarrow{0.75k_f} H_2 + CO$$

$$\xrightarrow{0.525k_f} 1.95\ HO_2\cdot + 0.048\ MEO_2 + CO + 0.048X \ .$$

In contrast, using the modified expression on page 53 with a = 0.75 and Killus and Whitten's relations $k_a = k_b = 2k_c$ gives rise to,

$$\text{CARB} + h\nu \xrightarrow{0.75k_f} H_2 + CO$$

$$\xrightarrow{0.875k_f} 1.86\ HO_2\cdot + 0.14\ MEO_2 + CO + 0.14X \ .$$

Also, we now use $k_f = 3.3\text{x}10^{-3}\ k_{NO_2}$ instead of the Killus and Whitten value of $k_f = 3.0\text{x}10^{-3}\ k_{NO_2}$. This new photolysis rate is consistent with the assumption of $k_a = \frac{3}{2} k_b = 10k_c = k_f$.

Making the above modifications to the Killus and Whitten mechanism has a marked affect on its predictions. The total number of NO to NO_2 conversions is reduced from 847 ppb to 659 ppb, which is much closer to the 591 ppb predicted by the master mechanism. Thus, we feel that updating the current treatment of carbonyl photolysis in the Killus and Whitten mechanism should be considered in future versions of that mechanism.

The fourth and final possible modification listed above is to treat acetone as an unreactive species, rather than as part paraffin and part carbonyl. Examination of the counter species results in Tables 4 to 6 shows that acetone accounts for very few NO to NO_2 conversions in the master mechanisms. For example, with initial condition set 1, the master mechanism attributes only five conversions to the initial acetone. In contrast, the Killus and Whitten mechanism derives 55 ppb of conversions from the initially present acetone, in this same case. If, in addition to the modifications described above, we treat acetone as an unreactive species, the counter species results for the Killus and Whitten mechanism agree very well with those of the master mechanism. These results are shown in Table 8.

3.5.3 Possible Modifications to the Killus and Whitten (1982) Mechanism

Based on our analysis we recommend the following modifications in future versions of the Killus and Whitten mechanism be considered:

(1) The photolysis rates of the DCRB and CARB species be updated to reflect the currently accepted values.

(2) Alternative reaction sequences be developed for the lumped group APRC.

(3) Acetone be classified as an unreactive compound.

TABLE 8

Counter Species Results for the Original and Modified Versions of the Killus and Whitten (1982) Mechanism Using Initial Condition Set 1 ($[RHC]_o/[NO_x]_o$ = 7.14)

The Modified Results were Obtained by Employing all of the Changes Discussed in Section 3.5.2

	NO TO NO_2 CONVERSIONS (ppb)		
ORGANIC CLASS	MASTER MECHANISM	ORIGINAL KILLUS AND WHITTEN	MODIFIED KILLUS AND WHITTEN
Aromatics	185	314	201
Alkanes	157	321	187
Alkenes	181	224	146
Aldehydes and Ketones	68	148	64
TOTAL	591	1007	598

3.6 The Demerjian (1982) Mechanism

3.6.1 Description of the Mechanism

A listing of the Demerjian (1982) mechanism as used in this study can be found in Table A6 of the Appendix. A number of lumped rate constants have been updated from the values listed in Table 4 of Part I (McRae et al., 1983). The reactions involved are numbers 26 through 31, 39, 44, and 45. These changes were made in response to our conversation with Ken Demerjian.

This mechanism uses molar weighted averaging to determine the lumped rate constants. For instance, initial condition set 1 contains 20 ppb of initial toluene and 50 ppb of initial m-xylene, and no other aromatics. In this case the rate constant employed in the Demerjian mechanism for the aromatic (HC4) plus OH reaction is

$$k_{HC4+OH} = \frac{20\ k_{\text{toluene + OH}} + 50\ k_{\text{m-xylene + OH}}}{20 + 50} \quad .$$

Since the initial conditions are specified for a given simulation, the only information needed to calculate the lumped rate constants is the rates for the individual hydrocarbon reactions. Demerjian indicated to us that he wanted the most up-to-date rates used in these calculations. Thus, the rates for reactions 26 through 29, 31, 39, and 45 were calculated using the individual hydrocarbon reaction rate constants recommended by Atkinson and Lloyd (1984). These are the same rates employed in the master mechanism. We note that substituting these updated rate constants could affect the original evaluation of the Demerjian mechanism using smog chamber data.

PHOTOLYSIS RATES: Rates for the photolysis reactions of O_3, HONO, and H_2O_2 (reactions 5, 12, and 25, respectively) were obtained in the same manner as with the Atkinson et al. (1982) mechanism. That is, these rates

were obtained by averaging over a zenith angle range of 30° to 60°. The data needed to calculate these averages were obtained from Demerjian et al. (1980). There are two additional photolysis reactions included in the Demerjian mechanism, reactions 30 and 44. Reaction 44 represents the photolysis of formaldehyde to stable products, and reaction 30 describes the photolysis of both formaldehyde and acetaldehyde to radical products,

$$\text{HC3} + h\nu \xrightarrow{k_{30}} 0.5\ RO_2 + 1.5\ HO_2\cdot + CO$$

$$\xrightarrow{k_{44}} CO + H_2 \quad .$$

The photolysis rates for these reactions were calculated as follows. First, the rates for the three explicit photolysis reactions were calculated by averaging over zenith angles as described above. Next, a correction factor was used to take into account the more recent quantum yields of Horowitz and Calvert (1982). These correction factors are shown below:

$$HCHO + h\nu \xrightarrow{k_1} H\cdot + H\dot{C}O \qquad k_A = 0.714\ k_1$$

$$HCHO + h\nu \xrightarrow{k_2} H_2 + CO \qquad k_B = 0.676\ k_2$$

$$CH_3CHO + h\nu \xrightarrow{k_3} \cdot CH_3 + H\dot{C}O \qquad k_C = 0.444\ k_3 \quad .$$

Finally, mole-weighted rate constants are calculated using the above rates and the initial amounts of formaldehyde and acetaldehyde,

$$k_{30} = \frac{k_A[HCHO]_o + k_C[CH_3CHO]_o}{[HCHO]_o + [CH_3CHO]_o}$$

$$k_{44} = \frac{[HCHO]_o}{[HCHO]_o + [CH_3CHO]_o}\ k_B \quad .$$

3.6.2 NO to NO_2 Conversion Results

The Demerjian mechanism consistently predicts a greater number of NO to NO_2 conversions than does the master mechanism. Although the discrepancies between the Demerjian and master mechanisms occur in all four organic classes, the greatest differences occur with the alkenes. For example, with initial condition set 1 the Demerjian mechanism predicts that the alkenes will lead to 346 ppb of NO to NO_2 conversions, 165 ppb more than predicted by the master mechanism. In the Demerjian treatment of alkene mechanisms ethene is not treated separately from the other olefins. Ethene reacts at a significantly slower rate than the higher alkenes, and in addition, its reaction products do not lead to as many NO to NO_2 conversions as do those from the higher alkenes. The lower reactivity of ethene is partially taken into account by the molar weighting used to obtain the lumped rate constants. However, this weighting is most effective early in the simulation. At later times the alkene distribution is much different from its initial form.

If we modify the Demerjian mechanism by simply separating ethene from the remaining alkenes, the results are in much better agreement with those of the master mechanism. In performing this test only the rate constants were changed, the reactants and products remained the same. The ethene reactions were assigned rates specific for ethene, while the lumped group HC1 (alkenes) was given rates determined by molar weighted averaging with propene and tr-2-butene. The results obtained with this modified Demerjian mechanism are shown in Table 9. Using initial condition set 1,

TABLE 9

Results of Separating Ethylene from the Remaining Olefins in the Demerjian (1982) Mechanism

These Results were Obtained Using Initial Condition Set 1 ($[RHC]_o/[NO_x]_o$ = 7.14)

ORGANIC CLASS	NO TO NO_2 CONVERSIONS (ppb) MASTER MECHANISM	ORIGINAL DEMERJIAN	MODIFIED DEMERJIAN
Aromatics	185	239	206
Alkanes	157	239	177
Alkenes	181	346	254
Aldehydes and Ketones	68	98	85
TOTAL	591	922	722

we find that the number of NO to NO_2 conversions attributable to ethene is reduced from 182 ppb to 88 ppb. At the same time, the number of conversions due to propene and tr-2-butene remains virtually unchanged. Separating ethene from the remaining olefins also has a substantial effect on the number of NO to NO_2 conversions due to the alkanes and aromatics. In fact, the total number of NO to NO_2 conversions is reduced from 922 ppb to 722 ppb. These differences can be explained by examining the radical concentrations present in each simulation. The rate of radical production is much slower in the case where ethene is treated explicitly.

Even after ethene is separated from the remaining olefins, the modified Demerjian mechanism still predicts 131 ppb, or 22 percent more NO to NO_2 conversions than does the master mechanism. This represents, in our view, a difference that is large enough to warrant investigation. It is important to remember that these discrepancies occur even though the same individual hydrocarbon rate constants have been used in both mechanisms. That leaves two possible explanations for the greater reactivity of the Demerjian mechanism:

(1) The molar weighted averaging technique gives rise to lumped rate constants that are too large. We expect that this is true since the more reactive species are depleted faster. Thus, the species with the larger rate constants are weighted too heavily at all times except at the beginning of the simulations. The fact that the Demerjian and master mechanisms are in much closer agreement when initial condition set 3 is used also indicates that this may be the problem. In that case ($[RHC]_o/[NO_x]_o = 1.79$), a much smaller amount of the initial hydrocarbons is consumed over the course of the

photooxidation. Thus, the lumped rate constants based on initial conditions apply for a much longer period of the simulation than for initial condition set 1.

(2) The actual mechanism is incorrect. For example, Killus and Whitten (1983) have found that assuming a yield of two peroxy radicals for the olefin plus ozone reaction introduces significant error into the Demerjian mechanism.

In order to determine which explanation is more responsible for the observed behavior, the Demerjian mechanism was modified as follows. First, remember that as part of the counter species analysis, each initially present hydrocarbon has a specific reaction written for itself. For example, we have two reactions for HC4 + OH present in the Demerjian mechanism used in the counter species analysis:

$$\text{HC41} + \text{OH} \xrightarrow{k} \text{R2O2} + 2\text{HC3} + \text{CO} \qquad k = 2.7\text{x}10^{4}\ \text{ppm}^{-1}\ \text{min}^{-1}$$

$$\text{HC42} + \text{OH} \xrightarrow{k} \text{R2O2} + 2\text{HC3} + \text{CO} \qquad k = 2.7\text{x}10^{4}\ \text{ppm}^{-1}\ \text{min}^{-1}.$$

The first reaction represents toluene chemistry, and the second, m-xylene chemistry. Similarly, there are three HC1 + O_3 reactions, one each for ethene, propene, and tr-2-butene. Thus, we can easily substitute the individual rate constants for each hydrocarbon. In this way, we are eliminating the problem of specifying a lumped rate constant.

The results obtained with this twice-modified Demerjian mechanism show that about one-half of the 131 ppb difference from the master mechanism is eliminated. The total number of predicted NO to NO_2 conversions

is reduced from 722 ppb to 663 ppb, in better agreement with the 591 ppb predicted by the master mechanism. The largest area of improvement is with the aromatic hydrocarbons. Thus, in this case, molar-weighted averaging with initial conditions is responsible for a significant fraction of the observed difference in reactivity between the Demerjian and master mechanisms.

Before summarizing our results concerning the Demerjian mechanism, we would like to discuss one additional aspect. We feel that it is important to note that the lumped group representing the carbonyls HC3 is present as a product in a large number of reactions. Since HC3 is a source of radicals, we might expect that the predictions of this mechanism would be especially sensitive to any inaccuracies in the photolysis rates of formaldehyde and acetaldehyde. To test this assumption, we modified the Demerjian mechanism as follows:

(1) Ethene was treated separately from the other olefins.

(2) The rate constants for the two HC3 photolysis steps were calculated using the Demerjian et al. (1980) rates for formaldehyde and acetaldehyde. In each of the earlier tests, these values were modified based on the work of Horowitz and Calvert (1982).

We can compare the results obtained with this mechanism to those obtained with the Demerjian mechanism in which the only modification is an explicit treatment of ethene chemistry. This comparison shows that the old photolysis rates lead to a 17 percent increase (722 ppb to 842 ppb) in the predicted number of NO to NO_2 conversions when initial conditions set 1 is used. In contrast, the Atkinson et al. (1982) "semi-lumped" mechanism, which contains more species, shows only a 10 percent difference when the same photolysis rate changes are made. We note that this sensitivity to

the aldehyde photolysis rates is not peculiar to the Demerjian mechanism, but is also present in some of the other lumped mechanisms in this study.

3.6.3 Possible Modifications to the Demerjian (1982) Mechanism

In summary, we recommend the following modifications in future versions of the Demerjian mechanism be considered:

(1) Ethene be treated separately from the other alkenes.

(2) The use of molar weighted averages based on initial conditions be thoroughly investigated with an aim toward possible modification.

(3) An improved treatment of aromatic chemistry be tested when future versions of this mechanism are developed. A great deal has been learned about aromatic hydrocarbon photooxidation since this mechanism was first formulated and this information can be incorporated.

(4) Acetone be treated as an unreactive species instead of as an alkane.

3.7 The McRae and Seinfeld (1983) Mechanism

3.7.1 Description of the Mechanism

The McRae and Seinfeld (1983) Mechanism as used in this study is shown in Table A.8 of the Appendix. A number of changes have been made from the mechanism shown in Table 10 of Part I (McRae et al., 1983). First, reaction 49, the O_3 wall loss term, has been eliminated. Also, the rate constant for reaction 50 has been changed from 8.28×10^3 to 7.45×10^3. This new value applies at an H_2O concentration of 15,500 ppm, the amount of water vapor present in our simulations. Rate constants for reactions involving the lumped species were calculated using molar-weighted averaging based on the initial hydrocarbon distribution, as in the Demerjian (1982) mechanism. The individual rate constants used in this calculation

were taken from McRae et al. (1982a). These explicit rates are close to those contained in the master mechanism. The reactions whose rate constants were calculated in this fashion are reactions 25, and 28 through 33.

PHOTOLYSIS RATES: The photolysis reactions appearing in the McRae and Seinfeld (1983) mechanism are reactions 20, 21, 22, 24, 35, and 51. The rates for these steps were taken from McRae et al. (1982a). They represent averages over daylight hours for Los Angeles, California.

3.7.2 NO to NO_2 Conversion Results

In each of the three test cases, the McRae and Seinfeld mechanism predicts significantly more NO to NO_2 conversions than does the master mechanism. In addition, the number of conversions predicted by this mechanism falls somewhere in the middle of the values predicted by the other lumped mechanisms. Examining Tables 4 to 6 shows that the predicted higher reactivity, relative to the master mechanism, occurs in each of the organic classes. The McRae and Seinfeld mechanism uses molar-weighted averaging based on initial concentrations to establish the lumped rate constants. From our analysis of the Demerjian mechanism, we are aware that this technique can lead to an overestimate of the total number of NO to NO_2 conversions. However, we expect that assigning each hydrocarbon its individual rate constant will only cause a small change in the predictions of this mechanism, similar in magnitude to the changes observed with the Demerjian mechanism. If we modify the McRae and Seinfeld mechanism to eliminate the molar-weighted averaging, we find that the total number of NO to NO_2 conversions predicted using initial condition set 1 is reduced from 813 ppb to 783 ppb, accounting for only a small percentage of the observed discrepancy from the predictions of the master mechanism.

Examining the counter species results for the McRae and Seinfeld mechanism shows more closely that the created carbonyl compounds are responsible for a large number of NO to NO_2 conversions. This is not unexpected since the lumped group RCHO is used to represent a wide variety of species. However, we also notice that the McRae and Seinfeld mechanism employs a large photolysis rate for these carbonyls. For example, the photolysis rate for RCHO used in this mechanism, $k_{RCHO} = 4.28 \times 10^{-3} \, k_{NO_2}$, is based on the upper limit reported by Demerjian et al. (1980) for acetaldehyde. This rate is ∿17 times faster than the currently accepted rate of $2.6 \times 10^{-4} \, k_{NO_2}$ (Horowitz and Calvert, 1982). The formaldehyde photolysis rates used by McRae and Seinfeld are also higher than the most recent values. Since the predictions of lumped mechanisms are particularly sensitive to these aldehyde photolysis rates, we expect that the predictions of this mechanism will change significantly if these photolysis rates are updated.

The counter species results obtained with a modified McRae and Seinfeld mechanism, having updated carbonyl photolysis rates and initial condition set 1, are given in Table 10. Also shown are the results for the original McRae and Seinfeld mechanism, and those for the master mechanism. Updating the aldehyde photolysis rates has an enormous effect on the performance of the McRae and Seinfeld mechanism. The total number of NO to NO_2 conversions has been reduced from 812 ppb to 426 ppb. This modified McRae and Seinfeld mechanism actually predicts fewer NO to NO_2 conversions than the master mechanism. These results illustrate the problems that can occur when rate constants are updated in lumped mechanisms. Including the updated photolysis rates renders the predictions of this mechanism

TABLE 10

Result of Updating the Aldehyde Photolysis Rates in the McRae and Seinfeld (1983) Mechanism

Results apply with Initial Condition Set 1 ($[RHC]_o/[NO_x]_o$ = 7.14)

ORGANIC CLASS	NO TO NO_2 CONVERSIONS (ppb) MASTER MECHANISM	ORIGINAL MCRAE AND SEINFELD	MODIFIED MCRAE AND SEINFELD
Aromatics	185	253	112
Alkanes	157	260	105
Alkenes	181	202	140
Aldehydes and Ketones	68	97	69
TOTAL	591	812	426

useless until its performance has been thoroughly reevaluated. On the other hand, using a mechanism with an aldehyde photolysis rate constant 17 times larger than its currently recommended value is not very appealing, in spite of the fact that this out-of-date version has been tested with smog chamber data.

Another problem with the McRae and Seinfeld mechanism arises from its simplified treatment of aromatic chemistry. Little was known regarding aromatic hydrocarbon photooxidation at the time this mechanism was formulated. Incorporating a few additional species, such as methyl glyoxal, into a new treatment of aromatic chemistry should improve its performance.

One possible aromatic reaction mechanism for the McRae and Seinfeld mechanism is:

$$\text{ARO} + \text{OH} \xrightarrow{1} 0.25\ \text{HO}_2\cdot + 0.75\ \text{ADD} \qquad k_1 = 2.76\text{x}10^4\ \text{ppm}^{-1}\text{-min}^{-1}$$

$$\text{ADD} + \text{NO} \xrightarrow{2} \text{NO}_2 + \text{HO}_2\cdot + \text{MGLY} \qquad k_2 = 1.04\text{x}10^4\ \text{ppm}^{-1}\text{-min}^{-1}$$

$$\text{MGLY} + h\nu \xrightarrow{3} 0.65\ \text{RCO}_3 + 0.35\ \text{RO}_2 + \text{HO}_2\cdot + 1.35\ \text{CO} \qquad k_3 = 0.019\ k_{\text{NO}_2}$$

$$\text{MGLY} + \text{OH} \xrightarrow{4} \text{RCO}_3 + \text{CO} \qquad k_4 = 2.5\text{x}10^4\ \text{ppm}^{-1}\text{-min}^{-1}.$$

This mechanism ignores many of the features of aromatic hydrocarbon photooxidation such as OH-abstraction pathways, cresol and dimethyl phenol formation, and the formation of conjugated-γ-dicarbonyls. However, it does provide a more up-to-date description of aromatic chemistry than does the current McRae and Seinfeld treatment, at the expense of only one additional non-steady-state species.

The results of substituting the above reaction sequence into the McRae and Seinfeld mechanism, along with the updated aldehyde photolysis rates discussed earlier, are shown in Table 11. The total number of NO to NO_2 conversions is increased from 426 ppb (see Table 11) to 514 ppb. This is much closer to the 591 ppb predicted by the master mechanism. Of course, we are not suggesting that the above reactions be adopted, as is, into the McRae and Seinfeld mechanism. We are merely pointing out that the current treatment of aromatic chemistry is not very representative of actual aromatic chemistry.

3.7.3 Possible Modifications to the McRae and Seinfeld (1983) Mechanism

In future versions of this mechanism, our major recommendations would include revising the out-of-date aldehyde photolysis rates, and developing a new treatment of aromatic chemistry. An improved treatment of aromatic chemistry will probably result in the addition of one or two new non-steady-state species.

3.8 The Penner and Walton (1982) Mechanism

3.8.1 Description of the Mechanism

The Penner and Walton (1982) mechanism as used in this study is shown in Table A.10 of the Appendix. Two changes have been made from the mechanism shown in Table 12 of Part I. First, the photolysis rates used in this mechanism were calculated using detailed tabulations furnished by

TABLE 11

Result of Replacing the Aromatic Reaction and Updating the Aldehyde Photolysis Rates in the McRae and Seinfeld (1983) Mechanism

These Results were Obtained Using Initial Condition Set 1. ($[RHC]_o/[NO_x]_o$ = 7.14)

ORGANIC CLASS	NO TO NO_2 CONVERSIONS (ppb) MASTER MECHANISM	ORIGINAL MCRAE AND SEINFELD	MODIFIED MCRAE AND SEINFELD
Aromatics	185	253	139
Alkanes	157	260	158
Alkenes	181	202	139
Aldehydes and Ketones	68	97	78
TOTAL	591	812	514

Joyce Penner. These rates represent averages over a zenith angle range of 30 to 60 degrees as was described earlier for the Atkinson et al. (1982) and Demerjian (1982) mechanisms. Second, the two wall loss terms, reactions 62 and 71, have been removed.

Before discussing the counter species results, we first present a brief discussion of reactivity weighting, a concept that is unique to the Penner and Walton mechanism. Reactivity weighting is used in the Penner and Walton mechanism to determine the initial conditions for a given simulation. This method is roughly equivalent to the molar weighting of individual rate constants that is used in the Demerjian and McRae and Seinfeld mechanisms. The technique works as follows. First, a representative species for each class of hydrocarbons is chosen. For example, propene is the representative alkene and n-butane is the representative alkane. Next, the reactions involving lumped groups are assigned rates that are equal to the rate for the reaction of the representative species of that group. For instance, the rate assigned for the alkane plus OH reaction (HC2+OH) is equal to the rate of the n-butane plus OH reaction. To take into account differences in reactivity among the members of a class, the initial concentration of each organic is weighted by its reaction rate relative to that of the representative species. Consider initial condition set 1 which contains initially 15 ppb of propane, 190 ppb of n-butane, and 110 ppb of 2,3-dimethylbutane. Since n-butane is the representative alkane, the initial conditions specified with the Penner and Walton mechanism become:

$$[\text{propane}]_o = \frac{15\ k_{\text{propane + OH}}}{k_{\text{n-butane + OH}}} \qquad [\text{butane}]_o = 190$$

$$[\text{2,3-dimethylbutane}]_o = \frac{110\ k_{\text{2,3-dimethylbutane + OH}}}{k_{\text{n-butane + OH}}} \ .$$

In order to calculate the initial conditions, the individual OH rate constants for each hydrocarbon comprising the class are needed. Joyce Penner indicated to us that she wanted the most up-to-date rate constants used in these calculations. Thus, the rate constants recommended by Atkinson and Lloyd (1984), which are employed in the master mechanism, were used in these calculations. However, the rate constants for the representative hydrocarbons that appear in the mechanism are those furnished to us by Joyce Penner. These rate constants are close to those recommended by Atkinson and Lloyd (1984).

3.8.2 NO to NO_2 Conversion Results

The performance of the Penner and Walton mechanism varies between the three test cases considered in this study. With initial conditions sets 1 and 2 ($[RHC]_o/[NO_x]_o$ = 7.14 and 28.6, respectively), the Penner and Walton mechanism predicts significantly more NO to NO_2 conversions than does the master mechanism. However, with initial condition set 3 ($[RHC]_o/[NO_x]_o$ = 1.79), there is excellent agreement between these two mechanisms. One reason for this behavior is the reactivity weighting of initial conditions used in the Penner and Walton mechanism. We will discuss the reactivity weighting technique in detail later in this section.

Examining Tables 4 to 6 shows that the greatest discrepancy between the master mechanism and the Penner and Walton mechanism occurs with the alkenes. Since the alkenes are a major source of aldehydes, (HC4), we

suspect that out-of-date aldehyde photolysis rates used in the Penner and Walton mechanism may be responsible for a large portion of this discrepancy. In addition, the methyl glyoxal photolysis rate used in this mechanism is a factor of approximately 2.5 times larger than the recently measured rate (Plum et al., 1983). The results of incorporating these changes into the Penner and Walton mechanism are shown in Table 12. The predicted total number of NO to NO_2 conversions in case 1 has been drastically reduced from 846 ppb to 540 ppb. This is actually ∿50 ppb fewer NO to NO_2 conversions than predicted by the master mechanism. The Penner and Walton mechanism now agrees very well with the master mechanism for case 2, but predicts many fewer NO to NO_2 conversions in case 3. Thus, we once again see the importance of the radical producing photolysis steps. Also, it is important to note that even though the total number of conversions predicted by the Penner and Walton mechanism agrees very well with the master mechanism in case 2, the numbers for each hydrocarbon class differ substantially. This is a cause for concern, since changing the initial hydrocarbon distributions could result in drastically different performance relative to the master mechanism.

The Penner and Walton mechanism, like the Demerjian mechanism, does not separate ethene from the higher olefins. Earlier, we noted that this led the Demerjian mechanism to overpredict the number of NO to NO_2 conversions attributable to the alkenes. One might expect that a similar effect is taking place with the Penner and Walton mechanism. However, when the Penner and Walton mechanism is modified so that ethene is treated separately, the predicted number of NO to NO_2 conversions is virtually unchanged. The

TABLE 12

Results Obtained by Updating the Methyl Glyoxal and Aldehyde Photolysis Rates in the Penner and Walton (1982) Mechanism

ORGANIC CLASS	NO TO NO_2 CONVERSIONS (ppb) MASTER MECHANISM	ORIGINAL PENNER AND WALTON	MODIFIED PENNER AND WALTON
INITIAL CONDITION SET 1 ($[RHC]_o/[NO_x]_o$ = 7.14):			
Aromatics	185	217	135
Alkanes	157	218	112
Alkenes	181	327	230
Aldehydes and Ketones	68	84	70
TOTAL	591	846	540
INITIAL CONDITION SET 2 ($[RHC]_o/[NO_x]_o$ = 28.6):			
Aromatics	175	188	147
Alkanes	197	179	148
Alkenes	232	349	300
Aldehydes and Ketones	60	70	55
TOTAL	664	786	650
INITIAL CONDITION SET 3 ($[RHC]_o/[NO_x]_o$ = 1.79):			
Aromatics	69	53	30
Alkanes	41	32	20
Alkenes	65	89	54
Aldehydes and Ketones	34	43	24
TOTAL	209	217	128

major effect of this modification is to increase slightly the number of conversions attributable to ethene.

The different behavior of these two mechanisms arises because of the different methods used to obtain the lumped rate constants. The Demerjian mechanism uses molar-weighted averaging of the individual rate constants. The Penner and Walton mechanism solves this problem indirectly by using the OH reactivity technique discussed earlier. This technique has several advantages over the molar weighting method used by Demerjian and McRae and Seinfeld. First, as we discussed earlier, the molar-weighting calculations lead to lumped rate constants that are too large for most of the simulation. Reactivity weighting does not lead to this problem. Secondly, reactivity weighting has the advantage of not requiring a new set of reaction rates each time the initial hydrocarbon distribution, or emission inventory, is changed.

One problem with this technique arises when large ozone concentrations are achieved. In this case, a significant fraction of the total alkene loss rate occurs through reaction with ozone. Since the initial alkene concentrations are determined using relative OH-reactivities, alkene decay may not be accurately represented in this situation. However, our tests indicate that this is not a serious problem. Nevertheless, there is an additional, and potentially more critical, problem with the reactivity weighting technique. It is this potential problem that is reponsible for the change in performance of the Penner and Walton mechanism as the $[RHC]_o/[NO_x]_o$ ratio changes. This problem is best illustrated with an extreme example.

Let us assume that there are three hydrocarbons that we wish to group into a single lumped class. Each hydrocarbon is present in about the same

concentration, say 5 ppb. Also assume that the OH-reaction rates of these three hydrocarbons are 0.1, 10, and 1000 in consistent units. Finally, assume that species 2 is the representative species for this lumped group. If we apply the reactivity weighting technique of Penner and Walton to this situation, we arrive at the following initial conditions:

Species	k_{OH}	actual initial concentration	reactivity weighted initial concentration
1	0.1	5	0.05
2	10	5	5
3	1000	5	500

The total initial concentration of this lumped group used in the Penner and Walton mechanism is 505.05 ppb, as opposed to the 15 ppb which would be used in an explicit mechanism. Thus, the potential for converting NO to NO_2 is much greater when reactivity weighting is used. Of course, species 3 is assigned a rate constant that is 100 times slower than its explicit rate, and the number of NO to NO_2 conversions is ultimately limited by NO_x availability. However, in cases where sufficient NO_x is present, and the opportunity exists for large amounts of primary hydrocarbon removal, this technique will over predict the total number of NO to NO_2 conversions.

The above example is an extreme case, but the same effects occur in the test cases used in this study. Based on the above reasoning, we would expect that as we change from initial condition set 3 to initial condition set 1, the Penner and Walton mechanism would predict more NO to NO_2 conversions relative to the master mechanism. Examination of Tables 4 to 6 and Table 12 shows this to be the case. This same effect occurs as we change from initial condition set 3 to initial condition set 2, except that the

disappearance of NO_x early in case 2 limits the number of conversions. Another way to illustrate this point is to modify the Penner and Walton mechanism by treating ethene and 2-butene explicitly. As expected, one finds that the number of conversions attributed to ethene increases, while those due to 2-butene decreases. However, the increase in the number of conversions attributable to 2-butene is seven times as large as the decrease in conversions due to ethene (for initial condition set 1). Since the conversions due to propene remain about the same, the total number of conversions due to the alkenes is much greater when reactivity weighting is applied.

3.8.3 Possible Modifications to the Penner and Walton (1982) Mechanism

Thus, we conclude that updating the aldehyde and methyl glyoxal photolysis rates renders the Penner and Walton mechanism very unreactive as compared to both the master mechanism and the other lumped mechanisms. However, the reactivity weighting of initial conditions (which can be considered a part of this mechanism) can result in large increases in the overall reactivity of the system. Thus, depending on the conditions, the actual predicted reactivity may or may not end up being in agreement with the other lumped mechanisms. Since reactivity weighting has such an important effect on the performance of this mechanism, we will not give any further suggestions for changes in the chemistry. We instead suggest that a thorough study of the reactivity weighting technique be carried out.

3.9 The Dodge (1977) Mechanism

3.9.1 Description of the Mechanism

Table A.12 of the Appendix contains a listing of the Dodge (1977) mechanism as used in this study. There are no changes from the mechanism

shown in Table 6 of Part I (McRae et al. (1983)). The photolysis rates used in this mechanism are based on Demerjian et al. (1980).

Before discussing the results for the Dodge mechanism, we note that this mechanism does not rely on the use of a detailed initial hydrocarbon distribution such as the one used in this study. Instead, the total reactive hydrocarbon concentration is calculated and then represented as 75 percent n-butane and 25 percent propene. The only organics contained in the Dodge reaction mechanism are these two hydrocarbons plus four aldehydes. Thus, each of the organics in initial condition sets 1 through 3 are represented in this mechanism by n-butane, propene, formaldehyde, and acetaldehyde.

3.9.2 NO to NO_2 Conversion Results

In each of the three test cases, the Dodge (1977) mechanism predicts more NO to NO_2 conversions than does the master mechanism. This mechanism also generally predicts more conversions than do the other lumped mechanisms. However, as pointed out in Section 3.3, the relationship between NO to NO_2 conversions and O_3 concentration in the Dodge (1977) mechanism is much different from that in the other lumped mechanisms. For example, in case 2, the Dodge (1977) mechanism predicts 40 ppb more of NO to NO_2 conversions than does the master mechanism. However, in this same case the Dodge (1977) mechanism predicts 115 ppb less ozone. Thus the counter species results, which were so useful when comparing the other lumped mechanisms, are not as meaningful when the Dodge (1977) mechanism is examined.

Since the Dodge (1977) mechanism was formulated several years ago, it contains many out-of-date rate constants. Updating these rate constants would, without doubt, significantly change the predictions of this mechanism. As an example, when the reactions involving PAN in the Dodge (1977) mechanism are updated, the maximum O_3 concentration obtained with initial

condition set 1 is reduced from 470 ppb to 280 ppb. Thus, it is clear that these old rate constants cannot be updated without a complete reevaluation of the entire mechanism.

Figures 4, 5, and 6 show that the Dodge (1977) mechanism, relative to the other mechanisms, derives a much higher percentage of its NO to NO_2 conversions from the alkanes. Since the initial hydrocarbon distributions used here contain a majority of alkanes, they give rise to the majority of the conversions predicted by the Dodge (1977) mechanism.

The results in Figures 4, 5, and 6 also show that the Dodge (1977) mechanism does a fair job of predicting the number of NO to NO_2 conversions attributable to the aromatics. This is true in spite of the fact that aromatic hydrocarbons are not included in the mechanism.

In summary, we find it difficult to compare the Dodge (1977) mechanism to the other lumped mechanisms. This difficulty arises because the counter species results for this mechanism cannot be compared to those for the other mechanisms, and because so much of the chemistry in the Dodge (1977) mechanism is out of date. We would be hesitant to recommend use of this mechanism in its current form because of the many out-of-date rate constants. At the same time, an updated version cannot be used until the entire mechanism has been reevaluated. Whether or not the effort involved

in developing and testing an updated version of this mechanism is worthwhile is questionable, since currently there exist mechanisms of similar nature, such as that of Atkinson et al. (1982), that contain updated chemistry.

3.10 Discussion of Results

In this chapter we have presented a quantitative analysis of six lumped reaction mechanisms for photochemical smog. There are several important points that should be considered when interpreting the results of this analysis.

First, even though the master mechanism is fairly detailed and represents our current understanding of the most important gas phase reactions occurring in the atmosphere, the state of the art of atmospheric chemistry is not good enough for the master mechanism to be assumed correct. Therefore, one cannot judge the accuracy of a lumped mechanism by how close its predictions lie to those of the master mechanism. The usefulness of the master mechanism is that it provides a common ground to which the lumped mechanism can be compared. Its purpose therefore is not to judge the adequacy of the lumped mechanisms.

Second, we reiterate that all chamber-dependent reactions were removed from the mechanisms before they were analyzed. As discussed in section 2.6, there is a great deal of disagreement over the magnitude of unknown chamber radical sources. Differences in the amount of "reactivity" predicted by the various mechanisms will continue to exist until the chamber radical source issue is resolved.

Third, it is important to remember that each of the lumped mechanisms has been tested against smog chamber data, and, to a certain extent, the parameters and reactions in the mechanism reflect values chosen within the

bounds of uncertainty that produce the best match of predicted and observed concentrations. Thus, changes in certain rate constants or reaction steps in a mechanism (such as those we have suggested) will require a complete re-analysis of the entire mechanism with respect to experimental chamber data in order to maintain the original degree of agreement.

Finally, remember that in choosing a mechanism one must consider not only how well the mechanism performs, but, if the mechanism is to be used in a full-scale atmospheric model, how many non-steady-state species it contains (McRae et al., 1983). The number of non-steady-state species is important because of computing time limitations.

3.11 Conclusions

In this chapter we have presented a quantitative analysis of the six lumped mechanisms under consideration in our study. The counter species analysis technique has been used to identify the key areas that lead to different predicted O_3 levels under identical initial conditions. Based on the results of our analysis, we have highlighted possible changes for each mechanism. It is clear that the predictions of these mechanisms will be in much closer agreement with each other if these modifications are adopted. We have not attempted to determine a "best" mechanism from among these six. Instead, we have determined why the predictions of each mechanism are so different, and have described changes that we believe will help to eliminate these discrepancies.

It is interesting to summarize this section by modifying each mechanism as per our suggestions, and once again performing a counter species analysis. The modifications that we have suggested for each mechanism are listed in Table 13. In each case, these modifications were made in order either to

TABLE 13

Summary of our Possible Modifications for all but the Dodge (1977) Mechanism

These Modifications are Used to Obtain the Results Shown in Table 14

MECHANISM	MODIFICATIONS (AS DESCRIBED IN CHAPTER 3)
Atkinson et al. (1982) (see Section 3.4.2)	1) 25 percent aromatic nitrate formation removed 2) Photolysis rates of methyl glyoxal, formaldehyde and acetaldehyde updated 3) Products of methylglyoxal photolysis changed from MGLY + hv ---> $CH_3C(O)O_2$ + CO + HO_2 to MGLY + hv ---> 0.65$CH_3C(O)O_2$ + 0.35CH_3O_2 + 1.35CO + HO_2
Killus and Whitten (1982) (see Section 3.5.2)	1) Photolysis rates for the lumped groups DCRB and HCHO updated 2) Atkinson et al. (1982) treatment of APRC reactions substituted in place of existing, first-order reactions 3) Correct mistake in product stoichiometric coefficients for the radical producing photolysis pathway from the aldehydes. Adjust parameter "a" from 0.33 to 0.75. Choose $k_f=k_a=1.5k_b=10k_c$ as opposed to $k_f=k_a=k_b=2k_c$ 4) Treat acetone as unreactive
Demerjian (1982) (see Section 3.6.2)	1) Separate ethene from the remaining alkenes 2) Treat acetone as unreactive
McRae and Seinfeld (1983) (see Section 3.7.2)	1) Update aldehyde photolysis rates 2) Substitute simple, but improved treatment of aromatic chemistry
Penner and Walton (1982) (see Section 3.8.2)	1) Update methyl glyoxal and aldehyde photolysis rates

(1) up-date an out-of-date component, or (2) "improve" the treatment of certain reactions. We have not included any possible changes for the Dodge (1977) mechanism in Table 13.

The counter species results for the modified mechanisms are shown in Table 14. Also shown in this table are the total number of NO to NO_2 conversions predicted by the original mechanisms. These same results are shown graphically in Figures 10, 11, and 12. In addition, Figures 13, 14, and 15 show the amount of O_3 predicted by the original and modified mechanisms. We see that, in nearly every case, the predictions of the modified mechanisms for both NO to NO_2 conversions and O_3 yield are in much better agreement with those of the master mechanism. This is true for each of the three sets of initial conditions. Just as important, we see that with only two exceptions, the lumped mechanisms now agree quite closely with each other. Thus, adopting the few modifications shown in Table 13 has eliminated most of the discrepancies between the predictions of these five mechanisms.

TABLE 14

Comparison of the Counter Species Results for the Original and Modified (in parenthesis) Versions of 5 Lumped Mechanisms

The Changes Made in Each of the Mechanisms are Shown in Table 13.

ORGANIC CLASS	MASTER	NO TO NO2 CONVERSIONS (ppb) ATKINSON ET AL.	KILLUS AND WHITTEN	DEMERJIAN	MC RAE AND SEINFELD	PENNER AND WALTON
		INITIAL CONDITION SET 1 ($[RHC]_o/[NO_x]_o$ = 7.14)				
Aromatics	185	157(146)	201(314)	199(239)	139(253)	135(217)
Alkanes	157	159(180)	187(321)	174(239)	158(260)	110(218)
Alkenes	181	160(191)	146(221)	248(346)	139(202)	227(327)
Aldehydes & Ketones	68	60 (74)	64(148)	71 (98)	78 (97)	60 (84)
TOTAL	591	536(591)	598(1007)	692(922)	514(812)	532(846)
		INITIAL CONDITION SET 2 ($[RHC]_o/[NO_x]_o$ = 28.6)				
Aromatics	175	162(142)	183(246)	246(231)	171(224)	147(188)
Alkanes	197	201(207)	217(223)	229(216)	226(230)	148(179)
Alkenes	232	220(229)	162(175)	358(474)	198(243)	299(349)
Aldehydes & Ketones	60	59 (64)	64(115)	73 (90)	67 (92)	54 (70)
TOTAL	664	642(642)	626(759)	906(1011)	662(789)	648(786)
		INITIAL CONDITION SET 3 ($[RHC]_o/[NO_x]_o$ = 1.79)				
Aromatics	69	68 (68)	82(133)	55 (59)	53 (95)	30 (53)
Alkanes	41	46 (54)	55 (88)	40 (44)	66 (76)	20 (32)
Alkenes	65	62 (74)	56 (95)	85(120)	41 (96)	53 (89)
Aldehydes & Ketones	34	30 (40)	32 (85)	33 (39)	34 (62)	24 (43)
TOTAL	209	206(236)	225(401)	213(262)	194(329)	127(217)

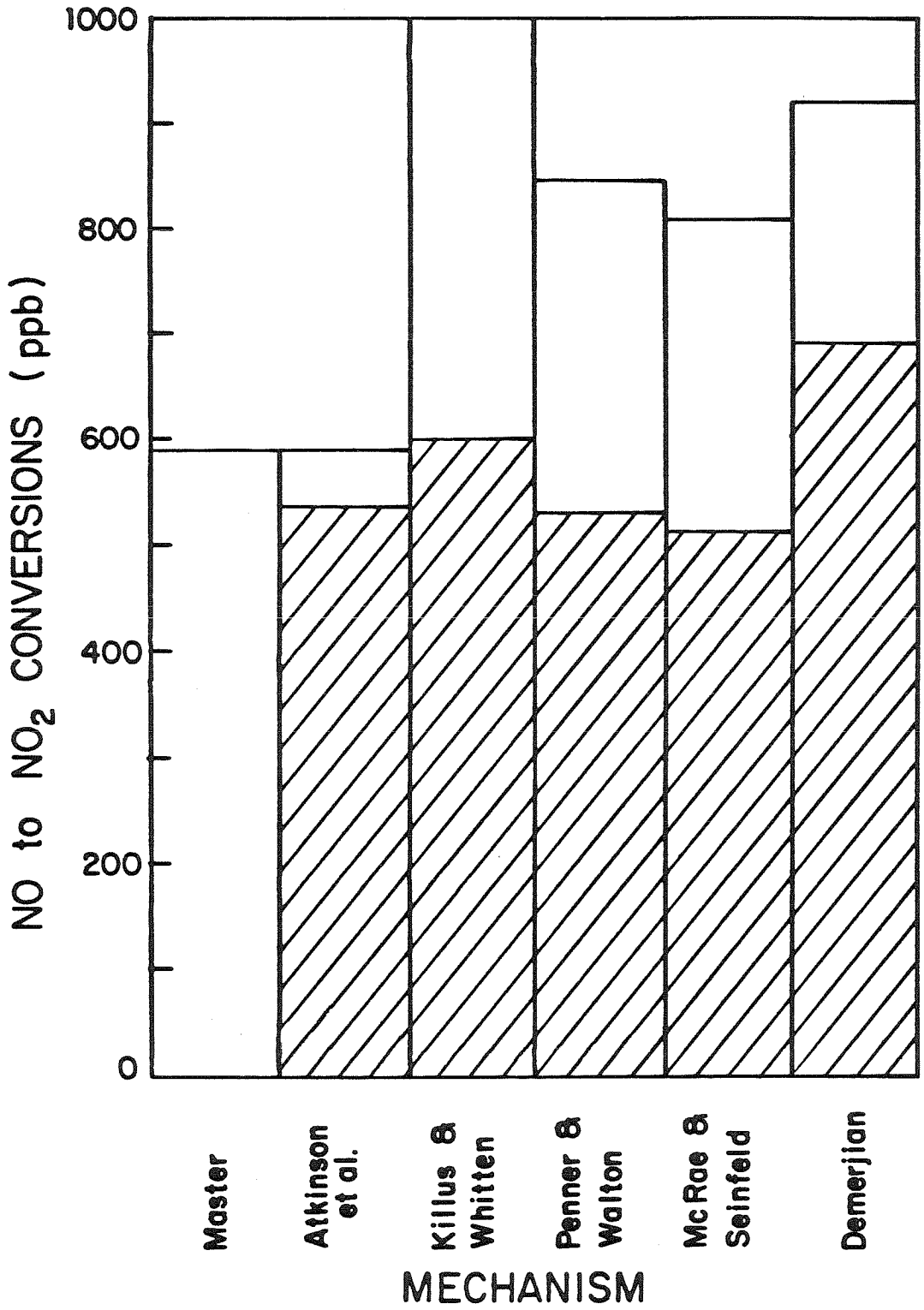

Figure 10. A Comparison of the Total Amount of NO to NO_2 Conversions Predicted by the Original (unshaded) and Modified (shaded) Versions of Five Lumped Mechanisms Using Initial Condition Set 1 ($[RHC]_o/[NO_x]_o$ = 7.14).

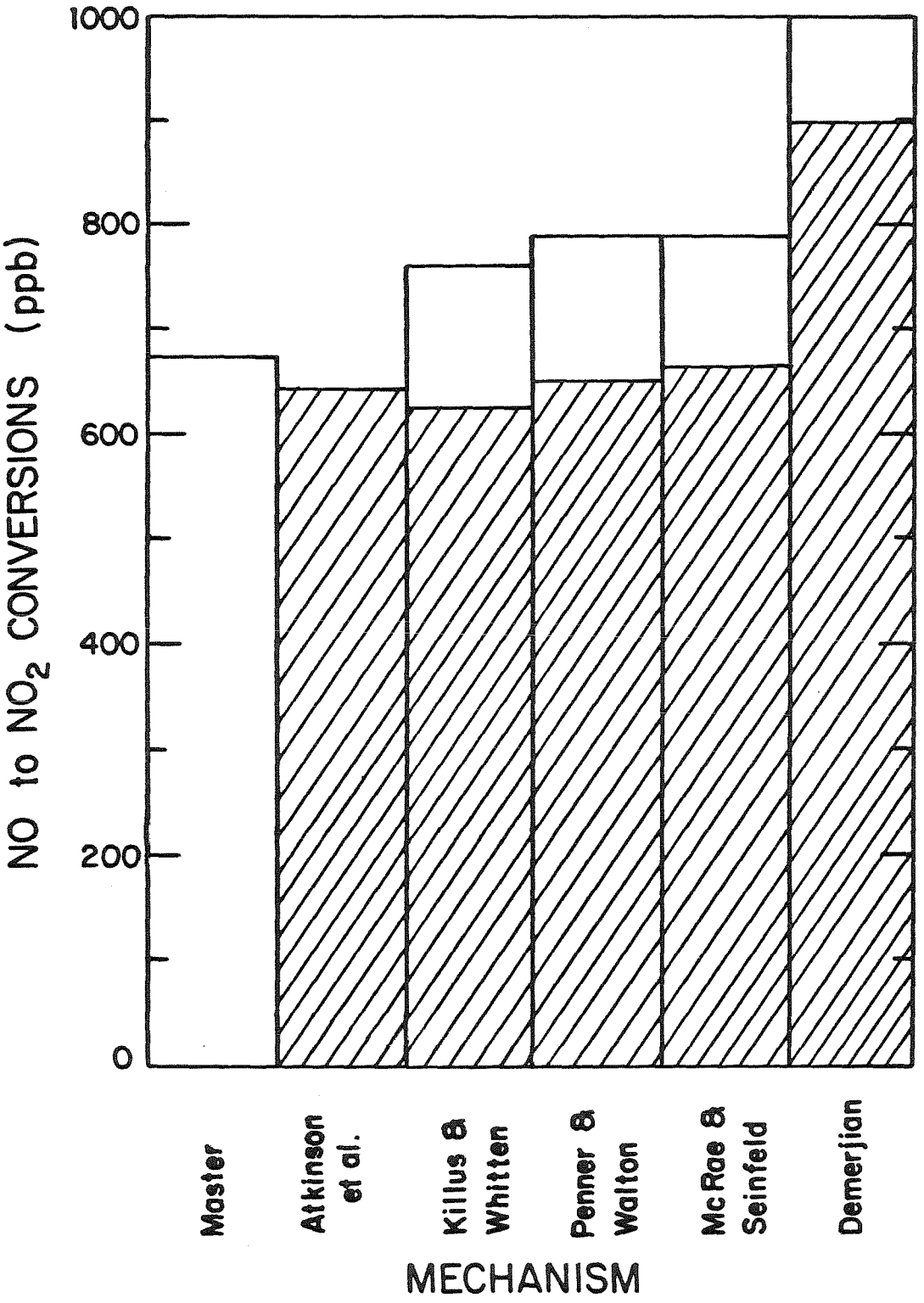

Figure 11. A Comparison of the Total Amount of NO to NO_2 Conversions Predicted by the Original (unshaded) and Modified (shaded) Versions of Five Lumped Mechanisms Using Initial Condition Set 2. $([RHC]_o/[NO_x]_o = 28.6)$.

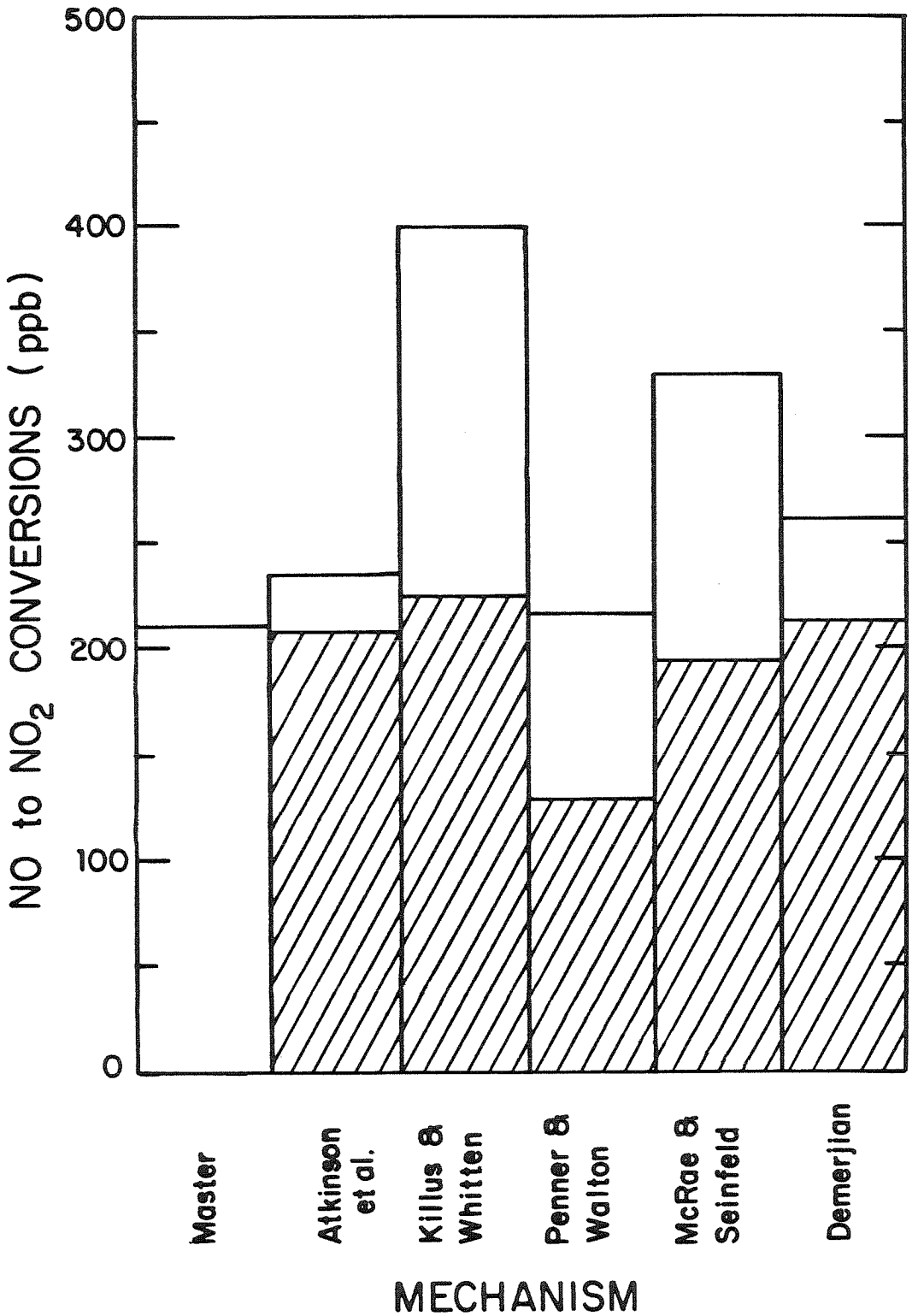

Figure 12. A Comparison of the Total Amount of NO to NO_2 Conversions Predicted by the Original (unshaded) and Modified (shaded) Versions of Five Lumped Mechanisms Using Initial Condition Set 3 ($[RHC]_o/[NO_x]_o = 1.79$).

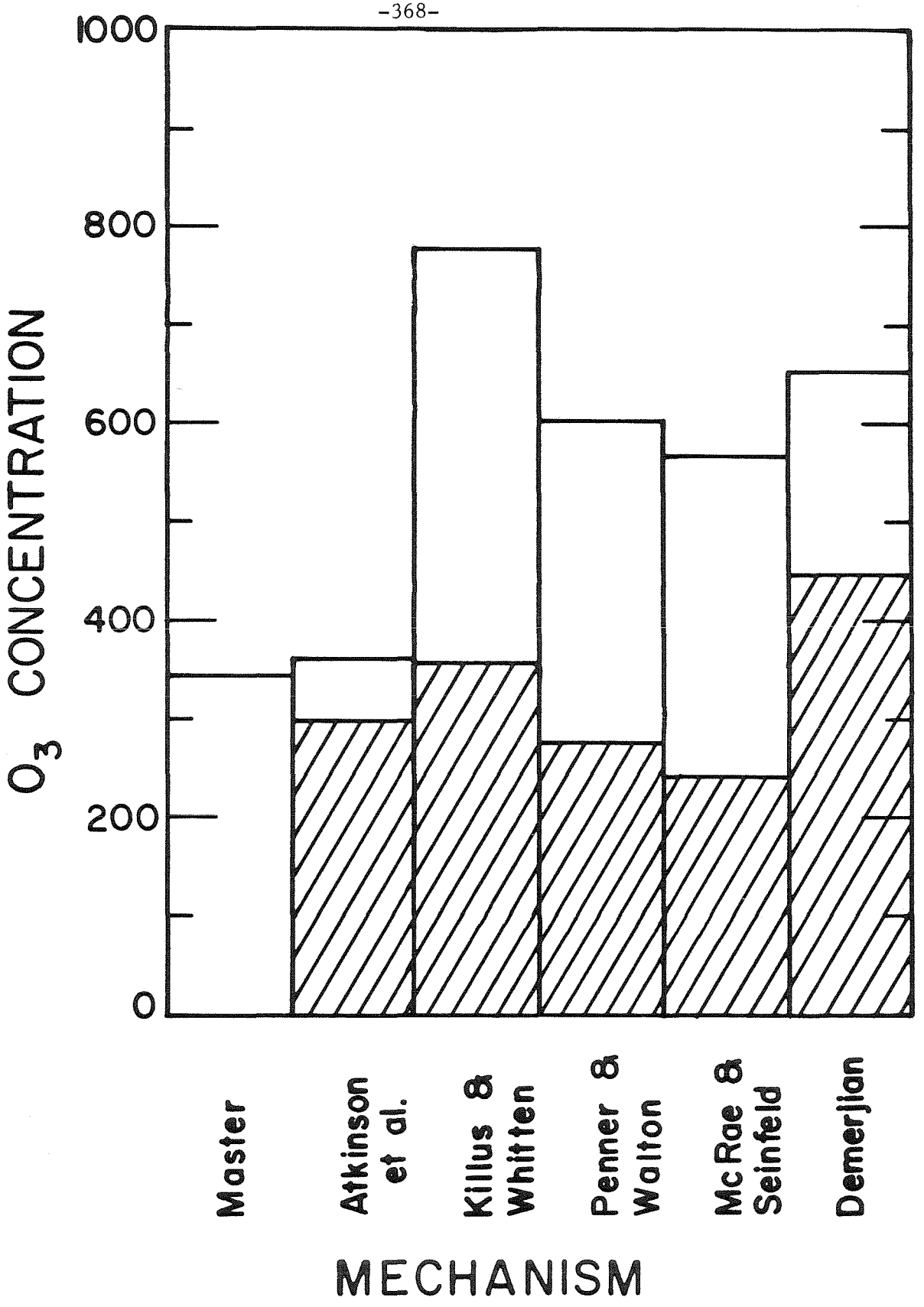

Figure 13. A Comparison of the O_3 Yield After 360 minutes of Simulation Predicted by the Original (unshaded) and Modified (shaded) Versions of Five Lumped Mechanisms Using Initial Condition Set 1.

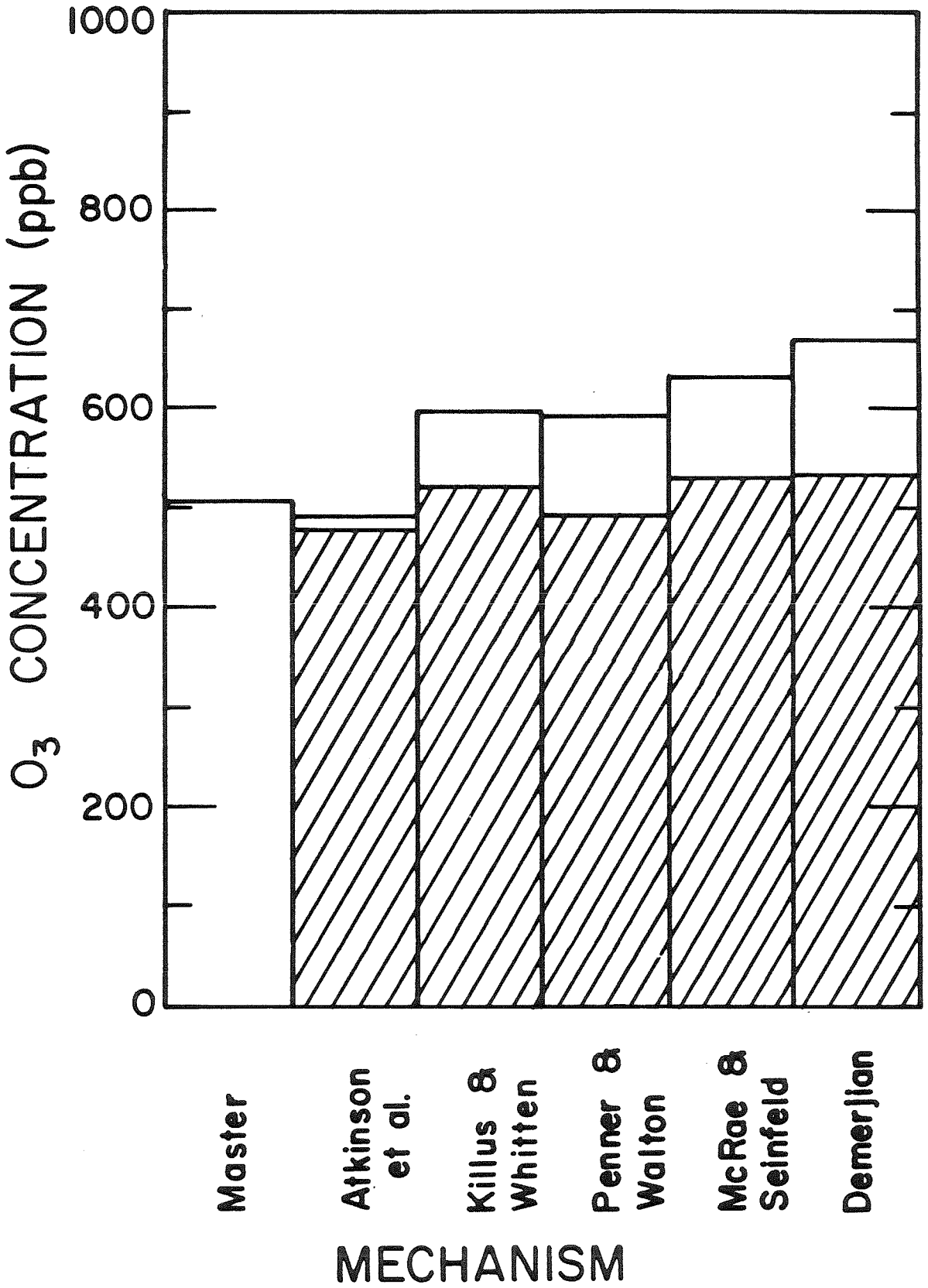

Figure 14. A Comparison of the O_3 Yield After 150 Minutes of Simulation Predicted by the Original (unshaded) and Modified (shaded) Versions of Five Lumped Mechanisms Using Initial Condition Set 2.

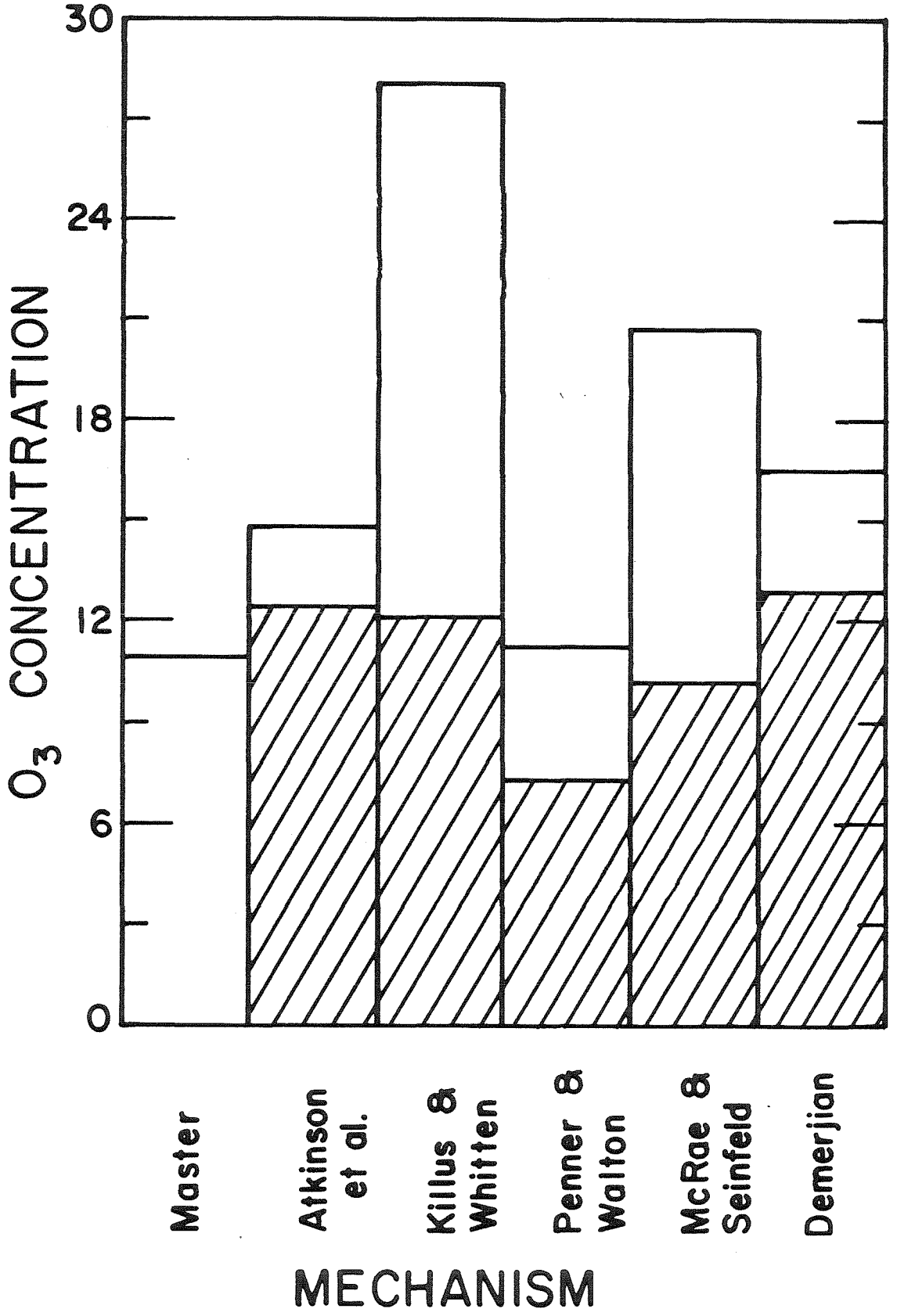

Figure 15. A Comparison of the O_3 Yield After 360 Minutes of Simulation Predicted by the Original (unshaded) and Modified (shaded) Versions of Five Lumped Mechanisms Using Initial Condition Set 3.

CHAPTER 4

CONCLUSIONS AND RECOMMENDATIONS

In this report we have presented a quantitative analysis of six lumped mechanisms describing photochemical smog. At the outset of this study, our goal was to determine why these mechanisms, under identical conditions, give rise to widely different predictions of peak O_3 levels. We have come a long way toward achieving this goal. Based on the results of this analysis, we have identified specific areas in each mechanism that are most responsible for the observed discrepancies in O_3 predictions. For each mechanism, several recommendations have been made that are aimed at eliminating these discrepancies (Table 13). Some of these recommendations amount merely to updating rate constants, while others involve developing completely new reaction sequences. When the lumped mechanisms are modified to include our suggestions, their predictions are in much closer agreement. Of course, changes such as those that we have suggested should not be adopted until the performance of the entire mechanism is reevaluated.

Several recommendations for future work are apparent upon completing this study. These would include recommending that:

- future work be directed at several important areas of atmospheric chemistry where our knowledge is lacking. Perhaps the most critical area needing improvement concerns the mechanism of aromatic ring opening. The products formed, when the aromatic-OH-O_2 adduct cleaves, are unknown. This aspect of the mechanism must be elucidated before any faith can be placed in the predictions of photochemical smog mechanisms. The photolysis products of the important α-dicarbonyls such as methyl glyoxal also represent a critical area of uncertainty in aromatic chemistry.

- much greater resources be devoted to the determination of the fundamental mechanism leading to chamber radical sources. It is an unfortunate fact that mechanisms cannot be unambiguously evaluated using chamber data or compared to each other until the radical source issue is resolved. It now appears that the only way to resolve this controversy is to determine the mechanism which gives rise to this radical source.
- the counter species analysis technique be used by each investigator when future versions of these mechanisms are developed. We have only applied this analysis to a single primary hydrocarbon distribution, at 3 RHC to NO_x ratios. Individual investigators should make use of counter species analysis to test their mechanisms with a variety of initial hydrocarbon distributions and RHC to NO_x ratios.
- future work in evaluating these lumped mechanisms include an analysis of the methods for establishing initial conditions when detailed hydrocarbon composition profiles are not available. The emission control requirements predicted by these lumped mechanisms should be evaluated under real world conditions of continuous pollutant emissions, continuous dilution, and in the presence of background pollutants. Problems of this type will be addressed in Part III of this study.
- that a significant effort be devoted toward measuring the composition and amounts of organics emitted into urban environments. Without this information, the uncertainties involved in specifying input data could nullify any improvements in the reaction mechanisms themselves.

REFERENCES

Atkinson, R. and Lloyd, A.C.(1984), "Evaluation of Kinetic and Mechanistic Data for Modeling of Photochemical Smog," J. Phys. Chem. Ref. Data, 13 (2) (in press).

Atkinson, R., Darnall, K.R., Lloyd, A.C., Winer, A.M. and Pitts, J.N. Jr. (1979), "Kinetics and Mechanisms of the Reaction of the Hydroxyl Radical with Organic Compounds in the Gas Phase," Advances in Photochemistry, 11, 375-488.

Atkinson, R., Carter, W.P.L., Darnall, K.R., Winer, A.M., and Pitts, J.N. Jr. (1980), "A Smog Chamber and Modeling Study of the Gas Phase NO_x-Air Photooxidation of Toluene and the Cresols," International Journal of Chemical Kinetics, 12, 779-837.

Atkinson, R., Lloyd, A.C. and Winges, L. (1982), "An Updated Chemical Mechanism for Hydrocarbons/NO_x/SO_2 Photooxidations Suitable for Inclusion in Atmospheric Simulation Models," Atmospheric Environment, 16, 1341-1355.

Baulch, D.L., Cox, R.A., Crutzen, P.J., Hampson, R.F., Kerr, J.A., Troe, J. and Watson, R.T. (1982), "Evaluated Kinetic and Photochemical Data for Atmospheric Chemistry: Supplement 1. CODATA Task Group on Chemical Kinetics," J. Physical and Chemical Reference Data, 11, 327-496.

Calvert, J.G., Su, F., Bottenheim, J.W. and Strausz, O.P. (1978), "Mechanism of the Homogeneous Oxidation of Sulfur Dioxide in the Troposphere," Atmospheric Environment, 12, 197-226.

Carter, W.P.L., Winer, A.M. and Pitts, J.N., Jr. (1982a) "Effect of Kinetic Mechanisms and Hydrocarbon Composition on Oxidant-Precursor Relationships Predicted by the EKMA Isopleth Technique," Atmospheric Environment 16, 113-120.

Carter, W.P.L., Atkinson, R., Winer, A.M. and Pitts, J.N. Jr., (1982b) "Experimental Investigation of Chamber-Dependent Radical Sources," International Journal of Chemical Kinetics, 14, 1071-1103.

Demerjian, K.L., Schere, K.L. and Peterson, J.T. (1980), "Theoretical Estimates of Actinic (Spherically Integrated) Flux and Photolytic Rate Constants of Atmospheric Species in the Lower Troposphere," Advances in Environmental Science and Technology, 10, 369-459.

Demerjian, K.L. (1982), Personal Communication.

DeMore, W.B., Watson, R.T., Howard, C.J., Golden, D.M., Molina, M.J., Hampson, R.F., Kurylo, M. and Ravishankara, A.R. (1982), Chemical Kinetics and Photochemical Data for Use in Stratospheric Modeling, Jet Propulsion Laboratory Publication 82-57, California Institue of Technology, Pasadena, California.

Dodge, M.C. (1977), "Combined Use of Modeling Techniques and Smog Chamber Data to Derive Ozone -Precursor Relationships," U.S. Environmental Protection Agency Report, EPA-600/3-77-001a, 881-889.

Durbin, P.A., Hecht, T.A. and Whitten, G.Z. (1975), "Mathematical Modeling of Simulated Photochemical Smog," U.S. Environmental Protection Agency Report, EPA-650/4-75-026.

Falls, A.H. and Seinfeld, J.H. (1978), "Continued Development of a Kinetic Mechanism for Photochemical Smog," Environmental Science and Technology, 12, 1398-1406.

Falls, A.H., McRae, G.J. and Seinfeld, J.H. (1979), "Sensitivity and Uncertainty of Reaction Mechanisms for Photochemical Air Pollution," Int. J. Chemical Kinetics, 11, 1137-1162.

Gelinas, R.J., Dickerson, R.P. and Grant, K.E. (1974), Solar Flux and Photodissociation Calculations for LLL Atmospheric Physics Programs, Lawrence Livermore Laboratory Report UCRL-74944 Rev. 1, Lawrence Livermore National Laboratory, University of California, Livermore, California

Gelinas, R.J. and Skewes-Cox, P.D. (1975), "Tropospheric-Photochemical Mechanisms," J. Physical Chemistry, 81, 2468-2479.

Graedel, T.E. (1977), "Functional Group Analysis of Large Chemical Kinetic Systems," J. Physical Chemistry, 81, 2372-2374.

Horowitz, A. and Calvert, J.G. (1982), "Wavelength Dependence of the Primary Processes in Acetaldehyde Photolysis," J. Physical Chemistry, 86, 3105-3114.

Jeffries, H.E., Sexton, K.G. and Salmi, C.N. (1981), "Effects of Chemistry and Meteorology on Ozone Control Calculations Using Simple Trajectory Models and the EKMA Procedure," Final Report to the U.S. Environmental Protection Agency Under Contract No. 68-02-3523, School of Public Health, University of North Carolina, Chapel Hill, North Carolina, 373 pp.

Killus, J.P. and Whitten, G.Z. (1982), A New Carbon-Bond Mechanism for Air Quality Modeling, U.S. Environmental Protection Agency Report No. EPA-600/3-82-041.

Killus, J.P. and Whitten, G.Z. (1983), Effects of Photochemical Kinetic Mechanisms on Oxidant Model Predictions, U.S. Environmental Protection Agency Report No. EPA-600/3-83-111.

Leone, J.A. and Seinfeld, J.H. (1983a) "Analysis of the Characteristic of Complex Chemical Reaction Mechanisms - Application to Photochemical Smog Chemistry," Environmental Science & Technology (in press).

Leone, J.A. and Seinfeld, J.H. (1983b), "An Updated Chemical Mechanism for the Atmospheric Photooxidation of Toluene," International Journal of Chemical Kinetics (in press).

Luther, F.M. and Gelinas, R.J. (1976), "Effects of Molecular Multiple Scattering and Surface Albedo on Atmospheric Photodissociation Rates," J. Geophysical Research, 81, 1125-1132.

MacCracken, M.C. and Sauter, G.C., eds. (1975), "Development of an Air Pollution Model for the San Francisco Bay Area," Final Report to the National Science Foundation, Lawrence Livermore Report UCRL-51920, 1169 pp.

McRae, G.J., Goodin, W.R. and Seinfeld, J.H. (1982a), Mathematical Modeling of Photochemical Air Pollution, California Institute of Technology, Environmental Quality Laboratory Report No. 18.

McRae, G.J., Goodin, W.R. and Seinfeld, J.H. (1982b), "Development of a Second-Generation Mathematical Model for Urban Air Pollution I. Model Formulation," Atmospheric Environment, 16, 679-696.

McRae, G.J. and Seinfeld, J.H. (1983), "Development of a Second-Generation Mathematical Model for Urban Pollution II: Model Performance Evaluation," Atmospheric Environment, 17, 501-523.

McRae, G.J., Leone, J.A. and Seinfeld, J.H. (1983) Evaluation of Chemical Reaction Mechanisms for Photochemical Smog - Part I. Mechanism Description and Documentation, U.S. Environmental Protection Agency Report No. EPA-600/3-83-086.

Penner, J.E. and Walton, J.J. (1982) Air Quality Model Update, Lawrence Livermore Laboratory Report UCID - 19300, Lawrence Livermore National Laboratory, University of California, Livermore, California, 55 pp.

Pitts, J.N., Winer, A.M., Darnall, K.R. et al. (1976), Chemical Consequences of Air Quality Standards and of Control Implementation Programs: Roles of Hydrocarbons, Oxides of Nitrogen, and Aged Smog in the Production of Photochemical Oxidant, Final Report to the California Air Resources Board under Contract Number 4-212, Statewide Air Pollution Research Center, University of California Riverside, California, 444 pp.

Pitts, J.N., Jr., Darnall , K., Carter, W.P.L., Winer, A.M. and Atkinson, R. (1979), Mechanisms of Photochemical Reactions in Urban Air - Final Report, U.S. Environmental Protection Agency Report No. EPA-600/3-79-110.

Plum, C.N., Sanhueza, E., Atkinson, R., Carter, W.P.L. and Pitts, J.N. (1983), "OH Radical Rate Constants and Photolysis Rates of Alpha-Dicarbonyls," Environmental Science and Technology (in press).

Schere, K.L. (1983), Personal Communcation - Letter dated 14 January.

Whitten, G.Z., Hogo, H. and Killus, J.P. (1980a), "The Carbon-Bond Mechanism: A Condensed Kinetic Mechanism for Photochemical Smog," Environmental Science and Technology, 14, 690-700.

Whitten, G.A., Hogo, H. and Killus, J.P. (1980b), Modeling of Simulated Photochemical Smog with Kinetic Mechanisms: Volume 1, U.S. Environmental Protection Agency Report No. EPA-600/3-80-028a, prepared by Systems Applications Inc., San Rafael, California, 362 pp.

Whitten, G.Z. (1981) Comments at U.S. Environmental Protection Agency Workshop on the Empirical Kinetic Modeling Approach, December 15-16, Research Triangle Park, NC.

Whitten, G.Z. (1983) Personal Communication.

APPENDIX

Table A.1. "Master" Reaction Mechanism

Reaction[1]	Rate Constant[2]	Activation Energy (K)	Note
Inorganic Reactions:			
1) $NO_2 + h\nu \rightarrow NO + O(^3P)$	*	-	
2) $O(^3P) + O_2 \rightarrow O_3$	2.6×10^1	-5.1×10^2	
3) $O_3 + NO \rightarrow NO_2 + O_2$	2.7×10^1	1.5×10^3	
4) $O(^3P) + NO_2 \rightarrow NO + O_2$	1.4×10^4	-	
5) $O_3 + NO_2 \rightarrow NO_3 + O_2$	4.7×10^{-2}	2.45×10^3	
6) $NO_3 + NO \rightarrow 2NO_2$	3.0×10^4	-	
7) $HO_2 + NO_2 \rightarrow HO_2NO_2$	1.6×10^3	-	
8) $NO_2 + OH \rightarrow HNO_3$	1.6×10^4	-	
9) $O_3 + OH \rightarrow HO_2 + O_2$	9.9×10^1	9.7×10^2	
10) $O_3 + HO_2 \rightarrow OH + 2O_2$	3.0×10^0	5.8×10^2	
11) $HO_2NO_2 \rightarrow HO_2 + NO_2$	5.1×10^0	1.042×10^4	
12) $HO_2 + NO \rightarrow NO_2 + OH$	1.2×10^4	-2.4×10^2	
13) $HO_2 + HO_2 \rightarrow H_2O_2\ O_2$	3.9×10^3	-1.2×10^3	
14) $HO_2 + HO_2 + H_2O \rightarrow H_2O_2 + O_2 + H_2O$	2.2×10^{-1}	-5.8×10^3	
15) $O_3 + h\nu \rightarrow O(^3P) + O_2$	$6.5 \times 10^{-2}\ k_{NO_2}$	-	1
16) $O_3 + h\nu \rightarrow O(^1D) + O_2$	$2.8 \times 10^{-3}\ K_{NO_2}$	-	1
17) $O(^1D) + O_2 \rightarrow O(^3P) + O_2$	4.3×10^4	-	
18) $O(^1D) + H_2O \rightarrow 2OH$	3.2×10^5	-	
19) $NO + OH \rightarrow HONO$	9.7×10^3	-	
20) $HONO + h\nu \rightarrow NO + OH$	$1.8 \times 10^{-1}\ k_{NO_2}$	-	1
21) $NO + NO + O_2 \rightarrow 2NO_2$	7.2×10^{-10}	-5.3×10^2	
22) $NO_3 + NO_2 \rightarrow NO + NO_2 + O_2$	5.9×10^{-1}	1.23×10^3	

Table A.1 (continued)

Reaction	Rate Constant	Activation Energy (K)	Note
23) $NO_3 + NO_2 \rightarrow N_2O_5$	1.6×10^3	-	
24) $N_2O_5 \rightarrow NO_2 + NO_3$	3.1×10^0	1.108×10^4	
25) $N_2O_5 + H_2O \rightarrow 2HNO_3$	0.0	-	
26) $H_2O_2 + OH \rightarrow HO_2 + H_2O$	2.5×10^3	-	
27) $H_2O_2 + h\nu \rightarrow 2OH$	$8.4 \times 10^{-4}\ k_{NO_2}$	-	
28) $CO + OH \xrightarrow{O_2} HO_2 + CO_2$	4.0×10^2	-	
29) $NO_3 + h\nu \rightarrow 0.3NO + 0.7NO_2 + 0.70(^3P)$	$1.55 \times 10^1\ k_{NO_2}$	-	
Aldehyde Reactions and PAN Formation:			
30) $CH_3CHO + h\nu \xrightarrow{2O_2} CH_3O_2\cdot + HO_2 + CO$	$2.58 \times 10^{-4}\ k_{NO_2}$	-	1
31) $CH_3CHO + OH \xrightarrow{O_2} CH_3C(O)O_2\cdot + H_2O$	2.4×10^4	-2.6×10^2	
32) $CH_3O_2\cdot + NO \rightarrow NO_2 + CH_3O\cdot$	1.1×10^4	-	
33) $CH_3O\cdot + O_2 \rightarrow HCHO + HO_2\cdot$	2.1×10^0	1.35×10^3	
34) $CH_3O\cdot + NO_2 \rightarrow CH_3ONO_2$	2.2×10^4	-	
35) $CH_3O_2\cdot + HO_2 \rightarrow CH_3OOH + O_2$	9.2×10^3	-1.3×10^3	
36) $CH_3C(O)O_2\cdot + NO \xrightarrow{2O_2} NO_2 + CH_3O_2\cdot + CO_2$	1.1×10^4	-	
37) $CH_3C(O)O_2\cdot + NO_2 \rightarrow PAN$	6.9×10^3	-	
38) $CH_3C(O)O_2\cdot + HO_2 \rightarrow CH_3C(O)O_2H + O_2$	4.4×10^3	-	
39) $PAN \rightarrow CH_3C(O)O_2\cdot + NO_2$	2.2×10^{-2}	1.354×10^4	
40) $HCHO + h\nu \rightarrow H_2 + CO$	$3.3 \times 10^{-3}\ k_{NO_2}$	-	1
41) $HCHO + h\nu \xrightarrow{2O_2} 2HO_2 + CO$	$2.35 \times 10^{-3}\ k_{NO_2}$	-	1

Table A.1 (continued)

Reaction[1]	Rate Constant[2]	Activation Energy (K)	Note
42) $HCHO + OH \xrightarrow{O_2} HO_2 + CO + H_2O$	1.6×10^4	-	
α-Dicarbonyl Chemistry:			
43) $CH_3C(O)CHO + OH \xrightarrow{O_2} CH_3C(O)O_2\cdot + CO + H_2O$	2.5×10^4	-	
44) $CH_3C(O)CHO + h\nu \xrightarrow{2O_2} CH_3C(O)O_2\cdot + HO_2 + CO$	$1.3\times10^{-2}\ k_{NO_2}$	-	
45) $CH_3C(O)CHO + h\nu \xrightarrow{2O_2} CH_3O_2\cdot + HO_2 + 2CO$	$6.0\times10^{-3}\ k_{NO_2}$	-	
46) $(CHO)_2 + OH \xrightarrow{O_2} HO_2 + 2CO + H_2O$	1.7×10^4	-	
47) $(CHO)_2 + h\nu \rightarrow 0.13HCHO + 0.87H_2 + 1.87CO$	$8.0\times10^{-3}\ k_{NO_2}$	-	
Toluene Abstraction Pathway:			
48) $C_6H_5\text{-}CH_3 + OH \xrightarrow{O_2} C_6H_5\text{-}CH_2O_2\cdot + H_2O$	7.5×10^2	-	
49) $C_6H_5\text{-}CH_2O_2\cdot + NO \rightarrow NO_2 + C_6H_5\text{-}CH_2O\cdot$	9.0×10^3	-	
50) $C_6H_5\text{-}CH_2O_2\cdot + NO \rightarrow C_6H_5\text{-}CH_2ONO_2$	1.0×10^3	-	
51) $C_6H_5\text{-}CH_2O\cdot + O_2 \rightarrow C_6H_5\text{-}CHO + HO_2$	1.0×10^1	6.9×10^2	
52) $C_6H_5\text{-}CH_2O\cdot + NO_2 \rightarrow C_6H_5\text{-}CH_2ONO_2$	1.9×10^4	-	
53) $C_6H_5\text{-}CHO + h\nu \rightarrow$ stable products	1.6×10^{-3}	-	
54) $C_6H_5\text{-}CHO + OH \xrightarrow{O_2} C_6H_5\text{-}C(O)O_2\cdot + H_2O$	1.9×10^4	-	
55) $C_6H_5\text{-}C(O)O_2\cdot + NO \xrightarrow{O_2} NO_2 + C_6H_5\text{-}O_2\cdot + CO_2$	1.0×10^4	-	

Table A.1 (continued)

Reaction[1]	Rate[2] Constant	Activation Energy (K)	Note
56) $C_6H_5\text{-}C(O)O_2\cdot + NO_2 \rightarrow C_6H_5\text{-}C(O)O_2NO_2$	6.9×10^3	-	
57) $C_6H_5\text{-}C(O)O_2NO_2 \rightarrow C_6H_5\text{-}C(O)O_2\cdot + NO_2$	9.6×10^{-3}	1.304×10^4	
58) $C_6H_5\text{-}O_2\cdot + NO \rightarrow NO_2 + C_6H_5\text{-}O\cdot$	9.0×10^3	-	
59) $C_6H_5\text{-}O_2\cdot + NO_2 \rightarrow NO_3 + C_6H_5\text{-}O\cdot$	1.0×10^4	-	
60) $C_6H_5\text{-}O\cdot + NO_2 \rightarrow$ 	2.2×10^4	-	
61) 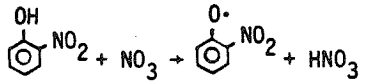	3.0×10^3	-	
62) 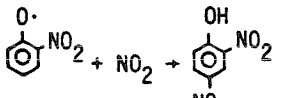	2.2×10^4	-	
63) 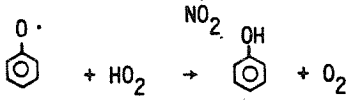	7.4×10^3	-	

Toluene Addition Pathway:

64) 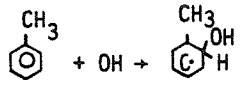	8.7×10^3	-	
65) 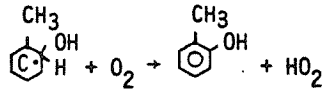	1.0×10^1	6.9×10^2	
66) 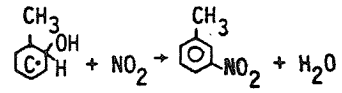	4.4×10^4	-	
67) 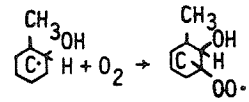	4.9×10^1	-	
68) 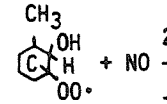 $+ NO \xrightarrow{2O_2} NO_2 + HO_2$ $+ CH_3C(O)CHO + CH(O)CH{=}CHCHO$	1.0×10^4	-	

Table A.1 (continued)

Reaction[1]	Rate Constant[2]	Activation Energy (K)	Note
Toluene addition path (continued)			
69) 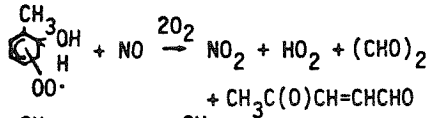	0.0	-	
70) 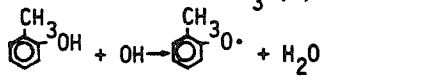	4.9×10^3	9.0×10^2	
71) 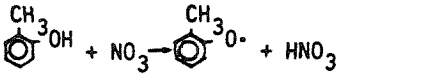	1.5×10^4	-	
72) 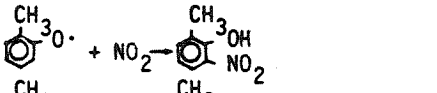	2.2×10^4	-	
73) 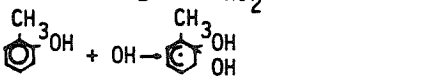	5.6×10^4	-	
74) 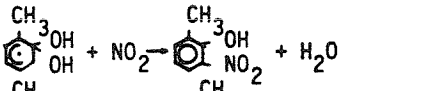	4.4×10^4	-	
75) 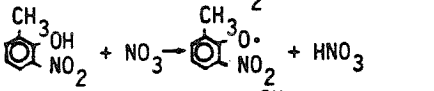	1.5×10^4	-	
76) 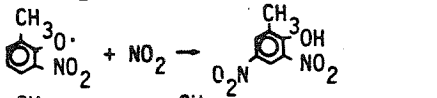	2.2×10^4	-	
77) 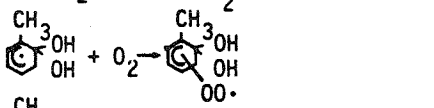	4.9×10^1	-	
78) 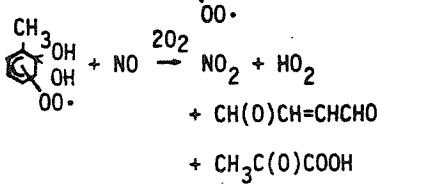	1.0×10^4	-	
79) 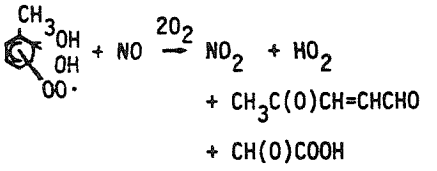	0.0	-	

Table A.1 (continued)

	Reaction[1]	Rate Constant[2]	Activation Energy(K)	Note
80)	$CH(O)COOH + OH \rightarrow HO_2 + H_2O + CO$	2.2×10^{4}	-	
81)	$CH_3C(O)COOH + h\nu \rightarrow CH_3CHO + CO_2$	1.4×10^{-2}	k_{NO_2}	-
	Conjugated γ-dicarbonyl chemistry			
82)	$HC(O)CH=CHCHO + OH \xrightarrow{O_2} HC(O)CH=CHC(O)O_2\cdot + H_2O$	4.4×10^{4}		-
83)	$HC(O)CH=CHC(O)O_2\cdot + NO \xrightarrow{O_2} NO_2 + CO_2 + HC(O)CH=CHO_2\cdot$	1.0×10^{4}		-
84)	$HC(O)CH=CHO_2\cdot + NO \xrightarrow{O_2} NO_2 + HC(O)CH(O_2\cdot)CHO$	1.0×10^{4}		-
85)	$HC(O)CH(O_2\cdot)CHO + NO \rightarrow HC(O)CH(ONO_2)CHO$	4.0×10^{2}		-
86)	$HC(O)CH=CHC(O)O_2\cdot + NO_2 \rightarrow HC(O)CH=CHCO_3NO_2$	6.9×10^{3}		-
87)	$HC(O)CH=CHCO_3NO_2 \rightarrow HC(O)CH=CHC(O)O_2\cdot + NO_2$	2.2×10^{-2}		-
88)	$HC(O)CH(O_2\cdot)CHO + NO \xrightarrow{O_2} (CHO)_2 + HO_2 + NO_2 + CO$	1.0×10^{4}		-
89)	$HC(O)CH=CHO_2\cdot + NO \rightarrow HC(O)CH=CHONO_2$	4.0×10^{2}		-
90)	$HC(O)CH=CHO_2\cdot + NO_2 \xrightarrow{O_2} HC(O)CH(O_2\cdot)CHO + NO_3$	1.0×10^{4}		-
91)	$CH_3C(O)CH=CHCHO + OH \xrightarrow{O_2} H_2O + CH_3C(O)CH=CHC(O)O_2\cdot$	2.2×10^{4}		-
92)	$CH_3C(O)CH=CHCHO + OH \xrightarrow{O_2} CH_3C(O)CH(OH)C(O_2\cdot)HCHO$	7.4×10^{3}		-
93)	$CH_3C(O)CH(OH)C(O_2\cdot)HCHO + NO \xrightarrow{O_2} NO_2 + HO_2 + CH_3C(O)CHO + (CHO)_2$	1.0×10^{4}		-
94)	$CH_3C(O)CH=CHC(O)O_2\cdot + NO \xrightarrow{O_2} NO_2 + CO_2 + CH_3C(O)CH=CHO_2\cdot$	1.0×10^{4}		-
95)	$CH_3C(O)CH=CHO_2\cdot + NO \xrightarrow{O_2} NO_2 + CH_3C(O)CH(O_2\cdot)CHO$	1.0×10^{4}		-
96)	$CH_3C(O)CH(O_2\cdot)CHO + NO \rightarrow CH_3C(O)CH(ONO_2)CHO$	8.0×10^{6}		-
97)	$CH_3C(O)CH=CHC(O)O_2\cdot + NO \rightarrow CH_3C(O)CH=CHCO_3NO_2$	6.9×10^{3}		-
98)	$CH_3C(O)CH=CHCO_3NO_2 \rightarrow CH_3C(O)CH=CHC(O)O_2\cdot + NO_2$	2.2×10^{-2}		-
99)	$CH_3C(O)CH(O_2\cdot)CHO + NO \xrightarrow{O_2} NO_2 + CH_3C(O)O_2\cdot + (CHO)_2$	5.0×10^{3}		-

Table A.1 (continued)

Reaction	Rate Constant	Activation Energy(K)	Note
Conjugated γ-dicarbonyl chemistry (continued)			
100) $CH_3C(O)CH(O_2\cdot)CHO+NO \xrightarrow{O_2} NO_2+HO_2+CH_3C(O)CHO+CO$	5.0×10^3	-	
101) $CH_3C(O)CH=CHO_2\cdot+NO \rightarrow CH_3C(O)CH=CHONO_2$	8.0×10^2	-	
102) $CH_3C(O)CH=CHO_2\cdot+NO_2 \xrightarrow{O_2} NO_3+CH_3C(O)CH(O_2\cdot)CHO$	1.0×10^4	-	
m-Xylene chemistry:			
103) 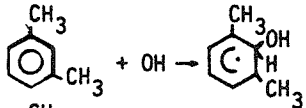	3.4×10^4	-	2
104) 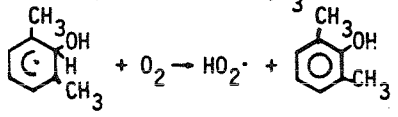	1.0×10^2	6.9×10^2	
105) 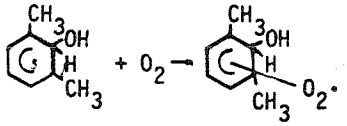	4.7×10^1	-	
106) 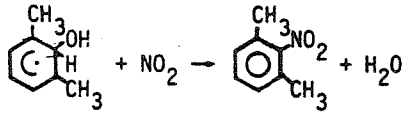	4.4×10^4	-	
107) 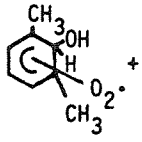 + NO → NO_2 + $HO_2\cdot$ + $CH_3C(O)CHO$ + 0.5 $CH_3C(O)CH=CHCHO$ + 0.5 $CH(O)CH=C(CH_3)CHO$	1.0×10^4	-	3
108) 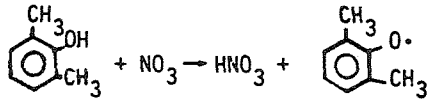	2.2×10^4	-	
109) 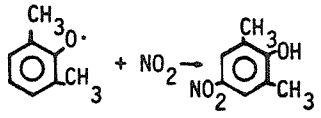	2.2×10^4	-	

Table A.1 (continued)

Reaction	Rate Constant	Activation Energy(K)	Note
m-Xylene chemistry (continued)			
110) 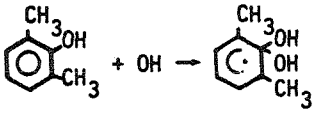	1.1×10^{5}	-	
111) 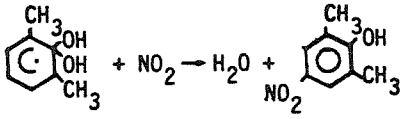	4.4×10^{4}	-	
112) 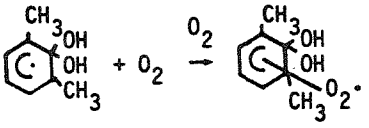	4.7×10^{1}	-	
113) 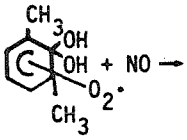 $+ NO \rightarrow NO_2 + HO_2 + CH_3COCOOH + 0.5\ CH_3COCH{=}CHCHO + 0.5\ CHOCH{=}C(CH_3)CHO$	1.0×10^{4}	-	3
114) $CHOCH{=}C(CH_3)CHO + OH \xrightarrow{O_2} HCOC(OH)HC^{\cdot}(CH_3)CHO_2^{\cdot}$	7.4×10^{3}	-	
115) $HCOC(OH)HC^{\cdot}(CH_3)CHO_2^{\cdot} + NO \xrightarrow{O_2} 0.88NO_2 + 0.88(CHO)_2 + 0.88\ HO_2^{\cdot}$	1.0×10^{4}	-	4
116) $CHOCHO{=}C(CH_3)CHO + OH \xrightarrow{O_2} HCOCH{=}C^{\cdot}(CH_3)CO_3^{\cdot} + H_2O$	4.4×10^{4}		
117) $HCOCH{=}C^{\cdot}(CH_3)CO_3^{\cdot} + NO \xrightarrow{O_2} NO_2 + HCOCH{=}C^{\cdot}(CH_3)CO_2^{\cdot} + CO_2$			
118) $HCOCH{=}C^{\cdot}(CH_3)CO_3^{\cdot} + NO_2 \rightarrow HCOCH{=}C^{\cdot}(CH_3)CO_3NO_2$	6.9×10^{3}	-	
119) $HCOCH{=}C^{\cdot}(CH_3)CO_3NO_2 \rightarrow NO_2 + HCOCH{=}C^{\cdot}(CH_3)CO_3^{\cdot}$	2.2×10^{-2}	1.354×10^{4}	

Table A.1 (continued)

Reaction	Rate Constant	Activation Energy(K)	Note
m-Xylene chemistry (continued)			
120) $HCOCH{=}\overset{CH_3}{\overset{|}{C}}O_2\cdot + NO \xrightarrow{O_2} NO_2 + CH_3(O)CH(O_2\cdot)CHO$	1.0×10^{4}	-	
121) $HCOCH{=}\overset{CH_3}{\overset{|}{C}}O_2\cdot + NO \rightarrow HCOCH{=}\overset{CH_3}{\overset{|}{C}}O_2NO_2$	8.0×10^{2}	-	
122) $HCOCH{=}\overset{CH_3}{\overset{|}{C}}O_2\cdot + NO_2 \rightarrow NO_3 + (CH_3C(O_2\cdot)(CHO)_2$	1×10^{4}	-	
123) $CH_3C(O_2\cdot)(CHO)_2 + NO \rightarrow CH_3C(ONO_2)(CHO)_2$	8.0×10^{2}	-	
124) $CH_3C(O_2\cdot)(CHO)_2 + NO \xrightarrow{O_2}$ 0.75 $HO_2\cdot$ + 0.75 CO + 0.75 CH_3COCHO + 0.25 $(CHO)_2$ + 0.25 $CH_3C(O)O_2\cdot$ + NO_2	1×10^{4}	-	
Ethene chemistry:			
125) $CH_2{=}CH_2 + OH \xrightarrow{O_2} HOCH_2CH_2O_2\cdot$	1.2×10^{4}	-3.82×10^{2}	
126) $HOCH_2CH_2O_2\cdot + NO \rightarrow NO_2 + HOCH_2CH_2O\cdot$	1×10^{4}		
127) $HOCH_2CH_2O\cdot \rightarrow HCHO + \cdot CH_2OH$	5.6×10^{6}		
128) $HOCH_2CH_2O\cdot + O_2 \rightarrow HOCH_2CHO + HO_2\cdot$	1.0×10^{1}	6.9×10^{2}	5
129) $\cdot CH_2OH + O_2 \rightarrow HCHO + HO_2\cdot$	$k_5=3\times10^{3}$		
130) $CH_2{=}CH_2 + O_3 \xrightarrow{O_2}$ HCHO + 0.4 $\check{C}H_2O\mathring{O}$ + 0.18 CO_2 + 0.42CO + 0.12 H_2 + 0.42 H_2O + 0.12 $HO_2\cdot$	2.5×10^{-3}	2.56×10^{3}	

Table A.1 (continued)

Reaction	Rate Constant	Activation Energy(K)	Note
Propene chemistry:			
131) $CH_3CHCH_2 + OH \rightarrow 0.65\ CH_3\dot{C}H\dot{C}H_2OH(O_2,O_2\cdot) + 0.35\ CH_3CH(OH)CH_2O_2\cdot$	3.7×10^{4}	-5.37×10^{2}	
132) $CH_3\dot{C}H\dot{C}H_2OH(O_2\cdot) + NO \rightarrow NO_2 + CH_3\dot{C}H\dot{C}H_2OH(O\cdot)$	1×10^{4}	-	
133) $CH_3\dot{C}H\dot{C}H_2OH(O\cdot) \rightarrow CH_3CHO + \cdot CH_2OH$	1×10^{5}	-	
134) $CH_3CH(OH)CH_2O\cdot \rightarrow HCHO + CH_3\dot{C}HOH$	1×10^{2}	-	
135) $CH_3\dot{C}H\dot{C}H_2OH(O_2\cdot) + NO \rightarrow CH_3\dot{C}H\dot{C}H_2OH(ONO_2)$	4.0×10^{2}	-	
136) $CH_3CH(OH)CH_2O_2\cdot + NO \rightarrow NO_2 + CH_3CH(OH)CH_2O\cdot$	1×10^{4}	-	
137) $CH_3CH(OH)CH_2O_2\cdot + NO \rightarrow CH_3CH(OH)CH_2ONO_2$	400	-	
138) $CH_3\dot{C}HOH + O_2 \rightarrow HO_2\cdot + CH_3CHO$	3×10^{3}	-	
139) $CH_3CHCH_2 + O_3 \rightarrow 0.5\ CH_3CHO + 0.2\ CH_3\dot{C}HO\mathring{O} + 0.06\ CH_4 + 0.27\ CO_2 + 0.33\ CO + 0.20\ HO_2\cdot + 0.1\ OH + 0.22\ CH_3O_2\cdot + 0.03\ CH_3O\cdot + 0.2\ \mathring{C}H_2O\mathring{O} + 0.06\ H_2 + 0.21\ H_2O$	1.6×10^{-2}	1.897×10^{3}	
tr-2-butene chemistry:			
140) $CH_3CH_2{=}CH_2CH_3 + OH \rightarrow CH_3CH(OH)\dot{C}HCH_3(O_2,OO\cdot)$	1.0×10^{5}	-5.42×10^{2}	
141) $CH_3CH(OH)\dot{C}HCH_3(OO\cdot) + NO \rightarrow NO_2 + CH_3\dot{C}H\dot{C}HCH_3(OH,O\cdot)$	1.0×10^{4}	-	

Table A.1 (continued)

	Reaction	Rate Constant	Activation Energy(K)	Note
	tr-2-butene chemistry (continued)			
142)	$CH_3CH(OH)\dot{C}HCH_3(OO\cdot) + NO \rightarrow CH_3\dot{C}HCH_3(OH)(ONO_2)$	8.0×10^{2}	-	
143)	$CH_3CH(OH)\dot{C}HCH_3(O\cdot) \rightarrow CH_3CHO + CH_3\dot{C}HOH$	1.0×10^{4}	-	
144)	$CH_3CH_2{=}CH_2CH_3 + O_3 \rightarrow CH_3CHO + 0.4\ CH_3\dot{C}HO\mathring{O} + 0.12\ CH_4 + 0.36\ CO_2 + 0.24\ CO + 0.29\ HO_2\cdot + 0.19\ OH + 0.05\ CH_3O\cdot + 0.43\ CH_3O_2\cdot$	2.7×10^{-1}	1.051×10^{3}	
145)	$C\dot{H}_2O\mathring{O} + NO \rightarrow NO_2 + HCHO$	1.0×10^{4}	-	
146)	$C\dot{H}_2O\mathring{O} + NO_2 \rightarrow NO_3 + HCHO$	1.0×10^{3}	-	
147)	$C\dot{H}_2O\mathring{O} + H_2O \rightarrow HCOOH + H_2O$	6.0×10^{-3}	-	
148)	$CH_3\dot{C}HO\mathring{O} + NO \rightarrow NO_2 + CH_3CHO$	1.0×10^{4}	-	
149)	$CH_3\dot{C}HO\mathring{O} + NO_2 \rightarrow NO_3 + CH_3CHO$	1.0×10^{3}	-	
150)	$CH_3\dot{C}HO\mathring{O} + H_2O \rightarrow CH_3COOH + H_2O$	6.0×10^{-3}	-	
	Propane chemistry:			
151)	$CH_3CH_2CH_3 + OH \rightarrow H_2O + 0.85\ CH_3\dot{C}HCH_3(OO\cdot) + 0.15\ CH_3CH_2CH_2O_2\cdot$	2.3E3	6.8×10^{2}	
152)	$CH_3\dot{C}HCH_3(OO\cdot) + NO \rightarrow NO_2 + CH_3\dot{C}HCH_3(O\cdot)$	1.1×10^{4}	-	
153)	$CH_3CH_2CH_2O_2\cdot + NO \rightarrow NO_2 + CH_3CH_2CHO\cdot$	1.1×10^{4}	-	

Table A.1 (continued)

	Reaction	Rate Constant	Activation Energy(K)	Note
	Propane chemistry (continued)			
154)	$CH_3\dot{C}HCH_3 + O_2 \rightarrow HO_2\cdot + CH_3C(O)CH_3$	4.4×10^{1}	-	
155)	$CH_3CH_2CH_2O\cdot + O_2 \rightarrow HO_2\cdot + CH_3CH_2CHO$	1.0×10^{2}	6.9×10^{2}	
	n-Butane chemistry:			
156)	$CH_3CH_2CH_2CH_3 + O(^3P) \xrightarrow{O_2} OH + 0.88\ CH_3CH_2\dot{C}HCH_3(OO\cdot) + 0.12\ CH_3CH_2CH_2CH_2O_2\cdot$	3.3×10^{1}	2.099×10^{3}	
157)	$CH_3CH_2CH_2CH_3 + OH \xrightarrow{O_2} H_2O + 0.86\ CH_3CH_2\dot{C}HCH_3(OO\cdot) + 0.14\ CH_3CH_2CH_2CH_2O_2\cdot$	3.8×10^{3}	5.59×10^{2}	
158)	$CH_3CH_2CH_2CH_2O_2\cdot + NO \rightarrow CH_3CH_2CH_2CH_2O\cdot + NO_2$	1.0×10^{4}	-	
159)	$CH_3CH_2CH_2CH_2O_2\cdot + NO \rightarrow CH_3CH_2CH_2CH_2ONO_2$	8.0×10^{2}	8.0×10^{2}	
160)	$CH_3CH_2CH_2CH_2O\cdot + O_2 \rightarrow HO_2\cdot + CH_3CH_2CH_2CHO$	1.0×10^{1}	6.90×10^{2}	
161)	$CH_3CH_2CH_2CH_2O\cdot \xrightarrow{O_2} \cdot OOCH_2CH_2CH_2CH_2OH$	7.2×10^{6}	4.200×10^{3}	
162)	$\cdot OOCH_2CH_2CH_2CH_2OH + NO \rightarrow NO_2 + \cdot OCH_2CH_2CH_2CH_2OH$	1.0×10^{4}	-	
163)	$\cdot OOCH_2CH_2CH_2CH_2OH + NO \rightarrow O_2NOCH_2CH_2CH_2CH_2OH$	8.0×10^{2}	-	
164)	$\cdot OCH_2CH_2CH_2CH_2OH \rightarrow HOCH_2CH_2CH_2\dot{C}HOH$	3.6×10^{7}	-	6
165)	$HOCH_2CH_2CH_2\dot{C}HOH + O_2 \rightarrow HO_2\cdot + OHCH_2CH_2CH_2CHO$	1.0×10^{1}	6.90×10^{2}	
166)	$CH_3CH_2\dot{C}HCH_3(OO\cdot) + NO \rightarrow NO_2 + CH_3CH_2\dot{C}HCH_3(O\cdot)$	1.0×10^{4}	-	

Table A.1 (continued)

Reaction	Rate Constant	Activation Energy(K)	Note
n-Butane chemistry (continued)			
167) $CH_3CH_2\overset{\overset{OO\cdot}{|}}{C}HCH_3 + NO \rightarrow CH_3CH_2\overset{\overset{ONO_2}{|}}{C}HCH_3$	8.0×10^{2}	-	
168) $CH_3CH_2\overset{\overset{O\cdot}{|}}{C}HCH_3 + O_2 \rightarrow CH_3CH_2C(O)CH_3 + HO_2\cdot$	4.4×10^{1}	-	
169) $CH_3CH_2\overset{\overset{O\cdot}{|}}{C}HCH_3 \xrightarrow{O_2} C_2H_5O_2\cdot + CH_3CHO$	4.0×10^{6}	7.0×10^{3}	
170) $C_2H_5O_2\cdot + NO \rightarrow C_2H_5O\cdot + NO_2$	1.1×10^{4}	-	
171) $C_2H_5O\cdot + NO_2 \rightarrow C_2H_5ONO_2$	2.2×10^{4}	-	
172) $C_2H_5O\cdot + NO \rightarrow C_2H_5ONO$	4.4×10^{4}	-	
173) $C_2H_5O\cdot + O_2 \rightarrow CH_3CHO + HO_2\cdot$	1.0×10^{1}	6.90×10^{2}	
2,3-dimethyl butane chemistry:			
174) $(CH_3)_2CHCH(CH_3)_2 + O(^3P) \rightarrow (CH_3)_2CHC(O_2\cdot)(CH_3)_2 + OH$	3.1×10^{2}	1.250×10^{3}	
175) $(CH_3)_2CHCH(CH_3)_2 + OH \rightarrow 0.14(CH_3)_2CHCH(CH_3)CH_2O_2\cdot + 0.86\ (CH_3)_2CHC(O_2\cdot)(CH_3)_2$	9.3×10^{3}	-	
176) $(CH_3)_2CHCH(CH_3)CH_2O_2\cdot + NO \rightarrow 0.9\ NO_2 + 0.9\ (CH_3)_2CHCH(CH_3)CH_2O\cdot + 0.1\ (CH_3)_2CHCH(CH_3)CH_2ONO_2$	1.0×10^{4}	-	
177) $(CH_3)_2CHCH(CH_3)CH_2O\cdot + O_2 \rightarrow HO_2\cdot + (CH_3)_2CHCH(CH_3)CHO$	1.0×10^{1}	6.90×10^{2}	
178) $(CH_3)_2CHCH(CH_3)CH_2O\cdot \xrightarrow{O_2} \cdot OOCH_2\overset{\overset{CH_3}{|}}{C}H\overset{\overset{CH_3}{|}}{C}HCH_2OH$	1.4×10^{7}	4.20×10^{3}	

Table A.1 (continued)

Reaction	Rate Constant	Activation Energy(K)	Note
2,3-dimethyl butane chemistry (continued)			
179) $\cdot OOCH_2\overset{CH_3}{\underset{}{C}}HCHCH_2OH + NO \rightarrow 0.9\ NO_2 + 0.9\ \cdot OCH_2\overset{CH_3}{\underset{}{C}}HCHCH_2OH + 0.1\ O_2NOCH_2\overset{CH_3}{\underset{}{C}}HCHCH_2OH$	1.0×10^{4}	-	
180) $\cdot OCH_2\overset{CH_3}{\underset{}{C}}HCHCH_2OH \xrightarrow{O_2} 0.8\ HOCH_2\overset{CH_3}{\underset{}{C}}HCHCHOH + 0.2\ HOCH_2\overset{CH_3}{\underset{}{C}}HCHCH_2OH$	1.4×10^{7}	4.200×10^{3}	
181) $HOCH_2\overset{CH_3}{\underset{}{C}}HCHCHOH + O_2 \rightarrow HO_2\cdot + HOCH_2\overset{CH_3}{\underset{}{C}}HCHCHO$	1.0×10^{1}	6.90×10^{2}	
182) $HOCH_2\overset{CH_3CH_2OO\cdot}{\underset{}{C}}HCHCH_2OH + NO \rightarrow 0.9\ NO_2 + 0.9\ HOCH_2\overset{CH_3CH_2O\cdot}{\underset{}{C}}HCHCH_2OH + 0.1\ HOCH_2\overset{CH_3CH_2ONO_2}{\underset{}{C}}HCHCH_2OH$	1.0×10^{4}	-	
183) $HOCH_2\overset{CH_3CH_2O\cdot}{\underset{}{C}}HCHCH_2OH \xrightarrow{O_2} 0.8\ HO\overset{CH_3CH_2OH}{\underset{}{C}}HCHCH_2OH + 0.2\ HOCH_2\overset{\cdot OOH_2C\ CH_2OH}{\underset{}{C}}HCHCH_2OH$	1.4×10^{7}	4.200×10^{3}	
184) $HO\overset{CH_3CH_2OH}{\underset{}{C}}HCHCH_2OH + O_2 \rightarrow HO_2\cdot + OHC\overset{CH_3CH_2OH}{\underset{}{C}}HCH_2OH$	1.0×10^{1}	6.90×10^{2}	
185) $HOCH_2\overset{\cdot OOH_2C\ CH_2OH}{\underset{}{C}}HCHCH_2OH + NO \xrightarrow{O_2} 0.9\ NO_2 + 0.9\ HO_2\cdot + 0.9\ (HOCH_2)_2CHCHCHO + 0.1\ HOCH_2\overset{O_2NOH_2C\ CH_2OH}{\underset{}{C}}HCHCH_2OH$	1.0×10^{4}	-	

Table A.1 (continued)

	Reaction	Rate Constant	Activation Energy	Note
	2,3-dimethyl butane chemistry (continued)			
186)	$(CH_3)_2CHC(O_2\cdot)(CH_3)_2 + NO \rightarrow 0.9\ NO_2 + 0.9\ (CH_3)_2CHC(O\cdot)(CH_3)_2 + 0.1\ (CH_3)_2CHC(ONO_2)(CH_3)_2$	1.0×10^{4}	-	
187)	$(CH_3)_2CHC(O\cdot)(CH_3)_2 \xrightarrow{O_2} CH_3C(O)CH_3 + CH_3CH(O_2\cdot)CH_3$	3.0×10^{7}	6.440×10^{3}	
188)	$CH_3CH(O_2\cdot)CH_3 + NO \rightarrow CH_3CH(ONO_2)CH_3$	4.0×10^{2}	-	
189)	$CH_3CH(O_2\cdot)CH_3 + NO \rightarrow NO_2 + CH_3CH(O\cdot)CH_3$	1.0×10^{4}	-	
190)	$CH_3CH(O\cdot)CH_3 + O_2 \rightarrow CH_3C(O)CH_3 + HO_2\cdot$	4.4×10^{1}	-	
	Propionaldehyde chemistry:			
191)	$C_2H_5CHO + OH \xrightarrow{O_2} H_2O + C_2H_5CO_3\cdot$	2.8×10^{4}	-2.5×10^{2}	
192)	$C_2H_5CHO + NO_3 \xrightarrow{O_2} HNO_3 + C_2H_5CO_3\cdot$	2.2×10^{0}	-	
193)	$C_2H_5CHO + h\nu \xrightarrow{O_2} C_2H_5O_2\cdot + HO_2\cdot + CO$	$8.4\times10^{-4}k_{NO_2}$	-	
194)	$C_2H_5CO_3\cdot + NO_2 \rightarrow C_2H_5CO_3NO_2$	6.9×10^{3}	-	
195)	$C_2H_5CO_3\cdot + NO \xrightarrow{O_2} C_2H_5O_2\cdot + NO_2 + CO$	1.1×10^{4}	-	
196)	$C_2H_5CO_3NO_2 \rightarrow C_2H_5CO_3\cdot + NO_2$	2.2×10^{-2}	1.354×10^{4}	
	Butyraldehyde chemistry:			
197)	$C_3H_7CHO + OH \xrightarrow{O_2} H_2O + C_3H_7CO_3\cdot$	3.7×10^{4}	-	
198)	$C_3H_7CHO + NO_3 \xrightarrow{O_2} HNO_3 + C_3H_7CO_3\cdot$	2.2×10^{0}	-	

Table A.1 (continued)

	Reaction	Rate Constant	Activation Energy	Note
	Butyraldehyde chemistry (continued)			
199)	$C_3H_7CHO + h\nu \xrightarrow{O_2} C_3H_7O_2\cdot + HO_2\cdot + CO$	$8.4\times10^{-4}k_{NO_2}$		-
200)	$C_3H_7CO_3\cdot + NO_2 \rightarrow C_3H_7CO_3NO_2$	6.9×10^{3}		-
201)	$C_3H_7CO_3\cdot + NO \xrightarrow{O_2} NO_2 + CO_2 + C_3H_7O_2\cdot$	1.1×10^{4}		-
202)	$C_3H_7CO_3NO_2 \rightarrow C_3H_7CO_3\cdot + NO_2$	2.2×10^{-2}	1.354×10^{4}	
203)	$C_3H_7O_2\cdot + NO \rightarrow NO_2 + C_3H_7O\cdot$	1.1×10^{4}		-
204)	$C_3H_7O\cdot + NO \rightarrow C_3H_7ONO$	4.4×10^{4}		-
205)	$C_3H_7O\cdot + NO_2 \rightarrow C_3H_7ONO_2$	2.2×10^{4}		-
206)	$C_3H_7O\cdot + O_2 \rightarrow HO_2\cdot + C_2H_5CHO$	1.0×10^{1}	6.90×10^{2}	
	Acetone chemistry:			
207)	$CH_3C(O)CH_3 + OH \xrightarrow{O_2} H_2O + CH_3C(O)CH_2O_2\cdot$	4.1×10^{2}	1.230×10^{3}	
208)	$CH_3C(O)CH_3 + h\nu \xrightarrow{O_2} CH_3CO_3\cdot + CH_3O_2\cdot$	$1.7\times10^{-4}k_{NO_2}$		
209)	$CH_3C(O)CH_2O_2\cdot + NO \rightarrow CH_3C(O)CH_2O\cdot + NO_2$	1.0×10^{4}		-
210)	$CH_3C(O)CH_2O_2\cdot + NO \rightarrow CH_3C(O)CH_2ONO_2$	4.0×10^{2}		-
211)	$CH_3C(O)CH_2O\cdot + O_2 \rightarrow HO_2\cdot + CH_3C(O)CHO$	1.0×10^{1}	6.9×10^{2}	

Table A.1 (continued)

	Reaction	Rate Constant	Activation Energy	Note
MEK chemistry:				
212)	$C_2H_5C(O)CH_3 + OH \xrightarrow{O_2} H_2O + CH_3\dot{C}HC(O)CH_3$ (OO·)	8.1×10^2	-	
213)	$C_2H_5C(O)CH_3 + h\nu \xrightarrow{O_2} CH_3CO_3\cdot + C_2H_5O_2\cdot$	$1.7\times10^{-3}k_{NO_2}$	-	
214)	$C_2H_5C(O)CH_3 + OH \rightarrow H_2O + C_2H_5\dot{C}(O)CH_2$	4.9×10^2	-	7
215)	$CH_3\dot{C}HC(O)CH_3 + NO \rightarrow NO_2 + CH_3\dot{C}HCOCH_3$ (OO· → O·)	1.0×10^4	-	
216)	$CH_3\dot{C}HC(O)CH_3 + NO \rightarrow CH_3\dot{C}HC(O)CH_3$ (OO· → ONO$_2$)	8.0×10^2	-	
217)	$CH_3\dot{C}HC(O)CH_3 \xrightarrow{O_2} CH_3CHO + CH_3CO_3\cdot$ (O·)	7.8×10^6	6.440×10^3	

* See Table 3

1 Only one isomer is shown, even when many are possible.

2 298K, ppm-min units

Notes:

(1) These photolysis rates represent averages over zenith angles ranging from 30 to 60 degrees.

(2) Abstraction pathway neglected.

(3) 50/50 split of the two γ-dicarbonyls is assumed.

(4) 12 percent nitrate formation assumed.

(5) Reactions of glycolaldehyde are ignored.

(6) Hydroxy substituted aldehydes are assumed to react the same as un-substituted aldehydes.

(7) Reactions of the $C_2H_5C(O)CH_2\cdot$ species are neglected.

TABLE A.2

The Atkinson et al. (1982) Reaction Mechanism as Used in this Study[a]

REACTION[b]	NUMBER	RATE CONSTANT[c] A	B	C	KEY
NO2 + HV —> NO + O3	(01)	d	0	0.	2
NO + O3 —> NO2 + O2	(02)	1.0E+6	-1	1450.	1
O3 + H2O + HV —> 2 OH + O2	(03)	2.3E-8	1	0.	3
OH + NO —> HONO	(04)	8.7E+8	-2	0.	1
OH + NO2 —> HNO3	(05)	1.5E+9	-2	0.	1
HONO + HV —> OH + NO	(06)	0.17	1	0.	3
HO2 + NO —> OH + NO2	(07)	3.7E+6	-1	0.	1
HO2 + NO2 —> HNO4	(08)	1.5E+8	-2	0.	1
HNO4 —> HO2 + NO2	(09)	7.8E+15	0	10420.	1
HO2 + HO2 —> H2O2 + O2	(10)	3.4E+4	-1	-1100.	1
HO2 + HO2 + H2O —> H2O2 + O2	(11)	5.8E-5	-2	-5800.	1
H2O2 + HV —> 2 OH	(12)	7.1E-4	1	0.	3
OH + CO —> HO2	(13)	1.3E+5	-1	0.	1
NO2 + O3 —> NO3	(14)	5.3E+4	-1	2450.	1
NO + NO3 —> 2 NO2	(15)	8.4E+6	-1	0.	1
NO2 + NO3 —> N2O5	(16)	3.1E+7	-1	1100.	1
N2O5 —> NO2 + NO3	(17)	3.5E+18	0	12280.	1
N2O5 + H2O —> 2 HNO3	(18)	0.	-1	0.	1
NO3 + HV —> 0.3 NO + 0.7 NO2 + 0.7 O3	(19)	15.5	1	0.	3
OH + O3 —> HO2	(20)	7.0E+5	-1	940.	1
HO2 + O3 —> OH	(21)	4.8E+3	-1	580.	1
HCHO + HV —> 2 HO2 + CO	(22)	3.1E-3	1	0.	3
HCHO + HV —> CO + H2	(23)	3.0E-3	1	0.	3
OH + HCHO —> HO2 + CO	(24)	4.4E+6	-1	0.	1
ALD2 + HV —> MPOX + HO2 + CO	(25)	6.0E-4	1	0.	3
OH + ALD2 —> ACOX	(26)	3.0E+6	-1	-250.	1
ACOX + NO2 —> PAN	(26)	2.1E+6	-1	0.	1
PAN —> ACOX + NO2	(28)	1.2E+18	0	13543.	1
ACOX + NO —> NO2 + MPOX	(29)	3.1E+6	-1	0.	1
MPOX + NO —> HCHO + HO2 + NO2	(30)	3.1E+6	-1	0.	1
OH + PRPA —> PO2	(31)	6.6E+6	-1	680.	1
PO2 + NO —> HO2 + NO2 + ACET	(32)	3.1E+6	-1	0.	1
OH + ALKA —> AO2	(33)	6.6E+6	-1	400.	1
AO2 + NO —> 1.7 NO2 + 0.9 HO2 + 0.15 HCHO + 0.3 ALD2 + 0.1 RCHO + 0.30 ACET + 0.45 MEK - 0.8 NO	(34)	3.1E+6	-1	0.	1
OH + RCHO —> RCO3	(35)	9.2E+6	-1	0.	1
RCO3 + NO2 —> PPN	(36)	2.1E+6	-1	0.	1
PPN —> RCO3 + NO2	(37)	1.2E+18	0	13543.	1
RCO3 + NO —> ETO2 + NO2	(38)	3.1E+6	-1	0.	1
ETO2 + NO —> ALD2 + HO2 + NO2	(39)	3.1E+6	-1	0.	1
RCHO + HV —> ETO2 + CO + HO2	(40)	8.4E-4	1	0.	3
OH + MEK —> XO2	(41)	4.4E+6	-1	330.	1

TABLE A.2 (Continued)

REACTION[b]	NUMBER	RATE CONSTANT[c] A	B	C	KEY
XO2 + NO —> NO2 + ALD2 + ACOX	(42)	3.1E+6	-1	0.	1
MEK + HV —> ACOX + ETO2	(43)	1.7E-3	1	0.	3
ACET + HV —> ACOX + MPOX	(44)	1.7E-4	1	0.	3
OH + ETHE —> NO2 + HO2 + 2.0 HCHO - 1.0 NO	(45)	9.7E+5	-1	-380.	1
OH + PRPE —> NO2 + HO2 + 1.0 HCHO + 1.0 ALD2 - 1.0 NO	(46)	1.8E+6	-1	-540.	1
OH + BUTE —> 0.9 NO2 + 0.9 HO2 + 1.8 ALD2 - 1.0 NO	(47)	5.0E+6	-1	-540.	1
O3 + ETHE —> HCHO + 0.4 CHO2 + 0.4 CO + 0.12 HO2	(48)	4.2E+3	-1	2560.	1
O3 + PRPE —> 0.5 HCHO + 0.5 ALD2 + 0.2 CHO2 + 0.2 CO + 0.3 CO + 0.2 HO2 + 0.1 OH + 0.2 MPOX	(49)	3.1E+3	-1	1900.	1
O3 + BUTE —> ALD2 + 0.40 CO + 0.3 HO2 + 0.2 OH + 0.45 MPOX + 0.2 CO	(50)	3.3E+3	-1	1050.	1
CHO2 + NO —> HCHO + HO2	(51)	3.1E+6	-1	0.	1
CHO2 + NO2 —> HCHO + NO3	(52)	3.1E+5	-1	0.	1
CHO2 + H2O —> PROD	(53)	1.5E+0	-1	0.	1
CO + NO —> ALD2 + HO2	(54)	3.1E+6	-1	0.	1
CO + NO2 —> ALD2 + NO3	(55)	3.1E+5	-1	0.	1
CO + H2O —> PROD	(56)	1.5E+0	-1	0.	1
OH + BENZ —> 0.25 CRES + 0.25 HO2 + 0.75 ADD	(57)	5.3E+5	-1	0.	1
OH + TOLU —> 0.15 ARO2 + 0.20 CRES + 0.65 ADD + 0.20 HO2	(58)	2.7E+6	-1	0.	1
OH + XYEN —> 0.25 CRES + 0.25 HO2 + 0.75 ADD	(59)	7.9E+6	-1	0.	1
ADD + NO —> 0.75 NO2 + 0.75 HO2 + 0.75 DIAL + BO1*GLY + BO2*MGLY	(60)	3.1E+6	-1	0.	1
OH + DIAL —> EL	(61)	1.3E+7	-1	0.	1
EL + NO2 —> ENO2	(62)	2.1E+6	-1	0.	1
ENO2 —> EL + NO2	(63)	1.2E+18	0	13543.	1
EL + NO —> 3 NO2 - 2 NO + BO3*HO2+BO3*GLY + BO4*ACOX + BO4*MGLY + BO3*CO	(64)	3.1E+6	-1	0.	1
OH + GLY —> HO2 + CO	(65)	8.8E+6	-1	0.	1
GLY + HV —> HCHO + CO	(66)	1.E-10	1	0.	3
OH + MGLY —> ACOX + CO	(67)	6.6E+6	-1	0.	1
MGLY + HV —> ACOX + HO2 + CO	(68)	0.15	1	0.	3
OH + CRES —> ADD2	(69)	1.9E+7	-1	0.	1
ADD2 + NO —> 0.75 NO2 + 0.75 HO2 + 0.75 DIAL	(70)	3.1E+6	-1	0.	1
NO3 + CRES —> HNO3 + PHEN	(71)	6.6E+6	-1	0.	1
PHEN + NO2 —> PRODN	(72)	6.6E+6	-1	0.	1
ARO2 + NO —> 0.75 NO2 + 0.75 HO2 + 0.75 ACHO	(73)	3.1E+6	-1	0.	1
ACHO + HV —> PROD	(74)	4.5E-3	1	0.	3
ACHO + OH —> ARC3	(75)	5.7E+6	-1	0.	1
ARC3 + NO2 —> PRZN	(76)	2.1E+6	-1	0.	1

TABLE A.2 (Continued)

REACTION[b]			RATE CONSTANT[c] NUMBER	A	B	C	KEY
PBZN	—> ARC3 +	NO2	(77)	1.0E+17	0	13025.	1
ARC3 + NO	—> PHO2 +	NO2	(78)	3.1E+6	-1	0.	1
PHO2 + NO	—> PHEN +	NO2	(79)	3.1E+6	-1	0.	1

Footnotes for Table A.2

(a) Mechanism documentation: Atkinson et al.(1979, 1982), Carter et al.(1979) A computer tape containing the reaction mechanism was obtained from F. Lurmann, Environmental Research and Technology, Inc., Westlake Village, California, on 8 July 1982. The original mechanism has been slightly modified for use in our study (see Section 3.4.1).

(b) See Section 3.4.1 for values of these coefficients.

(c) Reaction rate constants are of the form $k = A * TEMP^B * \exp(-C/TEMP)$ with units in terms of the ppm-min system. The explanation for the key is given in Table A.14.

(d) See Table 3.

TABLE A.3

Species Used in the Atkinson et al. (1982) Reaction Mechanism

NUMBER	CODE	SPECIES NAME
1	ACET	Acetone
2	ACHO	Benzaldehyde
3	ACOX	CH_3CO_3
4	ADD	OH-Aromatic-O_2 adducts
5	ADD2	OH-Aromatic-O_2 adducts
6	ALD2	Acetaldehyde
7	ALKA	>C3 alkanes
8	AO2	Alkyl peroxy radical
9	ARO2	Aromatic peroxy radical
10	ARC3	Peroxy benzoyl
11	BENZ	Benzene
12	BUTE	>C3 alkenes
13	CD	CH_3CHOO
14	CHO2	CH_2O_2
15	CO	Carbon monoxide
15	CONE	Wall source term for OH
17	CRES	Cresol
18	DIAL	Conjugated gamma dicarbonyls
19	EL	Radical formed from DIAL
20	ENO2	PAN analog from α-dicarbonyls
21	ETHE	Ethylene
22	ETO2	$C_2H_5O_2$
23	GLY	Glyoxal
24	HCHO	Formaldehyde
25	HNO3	Nitric acid
26	HNO4	Pernitric acid
27	HONO	Nitrous acid
28	HO2	Hydroperoxyl radical
29	H2O	Water vapor
30	H2O2	Hydrogen peroxide
31	MEK	Methylethylketone
32	MGLY	Methylglyoxal
33	MPOX	Methyl peroxy radical (CH_3O_2)
34	NO	Nitric oxide
35	NO2	Nitrogen dioxide
36	NO3	Nitrogen trioxide
37	N2O5	Nitrogen pentoxide
38	OH	Hydroxyl radical
39	O3	Ozone
40	PAN	Peroxyacetyl nitrate
41	PBZN	Peroxy Benzoyl nitrate
42	PHEN	Phenoxy Radical
43	PHO2	$C_6H_5O_2$ Radical
44	PO2	Propoxy Radical

TABLE A.3 (Continued)

NUMBER	CODE	SPECIES NAME
45	PPN	Higher PANS
46	PRPA	Propane
47	PRPE	Propylene
48	RCHO	C3–C5 aldehydes
49	RCO3	Acylperoxy
50	TOLU	Toluene
51	XO2	Peroxy radical
52	XYEN	>C7 aromatics

TABLE A.4

The Killus and Whitten (1982a) Reaction Mechanism as Used in this Study[a]

REACTION	NUMBER	RATE CONSTANT[b] A	B	C	KEY
NO2 + HV —> NO + O	(1)	c	0	0.	2
O —> O3	(2)	4.40E+6	0	0.	1
NO + O3 —> NO2 + O2	(3)	3.45E+3	0	1450.	1
NO2 + O3 —> NO3 + O2	(4)	1.79E+2	0	2450.	1
NO2 + O —> NO + O2	(5)	1.34E+4	0	0.	1
O3 + OH —> HO2 + O2	(6)	2.87E+1	0	1000.	1
O3 + HO2 —> OH + 2 O2	(7)	4.01E+2	0	1525.	1
OH + NO2 —> HNO3	(8)	1.60E+4	0	0.	1
OH + CO —> HO2	(9)	4.40E+2	0	0.	1
NO + NO —> 2 NO2	(10)	1.50E-4	0	0.	1
NO + NO3 —> 2 NO2	(11)	2.80E+4	0	0.	1
NO3 + NO2 + H2O —> 2 HNO3	(12)	5.56E-19	0	-10600.	1
NO + HO2 —> NO2 + OH	(13)	1.20E+4	0	0.	1
HO2 HO2 —> H2O2 + O2	(14)	1.50E+4	0	0.	1
X + PAR —>	(15)	1.00E+5	0	0.	1
OH + PAR —> MEO2 + H2O	(16)	8.51E+3	0	560.	1
O + OLE —> MEO2 + ACO3 + X	(17)	8.04E+3	0	325.	1
O + OLE —> CARB + PAR	(18)	8.04E+3	0	325.	1
OH + OLE —> RAO2	(19)	6.04E+3	0	-540.	1
O3 + OLE —> CARB + CRIG	(20)	4.70	0	1900.	1
O3 + OLE —> CARB + MCRG + X	(21)	4.70	0	1900.	1
O + ETH —> MEO2 + HO2 + CO	(22)	8.79E+3	0	800.	1
O + ETH —> CARB + PAR	(23)	8.79E+3	0	800.	1
OH + ETH —> RBO2	(24)	3.33E+3	0	-382.	1
O3 + ETH —> CARB + CRIG	(25)	1.29E+1	0	2560.	1
NO + ACO3 —> NO2 + MEO2 + CO2	(26)	1.04E+4	0	0.	1
NO + RBO2 —> NO2 + 2 CARB + HO2	(27)	1.20E+4	0	0.	1
NO + RAO2 —> NO2 + 2 CARB + HO2	(28)	1.20E+4	0	0.	1
NO + MEO2 —> NO2 + CARB + MEO2 + X	(29)	3.80E+3	0	0.	1
NO + MEO2 —> NO2 + CARB + HO2	(30)	7.70E+3	0	0.	1
NO + MEO2 —> NRAT	(31)	5.00E+2	0	0.	1
O3 + RBO2 —> 2 CARB + HO2 + O2	(32)	5.00	0	0.	1
O3 + RAO2 —> 2 CARB + HO2 + O2	(33)	2.00E+2	0	0.	1
OH + CARB —> CRO2 + X	(34)	5.00E+2	0	0.	1
OH + CARB —> HO2 + CO	(35)	7.00E+3	0	0.	1
OH + CARB —> ACO3 + X	(36)	6.00E+3	0	0.	1
CARB + HV —> CO + H2	(37)	1.0E-3	1	0.	3
CARB + HV —> 1.333 HO2 + CO + 0.667 MEO2 + 0.667 X	(38)	2.0E-3	1	0.	3
ACO3 + NO2 —> PAN	(39)	7.00E+3	0	0.	1
PAN —> ACO3 + NO2	(40)	1.04E+18	0	13500.	1
ACO3 + HO2 —> PRD1	(41)	1.50E+4	0	0.	1
MEO2 + HO2 —> PRD2	(42)	9.00E+3	0	0.	1
NO + CRIG —> NO2 + CARB	(43)	1.20E+4	0	0.	1

TABLE A.4 (Continued)

REACTION									NUMBER	RATE CONSTANT[b] A	B	C	KEY
NO2	+ CRIG	—>	NO3	+	CARB				(44)	8.00E+3	0	0.	1
CARB	+ CRIG	—>	OZD						(45)	2.00E+3	0	0.	1
NO	+ MCRG	—>	NO2	+	CARB				(46)	1.20E+4	0	0.	1
NO2	+ MCRG	—>	NO3	+	CARB	+	PAR		(47)	8.00E+3	0	0.	1
CARB	+ MCRG	—>	OZD						(48)	2.00E+3	0	0.	1
	CRIG	—>	CO	+	H2O				(49)	6.70E+2	0	0.	1
	CRIG	—>	PRD3						(50)	2.40E+2	0	0.	1
	CRIG	—>	2 NO2	+	CO2				(51)	9.00E+1	0	0.	1
	MCRG	—>	PRD4						(52)	1.50E+2	0	0.	1
	MCRG	—>	MEO2	+	OH	+	CO		(53)	3.40E+2	0	0.	1
	MCRG	—>	MEO2	+	HO2	+	CO2		(54)	4.25E+2	0	0.	1
	MCRG	—>	2 HO2	+	CARB	+	CO		(55)	8.50E+1	0	0.	1
ARO	+ OH	—>	RARO	+	H2O				(56)	5.99E+4	0	600.	1
ARO	+ OH	—>	OPEN	+	HO2				(57)	5.55E+4	0	400.	1
RARO	+ NO	—>	NO2	+	PHEN	+	HO2		(58)	4.00E+3	0	0.	1
OPEN	+ NO	—>	NO2	+	DCRB	+	X	+ APRC	(59)	6.00E+3	0	0.	1
APRC		—>	DCRB	+	CARB	+	CO	+ X	(60)	1.00E+4	0	0.	1
APRC		—>	2 CARB	+	2 CO				(61)	1.00E+4	0	0.	1
PHEN	+ NO3	—>	PHO	+	HNO3				(62)	5.00E+3	0	0.	1
PHO	+ NO2	—>	NPHN						(63)	4.00E+3	0	0.	1
PHO	+ HO2	—>	PHEN						(64)	5.00E+4	0	0.	1
OPEN	+ O3	—>	DCRB	+	APRC	+	X		(65)	4.00E+1	0	0.	1
PHEN	+ OH	—>	HO2	+	APRC	+	PAR	+ CARB	(66)	3.00E+4	0	0.	1
DCRB	+ HV	—>	HO2	+	0.5 ACO3	+							
			1.5 CO	+	0.5 MEO2				(67)	4.0E-2	1	0.	3
PHEN	+ OH	—>	PHO						(68)	1.00E+4	0	0.	1
CRO2	+ NO	—>	NO2	+	CARB	+	ACO3	+ X	(69)	1.20E+4	0	0.	1
DCRB	+ OH	—>	ACO3	+	CO				(70)	7.00E+3	0	0.	1
HONO	+ HV	—>	OH	+	NO				(71)	1.80E-1	1	0.	3
NO	+ OH	—>	HONO						(72)	9.77E+3	0	0.	1
O3	+ HV	—>	O1D						(73)	1.00E-3	1	0.	3
O1D		—>	O						(74)	4.44E+10	0	0.	1
O1D	+ H2O	—>	2 OH						(75)	3.40E+5	0	0.	1

Footnotes for Table A.4

(a) Mechanism documentation: Killus and Whitten (1982a) and Whitten et al. (1980a,b). The reaction mechanism was coded from Table 3 of Killus and Whitten (1982a) with the photolysis rates and wall terms obtained from a computer listing supplied by J.P. Killus on 25 August 1982. Reactions 26, 48, 54, 60, 69 and 70 have been corrected to maintain the overall carbon balance. The original mechanism has been slightly modified to adapt it for use in our study. *See* Section 3.5.1 for details.

(b) Reaction rate constants are of the form $k = A * TEMP^B * \exp(-C/TEMP)$ with units in terms of the ppm-min system. The explanation for the key is given in Table A.14.

(c) See Table 3.

TABLE A.5

Species Used in the Killus and Whitten (1982a) Reaction Mechanism

NUMBER	CODE[a]	SPECIES NAME
1	ACO3 (2)	Peroxyacyl radical (Two-carbon surrogate for RCO3)
2	APRC (4)	Free radical
3	ARO (6)	Reactive aromatic rings
4	CO (1)	Carbon monoxide
5	CO2 (1)	Carbon dioxide
6	CRIG (1)	Criegee intermediate
7	CRO2 (2)	Peroxy radical
8	DCRB (3)	Highly photolytic alpha-dicarbonyl compounds including methyl glyoxal and biacetyl
9	ETH (2)	Slow double bonds that are almost exclusively ethylene
10	CARB (1)	Carbonyl compounds such as aldehydes and ketones
11	HNO3	Nitric acid
12	HONO	Nitrous acid
13	HO2	Hydroperoxy radical
14	H2	Hydrogen
15	H2O	Water vapor
16	H2O2	Hydrogen peroxide
17	MCRG (2)	Criegee intermediate
18	MEO2 (1)	Peroxy radical (one-carbon surrogate for RO2)
19	NO	Nitric oxide
20	NO2	Nitrogen dioxide
21	NO3	Nitrogen trioxide (nitrate radical)
22	NPHN (6)	Nitrophenol
23	NRAT (1)	Nitrate
24	OLE (2)	Relatively reactive double-bonded carbon molecules
25	O	Atomic oxygen O(3P)
26	OH	Hydroxyl radical
27	OPEN (6)	Bicyclic peroxy radical
28	O1D	Atomic oxygen O(1D)
29	O2	Molecular oxygen
30	O3	Ozone
31	OZD (2)	Ozonide
32	OZON (1)	Ozonide
33	PAN (2)	Peroxyacetyl nitrate
34	PAR (1)	Single-bonded carbon atoms whose principal constituents are paraffinic carbon molecules
35	PHEN (6)	Phenol

TABLE A.5 (Continued)

NUMBER	CODE	SPECIES NAME
35	PHO (6)	C_6H_5O radical
36	RAO2 (2)	Peroxy radical
37	RARO (6)	Peroxy radical
38	RBO2 (2)	Peroxy radical
39	WNO3	Wall loss of NO_x species
40	X (-1)	Species introduced to maintain Carbon balance

Footnotes for Table A.5

(a) The values in brackets are the species carbon numbers.

TABLE A.6 (Continued)

REACTION	NUMBER	RATE CONSTANT[b] A	B	C	KEY
R1O2 + O3 —> RO2 + 2 O2	(43)	2.00E+0	0	0.	1
HC3 + HV —> CO	(44)	2.0E-3	1	0.	3
HC1 + O3 —> COOH + HC3	(45)	8.80E-3	0	0.	1

Footnotes for Table A.6

(a) Mechanism Documentation: Demerjian (1982) and Schere (1983) A computer tape containing the reaction mechanism was obtained from K. Schere, U.S. Environmental Protection Agency, Research Triangle Park, North Carolina, on 16 June 1982. The original mechanism has been modified to adapt it for use in our study. See section 3.6.1 for details.

(b) Reaction rate constants are of the form $k = A * TEMP^B * \exp(-C/TEMP)$ with units in terms of the ppm-min system. The explanation for the key is given in Table A.14.

(c) See Table 3.

TABLE A.6

The Demerjian (1982) Reaction Mechanism as Used in this Study[a]

REACTION	NUMBER	RATE CONSTANT[b] A	B	C	KEY
NO2 + HV —> NO + O	(01)	c	0	0.	2
O2 + O + M —> O3 + M	(02)	3.90E-6	0	-510.	1
O3 + NO —> NO2 + O2	(03)	3.40E+3	0	1450.	1
O3 + NO2 —> NO3 + O2	(04)	1.77E+2	0	2450.	1
O3 + HV —> O1D + O2	(05)	2.77E-3	1	0.	3
O1D + M —> O + M	(06)	6.68E+4	0	0.	1
O1D + H2O —> 2 OH	(07)	4.14E+5	0	0.	1
NO3 + NO —> 2 NO2	(08)	2.96E+4	0	0.	1
NO3 + NO2 —> N2O5	(09)	1.36E+16	-4.6	0.	1
N2O5 —> NO3 + NO2	(10)	1.30E+16	0	9700.	1
N2O5 + H2O —> 2 HNO3	(11)	1.92E-5	0	0.	1
HONO + HV —> HO + NO	(12)	1.80E-1	1	0.	3
HO + CO —> HO2 + CO2	(13)	4.10E+2	0	0.	1
HO2 + NO2 —> HONO + O2	(14)	4.40E+0	0	0.	1
HO2 + NO —> HO + NO2	(15)	6.36E+3	0	-200.	1
HO2 + NO2 + M —> HO4N + M	(16)	2.63E-3	0	0.	1
HO4N —> NO2 + NO2	(17)	5.21E+15	0	10420.	1
HO + HONO —> NO2 + H2O	(18)	9.75E+3	0	0.	1
HO + NO2 + M —> HNO3 + M	(19)	1.54E-2	0	0.	1
HO + NO + M —> HONO + M	(20)	7.39E-3	0	0.	1
HO + HNO3 —> H2O + NO3	(21)	1.26E+2	0	0.	1
HO2 + O3 —> HO + 2 O2	(22)	2.07E+1	0	600.	1
HO + O3 —> HO2 + O2	(23)	2.81E+3	0	1000.	1
HO2 + HO2 —> H2O2 + O2	(24)	3.40E+3	0	0.	1
H2O2 + HV —> 2 HO	(25)	8.37E-4	1	0.	3
HC1 + O —> RO2 + HC3 + HO2	(26)	1.20E+4	0	0.	1
HC1 + O3 —> RO2 + HC3 + HO2	(27)	7.90E-2	0	0.	1
HC1 + HO —> RO2 + HC3	(28)	4.50E+4	0	0.	1
HC2 + HO —> RO2	(29)	5.10E+3	0	0.	1
HC3 + HV —> 0.5 RO2 + 1.5 HO2 + CO	(30)	1.60E-3	1	0.	3
HC3 + HO —> 0.3 R1O2 + 0.7 HO2 + 0.7 CO	(31)	1.95E+4	0	0.	1
RO2 + NO —> RO + NO2	(32)	1.10E+4	0	0.	1
RO + O2 —> HC3 + HO2	(33)	7.39E+2	0	2000.	1
R1O2 + NO2 —> PAN	(34)	2.07E+3	0	0.	1
PAN —> R1O2 + NO2	(35)	4.77E+16	0	12516.	1
RO + NO2 —> RNO3	(36)	1.00E+2	0	0.	1
RO2 + O3 —> RO + 2 O2	(37)	2.00E+0	0	0.	1
R1O2 + NO —> RO2 + NO2	(38)	4.00E+3	0	0.	1
HC4 + HO —> R2O2 + 2 HC3 + CO	(39)	2.70E+4	0	0.	1
R2O2 + NO —> R2O + NO2	(40)	1.10E+4	0	0.	1
R2O + O2 —> HC3 + HO2 + 2 CO	(41)	8.87E-1	0	0.	1
R2O2 + O3 —> R2O + 2 O2	(42)	2.00E+0	0	0.	1

TABLE A.7

Species Used in the Demerjian (1982) Reaction Mechanism

NUMBER	CODE	SPECIES NAME
1	CO	Carbon monoxide
2	COOH	Criegee intermediate
3	CO2	Carbon dioxide
4	HC1	Olefins including C2H4
5	HC2	Alkanes (excluding methane)
6	HC3	Aldehydes
7	HC4	Aromatics
8	HNO3	Nitric acid
9	HO	Hydroxyl radical
10	HO4N	Pernitric acid
11	HONO	Nitrous acid
12	HO2	Hydroperoxyl radical
13	H2O	Water vapor
14	H2O2	Hydrogen peroxide
15	M	Third body for deactivation
16	NO	Nitric oxide
17	NO2	Nitrogen dioxide
18	NO3	Nitrogen trioxide (nitrate radical)
19	N2O5	Nitrogen pentoxide
20	O	Atomic oxygen
21	O1D	Singlet D oxygen
22	O2	Molecular oxygen
23	O3	Ozone
24	PAN	Peroxacetylnitrate
25	RNO3	Alkyl nitrate
26	RO	Alkoxyl radical
27	RO2	Alkylperoxy radical
28	R1O2	Peroxyacyl radical
29	R2O	Alkoxy radical
30	R2O2	Peroxy radical

TABLE A.8

The McRae and Seinfeld (1983) Reaction Mechanism as Used in this Study[a]

REACTION[b]	NUMBER	RATE CONSTANT[c] A	B	C	KEY
NO2 + HV —> NO + O3P	(1)	h	0	0.	2
O3P + O2 + M —> O3 + M	(2)	0.346	-2	-510.	1
O3 + NO —> NO2 + O2	(3)	9.24E+05	-1	1450.	1
NO2 + O3P —> NO + O2	(4)	3.99E+06	-1	0.	1
NO + O3P —> NO2	(5)	1.67E+05	-1	-584.	1
NO2 + O3P —> NO3	(6)	1.07E+06	-1	0.	1
O3 + NO2 —> NO3 + O2	(7)	5.19E+04	-1	2450.	1
NO3 + NO —> 2NO2	(8)	8.05E+06	-1	0.	1
NO + OH —> HONO	(9)	5.07E+06	-1	0.	1
HONO + HV —> OH + NO	(10)	1.86E-01	1	0.	3
HO2 + NO2 —> HONO + O2	(11)	1.73E+01	-1	-1006.	1
HONO + OH —> NO2 + H2O	(12)	2.91E+06	-1	0.	1
NO2 + HO2 —> HO2NO2	(13)	1.73E+04	-1	-1006.	1
HO2NO2 —> HO2 + NO2	(14)	1.80E+15	0	9950.	1
HO2 + NO —> NO2 + OH	(15)	3.58E+06	-1	0.	1
RO2 + NO —> NO2 + RO	(16)	3.58E+06	-1	0.	1
RCO3 + NO —> NO2 + RO2 + CO2	(17)	1.13E+06	-1	0.	1
NO2 + OH —> HONO2	(18)	4.53E+06	-1	0.	1
CO + OH —> HO2 + CO2	(19)	1.31E+05	-1	0.	1
O3 + HV —> O3P + O2	(20)	6.84E-02	1	0.	3
HCHO + HV —> 2 HO2 + CO	(21)	4.81E-03	1	0.	3
HCHO + HV —> H2 + CO	(22)	8.73E-03	1	0.	3
HCHO + OH —> HO2 + H2O + CO	(23)	4.14E+06	-1	0.	1
RCHO + HV —> RO2 + HO2 + CO	(24)	4.28E-03	1	0.	3
RCHO + OH —> RCO3	(25)	2.75E+04	0	0.	1
C2H4 + OH —> RO2	(26)	1.16E+04	0	0.	1
C2H4 + O3P —> RO2 + HO2	(27)	1.22E+03	0	0.	1
OLE + OH —> RO2	(28)	8.19E+04	0	0.	1
OLE + O3P —> RO2 + RCO3	(29)	2.44E+04	0	0.	1
OLE + O3 —> A01*RCHO + A02*HCHO + A03*HO2 + A04*RO2 + A05*OH + A06*RO	(30)	1.79E-01	0	0.	1
ALK + OH —> RO2	(31)	5.83E+03	0	0.	1
ALK + O3P —> RO2 + OH	(32)	1.58E+02	0	0.	1
ARO + OH —> RO2 + RCHO	(33)	2.76E+04	0	0.	1
RO —> B01*HO2 + B02*HCHO + B03*RCHO + B04*RO2	(34)	2.0E+05	0	0.	1
RONO + HV —> NO + RO	(35)	2.2E-01	1	0.	3
RO + NO —> RONO	(36)	4.38E+06	-1	0.	1
RO + NO2 —> RONO2	(37)	2.19E+06	-1	0.	1
RO + NO2 —> RCHO + HONO	(38)	6.39E+02	0	0.	1
NO2 + RO2 —> RO2NO2	(39)	1.64E+06	-1	0.	1
NO2 + RO2 —> RCHO + HONO2	(40)	1.64E+03	-1	0.	1
RO2NO2 —> NO2 + RO2	(41)	1.80E+15	0	9950.	1

TABLE A.8 (Continued)

REACTION[b]	NUMBER	RATE CONSTANT[c] A	B	C	KEY
RCO3 + NO2 —> PAN	(42)	6.17E+05	-1	0.	1
PAN —> RCO3 + NO2	(43)	4.77E+16	0	12516.	1
NO2 + NO3 —> N2O5	(44)	2.20E+06	-1	0.	1
N2O5 —> NO2 + NO3	(45)	3.44E+016	0	10600.	1
H2O + N2O5 —> 2 HONO2	(46)	4.47E-03	-1	0.	1
O3 + OH —> HO2 + O2	(47)	6.62E+05	-1	1000.	1
O3 + HO2 —> OH + 2 O2	(48)	4.85E+03	-1	580.	1
O3 —> WALL	(49)	0.	0	0.	1
HO2 + HO2 —> H2O2 + O2	(50)	7.45E+03	0	0.	1
H2O2 + HV —> 2 OH	(51)	2.89E-03	1	0.	3
RO2 + RO2 —> 2 RO	(52)	2.04E+04	-1	-223.	1

Footnotes for Table A.8

(a) Mechanism documentation: Falls and Seinfeld (1978) Falls et al. (1979), McRae et al. (1982b) and McRae and Seinfeld (1983). (15 November 1982) The original mechanism has been slightly modified to adapt it for our study. See Section 3.7.1 for details.

(b) In two reactions (30,34) the product stoichiometry varies as a function concentration. The functional forms for the coefficients A01 - A06 and B01-B04 are given by:

A01 = 0.5 A02 = 0.5 A03 = 0.304
A04 = 0.306 A05 = 0.136 A06 = 0.034

and

B01 = 1.0 B02 = 0.5 B03 = 0.5 .
B04 = (1-B01) = 0.0

(c) Reaction rate constants are of the form $k = A * TEMP^b * \exp(-C/TEMP)$ with units in terms of the ppm-min system. The key is explained in Table A.14.

(d) $k_{37}/(k_{37} + k_{38}) = 0.92$ for CH_3, $k_{38} = 0.087\ k_{37}$

(e) Rate constants for reactions 39 and 40 are based on the assumption that $k_{16}/(k_{39} + k_{40}) = 2.2$.

(f) Rate constant for reaction 18 determined from

$$1.477\times10^{15}\times10^{-(11.6T/(17.4+T))}\,SQRT(280/T)$$

(g) Rate constant for reaction 50 determined from

$$k_{50} = \frac{3.4\times10^{4}}{T}\exp(1100/T) + \frac{5.8\times10^{-5}}{T^2}\exp(5800/T)[H_2O]$$

at 298 °K, $[H_2O = 15500$ ppm$]$ $k_{50} = 7.45\times10^{3}$

(h) See Table 3.

TABLE A.9

Species Used in the McRae and Seinfeld (1983) Reaction Mechanism

NUMBER	CODE	SPECIES NAME
1	ALK	Alkanes (excluding CH4)
2	ARO	Aromatics
3	CO	Carbon monoxide
4	CO2	Carbon dioxide
5	ETH	Ethylene (C2H4)
6	HCHO	Formaldehyde
7	HNO2	Nitrous acid
8	HNO3	Nitric acid
9	HNO4	Pernitric acid
10	HO2	Hydroperoxyl radical
11	H2	Hydrogen
12	H2O	Water vapor
13	H2O2	Hydrogen peroxide
14	M	Third body for collisional deactivation
15	NO	Nitric oxide
16	NO2	Nitrogen dioxide
17	NO3	Nitrogen trioxide
18	N2O5	Dinitrogen pentoxide
19	OLE	Olefins excluding ethylene
20	O	Atomic oxygen (O(3P))
21	OH	Hydroxyl radical
22	O2	Molecular oxygen
23	O3	Ozone
24	PAN	Peroxacetylnitrate
25	RCHO	Higher aldehydes
26	RCO3	Peroxyacyl radical
27	RO	Alkoxyl radical
28	RONO	Alkyl nitrite
29	RNO4	Peroxyalkyl nitrate
30	RO2	Alkylperoxy radical
31	RNO3	Alkyl nitrate
32	WALL	Wall loss term

TABLE A.10

The Penner and Walton (1982) Reaction Mechanism as Used in this Study[a]

REACTION	NUMBER	RATE CONSTANT[b] A	B	C	KEY
:					
: Inorganic reactions (R1 - R23)					
:					
O + O2 + M —> O3 + M	(01)	3.90E-6	0	-510.	1
O3 + NO —> NO2 + O2	(02)	1.01E+6	-1	1450.	1
O + NO —> NO2	(03)	1.59E+7	-1.5	0.	1
O + NO2 —> NO + O2	(04)	4.09E+6	-1	0.	1
O + NO2 —> NO3	(05)	2.05E+8	-2	0.	1
O3 + NO2 —> NO3 + O2	(06)	5.28E+4	-1	2450.	1
NO3 + NO2 —> N2O5	(07)	6.05E+4	-0.7	0.	1
N2O5 —> NO2 + NO3	(08)	2.16E+18	-0.7	11180.	1
NO3 + NO —> 2 NO2	(09)	8.80E+6	-1	0.	1
N2O5 + H2O —> 2 HNO3[c]	(10)	1.32E-3	-1	0.	1
HO + NO2 —> HNO3	(11)	8.67E+7	-1.5	0.	1
HO + NO —> HNO2	(12)	4.99E+7	-1.5	0.	1
HO + CO —> HO2	(13)	1.19E+5	-1	0.	1
HO2 + NO —> HO + NO2	(14)	1.54E+6	-1	-250.	1
HNO2 + HO —> NO2	(26)	2.90E+6	-1	0.	1
HO2 + HO2 —> H2O2 + O2	(27)	3.70E+4	-1	-1250.	1
HO + HO2 —> H2O + O2	(36)	3.52E+7	-1	0.	1
HO + H2O2 —> HO2	(72)	7.04E+5	-1	0.	1
HO + HNO4 —> H2O + NO2 + O2	(93)	1.76E+6	-1	0.	1
HNO4 —> HO2 + NO2	(84)	3.00E+16	0	10720.	1
HO2 + NO2 —> HNO4	(34)	6.23E+15	-5	0.	1
HO + O3 —> HO2	(48)	7.04E+5	-1	940.	1
HO2 + O3 —> HO	(49)	4.84E+3	-1	580.	1
:					
: Reactions of HC1 (Alkenes, isoprene and mono-terpenes)					
:					
HC1 + HO —> RO2 + HC4	(17)	1.76E+7	-1	120.	1
HC1 + O3 —> HO2 + HC4	(16)	1.54E+3	-1	1900.	1
HC1 + O3 —> HC4	(47)	1.54E+3	-1	1900.	1
HC1 + O —> RO2 + RCO3	(15)	4.40E+6	-1	360.	1
HC1 + NO3 —> RO2 + RNO3	(40)	4.40E+5	-1	1400.	1
:					
: Reactions of HC2 (Alkanes)					
:					
HC2 + HO —> RO2 + H2O	(19)	2.20E+7	-1	900.	1
HC2 + O —> RO2 + HO	(18)	7.04E+6	-1	2000.	1
:					
: Reactions of HC4 (Aldehydes and Ketones)					
:					
HC4 + HO —> RCO3 + H2O	(20)	3.52E+6	-1	0.	1
HC4 + HO —> CO + HO2 + H2O	(37)	3.43E+6	-1	150.	1
HC4 + NO3 —> RCO3 + HNO3	(35)	1.32E+3	-1	200.	1

TABLE A.10 (Continued)

REACTION						NUMBER	RATE CONSTANT[b] A	B	C	KEY
:										
: Reactions of HC3 (Aromatics)										
:										
HC3	+ HO	—>	BRO2OHHH			(86)	1.76E+6	-1	0.	1
HC3	+ HO	—>	HO2			(87)	1.06E+6	-1	0.	1
NO	+ BRO2OHHH	—>	HO2	+ MGLY	+ NO2	(88)	8.80E+7	-1	0.	1
HO	+ MGLY	—>	H2O	+ RCO3	+ CO	(91)	7.04E+6	-1	0.	1
:										
: Reactions of Organic Radicals										
:										
RCO3	+ HO2	—>	RO2H			(41)	2.64E+6	-1	0.	1
RCO3	+ NO	—>	RO2	+ NO2		(22)	1.13E+6	-1	0.	1
RCO3	+ NO2	—>	PAN			(23)	5.98E+5	-1	0.	1
	PAN	—>	NO2	+ RCO3		(43)	4.74E+16	0	12516.	1
RO2	+ NO	—>	RO	+ NO2		(21)	3.08E+6	-1	0.	1
HO2	+ RO2	—>	RO2H	+ O2		(28)	1.19E+6	-1	0.	1
RO2	+ RO2	—>	2 RO	+ O2		(29)	1.76E+5	-1	0.	1
RO2	+ O3	—>	RO	+ O2		(38)	4.84E+3	-1	580.	1
RO	+ O2	—>	HO2	+ HC4		(24)	2.20E+5	-1	2000.	1
RO	+ NO2	—>	RNO3			(25)	4.40E+6	-1	0.	1
:										
: These terms are the Photolysis reaction steps (J1 - J12)										
:										
NO2	+ HV	—>	NO	+ O		(51)	d	0	0.	2
O3	+ HV	—>	O	+ O2		(58)	5.71E-2	1	0.	3
O3	+ HV	—>	O2	+ 2 HO		(59)	6.20E-4	1	0.	3
HNO2	+ HV	—>	HO	+ NO		(52)	2.20E-2	1	0.	3
H2O2	+ HV	—>	2 HO			(53)	1.18E-3	1	0.	3
NO3	+ HV	—>	NO2	+ O		(57)	1.56E+1	1	0.	3
NO3	+ HV	—>	NO	+ O2		(83)	1.90	1	0.	3
N2O5	+ HV	—>	2 NO2	+ O		(60)	3.90E-6	1	0.	3
HC4	+ HV	—>	CO			(42)	1.50E-3	1	0.	3
HC4	+ HV	—>	CO	+ 2 HO2		(50)	1.20E-3	1	0.	3
HC4	+ HV	—>	RO2	+ HO2	+ CO	(54)	1.20E-3	1	0.	3
MGLY	+ HV	—>	RCO3	+ HO2	+ CO	(90)	5.05E-2	1	0.	3

Footnotes for Table A.10

(a) Mechanism Documentation: Gelinas et al. (1974), Luther and Gelinas (1976), Gelinas and Skewes-Cox (1975), MacCracken and Sauter eds. (1975) and Penner and Walton (1982). A computer tape containing the reaction mechanism was obtained from J. Penner, Lawrence Livermore National Laboratory, Livermore, California, on 2 July 1982. Some minor modifications have been made to adapt this mechanism to our study. See Section 3.8.1 for details.

(b) Reaction rate constants are of the form $k = A * TEMP^B * \exp(-C/TEMP)$ with units in terms of the ppm-min system. Note that the values used in this table have been converted from the cgs system reported in Penner and Walton (1982). The key is explained in Table A.14.

(c) HNO_3, RNO_2, RNO_3, RO_2H, Wall, H_2O, M, and O_2 are not calculated in the PW mechanism.

(d) See Table 3.

TABLE A.11

Species Used in the Penner and Walton (1982) Reaction Mechanism

NUMBER	CODE	SPECIES NAME
1	BRO2OHHH	Oxygenated aromatic radical
2	CO	Carbon monoxide
3	HC1	Alkenes, isoprene and mono-terpenes
4	HC2	Alkanes
5	HC3	Aromatics
6	HC4	Aldehydes and ketones
7	HNO2	Nitrous acid
8	HNO3	Nitric acid
9	HNO4	Peroxy nitric acid
10	HO	Hydroxyl radical
11	HO2	Hydroperoxyl radical
12	H2O	Water vapor
13	H2O2	Hydrogen peroxide
14	M	Third body for deactivation
15	MGLY	Methylglyoxal
16	NO	Nitric Oxide
17	NO2	Nitrogen Dioxide
18	NO3	Nitrogen trioxide (nitrate radical)
19	N2O5	Dinitrogen pentoxide
20	O	Atomic oxygen
21	O2	Molecular oxygen
22	O3	Ozone
23	PAN	Peroxactyl nitrate
24	RCO3	Peroxyacyl radical
25	RNO2	Alkyl nitrite
26	RNO3	Alkyl nitrate
27	RO	Alkoxyl radical
28	RO2	Alkylperoxy radical
29	RO2H	Peroxide
30	WALL	Loss term

TABLE A.12

The Dodge (1977) Reaction Mechanism as Used in this Study[a]

REACTION	NUMBER	RATE CONSTANT[b] A	B	C	KEY
NO2 + HV —> NO + O	(1)	c	0	0.	2
O + O2 + M —> O3 + M	(2)	2.0E-5	0	0.	1
NO + O3 —> NO2	(3)	25.0	0	0.	1
O3 + NO2 —> NO3	(4)	0.045	0	0.	1
O + NO2 —> NO	(5)	1.3E+4	0	0.	1
NO + NO3 —> 2 NO2	(6)	1.3E+4	0	0.	1
NO3 + NO2 —> N2O5	(7)	5.6E+3	0	0.	1
N2O5 —> NO2 + NO3	(8)	22.0	0	0.	1
H2O + N2O5 —> 2 WHNO3	(9)	2.5E-6	0	0.	1
NO2 + NO + H2O —> 2 HONO	(10)	1.0E-9	0	0.	1
HONO + HONO —> NO + NO2	(11)	1.0E-3	0	0.	1
HONO + HV —> OH + NO	(12)	1.8E-1	1	0.	3
NO2 + OH —> HNO3	(13)	8.0E+3	0	0.	1
NO + OH —> HONO	(14)	3.0E+3	0	0.	1
NO + HO2 —> NO2 + OH	(15)	1.2E+3	0	0.	1
HO2 + HO2 —> HOOH + O2	(16)	8.4E+3	0	0.	1
HOOH + HV —> 2 OH	(17)	2.4E-3	1	0.	3
O3 + HV —> O1D	(18)	2.71E-3	1	0.	3
O3 + HV —> O	(19)	5.43E-3	1	0.	3
O1D + M —> O + M	(20)	8.7E+4	0	0.	1
O1D + H2O —> 2 OH	(21)	5.1E+5	0	0.	1
O3 + OH —> HO2 + O2	(22)	84.0	0	0.	1
HO2 + O3 —> OH	(23)	2.4	0	0.	1
OH + PROP —> ADD	(24)	2.5E+4	0	0.	1
NO + ADD —> X + NO2	(25)	1.0E+3	0	0.	1
ADD + ADD —> 2 X	(26)	1.2E+4	0	0.	1
MEO2 + ADD —> X + MEO	(27)	1.0E+3	0	0.	1
C2O2 + ADD —> X + C2O	(28)	1.0E+3	0	0.	1
C3O2 + ADD —> X + C3O	(29)	1.0E+3	0	0.	1
X —> HCHO + ALD2 + HO2	(30)	1.0E+5	0	0.	1
O3 + PROP —> OH + HO2 + ALD2	(31)	8.0E-3	0	0.	1
O3 + PROP —> OH + C2O3 + HCHO	(32)	8.0E-3	0	0.	1
OH + BUT —> SCO2	(33)	1.8E+3	0	0.	1
OH + BUT —> C4O2	(34)	1.8E+3	0	0.	1
C4O2 + NO —> NO2 + C4O	(35)	1.8E+3	0	0.	1
SCO2 + NO —> NO2 + SCO	(36)	1.8E+3	0	0.	1
C3O2 + NO —> NO2 + C3O	(37)	1.8E+3	0	0.	1
C2O2 + NO —> NO2 + C2O	(38)	1.8E+3	0	0.	1
MEO2 + NO —> NO2 + MEO	(39)	1.8E+3	0	0.	1
C4O —> HCHO + C3O2	(40)	7.5E+4	0	0.	1
SCO —> ALD2 + C2O2	(41)	1.0E+5	0	0.	1
C3O —> HCHO + C2O2	(42)	8.0E+3	0	0.	1

TABLE A.12 (Continued)

REACTION	NUMBER	RATE CONSTANT[b] A	B	C	KEY
C2O —> HCHO + MEO2	(43)	4.0E+3	0	0.	1
C4O + O2 —> ALD4 + HO2	(44)	0.7	0	0.	1
SCO + O2 —> MEK + HO2	(45)	1.4	0	0.	1
C3O + O2 —> ALD3 + HO2	(46)	0.5	0	0.	1
C2O + O2 —> ALD2 + HO2	(47)	0.4	0	0.	1
MEO + O2 —> HCHO + HO2	(48)	0.4	0	0.	1
HCHO + HV —> PROD	(49)	8.57E-3	1	0.	3
HCHO + HV —> 2 HO2	(50)	2.85E-3	1	0.	3
OH + HCHO —> HO2 + CO	(51)	1.5E+4	0	0.	1
ALD2 + HV —> PROD	(52)	1.2E-5	1	0.	3
ALD2 + HV —> MEO2 + HO2	(53)	2.8E-5	1	0.	3
OH + ALD2 —> C2O3	(54)	1.5E+4	0	0.	1
ALD3 + HV —> PROD	(55)	1.71E-4	1	0.	3
ALD3 + HV —> C2O2 + HO2	(56)	7.14E-3	1	0.	3
OH + ALD3 —> C3O3	(57)	4.5E+4	0	0.	1
ALD4 + HV —> PROD	(58)	1.71E-4	1	0.	3
ALD4 + HV —> C3O2 + HO2	(59)	5.42E-3	1	0.	3
OH + ALD4 —> C4O3	(60)	4.5E+4	0	0.	1
C4O2 + ADD —> X + C4O	(61)	1.0E+3	0	0.	1
SCO2 + ADD —> X + SCO	(62)	1.0E+3	0	0.	1
NO + C4O3 —> C3O2 + NO2	(63)	8.0E+2	0	0.	1
NO + C3O3 —> C2O3 + NO2	(64)	8.0E+2	0	0.	1
NO + C2O3 —> MEO2 + NO2	(65)	8.0E+2	0	0.	1
NO2 + C4O3 —> PAN	(66)	1.0E+2	0	0.	1
NO2 + C3O3 —> PAN	(67)	1.0E+2	0	0.	1
NO2 + C2O3 —> PAN	(68)	1.0E+2	0	0.	1
HO2 + C4O2 —> PROD	(69)	4.0E+3	0	0.	1
HO2 + C3O2 —> PROD	(70)	4.0E+3	0	0.	1
HO2 + SCO2 —> PROD	(71)	4.0E+3	0	0.	1
HO2 + C2O2 —> PROD	(72)	4.0E+3	0	0.	1
HO2 + MEO2 —> PROD	(73)	4.0E+3	0	0.	1
HO2 + C4O3 —> PROD	(74)	4.0E+3	0	0.	1
HO2 + C3O3 —> PROD	(75)	4.0E+3	0	0.	1
HO2 + C2O3 —> PROD	(76)	4.0E+3	0	0.	1

Footnotes for Table A.12

(a) Mechanism Documentation: Dodge (1977) and Durbin et al. (1975) The actual coding for the reactions and the rate constants were derived from the computer program: OZIPP - Isopleth Plotting Program obtained from H.L. Jeffries on 20 November 1982.

(b) Reaction rate constants are of the form $k = A * TEMP^B * \exp(-C/TEMP)$ with units in terms of the ppm-min system. The key is explained in Table A.14.

(c) See Table 3.

TABLE A.13

Species Used in the Dodge (1977) Reaction Mechanism

NUMBER	CODE	SPECIES NAME
1	ADD	$CH_3CH(OH)CH_2OO$
2	ALD2	CH_3CHO
3	ALD3	CH_3CH_2CHO
4	ALD4	$CH_3CH_2CH_2CHO$
5	BUT	n-Butane ($n\text{-}C_4H_{10}$)
6	C2O	CH_3CH_2O
7	C2O2	$CH_3CH_2O_2$
8	C2O3	$CH_3C(O)O_2$
9	C3O	$CH_3CH_2CH_2O$
10	C3O2	$CH_3CH_2CH_2O_2$
11	C3O3	$CH_3CH_2C(O)O_2$
12	C4O	$CH_3CH_2CH_2CH_2O$
13	C4O2	$CH_3CH_2CH_2CH_2O_2$
14	C4O3	$CH_3CH_2CH_2C(O)O_2$
15	HCHO	Formaldehyde
16	HNO3	Nitric acid
17	HONO	Nitrous acid
18	HO2	Hydroperoxyl radical
19	H2O	Water vapor
20	HOOH	Hydrogen peroxide
21	M	Third body
22	MEK	Methyl ethyl ketone
23	MEO	Methoxy radical
24	MEO2	Methyl peroxy radical
25	NO	Nitric oxide
26	NO2	Nitrogen dioxide
27	NO3	Nitrogen trioxide (nitrate radical)
28	N2O5	Nitrogen pentoxide
29	O	Atomic oxygen $O(^3P)$
30	OH	Hydroxyl radical
31	O1D	Singlet D oxygen
32	O2	Molecular oxygen
33	O3	Ozone
34	PAN	Peroxyacetyl nitrate
35	PROP	Propylene
36	SCO	$CH_3CH(O)CH_2CH_3$
37	SCO2	$CH_3CH(O_2)CH_2CH_3$
38	PROD	Stable products
39	X	$CH_3CH(OH)CH_2O$

TABLE A.14

Explanation of Rate Constant Format

KEY	RATE CONSTANT FORMAT
1	$k = A*TEMP^{B}*EXP(- C/T)$
2	Rate constant specified externally, this form is usually used only for photolysis steps.
3	Rate constant expressed as a proportion of another rate constant so that K = A*K(B) where B identifies the reaction number.

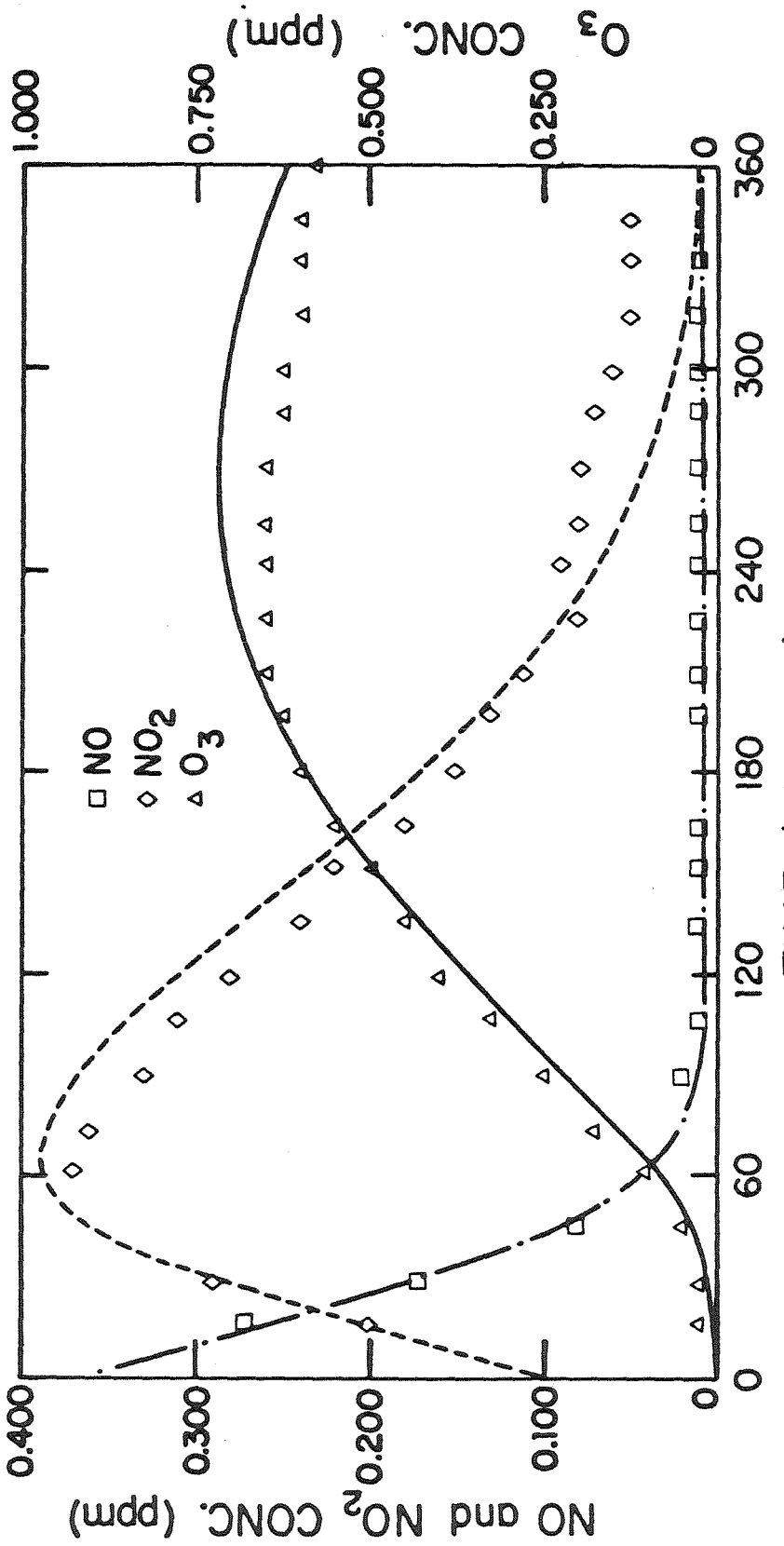

Figure A1a. Observed and Calculated Concentration-Time Profiles for 7-Hydrocarbon-NO_x Experiment EC-237

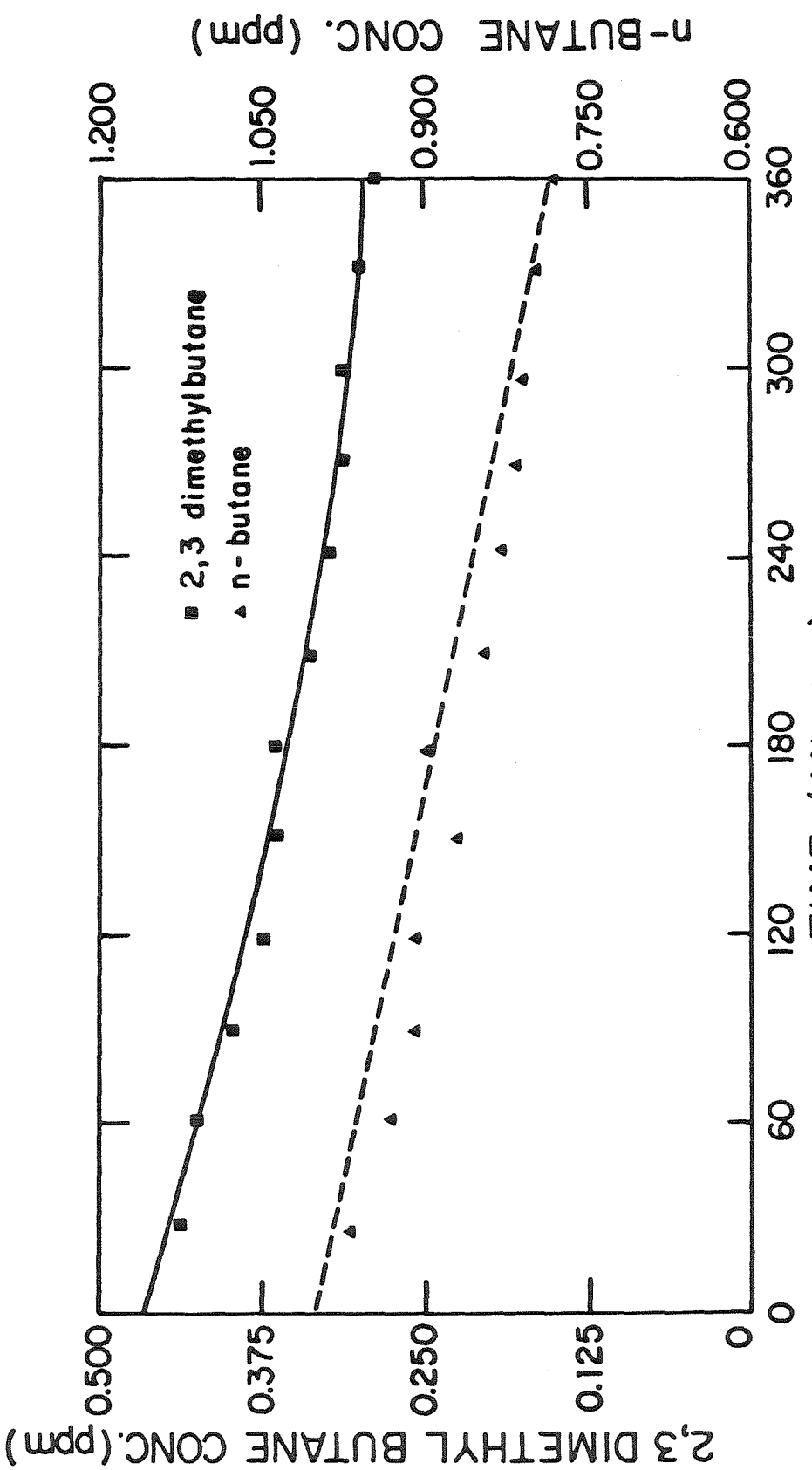

Figure A1b. Observed and Calculated Concentration-Time Profiles for 7-Hydrocarbon-NO_x Experiment EC-237

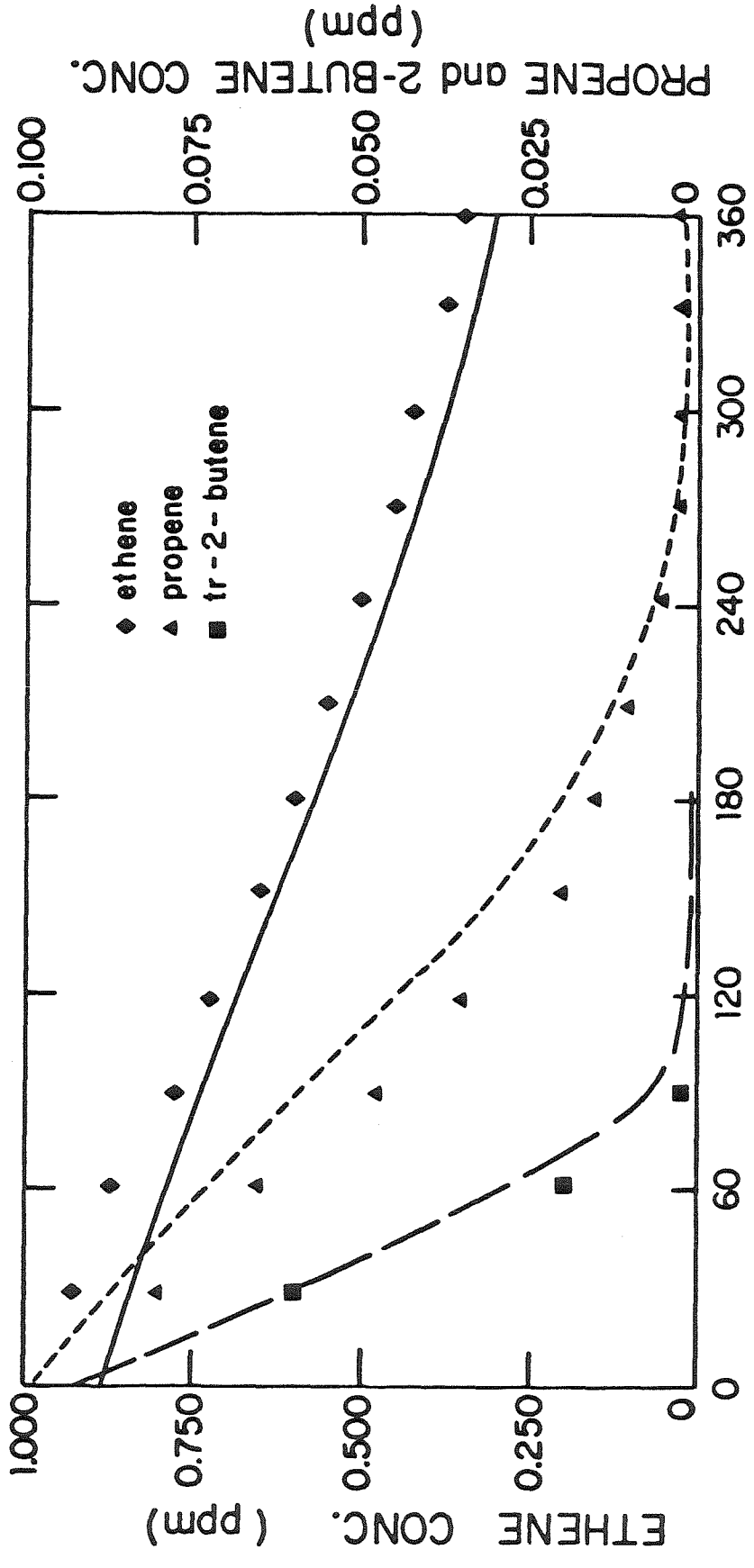

Figure A1c. Observed and Calculated Concentration-Time Profiles for 7-Hydrocarbon-NO_x Experiment EC-237

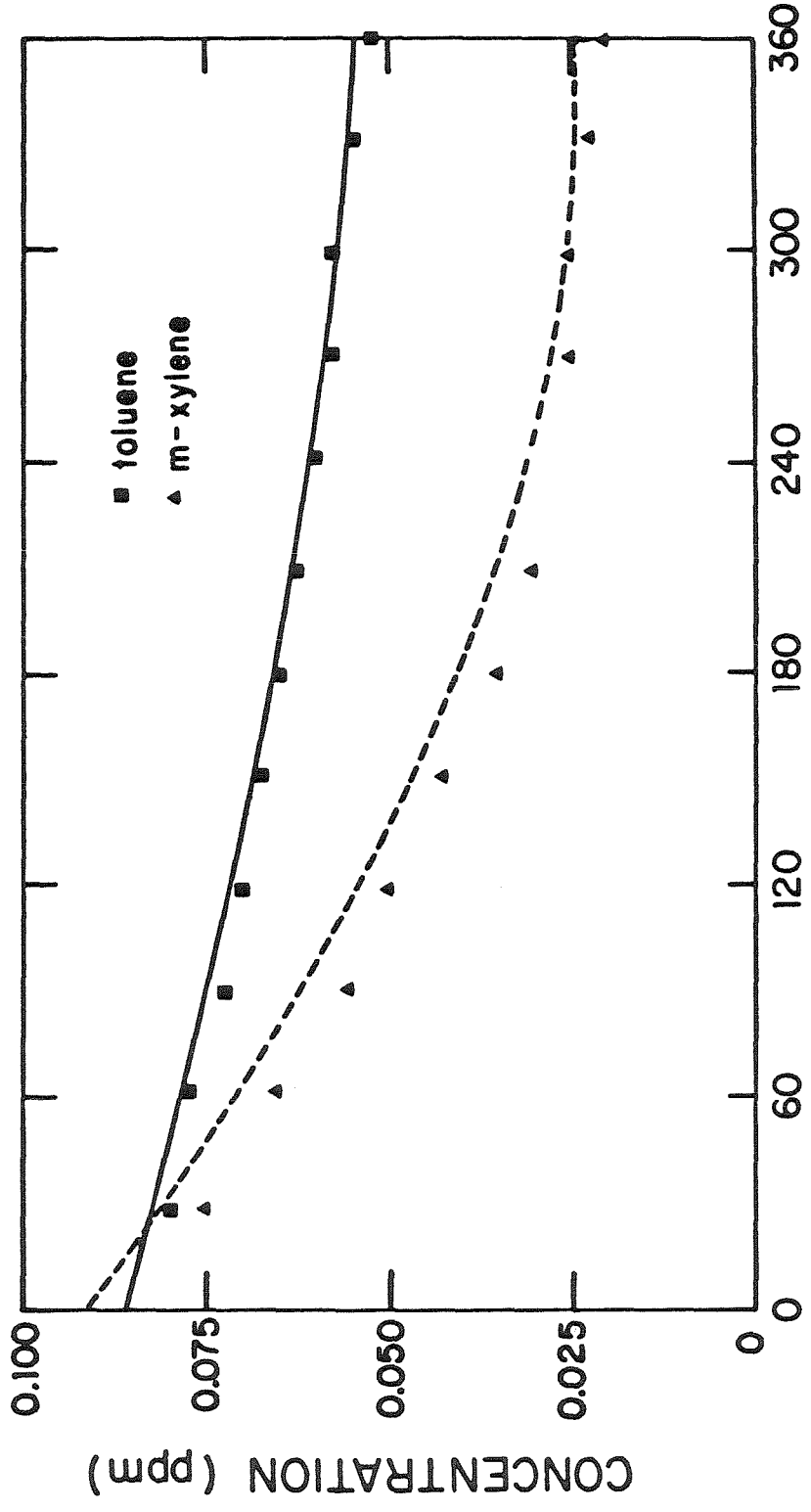

Figure A1d. Observed and Calculated Concentration-Time Profiles for 7-Hydrocarbon-NO_x Experiment-237

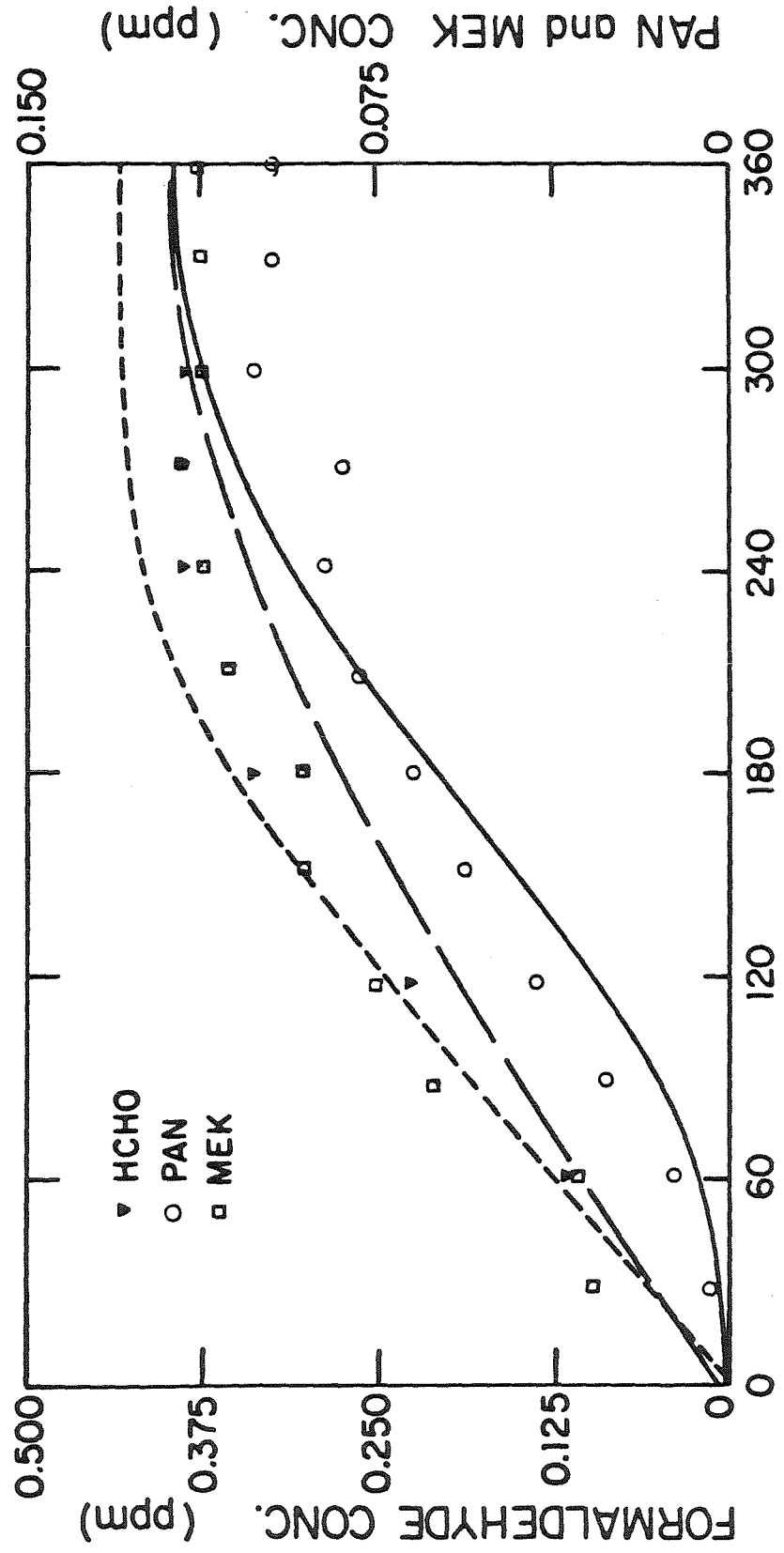

Figure A1e. Observed and Calculated Concentration-Time Profiles for 7-Hydrocarbon-NO_x Experiment EC-237

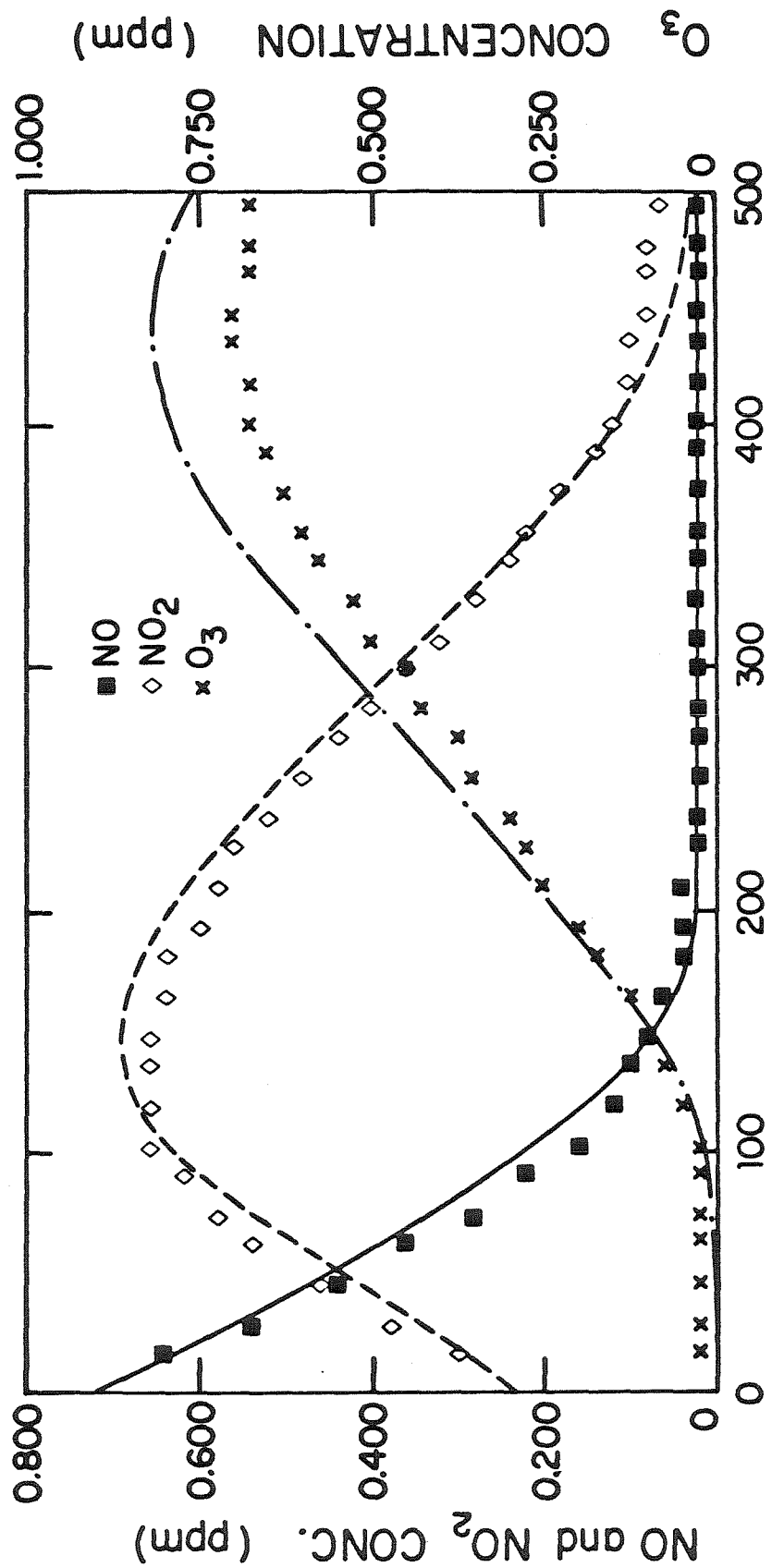

Figure A2a. Observed and Calculated Concentration-Time Profiles for 7-Hydrocarbon-NO_x Experiment EC-238

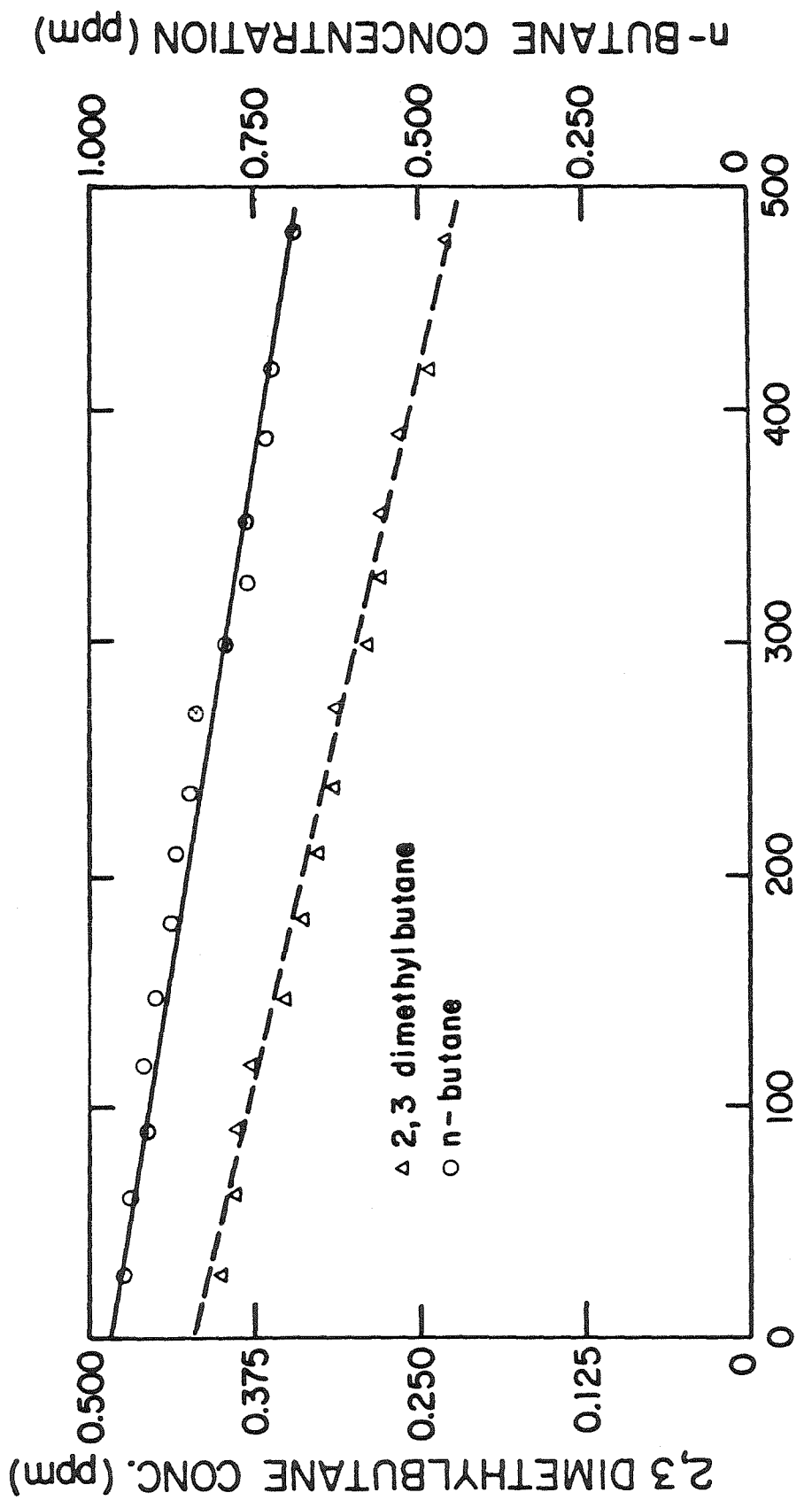

Figure A2b. Observed and Calculated Concentration-Time Profiles for 7-Hydrocarbon-NO_x Experiment EC-238

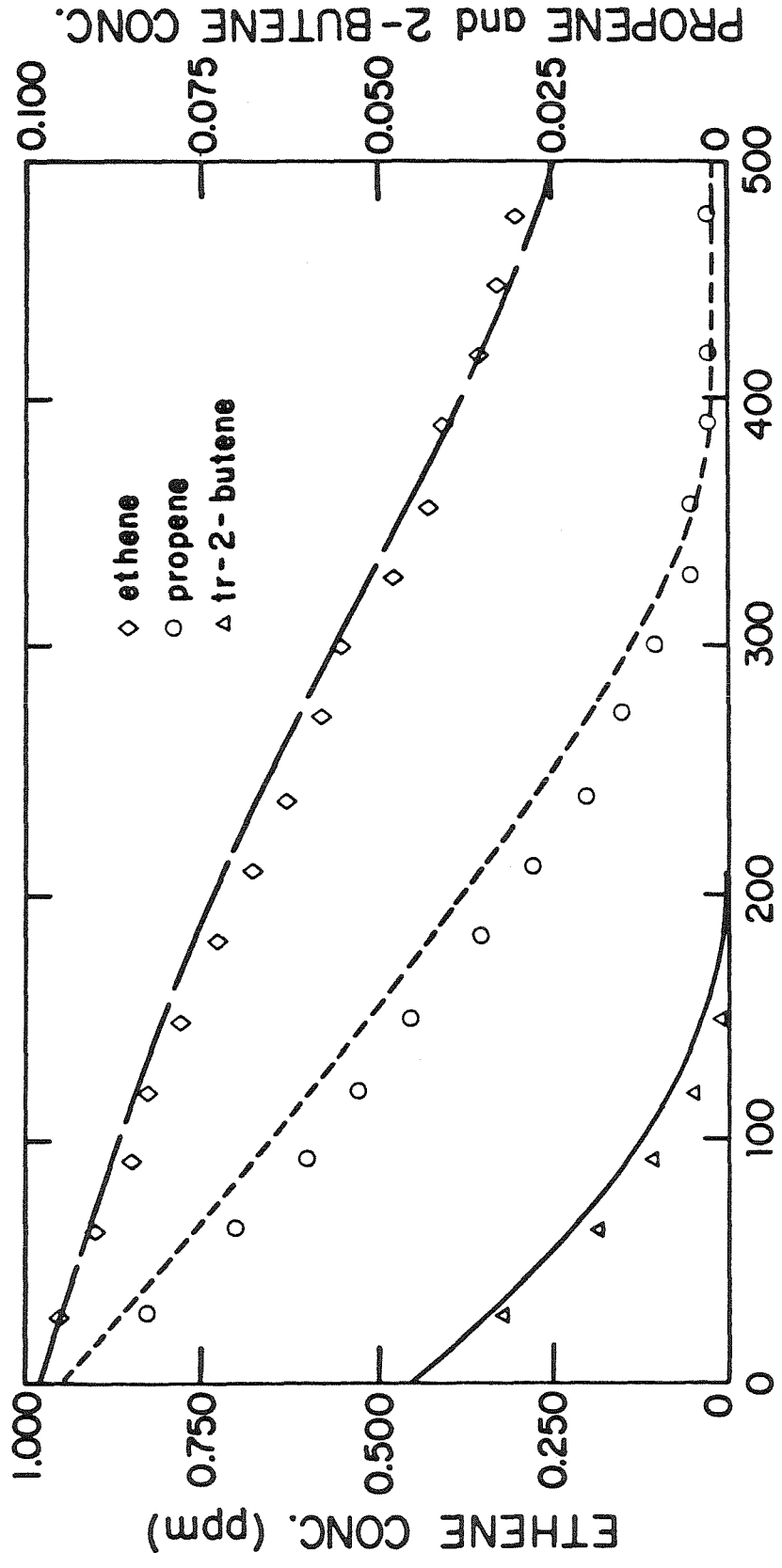

Figure A2c. Observed and Calculated Concentration-Time Profiles for 7-Hydrocarbon-NO_x Experiment EC-238

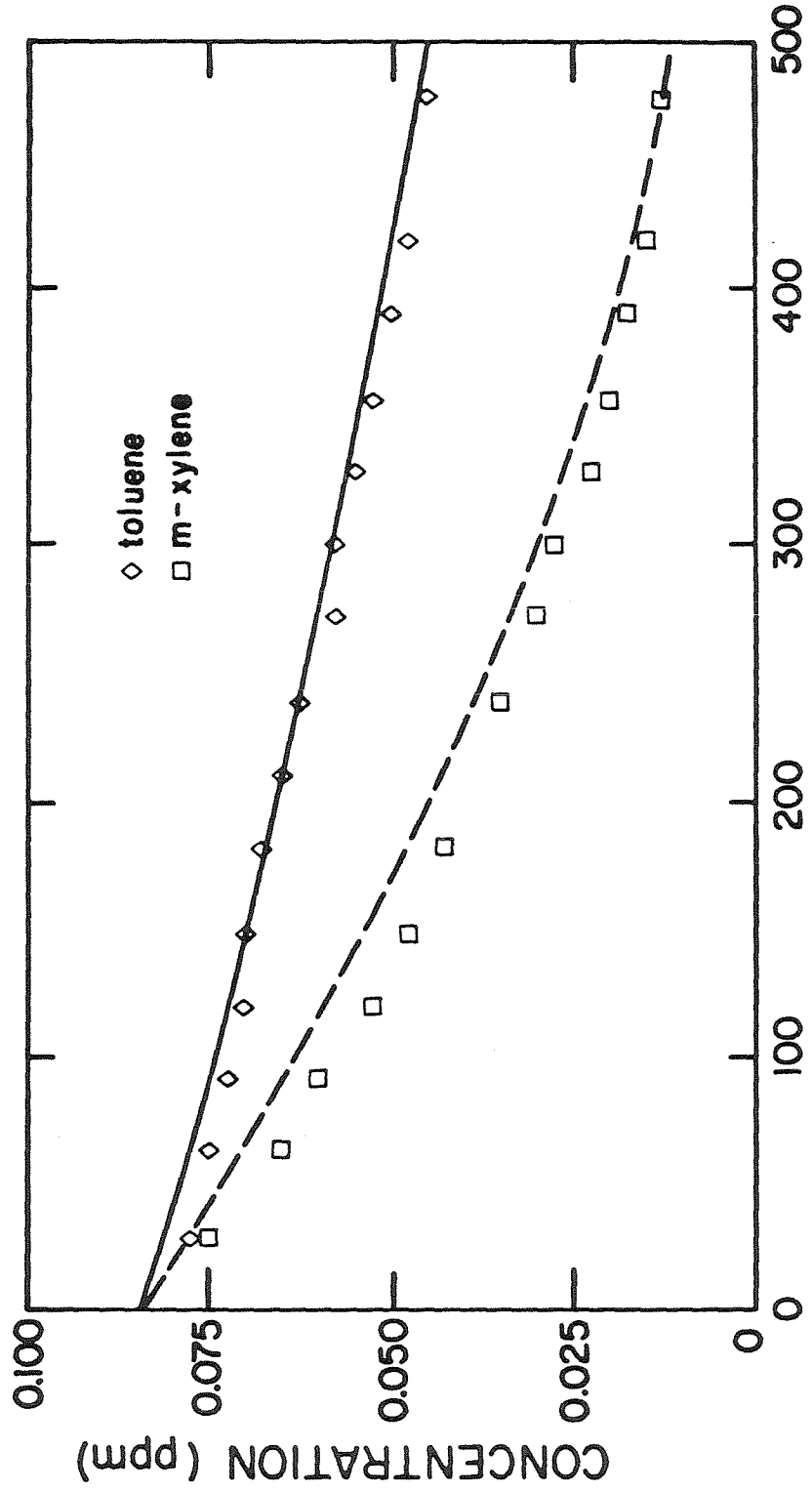

Figure A2d. Observed and Calculated Concentration-Time Profiles for 7-Hydrocarbon-NO_x Experiment EC-238

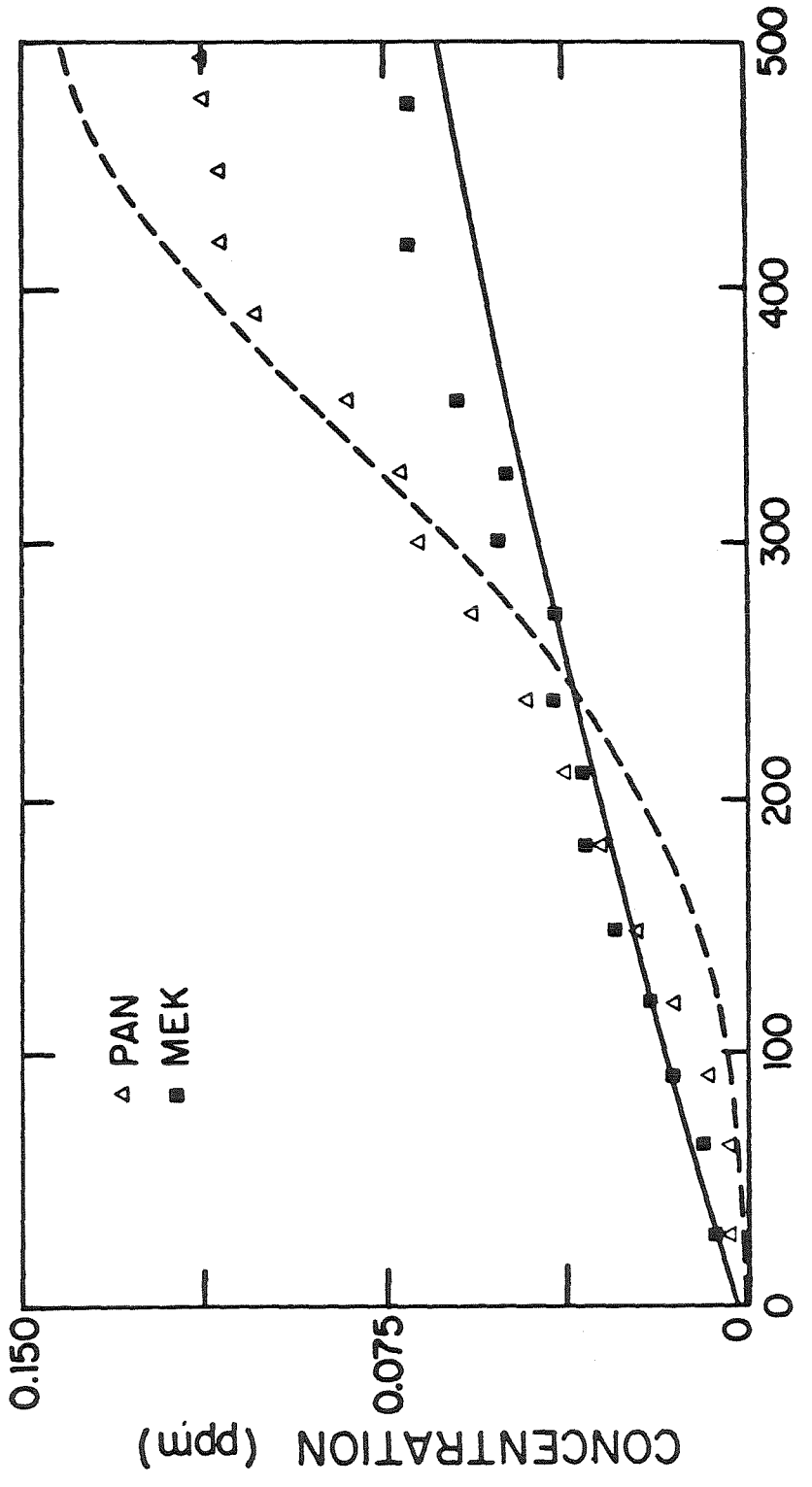

Figure A2e. Observed and Calculated Concentration-Time Profiles for 7-Hydrocarbon-NO_x Experiment EC-238

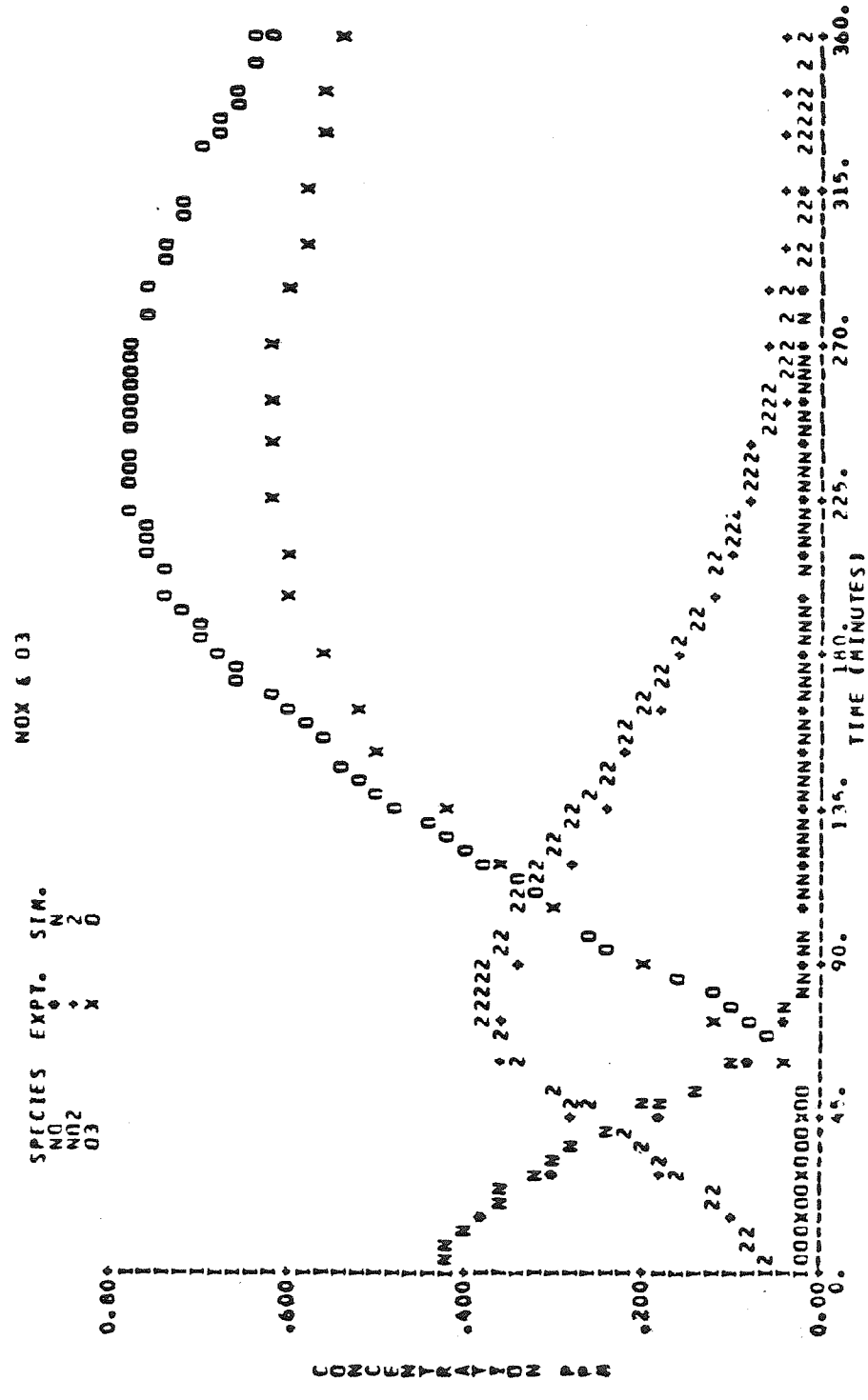

Figure A3a. Observed and Calculated Concentration-Time Profiles for 7-Hydrocarbon-NO_x Experiment EC-231

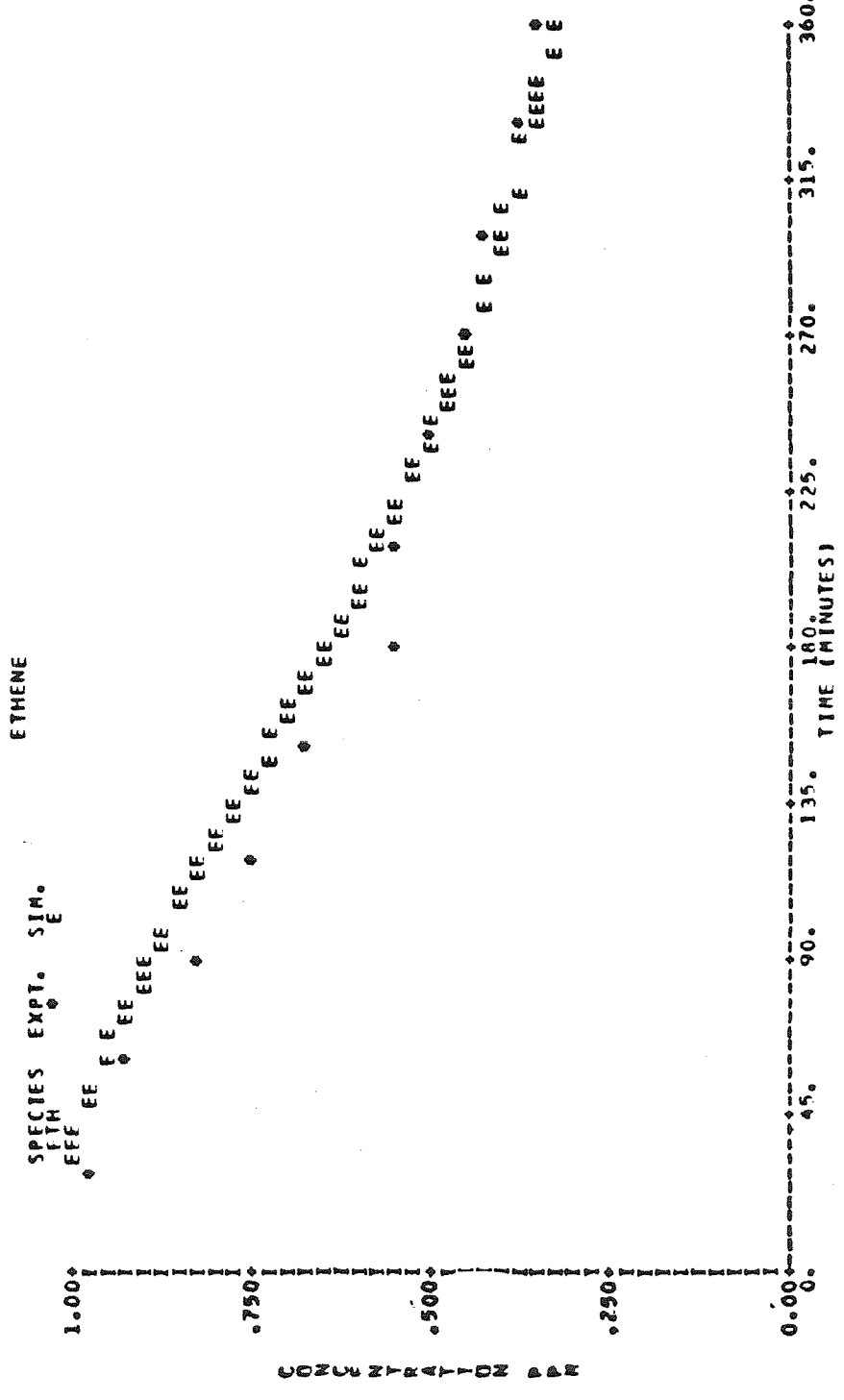

Figure A3b. Observed and Calculated Concentration-Time Profiles for 7-Hydrocarbon-NO_x Experiment EC-231

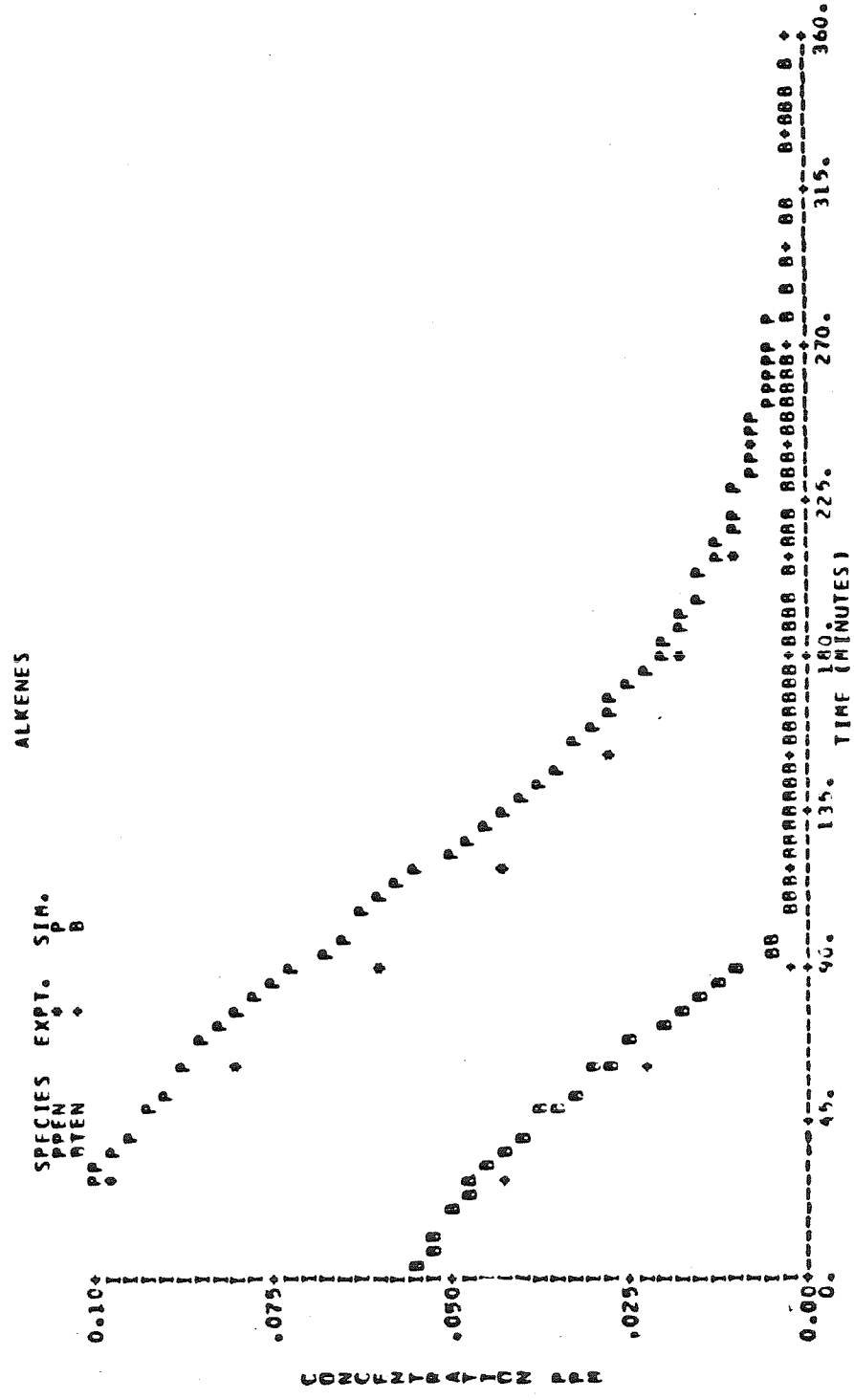

Figure A3c. Observed and Calculated Concentration-Time Profiles for 7-Hydrocarbon-NO_x Experiment EC-231

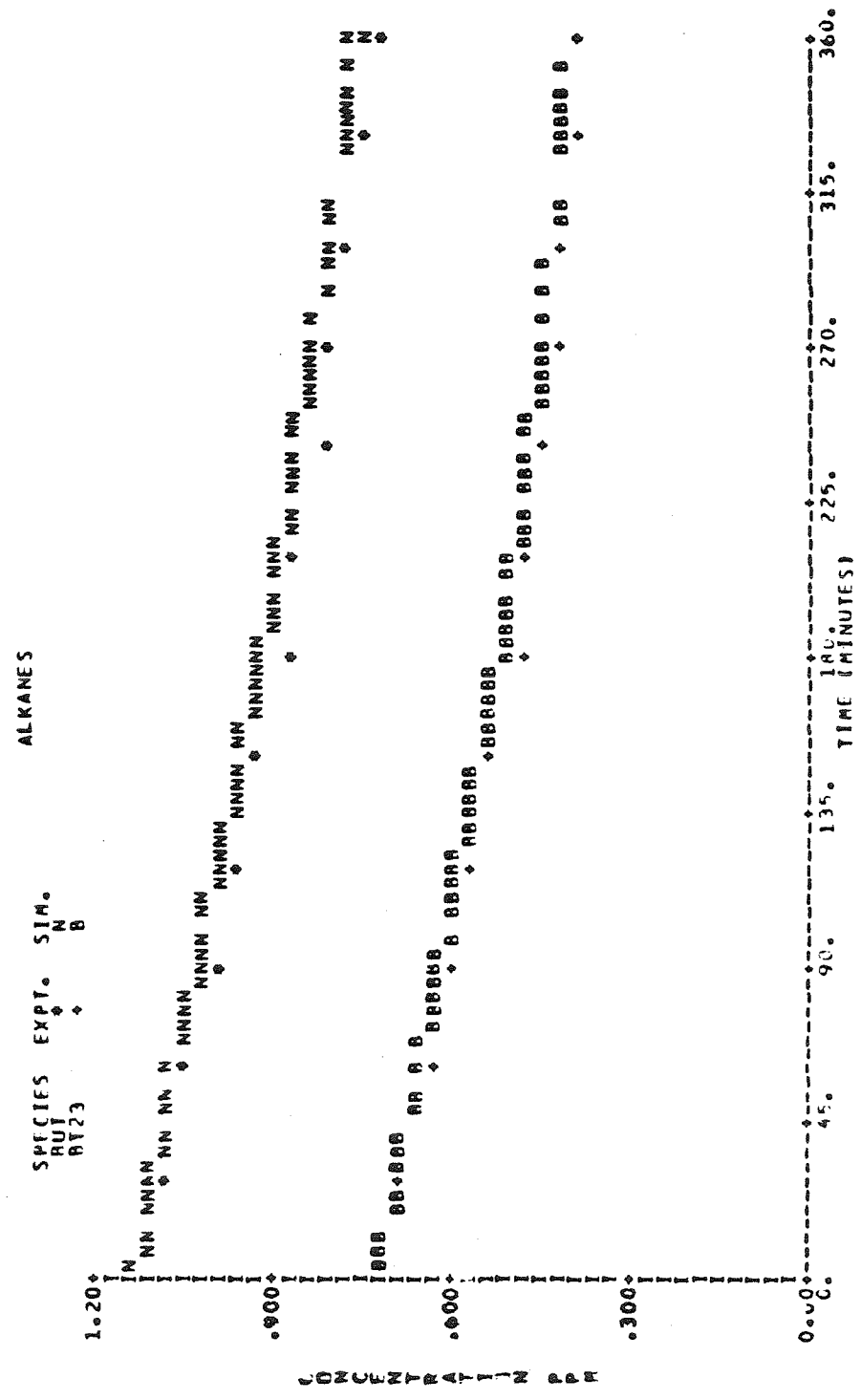

Figure A3d. Observed and Calculated Concentration-Time Profiles for 7-Hydrocarbon-NO_x Experiment EC-231

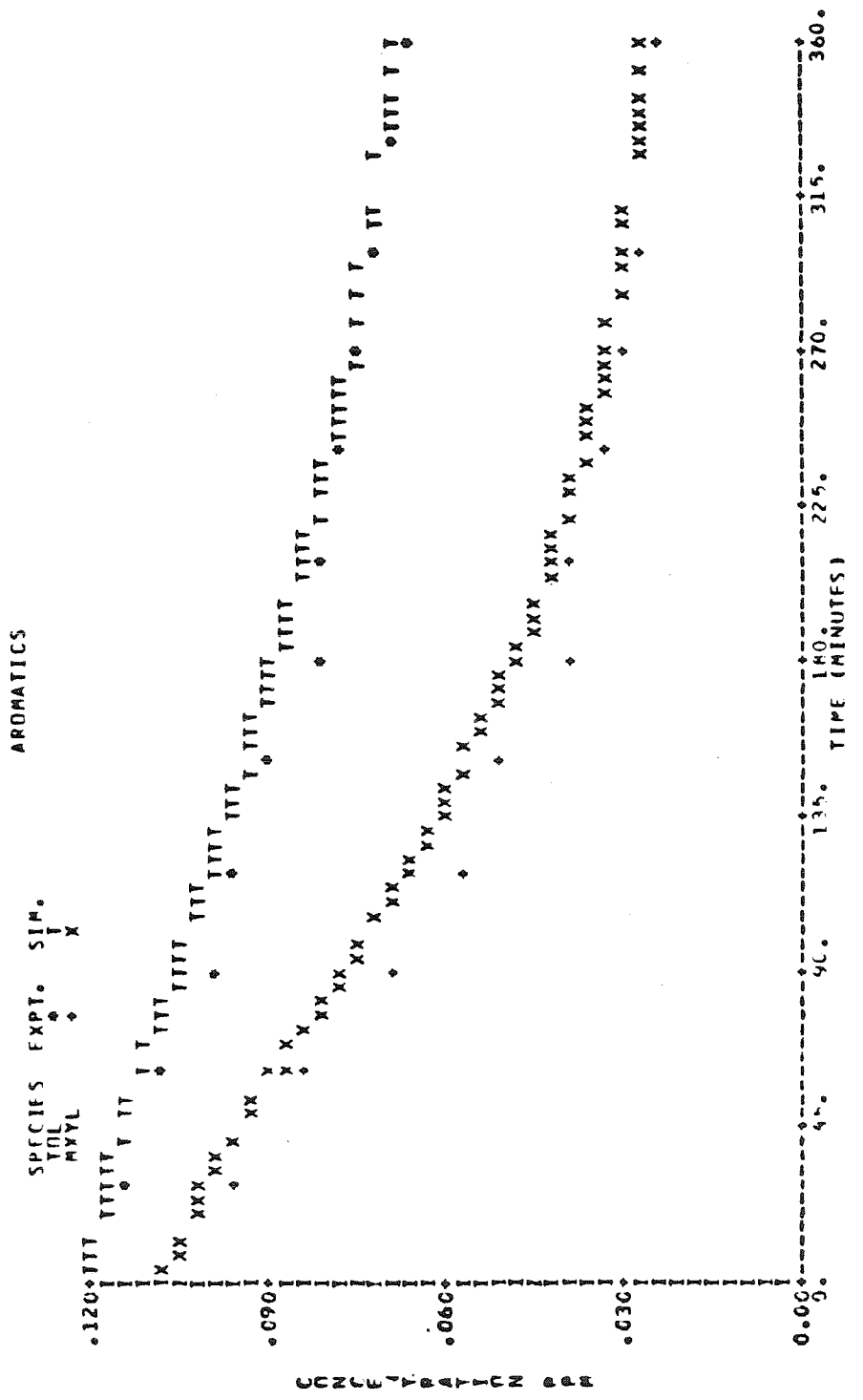

Figure A3e. Observed and Calculated Concentration-Time Profiles for 7-Hydrocarbon-NO_x Experiment EC-231

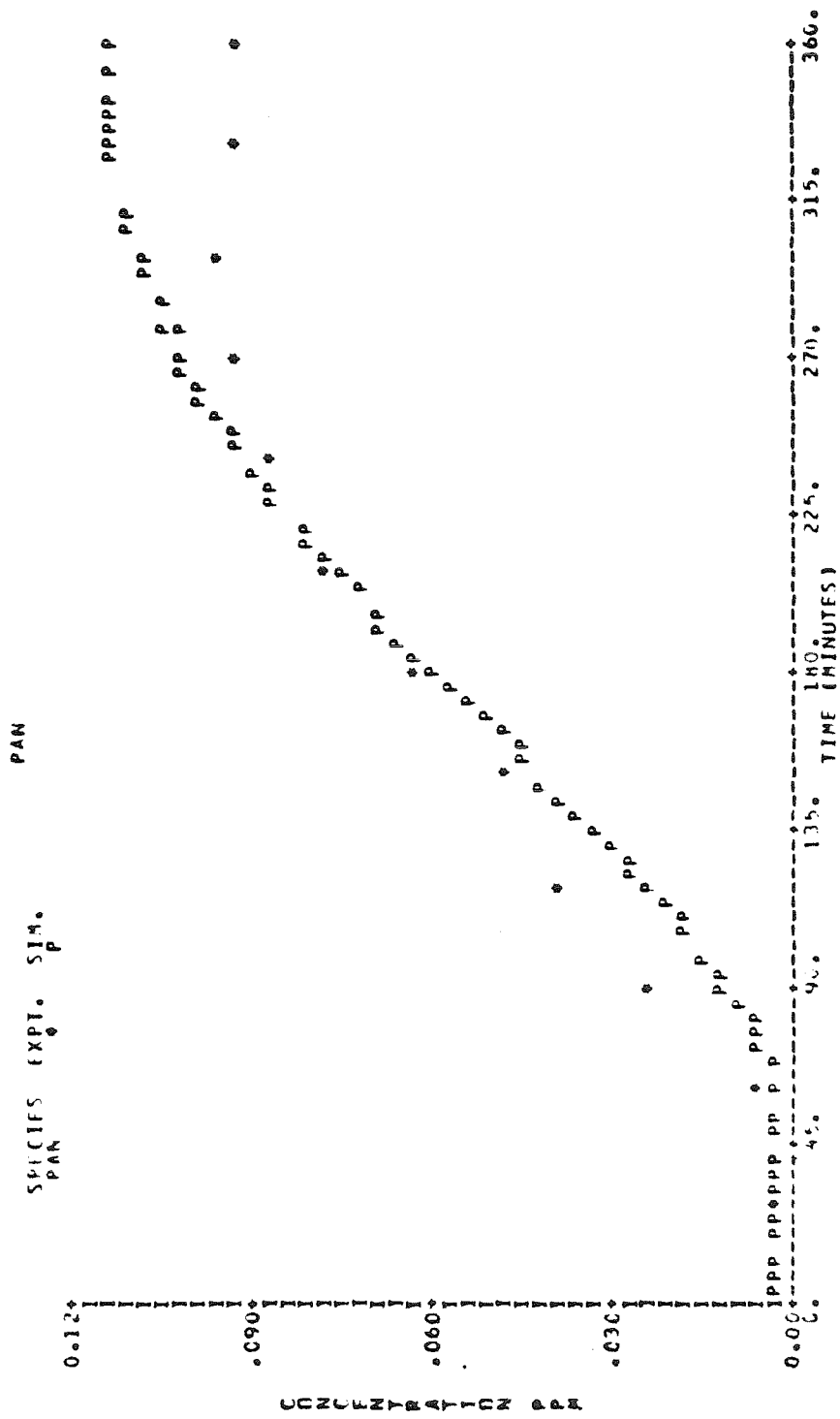

Figure A3f. Observed and Calculated Concentration-Time Profiles for 7-Hydrocarbon-NO_x Experiment EC-231

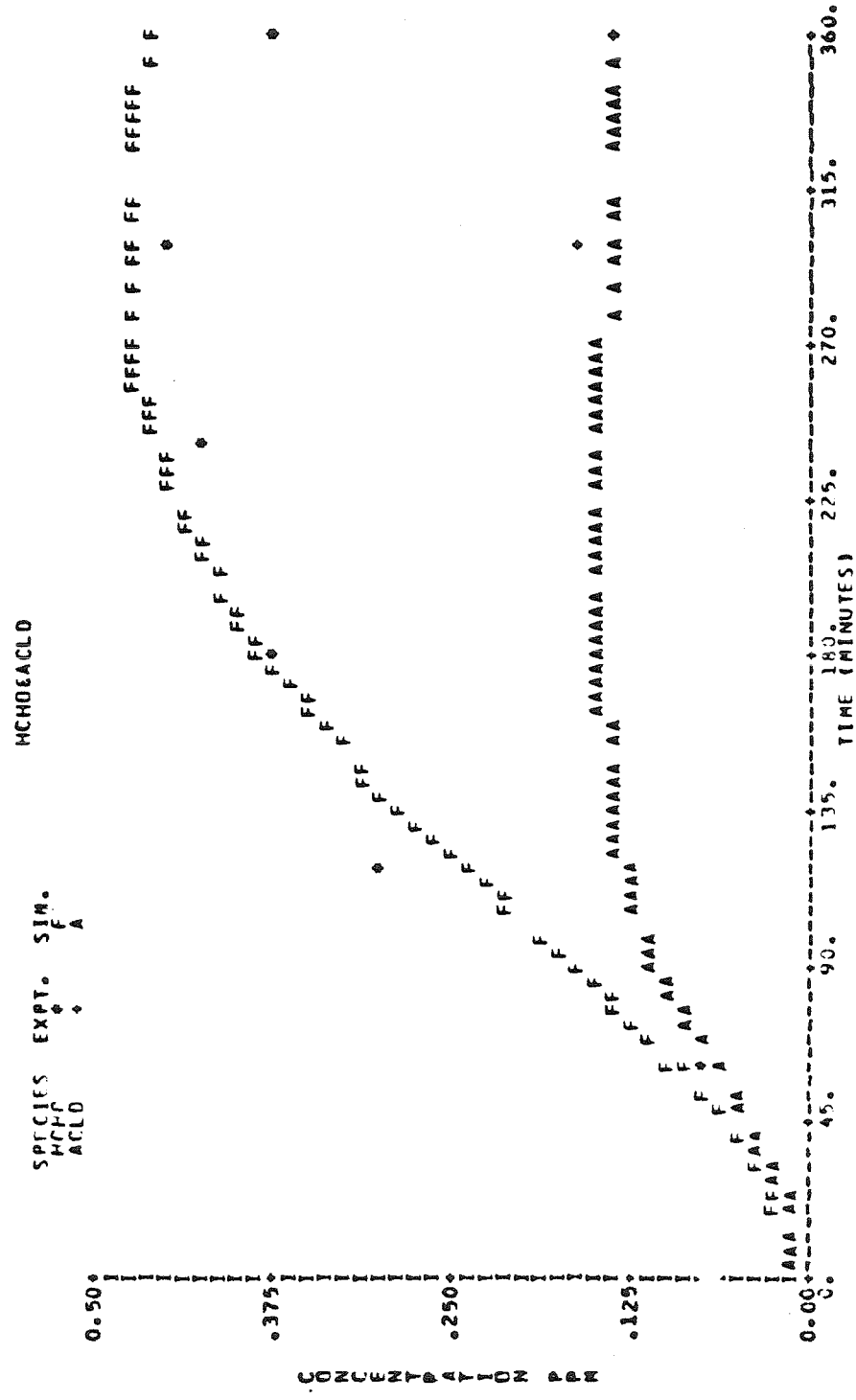

Figure A3g. Observed and Calculated Concentration-Time Profiles for 7-Hydrocarbon-NO_x Experiment EC-231

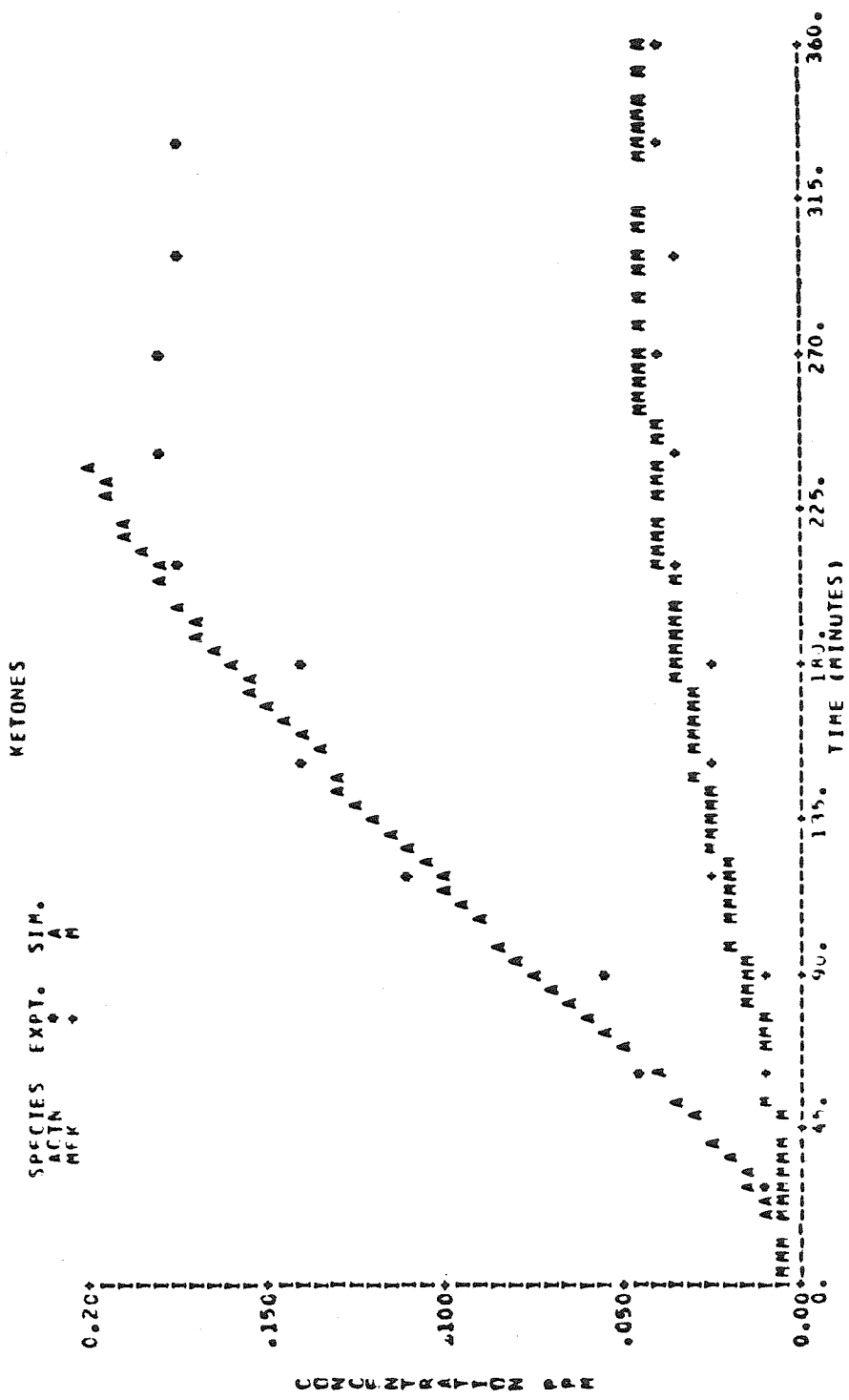

Figure A3h. Observed and Calculated Concentration-Time Profiles for 7-Hydrocarbon-NO_x Experiment EC-231

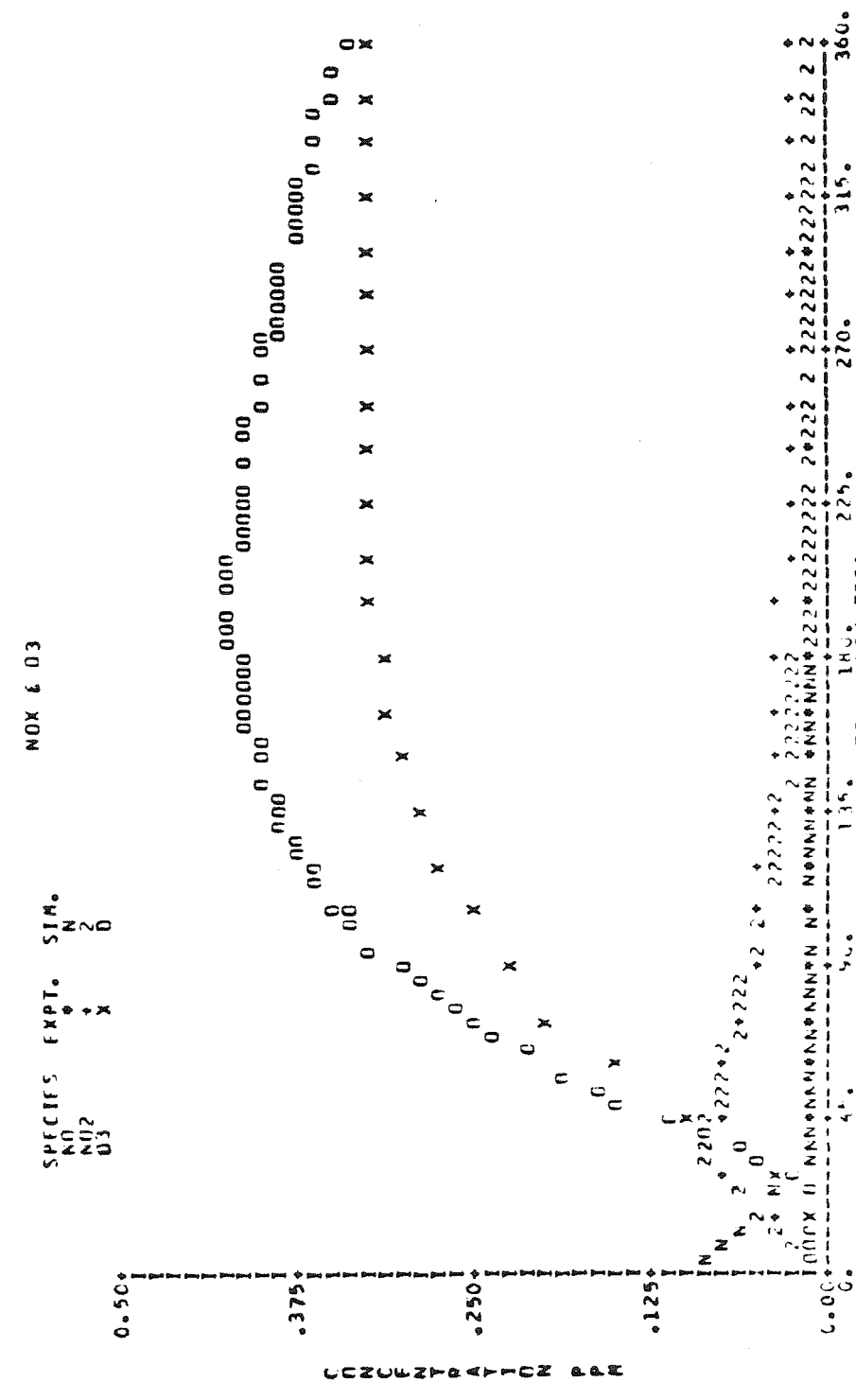

Figure A4a. Observed and Calculated Concentration-Time Profiles for 7-Hydrocarbon-NO_x Experiment EC-233.

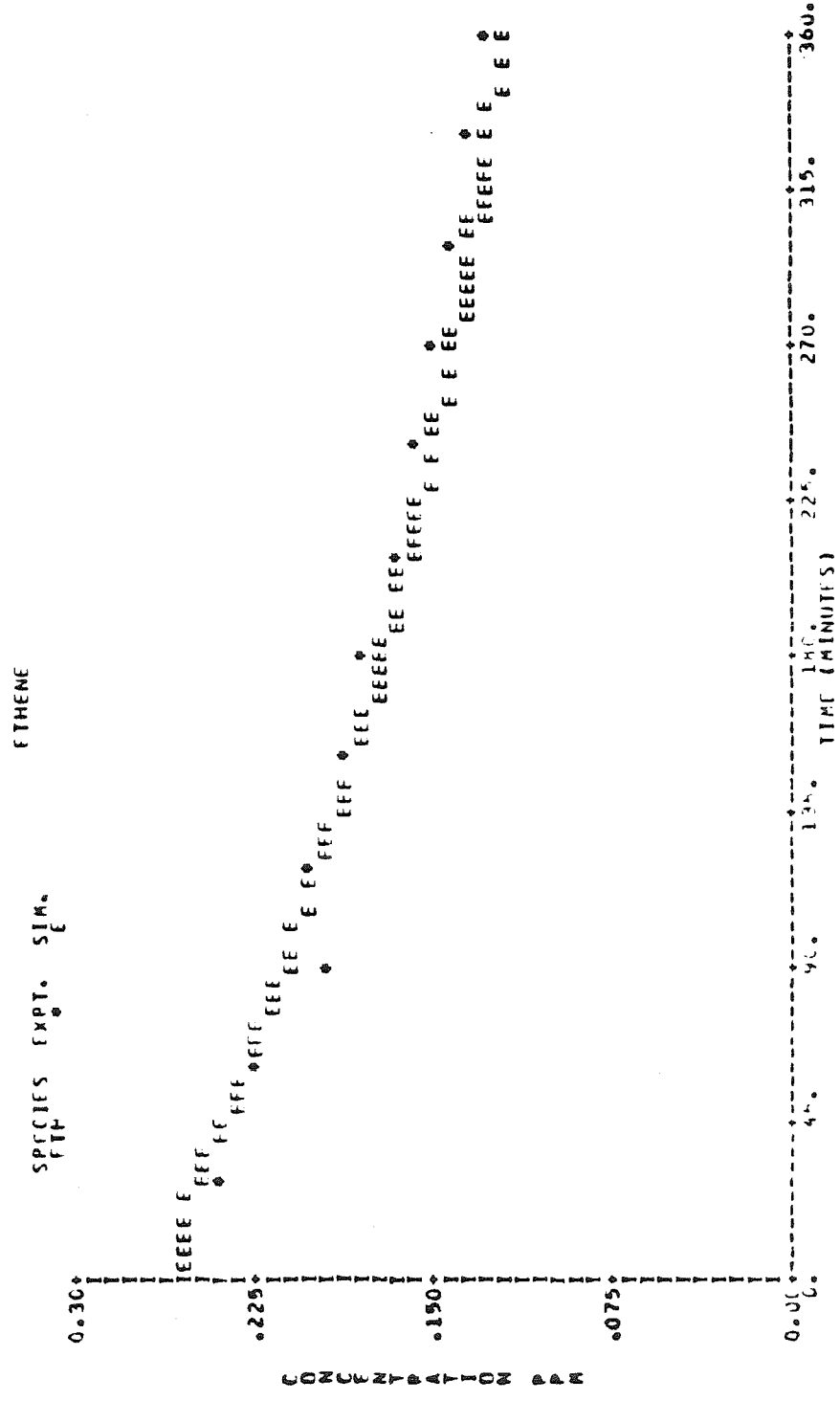

Figure A4b. Observed and Calculated Concentration-Time Profiles for 7-Hydrocarbon-NO_x Experiment EC-233.

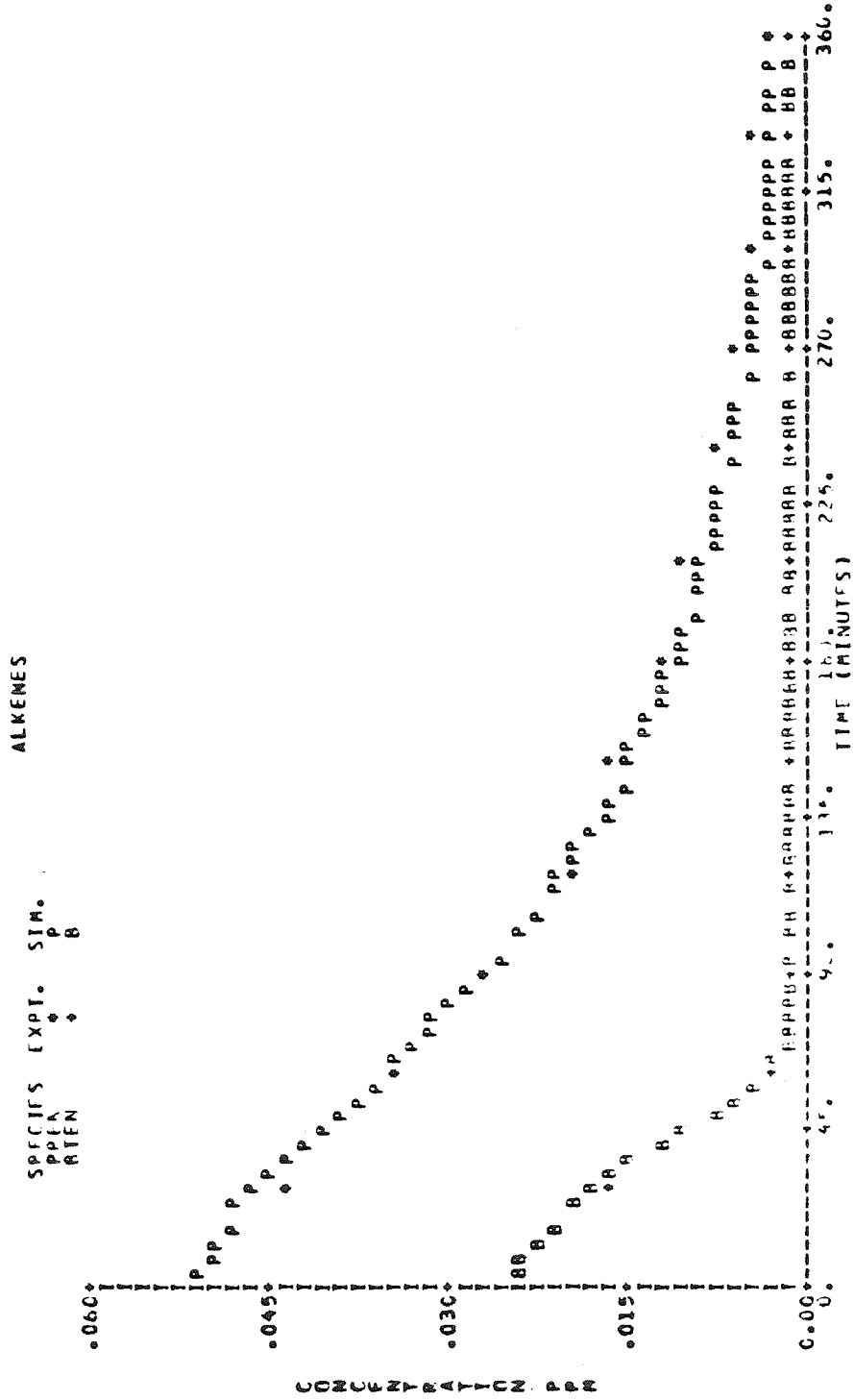

Figure A4c. Observed and Calculated Concentration-Time Profiles for 7-Hydrocarbon-NO_x Experiment EC-233.

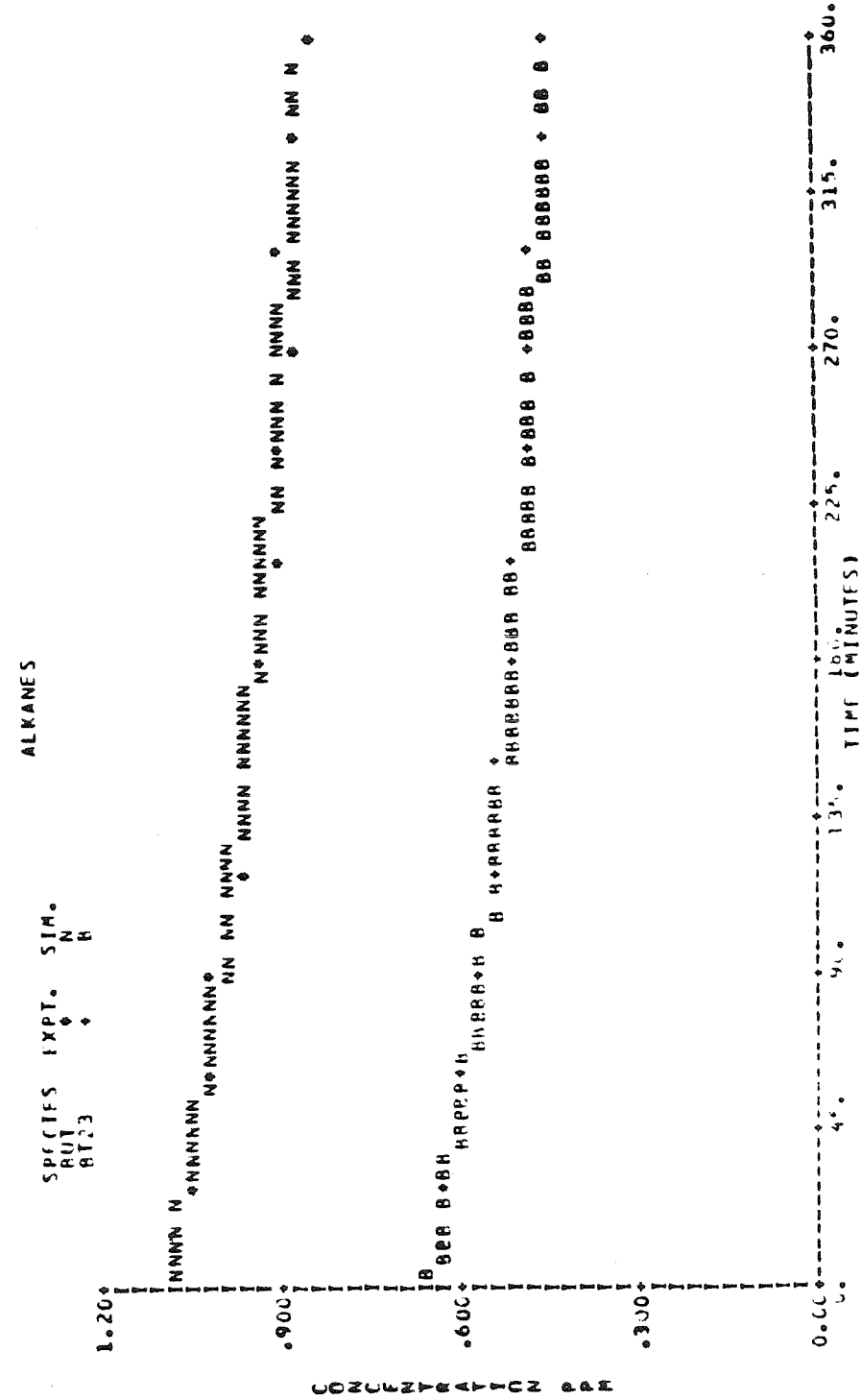

Figure A4d. Observed and Calculated Concentration-Time Profiles for 7-Hydrocarbon-NO_x Experiment EC-233.

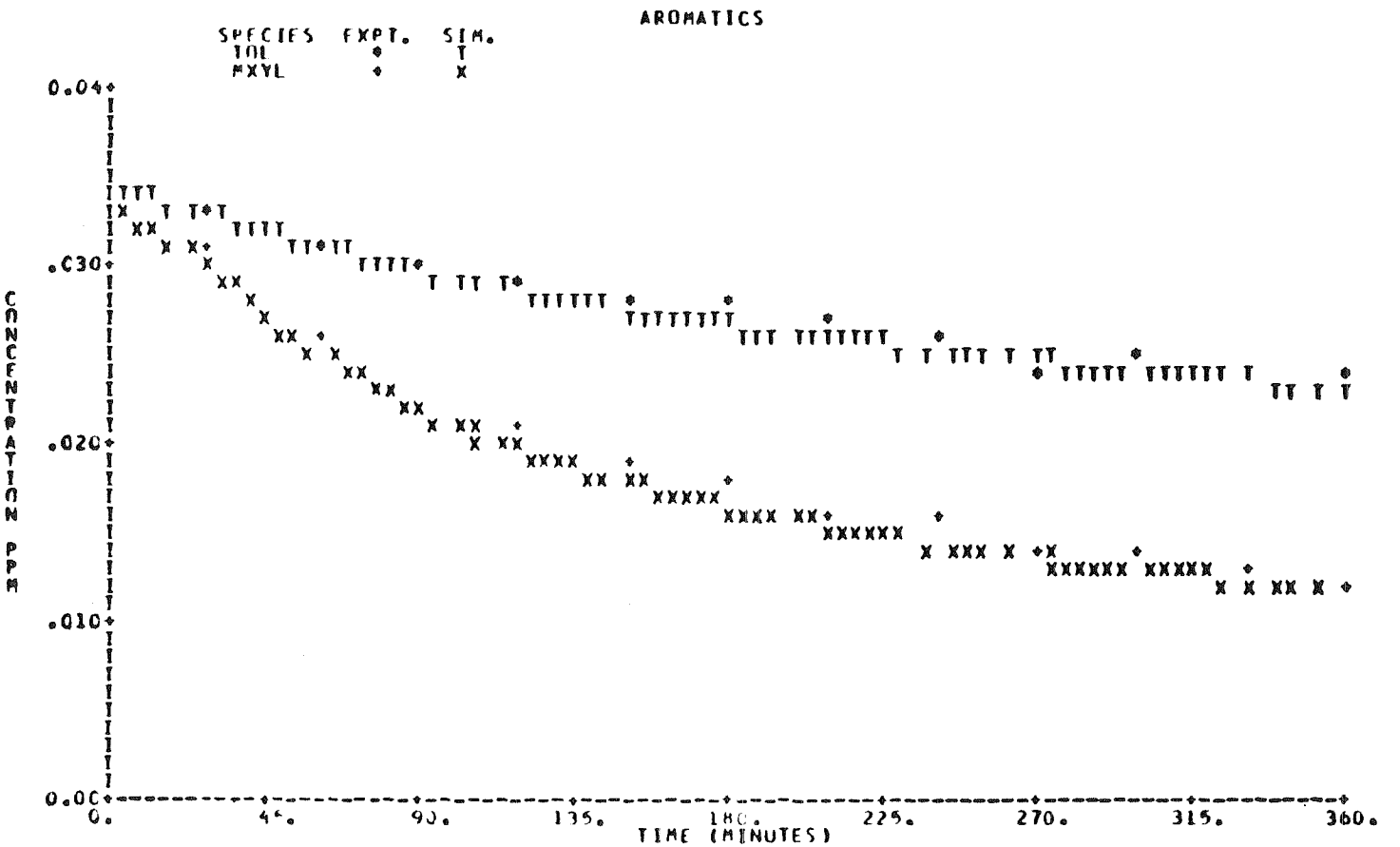

Figure A4e. Observed and Calculated Concentration-Time Profiles for 7-Hydrocarbon-NO_x Experiment EC-233.

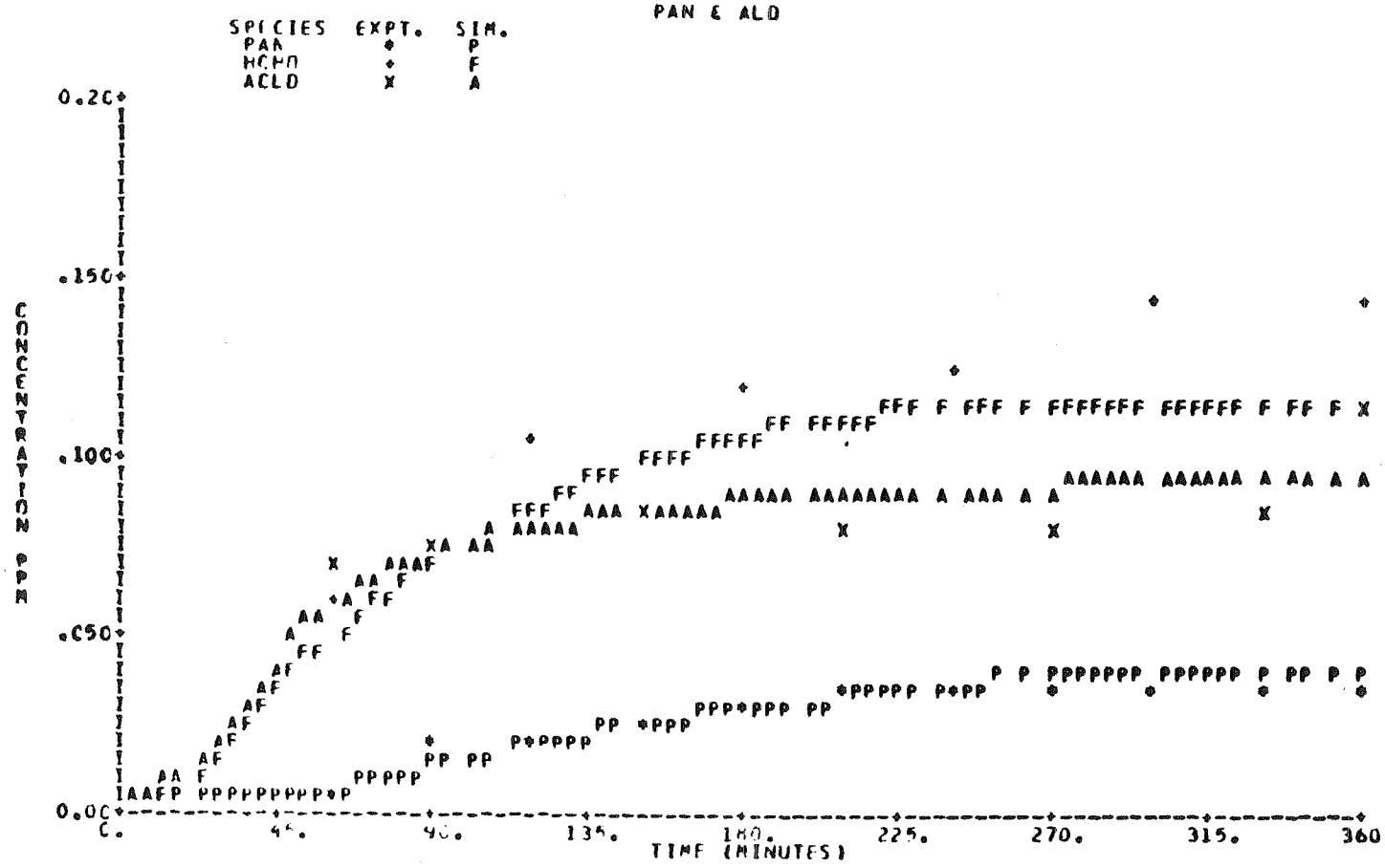

Figure A4f. Observed and Calculated Concentration-Time Profiles for 7-Hydrocarbon-NO_x Experiment EC-233.

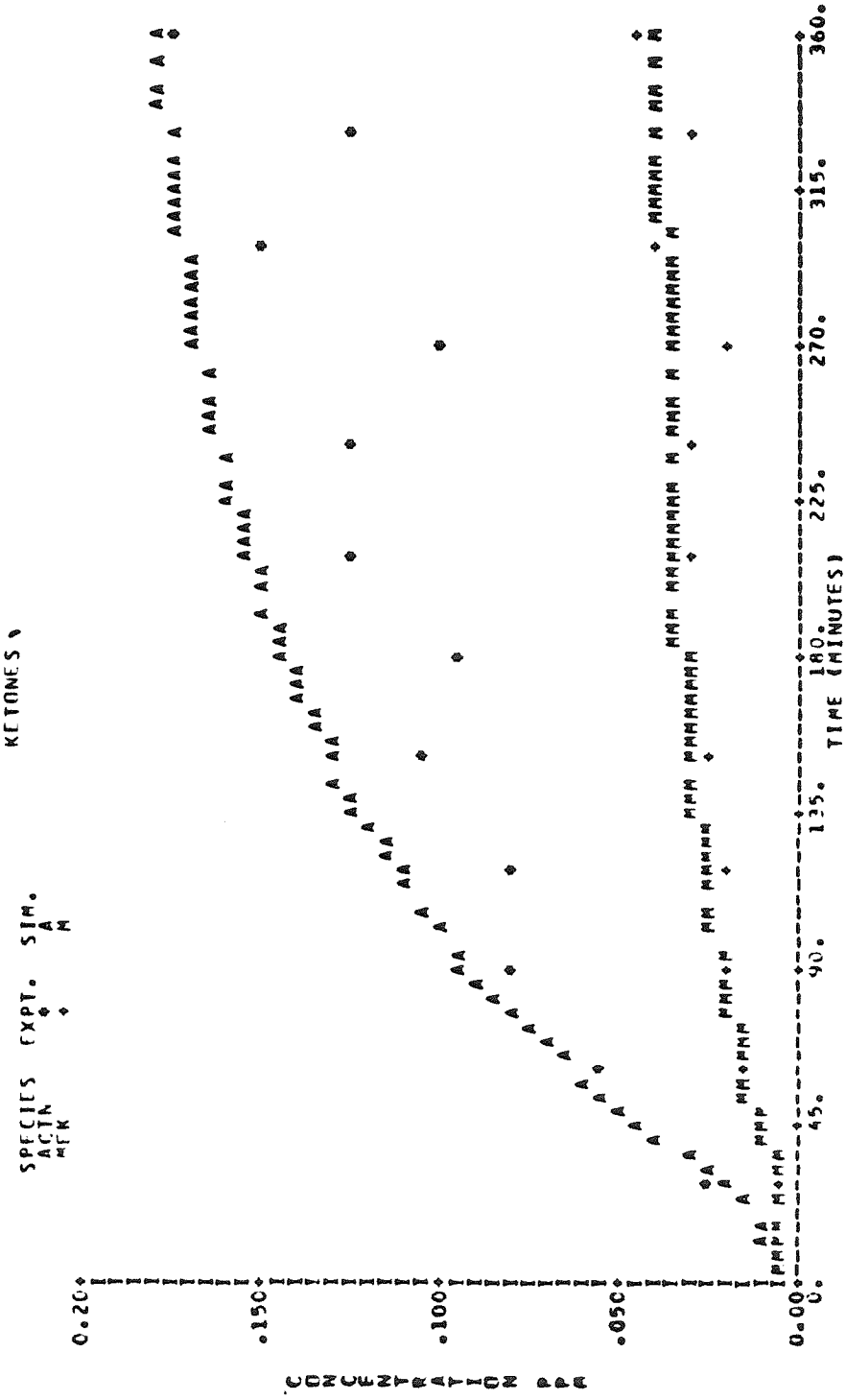

Figure A4g. Observed and Calculated Concentration-Time Profiles for 7-Hydrocarbon-NO_x Experiment EC-233.

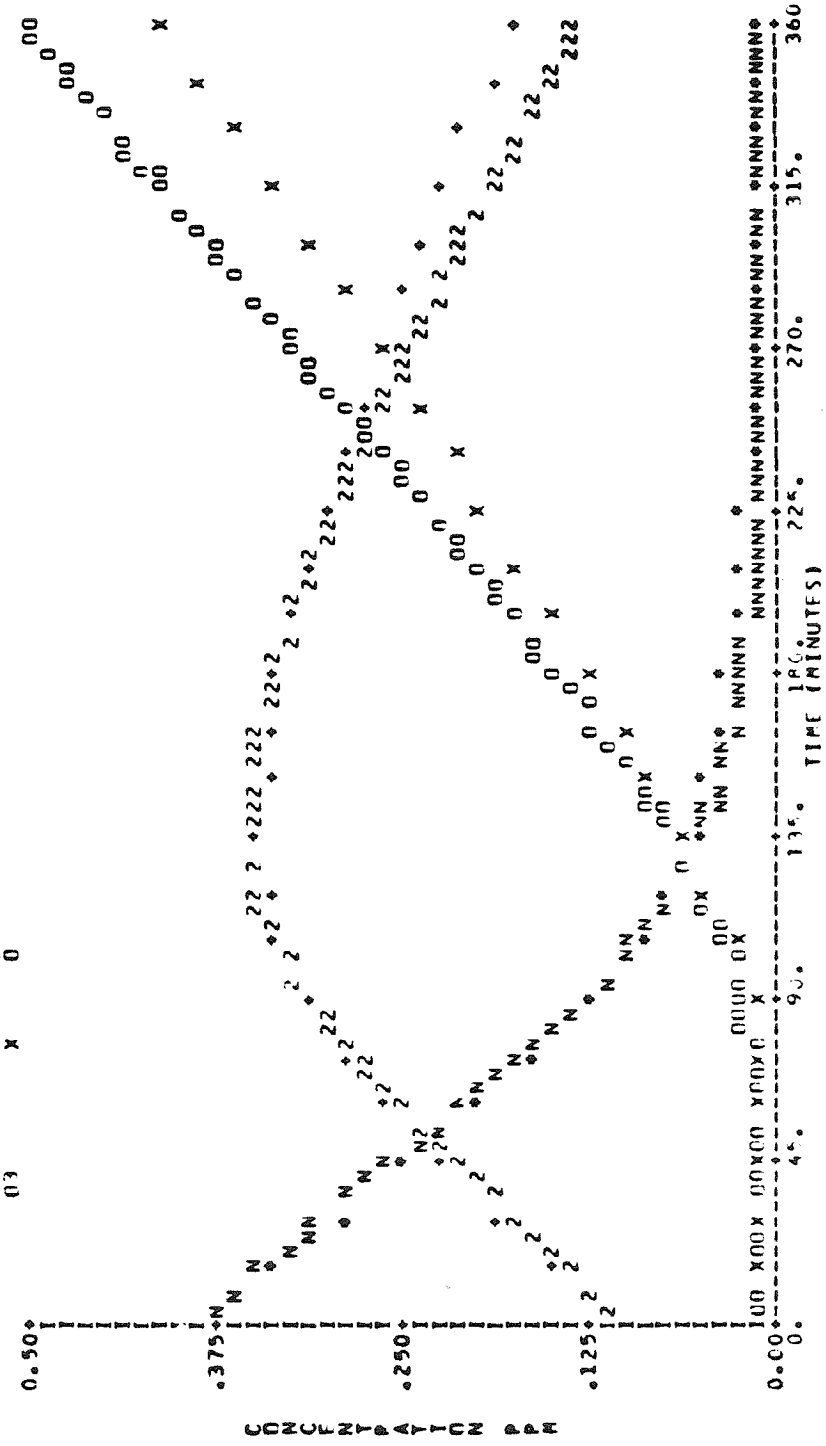

Figure A5a. Observed and Calculated Concentration-Time Profiles for 7-Hydrocarbon-NO_x Experiment EC-241.

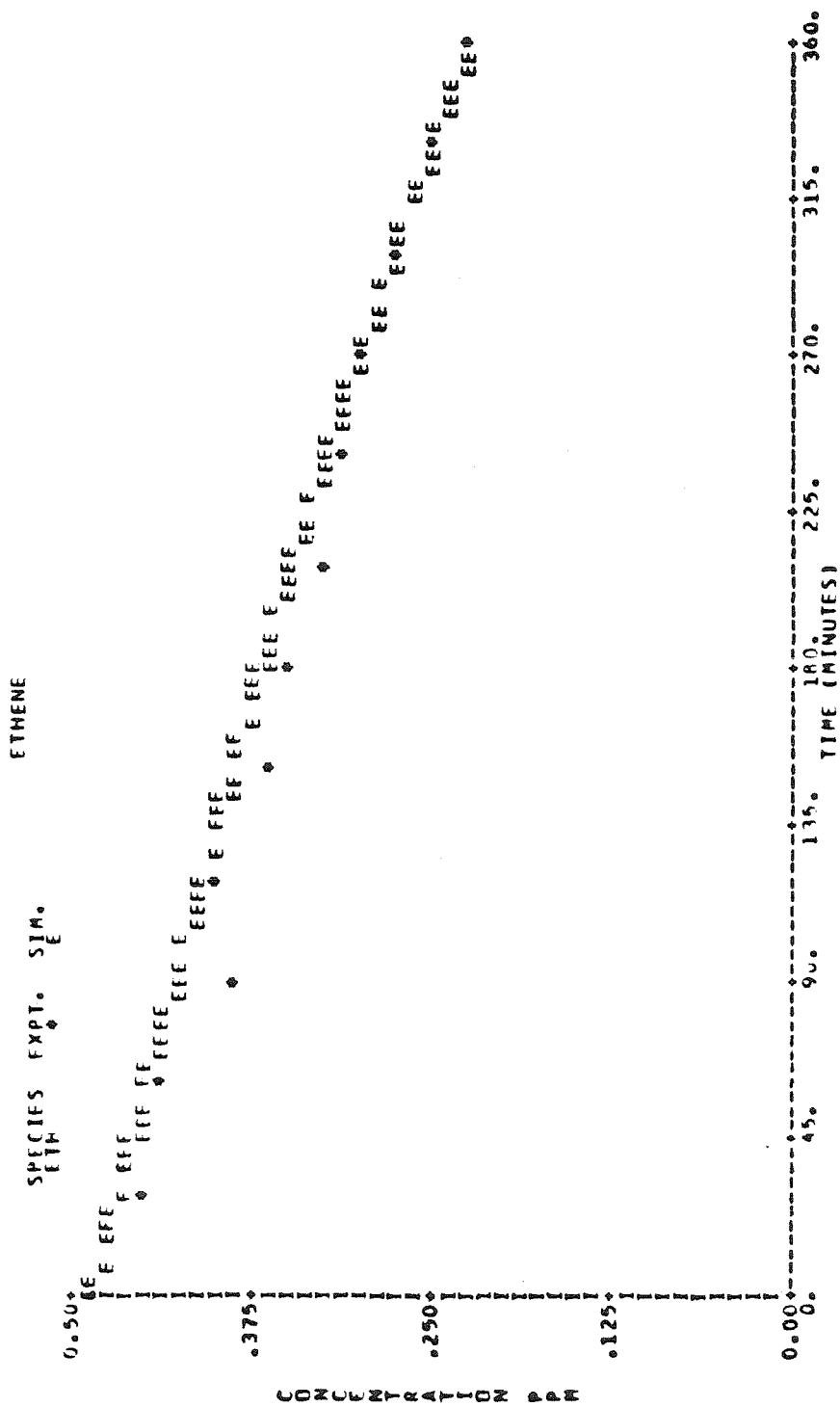

Figure A5b. Observed and Calculated Concentration-Time Profiles for 7-Hydrocarbon-NO_x Experiment EC-241.

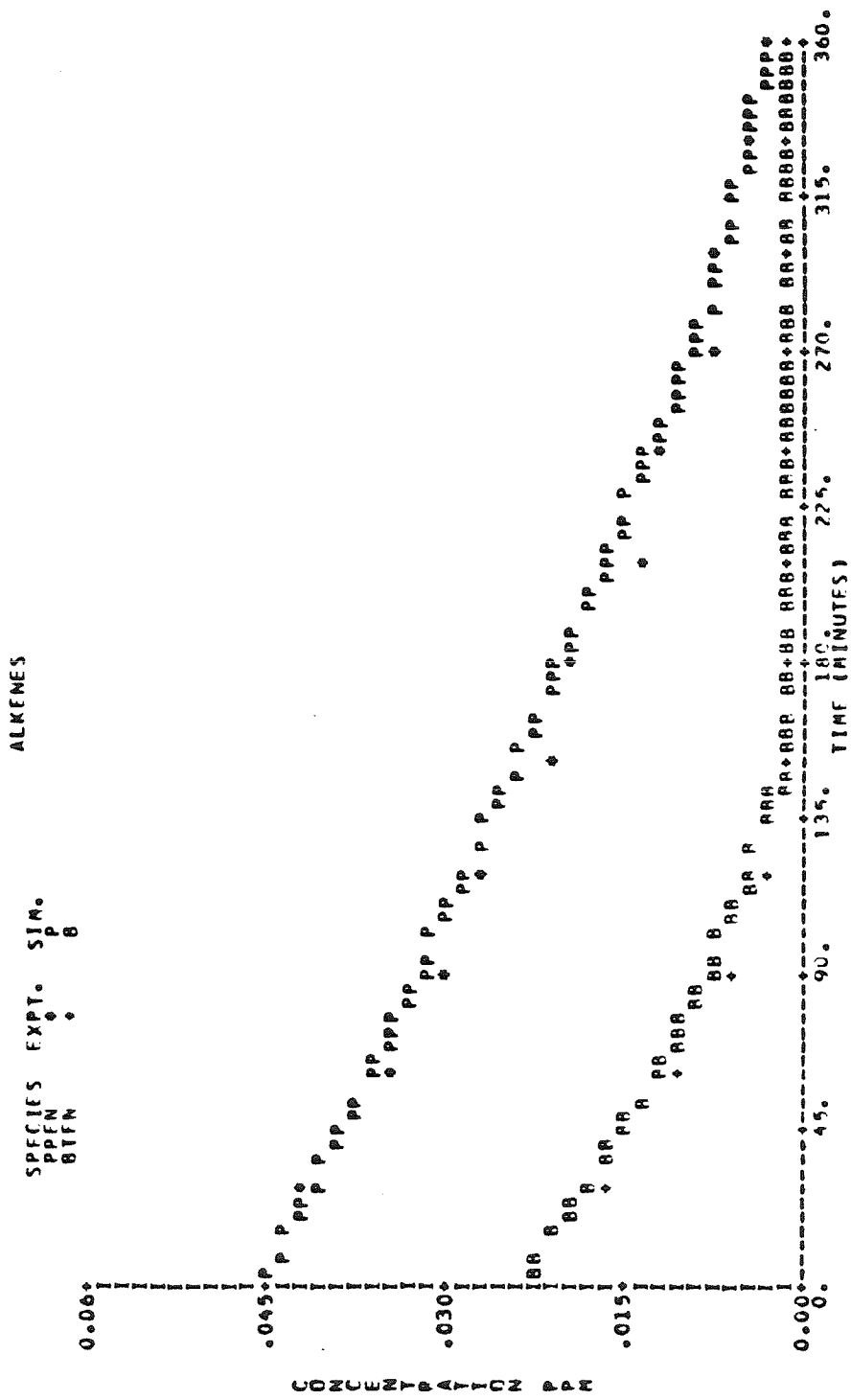

Figure A5c. Observed and Calculated Concentration-Time Profiles for 7-Hydrocarbon-NO_x Experiment EC-241.

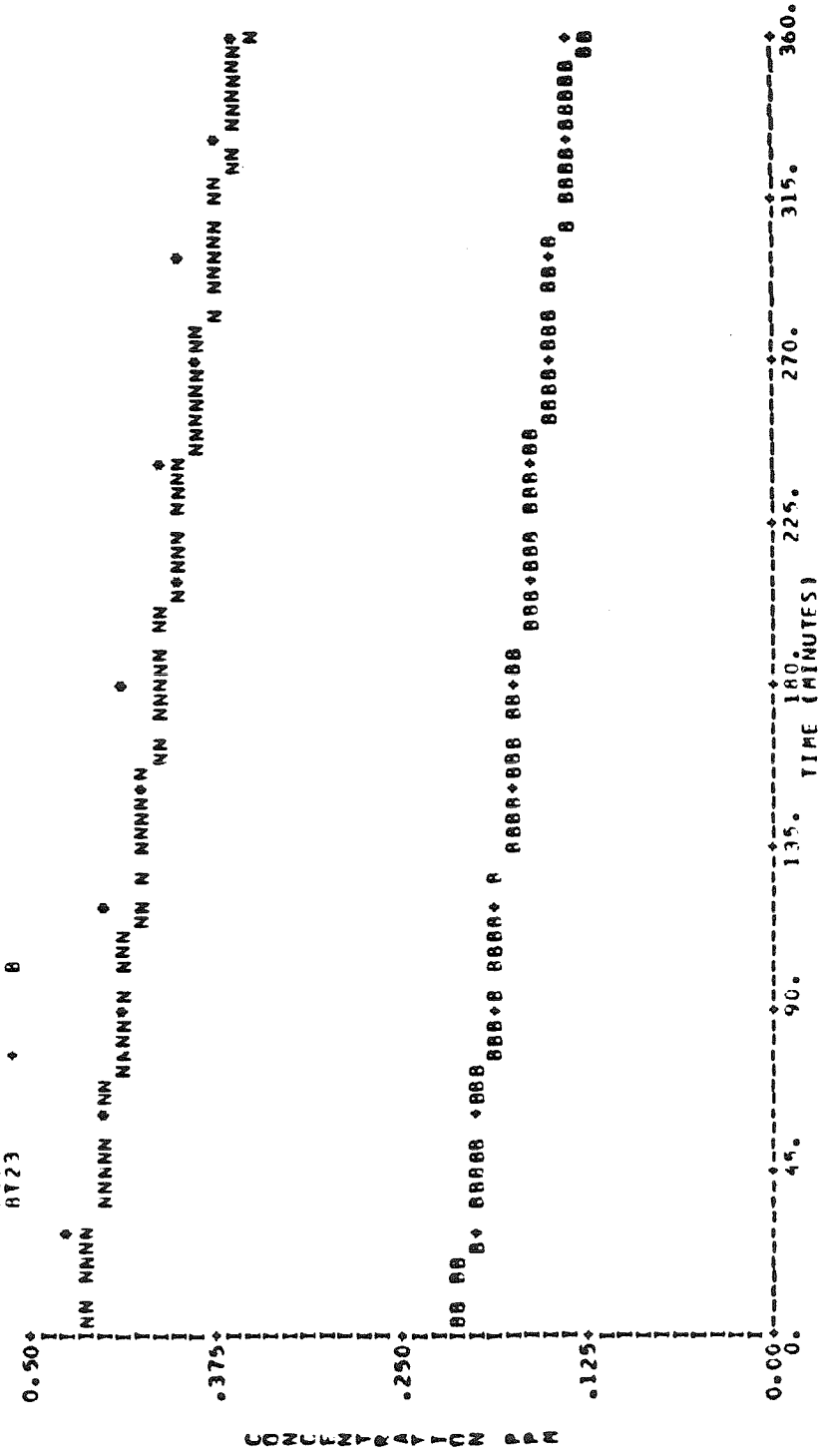

Figure A5d. Observed and Calculated Concentration-Time Profiles for 7-Hydrocarbon-NO_x Experiment EC-241.

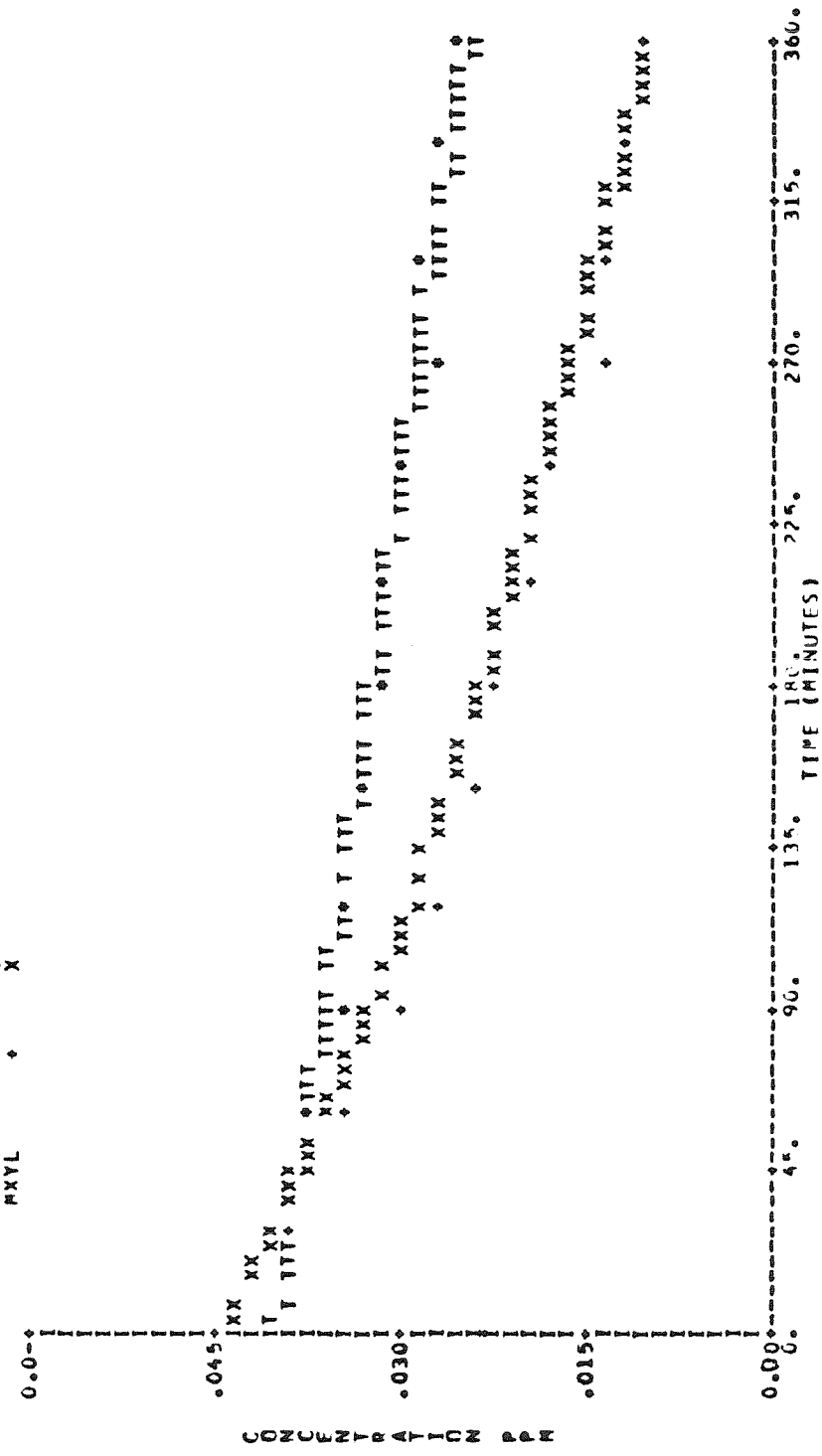

Figure A5e. Observed and Calculated Concentration-Time Profiles for 7-Hydrocarbon-NO_x Experiment EC-241.

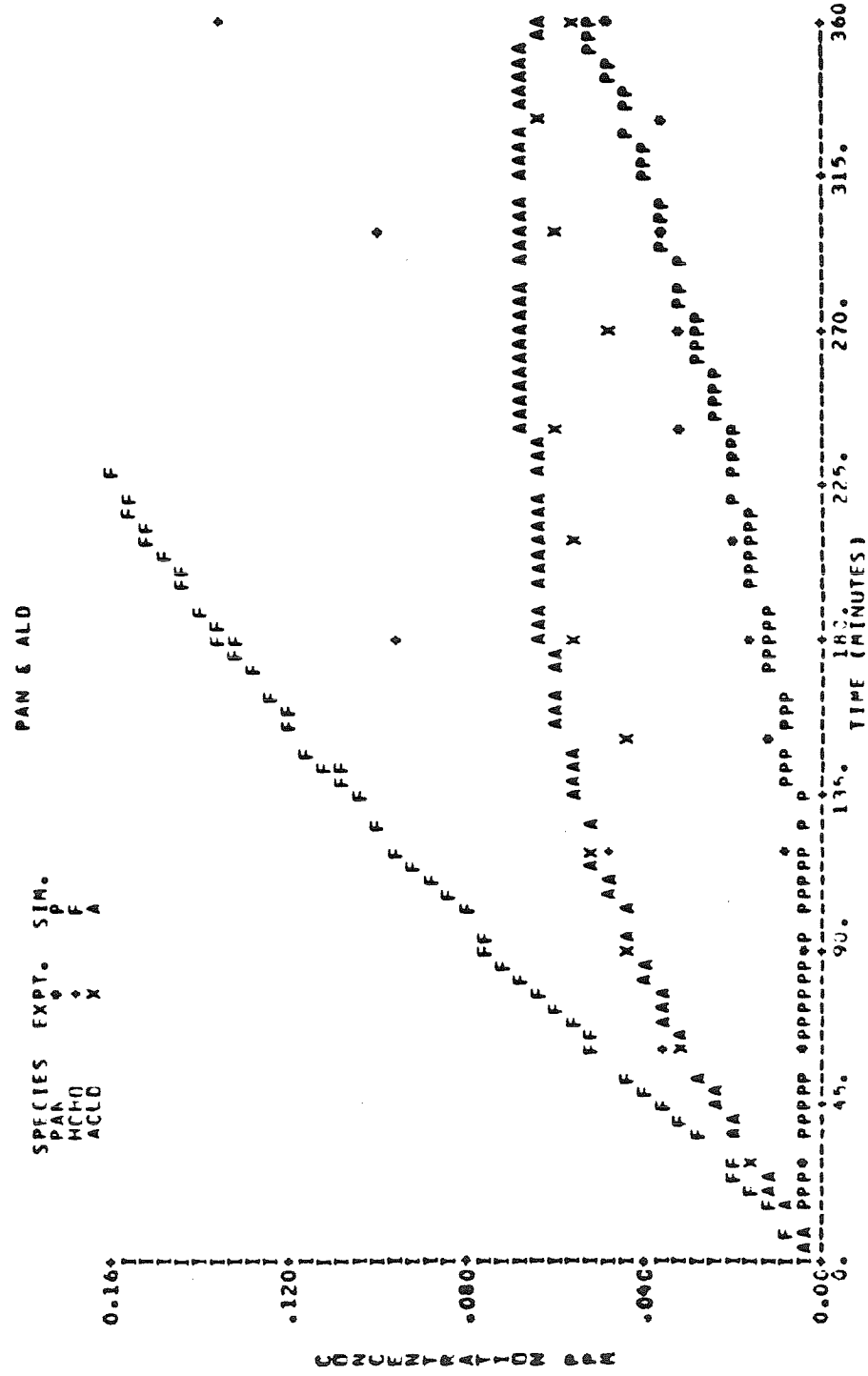

Figure A5f. Observed and Calculated Concentration-Time Profiles for 7-Hydrocarbon-NO_x Experiment EC-241.

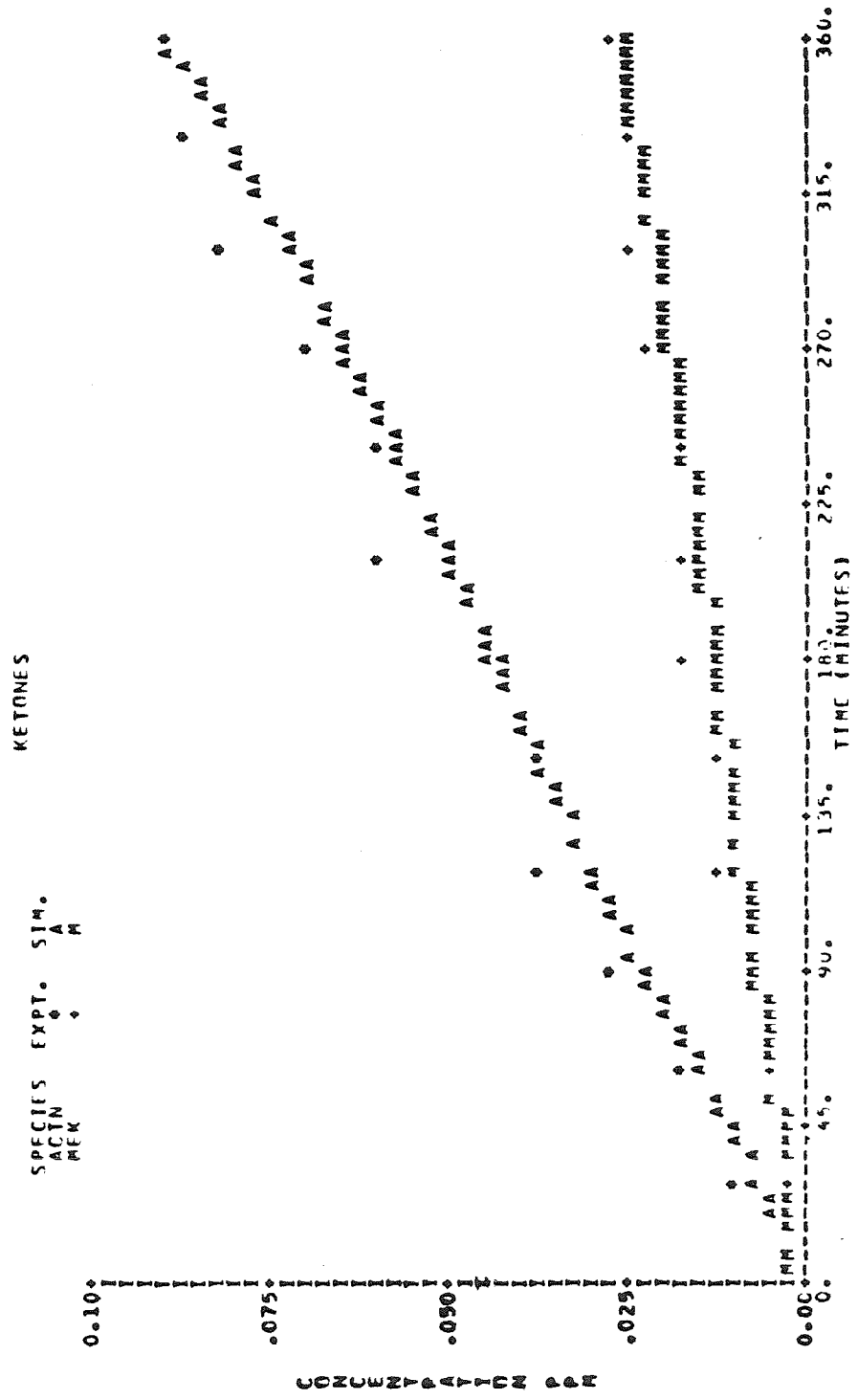

Figure A5g. Observed and Calculated Concentration-Time Profiles for 7-Hydrocarbon-NO_x Experiment EC-241.

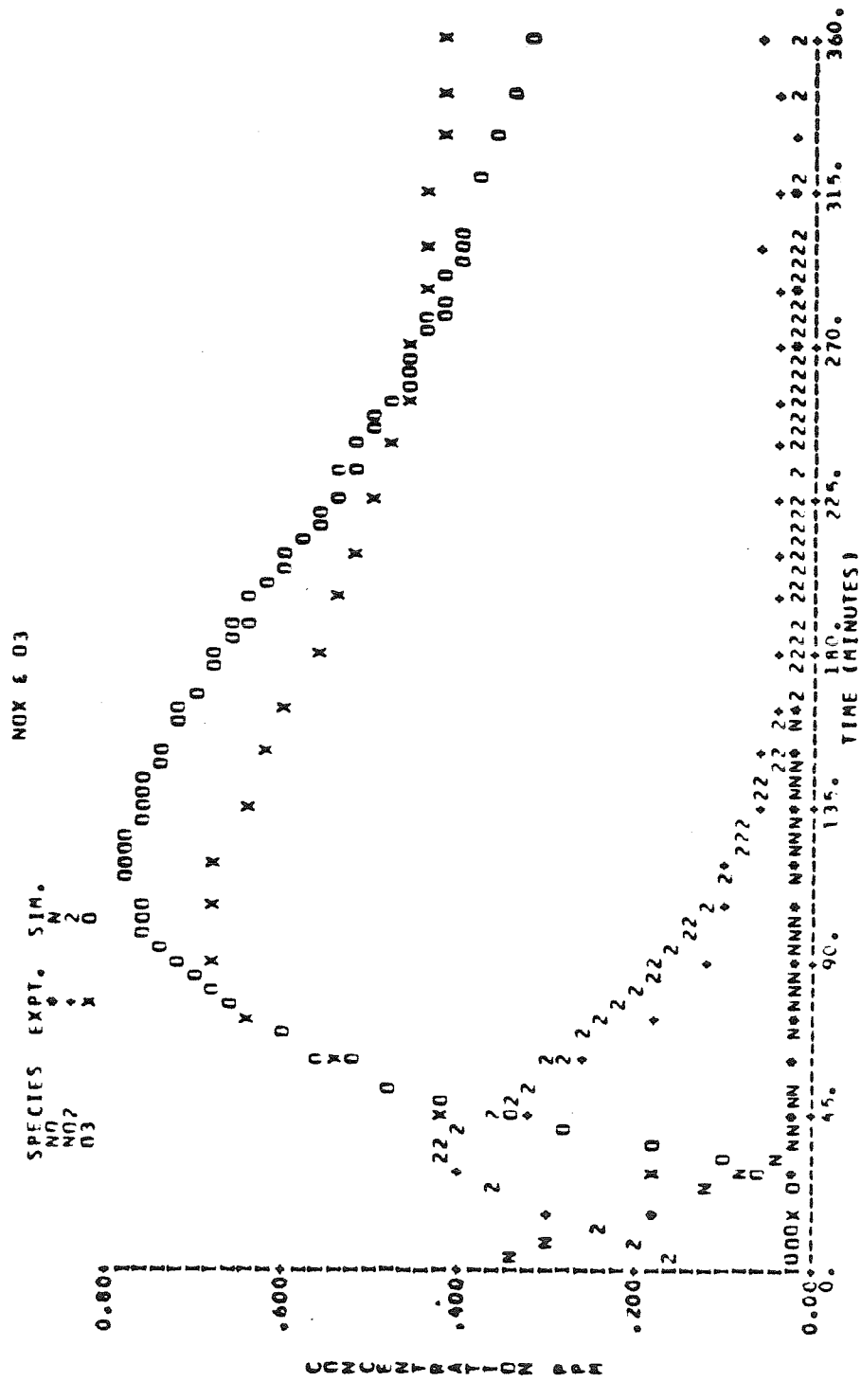

Figure A6a. Observed and Calculated Concentration-Time Profiles for 7-Hydrocarbon-NO_x Experiment EC-242.

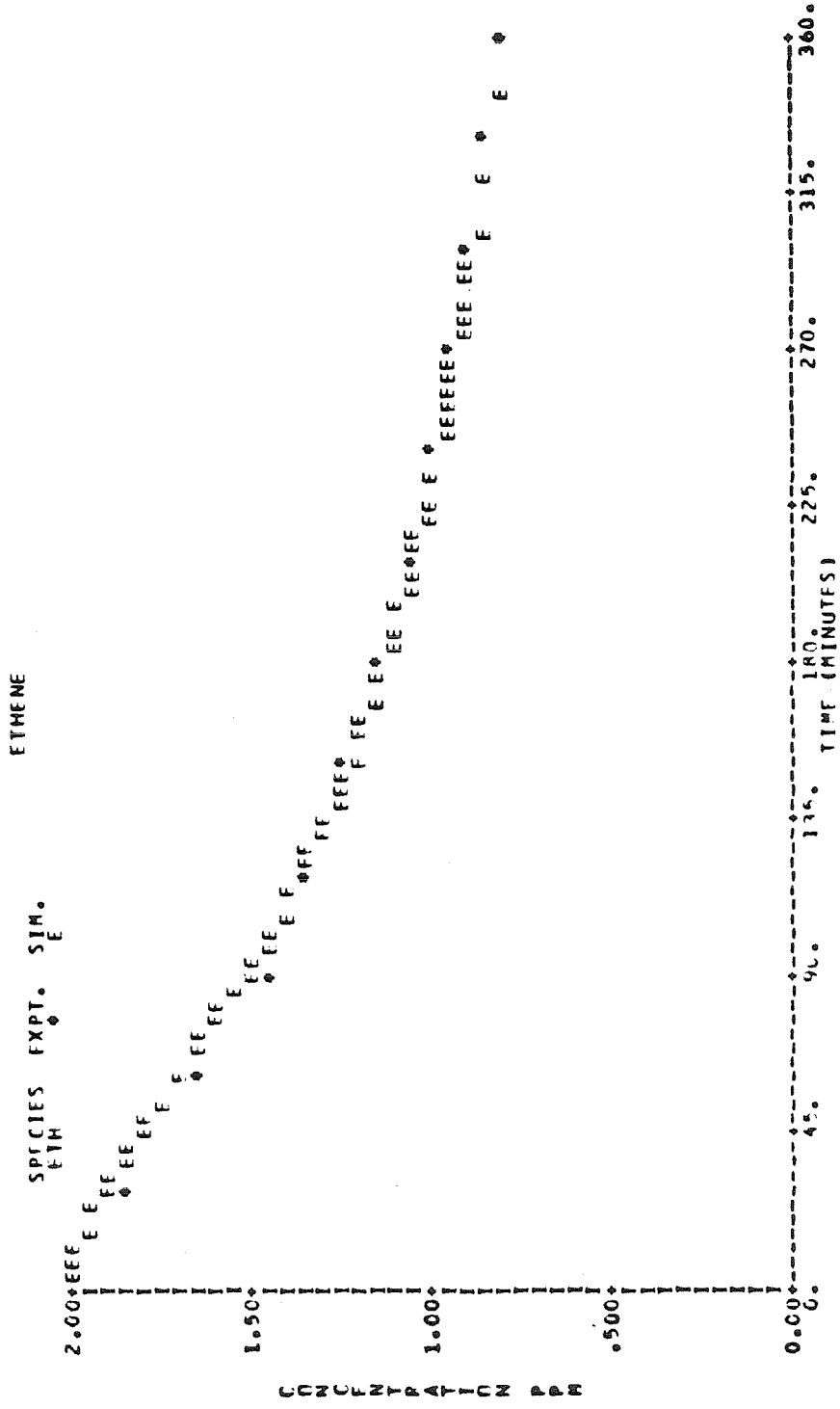

Figure A6b. Observed and Calculated Concentration-Time Profiles for 7-Hydrocarbon-NO_x Experiment EC-242.

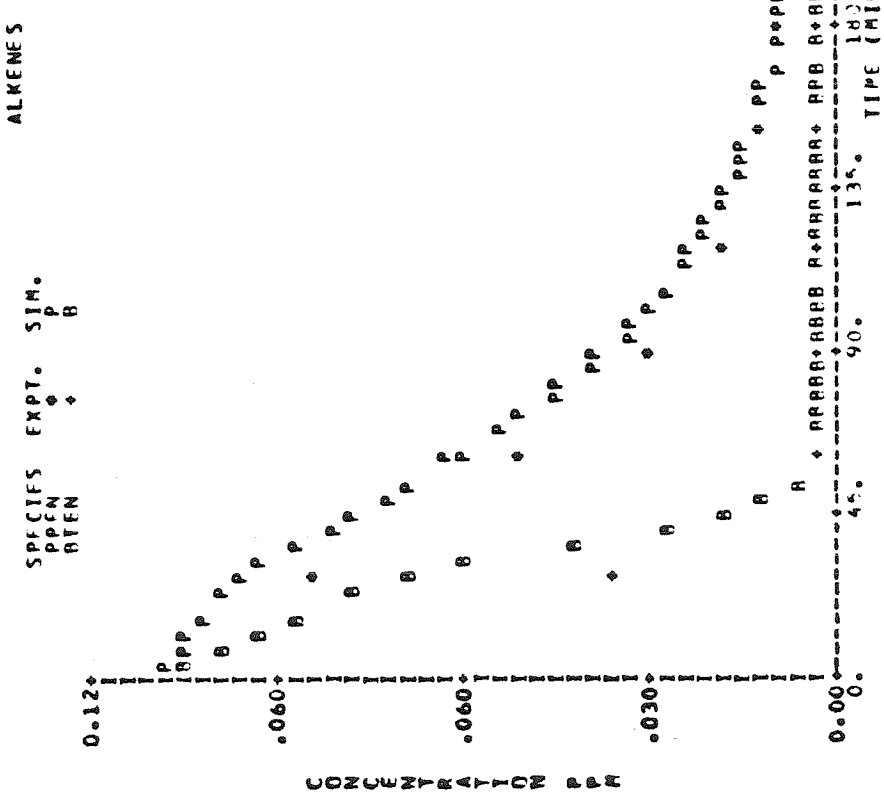

Figure A6c. Observed and Calculated Concentration-Time Profiles for 7-Hydrocarbon-NO_x Experiment EC-242.

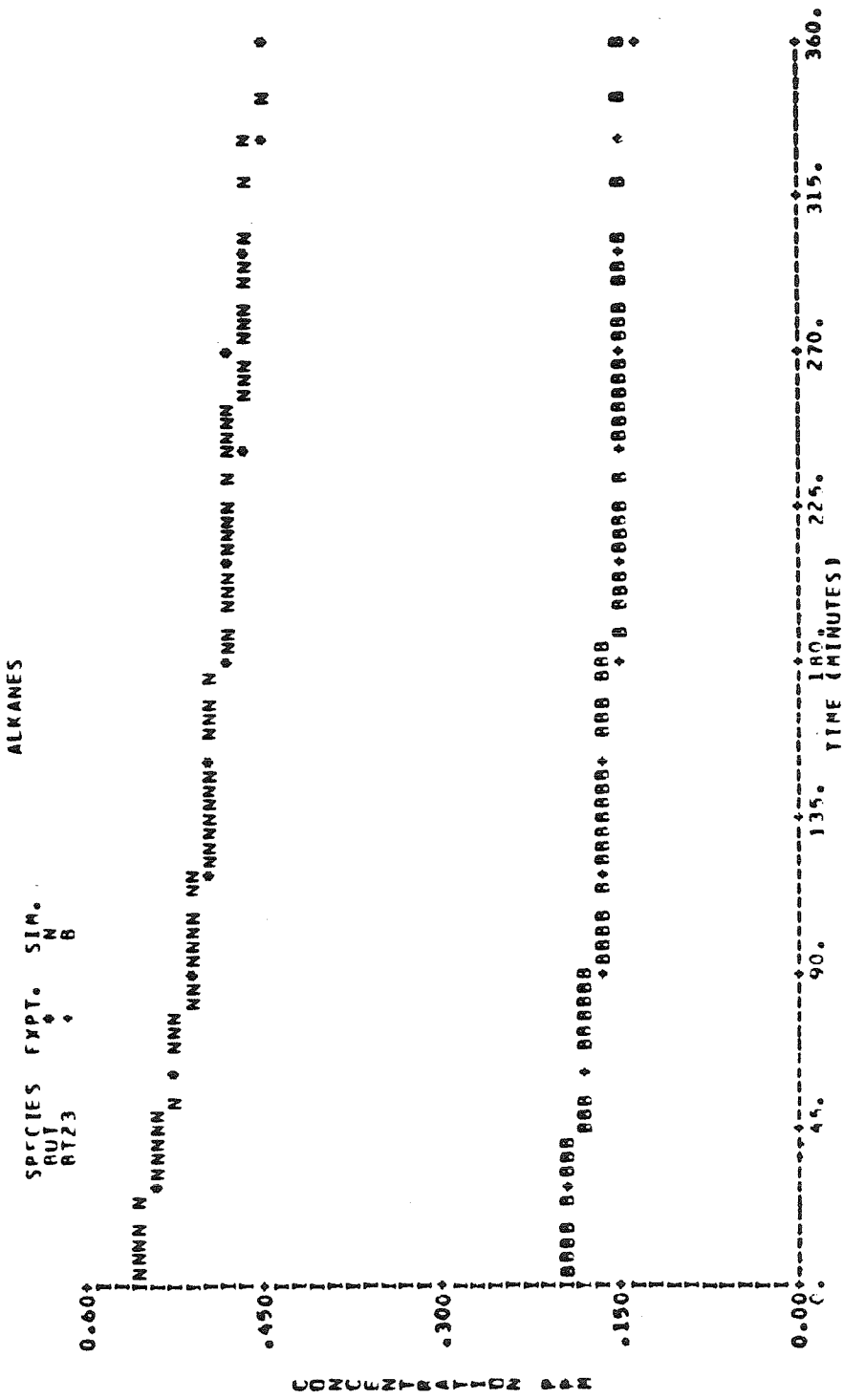

Figure A6d. Observed and Calculated Concentration-Time Profiles for 7-Hydrocarbon-NO_x Experiment EC-242.

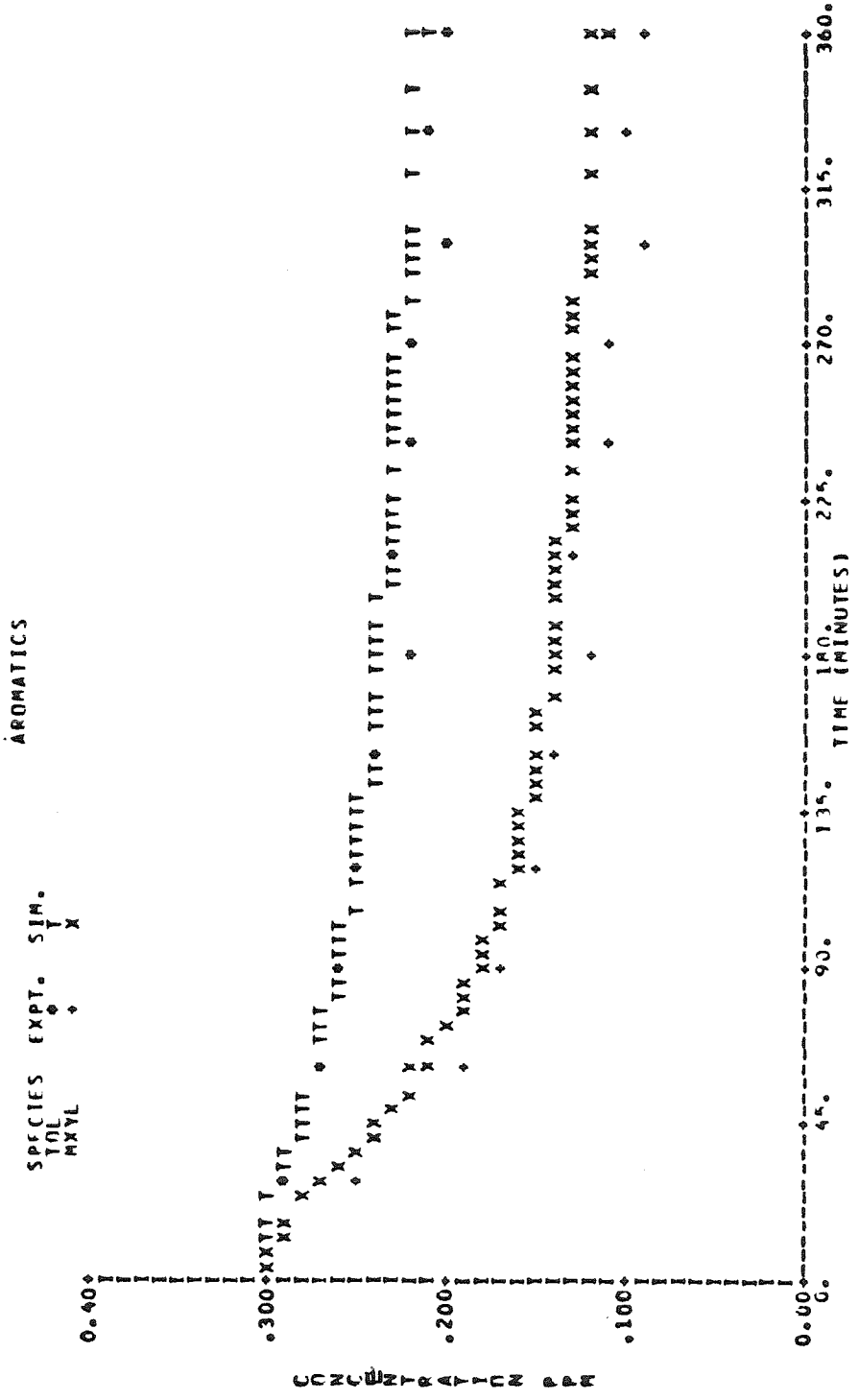

Figure A6e. Observed and Calculated Concentration-Time Profiles for 7-Hydrocarbon-NO_x Experiment EC-242.

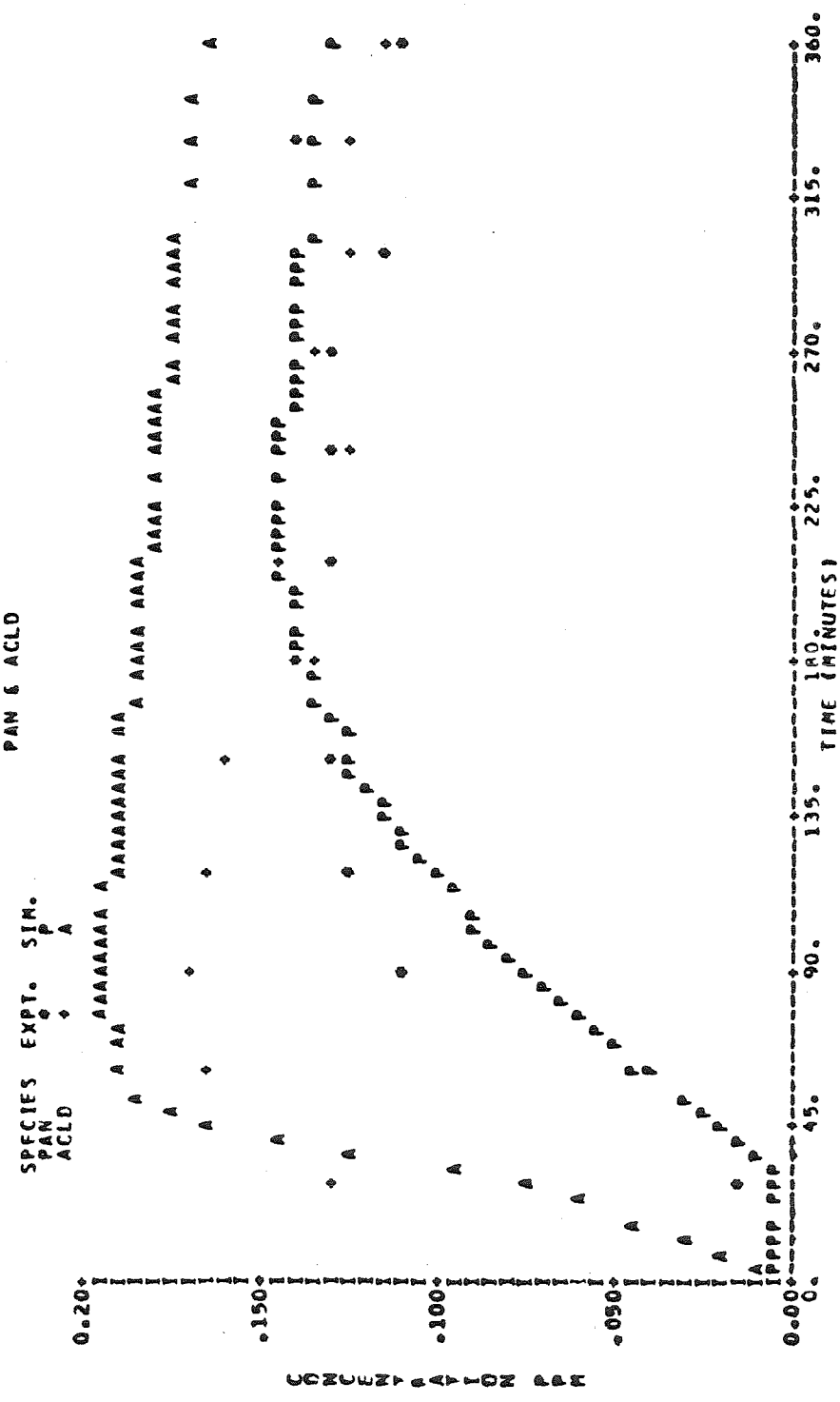

Figure A6f. Observed and Calculated Concentration-Time Profiles for 7-Hydrocarbon-NO_x Experiment EC-242.

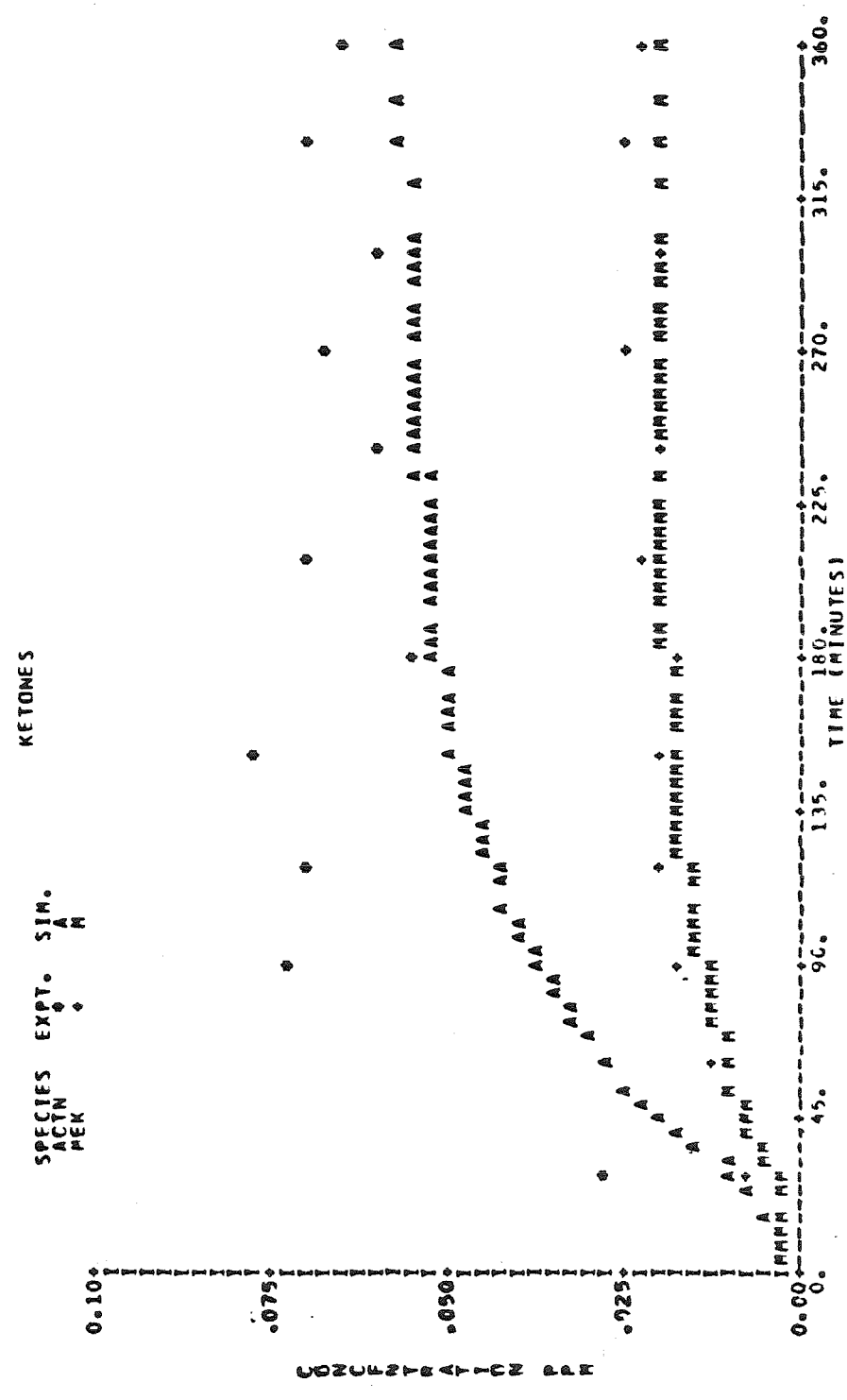

Figure A6g. Observed and Calculated Concentration-Time Profiles for 7-Hydrocarbon-NO_x Experiment EC-242.

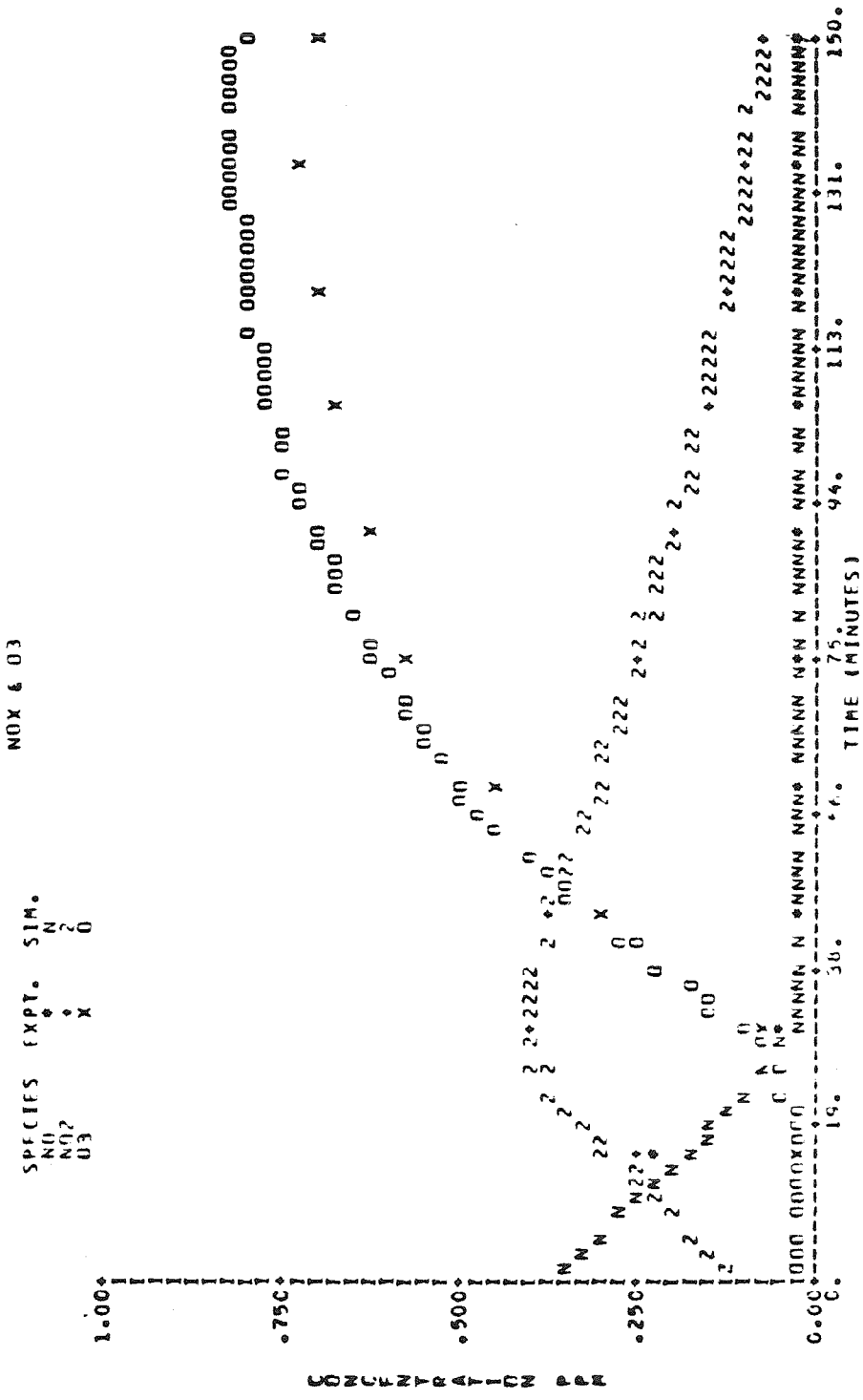

Figure A7a. Observed and Calculated Concentration-Time Profiles for 7-Hydrocarbon-NO_x Experiment EC-243.

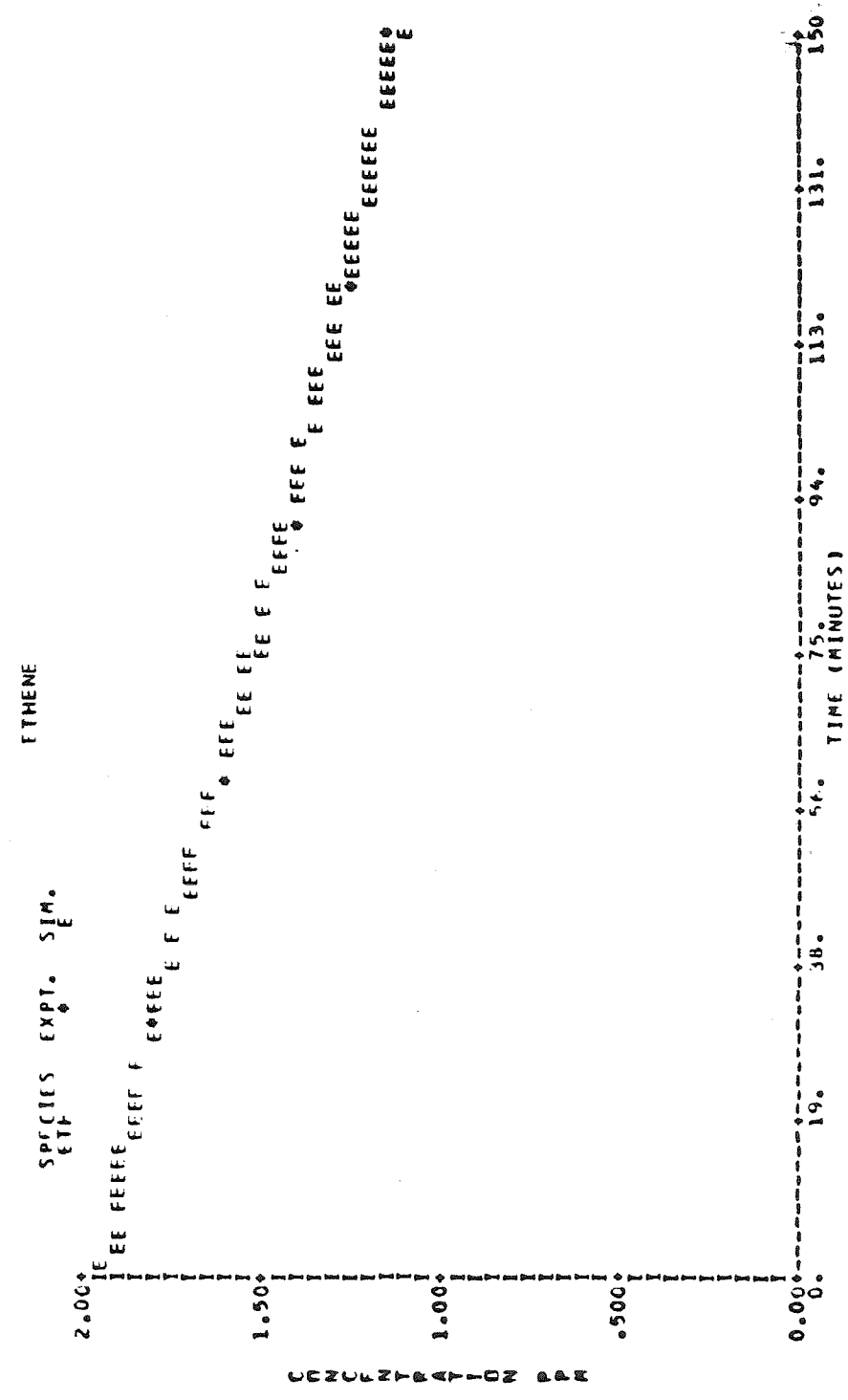

Figure A7b. Observed and Calculated Concentration-Time Profiles for 7-Hydrocarbon-NO_x Experiment EC-243.

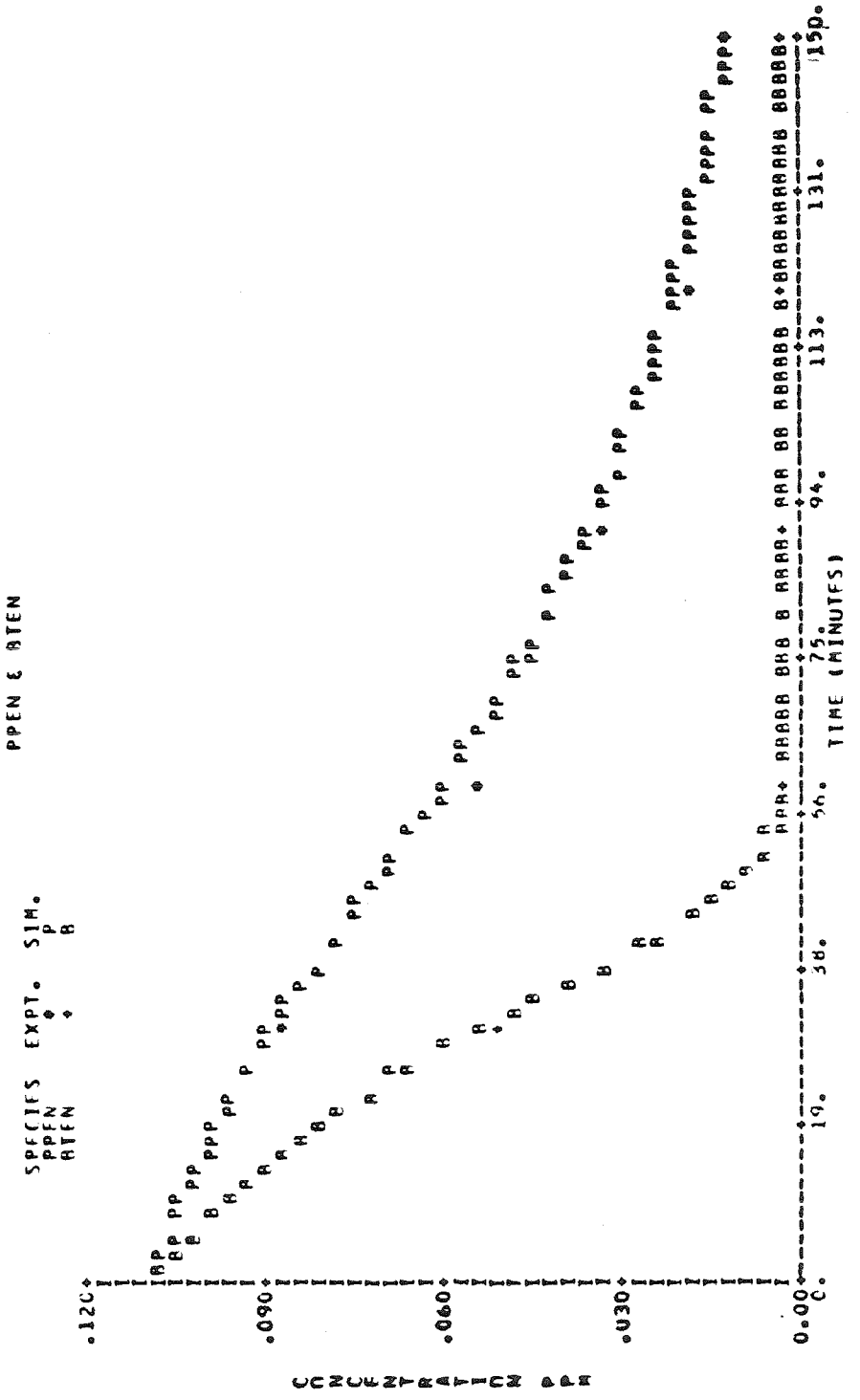

Figure A7c. Observed and Calculated Concentration-Time Profiles for 7-Hydrocarbon-NO_x Experiment EC-243.

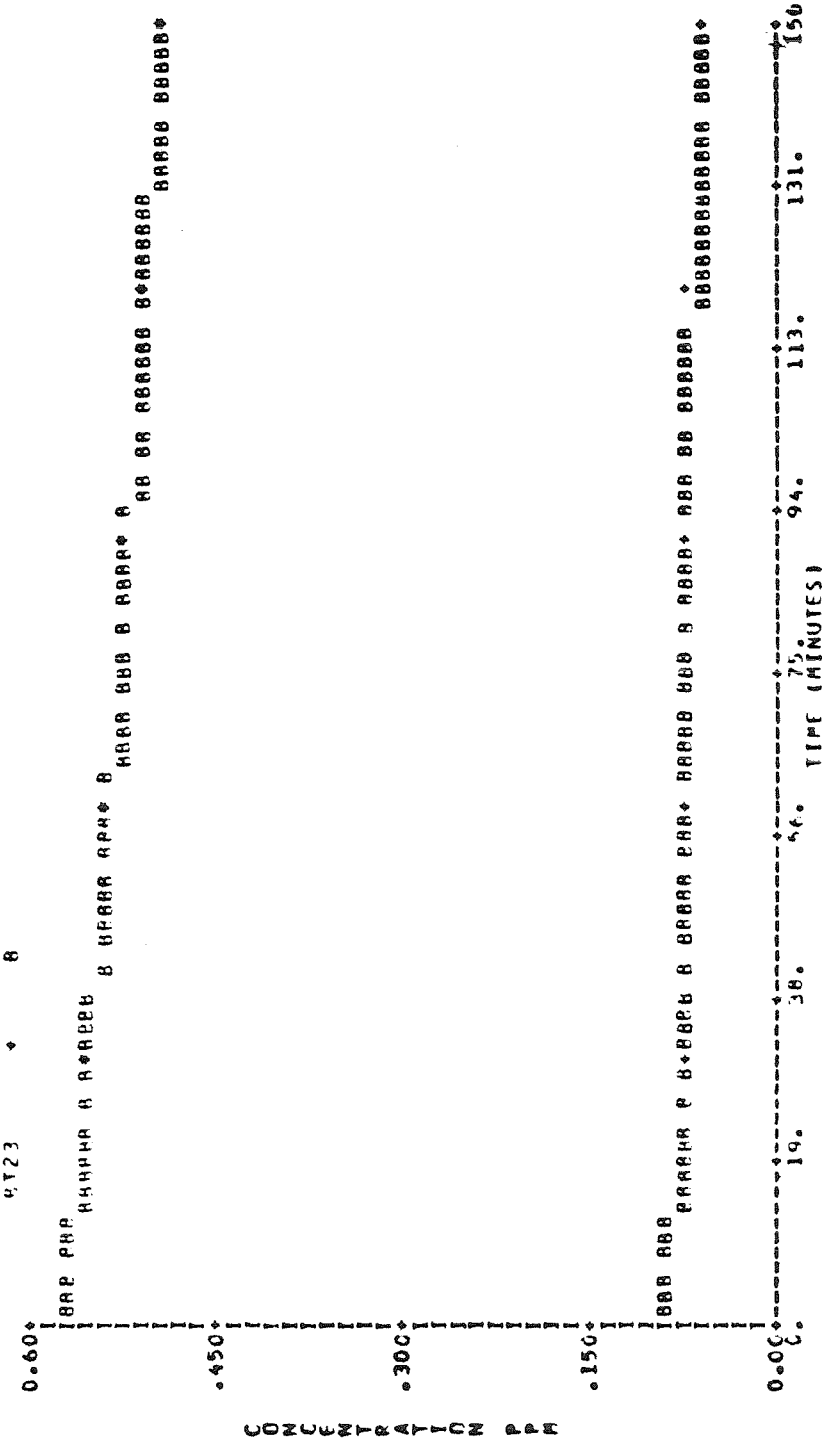

Figure A7d. Observed and Calculated Concentration-Time Profiles for 7-Hydrocarbon-NO_x Experiment EC-243.

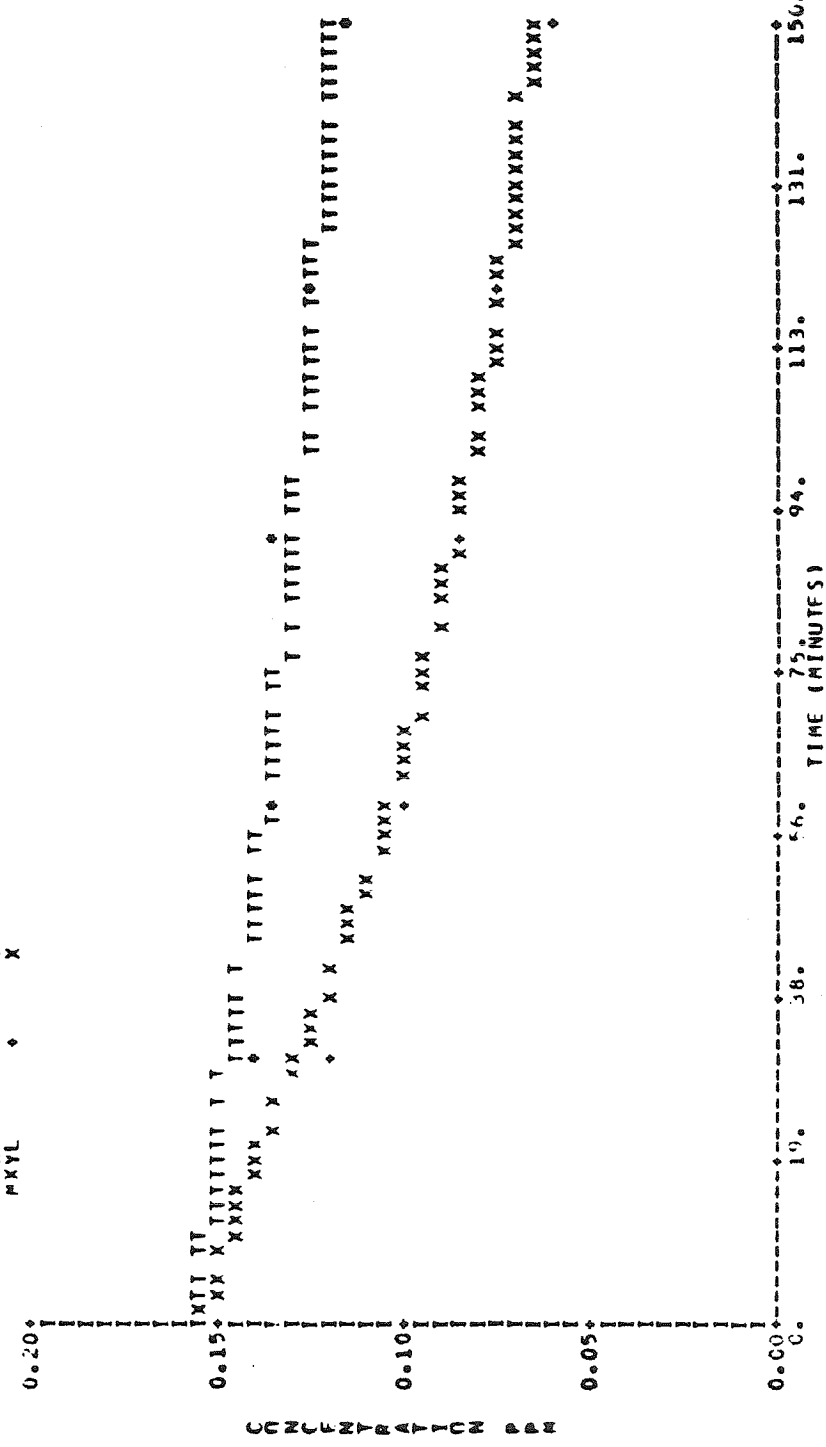

Figure A7e. Observed and Calculated Concentration-Time Profiles for 7-Hydrocarbon-NO_x Experiment EC-243.

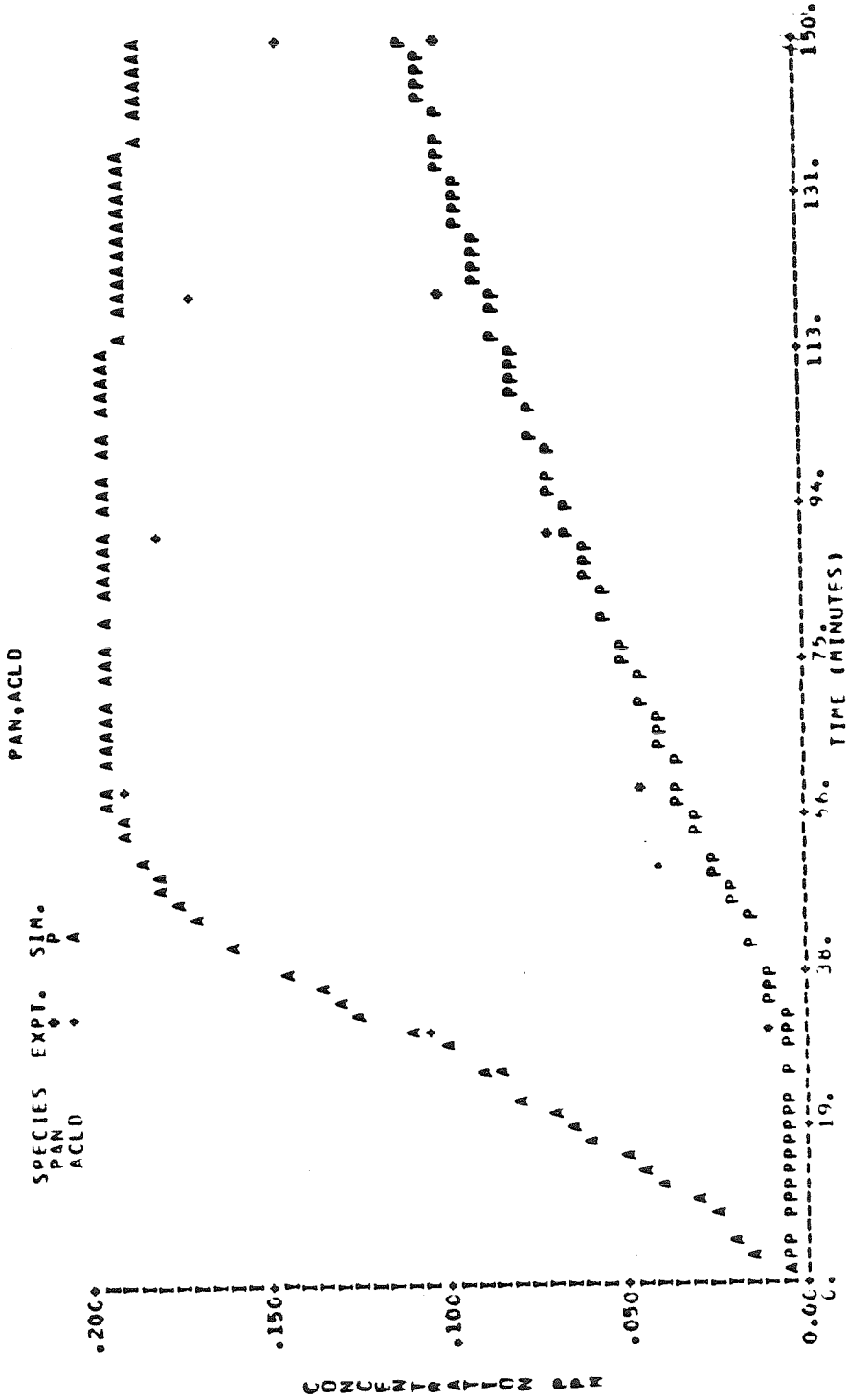

Figure A7f. Observed and Calculated Concentration-Time Profiles for 7-Hydrocarbon-NO_x Experiment EC-243.

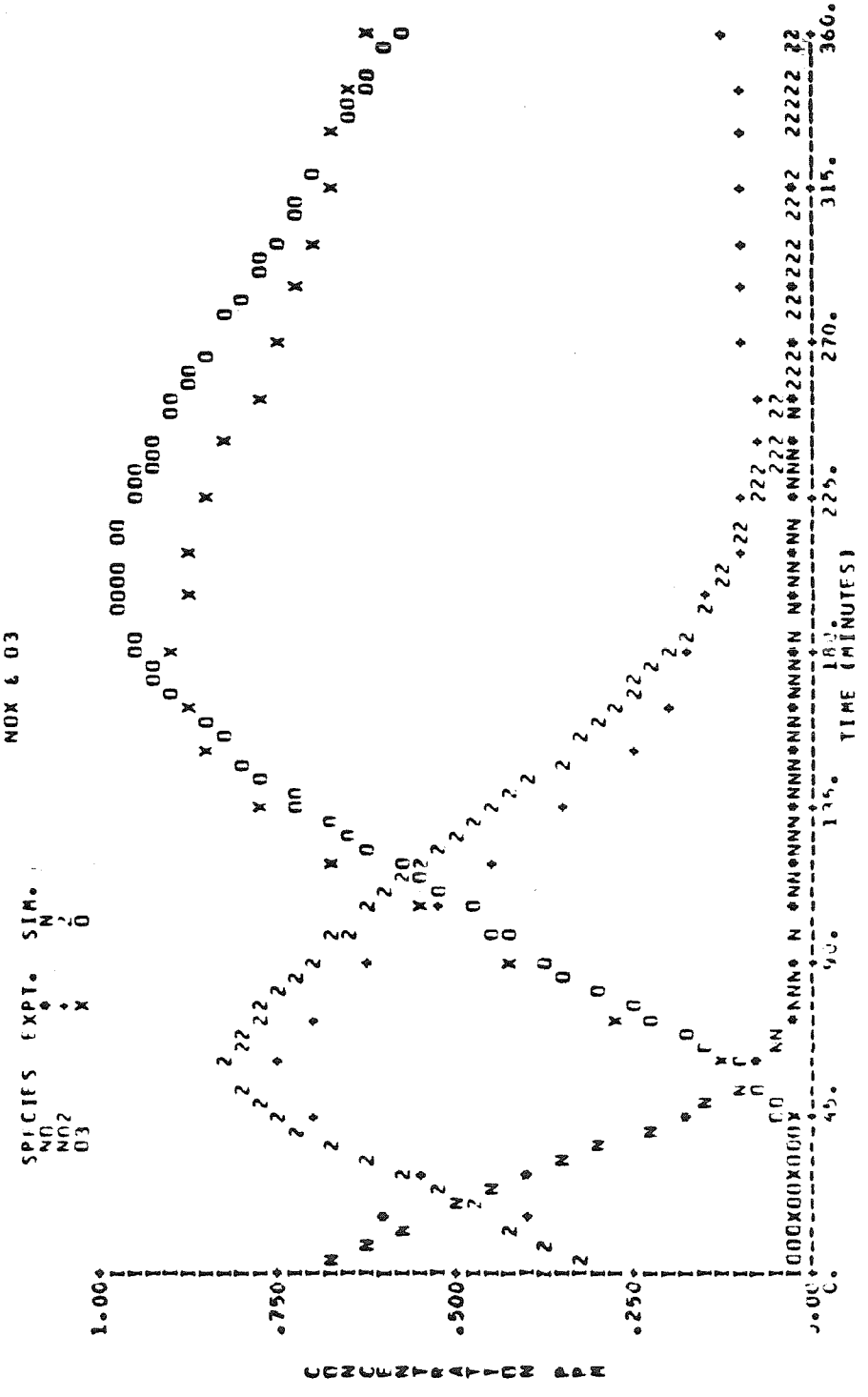

Figure A8a. Observed and Calculated Concentration-Time Profiles for 7-Hydrocarbon-NO_x Experiment EC-245.

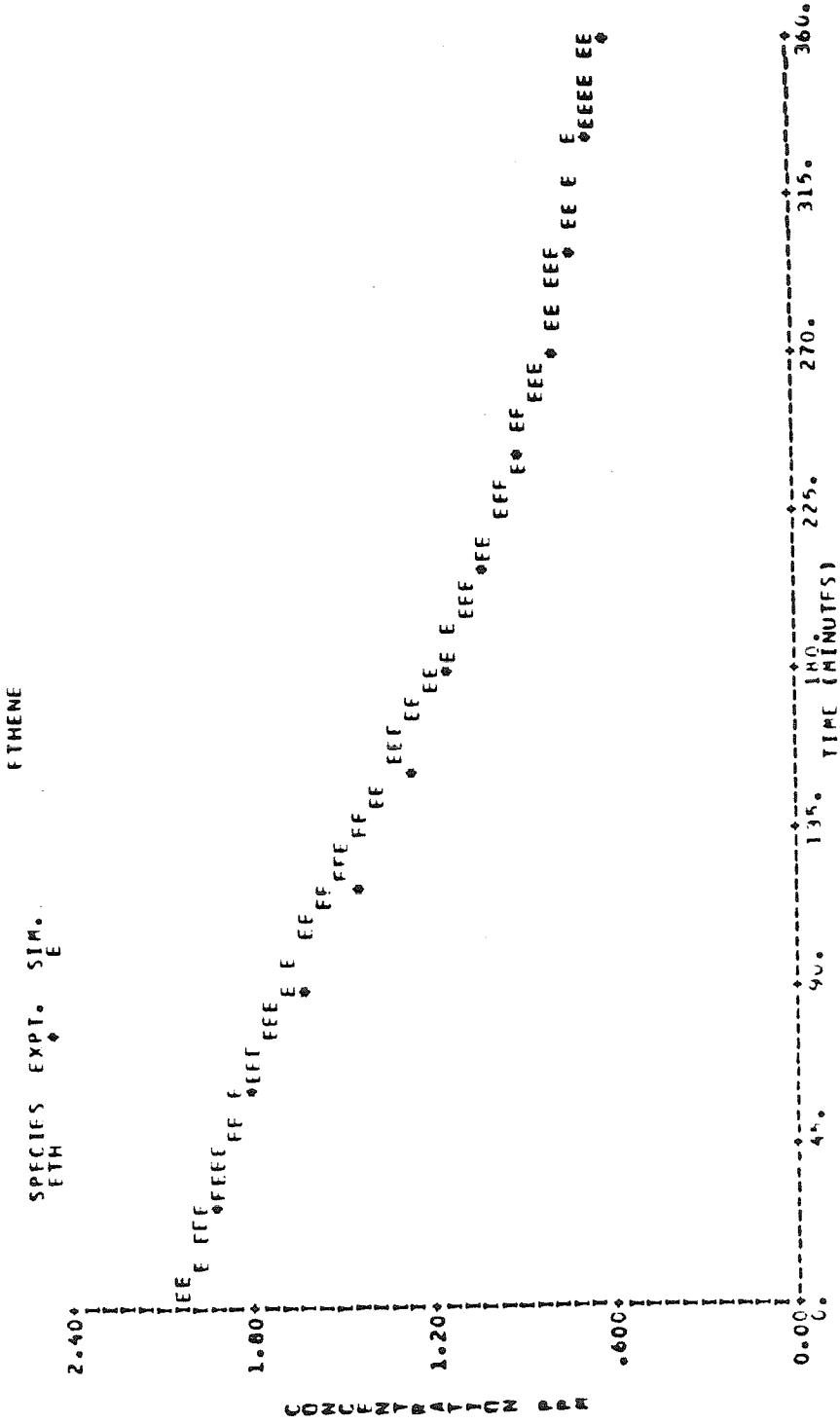

Figure A8b. Observed and Calculated Concentration-Time Profiles for 7-Hydrocarbon-NO_x Experiment EC-245.

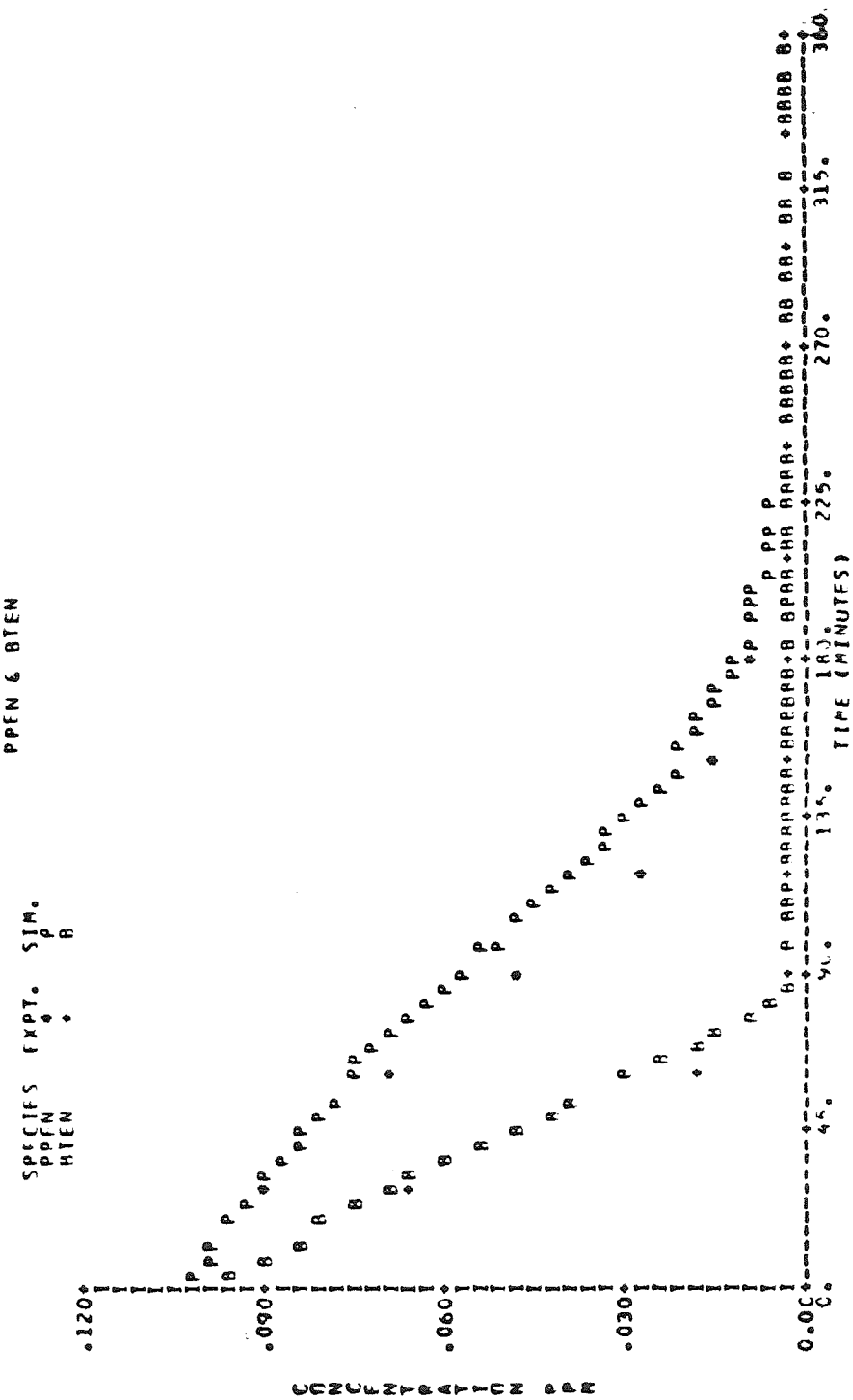

Figure A8c. Observed and Calculated Concentration-Time Profiles for 7-Hydrocarbon-NO_x Experiment EC-245.

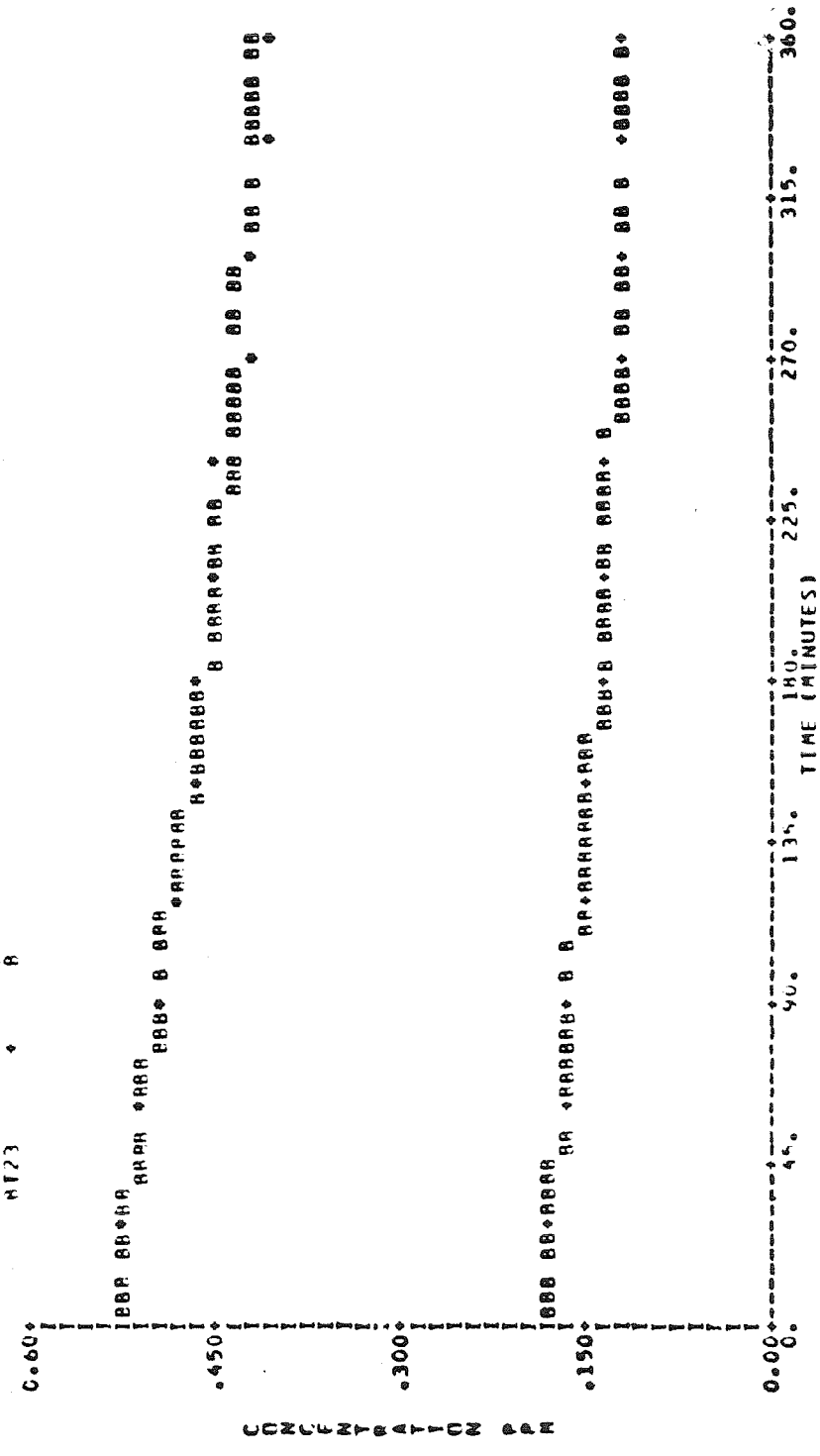

Figure A8d. Observed and Calculated Concentration-Time Profiles for 7-Hydrocarbon-NO_x Experiment EC-245.

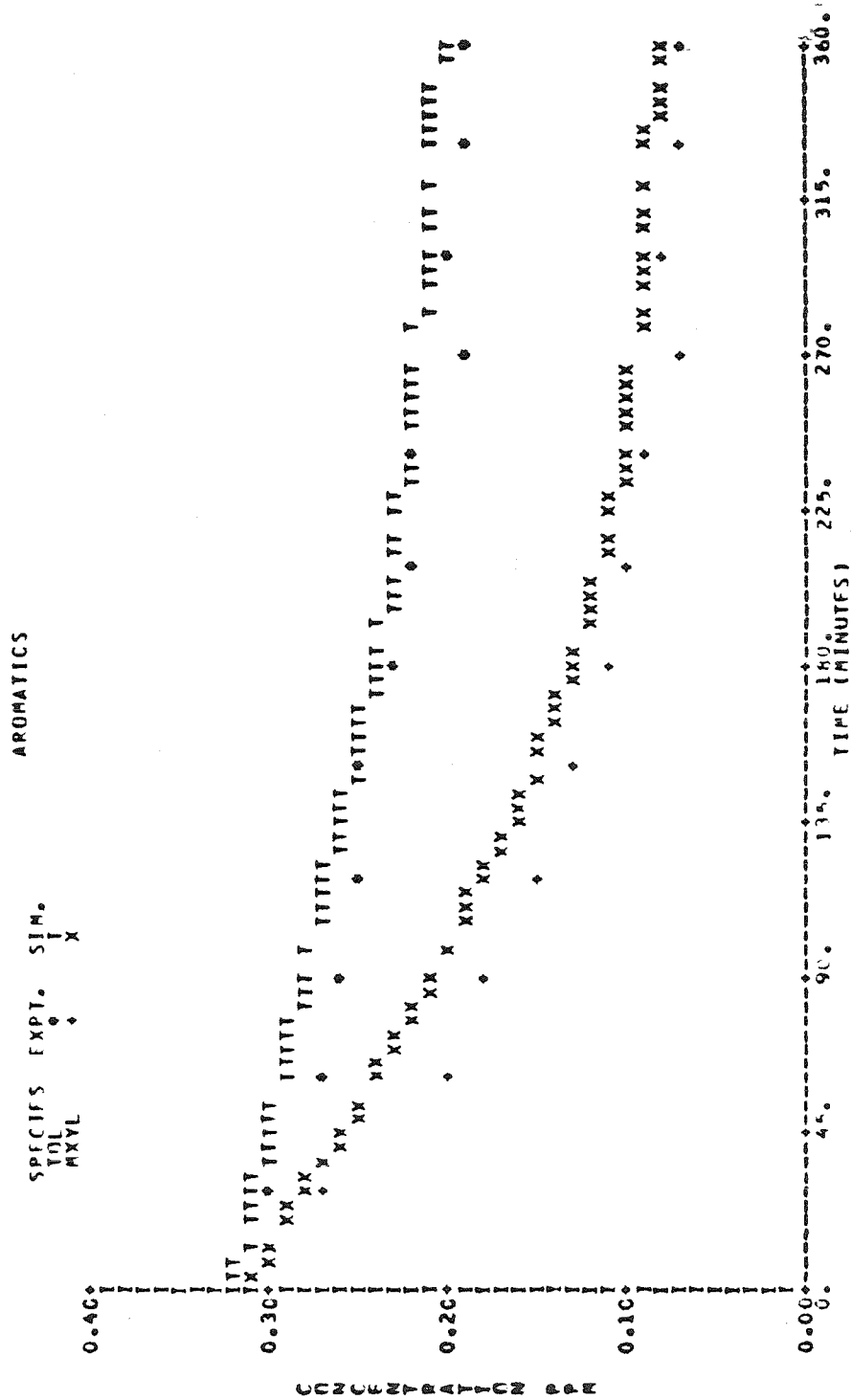

Figure A8e. Observed and Calculated Concentration-Time Profiles for 7-Hydrocarbon-NO_x Experiment EC-245.

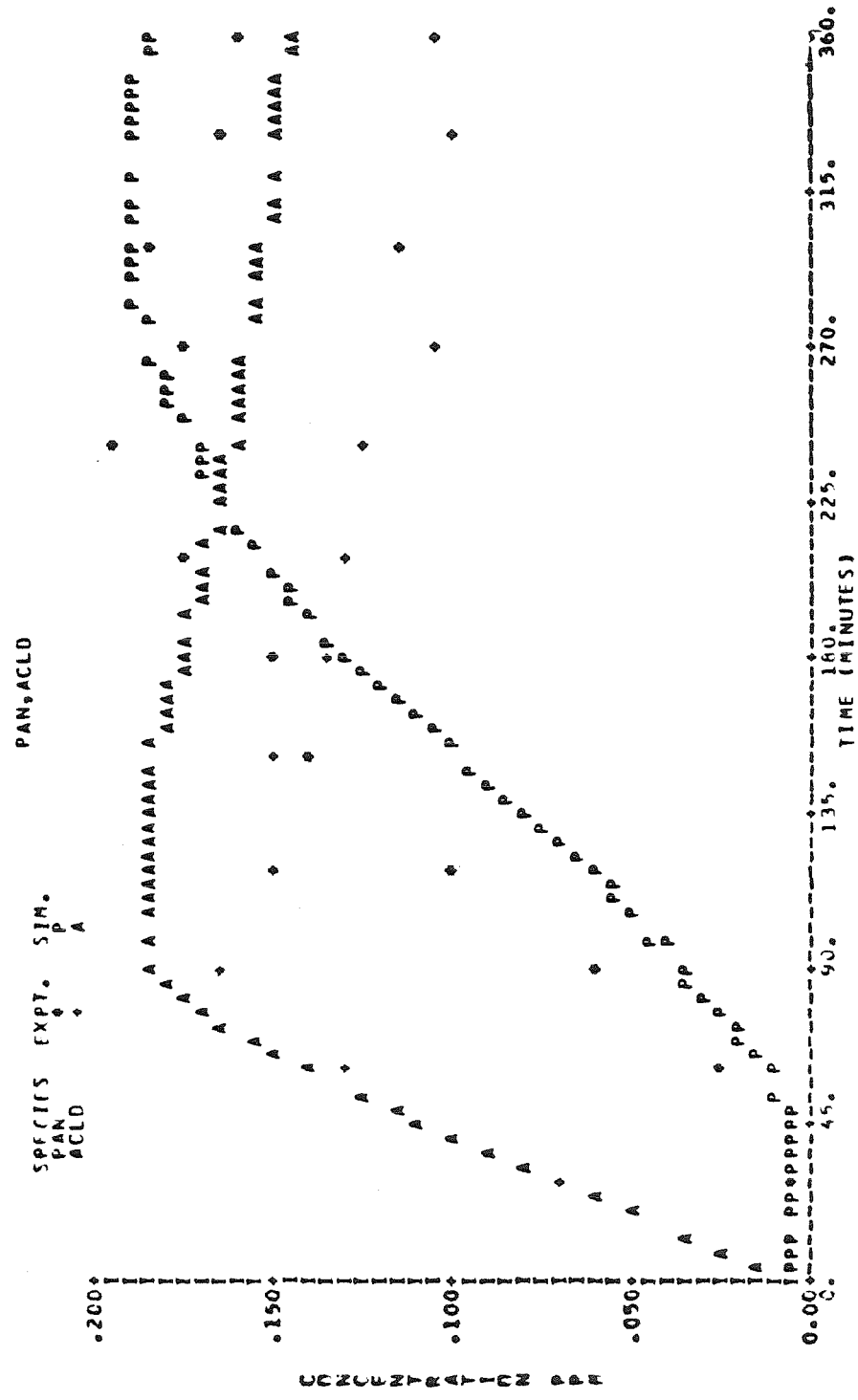

Figure A8f. Observed and Calculated Concentration-Time Profiles for 7-Hydrocarbon-NO_x Experiment EC-245.

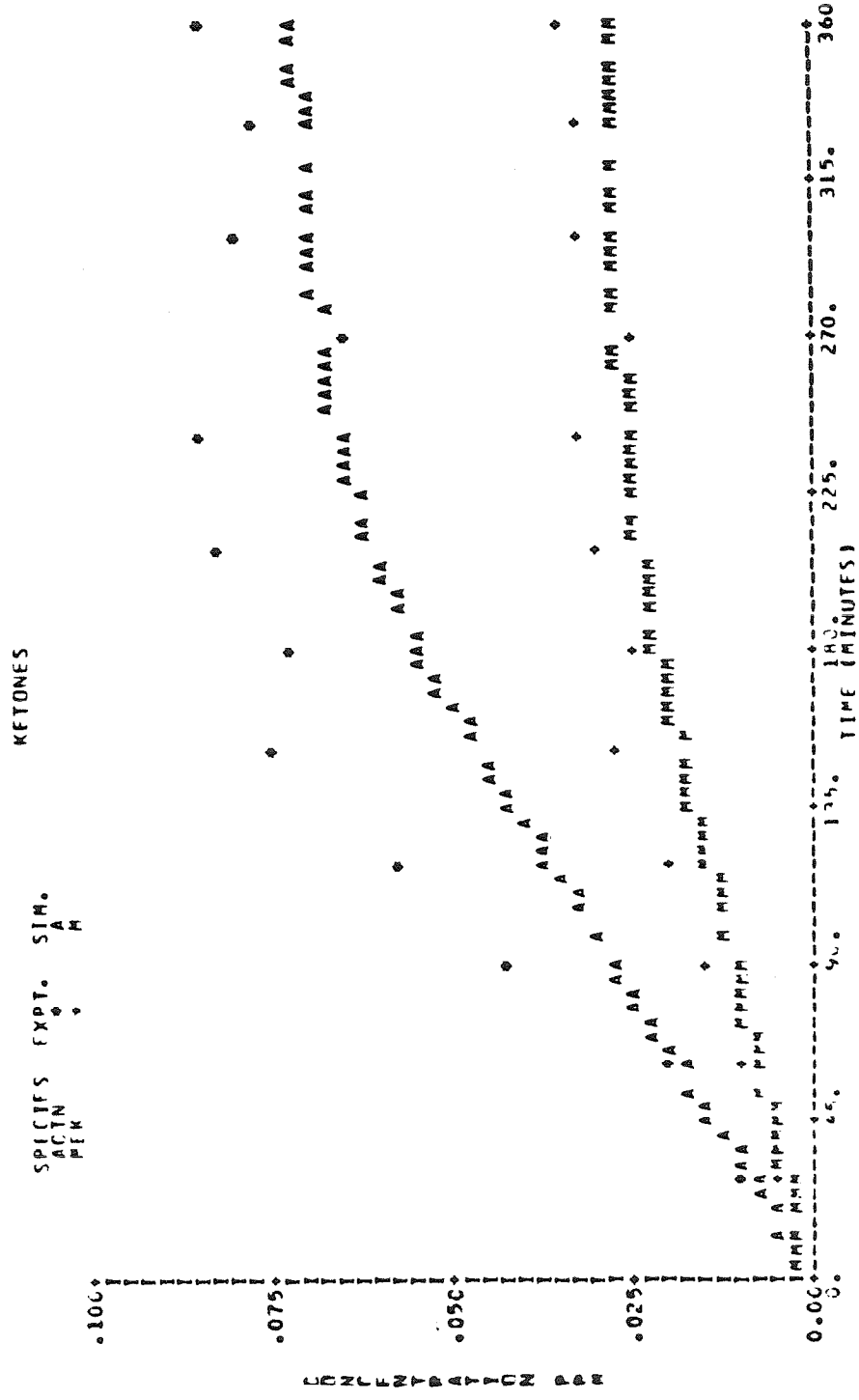

Figure A8g. Observed and Calculated Concentration-Time Profiles for 7-Hydrocarbon-NO_x Experiment EC-245.

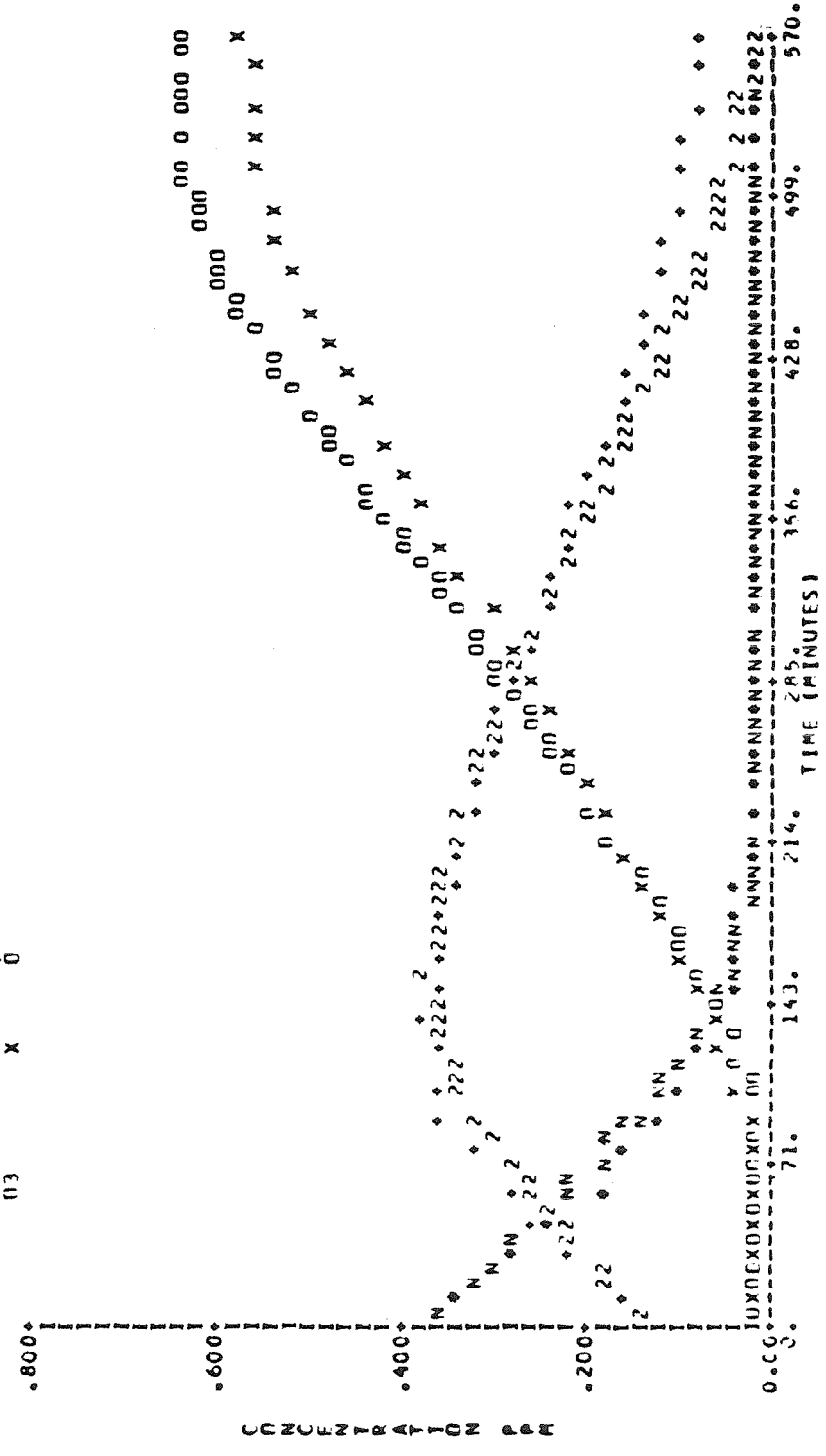

Figure A9a. Observed and Calculated Concentration-Time Profiles for 7-Hydrocarbon-NO_x Experiment EC-246.

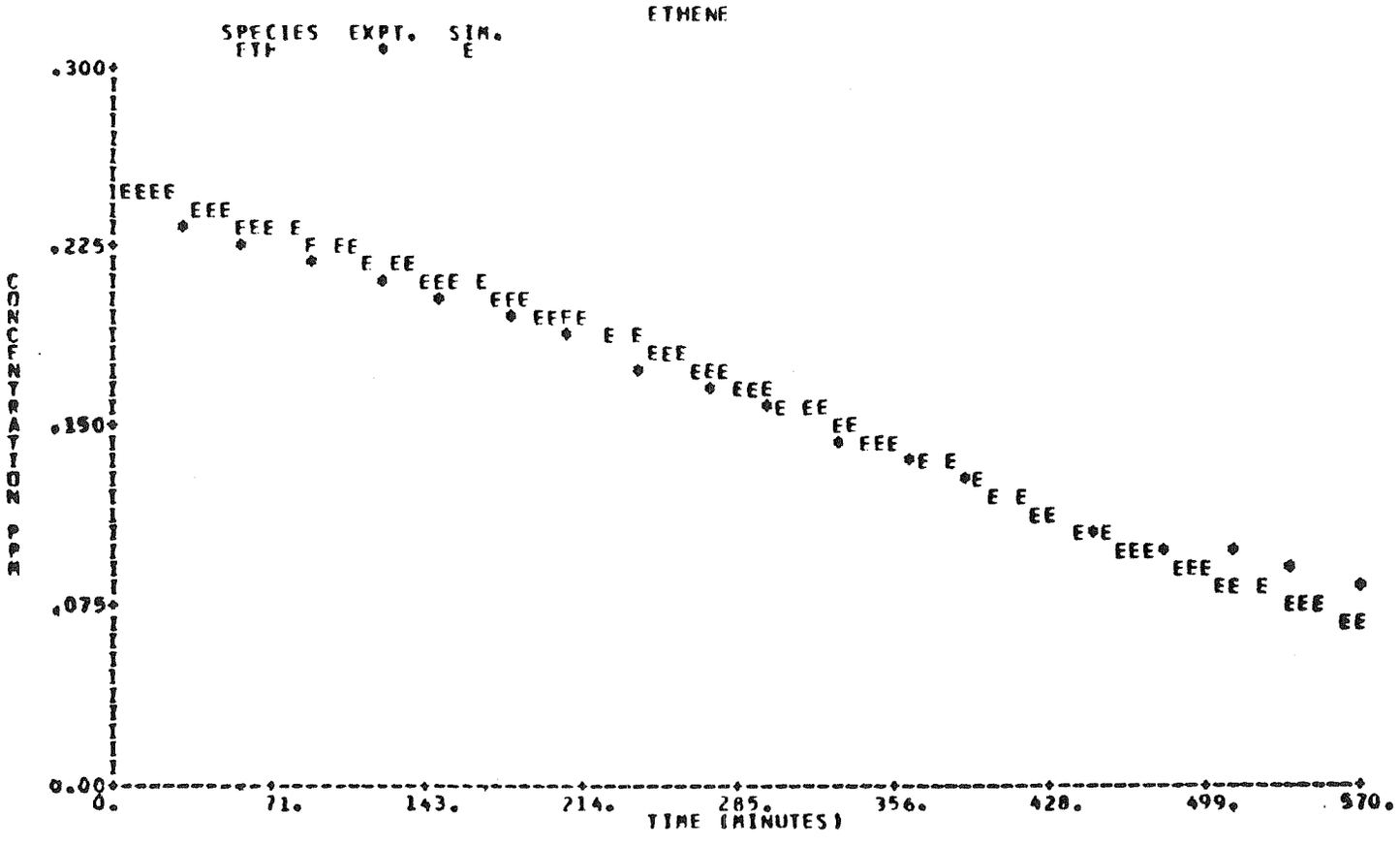

Figure A9b. Observed and Calculated Concentration-Time Profiles for 7-Hydrocarbon-NO_x Experiment EC-246.

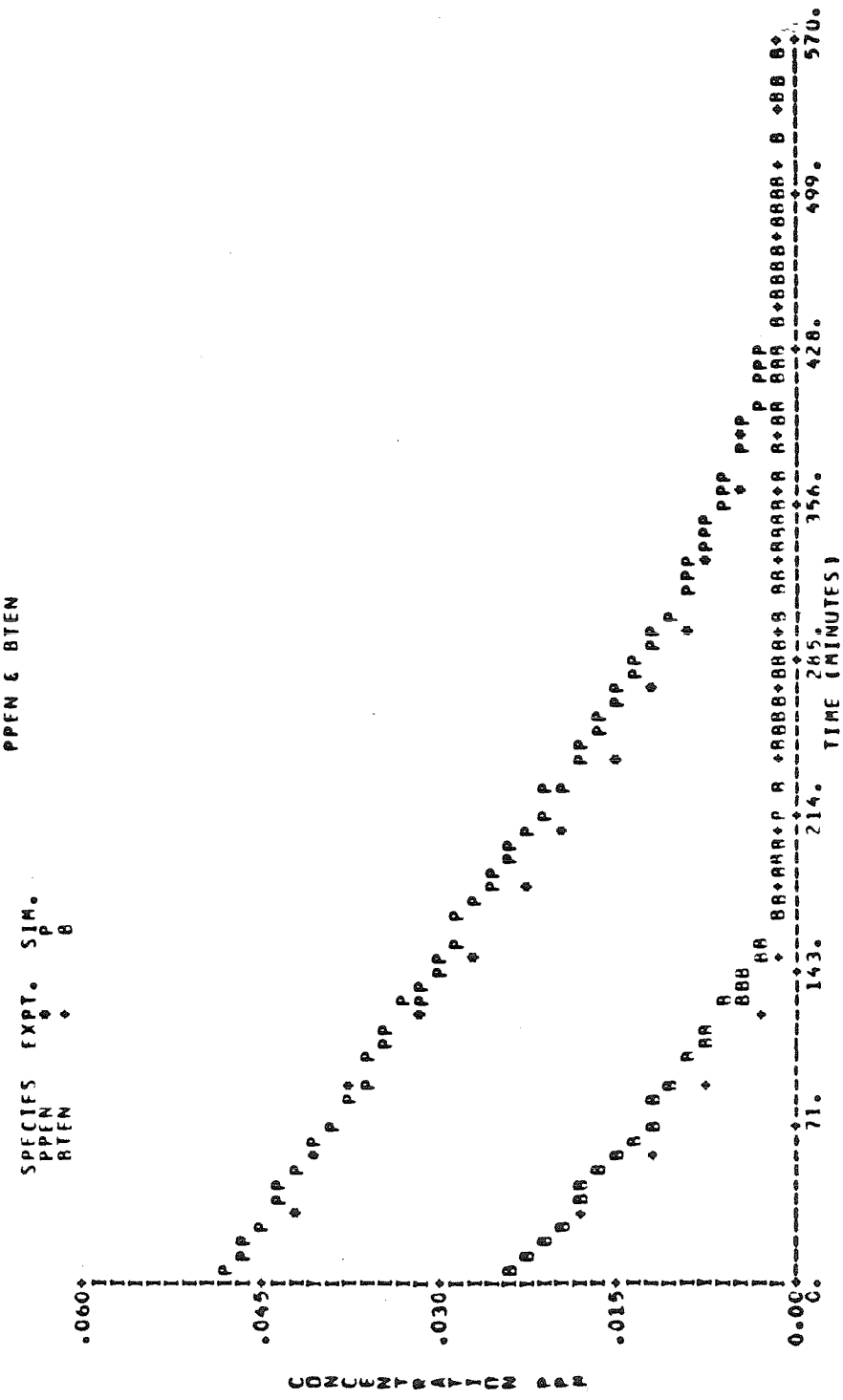

Figure A9c. Observed and Calculated Concentration-Time Profiles for 7-Hydrocarbon-NO_x Experiment EC-246.

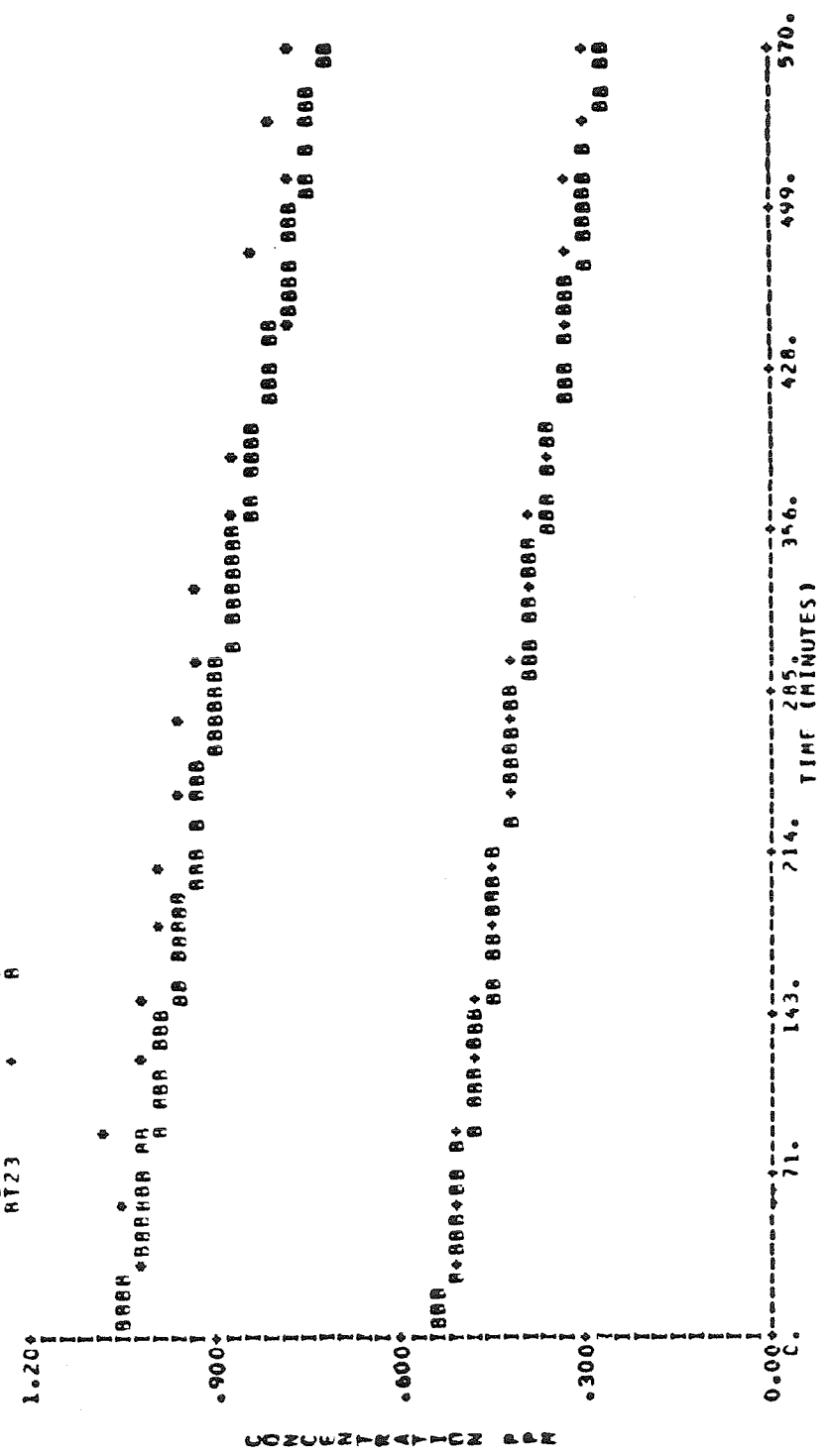

Figure A9d. Observed and Calculated Concentration-Time Profiles for 7-Hydrocarbon-NO_x Experiment EC-246.

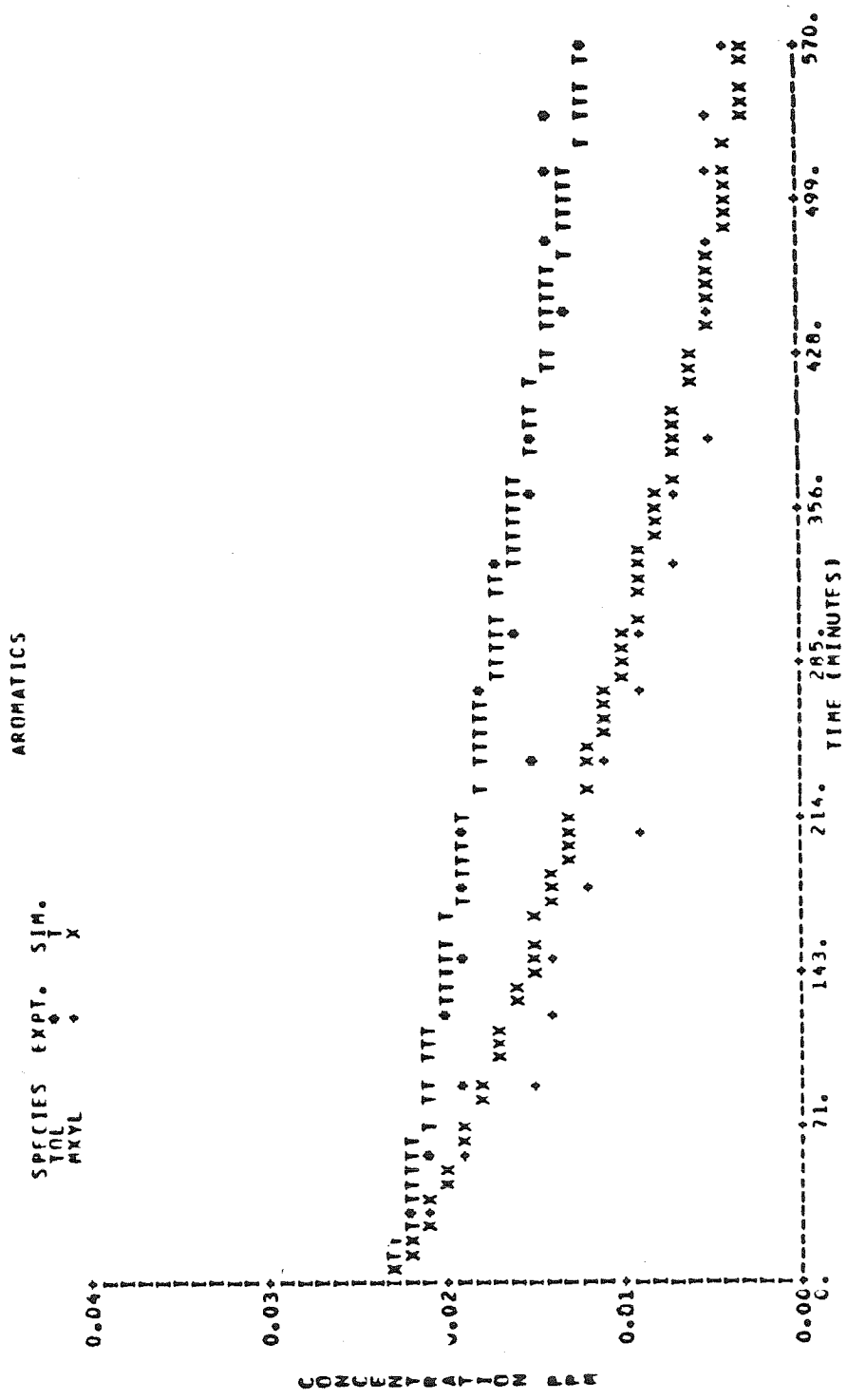

Figure A9e. Observed and Calculated Concentration-Time Profiles for 7-Hydrocarbon-NO_x Experiment EC-246.

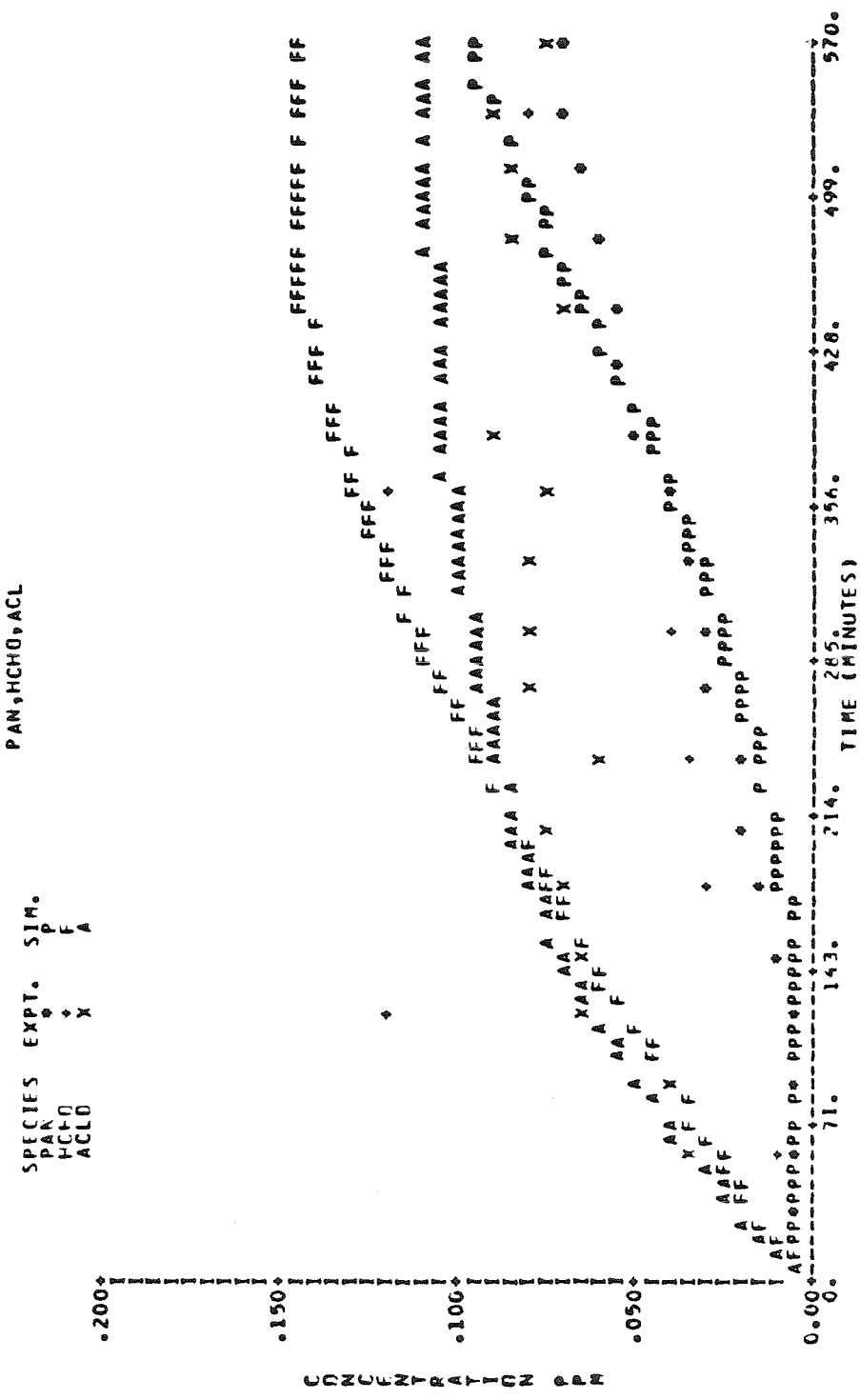

Figure A9f. Observed and Calculated Concentration-Time Profiles for 7-Hydrocarbon-NO_x Experiment EC-246.

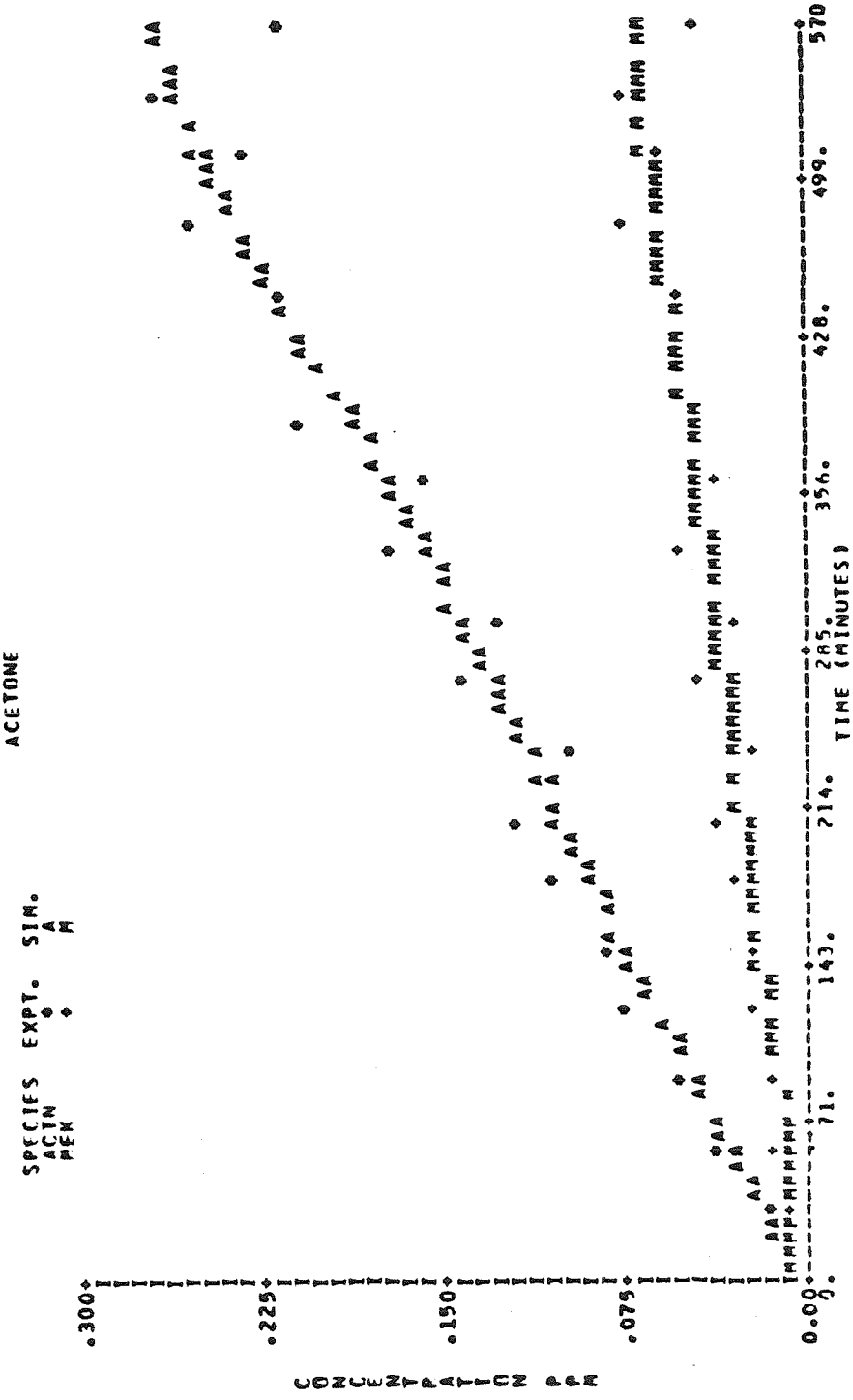

Figure A9g. Observed and Calculated Concentration-Time Profiles for 7-Hydrocarbon-NO_x Experiment EC-246.

CHAPTER 7

Development of a Surrogate Kinetic Mechanism for Photochemical Smog

DEVELOPMENT OF A SURROGATE KINETIC MECHANISM FOR PHOTOCHEMICAL SMOG

INTRODUCTION

There currently exist several reaction mechanisms that describe the organic chemistry of the urban atmosphere, and, at the same time, maintain a balance between chemical detail and mechanism length (1-6). These reaction mechanisms can be classified into two general categories, surrogate mechanisms and lumped mechanisms. In surrogate mechanisms the organic species in a particular class are represented by one or more members of that class, while in lumped mechanisms a generalized species is used to represent compounds of similar structure or reactivity. In general, lumped reaction mechanisms contain fewer non-steady-state species, making them more attractive from a computational point of view. An example of a generalized species lumped mechanism is the mechanism of Falls and Seinfeld (1), hereafter called the Caltech mechanism.

These condensed kinetic mechanisms are used in urban air quality models to determine how changes in emission levels will affect ambient air quality. Although each of the existing kinetic mechanisms for photochemical smog has been evaluated using the same body of experimental data, several investigators have shown that different mechanisms predict substantially different degrees of emission controls to achieve the same desired air quality under identical conditions (7-9). In a recent study, Leone and Seinfeld (10,11) have identified many of the reasons for these discrepancies in predictions. In that study, two major problems found with the Caltech mechanism are an inadequate treatment of atmospheric aromatic

chemistry, and the use of out-of-date rate constants and photolysis rates (particularly out-of-date aldehyde photolysis rates). When modifications were made to these reactions, the predictions of the Caltech mechanism were found to be in much closer agreement with those of a detailed explicit reaction mechanism for photochemical smog (10,11). Unfortunately, it is not possible to make use of this modified Caltech mechanism until a complete re-analysis of the entire mechanism with respect to experimental data has been performed.

The goal of this work is to develop a new condensed chemical reaction mechanism for photochemical smog that can replace the Caltech mechanism in the Caltech urban airshed model. Since condensed reaction mechanisms either lumped or surrogate, are derived from detailed, explicit chemistry, an effective approach to form a condensed mechanism for photochemical smog is by using surrogate species to eliminate or condense many of the least important species and reactions contained in the explicit mechanisms. This approach leads to the class of condensed mechanisms referred to as surrogate mechanisms which, because of their very nature, are easier to modify than lumped mechanisms when new experimental kinetic and mechanistic information become available. As noted earlier, the disadvantage of surrogate mechanisms in the past has been the large number of species that they contained. However, the recent work of Leone and Seinfeld (10,11) provides evidence that many of the species contained in surrogate mechanisms are not important from an ozone production point of view. That work also presents a counter species method of evaluating the contribution of individual species to the overall ozone production predicted by the mechanism. With this technique one can identify non-steady-state species that can be

eliminated with only minor effects on the predictive ability of the mechanism. Thus, it now appears possible to formulate a surrogate mechanism for photochemical smog that is suitable for use in air quality simulation models and could be easily updated when new kinetic or mechanistic data become available.

The approach taken in this study is therefore to first formulate a detailed explicit reaction mechanism for photochemical smog containing the chemistry of the important atmospheric organics. The formation of this explicit mechanism is summarized in the next section. After evaluating this explicit mechanism using smog chamber data, a surrogate condensed mechanism is formed by eliminating many of the fast reacting and less important species from the explicit mechanism. The resulting surrogate mechanism is similar in structure to the mechanism of Atkinson et al. (2). Next, the predictions of the explicit and surrogate condensed mechanisms are compared to determine if any significant loss of predictive ability has occurred. Following this, the counter species analysis technique mentioned above is applied to both the explicit and surrogate mechanisms to determine which additional non-steady-state species can be safely eliminated from the surrogate mechanism. The final version of the surrogate mechanism is then extensively evaluated against a variety of experimental data from both indoor and outdoor smog chamber facilities.

DEVELOPMENT AND TESTING OF THE EXPLICIT MECHANISM

The surrogate mechanism developed in this study represents an attempt to simplify the detailed chemistry of the atmospheric organic/NO_x system. For this reason, it is appropriate to compare the behavior of the surrogate mechanism to a detailed, explicit reaction mechanism containing as many of the important organic species as possible. In doing so, we can assess the degree to which each portion of the surrogate mechanism represents the detailed chemistry of the organic constituents included in the explicit mechanism. In addition, this explicit mechanism provides a convenient starting point from which to derive the surrogate mechanism.

Table 1 lists the range of concentrations measured for 50 organic species in a recent study of ambient Los Angeles air (29). Also shown in Table 1 is the initial composition of smog chamber experiment SUR-119J performed at the Statewide Air Pollution Research Center (SAPRC), University of California, Riverside (12). The individual species concentrations for this experiment were chosen to represent the 6-9 AM ambient pollutant burden in the Los Angeles atmosphere. If we exclude methane, acetylene, and ethane because of their low reactivity, we see that the remainder of the species in Table 1 are dominated by the presence of about 12 organics. Because of their importance, a great deal of kinetic and mechanistic data dealing with the atmospheric chemistry of these species has been obtained over the past decade. Thus, with this information, a realistic explicit reaction mechanism can be formulated for the key species in Table 1.

A listing of the explicit mechanism is given in Table A.1. The primary organics whose explicit chemistry is contained in the explicit mechanism are:

Table 1. Organic Composition of Ambient Los Angeles Air (29) and Smog Chamber Experiment SUR-119J (12).

Compound	Ambient Air Concentration Range (ppbv)	SUR-119J Concentration (ppbv)
Alkynes		
acetylene	26-94	46.4
Alkanes		
methane	-	2740.0
ethane	32-221	76.8
propane	11-99	17.0
isobutane	10-33	0.2
n-butane	21-70	166.0
isopentane	23-83	-
n-pentane	9-34	97.6
2,3-dimethylbutane	2-8	-
2-methylpentane	8-28	-
3-methylpentane	4-15	-
n-hexane	5-20	-
2,2,3-trimethylbutane	0-9	-
2,4-dimethylpentane	2-6	-
2,3-dimethylpentane	2-9	-
3-methylhexane	3-24	-
2,2,4-trimethylpentane	3-15	-
n-heptane	3-11	-
2,5-dimethylhexane	1-3	-
2,3,4-trimethylpentane	2-5	-
3-methylheptane	2-5	-
2,2,5-trimethylhexane	1-4	-
n-octane	1-5	-
n-nonane	1-3	-
n-decane	1-9	-
Cycloalkanes		
methylcyclopentane	4-16	-
cyclohexane	7-31	-
dimethylcyclopentane	1-19	-
methylcyclohexane	3-14	-
dimethylcyclohexane	0-1	-
Alkenes		
ethylene	32-91	43.2
propene	7-32	10.6
1-pentene	1-8	-
2-methyl-1-pentene	0-4	-

Table 1. Organic Composition of Ambient Los Angeles Air (29) and Smog Chamber Experiment SUR-119J (12) (Continued)

Compound	Ambient Air Concentration Range (ppbv)	SUR-119J Concentration (ppbv)
Alkenes (Continued)		
2-butene	-	13.7
2-methyl-2-butene	-	14.8
Aromatics		
benzene	12-29	1.6
toluene	20-68	16.8
ethylbenzene	3-12	6.4
m- and p-xylene	11-45	42.4
o-xylene	4-13	-
n-propylbenzene	1-3	0.1
p-ethyltoluene	4-12	-
o-ethyltoluene	1-3	-
1,3,5-trimethylbenzene	4-12	-
1,2,4-trimethylbenzene	4-12	-
1,2,3-trimethylbenzene	1-4	1.6
n-butylbenzene	0-2	-
isopropyl benzene	-	0.4
m-ethyltoluene	-	1.0
Carbonyls		
formaldehyde	4-86	38.0
acetaldehyde	2-39	20.0
propionaldehyde	-	3.2
propanal+acetone+acrolein	1-54	-
n-butanal	0-5	-
benzaldehyde	0-2	-

Alkanes:	Aromatics:
propane	toluene
n-butane	m-xylene
2,3-dimethylbutane	
Alkenes:	Carbonyls:
ethene	formaldehyde
propene	acetaldehyde
trans-2-butene	propionaldehyde
	acetone .

Excluding methane, acetylene, and ethane, 529.8 ppb of initial organics are present in SUR-119J. Of these, 503.7 ppb, or 95 percent is represented by the 12 organics included in the explicit mechanism. In the case of ambient Los Angeles air, these 12 species account for 538 ppb, or 49 per cent of the 1103 ppb of total reactive organics contained in the 50 major species*. Thus, we conclude that the explicit mechanism should provide a reasonable description of the chemistry occurring in a typical urban atmosphere. Since the reactions of species such as methane, ethane, acetylene, etc., are not included, the explicit mechanism is not suitable for use under clean tropospheric conditions.

The reactions and rate constants comprising the explicit mechanism were taken almost exclusively from four sources. The inorganic reactions were compiled using the recent reviews of Baulch et al. (13) and DeMore et al. (14). The aromatic reactions were taken mostly from the recent studies of Leone and Seinfeld (15) and Leone et al. (16). The vast majority of

*This calculation is based on the maximum concentrations measured by Grosjean and Fung (29).

the reactions and rate constants used in the explicit mechanism were taken from the review of Atkinson and Lloyd (17).

Even though the explicit mechanism represents the state of current understanding of atmospheric organic chemistry, there is still considerable uncertainty in many of the reactions and rate constants. In addition, we have only included in the explicit mechanism the reactions of a small number of the many organic species present in the typical urban troposphere. For these reasons, it is necessary to evaluate the explicit mechanism against experimental smog chamber data. The ability to model chamber data does not in any way guarantee that a mechanism is correct, especially with the uncertainty that exists in the magnitude of chamber radical sources. However, it does provide some evidence that the most important species and reactions are accounted for in the reaction mechanism.

We have chosen to test the explicit mechanism using series of 11 hydrocarbon-NO_x experiments performed at SAPRC (EC-231, EC-232, EC-233, EC-235, EC-237, EC-238, EC-241, EC-242, EC-243, EC-245, EC-246, and SUR-119J). These are multiple hydrocarbon-NO_x experiments in which both the initial hydrocarbon distribution and the $[RHC]_o/[NO_x]_o$ are varied. The initial conditions for each of these experiments are given in Table A.2. The chamber dependent reactions added to the explicit mechanism to adopt it for modeling chamber experiments are (18,19):

O_3 wall loss: $k = 1.65 \times 10^{-3}$ min^{-1}

NO wall source: $k = 1.0 \times 10^{-4}$ min^{-1}

OH radical source: $k = k_1 (0.39 + 1.37[NO_2])$ ppb-min^{-1}

heterogeneous HNO_3 formation: $k = 4.4 \times 10^{-6}$ ppm^{-1}-min^{-1}.

The results of simulating most of the above experiments with the explicit mechanism are shown in the Appendix (Figures A.1 through A.9)*. In nearly every case there is good agreement between the predictions of the explicit mechanism and the experimental data. In general, the O_3 and PAN peak heights are slightly over-predicted, while the NO_2 peak height is predicted very well. Both the timing of the NO_2 and O_3 peaks, and the hydrocarbon decay rates are predicted very well, indicating that the radical initiation and termination processes are represented adequately in the explicit mechanism. When examining the results in Figures A.1 through A.9, one should keep in mind that the explicit mechanism contains no adjustable parameters. Similarly, the chamber dependent terms are held constant and not varied as the initial conditions of the experiments change.

In summary, the explicit mechanism contains the reactions of the most important organic species found in the typical polluted urban atmosphere. Because there is considerable uncertainty in portions of this mechanism (particularly in the aromatic chemistry), the explicit mechanism should not be thought of as an exact description of atmospheric organic chemistry. In spite of this shortcoming, the explicit mechanism represents the state of the art in our understanding of atmospheric organic chemistry, and therefore provides a necessary starting point for the development of a surrogate condensed mechanism and for assessing the performance of this surrogate mechanism.

---

*Except for the updating of a few rate constants, the explicit mechanism is identical to the master mechanism discussed in the last chapter. Thus, Figures A.1 through A.9 are very similar to the master mechanism validations shown in the last chapter. For several reasons, including convenience to the reader, we choose to include both sets of validations in this thesis.

DEVELOPMENT OF A FIRST GENERATION SURROGATE MECHANISM

The explicit mechanism shown in Table A.1 serves as the starting point for the development of a new surrogate mechanism. The chemistry of each class of species (inorganics, alkanes, alkenes, aromatics, and carbonyls) is simplified by combining reactions and eliminating fast reacting or unimportant species. This simplification process is similar to that used by Atkinson et al. (2). The resulting mechanism, hereafter called SUR1, is shown in Table A.3. Many of the details regarding the formulation of the SUR1 mechanism can be found in the footnotes to Table A.3.

Inorganic Reactions

The only changes from the inorganic reactions appearing in the explicit mechanism are the elimination of $O(^3P)$, the combining of reactions 16-18 (2), and the elimination of reactions 21 and 22.

Alkene Reactions

The reactions of three alkenes are included in SUR1, ethene, propene, and trans-2-butene. Ethene is treated separately because of its relatively slow rate of reaction with both OH and O_3(10,11,17). The reactions of propene and trans-2-butene are used to represent the chemistry of the terminal and internal alkenes, respectively. By eliminating many of the free radical intermediates, the reactions of these three alkenes are reduced to those shown in Table A.3, section B.

Aromatic Reactions

Three aromatic hydrocarbons are included in SUR1, benzene, toluene, and xylene. Benzene is treated separately, while toluene represents the mono-alkylbenzenes and xylene represents the higher alkylbenzenes. The resulting reactions are shown in section C of Table A.3.

Alkane Reactions

The alkane chemistry contained in SUR1 has been taken directly from Atkinson et al. (2). Methane and ethane are neglected, while propane is treated explicitly. The C_4 and higher alkanes are represented by a lumped average alkane whose chemistry represents an average for the butanes, n- and isopentanes, n-hexane, and n-heptane (2).

Carbonyl Reactions

Formaldehyde, acetaldehyde, acetone, and methylethylketone are treated explicitly. Propionaldehyde is used to represent the C_3 and higher aldehydes. The resulting reactions are listed in part E of Table A.3.

QUANTITATIVE COMPARISON OF THE EXPLICIT AND SUR1 MECHANISMS

The SUR1 mechanism shown in Table A.3 is formulated in a straightforward manner from the explicit mechanism, and we therefore anticipate that these two mechanisms would perform similarly. Unfortunately, the SUR1 mechanism is still too large for use in multidimensional grid models, since it contains 31 non-steady-state species and 83 reactions. We could proceed by eliminating additional species from SUR1, creating a more condensed mechanism (SUR2), whose performance could then be compared to that of the explicit mechanism. However, if the predictions of the SUR2 and explicit mechanisms did not agree, we would not know which portion of the species elimination process was responsible for the error. Instead, we choose to first evaluate the performance of the SUR1 mechanism to insure that it is an adequate representation of the explicit mechanism. Included in this evaluation is a counter species analysis of both the explicit and SUR1 mechanisms. The results of this counter species analysis will be very useful in determining which species of the SUR1 mechanism can be eliminated without significantly affecting the performance of the mechanism. This is exactly the information that we would like to possess before beginning our formulation of a more condensed surrogate mechanism (SUR2).

Figures 1-4 illustrate how the explicit and SUR1 mechanisms compare in their predictions of maximum O_3, NO_2, and PAN concentrations, and the time of the ozone maximum. The same chamber-dependent terms (shown in Table A.6) were used with both reaction mechanisms to obtain these results. The initial conditions for these simulations correspond to the 10 multi-hydrocarbon-NO_x smog chamber experiments performed at SAPRC that were used to evaluate the explicit mechanism (EC-231 through EC-246). One can see

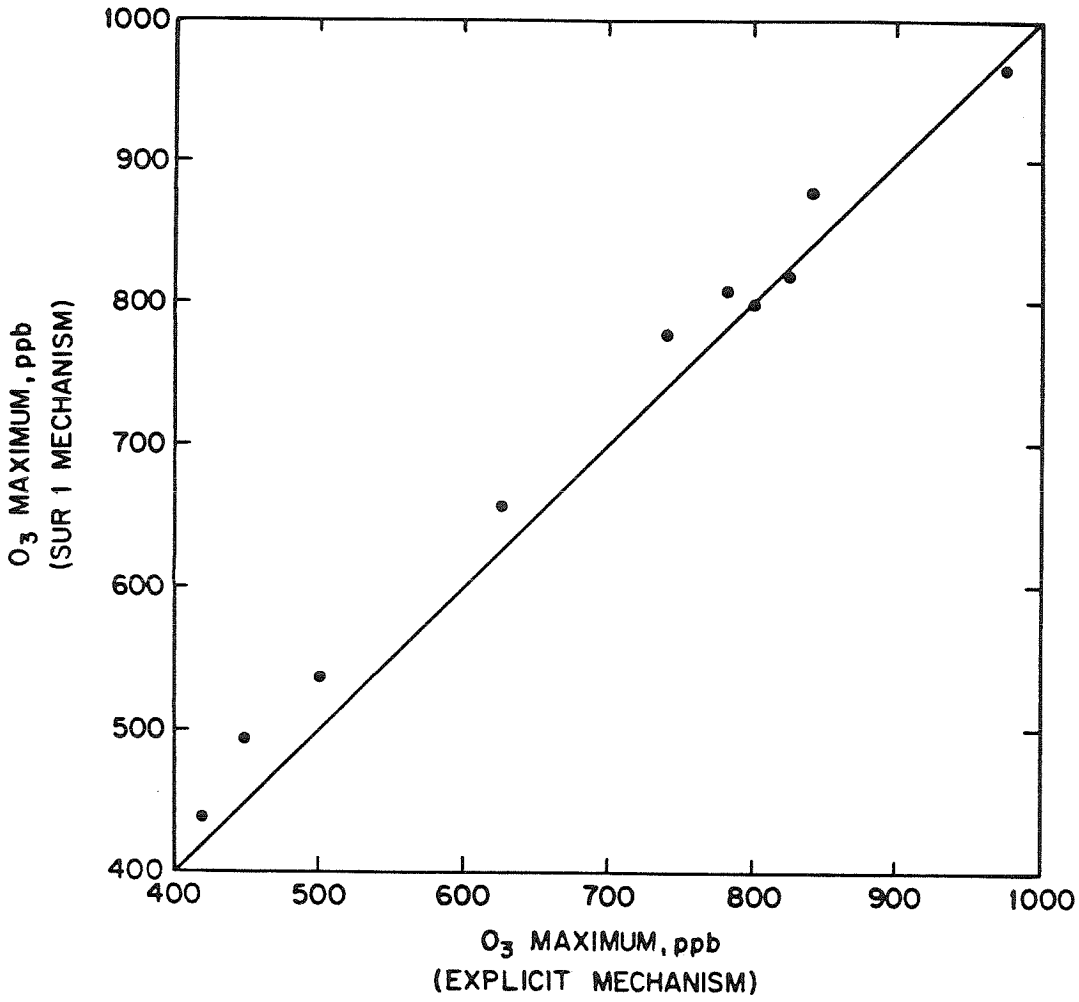

Figure 1. Comparison of peak O_3 concentrations predicted by the explicit and SUR1 mechanisms. Each point corresponds to one of the SAPRC multi-hydrocarbon-NO_x experiments EC-231 through EC-246.

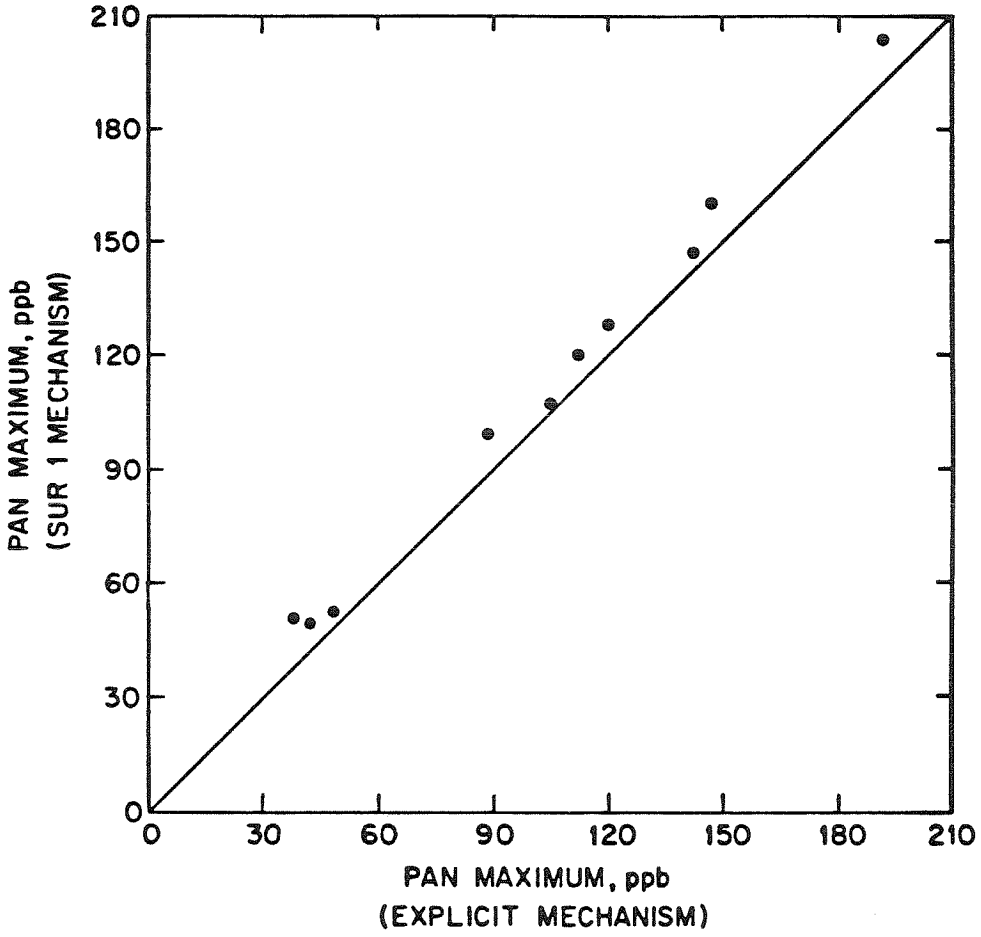

Figure 2. Comparison of peak PAN concentrations predicted by the explicit and SUR1 mechanisms. Each point corresponds to one of the SAPRC multi-hydrocarbon-NO_x experiments EC-231 through EC-246.

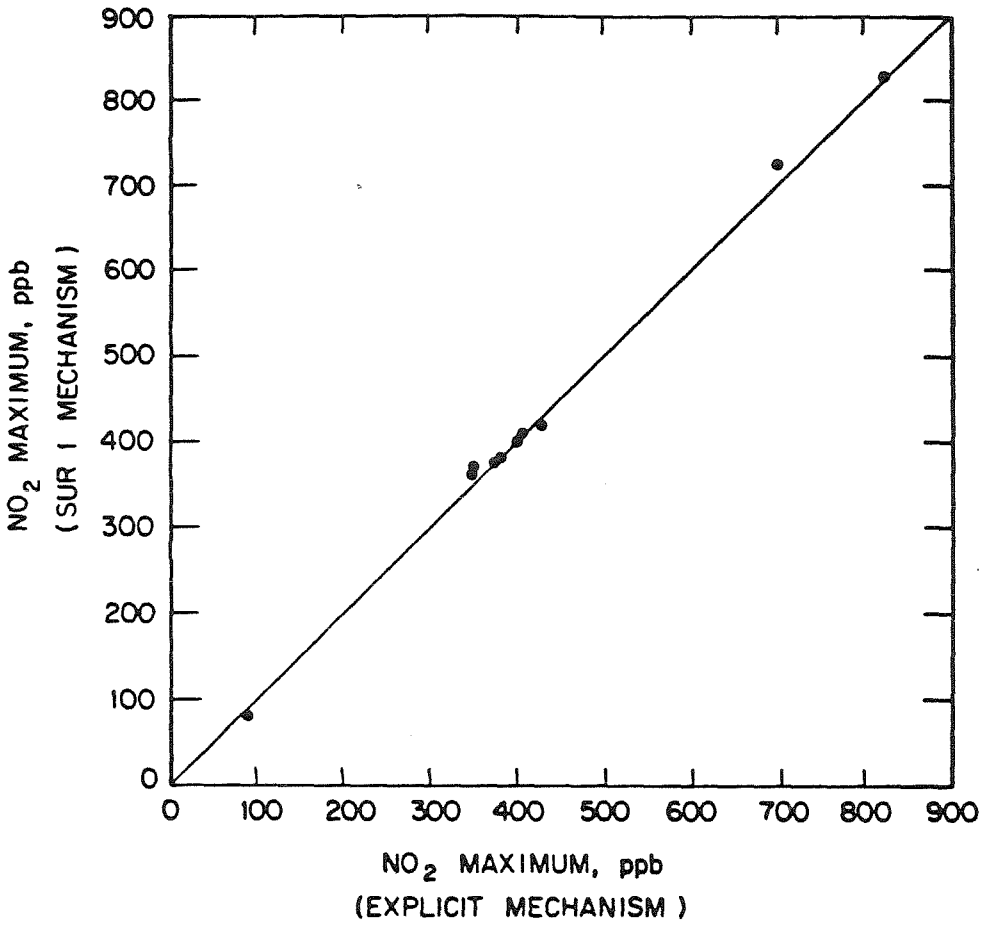

Figure 3. Comparison of peak NO_2 concentrations predicted by the explicit and SUR1 mechanisms. Each point corresponds to one of the SAPRC multi-hydrocarbon-NO_x experiments EC-231 through EC-246.

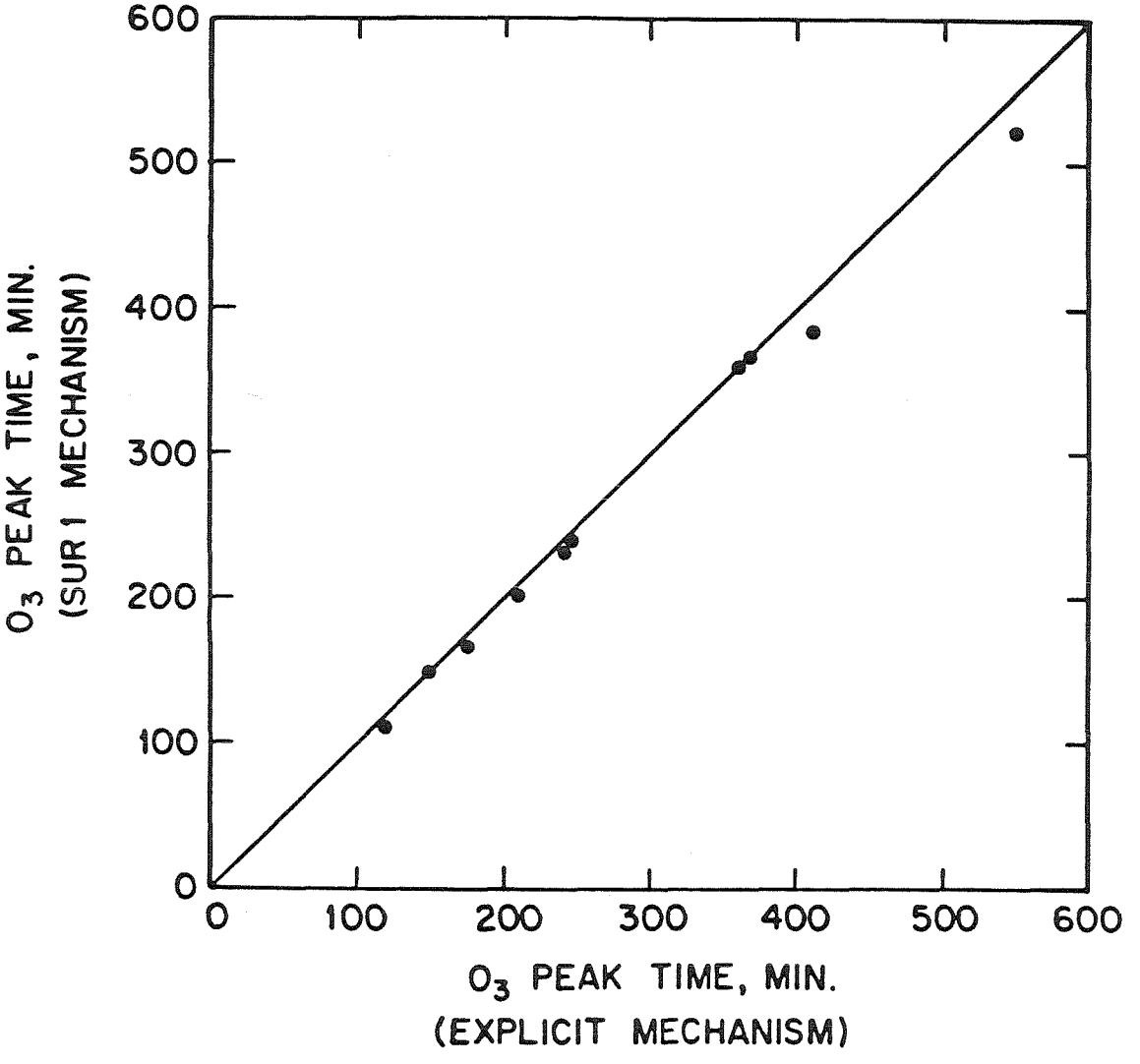

Figure 4. Comparison of peak O_3 times predicted by the explicit and SUR1 mechanisms. Each point corresponds to one of the SAPRC multi-hydrocarbon-NO_x experiments EC-231 through EC-246.

that the predictions of the SUR1 mechanism lie very close to those of the explicit mechanism. These results illustrate that the overall performance of the SUR1 mechanism compares well with the explicit mechanism; however, they tell us nothing of how the individual portions of the SUR1 mechanism correspond to their counterparts in the explicit mechanism. In order to gain this information we must use a counter species analysis.

The details of the counter species analysis technique are presented elsewhere (10,20), and are therefore not discussed here. The information provided by this analysis is the amount of NO to NO_2 conversions attributable to each of the important species appearing in a reaction mechanism. Since O_3 production is related to the amount of NO being converted to NO_2, this analysis provides us with an indirect way of assessing the amount of ozone production for which each of the initially present organics is responsible. By applying this analysis to both the explicit and SUR1 mechanisms, we can determine how well the simplified chemistry in SUR1 represents the explicit chemistry found in the explicit mechanism.

Some typical results of the counter species analysis are shown in Table 2 and Figures 5-8. Figure 5 shows that the total amount of NO to NO_2 conversions predicted by the two mechanisms agree very well. This agreement is expected, since we saw in Figure 1 that the two mechanisms predicted similar peak ozone levels. Table 2 shows the detailed counter species results for the simulations of experiments EC-231, EC-233, and EC-242. The results for the remaining seven simulations are very similar. Examination of these results shows that each portion of the SUR1 mechanism represents the NO to NO_2 conversion behavior of the explicit mechanism very well. In particular, the NO to NO_2 conversions attributable to the alkenes are very

Table 2. Comparison of Counter Species Results for the Explicit and SUR1 Mechanisms Using Initial Conditions from SAPRC Experiments EC-231, EC-233, and EC-242.

Experiment	EC-231		EC-233		EC-242	
Mechanism	Explicit	SUR1	Explicit	SUR1	Explicit	SUR1
I) AROMATICS						
toluene abstraction	4	4	1	1	7	7
toluene addition	45	59	10	14	86	103
m-xylene+OH	153	149	43	42	355	320
methyl glyoxal+hν	63	57	18	16	134	117
methyl glyoxal+OH	7	7	2	2	12	7
glyoxal	1	0	0	0	1	0
benzaldehyde	0	0	0	0	0	0
o-cresol	1	6	0	2	1	11
dimethyl phenol	3		1		6	
pyruvic acid	0	0	0	0	0	0
2-butene-1,4-dial	3	20	1	6	6	22
	10		3		20	
other γ-dicarbonyls	14		4		29	
TOTAL AROMATIC	202	212	54	57	448	430
II) ALKANES						
propane+OH	0	0	0	0	0	0
butane+OH	258	686	207	525	100	195
2,3-dimethylbutane+OH	387		299		90	
butane+O(^{3}P)	0	-	0	-	0	-
2,3-dimethylbutane+O(^{3}P)	2	-	0	-	0	-
TOTAL ALKANE	645	686	506	525	190	195
III) ALKENES						
ethene+OH	552	554	118	116	815	803
ethene+O_3	163	162	23	21	257	244
propene+OH	87	85	40	39	75	72
propene+O_3	41	45	15	18	36	41

Table 2. Comparison of Counter Species Results for the Explicit and SUR1 Mechanisms Using Initial Conditions from SAPRC Experiments EC-231, EC-233, and EC-242 (Continued)

Experiment	EC-231		EC-233		EC-242	
Mechanism	Explicit	SUR1	Explicit	SUR1	Explicit	SUR1
III) ALKENES (cont)						
butene+OH	40	40	18	17	70	66
butene+O_3	34	38	15	17	59	69
$\dot{C}H_2O\dot{O}$	70	72	5	5	82	81
$CH_3\dot{C}HO\dot{O}$	15	16	4	4	22	23
TOTAL ALKENE	917	924	229	228	1312	1295
IV) CARBONYLS						
initial HCHO	8	7	2	2	9	8
initial CH_3CHO	0	0	0	0	0	0
initial C_2H_5CHO	0	0	0	0	0	0
initial $CH_3C(O)CH_3$	0	0	0	0	0	0
created HCHO	233	267	49	59	324	343
created CH_3CHO	47	48	25	25	42	27
created C_2H_5CHO	0	4	0	4	0	1
created C_3H_7CHO	9		8		3	
created $CH_3C(O)CH_3$	10	2	7	2	1	1
TOTAL ALDEHYDE	8	7	2	2	9	8
V) INITIAL CO	15	15	8	8	7	7
TOTAL	1787	1844	799	820	1966	1935

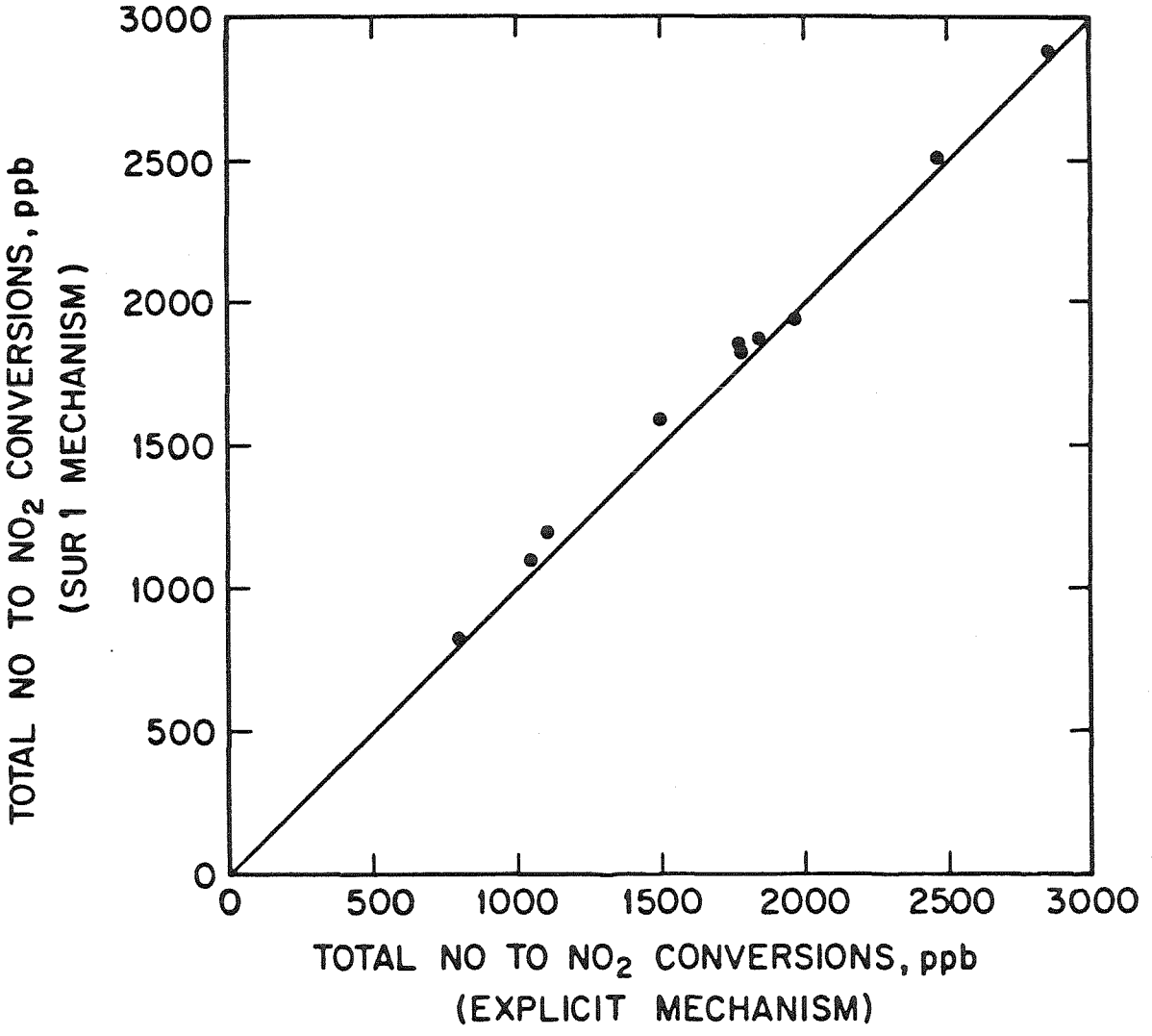

Figure 5. Comparison of the total amount of NO to NO_2 conversions predicted by the explicit and SUR1 mechanisms. Each point corresponds to one of the SAPRC multi-hydrocarbon-NO_x experiments EC-231 through EC-246.

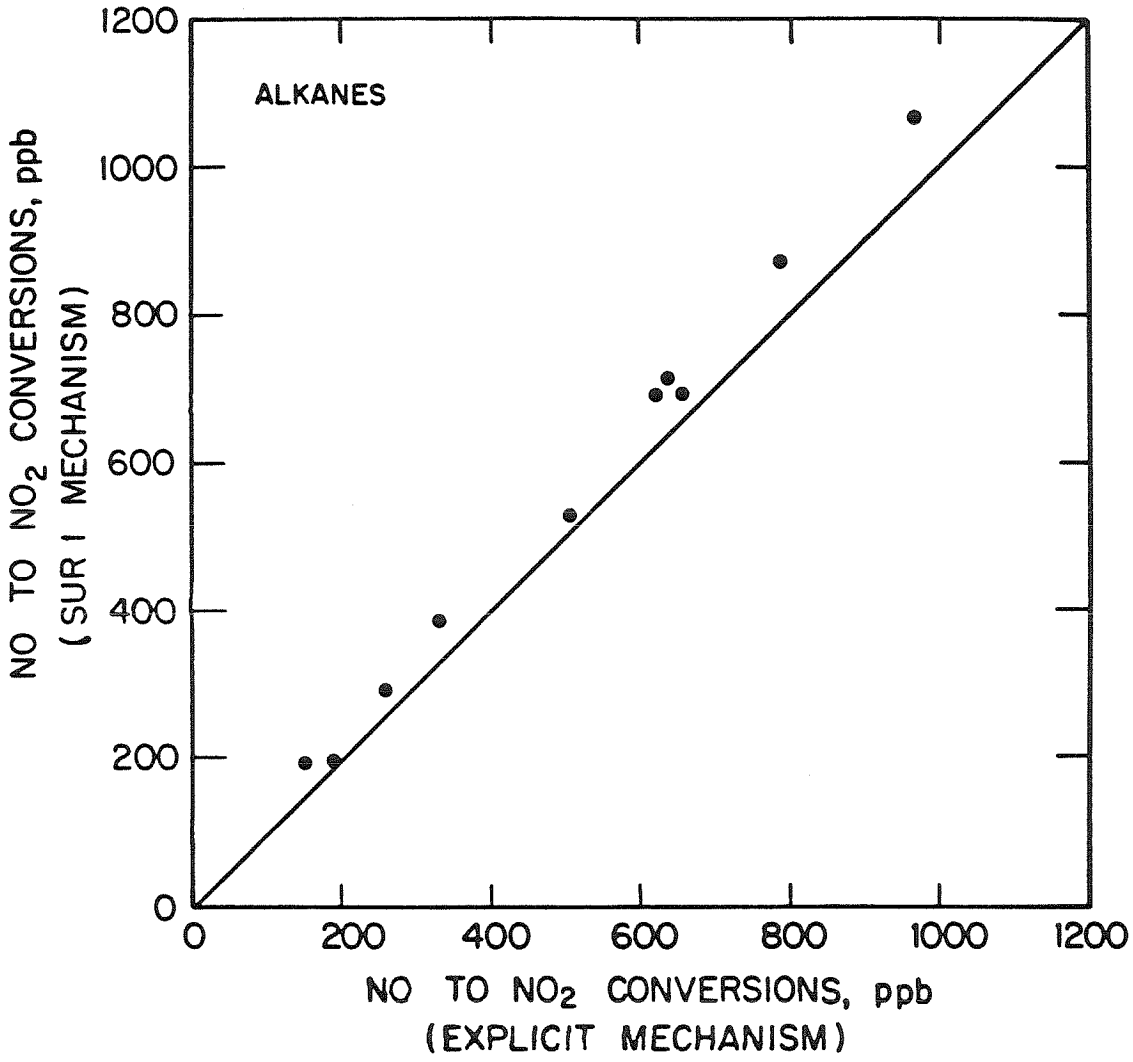

Figure 6. Comparison of the counter species results for the alkanes between the explicit and SUR1 mechanisms. Each point corresponds to one of the SAPRC multi-hydrocarbon-NO_x experiments EC-231 through EC-246.

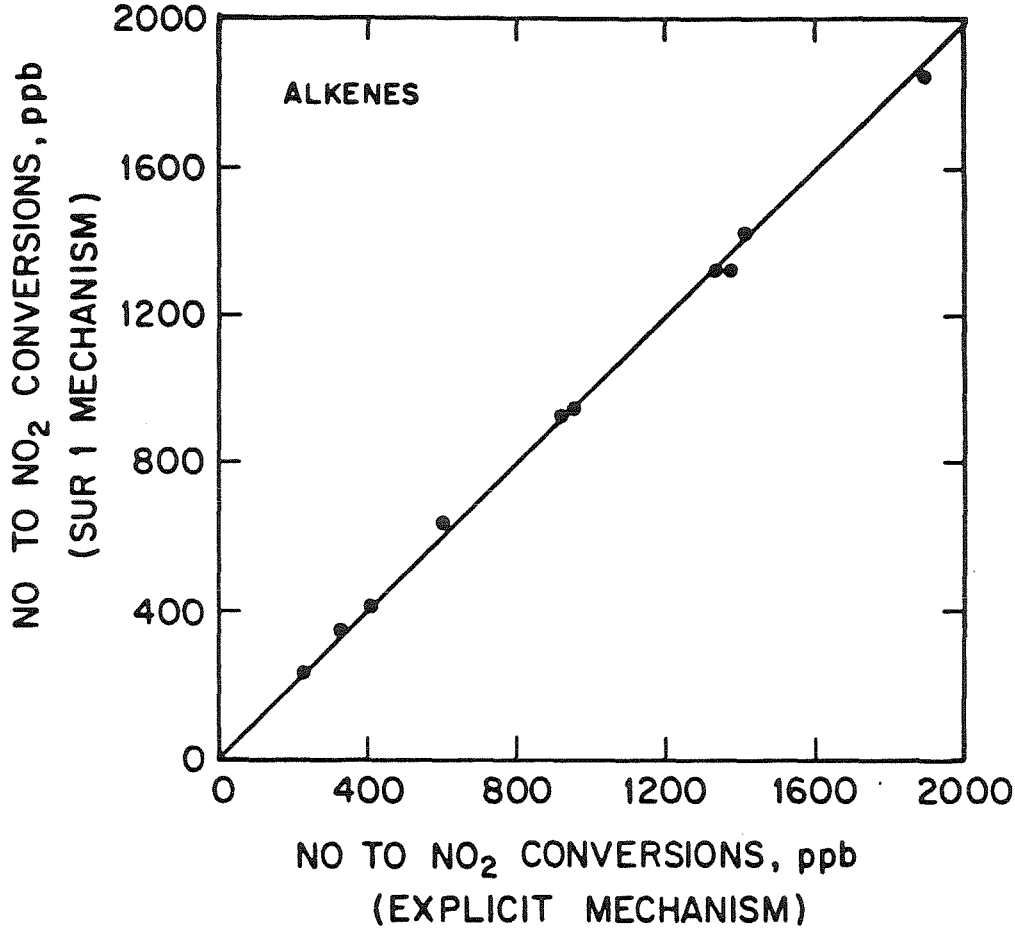

Figure 7. Comparison of the counter species results for the alkenes between the explicit and SUR1 mechanisms. Each point corresponds to one of the SAPRC multi-hydrocarbon-NO_x experiments EC-231 through EC-246.

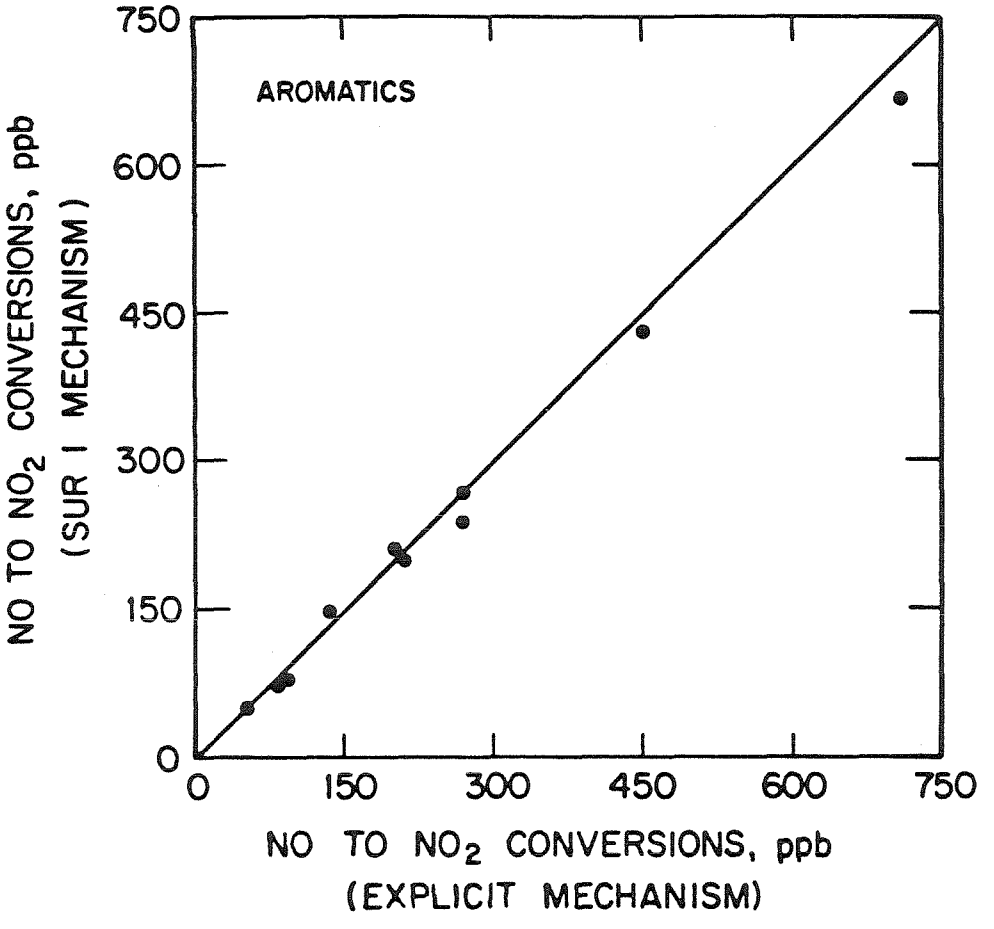

Figure 8. Comparison of the counter species results for the aromatics between the explicit and SUR1 mechanisms. Each point corresponds to one of the SAPRC multi-hydrocarbon-NO_x experiments EC-231 through EC-246.

similar for the two mechanisms. The agreement for the aromatics and alkanes is not quite as close, but the amount of simplification in going from the explicit to condensed treatments is much greater for these species. Figures 6-8 show the counter species results for each of the 10 simulations in an alternate form. Once again, we see that each portion of the surrogate mechanism represents the explicit chemistry very well.

The above results are important because they show that the overall performance of the SUR1 mechanism, as shown in Figures 1-4, is not fortuitous. Accurate overall results can be obtained even if individual portions of the surrogate mechanism contain inaccurate representations of the chemistry. For example, an over-reactive surrogate treatment of alkane chemistry could be hidden by an under-reactive representation of aromatic chemistry. Such compensating errors could cause serious problems when the mechanism is applied under a different set of conditions. The counter species results show that this type of error is not occurring under the conditions in which we have evaluated SUR1.

DEVELOPMENT OF A SECOND GENERATION SURROGATE MECHANISM

The number of non-steady-state species contained in the SUR1 mechanism must be reduced if it is to be practical for use in multidimensional urban air quality models. The results of the counter species analysis, such as those shown in Table 2, provide the information needed to determine which species can be safely eliminated. Examining these results shows that acetone, methyl ethyl ketone, benzaldehyde, peroxybenzoyl nitrate, glyoxal, pyruvic acid, propane*, propionaldehyde, and peroxypropionyl nitrate ($C_2H_5CO_3NO_2$) can be eliminated with only minor effects on mechanism predictions. In addition, we can eliminate two species by lumping together propene and butene, and toluene and xylene, as shown below.

Alkenes: Reactions 25 and 27 of the SUR1 mechanism become,

$$(25)\quad OLE + OH \rightarrow 0.95\gamma HCHO + (1.8-0.85\gamma)CH_3CHO + (0.9 + 0.05\gamma)(HO_2\cdot + NO_2) - NO$$

$$k_{25} = 3.7\times10^{4}\gamma + 1.0\times10^{5}(1-\gamma)$$

where,

$$\gamma = \frac{[propene]_o}{[propene]_o+[butene]_o}$$

Reactions 26 and 28 of the SUR1 mechanism become,

$$(26)\quad OLE + O_3 \rightarrow (1-0.5\gamma)CH_3CHO + (0.4-0.2\gamma)CH_3\dot{C}HO\dot{O} + (0.24+0.09\gamma)CO + (0.29-0.09\gamma)HO_2\cdot + (0.19-0.09\gamma)OH + (0.43-0.21\gamma)CH_3O_2\cdot + (0.05-0.03\gamma)CH_3O\cdot + 0.2\gamma\dot{C}H_2O\dot{O}$$

$$k_{26} = 1.6\times10^{-2}\gamma + 2.7\times10^{-1}(1-\gamma) \quad .$$

*Propane should not be eliminated in cases where long range transport is being studied.

Aromatics: Reactions 36 and 37 of the SUR1 mechanism become,

(34) ARO + OH → (0.25-0.05β) 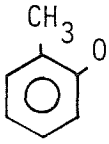 + (1-0.1β)HO_2·

(lumped xylene)

+ (0.75-0.05β)(NO_2 - NO + CH(O)CH=CHCHO)

+ (0.68 + 0.02β)$CH_3C(O)CH_O$ + (0.08-0.08β)$(CHO)_2$ + 0.1β 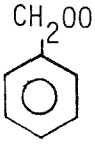

ARO + OH → (0.25-0.05β) 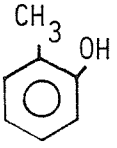 + (1-0.1β)HO_2·

(m-xylene)

+ (0.75-0.05β)(NO_2-NO + CH(O)CH=CHCHO)

+ (0.75-0.05β)$CH_3C(O)CH$O + 0.1β 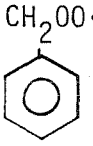

$k_{34} = 9.4x10^3\beta + 2.7x10^4(1-\beta)$ for lumped xylene

$k_{34} = 9.4x10^3\beta + 3.4x10^4(1-\beta)$ for m-xylene

$$\beta = \frac{[\text{toluene}]_o}{[\text{toluene}]_o+[\text{xylene}]_o}$$

Since the molar weighted average rate constants shown above are based on initial conditions, they strictly apply only at the start of a simulation. The use of these rate constants introduces some error into the mechanism; however, tests indicate that the magnitude of these errors is small as long as the species that are lumped together do not have large differences in rate constants or concentrations (10). For this reason, we choose not to lump benzene together with toluene and xylene, i.e., benzene reacts at a much slower rate in the atmosphere.

The mechanism that results after the above changes are made is shown in Table A.4. This new mechanism, which we call SUR2, contains 58 reactions and 20 non-steady-state species* and is therefore compact enough for use in grid models of urban air pollution. A list of the non-steady-state species appearing in SUR2 is shown in Table A.5. Since propionaldehyde is not treated in the SUR2 mechanism, acetaldehyde now represents all $\geq$C2 aldehydes. However, even though propane has been removed, the lumped group ALK still represents $\geq$C4 alkanes.

QUANTITATIVE COMPARISON OF THE EXPLICIT AND SUR2 MECHANISMS

The performance of the SUR2 mechanism is compared to that of the explicit mechanism in Figures 9-16. Figures 9-11 compare the two mechanisms in their predictions of O_3, PAN, and NO_2 maxima, while Figure 12 compares the timing of the O_3 peak. The initial conditions for these simulations correspond once again to those of SAPRC experiments EC-231 through EC-246. Examination of Figures 9-12 shows that the predictions of the SUR2 mechanism are in good agreement with those of the explicit mechanism. In fact, comparing Figures 9-12 with Figures 1-4 shows that the predictions of the SUR2 mechanism actually differ only slightly from those of the SUR1 mechanism. This is not surprising since the counter species analysis showed that the species that were eliminated from SUR1 were not important from an ozone production point of view.

The counter species results for the SUR2 and explicit mechanisms are compared in Figures 13-16. Once again the best agreement between the

*See the footnote to Table A.5.

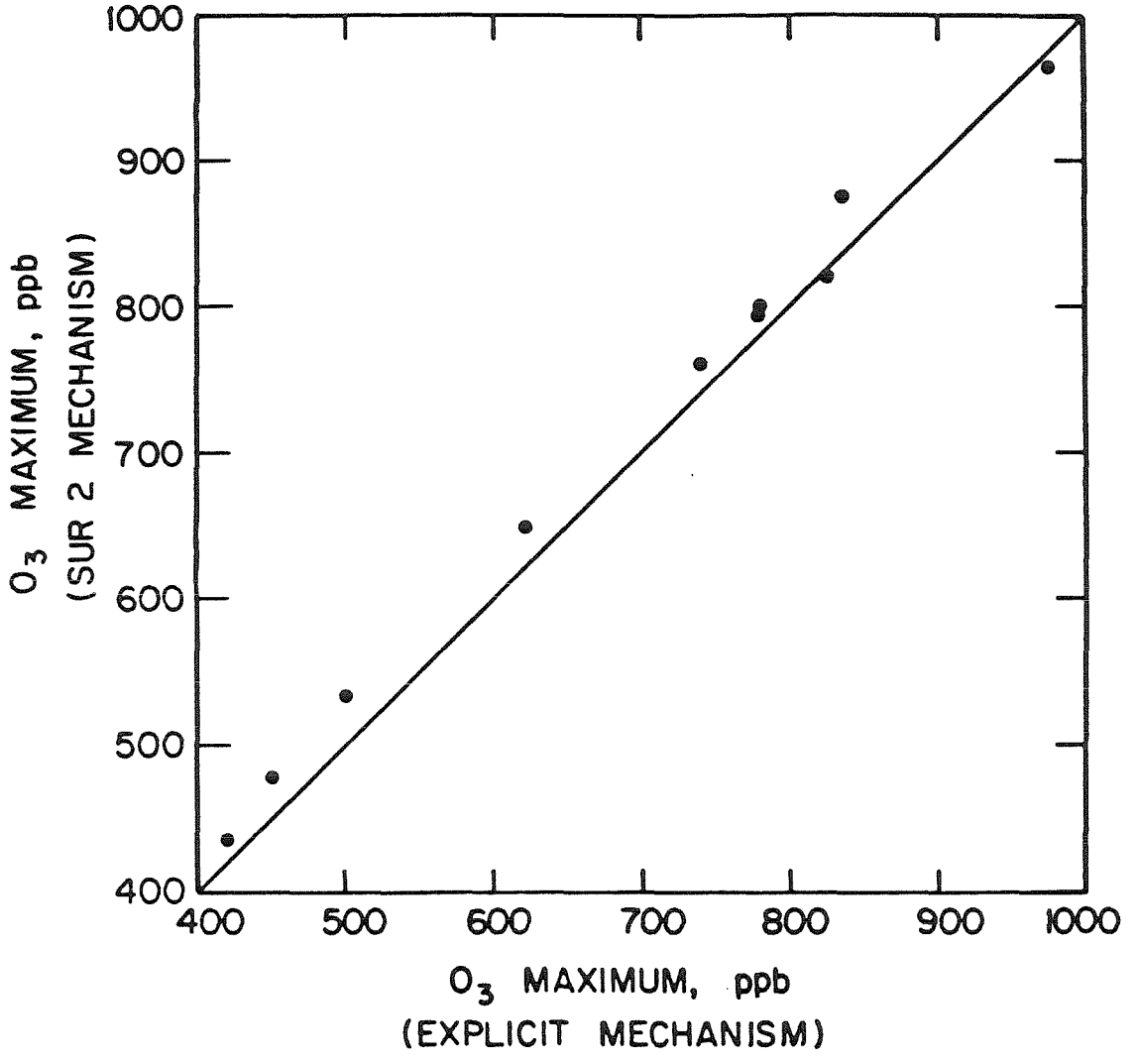

Figure 9. Comparison of peak O_3 concentrations predicted by the explicit and SUR2 mechanisms. Each point corresponds to one of the SAPRC multi-hydrocarbon-NO_x experiments EC-231 through EC-246.

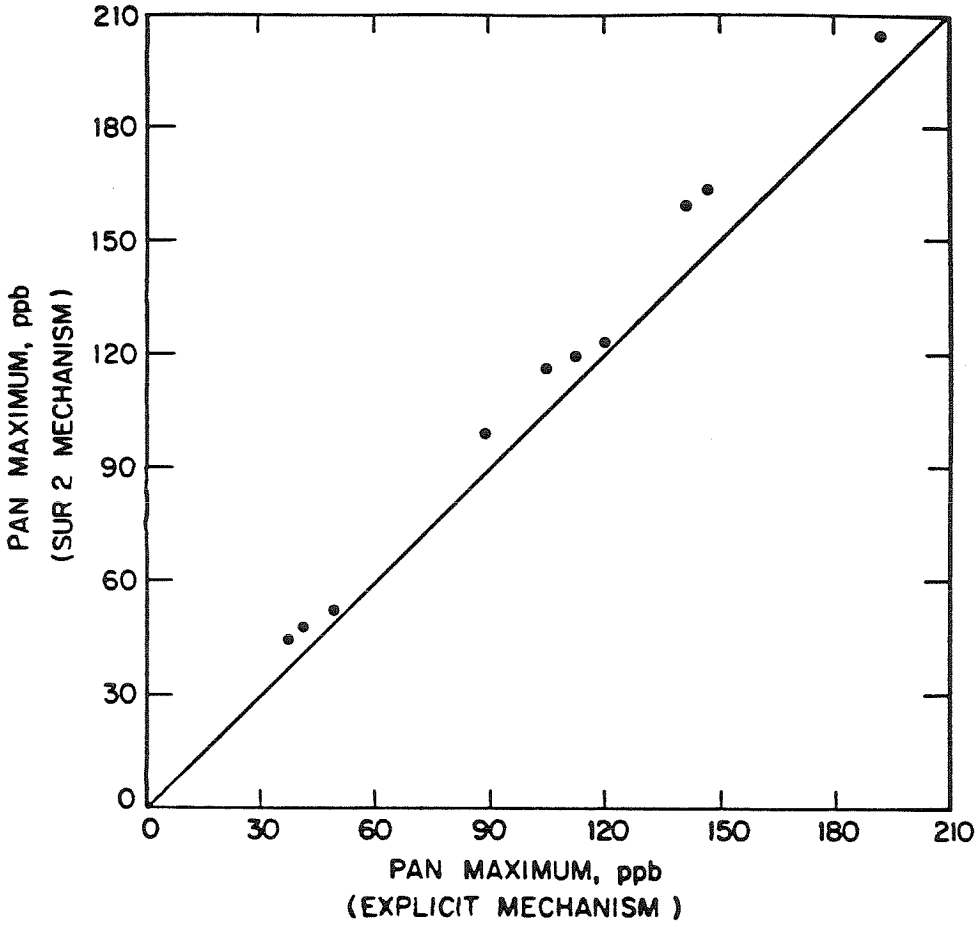

Figure 10. Comparison of peak PAN concentrations predicted by the explicit and SUR2 mechanisms. Each point corresponds to one of the SAPRC multi-hydrocarbon-NO_x experiments EC-231 through EC-246.

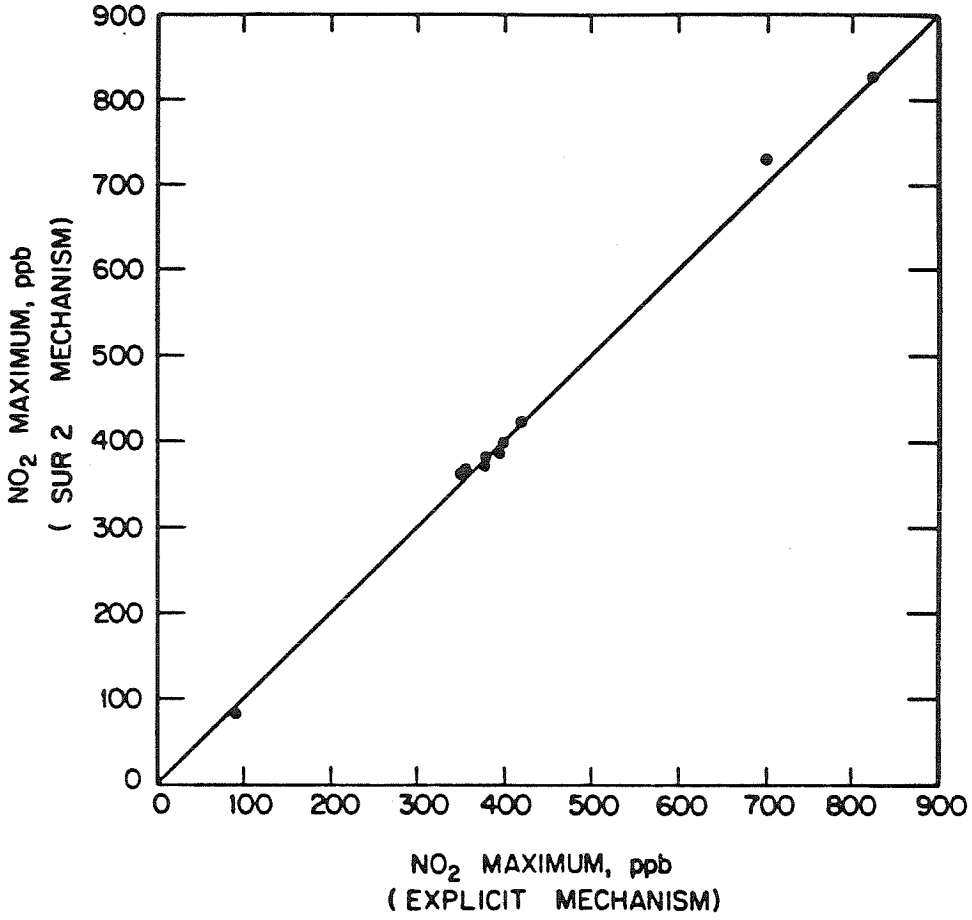

Figure 11. Comparison of peak NO_x concentrations predicted by the explicit and SUR2 mechanisms. Each point corresponds to one of the SAPRC multi-hydrocarbon-NO_x experiments EC-231 through EC-246.

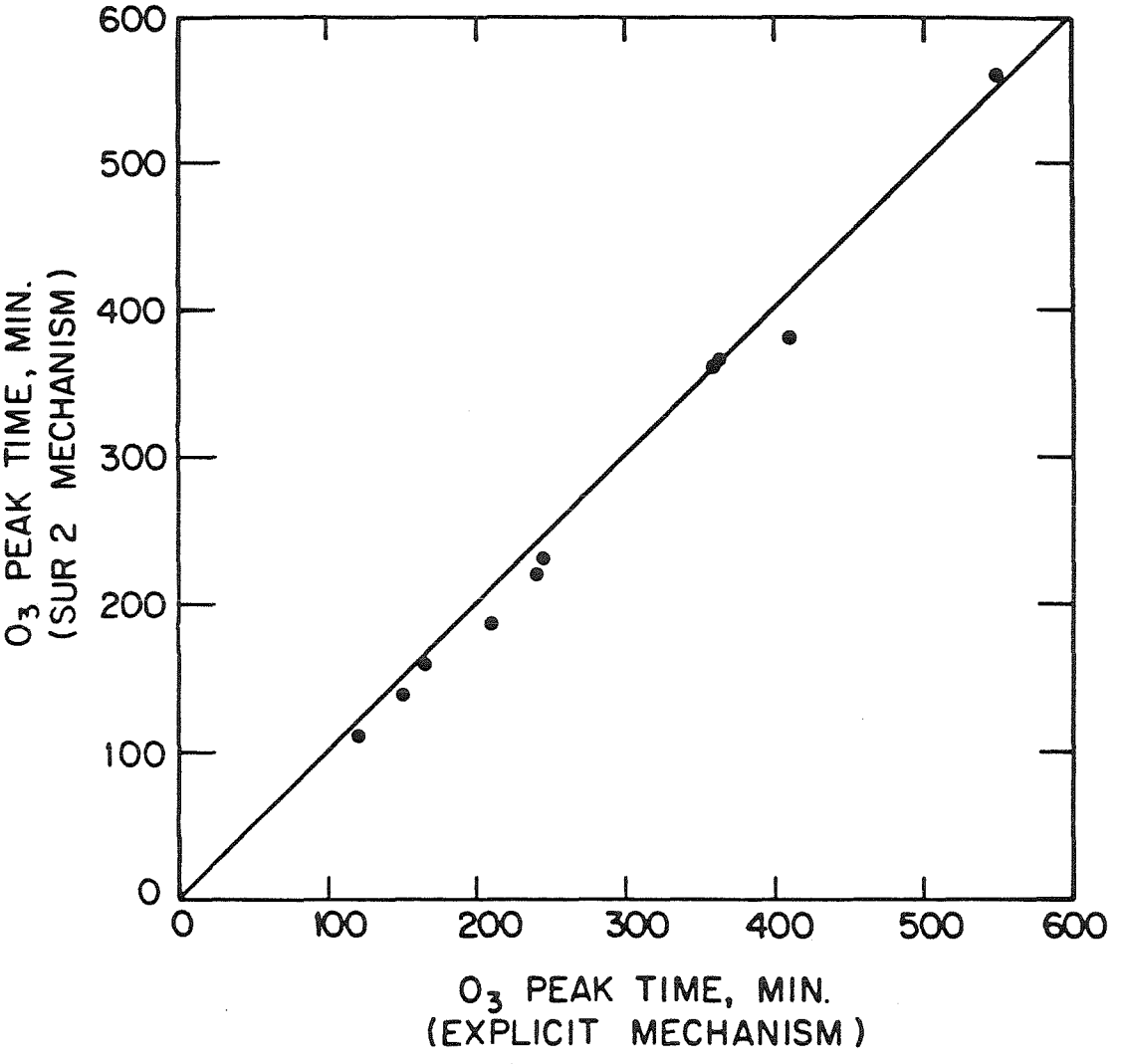

Figure 12. Comparison of peak O_3 times predicted by the explicit and SUR2 mechanisms. Each point corresponds to one of the SAPRC multi-hydrocarbon-NO_x experiments EC-231 through EC-246.

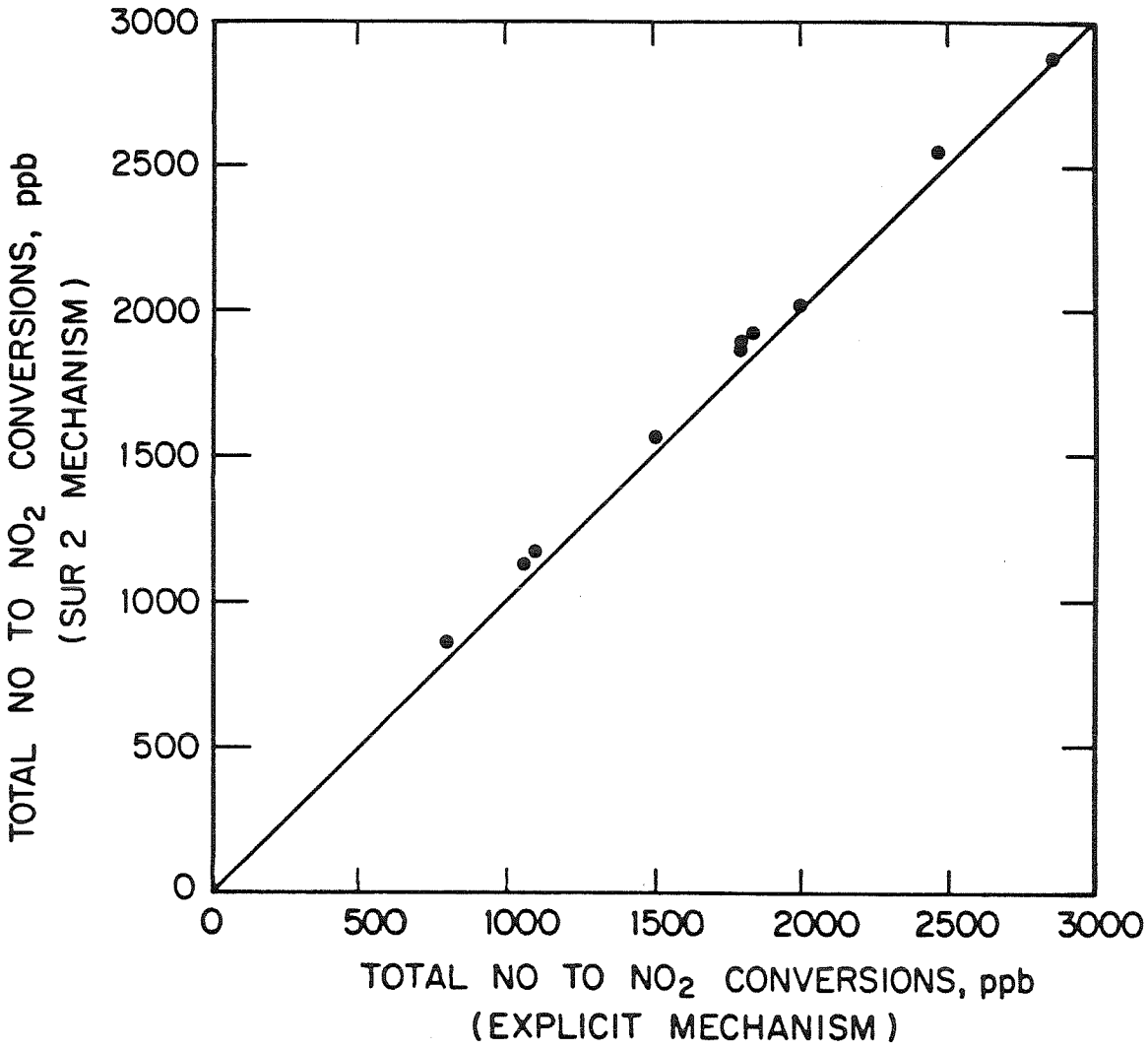

Figure 13. Comparison of the total amount of NO to NO_2 conversions predicted by the explicit and SUR2 mechanisms. Each point corresponds to one of the SAPRC multi-hydrocarbon-NO_x experiments EC-231 through EC-246.

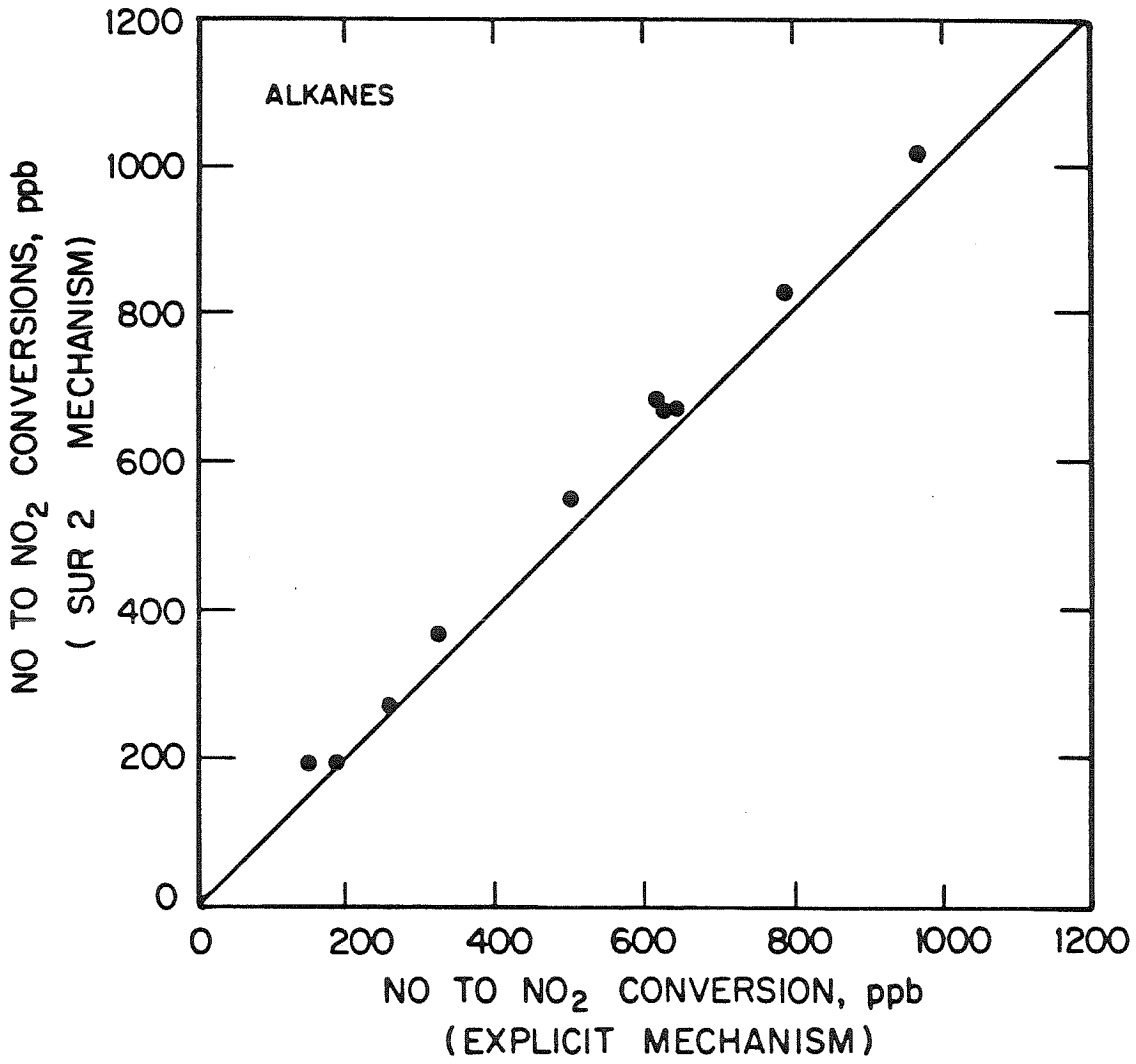

Figure 14. Comparison of the counter species results for the alkanes between the explicit and SUR2 mechanisms. Each point corresponds to one of the SAPRC multi-hydrocarbon-NO_x experiments EC-231 through EC-246.

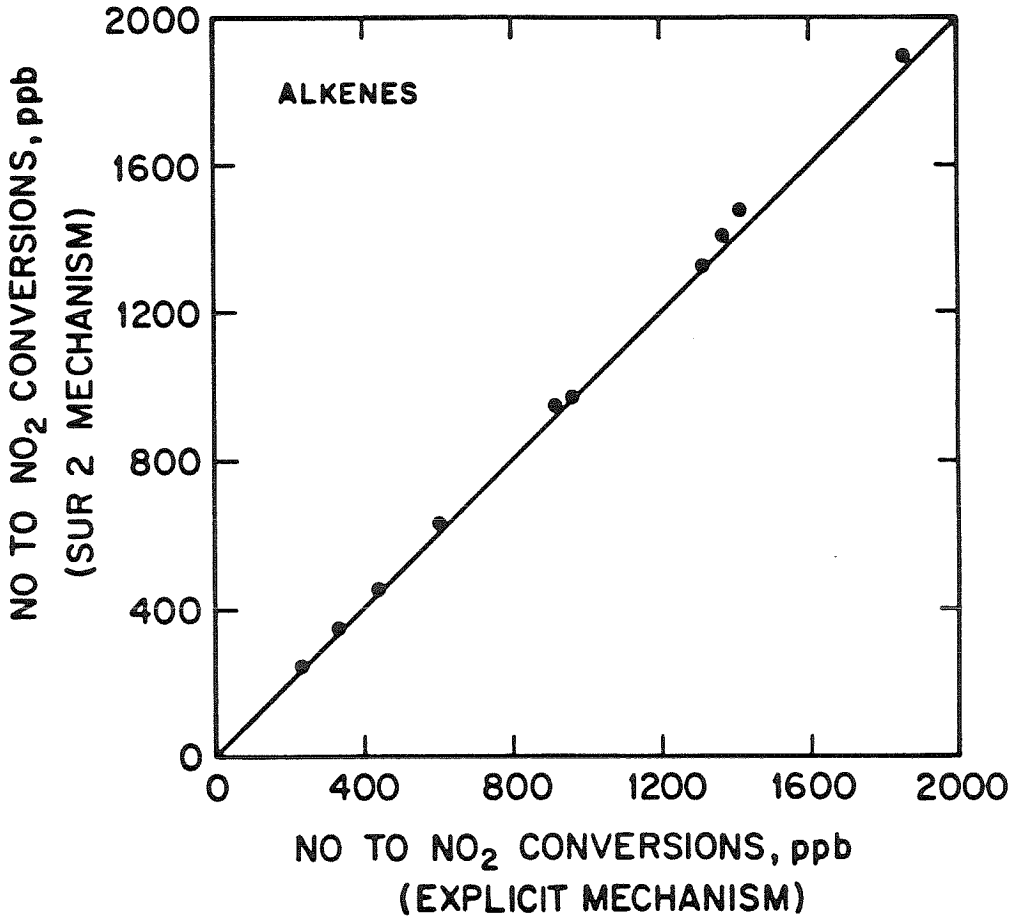

Figure 15. Comparison of the counter species results for the alkenes between the explicit and SUR2 mechanisms. Each point corresponds to one of the SAPRC multi-hydrocarbon-NO_x experiments EC-231 through EC-246.

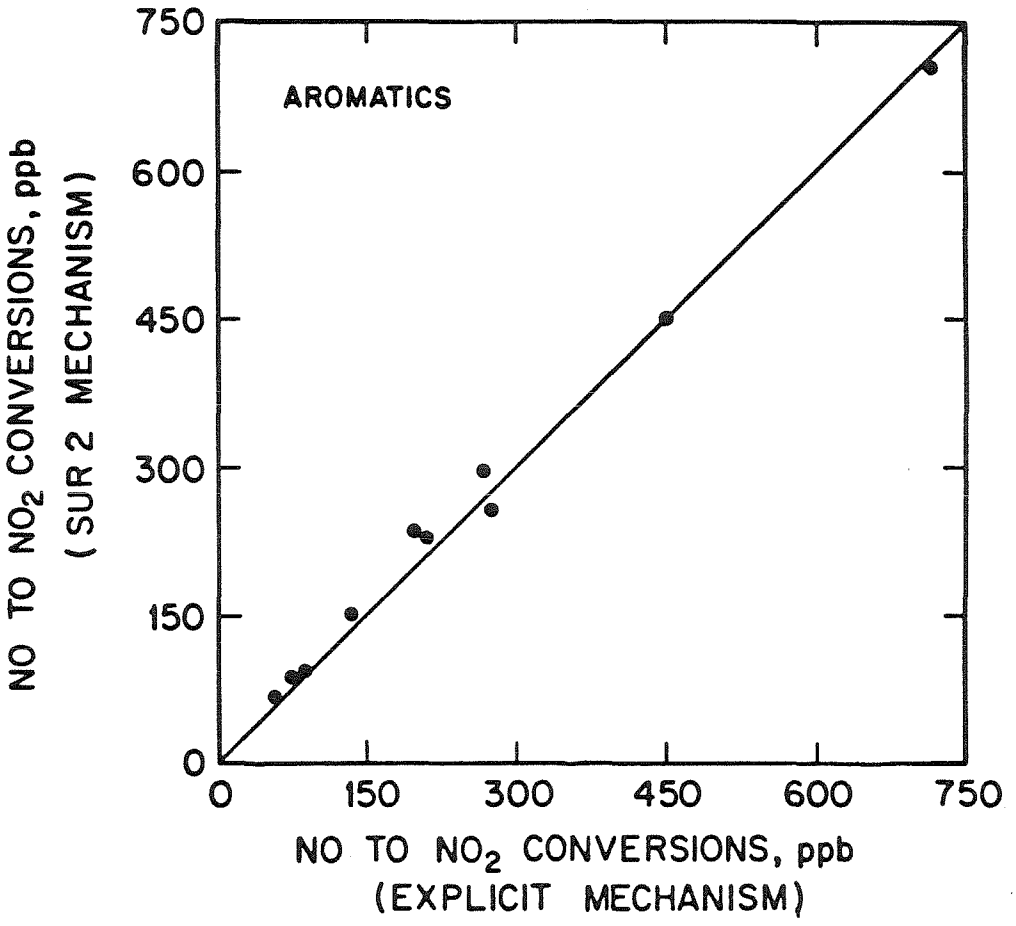

Figure 16. Comparison of the counter species results for the aromatics between the explicit and SUR2 mechanisms. Each point corresponds to one of the SAPRC multi-hydrocarbon-NO_x experiments EC-231 through EC-246.

surrogate and explicit mechanisms is obtained with the alkenes, but very good agreement is also found for the alkanes and aromatics. This type of agreement for each class of organic indicates that the SUR2 mechanism represents the chemistry found in the explicit mechanism very well.

Tests with the SUR2 mechanism indicate that one additional non-steady-state species, o-cresol, can be eliminated with less than a five percent effect on the predictions of the mechanism. This elimination would reduce the number of non-steady-state species from 20 to 19. However, with recently developed solution techniques, the amount of CPU time required for solution increases approximately linearly with the number of non-steady-state species (21,22). Thus, it is no longer crucial that the number of species be kept to an absolute minimum. With this in mind, we have decided not to remove o-cresol from the SUR2 mechanism.

EVALUATION OF THE SUR2 MECHANISM

The first step in evaluating the SUR2 mechanism for use in urban air quality models is to evaluate the performance of the mechanism against smog chamber data. In addition to testing the ozone formation aspect of the SUR2 mechanism, these evaluations will indicate how well the mechanism can predict important characteristics such as organic decay rates. In evaluating mechanisms with experimental data, it is very important to make use of data from more than one smog chamber facility, especially because of the different magnitudes of chamber specific radical sources in different facilities. We have chosen therefore to model experiments from two quite different smog chamber facilities, the evacuable chamber at SAPRC, and the outdoor chamber at the University of North

Carolina (UNC). The indoor chamber at SAPRC is relatively small ($5.8m^3$), makes use of artificial solar radiation, operates under conditions of constant temperature and light intensity, and appears to supply a relatively large source of free radicals to the chamber contents (18). In contrast, the UNC chamber is very large ($\sim 100m^3$ per side of a dual chamber), uses natural sunlight, operates near ambient temperature, and apparently has a considerably smaller wall radical source than the SAPRC chamber (27).

In order to adapt the SUR2 mechanism for modeling chamber experiments it is necessary to add several reactions to the mechanism, which are summarized in Table A.6. The SAPRC experiments we have chosen to model are once again the 10 multi-hydrocarbon-NO_x experiments EC-231 through EC-246. The initial conditions and physical parameters for these experiments have been given in Table A.2. Six experiments from the outdoor UNC chamber will also be simulated. These experiments are also multi-hydrocarbon-NO_x runs in which both the initial hydrocarbon distribution and the $[RHC]_o/[NO_x]_o$ ratio are varied. The initial conditions for these six experiments are given in Table A.7.

Many of the results of modeling these 16 experiments with the SUR2 mechanism are shown in Figures A.10 through A.23. The agreement between experiment and prediction is good with both sets of experimental data. The results for the SAPRC experiments (Figures A.10 through A.17) are very close to those obtained with the explicit mechanism (Figures A.1 through A.9), a further indication that the SUR2 mechanism is a good representation of the explicit chemistry in the explicit mechanism. In the experiments at SAPRC, the SUR2 mechanism, like the explicit mechanism, tends to over-predict the O_3 peak heights and slightly over-predict the PAN peak

height. The time of the NO_2 and O_3 peaks, the height of the NO_2 peak, and the hydrocarbon decay rates are all predicted very well. In the experiments performed at UNC*, the SUR2 mechanism does very well in predicting O_3 and PAN peak heights, with the typical O_3 peak being slightly under-predicted. Once again, the time of the ozone peak and the hydrocarbon decay rates lie very close to the experimental data. We repeat that, while chamber effects are used in these simulations, each chamber dependent term is set at the value recommended by either SAPRC or UNC, and not varied as the initial conditions of the experiments changed.

APPLICATION TO THE ATMOSPHERE

Up to this point, the SUR2 mechanism has only been applied under conditions, such as a smog chamber experiment, where the initial organic distribution is known exactly. In the atmosphere the organic distribution is not well defined, and fresh emissions are continuously being added. In this case, one needs a way of formulating a set of initial conditions that will accurately represent the complicated atmospheric mix. Although relatively few studies of ambient organic concentrations have been performed to date, many major cities now have some information available on both ambient organic distributions and emissions inventories. When ambient organic data are available for the city of interest, these data should be used with measurements of total NMHC and the information in Table 3 to obtain the initial conditions for use with the SUR2 mechanism. This is the standard method of obtaining initial conditions for atmospheric applications of lumped

*PAN was not measured in some of the UNC experiments, so the experimental NO_2 data actually correspond to the sum of NO_2 and PAN.

Table 3. Surrogate Species Used with the SUR2 Mechanism and the Compounds They Represent[1]

Surrogate Species	Compounds Represented
ALK	All C_4 and greater alkanes
propene	All C_3 and greater terminal alkenes
trans-2-butene	All C_4 and greater internal alkenes
toluene	All mono-alkylbenzenes
xylene	All di- and tri-alkylbenzenes
acetaldehyde	All C_2 and greater aldehydes
formaldehyde	formaldehyde
benzene	benzene
ethene	ethene

[1] In the SUR2 mechanism, propene and butene are lumped into the OLE group, and toluene and xylene are lumped into the ARO group. However, the individual concentrations of the surrogate species (propene, butene, toluene, and xylene) must be calculated in order to determine the stoichiometric coefficients and rate constants for the reactions involving the OLE and ARO groups.

mechanisms. If no detailed organic composition data are available for the city of interest, a distribution of organics must be assumed. Experimental studies of organics in urban air, such as the investigation of Grosjean and Fung (29), should be helpful in this matter. Obviously, more work is needed in order to both better characterize the distribution of ambient organics and to understand the effects of varying this distribution on the predictions of chemical mechanisms.

CONCLUSIONS

A surrogate condensed chemical reaction mechanism for photochemical smog containing the latest available kinetic and mechanistic data is developed here and is extensively tested against experimental data from two smog chamber facilities. In addition, a counter species analysis has shown that the predictions of the individual portions of the surrogate mechanism are in good agreement with those of a detailed explicit mechanism for photochemical smog. The new mechanism contains 20 non-steady-state species, making it compact enough for use in multidimensional grid models of urban air pollution. A major advantage of the new mechanism is the ease with which it can be modified to incorporate new kinetic or mechanistic information because of the straightforward manner in which the mechanism was formulated from the detailed explicit chemistry.

Future work should concentrate on the atmospheric application of the new mechanism. Ozone isopleths generated with the new mechanism should be compared to those obtained using the existing mechanisms for photochemical smog. The effects of dilution, hydrocarbons aloft, and aldehydes aloft on the predictions of the new mechanism should be studied. In addition, more

attention should be directed toward the specification of initial conditions using measurements of atmospheric hydrocarbon distributions and emission inventories.

REFERENCES

(1) Falls, A.H. and Seinfeld, J. H. (1978), "Continued Development of a Kinetic Mechanism for Photochemical Smog," Environmental Science and Technology, 12, 1398-1406.

(2) Atkinson, R., Lloyd, A.C. and Winges, L. (1982), "An Updated Chemical Mechanism for Hydrocarbons/NO_x/SO_2 Photooxidations Suitable for Inclusion in Atmospheric Simulation Models," Atmospheric Environment, 16, 1341-1355.

(3) Killus, J.P. and Whitten, G.Z. (1982), A New Carbon-Bond Mechanism for Air Quality Modeling, U.S. Environmental Protection Agency Report No. EPA-600/3-82-041.

(4) Dodge, M.C. (1977), Combined Use of Modeling Techniques and Smog Chamber Data to Derive Ozone-Precursor Relationships, U.S. Environmental Protection Agency Report, EPA-600/3-77-001a, 881-889.

(5) Demerjian, K.L. (1982), "Personal Communication."

(6) Penner, J.E. and Walton, J.J. (1982) Air Quality Model Update, Lawrence Livermore Laboratory Report UCID - 19300, Lawrence Livermore National Laboratory, University of California, Livermore, California, 55 pp.

(7) Jeffries, H.E., Sexton, K.G. and Salmi, C.N. (1981), Effects of Chemistry and Meteorology on Ozone Control Calculations Using Simple Trajectory Models and the EKMA Procedure, Final Report to the U.S. Environmental Protection Agency Under Contract No. 68-02-3523, School of Public Health, University of North Carolina, Chapel Hill, North Carolina, 373 pp.

(8) Whitten, G.Z. (1981) Comments at U.S. Environmental Protection Agency Workshop on the Empirical Kinetic Modeling Approach, December 15-16, Research Triangle Park, NC.

(9) Carter, W.P.L., Winer, A.M. and Pitts, J.N., Jr. (1982) "Effect of Kinetic Mechanisms and Hydrocarbon Composition on Oxidant-Precursor Relationships Predicted by the EKMA Isopleth Technique," Atmospheric Environment 16, 113-120.

(10) Leone, J.A. and Seinfeld, J.H. (1983) Evaluation of Chemical Reaction Mechanisms for Photochemical Smog - Part II. Quantitative Evaluation of the Mechanisms, U.S. Environmental Protection Agency Report (in press).

(11) Leone, J.A. and Seinfeld, J.H. (1984) "Comparative Analysis of Chemical Reaction Mechanisms for Photochemical Smog," Atmospheric Environment (in press).

(12) Pitts, J.N., Winer, A.M., Darnall, K.R. et al. (1976), Chemical Consequences of Air Quality Standards and of Control Implementation Programs: Roles of Hydrocarbons, Oxides of Nitrogen, and Aged Smog in the Production of Photochemical Oxidant, Final Report to the California Air Resources Board under Contract Number 4-212, Statewide Air Pollution Research Center, University of California Riverside, California, 444 pp.

(13) Baulch, D.L., Cox, R.A., Crutzen, P.J., Hampson, R.F., Kerr, J.A., Troe, J. and Watson, R.T. (1982), "Evaluated Kinetic and Photochemical Data for Atmospheric Chemistry: Supplement 1. CODATA Task Group on Chemical Kinetics," J. Physical and Chemical Reference Data, 11, 327-496.

(14) DeMore, W.B., Watson, R.T., Howard, C.J., Golden, D.M., Molina, M.J., Hampson, R.F., Kurylo, M. and Ravishankara, A.R. (1982), Chemical Kinetics and Photochemical Data for Use in Stratospheric Modeling, Jet Propulsion Laboratory Publication 82-57, California Institute of Technology, Pasadena, California.

(15) Leone, J.A. and Seinfeld, J.H. (1983), "An Updated Chemical Mechanism for the Atmospheric Photooxidation of Toluene," International Journal of Chemical Kinetics, 16, 159-193.

(16) Leone, J.A., Flagan, R.C., Grosjean, D. and Seinfeld, J.H. (1984), "An Outdoor Smog Chamber and Modeling Study of Toluene-NO_x Photooxidation," International Journal of Chemical Kinetics, (in press).

(17) Atkinson, R. and Lloyd, A.C. (1984), "Evaluation of Kinetic and Mechanistic Data for Modeling of Photochemical Smog," J. Phys. Chem. Ref. Data, 13 (2), in press.

(18) Carter, W.P.L., Atkinson, R., Winer, A.M. and Pitts, J.N. Jr., (1982) "Experimental Investigation of Chamber-Dependent Radical Sources," International Journal of Chemical Kinetics, 14, 1071-1103.

(19) Atkinson, R., Carter, W.P.L., Darnall, K.R., Winer, A.M., and Pitts, J.N. Jr. (1980), "A Smog Chamber and Modeling Study of the Gas Phase NO_x-Air Photooxidation of Toluene and the Cresols," International Journal of Chemical Kinetics, 12, 779-837.

(20) Leone, J.A. and Seinfeld, J.H. (1983), "Analysis of the Characteristics of Complex Chemical Reaction Mechanisms - Application to Photochemical Smog Chemistry," Environmental Science & Technology, 18, 280-287.

(21) Russell, A. (1984), "Personal Communication."

(22) Young, T.R. and Boris, J.P. (1977), "A Numerical Technique for Solving Stiff Ordinary Differential Equations Associated with the Chemical Kinetics of Reactive-Flow Problems," Journal of Physical Chemistry, 81, 2423-2427.

(23) Pitts, J.N., Jr., Darnall, K., Carter, W.P.L., Winer, A.M. and Atkinson, R. (1979), Mechanisms of Photochemical Reactions in Urban Air - Final Report, U.S. Environmental Protection Agency Report No. EPA-600/3-79-110.

(24) Demerjian, K.L., Schere, K.L. and Peterson, J.T. (1980), "Theoretical Estimates of Actinic (Spherically Integrated) Flux and Photolytic Rate Constants of Atmospheric Species in the Lower Troposphere," Advances in Environmental Science and Technology, 10, 369-459.

(25) Grosjean, D. (1983), "Atmospheric Reactions of Pyruvic Acid," Atmospheric Environment, 17, 2379-2382.

(26) Horowitz, A. and Calvert, J.G. (1982), "Wavelength Dependence of the Primary Processes in Acetaldehyde Photolysis," J. Physical Chemistry, 86, 3105-3114.

(27) Jeffries, H.E., Kamens, R.M., Sexton, K.G. and Gerhardt, A.A. (1982), Outdoor Smog Chamber Experiment to Test Photochemical Models, U.S. Environmental Protection Agency Report.

(28) Plum, C.N., Sanhueza, E., Atkinson, R., Carter, W.P.L. and Pitts, J.N., Jr., "OH Radical Rate Constants and Photolysis Rates of α-Dicarbonyls," Environmental Science and Technology, 17, 479.

(29) Grosjean, D. and Fung, K. (1984), "Hydrocarbons and Carbonyls in Los Angeles Air," Journal Air Pollution Control Association, 34, 537-543.

APPENDIX

Table A.1. Explicit Reaction Mechanism

Reaction[1,2]	Rate Constant[3]	Activation Energy (K)	Note
Inorganic Reactions (13,14,17):			
1) $NO_2 + h\nu \rightarrow NO + O(^3P)$	0.30	-	1
2) $O(^3P) + O_2 \rightarrow O_3$	2.6×10^{1}	-5.1×10^{2}	
3) $O_3 + NO \rightarrow NO_2 + O_2$	2.7×10^{1}	1.5×10^{3}	
4) $O(^3P) + NO_2 \rightarrow NO + O_2$	1.4×10^{4}	-	
5) $O_3 + NO_2 \rightarrow NO_3 + O_2$	4.7×10^{-2}	2.45×10^{3}	
6) $NO_3 + NO \rightarrow 2NO_2$	3.0×10^{4}	-	
7) $HO_2 + NO_2 \rightarrow HO_2NO_2$	1.6×10^{3}	-	
8) $NO_2 + OH \rightarrow HNO_3$	1.6×10^{4}	-	
9) $O_3 + OH \rightarrow HO_2 + O_2$	9.9×10^{1}	9.7×10^{2}	
10) $O_3 + HO_2 \rightarrow OH + 2O_2$	3.0×10^{0}	5.8×10^{2}	
11) $HO_2NO_2 \rightarrow HO_2 + NO_2$	5.1×10^{0}	1.042×10^{4}	
12) $HO_2 + NO \rightarrow NO_2 + OH$	1.2×10^{4}	-2.4×10^{2}	
13) $HO_2 + HO_2 \rightarrow H_2O_2 + O_2$	3.9×10^{3}	-1.2×10^{3}	
14) $HO_2 + HO_2 + H_2O \rightarrow H_2O_2 + O_2 + H_2O$	2.2×10^{-1}	-5.8×10^{3}	
15) $O_3 + h\nu \rightarrow O(^3P) + O_2$	$6.5 \times 10^{-2}\ k_{NO_2}$	-	2
16) $O_3 + h\nu \rightarrow O(^1D) + O_2$	$2.8 \times 10^{-3}\ K_{NO_2}$	-	2
17) $O(^1D) + O_2 \rightarrow O(^3P) + O_2$	4.3×10^{4}	-	
18) $O(^1D) + H_2O \rightarrow 2OH$	3.2×10^{5}	-	
19) $NO + OH \rightarrow HONO$	9.7×10^{3}	-	
20) $HONO + h\nu \rightarrow NO + OH$	$1.8 \times 10^{-1}\ k_{NO_2}$	-	2
21) $NO + NO + O_2 \rightarrow 2NO_2$	7.2×10^{-10}	-5.3×10^{2}	
22) $NO_3 + NO_2 \rightarrow NO + NO_2 + O_2$	5.9×10^{-1}	1.23×10^{3}	

Table A.1 (continued)

Reaction [1,2]	Rate Constant[3]	Activation Energy (K)	Note
23) $NO_3 + NO_2 \rightarrow N_2O_5$	1.6×10^3	-	
24) $N_2O_5 \rightarrow NO_2 + NO_3$	3.1×10^0	1.108×10^4	
25) $N_2O_5 + H_2O \rightarrow 2HNO_3$	4.4×10^{-6}	-	1
26) $H_2O_2 + OH \rightarrow HO_2 + H_2O$	2.5×10^3	-	
27) $H_2O_2 + h\nu \rightarrow 2OH$	$8.4 \times 10^{-4}\ k_{NO_2}$	-	2
28) $CO + OH \xrightarrow{O_2} HO_2 + CO_2$	4.0×10^2	-	
29) $NO_3 + h\nu \rightarrow 0.3NO + 0.7NO_2 + 0.70(^3P)$	$1.55 \times 10^1\ k_{NO_2}$	-	3

Aldehyde Reactions and PAN Formation (17):

30) $CH_3CHO + h\nu \xrightarrow{2O_2} CH_3O_2\cdot + HO_2 + CO$	$2.58 \times 10^{-4}\ k_{NO_2}$	-	4
31) $CH_3CHO + OH \xrightarrow{O_2} CH_3C(O)O_2\cdot + H_2O$	2.4×10^4	-2.6×10^2	
32) $CH_3O_2\cdot + NO \rightarrow NO_2 + CH_3O\cdot$	1.1×10^4	-	
33) $CH_3O\cdot + O_2 \rightarrow HCHO + HO_2\cdot$	2.1×10^0	1.35×10^3	
34) $CH_3O\cdot + NO_2 \rightarrow CH_3ONO_2$	2.2×10^4	-	
35) $CH_3O_2\cdot + HO_2 \rightarrow CH_3OOH + O_2$	9.2×10^3	-1.3×10^3	
36) $CH_3C(O)O_2\cdot + NO \xrightarrow{2O_2} NO_2 + CH_3O_2\cdot + CO_2$	1.1×10^4	-	
37) $CH_3C(O)O_2\cdot + NO_2 \rightarrow PAN$	6.9×10^3	-	
38) $CH_3C(O)O_2\cdot + HO_2 \rightarrow CH_3C(O)O_2H + O_2$	4.4×10^3	-	
39) $PAN \rightarrow CH_3C(O)O_2\cdot + NO_2$	2.2×10^{-2}	1.354×10^4	
40) $HCHO + h\nu \rightarrow H_2 + CO$	$3.3 \times 10^{-3}\ k_{NO_2}$	-	4
41) $HCHO + h\nu \xrightarrow{2O_2} 2HO_2 + CO$	$2.35 \times 10^{-3}\ k_{NO_2}$	-	4

Table A.1 (continued)

Reaction[1,2]	Rate Constant[3]	Activation Energy (K)	Note
42) $HCHO + OH \xrightarrow{O_2} HO_2 + CO + H_2O$	1.6×10^4	-	
α-Dicarbonyl Chemistry (17,28):			
43) $CH_3C(O)CHO + OH \xrightarrow{O_2} CH_3C(O)O_2\cdot + CO + H_2O$	2.5×10^4	-	
44) $CH_3C(O)CHO + h\nu \xrightarrow{2O_2} CH_3C(O)O_2\cdot + HO_2 + CO$	$1.3\times10^{-2}\ k_{NO_2}$	-	
45) $CH_3C(O)CHO + h\nu \xrightarrow{2O_2} CH_3O_2\cdot + HO_2 + 2CO$	$6.0\times10^{-3}\ k_{NO_2}$	-	
46) $(CHO)_2 + OH \xrightarrow{O_2} HO_2 + 2CO + H_2O$	1.7×10^4	-	
47) $(CHO)_2 + h\nu \rightarrow 0.13HCHO + 0.87H_2 + 1.87CO$	$8.0\times10^{-3}\ k_{NO_2}$	-	
Toluene Abstraction Pathway (15,16)			
48) $C_6H_5\text{-}CH_3 + OH \xrightarrow{O_2} C_6H_5\text{-}CH_2O_2\cdot + H_2O$	7.5×10^2	-	
49) $C_6H_5\text{-}CH_2O_2\cdot + NO \rightarrow NO_2 + C_6H_5\text{-}CH_2O\cdot$	9.0×10^3	-	
50) $C_6H_5\text{-}CH_2O_2\cdot + NO \rightarrow C_6H_5\text{-}CH_2ONO_2$	1.0×10^3	-	
51) $C_6H_5\text{-}CH_2O\cdot + O_2 \rightarrow C_6H_5\text{-}CHO + HO_2$	1.0×10^1	6.9×10^2	
52) $C_6H_5\text{-}CH_2O\cdot + NO_2 \rightarrow C_6H_5\text{-}CH_2ONO_2$	1.9×10^4	-	
53) $C_6H_5\text{-}CHO + h\nu \rightarrow$ stable products	1.6×10^{-3}	-	
54) $C_6H_5\text{-}CHO + OH \xrightarrow{O_2} C_6H_5\text{-}C(O)O_2\cdot + H_2O$	1.9×10^4	-	
55) $C_6H_5\text{-}C(O)O_2\cdot + NO \xrightarrow{O_2} NO_2 + C_6H_5\text{-}O_2\cdot + CO_2$	1.0×10^4	-	

Table A.1 (continued)

Reaction[1,2]	Rate Constant[3]	Activation Energy (K)	Note
56) $C_6H_5\text{-}C(O)O_2\cdot + NO_2 \rightarrow C_6H_5\text{-}C(O)O_2NO_2$	6.9×10^3	-	
57) $C_6H_5\text{-}C(O)O_2NO_2 \rightarrow C_6H_5\text{-}C(O)O_2\cdot + NO_2$	9.6×10^{-3}	1.304×10^4	
58) $C_6H_5\text{-}O_2\cdot + NO \rightarrow NO_2 + C_6H_5\text{-}O\cdot$	9.0×10^3	-	
59) $C_6H_5\text{-}O_2\cdot + NO_2 \rightarrow NO_3 + C_6H_5\text{-}O\cdot$	1.0×10^4	-	
60) $C_6H_5\text{-}O\cdot + NO_2 \rightarrow$ 	2.2×10^4	-	
61) 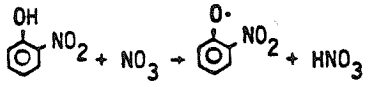	3.0×10^3	-	
62) 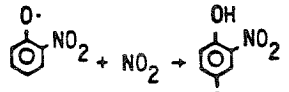	2.2×10^4	-	
63) 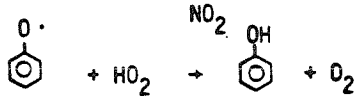	7.4×10^3	-	

Toluene Addition Pathway (15,16):

64) 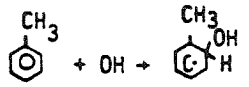	8.7×10^3	-	
65) 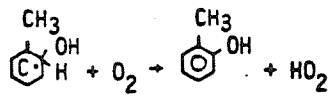	1.0×10^1	6.9×10^2	
66) 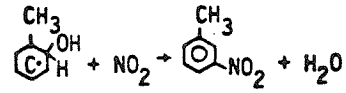	4.4×10^4	-	
67) 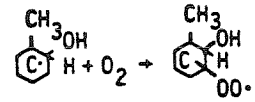	4.9×10^1	-	
68) 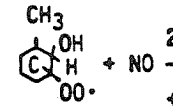 $\xrightarrow{2O_2}$ $NO_2 + HO_2$ + $CH_3C(O)CHO$ + $CH(O)CH{=}CHCHO$	1.0×10^4	-	

Table A.1 (continued)

Reaction[1,2]	Rate Constant[3]	Activation Energy (K)	Note
Toluene addition path (continued)			
69) 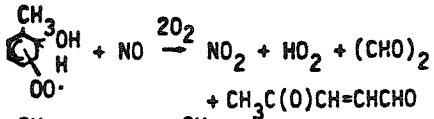	0.0	-	
70) 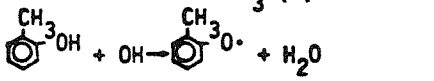	4.9×10^3	9.0×10^2	
71) 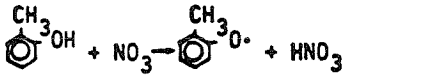	1.5×10^4	-	
72) 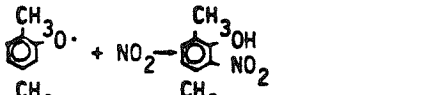	2.2×10^4	-	
73) 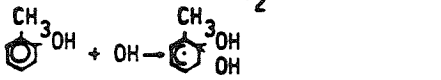	5.6×10^4	-	
74) 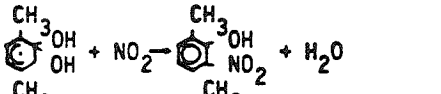	4.4×10^4	-	
75) 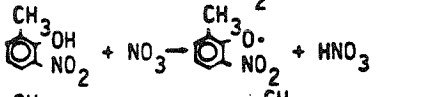	1.5×10^4	-	
76) 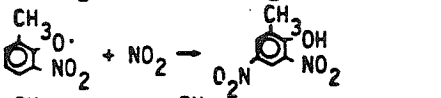	2.2×10^4	-	
77) 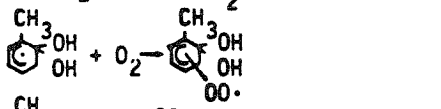	4.9×10^1	-	
78) 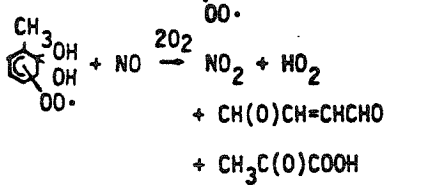	1.0×10^4	-	
79) 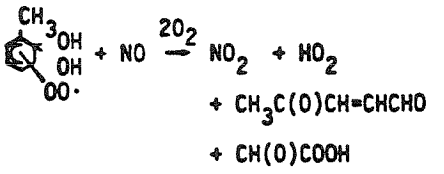	0.0	-	

Table A.1 (continued)

Reaction[1,2]	Rate Constant[3]	Activation Energy(K)	Note
80) $CH(O)COOH + OH \xrightarrow{O_2} HO_2 + H_2O + CO + CO_2$	2.2×10^{4}	-	
81) $CH_3C(O)COOH + h\nu \rightarrow CH_3CHO + CO_2$	$3.6\times10^{-2}\ k_{NO_2}$	-	5
Conjugated γ-dicarbonyl chemistry (15-17)			
82) $HC(O)CH=CHCHO + OH \xrightarrow{O_2} HC(O)CH=CHC(O)O_2\cdot + H_2O$	4.4×10^{4}	-	
83) $HC(O)CH=CHC(O)O_2\cdot + NO \xrightarrow{O_2} NO_2 + CO_2 + HC(O)CH=CHO_2\cdot$	1.0×10^{4}	-	
84) $HC(O)CH=CHO_2\cdot + NO \xrightarrow{O_2} NO_2 + HC(O)CH(O_2\cdot)CHO$	1.0×10^{4}	-	
85) $HC(O)CH(O_2\cdot)CHO + NO \rightarrow HC(O)CH(ONO_2)CHO$	4.0×10^{2}	-	
86) $HC(O)CH=CHC(O)O_2\cdot + NO_2 \rightarrow HC(O)CH=CHCO_3NO_2$	6.9×10^{3}	-	
87) $HC(O)CH=CHCO_3NO_2 \rightarrow HC(O)CH=CHC(O)O_2\cdot + NO_2$	2.2×10^{-2}	-	
88) $HC(O)CH(O_2\cdot)CHO + NO \xrightarrow{O_2} (CHO)_2 + HO_2 + NO_2 + CO$	1.0×10^{4}	-	
89) $HC(O)CH=CHO_2\cdot + NO \rightarrow HC(O)CH=CHONO_2$	4.0×10^{2}	-	
90) $HC(O)CH=CHO_2\cdot + NO_2 \xrightarrow{O_2} HC(O)CH(O_2\cdot)CHO + NO_3$	1.0×10^{4}	-	
91) $CH_3C(O)CH=CHCHO + OH \xrightarrow{O_2} H_2O + CH_3C(O)CH=CHC(O)O_2\cdot$	2.2×10^{4}	-	
92) $CH_3C(O)CH=CHCHO + OH \xrightarrow{O_2} CH_3C(O)CH(OH)C(O_2\cdot)HCHO$	7.4×10^{3}	-	
93) $CH_3C(O)CH(OH)C(O_2\cdot)HCHO + NO \xrightarrow{O_2} NO_2 + HO_2 + CH_3C(O)CHO + (CHO)_2$	1.0×10^{4}	-	
94) $CH_3C(O)CH=CHC(O)O_2\cdot + NO \xrightarrow{O_2} NO_2 + CO_2 + CH_3C(O)CH=CHO_2\cdot$	1.0×10^{4}	-	
95) $CH_3C(O)CH=CHO_2\cdot + NO \xrightarrow{O_2} NO_2 + CH_3C(O)CH(O_2\cdot)CHO$	1.0×10^{4}	-	
96) $CH_3C(O)CH(O_2\cdot)CHO + NO \rightarrow CH_3C(O)CH(ONO_2)CHO$	8.0×10^{6}	-	
97) $CH_3C(O)CH=CHC(O)O_2\cdot + NO \rightarrow CH_3C(O)CH=CHCO_3NO_2$	6.9×10^{3}	-	
98) $CH_3C(O)CH=CHCO_3NO_2 \rightarrow CH_3C(O)CH=CHC(O)O_2\cdot + NO_2$	2.2×10^{-2}	-	
99) $CH_3C(O)CH(O_2\cdot)CHO + NO \xrightarrow{O_2} NO_2 + CH_3C(O)O_2\cdot + (CHO)_2$	5.0×10^{3}	-	

Table A.1 (continued)

Reaction[1,2]	Rate Constant[3]	Activation Energy(K)	Note
Conjugated γ-dicarbonyl chemistry (continued)			
100) $CH_3C(O)CH(O_2\cdot)CHO+NO \xrightarrow{O_2} NO_2+HO_2+CH_3C(O)CHO+CO$	5.0×10^3	-	
101) $CH_3C(O)CH=CHO_2\cdot+NO \rightarrow CH_3C(O)CH=CHONO_2$	8.0×10^2	-	
102) $CH_3C(O)CH=CHO_2\cdot+NO_2 \xrightarrow{O_2} NO_3+CH_3C(O)CH(O_2\cdot)CHO$	1.0×10^4	-	
m-Xylene chemistry (15-17):			
103) 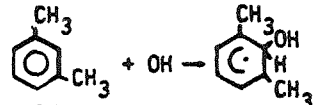	3.4×10^4	-	6
104) 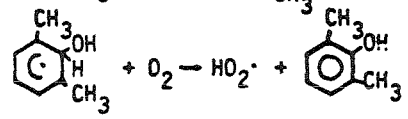	1.0×10^2	6.9×10^2	
105) 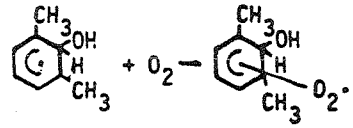	4.7×10^1	-	
106) 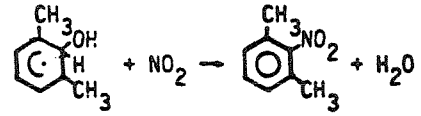	4.4×10^4	-	
107) 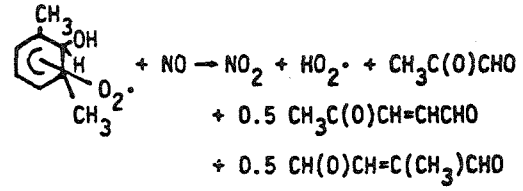	1.0×10^4	-	7
108) 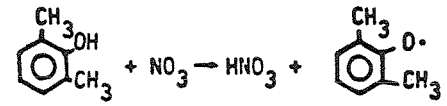	2.2×10^4	-	
109) 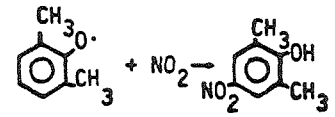	2.2×10^4	-	

Table A.1 (continued)

	Reaction[1,2]	Rate Constant[3]	Activation Energy(K)	Note
	m-Xylene chemistry (continued)			
110)	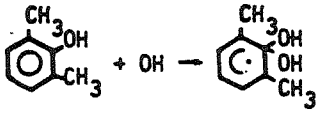	1.1×10^{5}	-	
111)	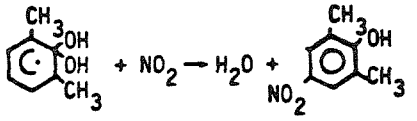	4.4×10^{4}	-	
112)	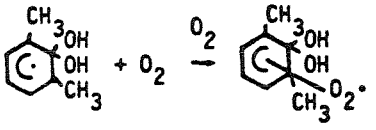	4.7×10^{1}	-	
113)	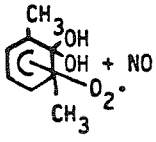 $+ NO \rightarrow NO_2 + HO_2 + CH_3COCOOH + 0.5\ CH_3COCH{=}CHCHO + 0.5\ CHOCH{=}C(CH_3)CHO$	1.0×10^{4}	-	7
114)	$CHOCH{=}C(CH_3)CHO + OH \xrightarrow{O_2} HCOC(OH)HC^{\cdot}(CH_3)CHO_2^{\cdot}$	7.4×10^{3}	-	
115)	$HCOC(OH)HC^{\cdot}(CH_3)CHO_2^{\cdot} + NO \xrightarrow{O_2} 0.88NO_2 + 0.88(CHO)_2 + 0.88\ HO_2^{\cdot}$	1.0×10^{4}	-	8
116)	$CHOCHO{=}C(CH_3)CHO + OH \xrightarrow{O_2} HCOCH{=}C^{\cdot}(CH_3)CO_3^{\cdot} + H_2O$	4.4×10^{4}		
117)	$HCOCH{=}C^{\cdot}(CH_3)CO_3^{\cdot} + NO \xrightarrow{O_2} NO_2 + HCOCH{=}C^{\cdot}(CH_3)CO_2^{\cdot} + CO_2$			
118)	$HCOCH{=}C^{\cdot}(CH_3)CO_3^{\cdot} + NO_2 \rightarrow HCOCH{=}C^{\cdot}(CH_3)CO_3\ NO_2$	6.9×10^{3}	-	
119)	$HCOCH{=}C^{\cdot}(CH_3)CO_3NO_2 \rightarrow NO_2 + HCOCH{=}C^{\cdot}(CH_3)CO_3^{\cdot}$	2.2×10^{-2}	1.354×10^{4}	

Table A.1 (continued)

Reaction[1,2]	Rate Constant[3]	Activation Energy(K)	Note
m-Xylene chemistry (continued)			
120) $HCOCH{=}\overset{CH_3}{\overset{|}{C}}O_2\cdot + NO \xrightarrow{O_2} NO_2 + CH_3(O)CH(O_2\cdot)CHO$	1.0×10^4	-	
121) $HCOCH{=}\overset{CH_3}{\overset{|}{C}}O_2\cdot + NO \rightarrow HCOCH{=}\overset{CH_3}{\overset{|}{C}}CO_2NO_2$	8.0×10^2	-	
122) $HCOCH{=}\overset{CH_3}{\overset{|}{C}}O_2\cdot + NO_2 \rightarrow NO_3 + CH_3C(O_2\cdot)(CHO)_2$	1×10^4	-	
123) $CH_3C(O_2\cdot)(CHO)_2 + NO \rightarrow CH_3C(ONO_2)(CHO)_2$	8.0×10^2	-	
124) $CH_3C(O_2\cdot)(CHO)_2 + NO \xrightarrow{O_2} 0.75\ HO_2\cdot + 0.75\ CO + 0.75\ CH_3COCHO + 0.25\ (CHO)_2 + 0.25\ CH_3C(O)O_2\cdot + NO_2$	1×10^4	-	
Ethene chemistry (17):			
125) $CH_2{=}CH_2 + OH \xrightarrow{O_2} HOCH_2CH_2O_2\cdot$	1.2×10^4	-3.82×10^2	
126) $HOCH_2CH_2O_2\cdot + NO \rightarrow NO_2 + HOCH_2CH_2O\cdot$	1×10^4		
127) $HOCH_2CH_2O\cdot \rightarrow HCHO + \cdot CH_2OH$	5.6×10^6		
128) $HOCH_2CH_2O\cdot + O_2 \rightarrow HOCH_2CHO + HO_2\cdot$	1.0×10^1	6.9×10^2	9
129) $\cdot CH_2OH + O_2 \rightarrow HCHO + HO_2\cdot$	$k_5=3\times10^3$		
130) $CH_2{=}CH_2 + O_3 \xrightarrow{O_2} HCHO + 0.4\ \dot{C}H_2O\dot{O} + 0.18\ CO_2 + 0.42CO + 0.12\ H_2 + 0.42\ H_2O + 0.12\ HO_2\cdot$	2.5×10^{-3}	2.56×10^3	

Table A.1 (continued)

Reaction [1,2]	Rate Constant [3]	Activation Energy(K)	Note
Propene chemistry (17):			
131) $CH_3CHCH_2 + OH \xrightarrow{O_2} 0.65\ CH_3\dot{C}HCH_2OH(O_2\cdot) + 0.35\ CH_3CH(OH)CH_2O_2\cdot$	3.7×10^4	-5.37×10^2	
132) $CH_3\dot{C}HCH_2OH(O_2\cdot) + NO \rightarrow NO_2 + CH_3\dot{C}HCH_2OH(O\cdot)$	1×10^4	-	
133) $CH_3\dot{C}HCH_2OH(O\cdot) \rightarrow CH_3CHO + \cdot CH_2OH$	1×10^5	-	
134) $CH_3CH(OH)CH_2O\cdot \rightarrow HCHO + CH_3\dot{C}HOH$	1×10^2	-	
135) $CH_3\dot{C}HCH_2OH(O_2\cdot) + NO \rightarrow CH_3\dot{C}HCH_2OH(ONO_2)$	4.0×10^2	-	
136) $CH_3CH(OH)CH_2O_2\cdot + NO \rightarrow NO_2 + CH_3CH(OH)CH_2O\cdot$	1×10^4	-	
137) $CH_3CH(OH)CH_2O_2\cdot + NO \rightarrow CH_3CH(OH)CH_2ONO_2$	400	-	
138) $CH_3\dot{C}HOH + O_2 \rightarrow HO_2\cdot + CH_3CHO$	3×10^3	-	
139) $CH_3CHCH_2 + O_3 \rightarrow 0.5\ CH_3CHO + 0.2\ CH_3\dot{C}HO\delta + 0.06\ CH_4 + 0.27\ CO_2 + 0.33\ CO + 0.20\ HO_2\cdot + 0.1\ OH + 0.22\ CH_3O_2\cdot + 0.03\ CH_3O\cdot + 0.2\ \dot{C}H_2O\delta + 0.06\ H_2 + 0.21\ H_2O$	1.6×10^{-2}	1.897×10^3	
tr-2-butene chemistry (17):			
140) $CH_3CH=CHCH_3 + OH \xrightarrow{O_2} CH_3CH(OH)\dot{C}HCH_3(OO\cdot)$	1.0×10^5	-5.42×10^2	
141) $CH_3CH(OH)\dot{C}HCH_3(OO\cdot) + NO \rightarrow NO_2 + CH_3\dot{C}HCH_3(OH\ O\cdot)$	1.0×10^4	-	

Table A.1 (continued)

Reaction[1,2]	Rate Constant[3]	Activation Energy(K)	Note
tr-2-butene chemistry (continued)			
142) $CH_3CH(OO\cdot)CHCH_3 + NO \rightarrow CH_3CH(OH)CH(ONO_2)CH_3$	8.0×10^{2}	-	
143) $CH_3CH(O\cdot)CHCH_3 \rightarrow CH_3CHO + CH_3\dot{C}HOH$	1.0×10^{4}	-	
144) $CH_3CH_2{=}CH_2CH_3 + O_3 \rightarrow CH_3CHO + 0.4\ CH_3\dot{C}HOO\delta$ $+ 0.12\ CH_4 + 0.36\ CO_2$ $+ 0.24\ CO + 0.29\ HO_2\cdot$ $+ 0.19\ OH + 0.05\ CH_3O\cdot$ $+ 0.43\ CH_3O_2\cdot$	2.7×10^{-1}	1.051×10^{3}	
145) $C\dot{H}_2OO\delta + NO \rightarrow NO_2 + HCHO$	1.0×10^{4}	-	
146) $C\dot{H}_2OO\delta + NO_2 \rightarrow NO_3 + HCHO$	1.0×10^{3}	-	
147) $C\dot{H}_2OO\delta + H_2O \rightarrow HCOOH + H_2O$	6.0×10^{-3}	-	
148) $CH_3\dot{C}HOO\delta + NO \rightarrow NO_2 + CH_3CHO$	1.0×10^{4}	-	
149) $CH_3\dot{C}HOO\delta + NO_2 \rightarrow NO_3 + CH_3CHO$	1.0×10^{3}	-	
150) $CH_3\dot{C}HOO\delta + H_2O \rightarrow CH_3COOH + H_2O$	6.0×10^{-3}	-	
Propane chemistry (17):			
151) $CH_3CH_2CH_3 + OH \rightarrow H_2O + 0.85\ CH_3\dot{C}H(OO\cdot)CH_3$ $+ 0.15\ CH_3CH_2CH_2O_2\cdot$	2.3E3	6.8×10^{2}	
152) $CH_3\dot{C}H(OO\cdot)CH_3 + NO \rightarrow NO_2 + CH_3\dot{C}H(O\cdot)CH_3$	1.1×10^{4}	-	
153) $CH_3CH_2CH_2O_2\cdot + NO \rightarrow NO_2 + CH_3CH_2CHO\cdot$	1.1×10^{4}	-	

Table A.1 (continued)

Reaction[1,2]	Rate Constant[3]	Activation Energy(K)	Note
Propane chemistry (continued)			
154) $CH_3\dot{C}HCH_3 + O_2 \rightarrow HO_2\cdot + CH_3C(O)CH_3$	4.4×10^{1}	-	
155) $CH_3CH_2CH_2O\cdot + O_2 \rightarrow HO_2\cdot + CH_3CH_2CHO$	1.0×10^{2}	6.9×10^{2}	
n-Butane chemistry (17):			
156) $CH_3CH_2CH_2CH_3 + O(^3P) \xrightarrow{O_2} OH + 0.88\ CH_3CH_2\dot{C}HCH_3(OO\cdot) + 0.12\ CH_3CH_2CH_2CH_2O_2\cdot$	3.3×10^{1}	2.099×10^{3}	
157) $CH_3CH_2CH_2CH_3 + OH \xrightarrow{O_2} H_2O + 0.86\ CH_3CH_2\dot{C}HCH_3(OO\cdot) + 0.14\ CH_3CH_2CH_2CH_2O_2\cdot$	3.8×10^{3}	5.59×10^{2}	
158) $CH_3CH_2CH_2CH_2O_2\cdot + NO \rightarrow CH_3CH_2CH_2CH_2O\cdot + NO_2$	1.0×10^{4}	-	
159) $CH_3CH_2CH_2CH_2O_2\cdot + NO \rightarrow CH_3CH_2CH_2CH_2ONO_2$	8.0×10^{2}	8.0×10^{2}	
160) $CH_3CH_2CH_2CH_2O\cdot + O_2 \rightarrow HO_2\cdot + CH_3CH_2CH_2CHO$	1.0×10^{1}	6.90×10^{2}	
161) $CH_3CH_2CH_2CH_2O\cdot \xrightarrow{O_2} \cdot OOCH_2CH_2CH_2CH_2OH$	7.2×10^{6}	4.200×10^{3}	
162) $\cdot OOCH_2CH_2CH_2CH_2OH + NO \rightarrow NO_2 + \cdot OCH_2CH_2CH_2CH_2OH$	1.0×10^{4}	-	
163) $\cdot OOCH_2CH_2CH_2CH_2OH + NO \rightarrow O_2NOCH_2CH_2CH_2CH_2OH$	8.0×10^{2}	-	
164) $\cdot OCH_2CH_2CH_2CH_2OH \rightarrow HOCH_2CH_2CH_2\dot{C}HOH$	3.6×10^{7}	-	
165) $HOCH_2CH_2CH_2\dot{C}HOH + O_2 \rightarrow HO_2\cdot + OHCH_2CH_2CH_2CHO$	1.0×10^{1}	6.90×10^{2}	10
166) $CH_3CH_2\dot{C}HCH_3(OO\cdot) + NO \rightarrow NO_2 + CH_3CH_2\dot{C}HCH_3(O\cdot)$	1.0×10^{4}	-	

Table A.1 (continued)

Reaction[1,2]	Rate Constant[3]	Activation Energy(K)	Note
n-Butane chemistry (continued)			
167) $CH_3CH_2\overset{\overset{OO\cdot}{|}}{C}HCH_3 + NO \rightarrow CH_3CH_2\overset{\overset{ONO_2}{|}}{C}HCH_3$	8.0×10^{2}	-	
168) $CH_3CH_2\overset{\overset{O\cdot}{|}}{C}HCH_3 + O_2 \rightarrow CH_3CH_2C(O)CH_3 + HO_2\cdot$	4.4×10^{1}	-	
169) $CH_3CH_2\overset{\overset{O\cdot}{|}}{C}HCH_3 \xrightarrow{O_2} C_2H_5O_2\cdot + CH_3CHO$	4.0×10^{6}	7.0×10^{3}	
170) $C_2H_5O_2\cdot + NO \rightarrow C_2H_5O\cdot + NO_2$	1.1×10^{4}	-	
171) $C_2H_5O\cdot + NO_2 \rightarrow C_2H_5ONO_2$	2.2×10^{4}	-	
172) $C_2H_5O\cdot + NO \rightarrow C_2H_5ONO$	4.4×10^{4}	-	
173) $C_2H_5O\cdot + O_2 \rightarrow CH_3CHO + HO_2\cdot$	1.0×10^{1}	6.90×10^{2}	
2,3-dimethyl butane chemistry (17):			
174) $(CH_3)_2CHCH(CH_3)_2 + O(^3P) \rightarrow (CH_3)_2CHC(O_2\cdot)(CH_3)_2 + OH$	3.1×10^{2}	1.250×10^{3}	
175) $(CH_3)_2CHCH(CH_3)_2 + OH \rightarrow 0.14(CH_3)_2CHCH(CH_3)CH_2O_2\cdot + 0.86\ (CH_3)_2CHC(O_2\cdot)(CH_3)_2$	9.3×10^{3}	-	
176) $(CH_3)_2CHCH(CH_3)CH_2O_2\cdot + NO \rightarrow 0.9\ NO_2 + 0.9\ (CH_3)_2CHCH(CH_3)CH_2O\cdot + 0.1\ (CH_3)_2CHCH(CH_3)CH_2ONO_2$	1.0×10^{4}	-	
177) $(CH_3)_2CHCH(CH_3)CH_2O\cdot + O_2 \rightarrow HO_2\cdot + (CH_3)_2CHCH(CH_3)CHO$	1.0×10^{1}	6.90×10^{2}	
178) $(CH_3)_2CHCH(CH_3)CH_2O\cdot \xrightarrow{O_2} \cdot OOCH_2\overset{\overset{CH_3CH_3}{|}}{C}HCHCH_2OH$	1.4×10^{7}	4.20×10^{3}	

Table A.1 (continued)

Reaction[1,2]	Rate Constant[3]	Activation Energy(K)	Note
2,3-dimethyl butane chemistry (continued)			
179) $\cdot OOCH_2\overset{CH_3}{\underset{}{C}}HCH\overset{CH_3}{\underset{}{C}}H_2OH + NO \rightarrow 0.9\ NO_2 + 0.9\ \cdot OCH_2\overset{CH_3}{\underset{}{C}}HCH\overset{CH_3}{\underset{}{C}}H_2OH + 0.1\ O_2NOCH_2\overset{CH_3}{\underset{}{C}}HCH\overset{CH_3}{\underset{}{C}}H_2OH$	1.0×10^{4}	-	
180) $\cdot OCH_2\overset{CH_3}{\underset{}{C}}HCH\overset{CH_3}{\underset{}{C}}H_2OH \xrightarrow{O_2} 0.8\ HOCH_2\overset{CH_3}{\underset{}{C}}HCH\overset{CH_3}{\underset{}{C}}HOH + 0.2\ HOCH_2\overset{CH_3CH_2OO\cdot}{\underset{}{C}}HCH\overset{CH_3}{\underset{}{C}}H_2OH$	1.4×10^{7}	4.200×10^{3}	
181) $HOCH_2\overset{CH_3}{\underset{}{C}}HCH\overset{CH_3}{\underset{}{C}}HOH + O_2 \rightarrow HO_2\cdot + HOCH_2\overset{CH_3}{\underset{}{C}}HCH\overset{CH_3}{\underset{}{C}}HO$	1.0×10^{1}	6.90×10^{2}	
182) $HOCH_2\overset{CH_3CH_2OO\cdot}{\underset{}{C}}HCH\overset{CH_3}{\underset{}{C}}H_2OH + NO \rightarrow 0.9\ NO_2 + 0.9\ HOCH_2\overset{CH_3CH_2O\cdot}{\underset{}{C}}HCH\overset{CH_3}{\underset{}{C}}H_2OH + 0.1\ HOCH_2\overset{CH_3CH_2ONO_2}{\underset{}{C}}HCH\overset{CH_3}{\underset{}{C}}H_2OH$	1.0×10^{4}	-	
183) $HOCH_2\overset{CH_3CH_2O\cdot}{\underset{}{C}}HCH\overset{CH_3}{\underset{}{C}}H_2OH \xrightarrow{O_2} 0.8\ HOCH_2\overset{CH_3CH_2OH}{\underset{}{C}}HCH\overset{CH_3}{\underset{}{C}}H_2OH + 0.2\ HOCH_2\overset{\cdot OOH_2C\ CH_2OH}{\underset{}{C}}HCH\overset{CH_3}{\underset{}{C}}H_2OH$	1.4×10^{7}	4.200×10^{3}	
184) $HOCH_2\overset{CH_3CH_2OH}{\underset{}{C}}HCH\overset{CH_3}{\underset{}{C}}H_2OH + O_2 \rightarrow HO_2\cdot + OHCCH_2\overset{CH_3CH_2OH}{\underset{}{C}}HCH\overset{CH_3}{\underset{}{C}}H_2OH$	1.0×10^{1}	6.90×10^{2}	
185) $HOCH_2\overset{\cdot OOH_2C\ CH_2OH}{\underset{}{C}}HCH\overset{CH_3}{\underset{}{C}}H_2OH + NO \xrightarrow{O_2} 0.9\ NO_2 + 0.9\ HO_2\cdot + 0.9\ (HOCH_2)_2CHCHCHO\ (CH_2OH) + 0.1\ HOCH_2\overset{CH_3}{\underset{}{C}}HCH\overset{CH_3}{\underset{}{C}}H_2OH\ (O_2NOH_2C\ CH_2OH)$	1.0×10^{4}	-	

Table A.1 (continued)

Reaction [1,2]	Rate Constant[3]	Activation Energy	Note
2,3-dimethyl butane chemistry (continued)			
186) $(CH_3)_2CHC(O_2\cdot)(CH_3)_2 + NO \rightarrow 0.9\ NO_2 + 0.9\ (CH_3)_2CHC(O\cdot)(CH_3)_2 + 0.1\ (CH_3)_2CHC(ONO_2)(CH_3)_2$	1.0×10^{4}	-	
187) $(CH_3)_2CHC(O\cdot)(CH_3)_2 \xrightarrow{O_2} CH_3C(O)CH_3 + CH_3CH(O_2\cdot)CH_3$	3.0×10^{7}	6.440×10^{3}	
188) $CH_3CH(O_2\cdot)CH_3 + NO \rightarrow CH_3CH(ONO_2)CH_3$	4.0×10^{2}	-	
189) $CH_3CH(O_2\cdot)CH_3 + NO \rightarrow NO_2 + CH_3CH(O\cdot)CH_3$	1.0×10^{4}	-	
190) $CH_3CH(O\cdot)CH_3 + O_2 \rightarrow CH_3C(O)CH_3 + HO_2\cdot$	4.4×10^{1}	-	
Propionaldehyde chemistry (17):			
191) $C_2H_5CHO + OH \xrightarrow{O_2} H_2O + C_2H_5CO_3\cdot$	2.8×10^{4}	-2.5×10^{2}	
192) $C_2H_5CHO + NO_3 \xrightarrow{O_2} HNO_3 + C_2H_5CO_3\cdot$	2.2×10^{0}	-	
193) $C_2H_5CHO + h\nu \xrightarrow{O_2} C_2H_5O_2\cdot + HO_2\cdot + CO$	$8.4\times10^{-4}k_{NO_2}$	-	11
194) $C_2H_5CO_3\cdot + NO_2 \rightarrow C_2H_5CO_3NO_2$	6.9×10^{3}	-	
195) $C_2H_5CO_3\cdot + NO \xrightarrow{O_2} C_2H_5O_2\cdot + NO_2 + CO$	1.1×10^{4}	-	
196) $C_2H_5CO_3NO_2 \rightarrow C_2H_5CO_3\cdot + NO_2$	2.2×10^{-2}	1.354×10^{4}	
Butyraldehyde chemistry (17):			
197) $C_3H_7CHO + OH \xrightarrow{O_2} H_2O + C_3H_7CO_3\cdot$	3.7×10^{4}	-	
198) $C_3H_7CHO + NO_3 \xrightarrow{O_2} HNO_3 + C_3H_7CO_3\cdot$	2.2×10^{0}	-	

Table A.1 (continued)

Reaction[1,2]	Rate Constant[3]	Activation Energy	Note
Butyraldehyde chemistry (continued)			
199) $C_3H_7CHO + h\nu \xrightarrow{O_2} C_3H_7O_2\cdot + HO_2\cdot + CO$	$8.4\times10^{-4}k_{NO_2}$	-	11
200) $C_3H_7CO_3\cdot + NO_2 \rightarrow C_3H_7CO_3NO_2$	6.9×10^{3}	-	
201) $C_3H_7CO_3\cdot + NO \xrightarrow{O_2} NO_2 + CO_2 + C_3H_7O_2\cdot$	1.1×10^{4}	-	
202) $C_3H_7CO_3NO_2 \rightarrow C_3H_7CO_3\cdot + NO_2$	2.2×10^{-2}	1.354×10^{4}	
203) $C_3H_7O_2\cdot + NO \rightarrow NO_2 + C_3H_7O\cdot$	1.1×10^{4}	-	
204) $C_3H_7O\cdot + NO \rightarrow C_3H_7ONO$	4.4×10^{4}	-	
205) $C_3H_7O\cdot + NO_2 \rightarrow C_3H_7ONO_2$	2.2×10^{4}	-	
206) $C_3H_7O\cdot + O_2 \rightarrow HO_2\cdot + C_2H_5CHO$	1.0×10^{1}	6.90×10^{2}	
Acetone chemistry (17):			
207) $CH_3C(O)CH_3 + OH \xrightleftharpoons{O_2} H_2O + CH_3C(O)CH_2O_2\cdot$	4.1×10^{2}	1.230×10^{3}	
208) $CH_3C(O)CH_3 + h\nu \xrightarrow{O_2} CH_3CO_3\cdot + CH_3O_2\cdot$	$1.7\times10^{-4}k_{NO_2}$		12
209) $CH_3C(O)CH_2O_2\cdot + NO \rightarrow CH_3C(O)CH_2O\cdot + NO_2$	1.0×10^{4}	-	
210) $CH_3C(O)CH_2O_2\cdot + NO \rightarrow CH_3C(O)CH_2ONO_2$	4.0×10^{2}	-	
211) $CH_3C(O)CH_2O\cdot + O_2 \rightarrow HO_2\cdot + CH_3C(O)CHO$	1.0×10^{1}	6.9×10^{2}	

Table A.1 (continued)

	Reaction[1,2]	Rate Constant[3]	Activation Energy	Note
MEK chemistry (17):				
212)	$C_2H_5C(O)CH_3 + OH \xrightarrow{O_2} H_2O + CH_3\dot{C}HC(O)CH_3$ (OO·)	8.1×10^{2}	-	
213)	$C_2H_5C(O)CH_3 + h\nu \xrightarrow{O_2} CH_3CO_3\cdot + C_2H_5O_2\cdot$	$1.7\times10^{-3}k_{NO_2}$	-	12
214)	$C_2H_5C(O)CH_3 + OH \rightarrow H_2O + C_2H_5\dot{C}(O)CH_2$	4.9×10^{2}	-	13
215)	$CH_3\dot{C}HC(O)CH_3$ (OO·) $+ NO \rightarrow NO_2 + CH_3\dot{C}HCOCH_3$ (O·)	1.0×10^{4}	-	
216)	$CH_3\dot{C}HC(O)CH_3$ (OO·) $+ NO \rightarrow CH_3\dot{C}HC(O)CH_3$ (ONO_2)	8.0×10^{2}	-	
217)	$CH_3\dot{C}HC(O)CH_3$ (O·) $\xrightarrow{O_2} CH_3CHO + CH_3CO_3\cdot$	7.8×10^{6}	6.440×10^{3}	

[1]Only one isomer is shown, even when several are possible

[2]Reaction formulated from Atkinson and Lloyd (2) unless otherwise noted.

[3]298K, ppm-min units

Notes:

(1) Rate constant is specific for SAPRC smog chamber experiments.

(2) Photolysis rates calculated by averaging over zenith angles between 30° and 60° using the results of Demerjian et al. (24)

(3) Reaction taken from Atkinson et al. (2)

(4) Photolysis rates calculated by averaging over zenith angles between 30° and 60° using the results of Demerjian et al. (24), followed by correction based on the results of Horowitz and Calvert (26).

(5) Rate constant from Grosjean (25), this rate constant has been updated from the master mechanism.

(6) Abstraction pathway neglected.

(7) 50/50 split of the two γ-dicarbonyls is assumed.

(8) 12 percent nitrate formation is assumed.

(9) Reactions of glycolaldehyde are ignored.

(10) Hydroxy substituted aldehydes are assumed to react the same as un-substituted aldehydes.

(11) Photolysis rate assumed to be the same as acetaldehyde.

(12) Photolysis rate from Atkinson et al. (2).

(13) Reactions of the $C_2H_5C(O)CH_2\cdot$ species are neglected.

Table A.2. Initial Conditions and Physical Parameters for the SAPRC Smog Chamber Experiments[1,2]

	Concentration (ppb)									
Experiment	EC-231	EC-232	EC-233	EC-237	EC-238	EC-241	EC-242	EC-243	EC-245	EC-246
NO	440	469	96	377	718	379	377	366	743	386
NO_2	52	24	7	106	234	110	125	115	259	122
ethene	1,051	258	260	875	982	484	2,014	1,939	2,055	253
propene	108	51	51	100	93	45	109	109	104	49
n-butane	1,130	1,102	1,085	1,025	966	464	558	568	534	1,058
trans-2-butene	55	26	25	50	47	24	108	110	102	26
2,3-dimethylbutane	715	612	648	463	420	211	203	84	185	538
toluene	121	32	34	86	83	40	306	155	321	23
m-xylene	108	29	33	91	84	44	306	154	317	23
CO	1,630	1,742	1,299	956	677	1,296	1,021	608	2,510	-
HCHO	20	9	4	1	26	18	28	-	16	-
acetone	1	1	1	3	4	2	4	2	-	2
H_2O (ppm)	$1.621.10^4$	$1.871x10^4$	$2,138x10^4$	$2.348x10^4$	$2.547x10^4$	$2.076x10^4$	$2.4755x10^4$	$1.710x10^4$	$9.217x10^5$	$2.225x10^4$
Temp (K)	302.8	302.5	302.7	303.1	303.6	303.3	303.1	301.8	302.6	303.3
Dilution Rate (min^{-1})	$6.9x10^{-4}$	$3.9x10^{-4}$	$3.9x10^{-4}$	$2.9x10^{-4}$	$2.8x10^{-4}$	$2.9x10^{-4}$	$3.0x10^{-4}$	$2.8x10^{-4}$	$2.9x10^{-4}$	$2.8x10^{-4}$

[1] $k_1 = 0.30\ min^{-1}$ for each experiment

[2] Detailed data tabulations for these experiments can be found in Pitts et al. (23)

Table A.3. SUR1 Reaction Mechanism

	Reaction[1,2]	Rate Constant[3]	Activation Energy (K)	Note
A) Inorganic Reactions:				
1)	$NO_2 + h\nu \rightarrow NO + O_3$	3.0×10^{-1}	-	1
2)	$O_3 + NO \rightarrow NO_2 + O_2$	2.7×10^{1}	1.5×10^{3}	2
3)	$O_3 + NO_2 \rightarrow NO_3 + O_2$	4.7×10^{-2}	2.45×10^{3}	2
4)	$NO_3 + NO \rightarrow 2NO_2$	3.0×10^{4}	-	2
5)	$HO_2 + NO_2 \rightarrow HO_2NO_2$	1.6×10^{3}	-	2
6)	$NO_2 + OH \rightarrow HNO_3$	1.6×10^{4}	-	2
7)	$O_3 + OH \rightarrow HO_2 + O_2$	9.9×10^{1}	9.7×10^{2}	2
8)	$O_3 + HO_2 \rightarrow OH + 2O_2$	3.0×10^{0}	5.8×10^{2}	2
9)	$HO_2NO_2 \rightarrow HO_2 + NO_2$	5.1×10^{0}	1.042×10^{4}	2
10)	$HO_2 + NO \rightarrow NO_2 + OH$	1.2×10^{4}	-2.4×10^{2}	2
11)	$HO_2 + HO_2 \rightarrow H_2O + O_2$	3.9×10^{3}	-1.2×10^{3}	2
12)	$HO_2 + HO_2 + H_2O \rightarrow H_2O_2 + O_2 + H_2O$	2.2×10^{-1}	-5.8×10^{3}	2
13)	$O_3 + H_2O + h\nu \rightarrow 2OH$	$2.8 \times 10^{-3}\ K_{NO_2}$	-	3
14)	$NO + OH \rightarrow HONO$	9.7×10^{3}	-	2
15)	$HONO + h\nu \rightarrow NO + OH$	$1.8 \times 10^{-1}\ k_{NO_2}$	-	4
16)	$NO_3 + NO_2 \rightarrow N_2O_5$	1.6×10^{3}	-	2
17)	$N_2O_5 \quad NO_2 + NO_3$	3.1×10^{0}	1.108×10^{4}	2
18)	$N_2O_5 + H_2O \rightarrow 2HNO_3$	4.4×10^{-6}	-	5
19)	$H_2O_2 + OH \rightarrow HO_2 + H_2O$	2.5×10^{3}	-	2
20)	$H_2O_2 + h\nu \rightarrow 2OH$	$8.4 \times 10^{-4}\ k_{NO_2}$	-	4
21)	$CO + OH \xrightarrow{O_2} HO_2 + CO_2$	4.0×10^{2}	-	2
22)	$NO_3 + h\nu \rightarrow 0.3NO + 0.7NO_2 + 0.70\ O_3$	$1.55 \times 10^{1}\ k_{NO_2}$	-	6

Table A.3 SUR1 Reaction Mechanism (continued)

	Reaction[1,2]	Rate Constant[3]	Activation Energy (K)	Note
B) Alkene Reactions:				
23)	$CH_2=CH_2 + OH \rightarrow NO_2\text{-}NO + 2HCHO + HO_2\cdot$	1.2×10^{4}	-3.8×10^{2}	7
24)	$CH_2=CH_2 + O_3 \rightarrow HCHO + 0.42CO + 0.12HO_2\cdot + 0.4\dot{C}H_2O\dot{O} + 0.18CO_2 + 0.12H_2 + 0.42H_2O$	2.5×10^{-3}	2.56×10^{3}	2
25)	$CH_3CHCH_2 + OH \rightarrow 0.95(NO_2\cdot + HO_2\cdot + HCHO + CH_3CHO) - NO$	3.7×10^{4}	-5.37×10^{2}	8
26)	$CH_3CHCH_2 + O_3 \rightarrow 0.5CH_3CHO + 0.2CH_3\dot{C}HO\dot{O} + 0.33CO + 0.20HO_2\cdot + 0.10H + 0.2CH_3O_2\cdot + 0.03CH_3O\cdot + 0.2\dot{C}H_2O\dot{O} + 0.06CH_4 + 0.27CO_2 + 0.06H_2 + 0.21H_2O$	1.6×10^{-2}	1.897×10^{3}	2
27)	$CH_3CH=CHCH_3 + OH \rightarrow 0.9NO_2 + 0.9HO_2\cdot + 1.8CH_3CHO -NO + 0.1$ Nitrate	1.0×10^{5}	-5.42×10^{2}	9
28)	$CH_3CH=CHCH_3 + O_3 \rightarrow CH_3CHO + 0.4CH_3\dot{C}HO\dot{O} + 0.24CO + 0.29HO_2\cdot + 0.19OH + 0.05CH_3O\cdot + 0.43CH_3O_2\cdot + 0.12CH_4 + 0.36CO_2$	2.7×10^{-1}	1.051×10^{3}	2
29)	$\dot{C}H_2O\dot{O} + NO \rightarrow NO_2 + HCHO$	1.0×10^{4}	-	2
30)	$\dot{C}H_2O\dot{O} + NO_2 \rightarrow NO_3 + HCHO$	1.0×10^{3}	-	2

Table A.3. SUR1 Reaction Mechanism (continued)

	Reaction[1,2]	Rate Constant[3]	Activation Energy (K)	Note
31)	$\mathring{C}H_2O\mathring{O}$ + H_2O → HCOOH + H_2O	6.0×10^{-3}	-	2
32)	$CH_3\mathring{C}HO\mathring{O}$ + NO → NO_2 + CH_3CHO	1.0×10^{4}	-	2
33)	$CH_3\mathring{C}HO\mathring{O}$ + NO_2 → NO_3 + CH_3CHO	1.0×10^{3}	-	2
34)	$CH_3\mathring{C}H\mathring{O}\mathring{O}$ + H_2O → CH_3COOH + H_2O	6.0×10^{-3}	-	2
C)	*Aromatic Reactions:*			
35)	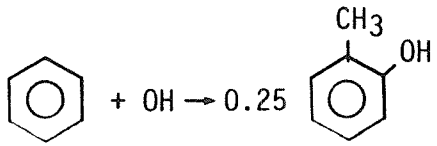 + 0.75 CH(O)CH=CHCHO + 0.75 $(CHO)_2$	1.8×10^{3}	-	10
36)	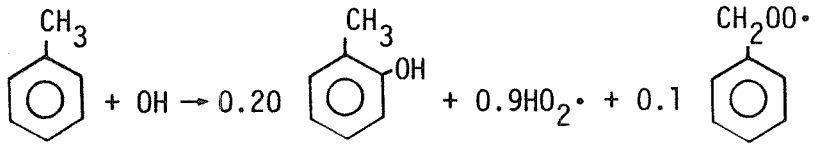 + 0.7 CH(O)CH=CHCHO - 0.7NO	9.1×10^{3}	-	10
37)	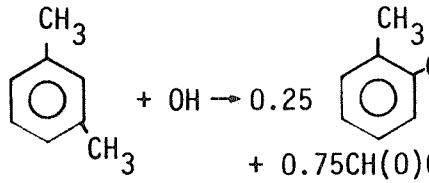 + 0.68$CH_3C(O)CHO$ + 0.07$(CHO)_2$	2.65×10^{4}	-	10

Table A.3 SUR1 Reaction Mechanism (continued)

	Reaction[1,2]	Rate Constant[3]	Activation Energy (K)	Note
38)	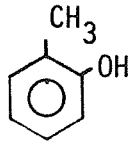 + OH → NO_2 - NO + HO_2· + CH(O)CH=CHCHO + $CH_3C(O)COOH$	8.0×10^4	-	11
39)	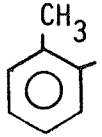 + NO_3 → 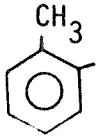 + HNO_3	1.5×10^4	-	2
40)	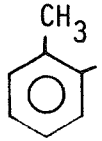 + NO_2 → Product	2.2×10^4	-	2
41)	CH(O)CH=CHCHO + OH → CH(O)CH=CHC(O)O_2· + H_2O	4.4×10^4	-	12
42)	CH(O)CH=CHC(O)O_2· + NO_2 → CH(O)CH=CHC(O)O_2NO_2	6.9×10^3	-	12
43)	CH(O)CH=CHC(O)O_2NO_2 → CH(O)CH=CHC(O)O_2· + NO_2	2.2×10^{-2}	1.354×10^4	12
44)	CH(O)CH=CHC(O)O_2· + NO → $3NO_2$ - 2NO + α(HO_2· + $(CHO)_2$+CO)+(1-α)(CH_3CO_3· + $CH_3C(O)CHO$)	1.1×10^4	-	12

Table A.3 SUR1 Reaction Mechanism (continued)

	Reaction[1,2]	Rate Constant[3]	Activation Energy (K)	Note
45)	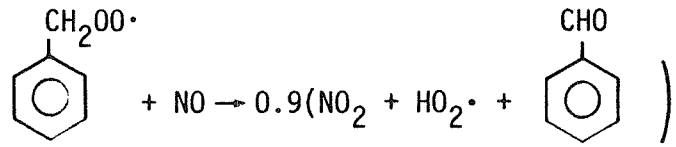	1.1×10^{4}	-	13
46)	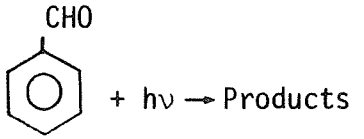	$5.3 \times 10^{-3} k_1$	-	14
47)	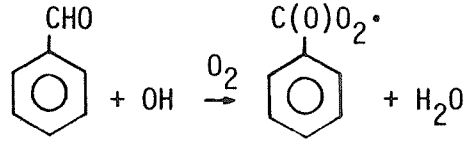	1.9×10^{4}	-	2
48)	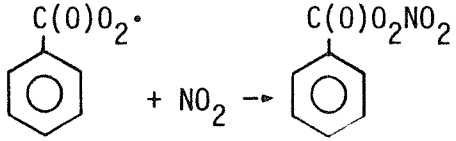	6.9×10^{3}	-	2
49)	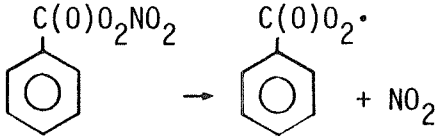	9.6×10^{-3}	1.304×10^{4}	2

Table A.3 SUR1 Reaction Mechanism (continued)

	Reaction[1,2]	Rate Constant[3]	Activation Energy (K)	Note
50)	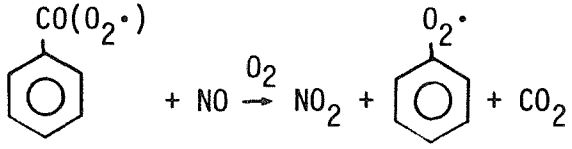	1.0×10^{4}	-	2
51)	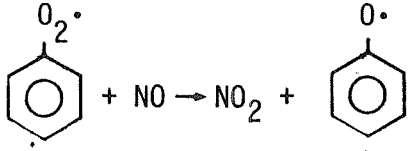	9.0×10^{3}	-	2
52)	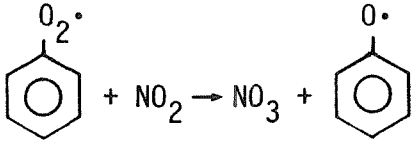	1.0×10^{4}	-	2
53)	$CH_3C(O)COOH + h\nu \rightarrow CH_3CHO + CO_2$	$3.6 \times 10^{-2} k_{NO_2}$	-	15
54)	$CH_3C(O)CHO + OH \xrightarrow{O_2} CH_3C(O)O_2\cdot + CO + H_2O$	2.5×10^{4}	-	2
55)	$CH_3C(O)CH) + h\nu \xrightarrow{2O_2} CH_3C(O)O_2\cdot + HO_2\cdot + CO$	$1.3 \times 10^{-2} k_{NO_2}$	-	2
56)	$CH_3C(O)CHO + h\nu \xrightarrow{2O_2} CH_3O_2\cdot + HO_2\cdot + 2CO$	$6.0 \times 10^{-3} k_{NO_2}$	-	2

Table A.3 SUR1 Reaction Mechanism (continued)

	Reaction[1,2]	Rate Constant[3]	Activation Energy (K)	Note
57)	$(CHO)_2 + OH \xrightarrow{O_2} HO_2\cdot + 2CO + H_2O$	1.7×10^{4}	-	2
58)	$(CHO)_2 + h\nu \rightarrow 0.13HCHO + 0.87H_2 + 1.87CO$	$8.0\times10^{-3}k_{NO_2}$	-	2
D) Alkane Reactions:				
59)	$CH_3CH_2CH_3 + OH \xrightarrow{O_2} CH_3CH(O_2\cdot)CH_3 + H_2O$	2.3×10^{3}	6.8×10^{2}	2
60)	$CH_3CH(O_2\cdot)CH_3 + NO \rightarrow NO_2 + HO_2\cdot + 0.15CH_3CH_2CHO + 0.85CH_3C(O)CH_3$		1.0×10^{4}	16
61)	$ALK + OH \xrightarrow{O_2} RO_2\cdot + H_2O$	5.8×10^{3}	4.0×10^{2}	17
62)	$RO_2\cdot + NO \rightarrow 1.7NO_2 - 0.8NO + 0.9HO_2\cdot + 0.15HCHO + 0.3CH_3CHO + 0.10CH_3CH_2CHO + 0.30CH_3C(O)CH_3 + 0.45C_2H_5C(O)CH_3$	1.0×10^{4}	-	17
E) Carbonyl Reactions:				
63)	$HCHO + h\nu \rightarrow H_2 + CO$	$3.3\times10^{-3}k_{NO_2}$	-	18
64)	$HCHO + h\nu \xrightarrow{2O_2} 2HO_2\cdot + CO$	$2.35\times10^{-3}k_{NO_2}$	-	18
65)	$HCHO + OH \xrightarrow{O_2} HO_2\cdot + CO + H_2O$	1.6×10^{4}	-	2
66)	$CH_3CHO + h\nu \xrightarrow{2O_2} CH_3O_2\cdot + HO_2\cdot + CO$	$2.58\times10^{-4}k_{NO_2}$	-	18
67)	$CH_3CHO + OH \xrightarrow{O_2} CH_3C(O)O_2\cdot + H_2O$	2.4×10^{4}	-2.6×10^{2}	2

Table A.3 SUR1 Reaction Mechanism (continued)

	Reaction[1,2]	Rate Constant[3]	Activation Energy (K)	Note
68)	$CH_3O_2\cdot + NO \rightarrow NO_2 + CH_3O\cdot$	1.1×10^{4}	-	2
69)	$CH_3O\cdot + O_2 \rightarrow HCHO + HO_2\cdot$	2.1×10^{0}	1.35×10^{3}	2
70)	$CH_3O\cdot + NO_2 \rightarrow CH_3ONO_2$	2.2×10^{4}	-	2
71)	$CH_3C(O)O_2\cdot + NO \xrightarrow{2O_2} NO_2 + CH_3O_2\cdot + CO_2$	1.1×10^{4}	-	2
72)	$CH_3C(O)O_2\cdot + NO_2 \rightarrow PAN$	6.9×10^{3}	-	2
73)	$PAN \rightarrow CH_3C(O)O_2\cdot + NO_2$	2.2×10^{-2}	1.354×10^{4}	2
74)	$C_2H_5CHO + OH \xrightarrow{O_2} H_2O + C_2H_5CO_3\cdot$	2.8×10^{4}	-2.5×10^{2}	2
75)	$C_2H_5CHO + h\nu \xrightarrow{O_2} C_2H_5O_2\cdot + HO_2\cdot + CO$	$2.6\times10^{-4}k_{NO_2}$	-	19
76)	$C_2H_5CO_3\cdot + NO_2 \rightarrow C_2H_5CO_3NO_2$	6.9×10^{3}	-	2
77)	$C_2H_5CO_3\cdot + NO \xrightarrow{O_2} C_2H_5O_2\cdot + NO_2 + CO$	1.1×10^{4}	-	2
78)	$C_2H_5CO_3NO_2 \rightarrow C_2H_5CO_3\cdot + NO_2$	2.2×10^{-2}	1.354×10^{4}	2
79)	$C_2H_5O_2\cdot + NO \rightarrow NO_2 + HO_2\cdot + CH_3CHO$	1.1×10^{4}	-	20
80)	$CH_3C(O)CH_3 + h\nu \xrightarrow{O_2} CH_3CO_3\cdot + CH_3O_2\cdot$	$1.7\times10^{-4}k_{NO_2}$	-	21
81)	$C_2H_5C(O)CH_3 + h\nu \xrightarrow{O_2} CH_3CO_3\cdot + C_2H_5O_2\cdot$	$1.7\times10^{-3}k_{NO_2}$	-	21
82)	$C_2H_5C(O)CH_3 + OH \rightarrow CH_3\dot{C}HC(O)CH_3 + H_2O$ (OO· on the $\dot{C}H$)	1.3×10^{3}	-	22
83)	$CH_3\dot{C}HC(O)CH_3 + NO \rightarrow 0.9NO_2 + 0.9CH_3CHO + 0.9CH_3CO_3\cdot$ (OO· on the $\dot{C}H$)	1.1×10^{4}	-	23

[1] One isomer is shown, even when several are possible

[2] CH_3CHCH_2 represents all terminal alkenes, $CH_3CH{=}CHCH_3$ represents all internal alkenes, toluene represents all mono-alkylbenzenes, xylene represents all di-

Table A.3 SUR1 Reaction Mechanism (continued)

and tri-alkylbenzenes, o-cresol represents phenol, o-cresol, and dimethylphenols, CH(O)CH=CHCHO represents all γ-dicarbonyls, C_4H_{10} represents all $\geq C_4$ alkanes, C_2H_5CHO represents all $\geq C_3$ aldehydes.

[3]Rate constants are for 298K, in ppm-min units.

Notes:

(1) For experiments EC-231 to EC-246, k_1 was measured at 0.30 min^{-1}.

(2) Reaction taken directly from the explicit mechanism.

(3) This reaction is formulated by combining reactions 16-18 of the explicit mechanism as suggested by Atkinson et al. (2).

(4) Rate constant obtained by averaging over zenith angles between 30° and 60° using the results of Demerjian et al. (24).

(5) Rate constant is specific for the evacuable chamber at SAPRC (19).

(6) Rate constant from Atkinson et al. (2).

(7) Represents reactions 125-129 of the explicit mechanism.

(8) Represents reactions 131-138 of the explicit mechanism. Five percent nitrate formation is assumed.

(9) Represents reactions 140-143 of the explicit mechanism. Ten percent nitrate formation is assumed.

(10) Ortho cresol is used to represent both phenol and the dimethylphenols and cis-2-butene-1,4-dial represents all γ-dicarbonyls. Ten percent of the initial toluene-OH reaction is assumed to proceed via OH abstraction. The abstraction pathway is neglected for both benzene and xylene. The rate constant and products shown for the xylene + OH reaction are for a lumped average xylene (2). If only m-xylene is present (as in experiments EC-231 to EC-246) the reaction should read

m-xylene + OH → 0.25 o-cresol + $HO_2\cdot$ + 0.75NO_2
+ 0.75 CH(O)CH=CHCHO + 0.75$CH_3C(O)CHO$

with $k_{37} = 3.4 \times 10^4$ ppm^{-1} min^{-1}

(11) Rate constant for reaction 38 is an average OH rate constant for o-cresol and dimenthylphenol.

(12) Reactions 41-44 are taken from Atkinson et al. (2) and represent reactions 82 through 90 of the explicit mechanism

$$\alpha = \frac{k_{35}[\text{benzene}]_o + k_{36}[\text{toluene}]_o + 0.5k_{37}[\text{xylene}]_o}{k_{35}[\text{benzene}]_o + k_{36}[\text{toluene}]_o + k_{37}[\text{xylene}]_o}$$

Table A.3 SUR1 Reaction Mechanism (continued)

Notes: (continued)

(12) See Atkinson et al. (2) for a discussion of these reactions.

(13) Represents reactions 49 through 51 of the explicit mechanism.

(14) Rate constant from Leone and Seinfeld (15).

(15) Based on measurements in sunlight by Grosjean (25).

(16) Represents reactions 152 through 155 of the explicit mechanism.

(17) ALK represents all $\geq C_4$ alkanes. See Atkinson et al. (2) for a discussion of these reactions. For explicit n-butane use (2):

$k_{61} = 4.1 \times 10^3$ ppm^{-1} min^{-1} $\quad A_{61} = 560K$

$$RO_2\cdot + NO \xrightarrow{62} 1.3NO_2 - 0.4NO + 0.9HO_2\cdot + 0.6CH_3CHO + 0.1\ C_2H_5CHO + 0.5\ C_2H_5C(O)CH_3$$

(18) Photolysis rates calculated by averaging over zenith angles between 30° and 60° using the results of Demerjian et al. (24) followed by corrections based on the results of Horowitz and Calvert (26).

(19) Photolysis rate assumed to be similar to that of acetaldehyde.

(20) Represents reactions 170 and 173 of the explicit mechanism (reactions 171 and 172 are neglected).

(21) Photolysis rates from Atkinson et al. (2).

(22) Represents reactions 212 and 214 of the explicit mechanism.

(23) Represents reactions 215 through 217 of the explicit mechanism. Ten percent nitrate formation is assumed.

Table A.4. SUR2 Reaction Mechanism

Reaction[1,2]	Rate Constant[3,4]	Activation Energy (K)	Note
A) Inorganic Reactions:			
1) $NO_2 + h\nu \rightarrow NO + O_3$	*	-	1
2) $O_3 + NO \rightarrow NO_2 + O_2$	2.7×10^{1}	1.5×10^{3}	2
3) $O_3 + NO_2 \rightarrow NO_3 + O_2$	4.7×10^{-2}	2.45×10^{3}	2
4) $NO_3 + NO \rightarrow 2NO_2$	3.0×10^{4}	-	2
5) $HO_2 + NO_2 \rightarrow HO_2NO_2$	1.6×10^{3}	-	2
6) $NO_2 + OH \rightarrow HNO_3$	1.6×10^{4}	-	2
7) $O_3 + OH \rightarrow HO_2 + O_2$	9.9×10^{1}	9.7×10^{2}	2
8) $O_3 + HO_2 \rightarrow OH + 2O_2$	3.0×10^{0}	5.8×10^{2}	2
9) $HO_2NO_2 \rightarrow HO_2 + NO_2$	5.1×10^{0}	1.042×10^{4}	2
10) $HO_2 + NO \rightarrow NO_2 + OH$	1.2×10^{4}	-2.4×10^{2}	2
11) $HO_2 + HO_2 \rightarrow H_2O + O_2$	3.9×10^{3}	-1.2×10^{3}	2
12) $HO_2 + HO_2 + H_2O \rightarrow H_2O_2 + O_2 + H_2O$	2.2×10^{-1}	-5.8×10^{3}	2
13) $O_3 + H_2O + h\nu \rightarrow 2OH$	$2.8 \times 10^{-3}\ k_{NO_2}$		3
14) $NO + OH \rightarrow HONO$	9.7×10^{3}		2
15) $HONO + h\nu \rightarrow NO + OH$	$1.8 \times 10^{-1}\ k_{NO_2}$		4
16) $NO_3 + NO_2 \rightarrow N_2O_5$	1.6×10^{3}	-	2
17) $N_2O_5 \quad NO_2 + NO_3$	3.1×10^{0}	1.108×10^{4}	2
18) $N_2O_5 + H_2O \rightarrow 2HNO_3$	*	-	5
19) $H_2O_2 + OH \rightarrow HO_2 + H_2O$	2.5×10^{3}	-	2
20) $H_2O_2 + h\nu \rightarrow 2OH$	$8.4 \times 10^{-4}\ k_{NO_2}$	-	4
21) $CO + OH \xrightarrow{O_2} HO_2 + CO_2$	4.0×10^{2}	-	2
22) $NO_3 + h\nu \rightarrow 0.3NO + 0.7NO_2 + 0.70(^3P)$	$1.55 \times 10^{2}\ k_{NO_2}$	-	6

Table A.4. SUR2 Reaction Mechanism (continued)

	Reaction[1,2]	Rate Constant[3,4]	Activation Energy (K)	Note
	Alkene Reactions			
23)	$CH_2{=}CH_2 + OH \rightarrow NO_2 - NO + 2HCHO + HO_2\cdot$	1.2×10^{4}	-3.8×10^{2}	7
24)	$CH_2{=}CH_2 + O_3 \rightarrow HCHO + 0.42CO + 0.12HO_2\cdot + 0.4\dot{C}H_2O\dot{O} + 0.18CO_2 + 0.12H_2 + 0.42H_2O$	2.5×10^{-3}	2.56×10^{3}	2
25)	$OLE + OH \rightarrow 0.95\gamma HCHO + (1.8-0.85\gamma)CH_3CHO + (0.9 + 0.05\gamma)(HO_2\cdot + NO_2) - NO$	*	-5.4×10^{2}	8
26)	$OLE + O_3 \rightarrow (1-0.5\gamma)CH_3CHO + (0.4-0.2\gamma)CH_3\dot{C}HO\dot{O} + (0.24 + 0.09\gamma)CO + (0.29-0.09\gamma)HO_2\cdot + (0.19-0.09\gamma)OH + (0.43-0.21\gamma)CH_3O_2\cdot + (0.05-0.03\gamma)CH_3O\cdot + 0.2\gamma\dot{C}H_2O\dot{O}$	*	1.9×10^{3}	8,9
27)	$\dot{C}H_2O\dot{O} + NO \rightarrow NO_2 + HCHO$	1.0×10^{4}	-	2
28)	$\dot{C}H_2O\dot{O} + NO_2 \rightarrow NO_3 + HCHO$	1.0×10^{3}	-	2
29)	$\dot{C}H_2O\dot{O} + H_2O \rightarrow HCOOH + H_2O$	6.0×10^{-3}	-	2
30)	$CH_3\dot{C}HO\dot{O} + NO \rightarrow NO_2 + CH_3CHO$	1.0×10^{4}	-	2
31)	$CH_3\dot{C}HO\dot{O} + NO_2 \rightarrow NO_3 + CH_3CHO$	1.0×10^{3}	-	2
32)	$CH_3\dot{C}HO\dot{O} + H_2O \rightarrow CH_3COOH + H_2O$	6.0×10^{-3}	-	2

Table A.4. SUR2 Reaction Mechanism (continued)

	Reaction[1,2]	Rate Constant[3,4]	Activation Energy (K)	Note
	Aromatic Reactions:			
33)	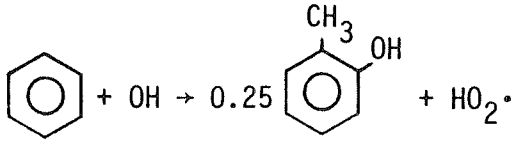 + 0.75CH(O)CH=CHCHO + 0.75$(CHO)_2$	1.8×10^3	-	10
34)	ARO + OH → (0.25-0.05β) 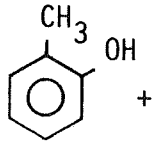 + (1-0.1β)HO_2·	*	-	10,11
	(lumped xylene) + (0.75-0.05β)(NO_2 + CH(O)CH=CHCHO - NO) + (0.68 + 0.02β)$CH_3C(O)CHO$ + (0.08 - 0.08β)$(CHO)_2$ + 0.1β 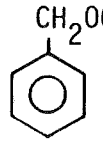			
	(m-xylene) → (0.25-0.05β) 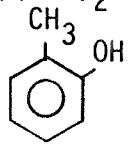 + (1-0.1β)HO_2·	*	-	
	+ (0.75-0.05β)(NO_2 + CH(O)CH=CHCHO - NO) + (0.75-0.05β)$CH_3C(O)CHO$ + 0.1β 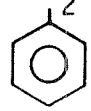			

Table A.4. SUR2 Reaction Mechanism (continued)

	Reaction[1,2]	Rate Constant[3,4]	Activation Energy (K)	Note
35)	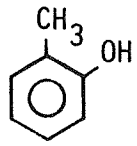 + OH → NO_2 - NO + HO_2· + CH(O)CH=CHCHO + $CH_3C(O)COOH$	8.0×10^4	-	12
36)	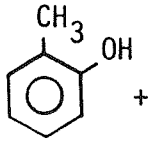 + NO_3 → 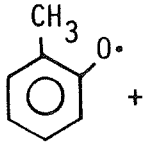 + HNO_3	1.5×10^4	-	2
37)	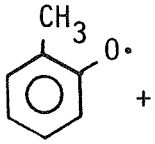 + NO_2 → Product	2.2×10^4	-	2
38)	CH(O)CH=CHCHO + OH → CH(O)CH=CHC(O)O_2· + H_2O	4.4×10^4	-	13
39)	CH(O)CH=CHC(O)O_2· + NO_2 → CH(O)CH=CHC(O)O_2NO_2	6.9×10^3	-	13
40)	CH(O)CH=CHC(O)O_2NO_2 → CH(O)CH=CHC(O)O_2· + NO_2	2.2×10^{-2}	1.354×10^4	13
41)	CH(O)CH=CHC(O)O_2· + NO → $3NO_2$-2NO + α(HO_2· + $(CHO)_2$ + CO) + (1-α)(CH_3CO_3· + $CH_3C(O)CHO$)	1.1×10^4	-	13

Table A.4. SUR2 Reaction Mechanism (continued)

	Reaction[1,2]	Rate Constant[3,4]	Activation Energy (K)	Note
42)	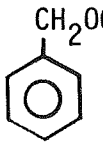 + NO → $0.9NO_2$ + $0.9HO_2\cdot$	1.1×10^{4}	-	14
43)	$CH_3C(O)CHO + OH \xrightarrow{O_2} CH_3C(O)O_2\cdot + CO + H_2O$	2.5×10^{4}	-	2
44)	$CH_3C(O)CHO + h\nu \xrightarrow{2O_2} CH_3C(O)O_2\cdot + HO_2\cdot + CO$	$1.3\times10^{-2}k_{NO_2}$	-	2
45)	$CH_3C(O)CHO + h\nu \xrightarrow{2O_2} CH_3O_2\cdot + HO_2\cdot + 2CO$	$6.0\times10^{-3}k_{NO_2}$	-	2
	Alkane Reactions:			
46)	$ALK + OH \xrightarrow{O_2} RO_2\cdot$	5.8×10^{3}	4.0×10^{2}	15
47)	$RO_2\cdot$ + NO → $1.7NO_2$-$0.8NO$ + $0.9HO_2\cdot$ + $0.15HCHO$ + $0.4CH_3CHO$	1.1×10^{4}	-	15

Table A.4. SUR2 Reaction Mechanism (continued)

	Reaction [1,2]	Rate Constant [3,4]	Activation Energy (K)	Note
	Carbonyl Reactions:			
48)	$HCHO + h\nu \rightarrow H_2 + CO$	$3.3\times10^{-3} k_{NO_2}$	-	16
49)	$HCHO + h\nu \xrightarrow{2O_2} 2HO_2\cdot + CO$	$2.35\times10^{-3} k_{NO_2}$	-	16
50)	$HCHO + OH \xrightarrow{O_2} HO_2\cdot + CO + H_2O$	1.6×10^{4}	-	2
51)	$CH_3CHO + h\nu \xrightarrow{2O_2} CH_3O_2\cdot + HO_2\cdot + CO$	$2.58\times10^{-4} k_{NO_2}$	-	16
52)	$CH_3CHO + OH \xrightarrow{O_2} CH_3C(O)O_2\cdot + H_2O$	2.4×10^{4}	-2.6×10^{2}	2
53)	$CH_3O_2\cdot + NO \rightarrow NO_2 + CH_3O\cdot$	1.1×10^{4}	-	2
54)	$CH_3O\cdot + O_2 \rightarrow HCHO + HO_2\cdot$	2.1×10^{0}	1.35×10^{3}	2
55)	$CH_3O\cdot + NO_2 \rightarrow CH_3ONO_2$	2.2×10^{4}	-	2
56)	$CH_3C(O)O_2\cdot + NO \xrightarrow{2O_2} NO_2 + CH_3O_2\cdot + CO_2$	1.1×10^{4}	-	2
57)	$CH_3C(O)O_2\cdot + NO_2 \rightarrow PAN$	6.9×10^{3}		
58)	$PAN \rightarrow CH_3C(O)O_2\cdot + NO_2$	2.2×10^{-2}	1.354×10^{4}	2

[1] One isomer is shown even when several are possible.

Table A.4. SUR2 Reaction Mechanism (Continued)

[2] o-cresol represents phenol, o-cresol, and dimethylphenols, CH(O)CH=CHCHO represents all γ-dicarbonyls, ALK represents all $\geq C_4$ alkanes, CH_3CHO represents all $\geq C_2$ aldehydes.

[3] 298K, ppm-min units

[4] For rate constants marked *, see the appropriate note.

Notes:

(1) See Table A.2 for the k_1 values used in simulations of the SAPRC smog chamber experiments.

(2) Reaction taken directly from the explicit mechanism.

(3) This reaction is formulated by combining reactions 16-18 of the explicit mechanism as suggested by Atkinson et al. (2).

(4) Rate constant obtained by averaging over zenith angles between 30° and 60° using the results of Demerjian et al. (24).

(5) $k_{18} = 4.4 \times 10^{-6}$ ppm^{-1} - min^{-1} for SAPRC evacuable chamber
$k_{18} = 1.5 \times 10^{-5}$ ppm^{-1} - min^{-1} for UNC chamber.

(6) Rate constant from Atkinson et al. (2).

(7) Represents reactions 125-129 of the explicit mechanism.

(8) Represents reactions 131-138 and 140-143 of the explicit mechanism

$$\gamma = \frac{[\text{propene}]_o}{[\text{propene}]_o + [\text{butene}]_o}$$

where,
$[\text{propene}]_o \equiv$ initial concentration of terminal alkenes
$[\text{butene}]_o \equiv$ initial concentration of internal alkenes

$$k_{25} = 3.7 \times 10^{4} \gamma + 1.0 \times 10^{5} (1-\gamma)$$

(9) Represents reactions 139 and 144 of the explicit mechanism.

$$k_{26} = 1.6 \times 10^{-2} \gamma + 2.7 \times 10^{-1} (1-\gamma)$$

(10) Ortho-cresol is used to represent both phenol and the dimethylphenols, and cis-2-butene-1,4-dial represents all γ-dicarbonyls. The abstraction pathway for benzene is neglected.

Table A.4. SUR2 Reaction Mechanism (continued)

(11) Represents reactions 36 and 37 of the SUR1 mechanism.

$$\beta = \frac{[\text{toluene}]_o}{[\text{toluene}]_o + [\text{xylene}]_o}$$

where,
$[\text{toluene}]_o \equiv$ initial concentration of mono-alkylbenzenes
$[\text{xylene}]_o \equiv$ initial concentration of di- and tri-alkylbenzenes

$k_{34} = 9.1\text{x}10^3\beta + 2.65\text{x}10^4(1-\beta)$ for lumped xylene
$k_{34} = 9.1\text{x}10^3\beta + 3.4\text{x}10^4(1-\beta)$ for m-xylene

(12) k_{35} is an average OH rate constant for o-cresol and dimethylphenol.

(13) Reactions 38-41 are taken from Atkinson et al. (2) and represent reactions 82 through 90 of the explicit mechanism.

for lumped xylene, $$\alpha = \frac{1.8\text{x}10^3[\text{benzene}]_o + 9.1\text{x}10^3[\text{toluene}]_o + 1.35\text{x}10^4[\text{xylene}]_o}{1.8\text{x}10^3[\text{benzene}]_o + 9.1\text{x}10^3[\text{toluene}]_o + 2.65\text{x}10^4[\text{xylene}]_o}$$

where,
$[\text{toluene}]_o \equiv$ initial concentration of mono-alkylbenzenes
$[\text{xylene}]_o \equiv$ initial concentration of di- and tri-alkylbenzenes

(14) Benzaldehyde formation is neglected.

(15) ALK represents all $\geq C_4$ alkanes. See Atkinson et al. (2) for a discussion of these reactions. For explicit n-butane use (2):

$$k_{46} = 4.1\text{x}10^3 \text{ ppm}^{-1}\text{-min}^{-1} \qquad A_{61} = 560\text{K}$$

$$C_4H_{11}O_3\cdot + NO \rightarrow 1.3NO_2 - 0.4NO + 0.9HO_2\cdot + 0.7CH_3CHO$$

(16) Photolysis rates calculated by averaging over zenith angles between 30° and 60° using the results of Demerjian et al. (24) followed by corrections based on the results of Horowitz and Calvert (26). CH_3CHO represents all $\geq C_2$ aldehydes.

Table A.5 Non-Steady-State Species Appearing in the SUR2 Mechanism[1]

NO	HONO	ARO	$CH_3C(O)CHO$
NO_2	N_2O_5	CH(O)CH=CHCHO	ALK
O_3	CO	benzene	HCHO
HO_2NO_2	ethene	o-cresol	CH_3CHO
H_2O_2	OLE	$CH(O)CH=CHC(O)O_2NO_2$	PAN

[1] In most cases the additional non-steady-state species appearing in the SUR2 mechanism (H_2O,HCOOH, etc.) would either be held constant or ignored. There are cases where one would include additional non-steady state species. For instance, HNO_3 would definitely be included in studies on acid rain.

Table A.6 Chamber Dependent Reactions for the SAPRC and UNC Chambers[1]

Reaction	Rate Constant[2,3] SAPRC	UNC
$O_3 \rightarrow$ wall	1.65×10^{-3}	1.5×10^{-4}
$N_2O_5 + H_2O \xrightarrow{\text{wall}} 2HNO_3$	4.4×10^{-6}	1.5×10^{-5}
Wall $\rightarrow HO_2\cdot$	-	$1.5 \times 10^{-4} k_1$
wall $\rightarrow$ OH	$0.39 k_1$	-
$NO_2 \xrightarrow{\text{wall}}$ OH	$1.37 k_1$	-
Wall $\rightarrow$ NO	1.0×10^{-4}	-

[1]The reactions shown here are the chamber dependent reactions recommended by the chamber operators (18,19,27).

[2]ppm-min units

[3]k_1 is the NO_2 photolysis rate.

Table A.7 Initial Conditions and Physical Parameters for University of North Carolina Smog Chamber Experiments.[1-4]

Experiment	Concentration (ppbC)[5] 7/8/82-Red	7/8/82-Blue	8/26/81-Blue	9/2/81-Red	10/14/81-Red	8/26/81-Red
NO	212	210	182	191	174	184
NO_2	78	73	51	55	106	47
n-butane	863	801	582	-	-	840
propene	327	278	171	143	71	259
toluene	370	220	293	194	-	-
m-xylene	365	170	214	176	685	-
ethene	-	-	235	230	216	346
HCHO	4	4	-	-	-	-
CO	355	300	355[6]	355[6]	300[6]	355[6]
H_2O(ppm)	15,000	15,500	17,500	21,000	5,500	20,000
n-propylbenzene	-	183	-	-	-	-
1,2,4-trimethylbenzene	160	287	-	-	-	-
sec-butylbenzene	-	172	-	-	-	-
n-pentane	-	442	-	419	519	665
2,4-dimethylpentane	-	-	-	275	353	-
2,2,4-trimethylpentane	-	-	-	184	270	-
1-butene	-	-	-	61	67	-
cis-2-butene	-	-	-	56	53	-
isopentane	-	-	-	250	317	-

Table A.7 Initial Conditions and Physical Parameters for University of North Carolina Smog Chamber Experiments.[1-4] (continued)

	Concentration (ppbC)[5]					
Experiment	7/8/82-Red	7/8/82-Blue	8/26/81-Blue	9/2/81-Red	10/14/81-Red	8/26/81-Red
2-methyl-1-butene	-	-	-	73	88	-
2-methyl-2-butene	-	-	-	110	92	-
2-methylpentane	-	-	-	226	339	-
Start time (EDT)	06:00	06:00	06:00	06:55	07:30	06:30
Dilution Rate (min^{-1})[7]	$3.7x10^{-4}$	$4.8x10^{-4}$	$3.6x10^{-4}$	$3.6x10^{-4}$	$9.6x10^{-5}$	$3.6x10^{-4}$

[1]The UNC chamber has two sides, one is labeled red, the other blue.

[2]Since the chamber temperature varied throughout the experiment, no temperature data are presented presented here. Consult Jeffries et al. (27).

[3]k_1 is not given because it varied throughout the experiment. The k_1 values used in our simulations were calculated as k_1 = 0.4 x total solar radiation, increased by 15 percent between 9 AM and 3 PM (27).

[4]5 ppb of initial HONO is assumed in each simulation.

[5]Note that the units of concentration are ppbC for the organics, ppb for NO and NO_2.

[6]CO was not measured in these experiments, so the initial CO concentration had to be estimated.

[7]The average dilution rate recommended by Jeffries et al. (27), $3.6x10^{-4}$ min^{-1}, was used if detailed dilution data was not available.

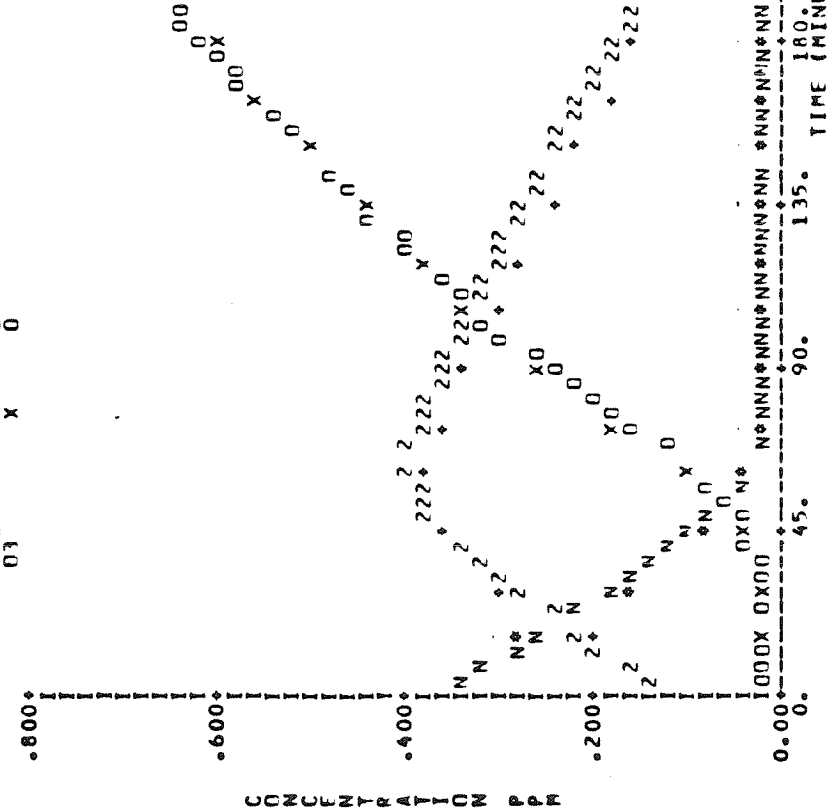

Figure A.1.a Comparison of Concentration-Time Profiles Predicted by the Explicit Mechanism with Experimental Data from SAPRC Experiment EC-237.

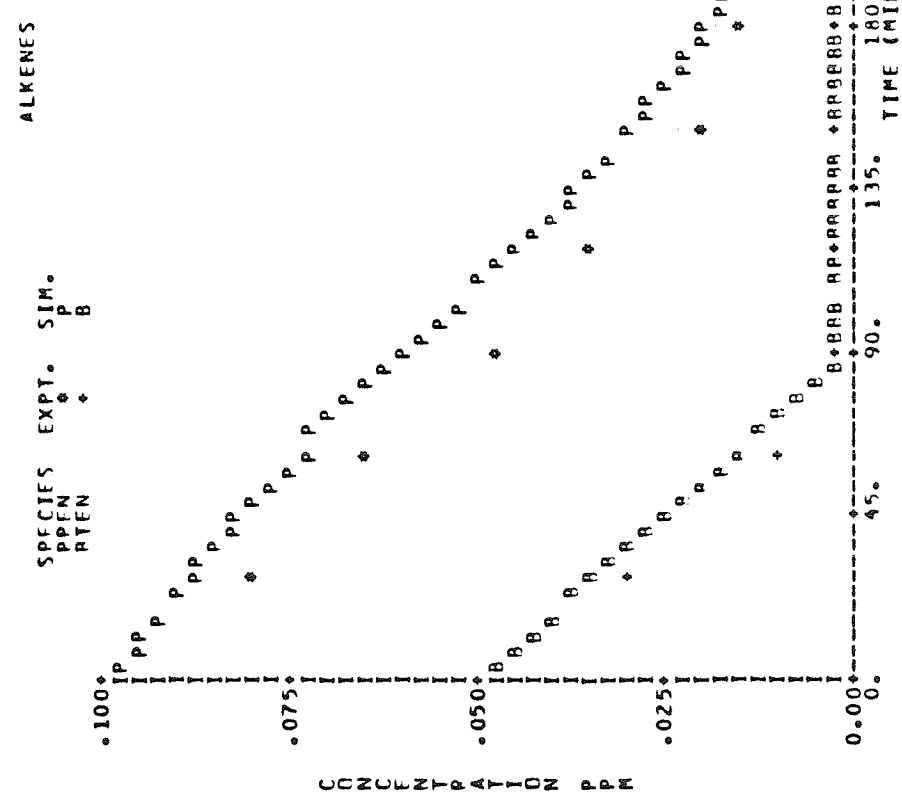

Figure A.1.b Comparison of Concentration-Time Profiles Predicted by the Explicit Mechanism with Experimental Data from SAPRC Experiment EC-237.

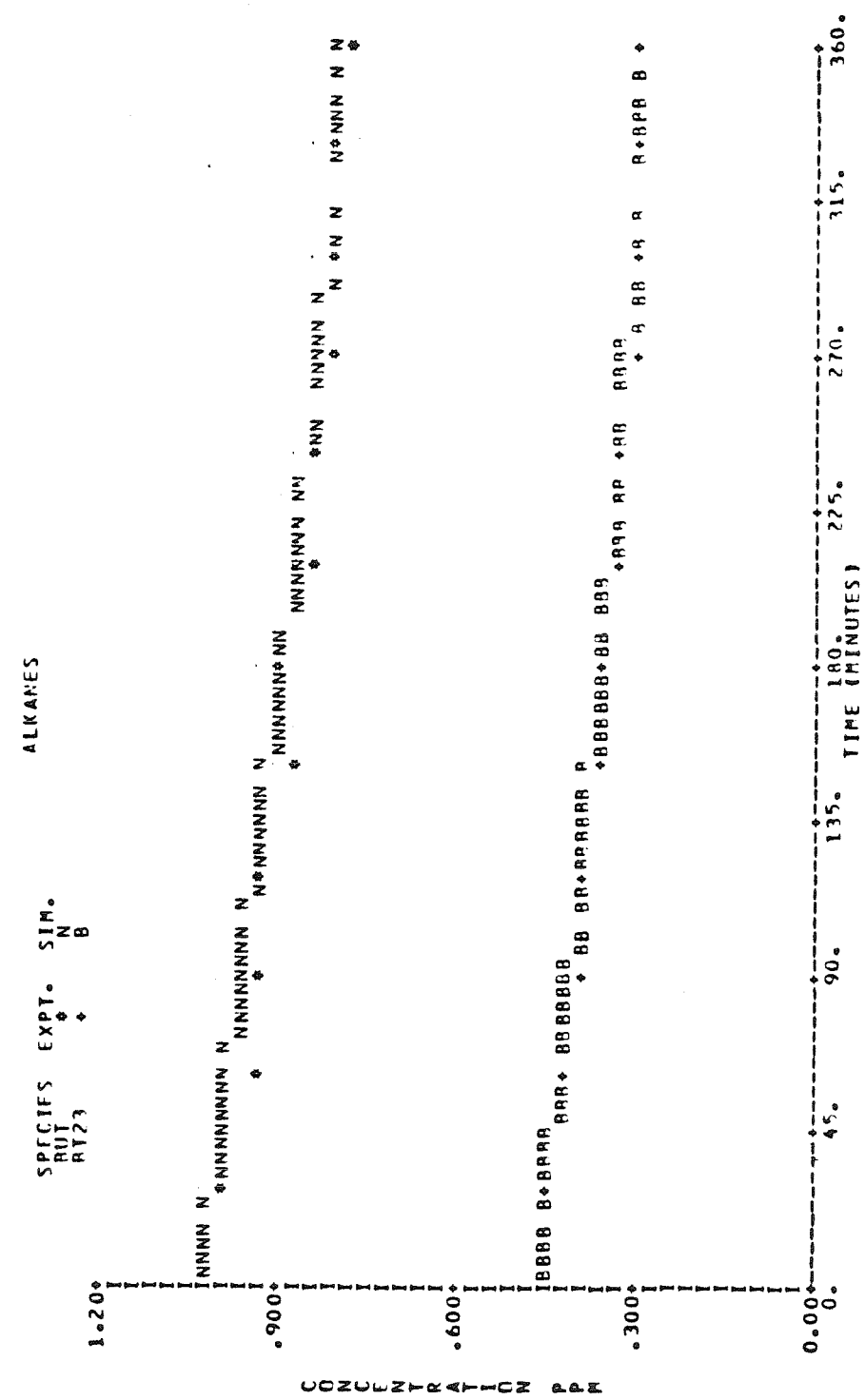

Figure A.1.c Comparison of Concentration-Time Profiles Predicted by the Explicit Mechanism with Experimental Data from SAPRC Experiment EC-237.

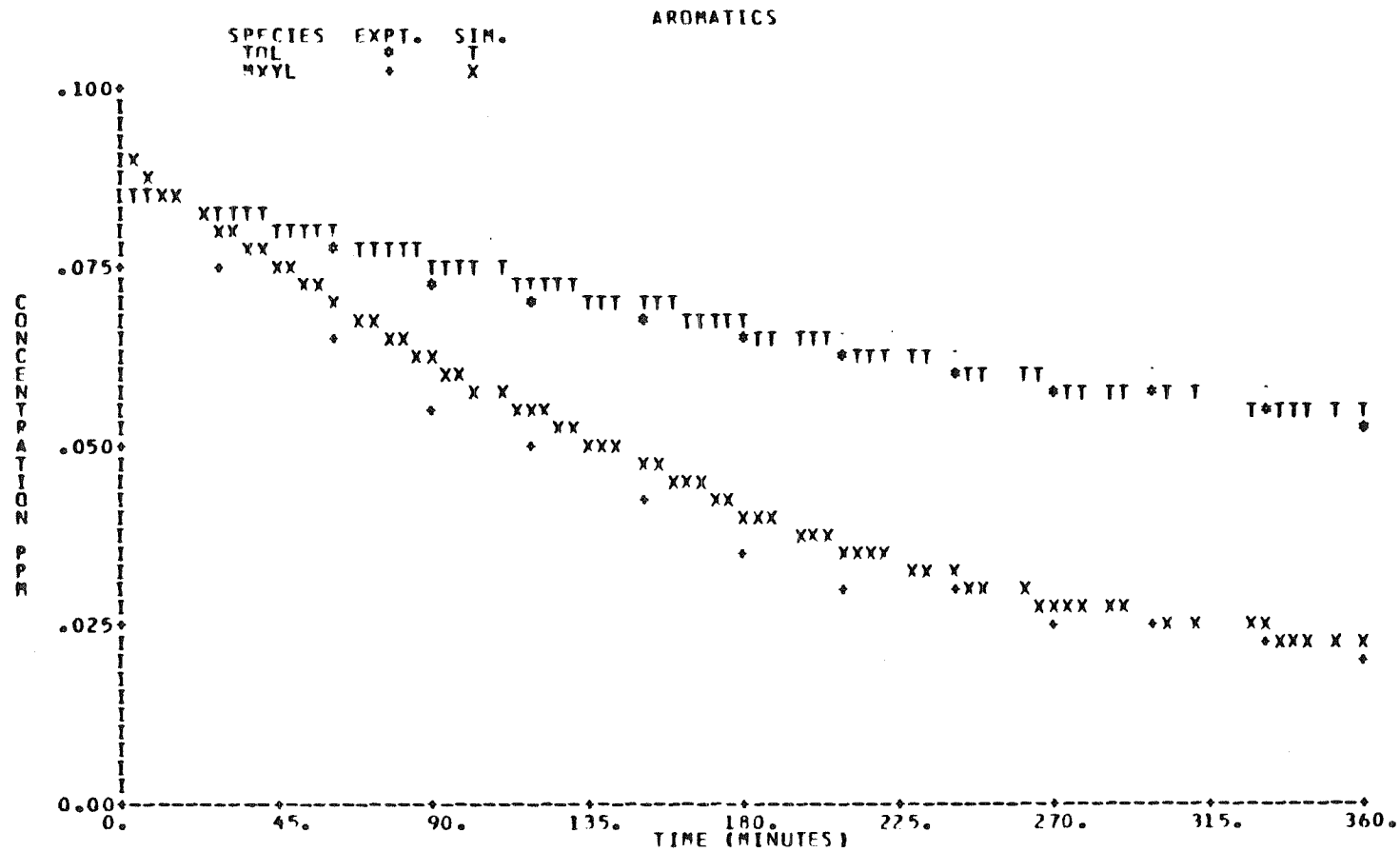

Figure A.1.d Comparison Concentration-Time Profiles Predicted by the Explicit Mechanism with Experimental Data from SAPRC Experiment EC-237.

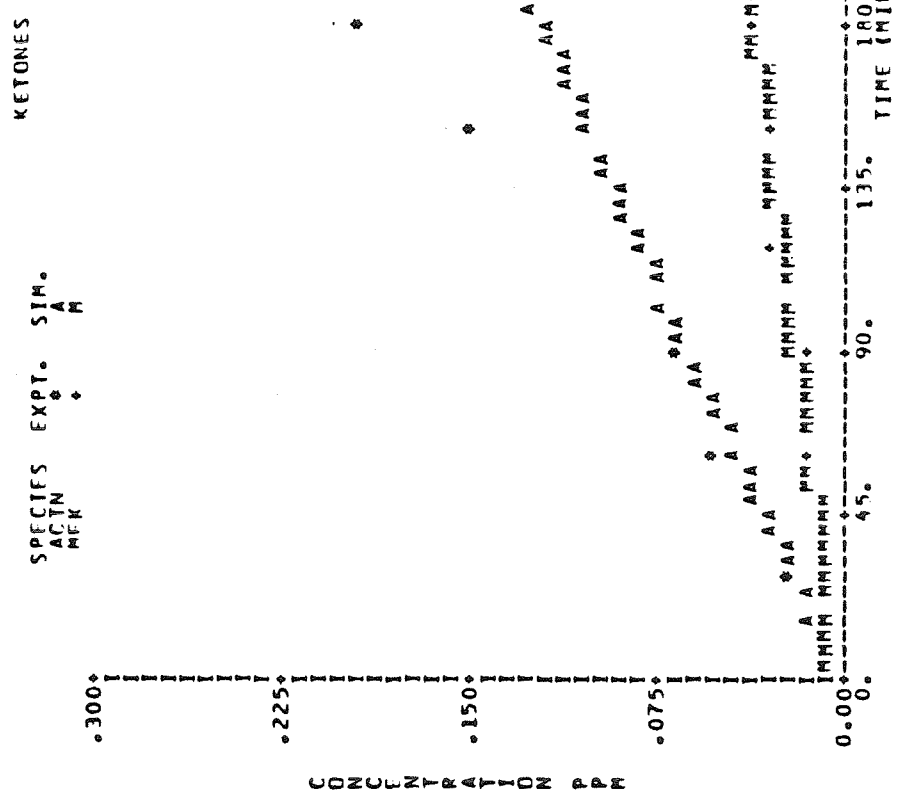

Figure A.1.e. Comparison of Concentration-Time Profiles Predicted by the Explicit Mechanism with Experimental Data from SAPRC Experiment EC-237.

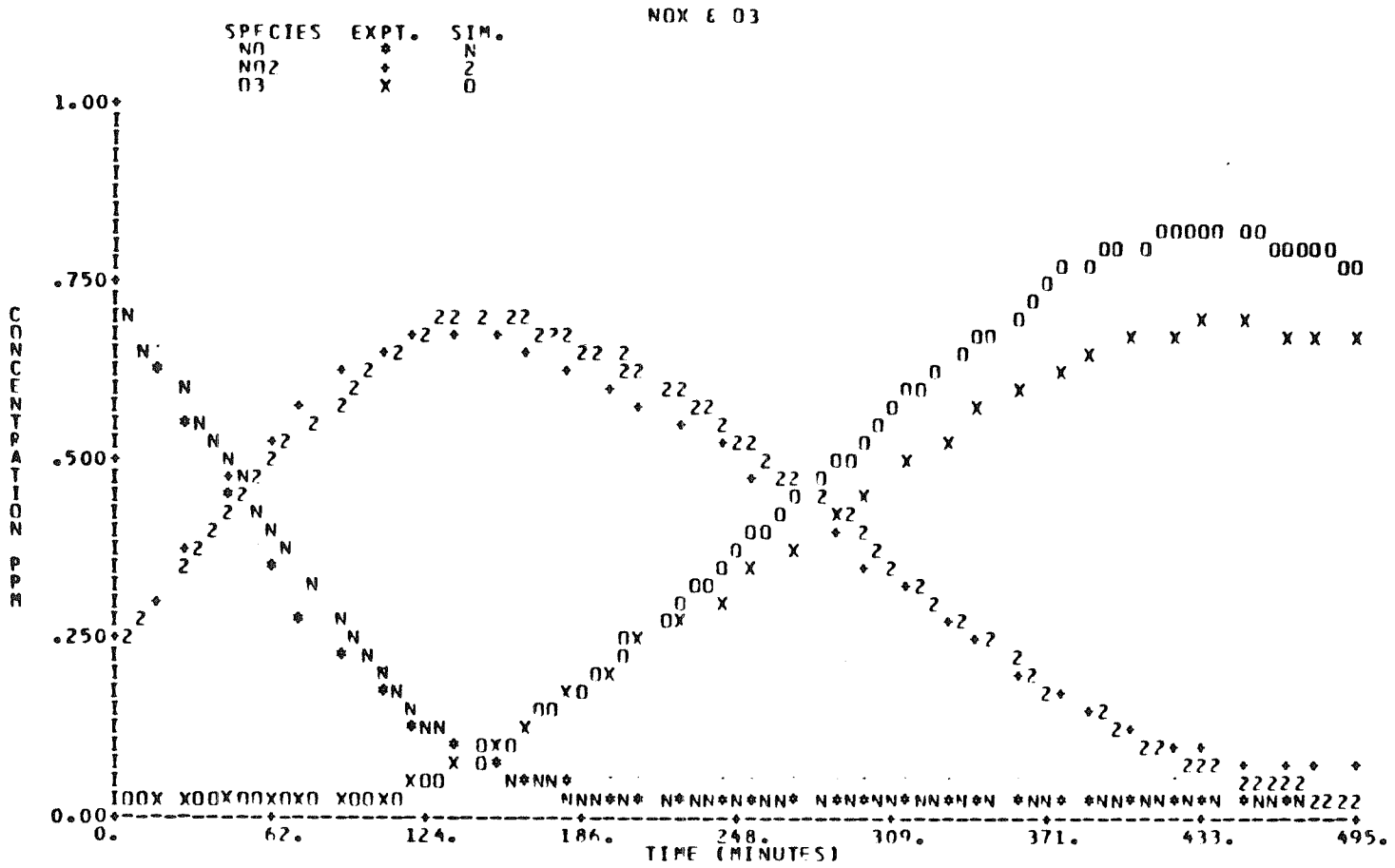

Figure A.2.a Comparison of Concentration-Time Profiles Predicted by the Explicit Mechanism with Experimental Data from SAPRC EC-238.

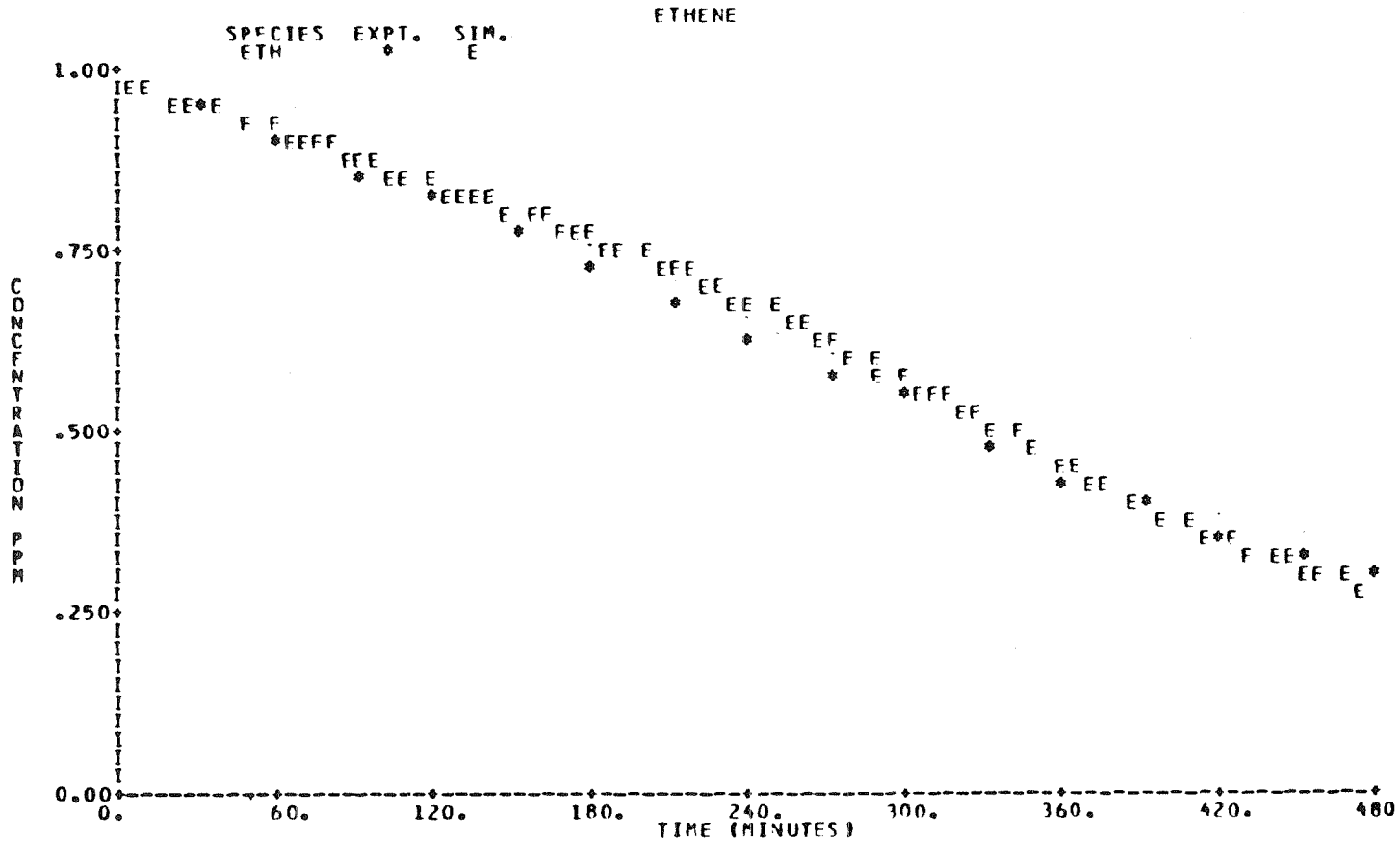

Figure A.2.b Comparison of Concentration-Time Profiles Predicted by the Explicit Mechanism with Experimental Data from SAPRC Experiment EC-238.

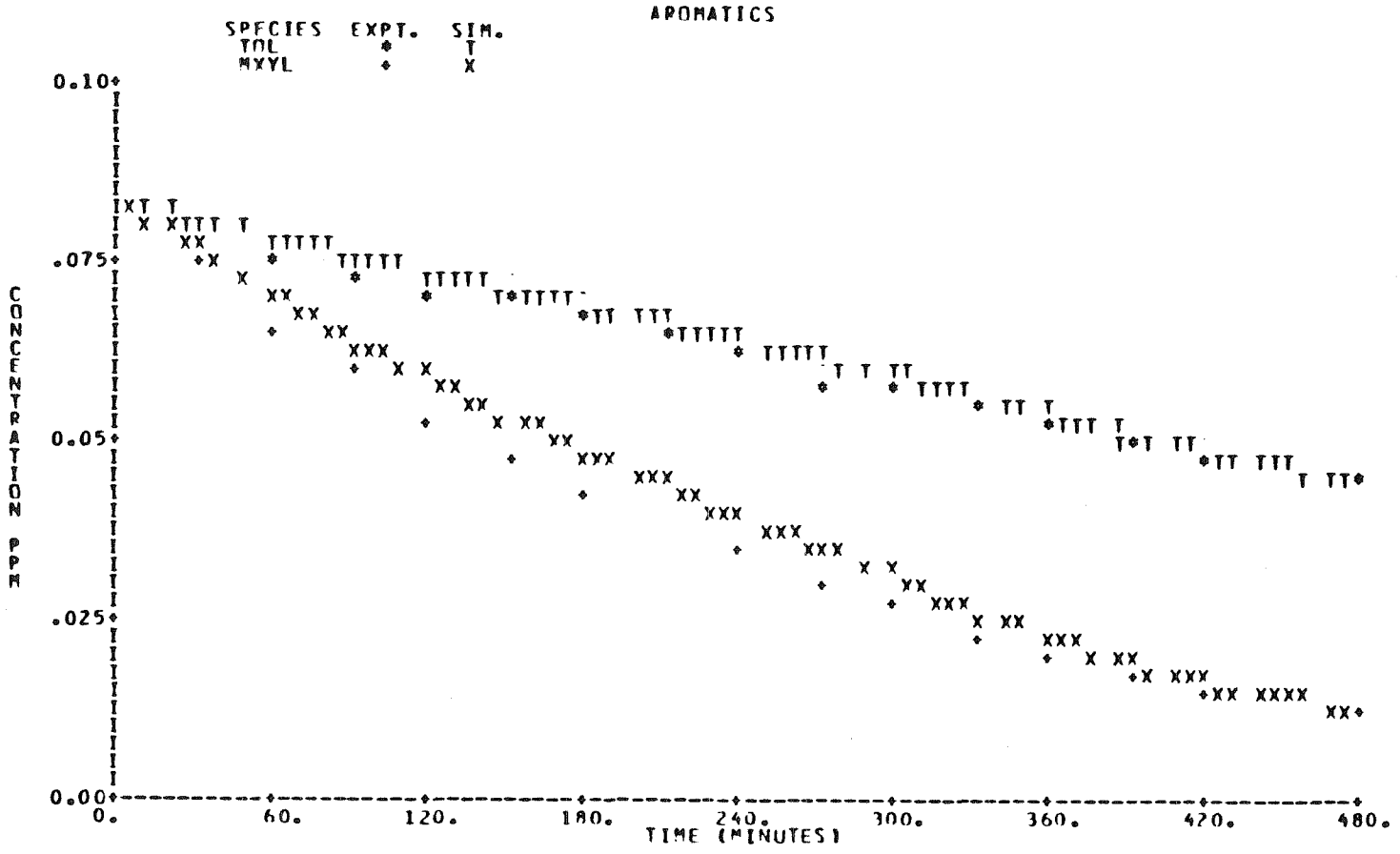

Figure A.2.c. Comparison of Concentration-Time Profiles Predicted by the Explicit Mechanism with Experimental Data from SAPRC Experiment EC-238.

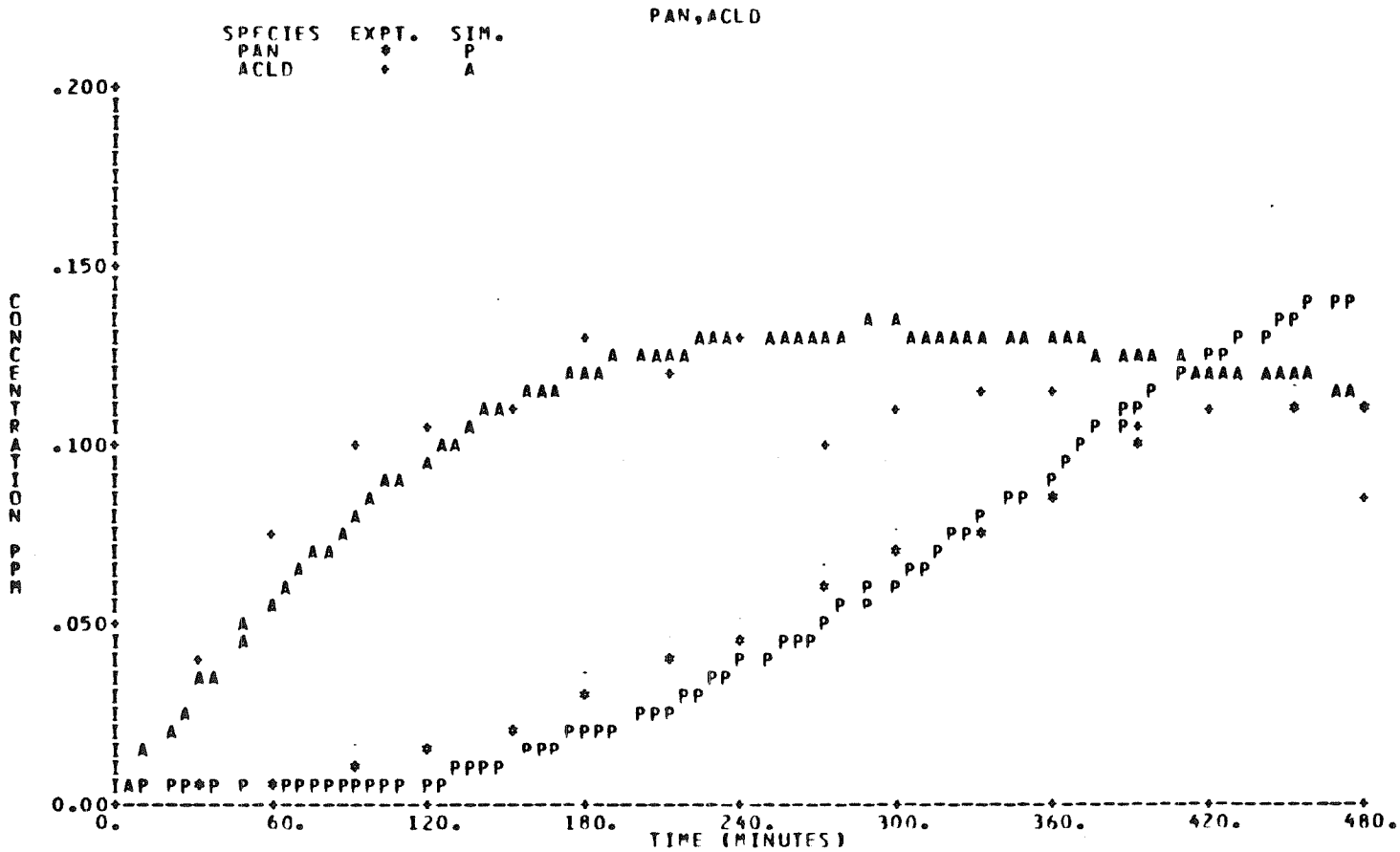

Figure A.2.d. Comparison of Concentration-Time Profiles Predicted by the Explicit Mechanism wtih Experimental Data from SAPRC Experiment EC-238.

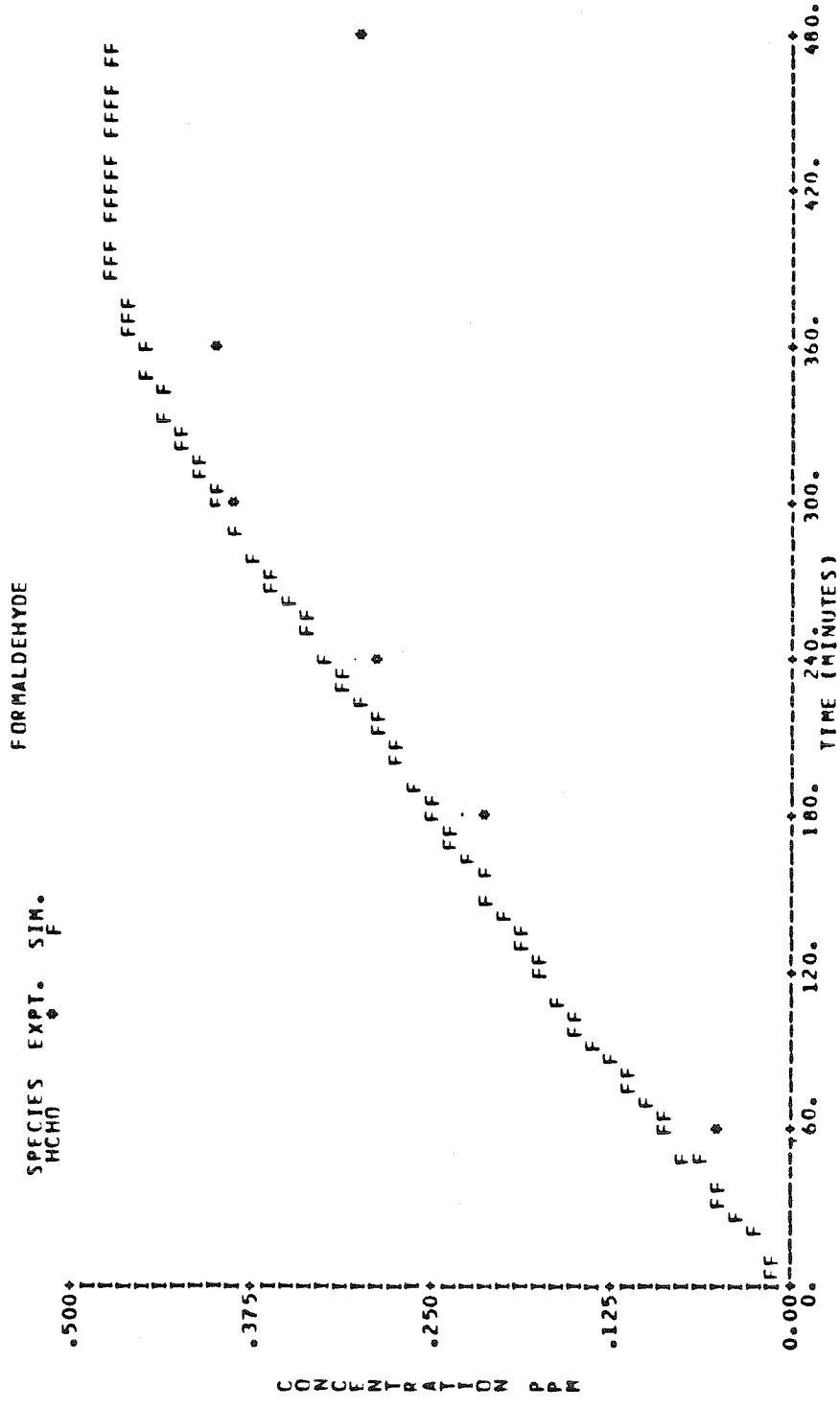

Figure A.2.e. Comparison of Concentration-Time Profiles Predicted by the Explicit Mechanism with Experimental Data from SAPRC Experiment EC-238.

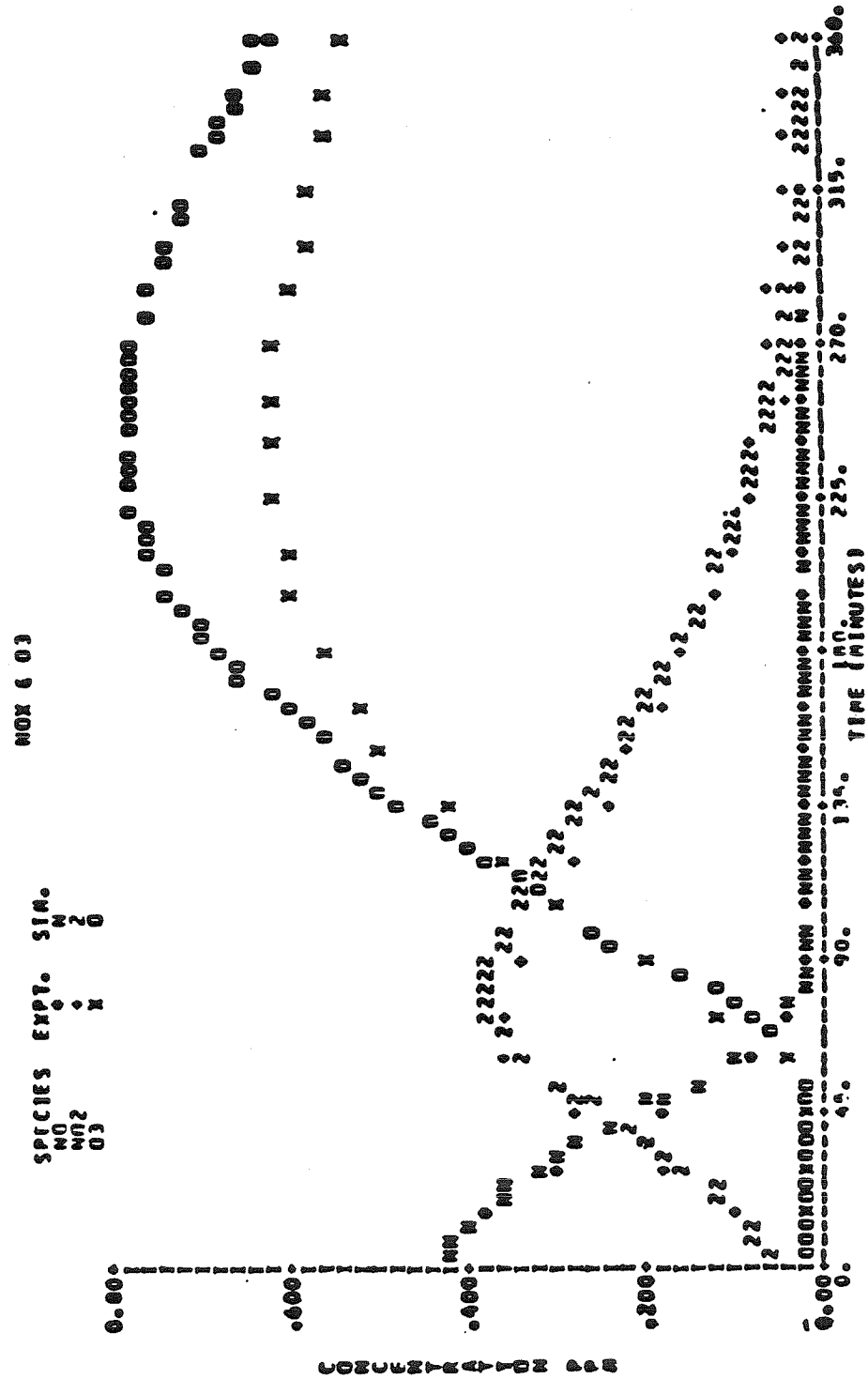

Figure A.3.a Comparison of Concentration-Time Profiles Predicted by the Explicit Mechanism with Experimental Data from SAPRC Experiment EC-231.

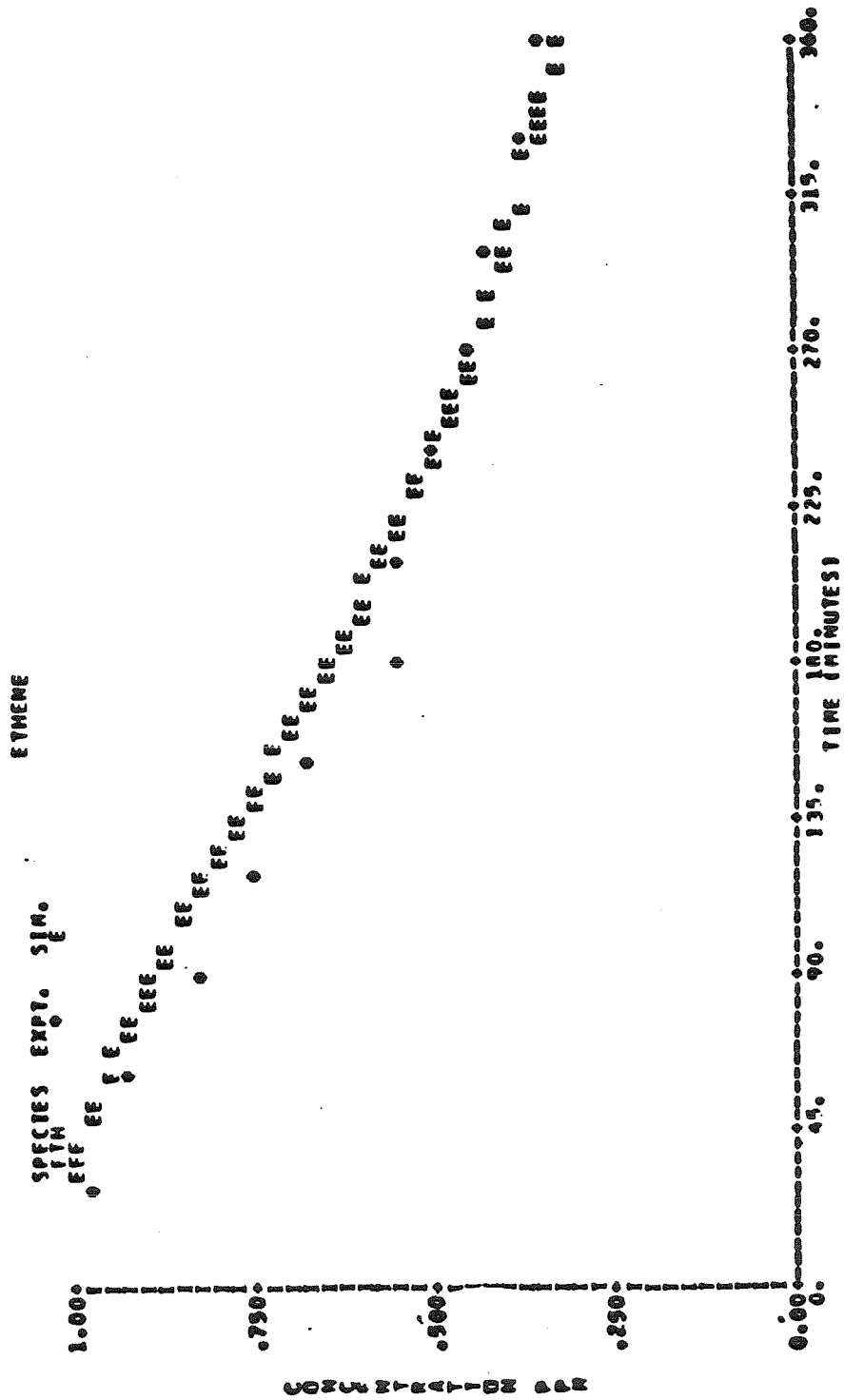

Figure A.3.b. Comparison of Concentration-Time Profiles Predicted by the Explicit Mechanism with Experimental Data from SAPRC Experiment EC-231.

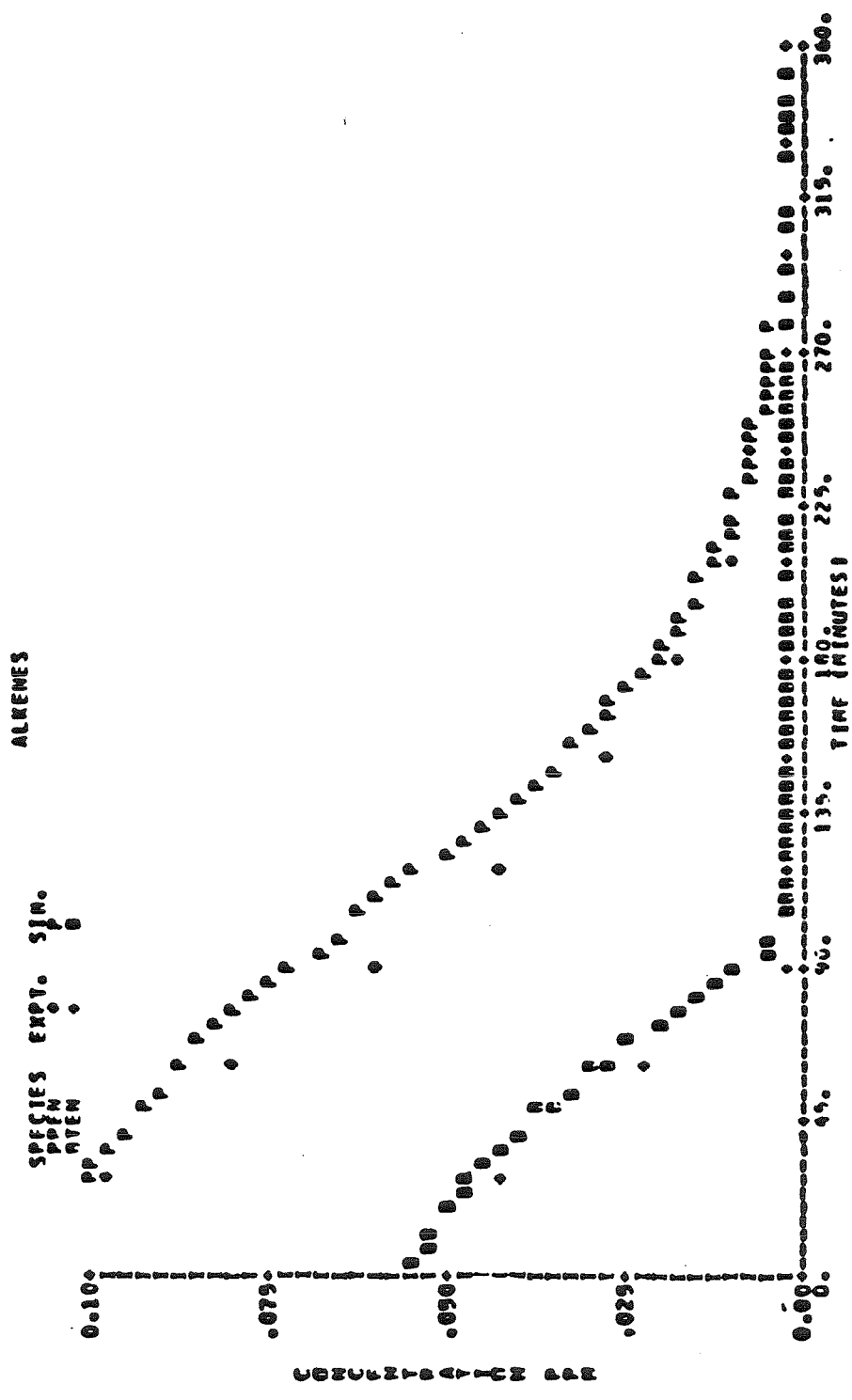

Figure A.3.c. Comparison of Concentration-Time Profiles Predicted by the Explicit Mechanism with Experimental Data from SAPRC Experiment EC-231.

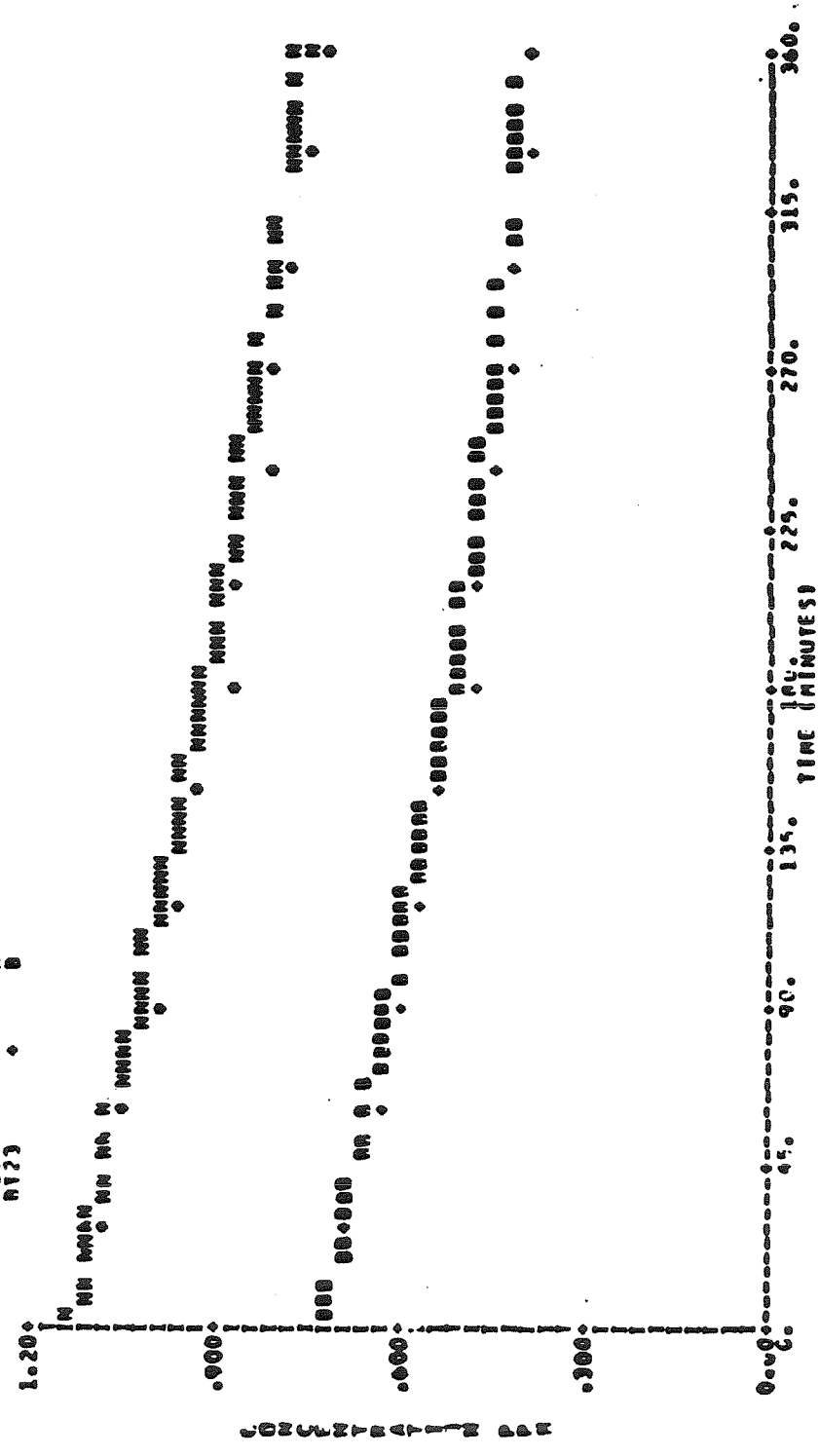

Figure A.3.d. Comparison of Concentration-Time Profiles Predicted by the Explicit Mechanism with Experimental Data from SAPRC Experiment EC-231.

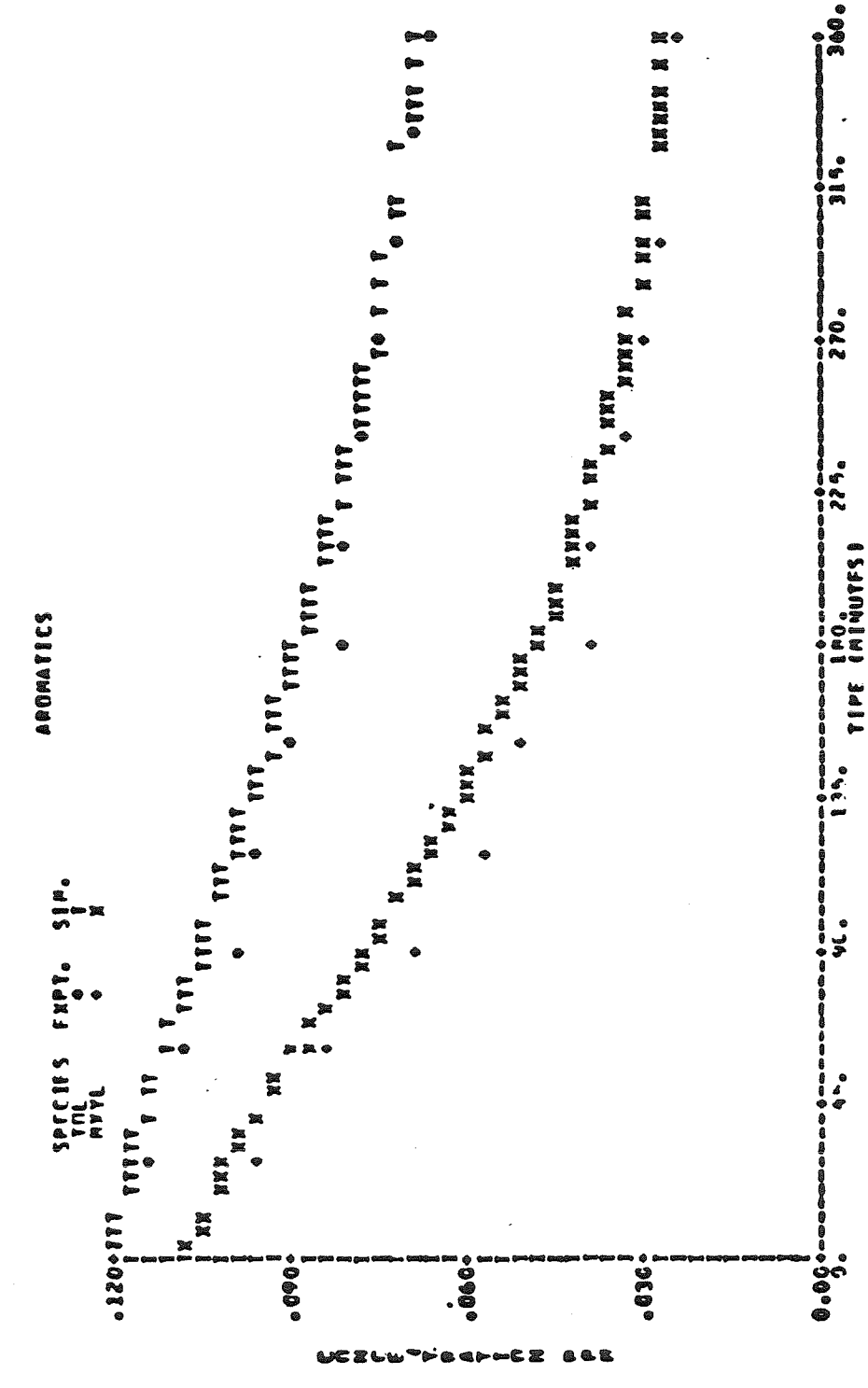

Figure A.3.e. Comparison of Concentration-Time Profiles Predicted by the Explicit Mechanism with Experimental Data from SAPRC Experiment EC-231.

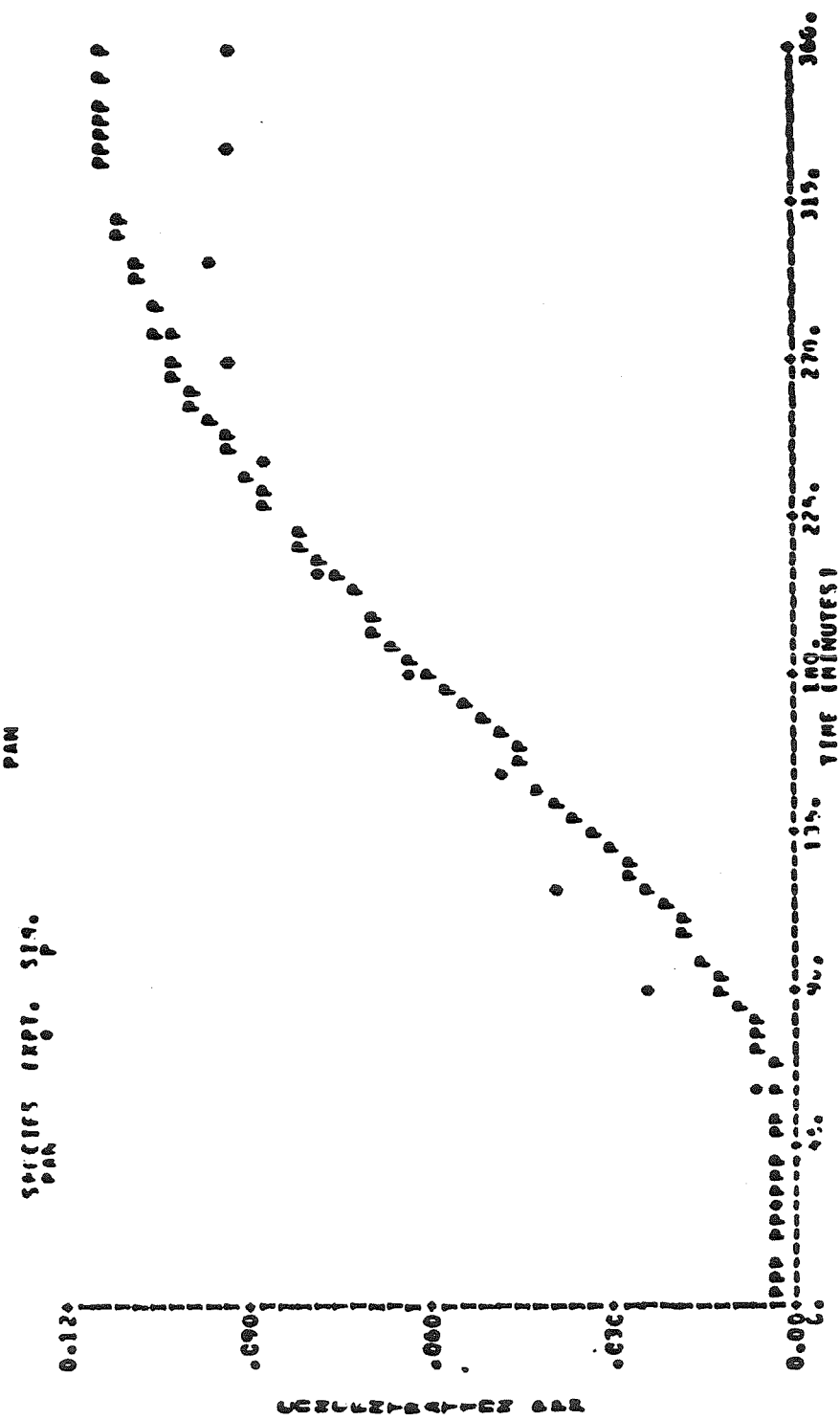

Figure A.3.f. Comparison of Concentration-Time Profiles Predicted by the Explicit Mechanism with Experimental Data from SAPRC Experiment EC-231.

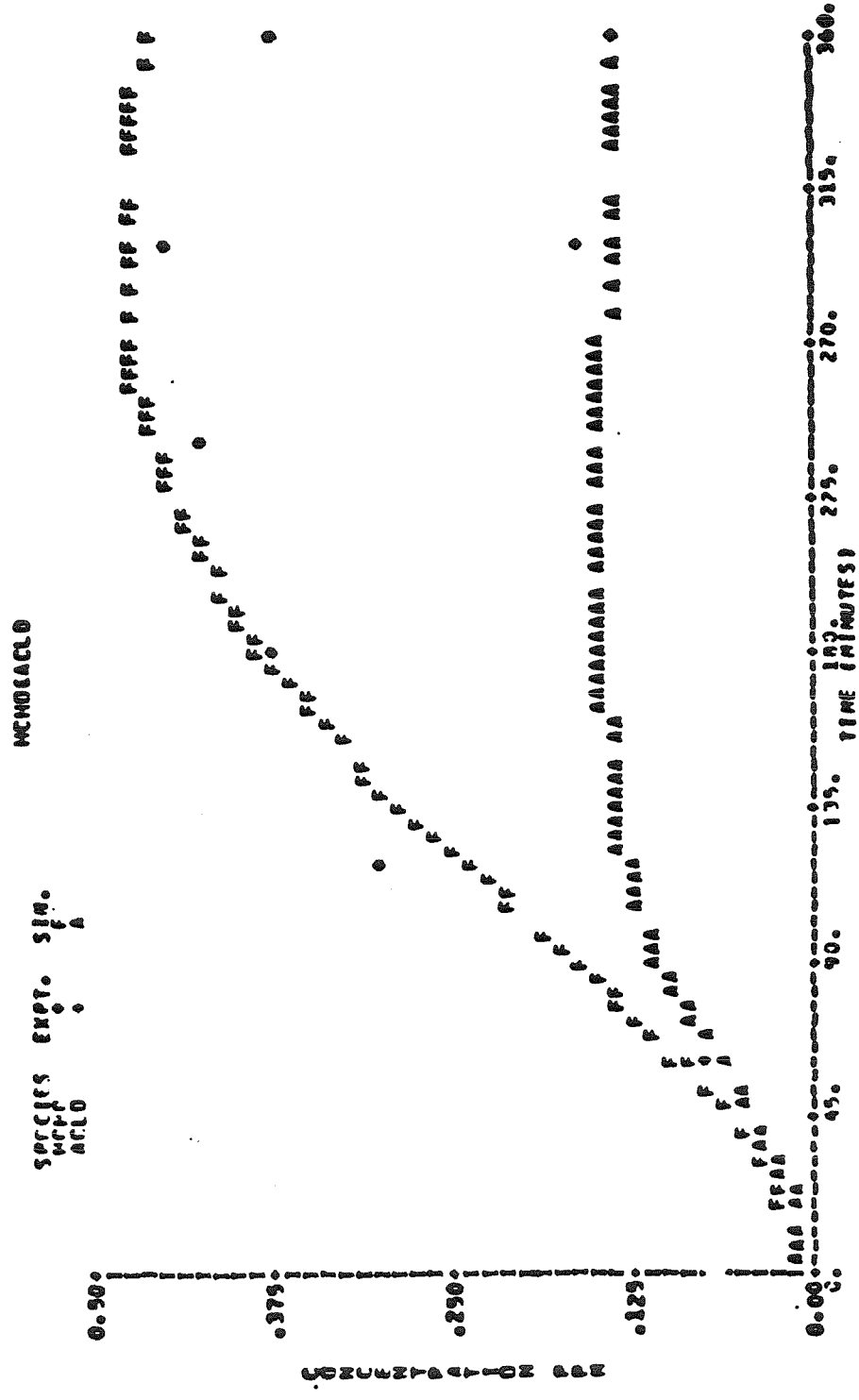

Figure A.3.g. Comparison of Concentration-Time Profiles Predicted by the Explicit Mechanism with Experimental Data from SAPRC Experiment EC-231.

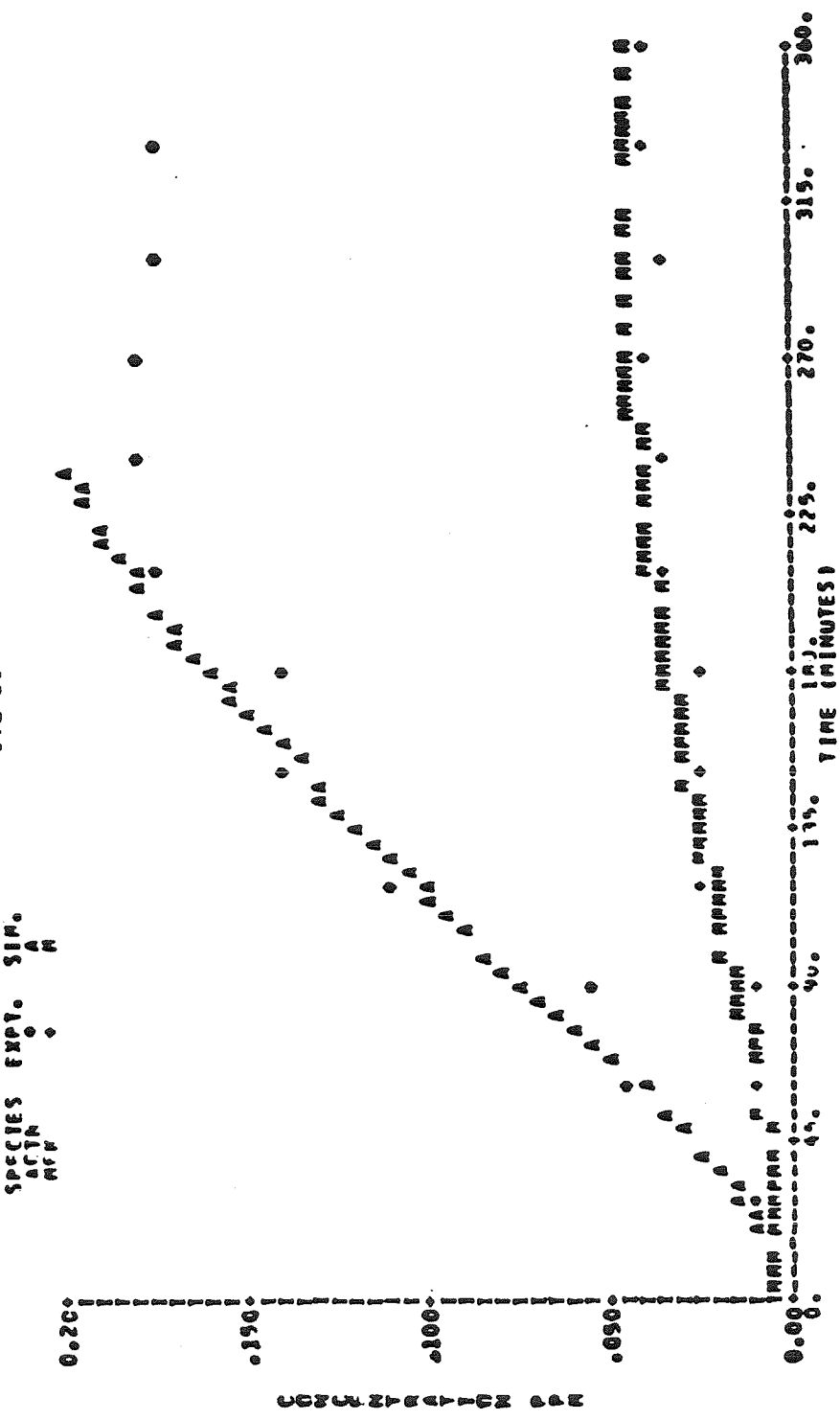

Figure A.3.h. Comparison of Concentration-Time Profiles Predicted by the Explicit Mechanism with Experimental Data from SAPRC Experiment EC-231.

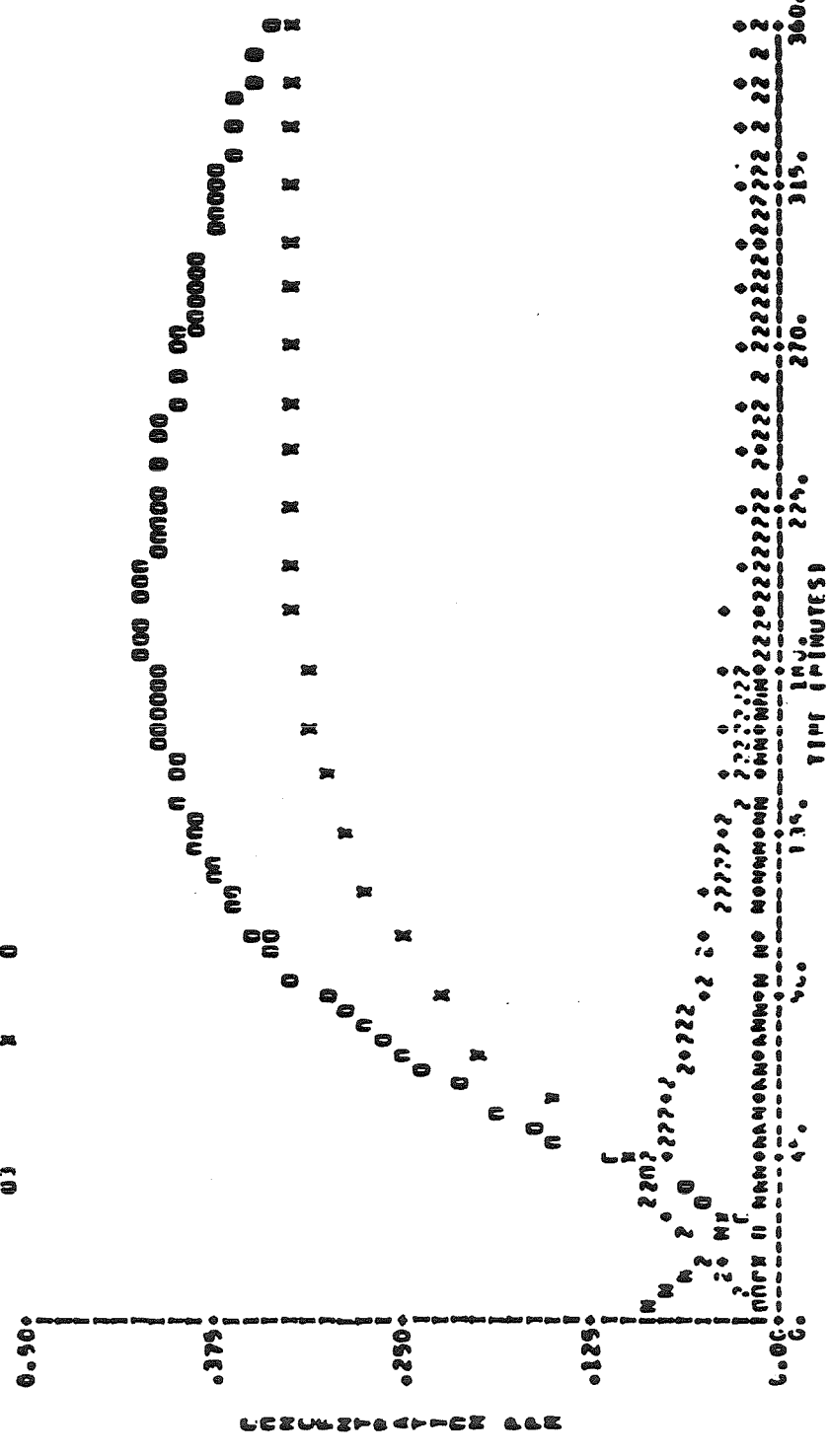

Figure A.4.a. Comparison of Concentration-Time Profiles Predicted by the Explicit Mechanism with Experimental Data from SAPRC Experiment EC-233.

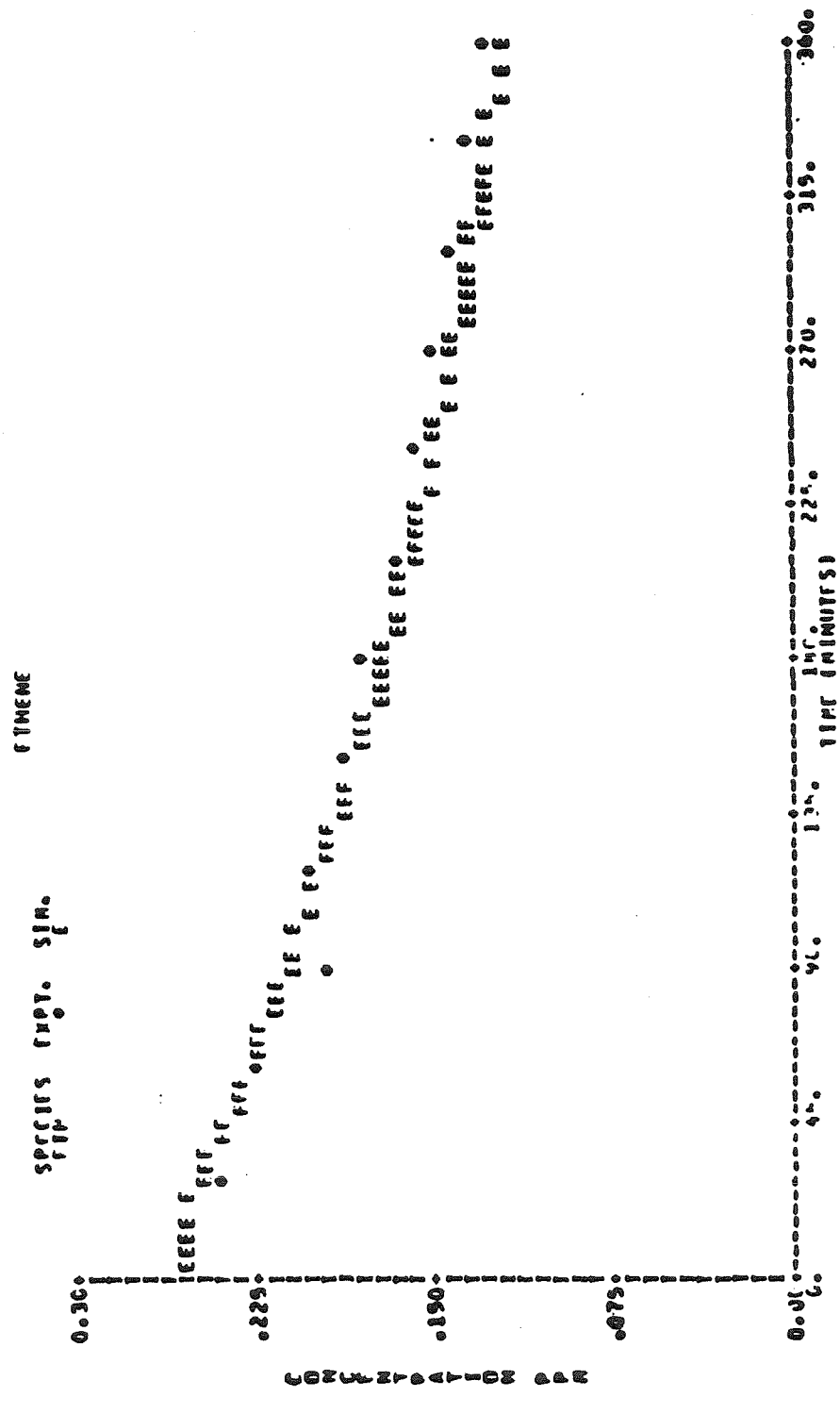

Figure A.4.b. Comparison of Concentration-Time Profiles Predicted by the Explicit Mechanism with Experimental Data from SAPRC Experiment EC-233.

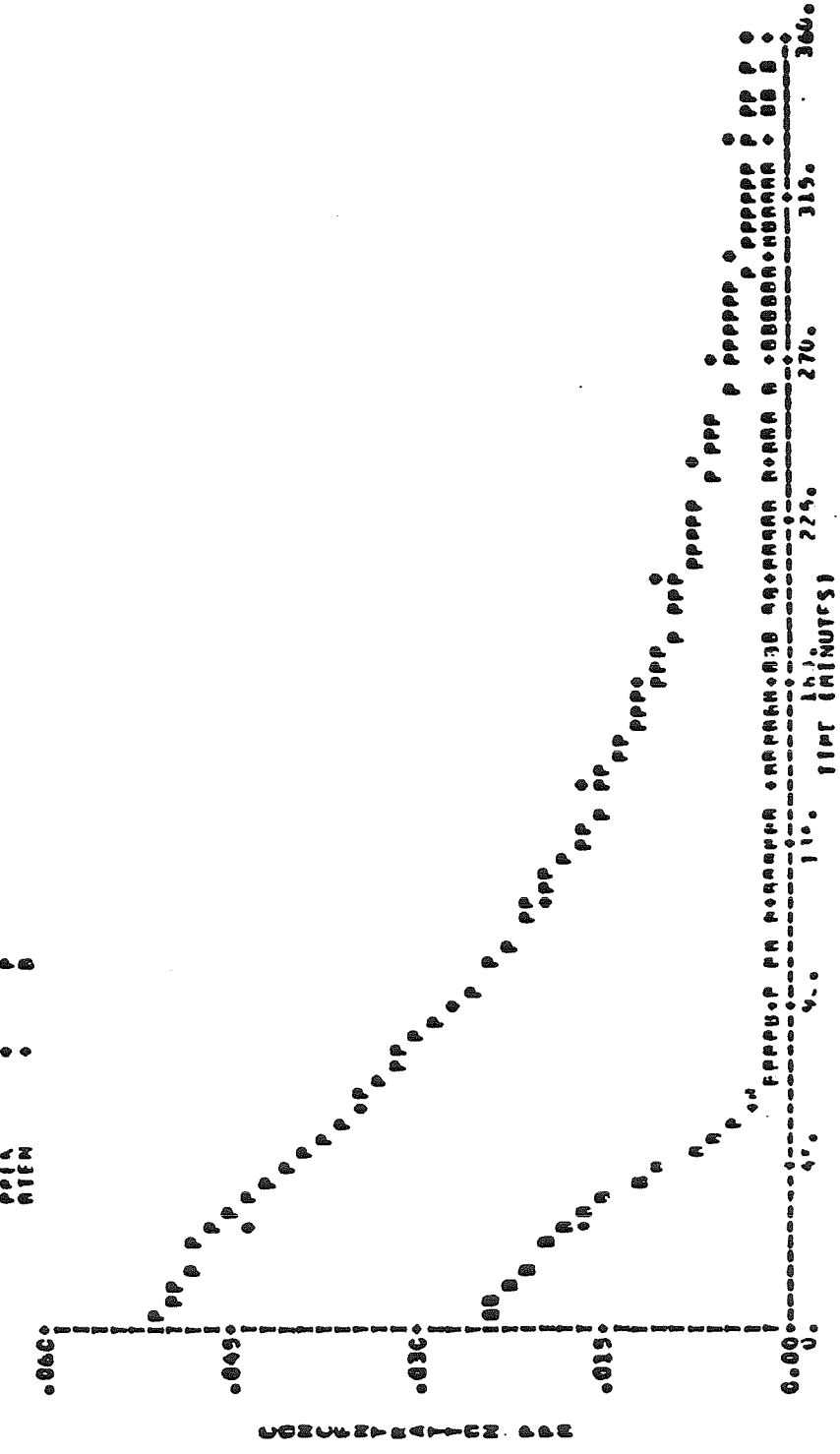

Figure A.4.c. Comparison of Concentration-Time Profiles Predicted by the Explicit Mechanism with Experimental Data from SAPRC Experiment EC-233.

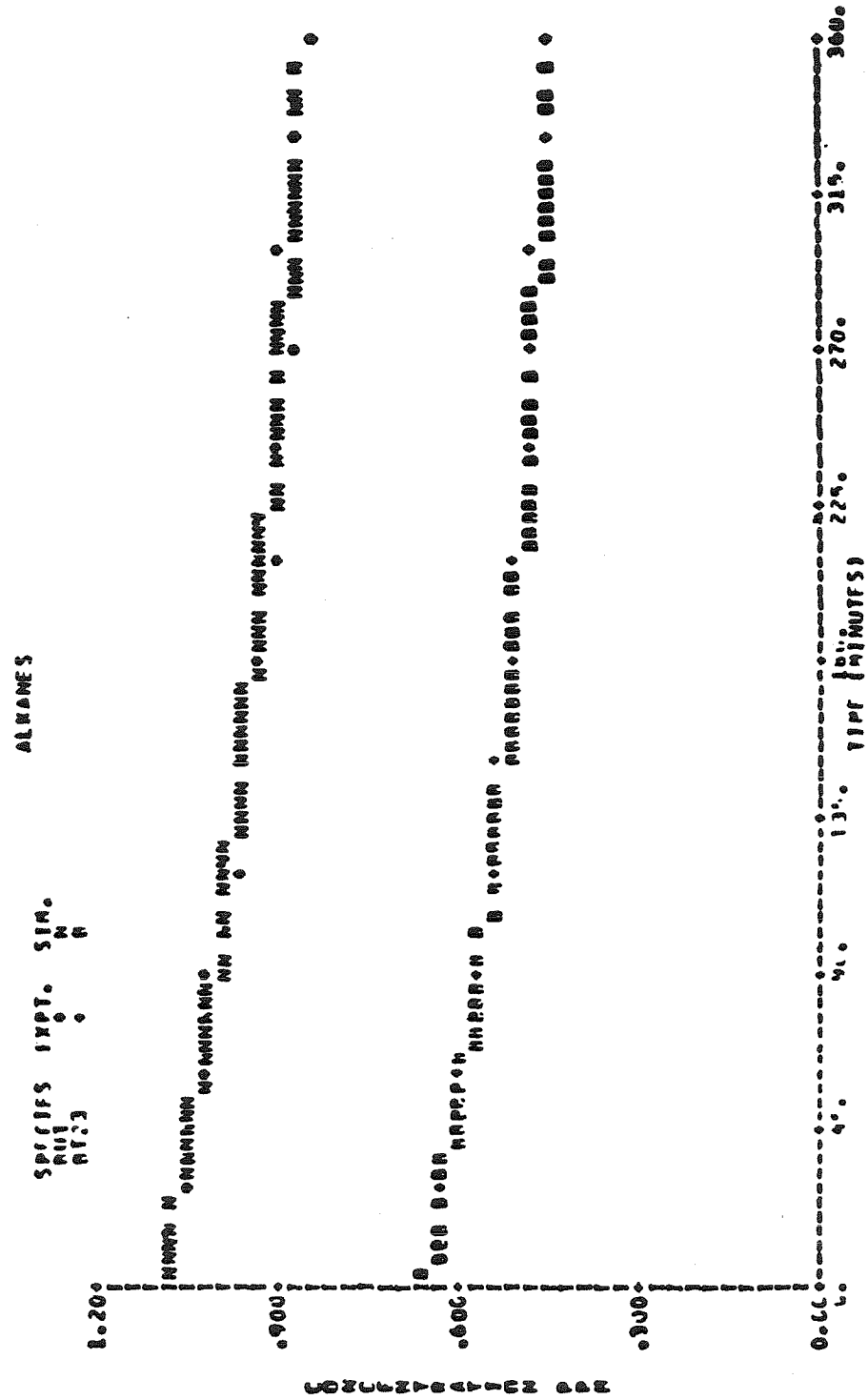

Figure A.4.d. Comparison of Concentration-Time Profiles Predicted by the Explicit Mechanism with Experimental Data from SAPRC Experiment EC-233.

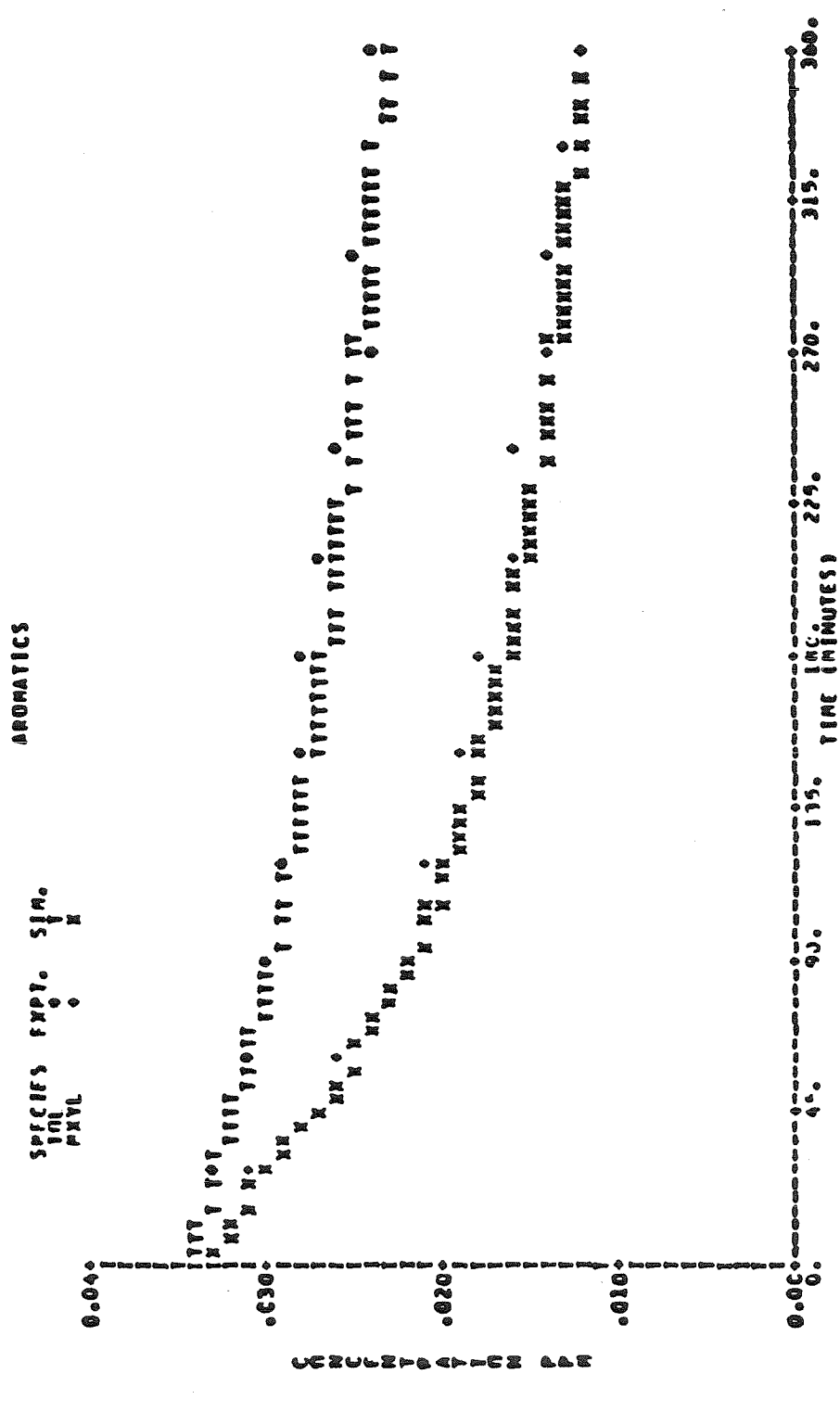

Figure A.4.e. Comparison of Concentration-Time Profiles Predicted by the Explicit Mechanism with Experimental Data from SAPRC Experiment EC-233.

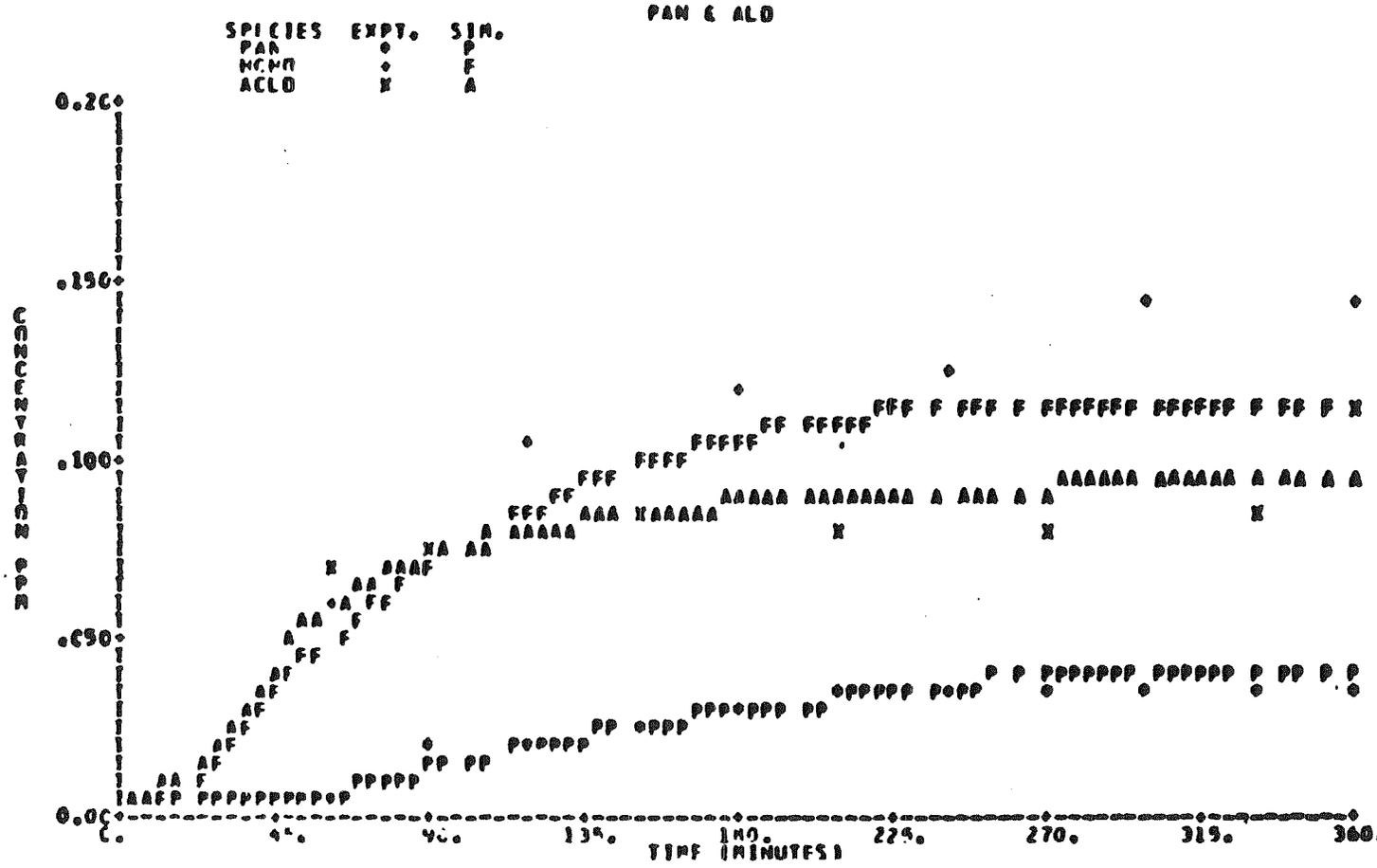

Figure A.4.f. Comparison of Concentration-Time Profiles Predicted by the Explicit Mechanism with Experimental Data from SAPRC Experiment EC-233.

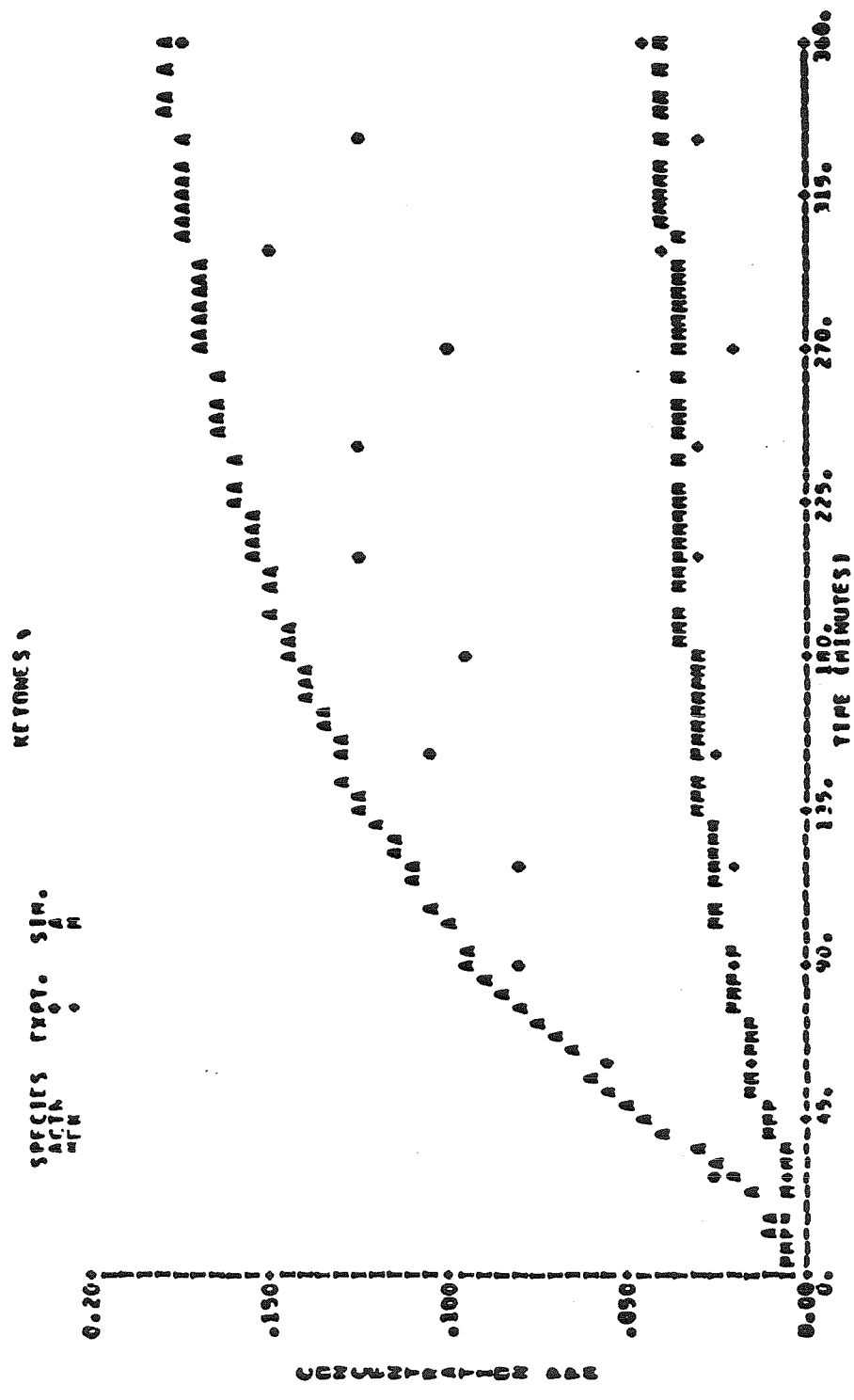

Figure A.4.g. Comparison of Concentration-Time Profiles Predicted by the Explicit Mechanism with Experimental Data from SAPRC Experiment EC-233.

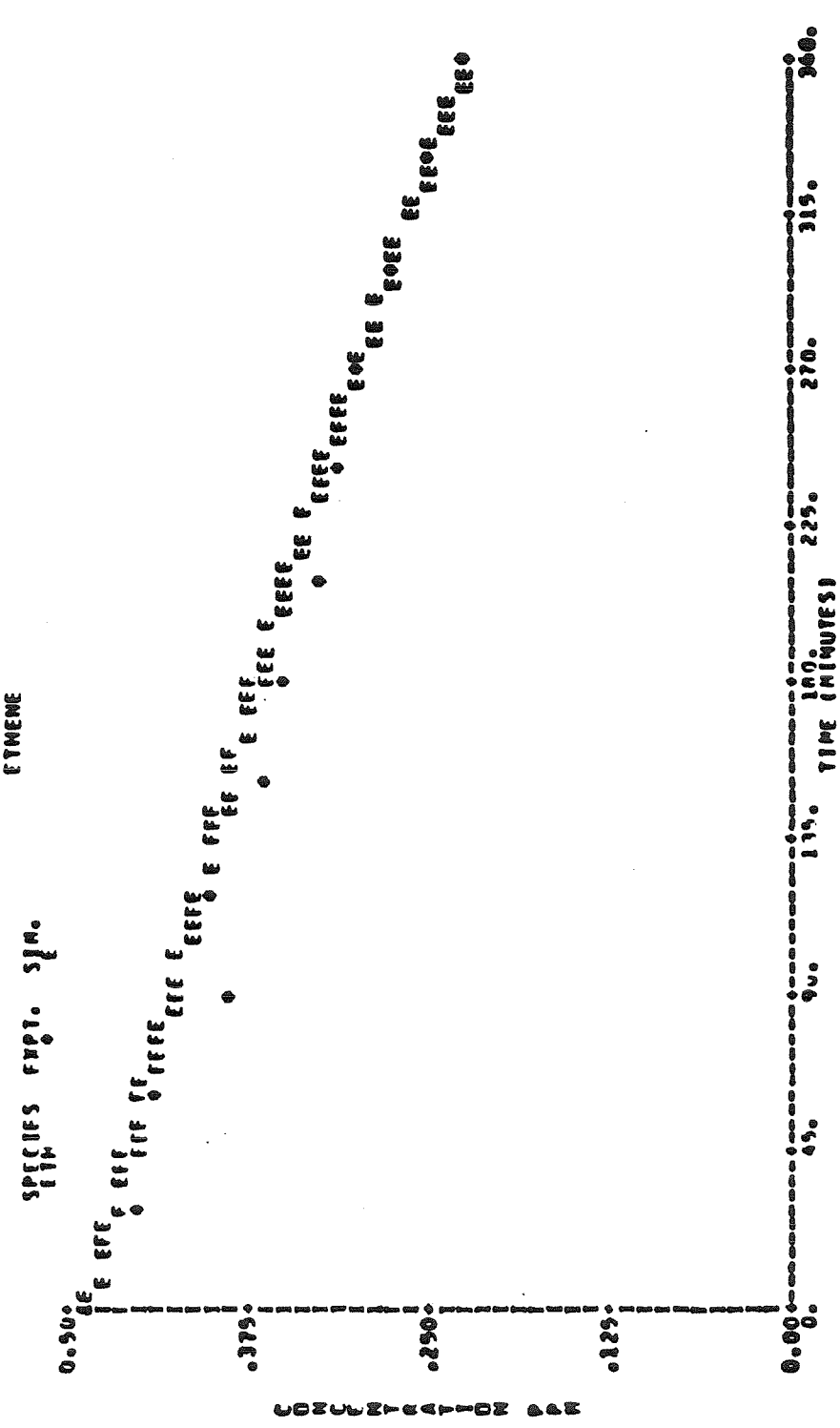

Figure A.5.b. Comparison of Concentration-Time Profiles Predicted by the Explicit Mechanism with Experimental Data from SAPRC Experiment EC-241.

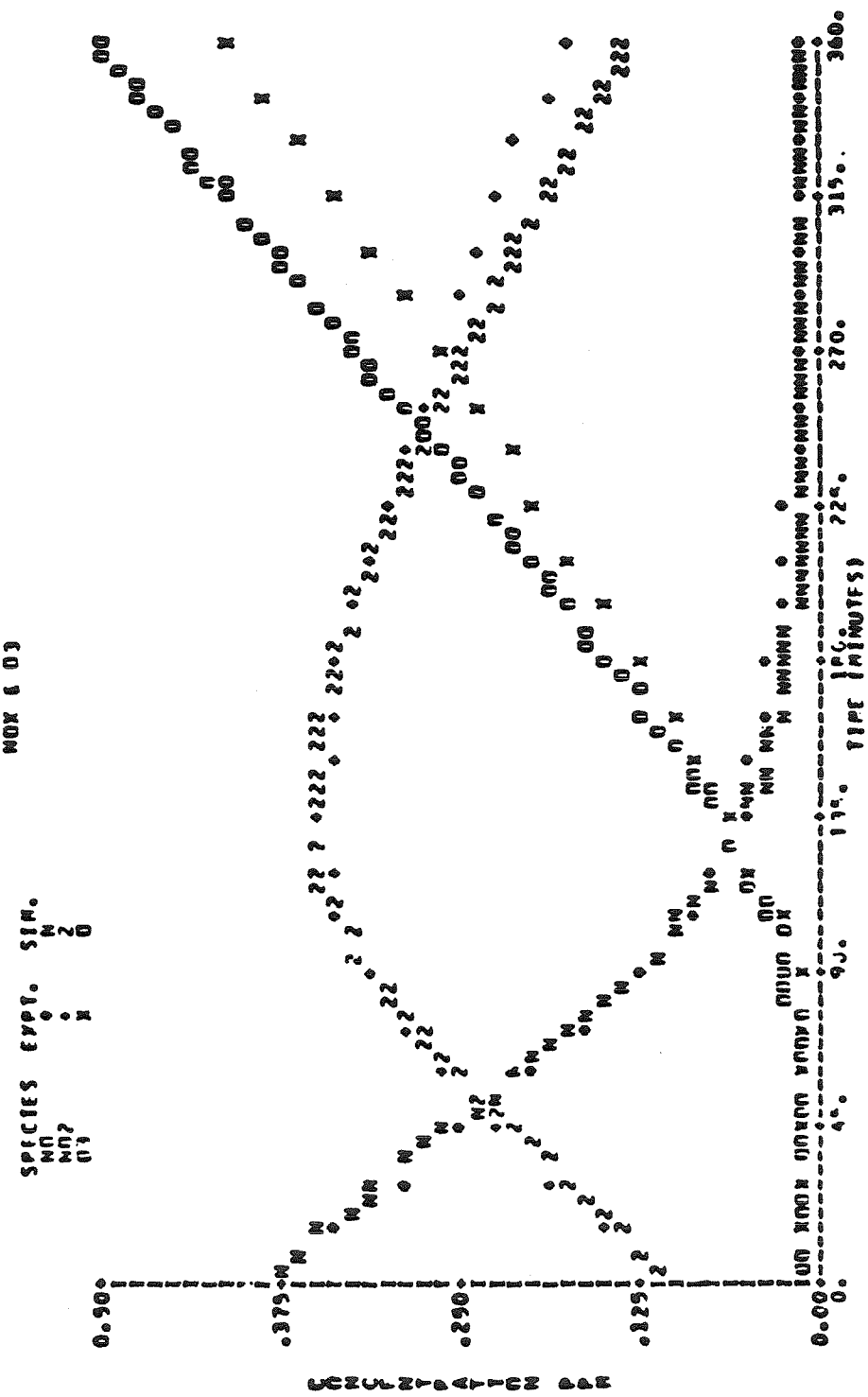

Figure A.5.a. Comparison of Concentration-Time Profiles Predicted by the Explicit Mechanism with Experimental Data from SAPRC Experiment EC-241.

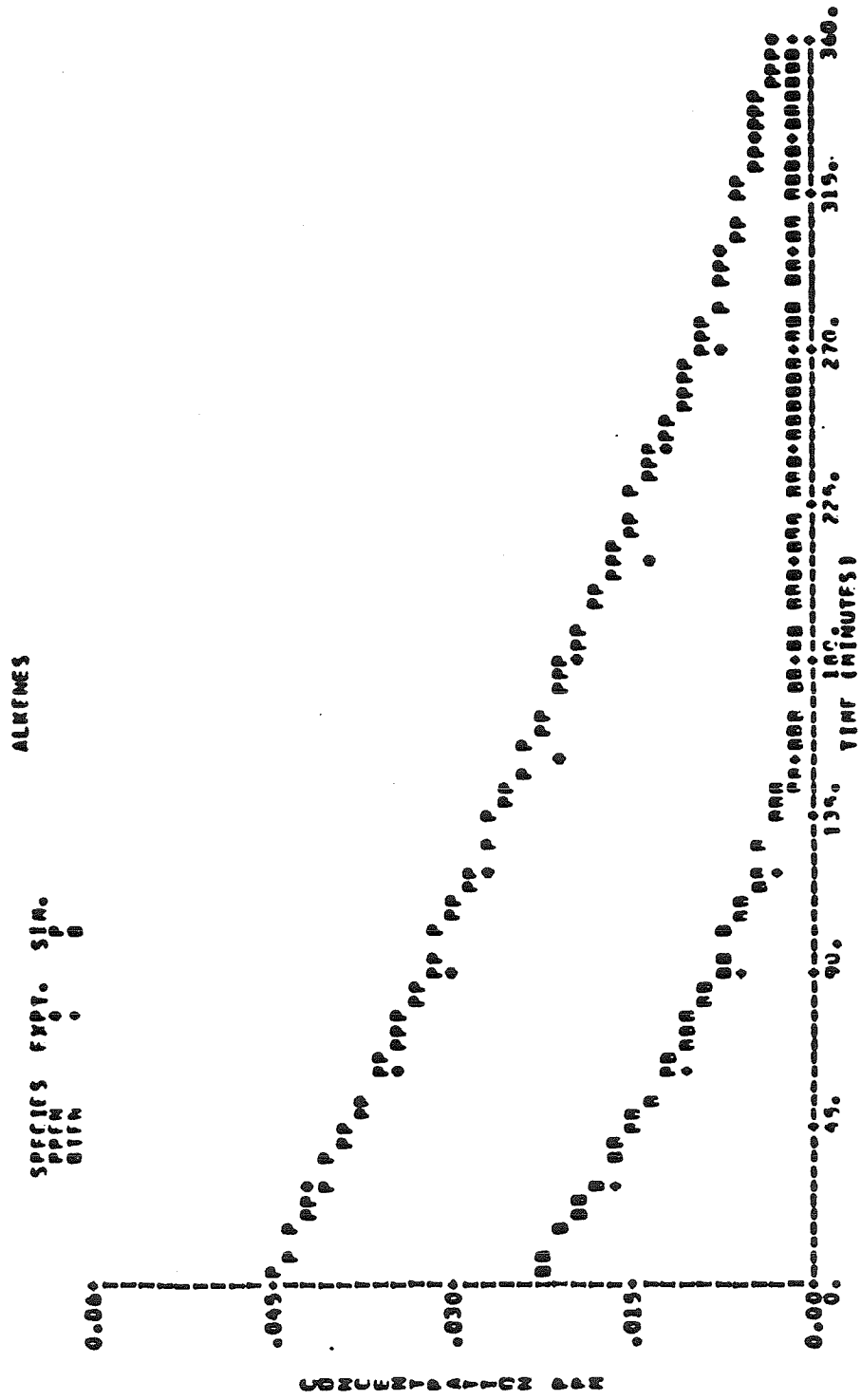

Figure A.5.c. Comparison of Concentration-Time Profiles Predicted by the Explicit Mechanism with Experimental Data from SAPRC Experiment EC-241.

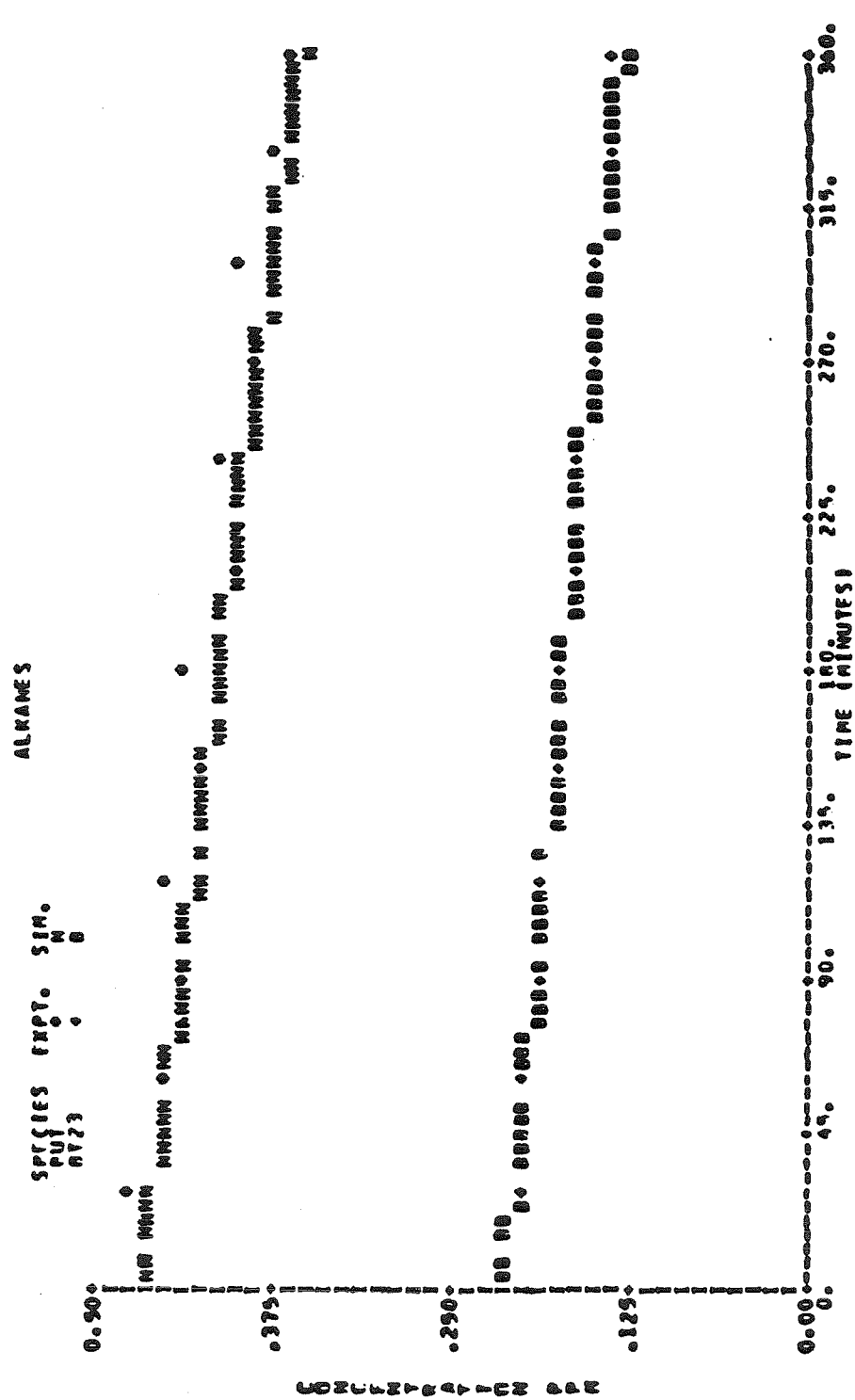

Figure A.5.d. Comparison of Concentration-Time Profiles Predicted by the Explicit Mechanism with Experimental Data from SAPRC Experiment EC-241.

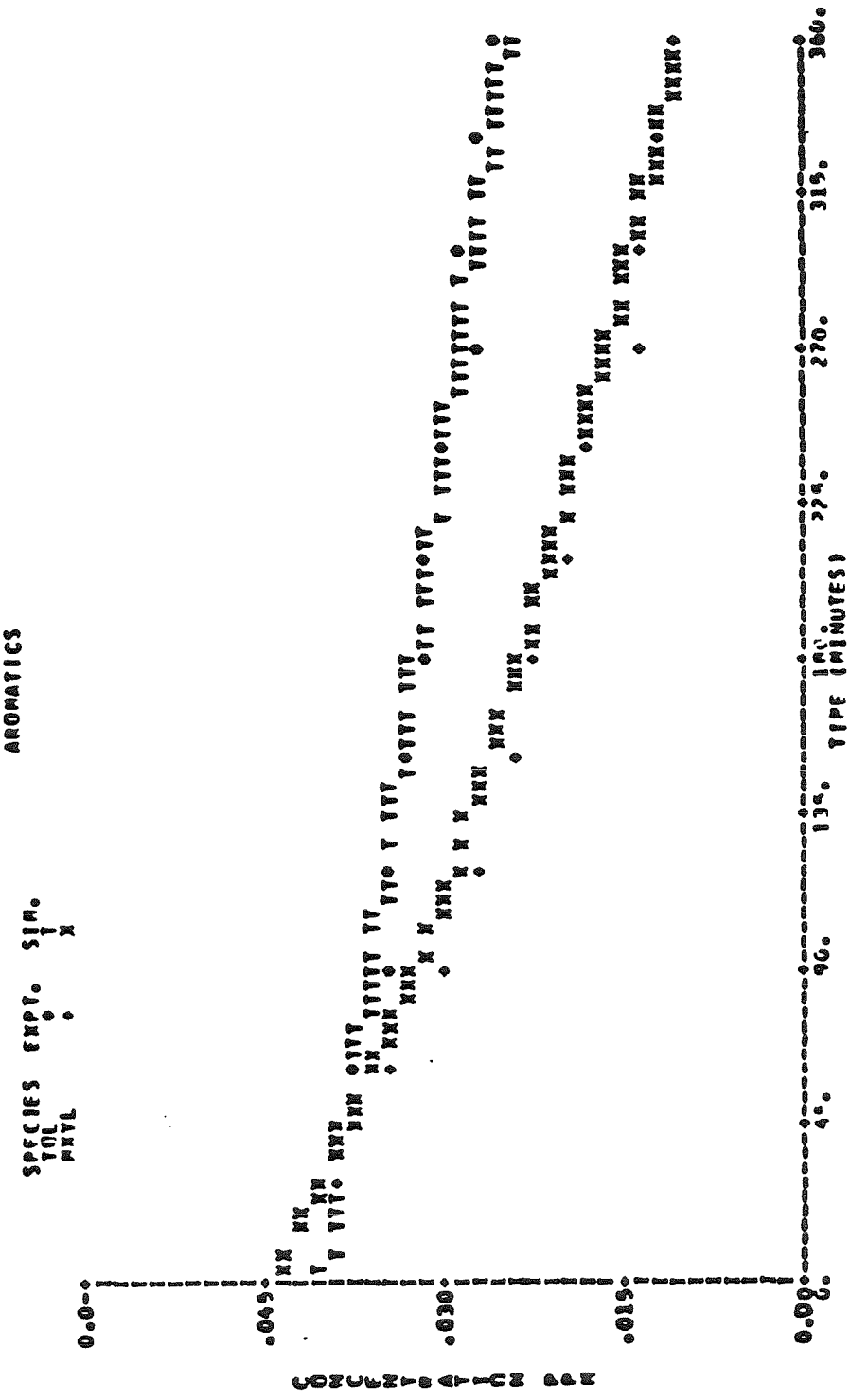

Figure A.5.e. Comparison of Concentration-Time Profiles Predicted by the Explicit Mechanism with Experimental Data from SAPRC Experiment EC-241.

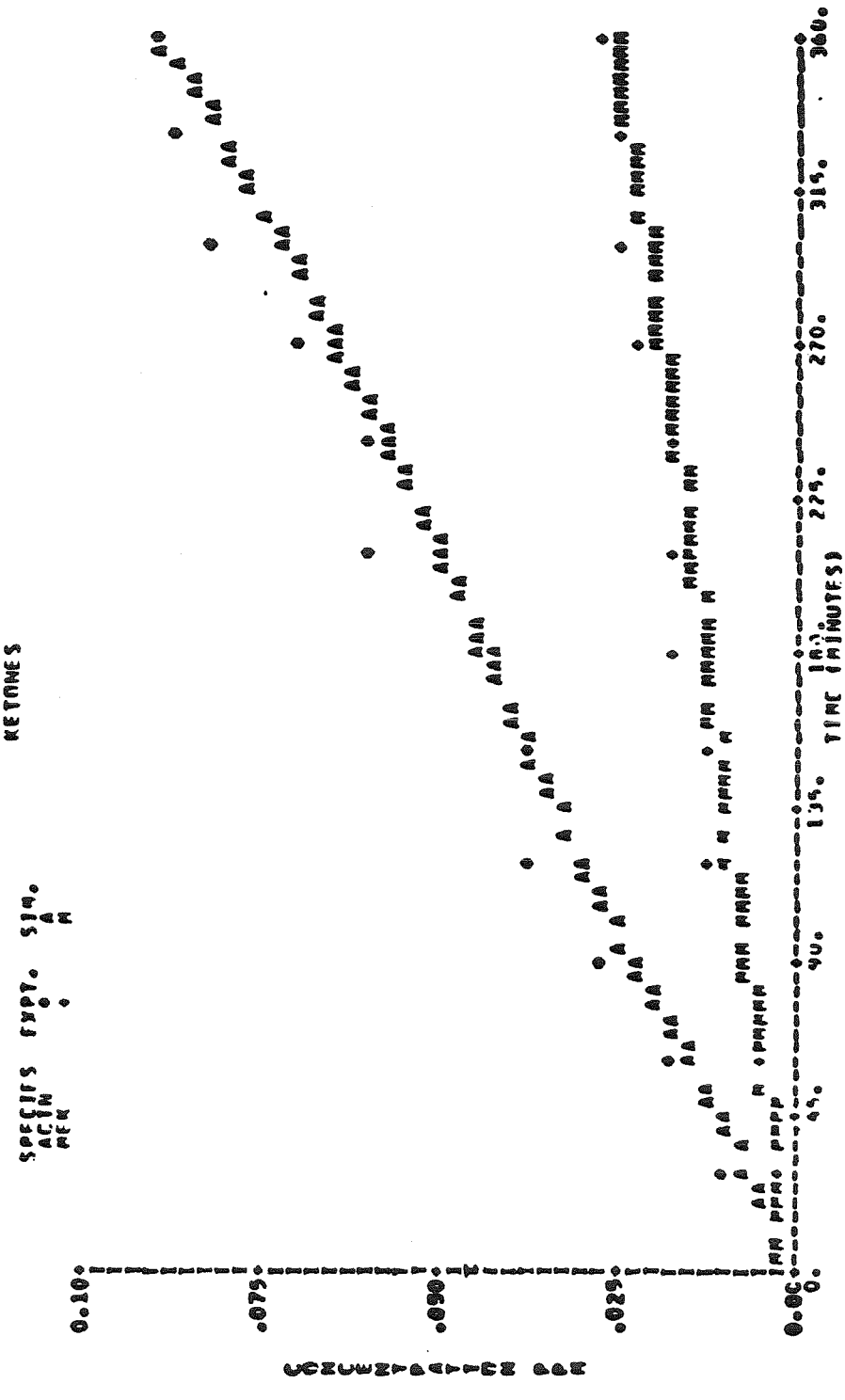

Figure A.5.f. Comparison of Concentration-Time Profiles Predicted by the Explicit Mechanism with Experimental Data from SAPRC Experiment EC-241.

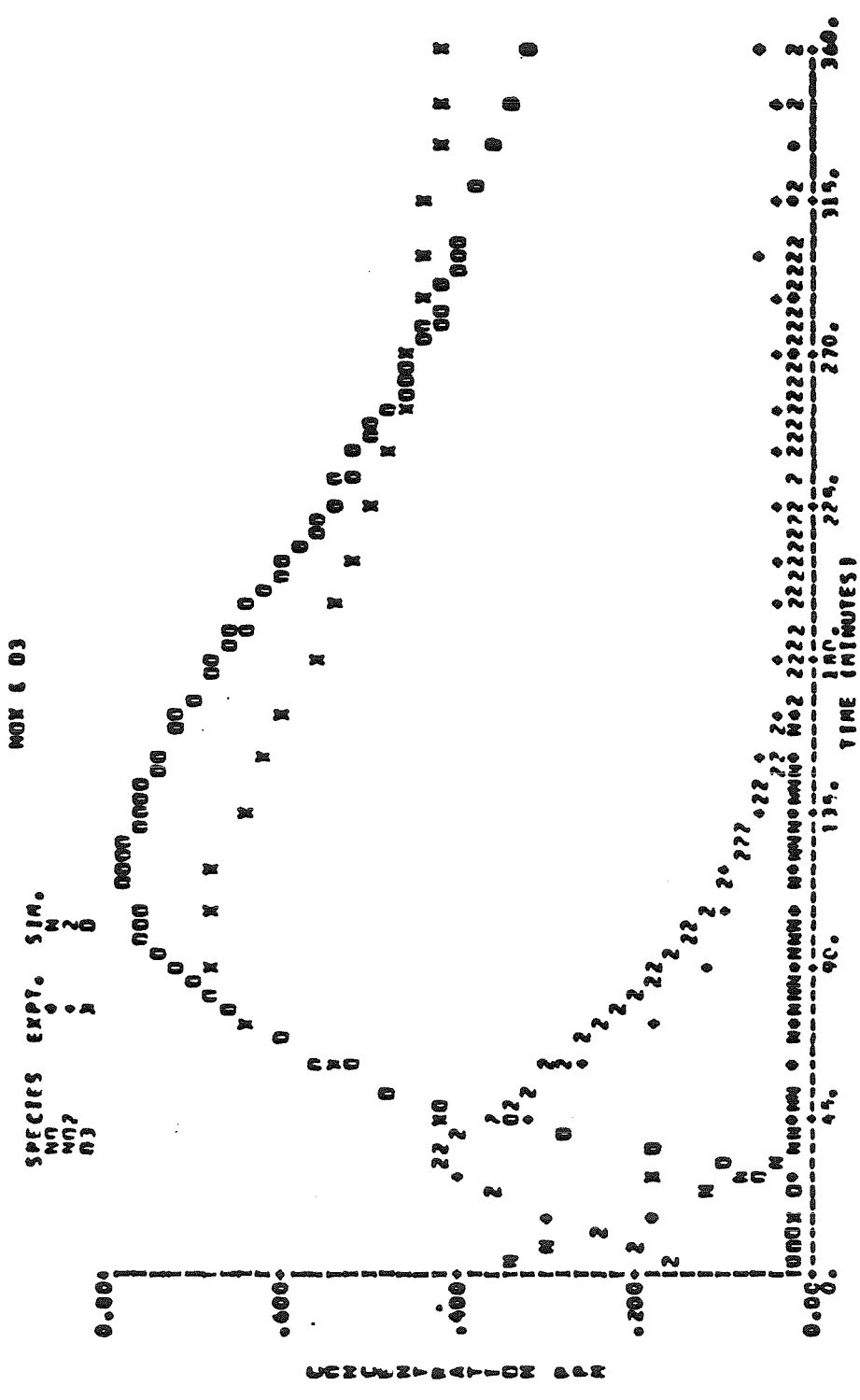

Figure A.6.a. Comparison of Concentration-Time Profiles Predicted by the Explicit Mechanism with Experimental Data from SAPRC Experiment EC-242.

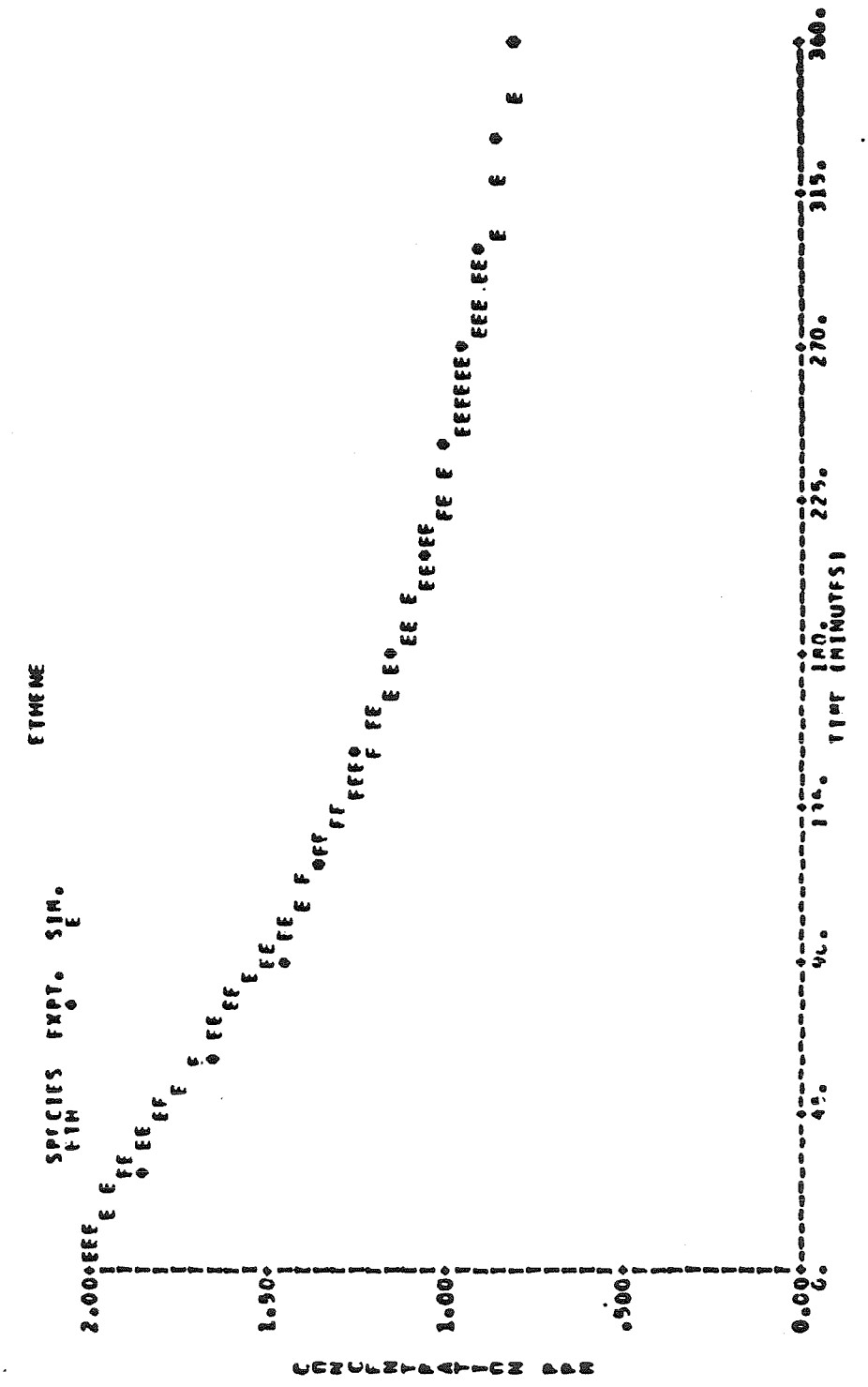

Figure A.6.b. Comparison of Concentration-Time Profiles Predicted by the Explicit Mechanism with Experimental Data from SAPRC Experiment EC-242.

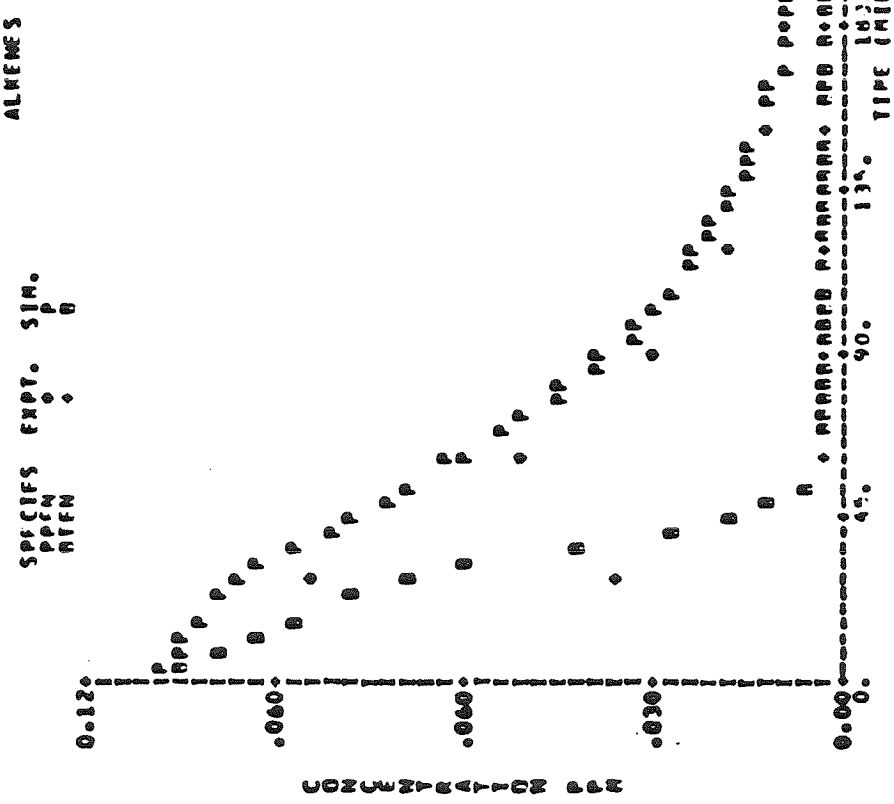

Figure A.6.c. Comparison of Concentration-Time Profiles Predicted by the Explicit Mechanism with Experimental Data from SAPRC Experiment EC-242.

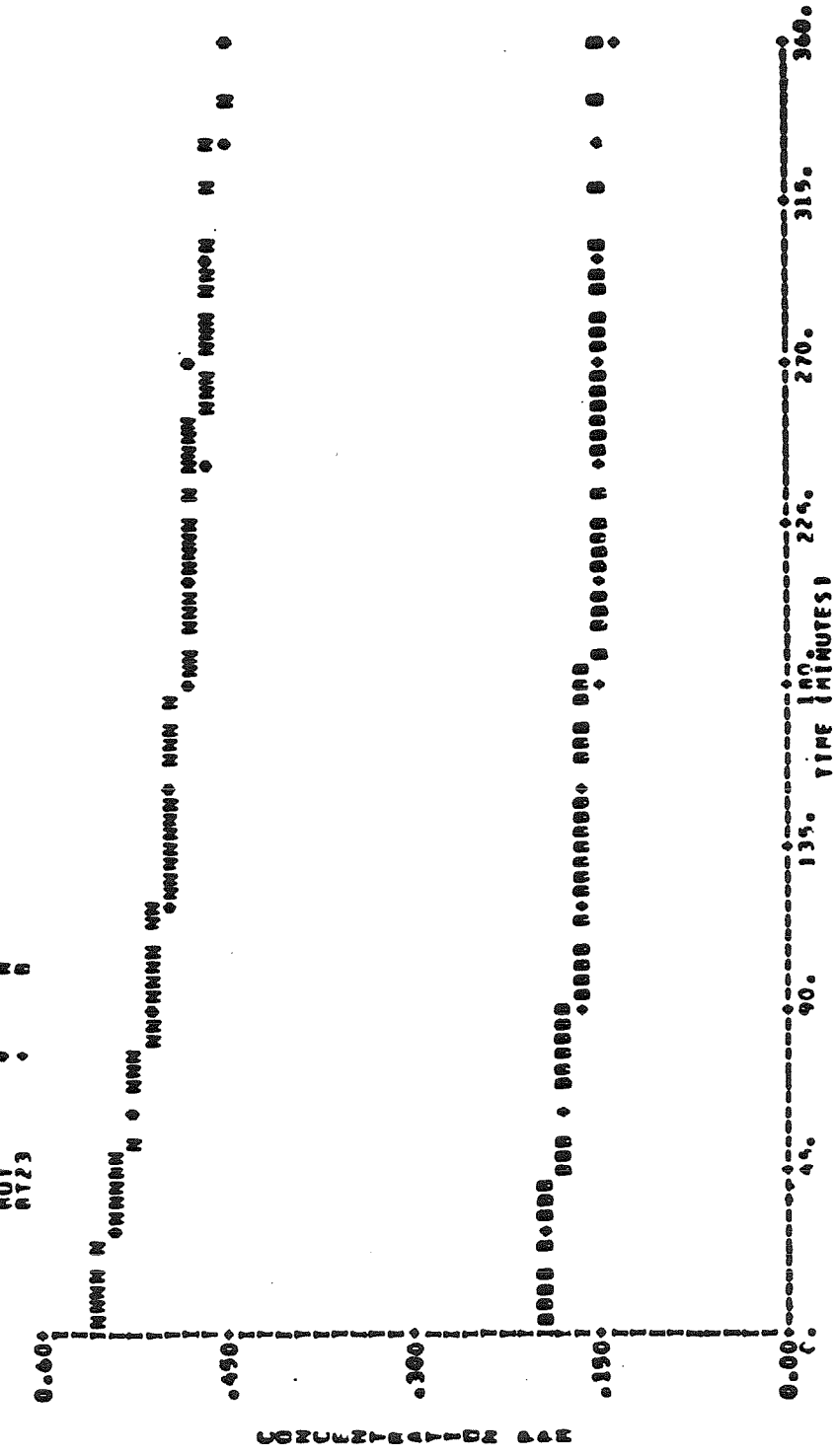

Figure A.6.d. Comparison of Concentration-Time Profiles Predicted by the Explicit Mechanism with Experimental Data from SAPRC Experiment EC-242.

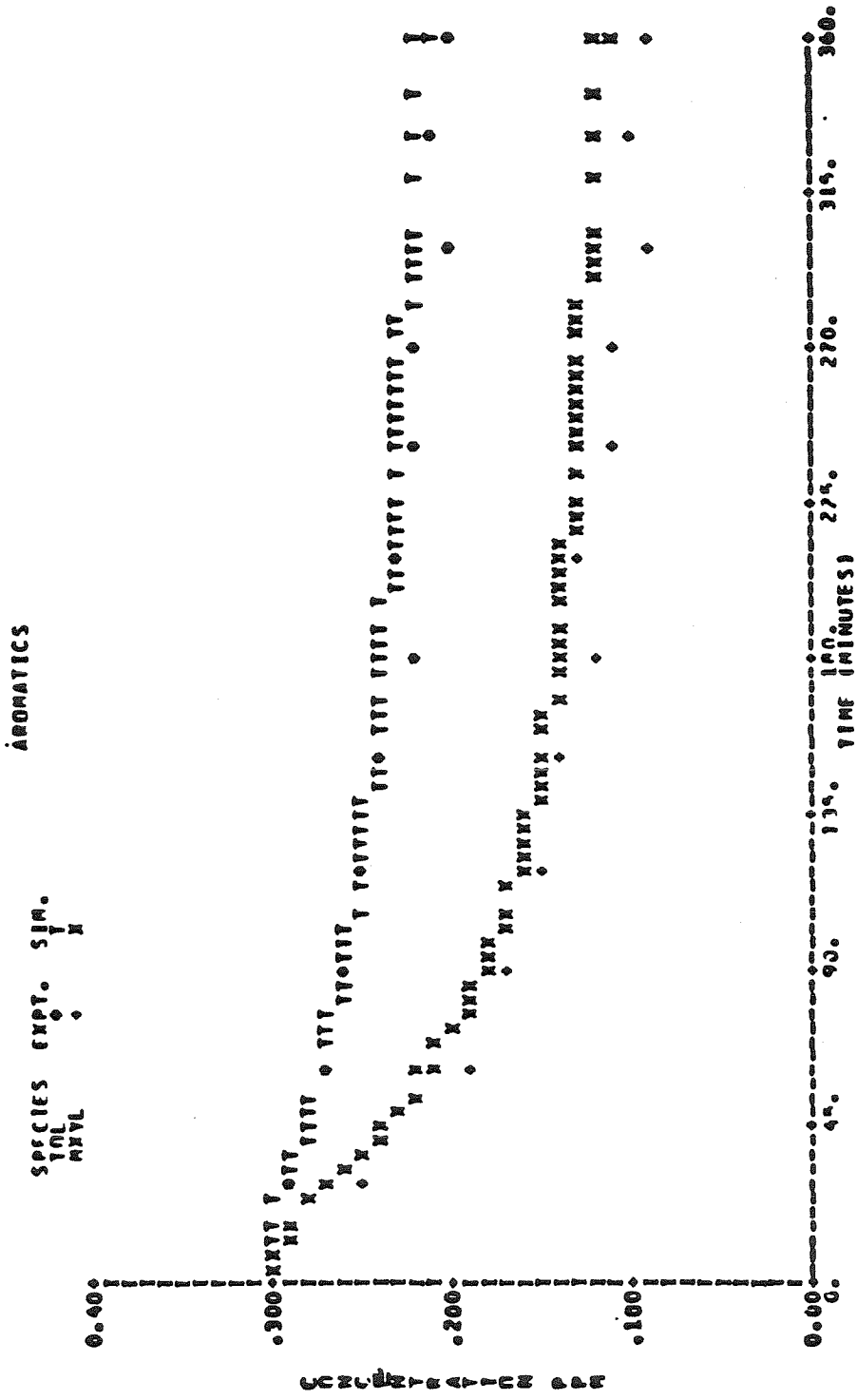

Figure A.6.e. Comparison of Concentration-Time Profiles Predicted by the Explicit Mechanism with Experimental Data from SAPRC Experiment EC-242.

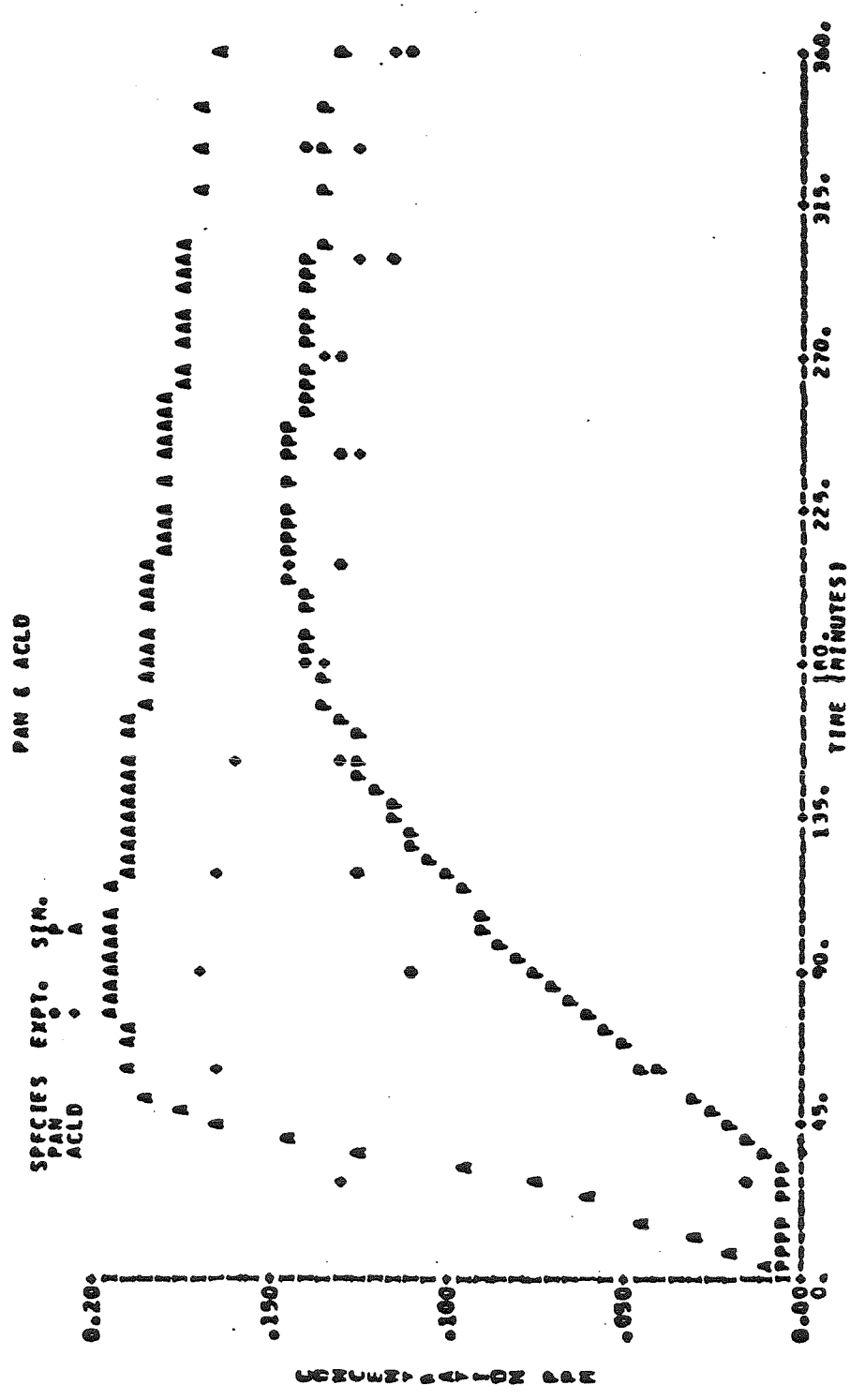

Figure A.6.f. Comparison of Concentration-Time Profiles Predicted by the Explicit Mechanism with Experimental Data from SAPRC Experiment EC-242.

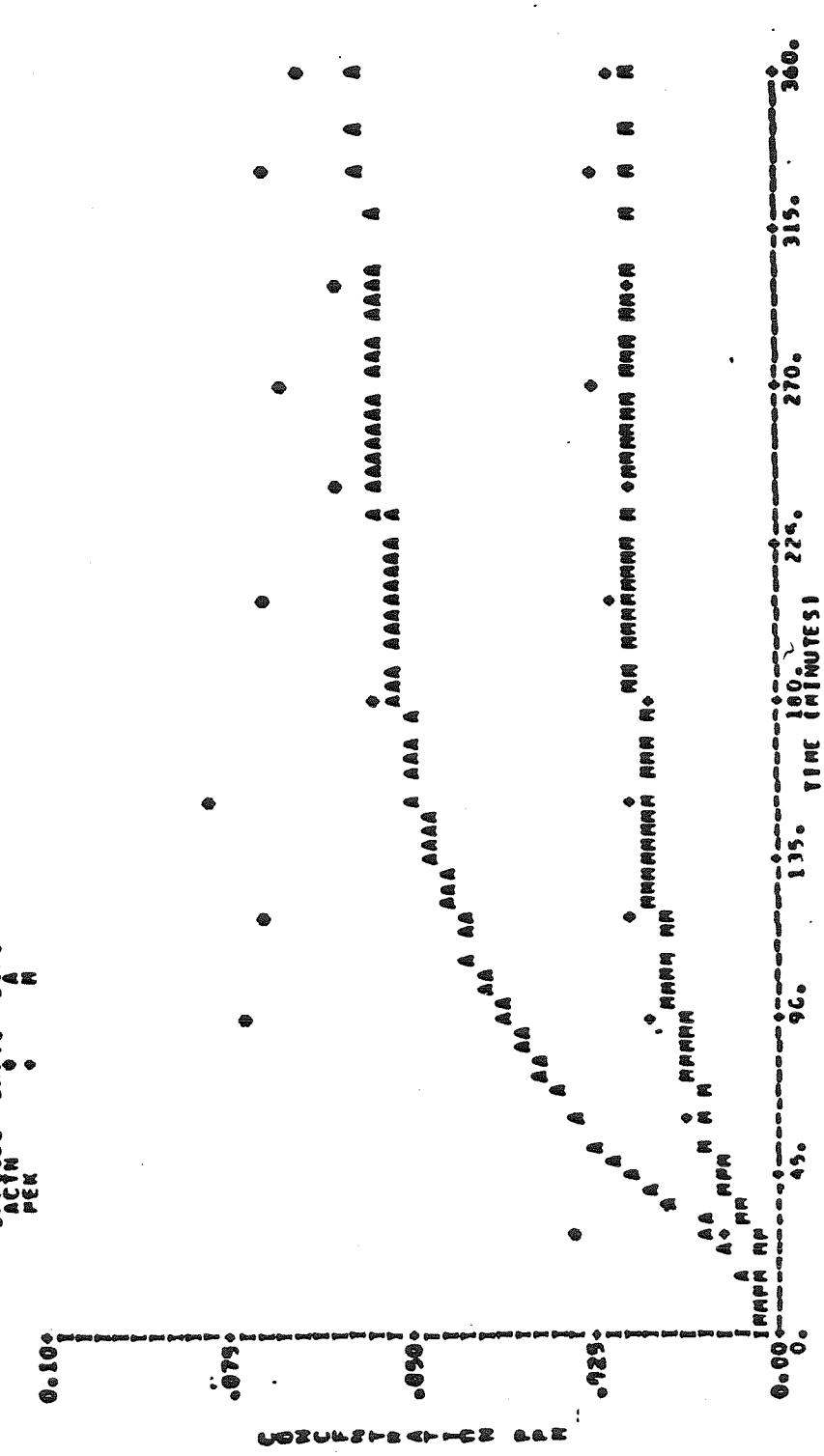

Figure A.6.g. Comparison of Concentration-Time Profiles Predicted by the Explicit Mechanism with Experimental Data from SAPRC Experiment EC-242.

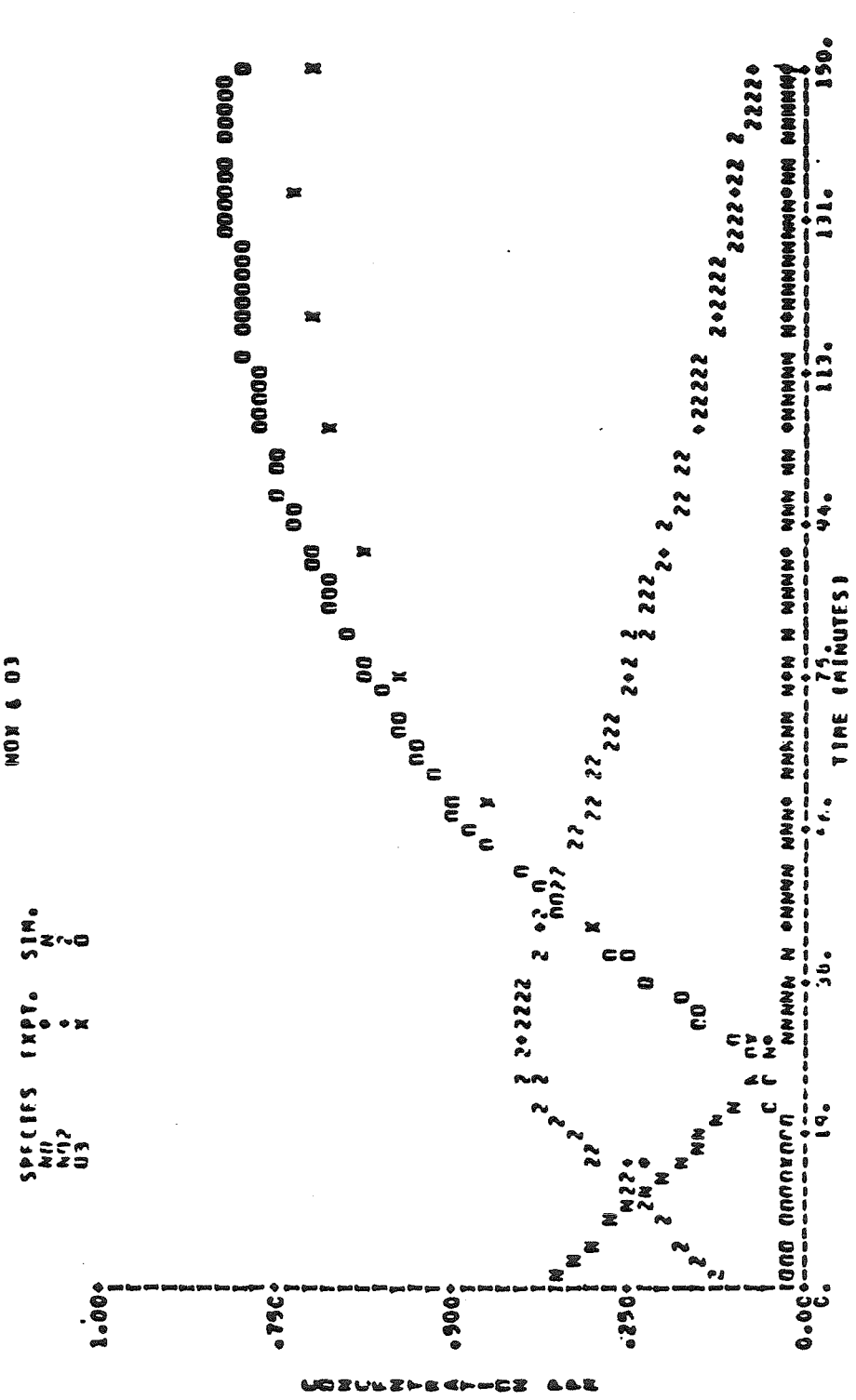

Figure A.7.a. Comparison of Concentration-Time Profiles Predicted by the Explicit Mechanism with Experimental Data from SAPRC Experiment EC-243.

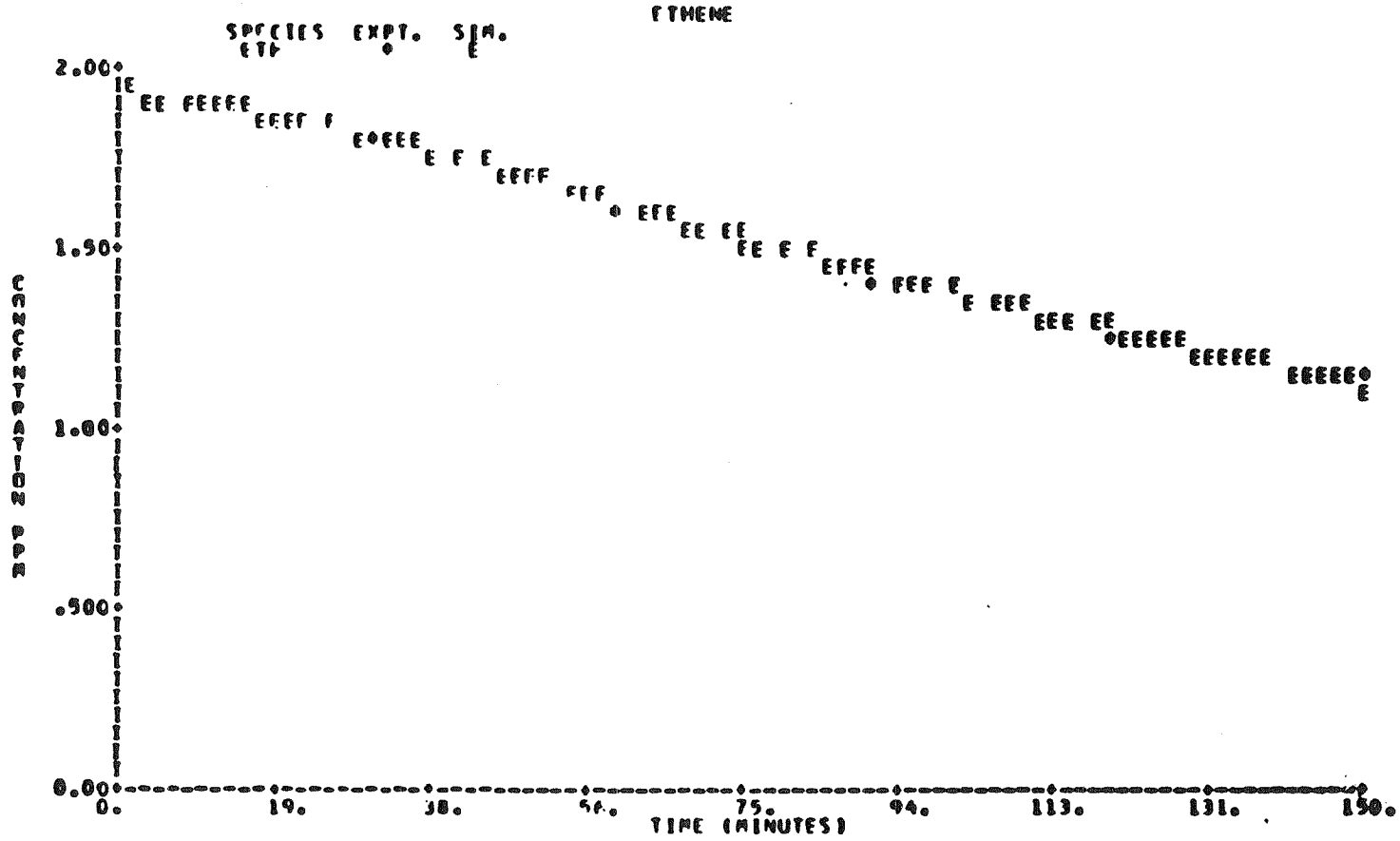

Figure A.7.b. Comparison of Concentration-Time Profiles Predicted by the Explicit Mechanism with Experimental Data from SAPRC Experiment EC-243.

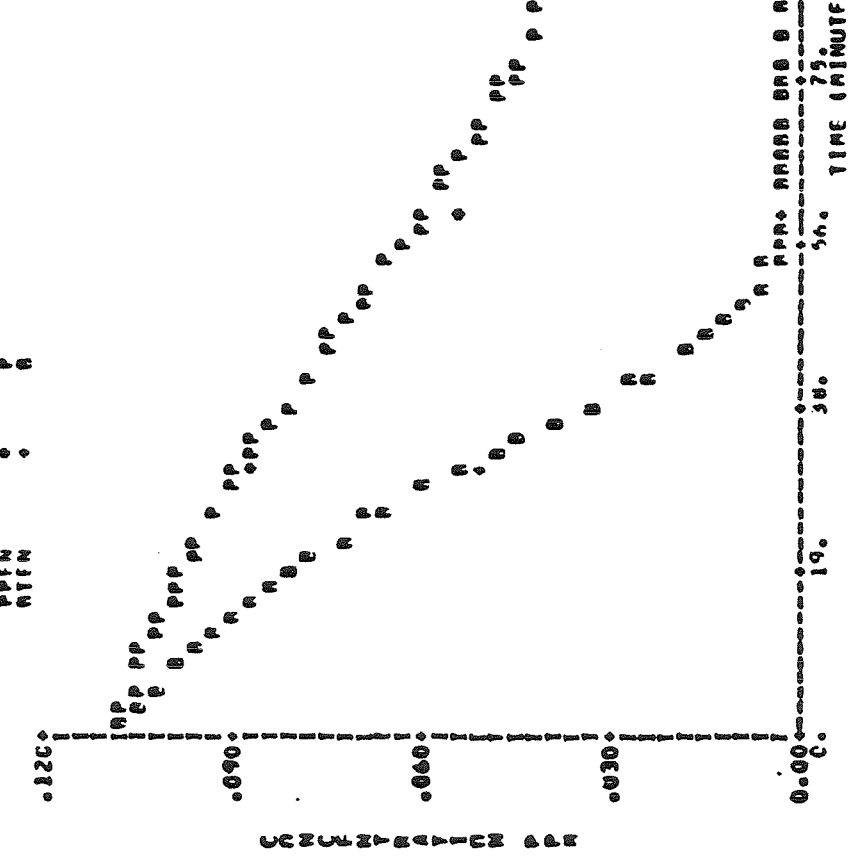

Figure A.7.c. Comparison of Concentration-Time Profiles Predicted by the Explicit Mechanism with Experimental Data from SAPRC Experiment EC-243.

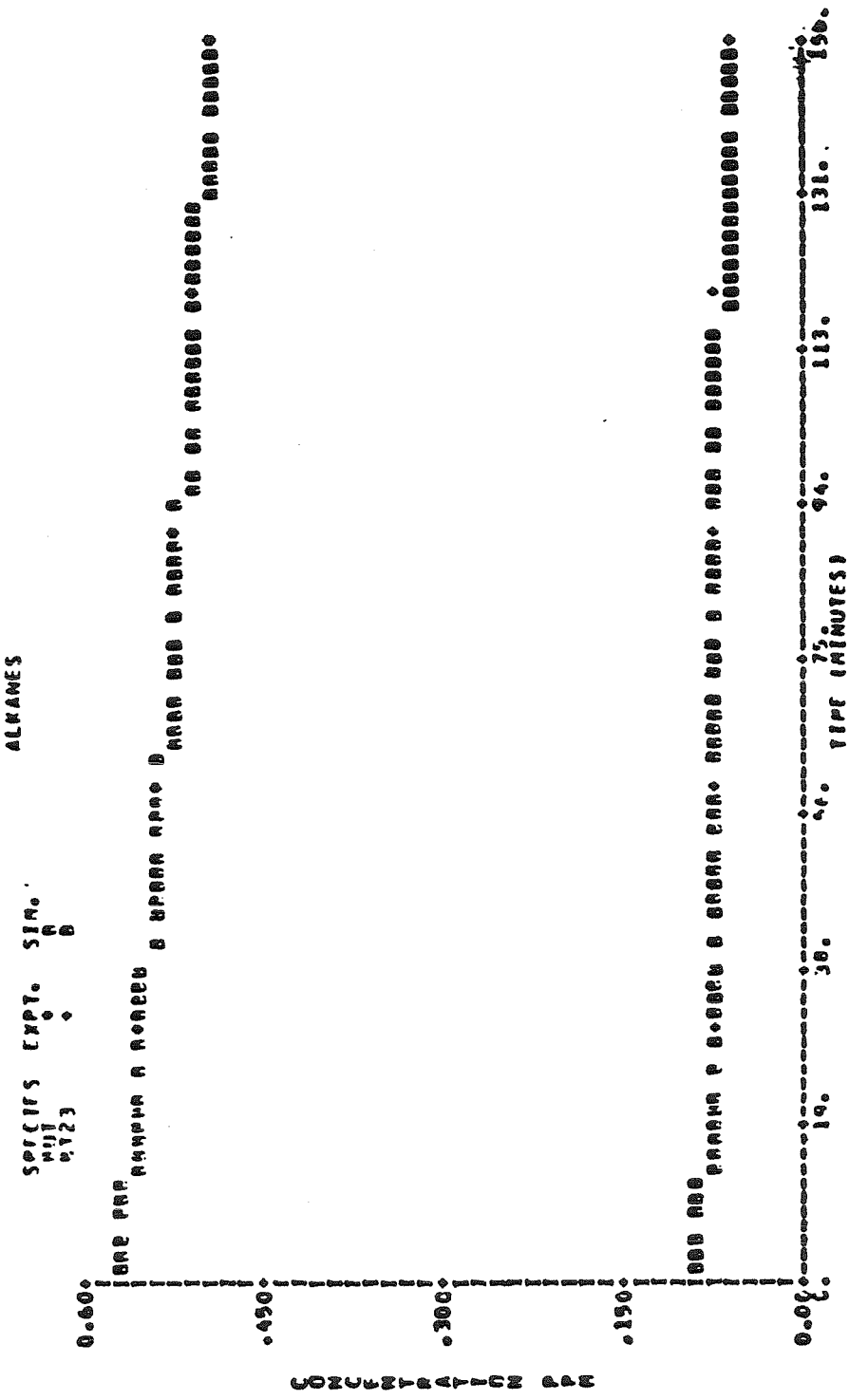

Figure A.7.d. Comparison of Concentration-Time Profiles Predicted by the Explicit Mechanism with Experimental Data from SAPRC Experiment EC-243.

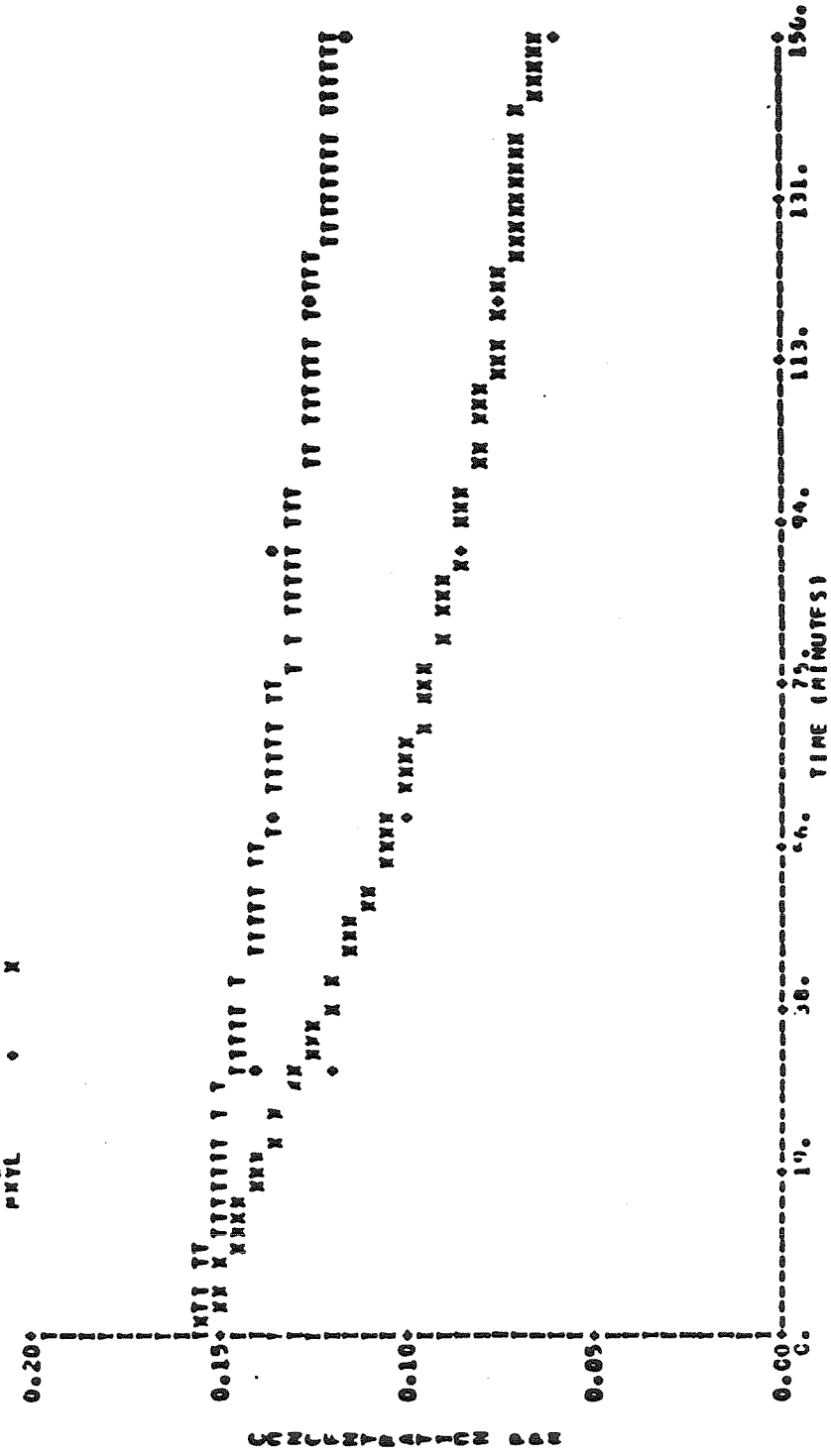

Figure A.7.e. Comparison of Concentration-Time Profiles Predicted by the Explicit Mechanism with Experimental Data from SAPRC Experiment EC-243.

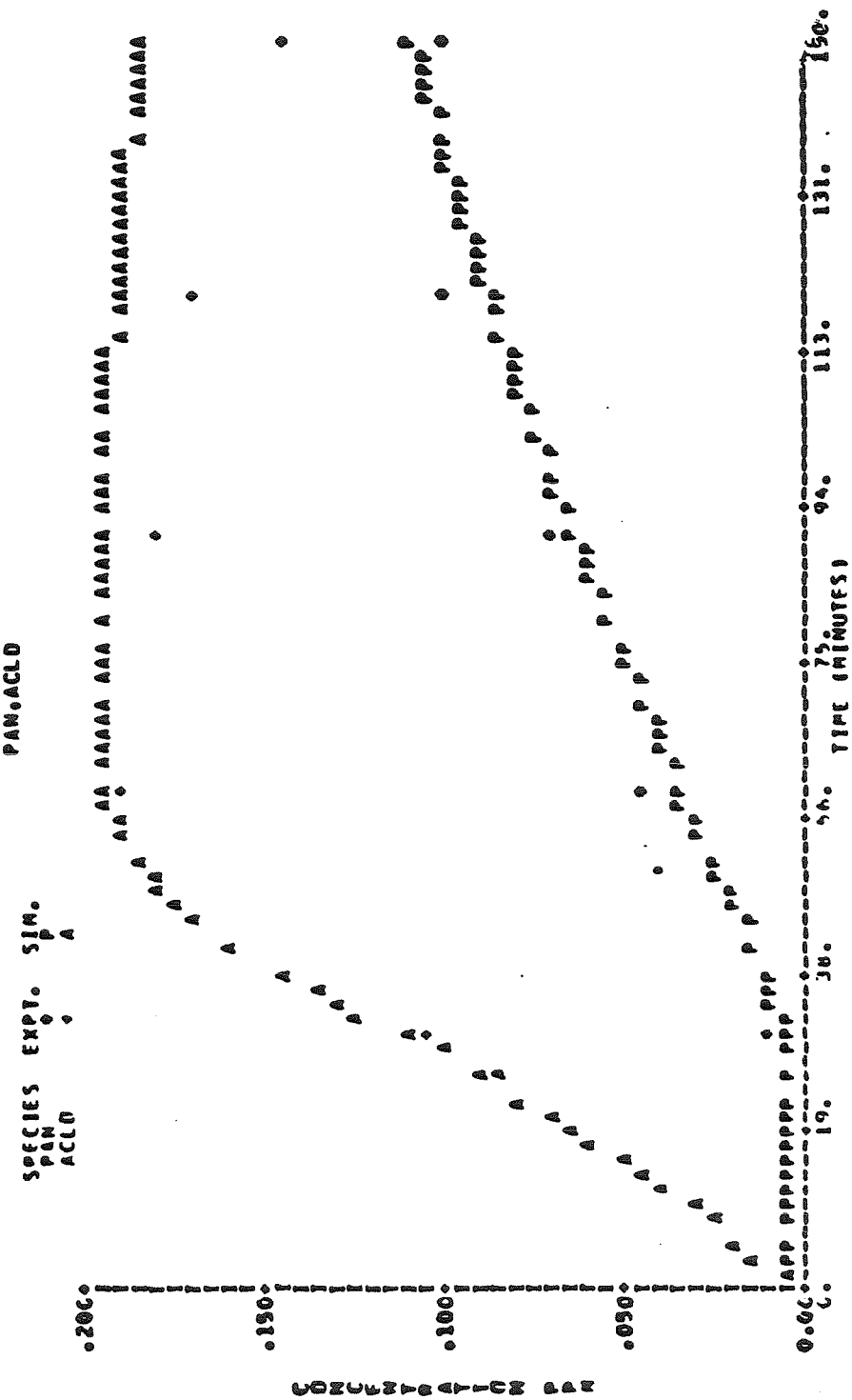

Figure A.7.f. Comparison of Concentration-Time Profiles Predicted by the Explicit Mechanism with Experimental Data from SAPRC Experiment EC-243.

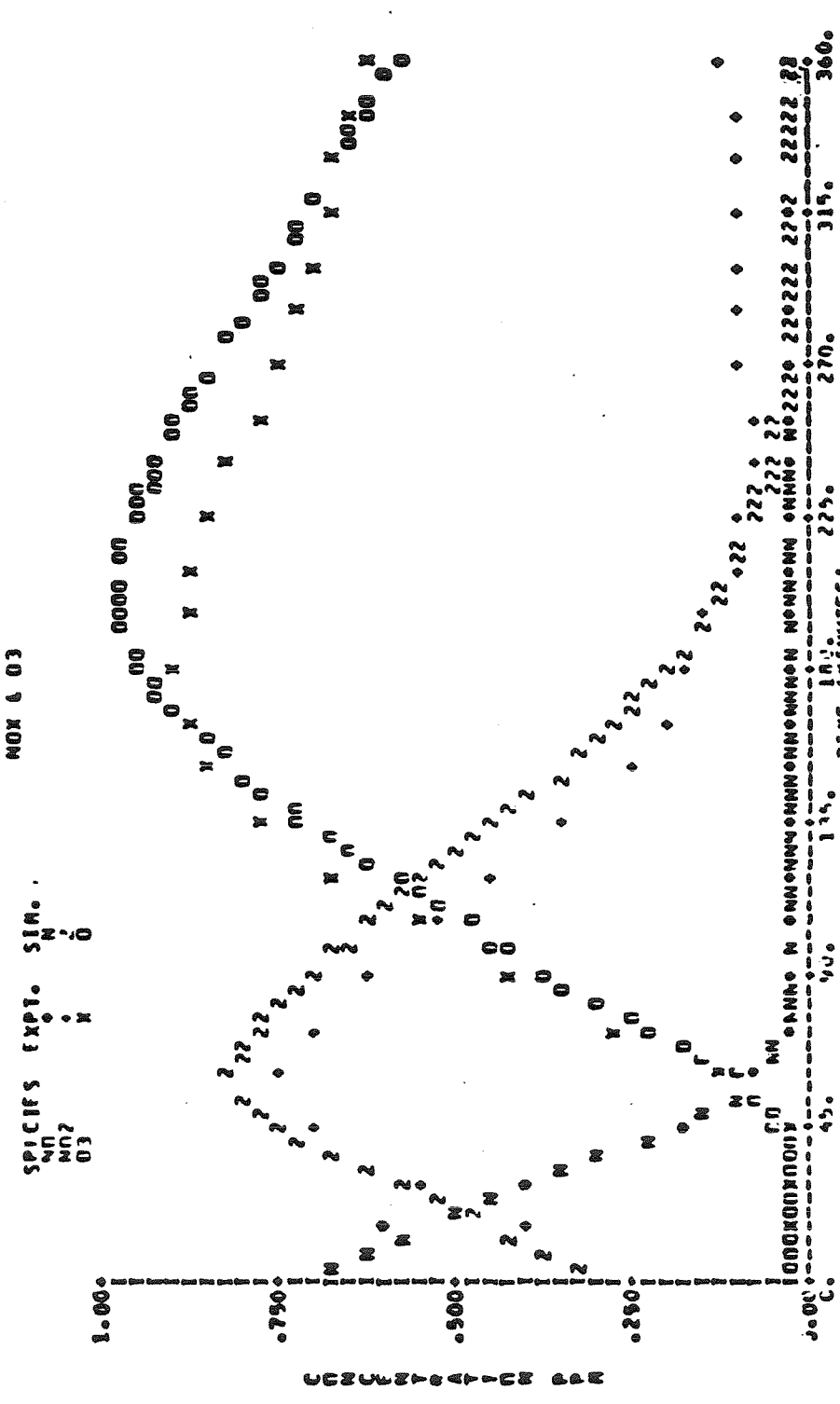

Figure A.8.a. Comparison of Concentration-Time Profiles Predicted by the Explicit Mechanism with Experimental Data from SAPRC Experiment EC-245.

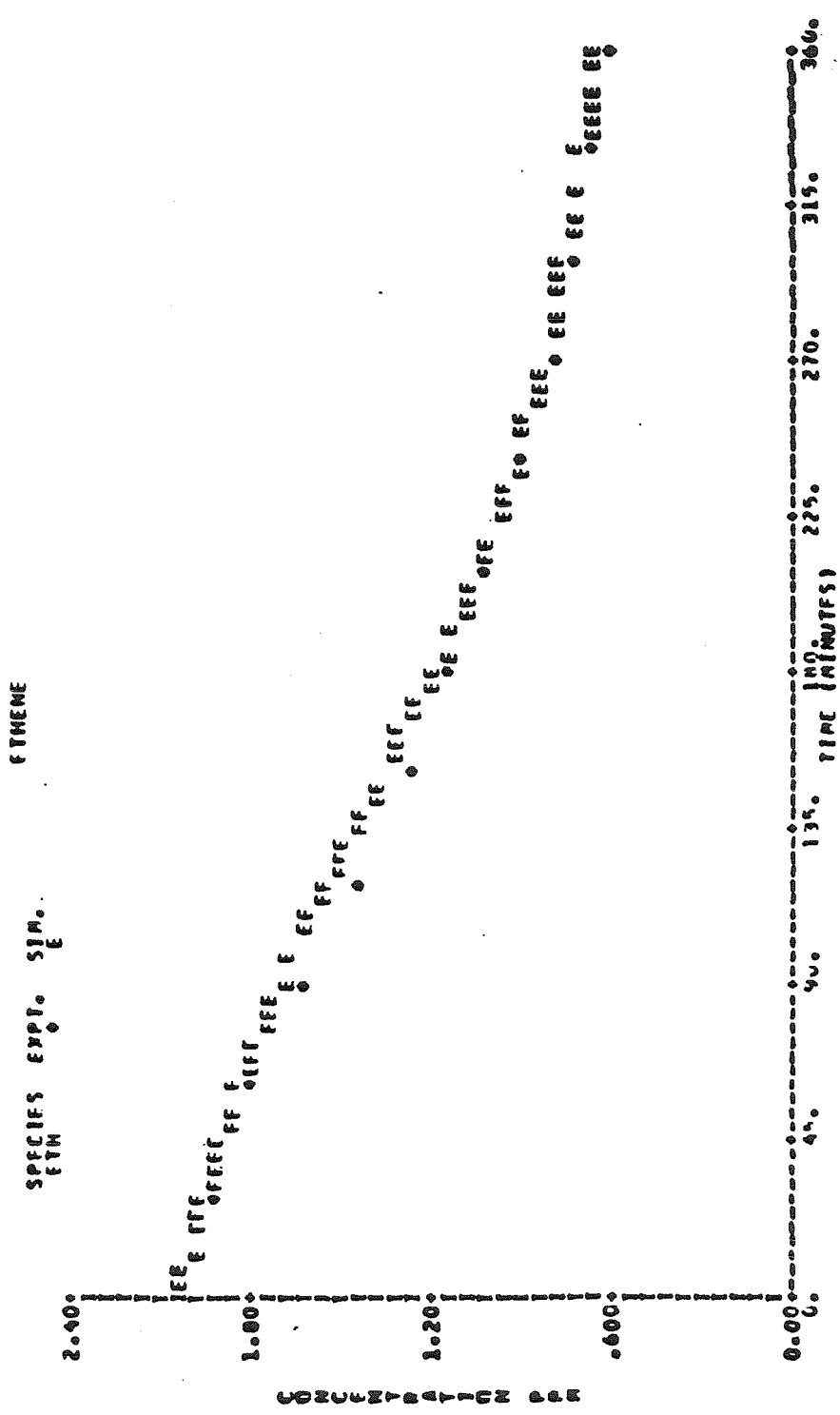

Figure A.8.b. Comparison of Concentration-Time Profiles Predicted by the Explicit Mechanism with Experimental Data from SAPRC Experiment EC-245.

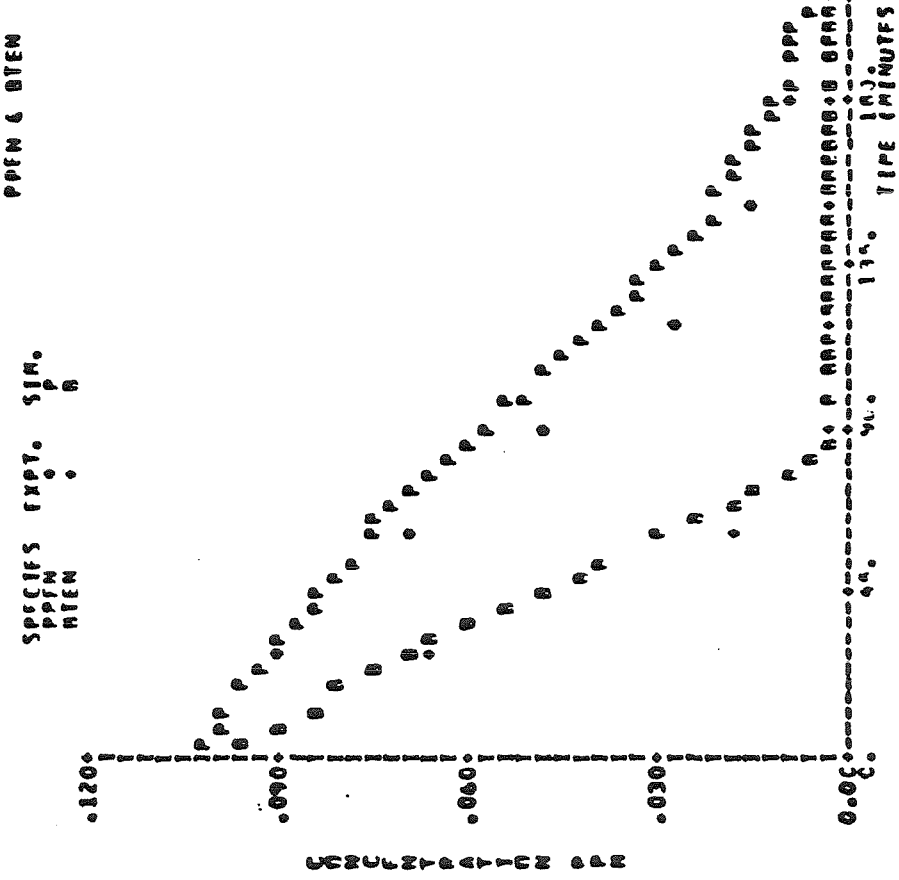

Figure A.8.c. Comparison of Concentration-Time Profiles Predicted by the Explicit Mechanism with Experimental Data from SAPRC Experiment EC-245.

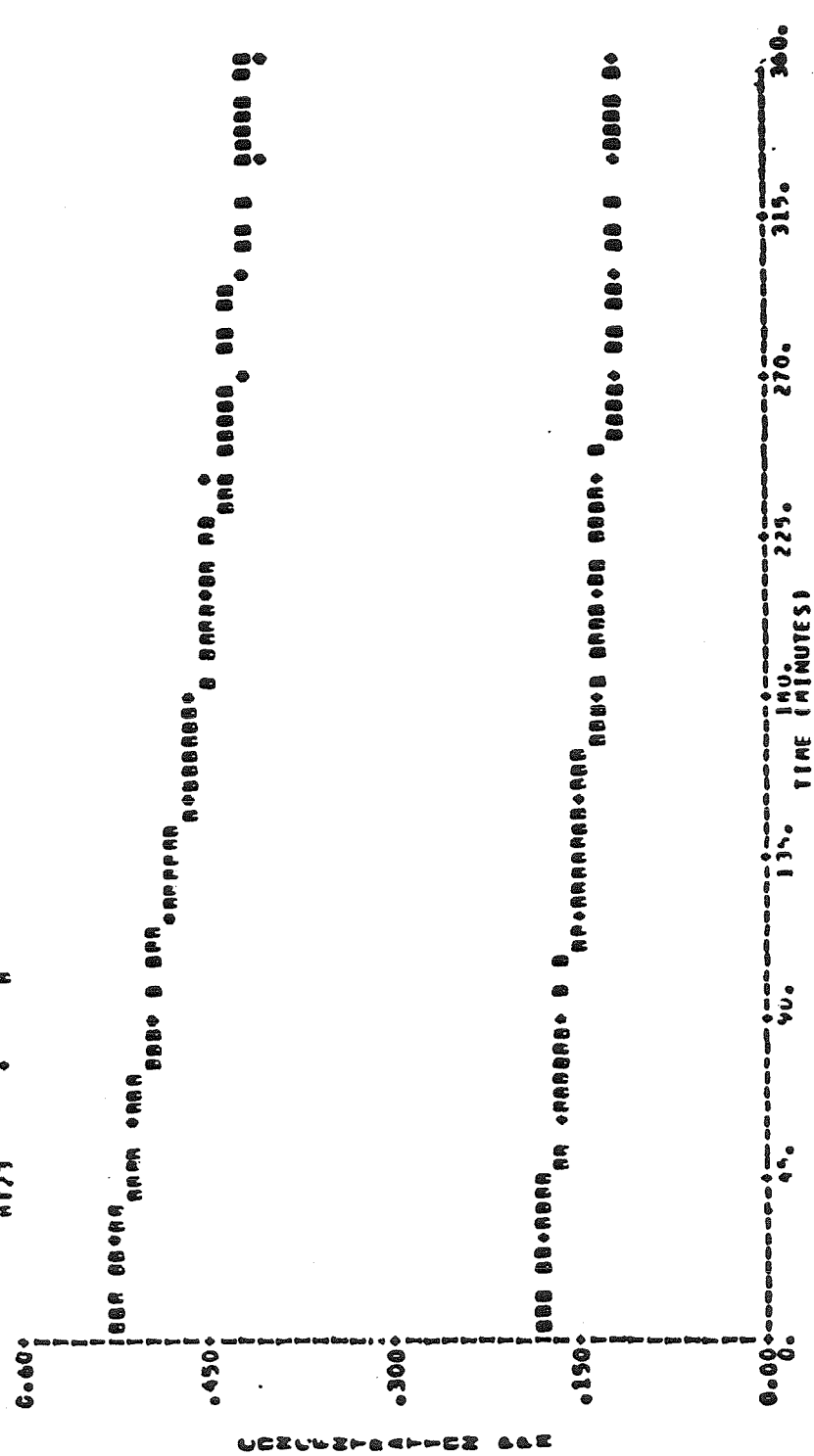

Figure A.8.d. Comparison of Concentration-Time Profiles Predicted by the Explicit Mechanism with Experimental Data from SAPRC Experiment EC-245.

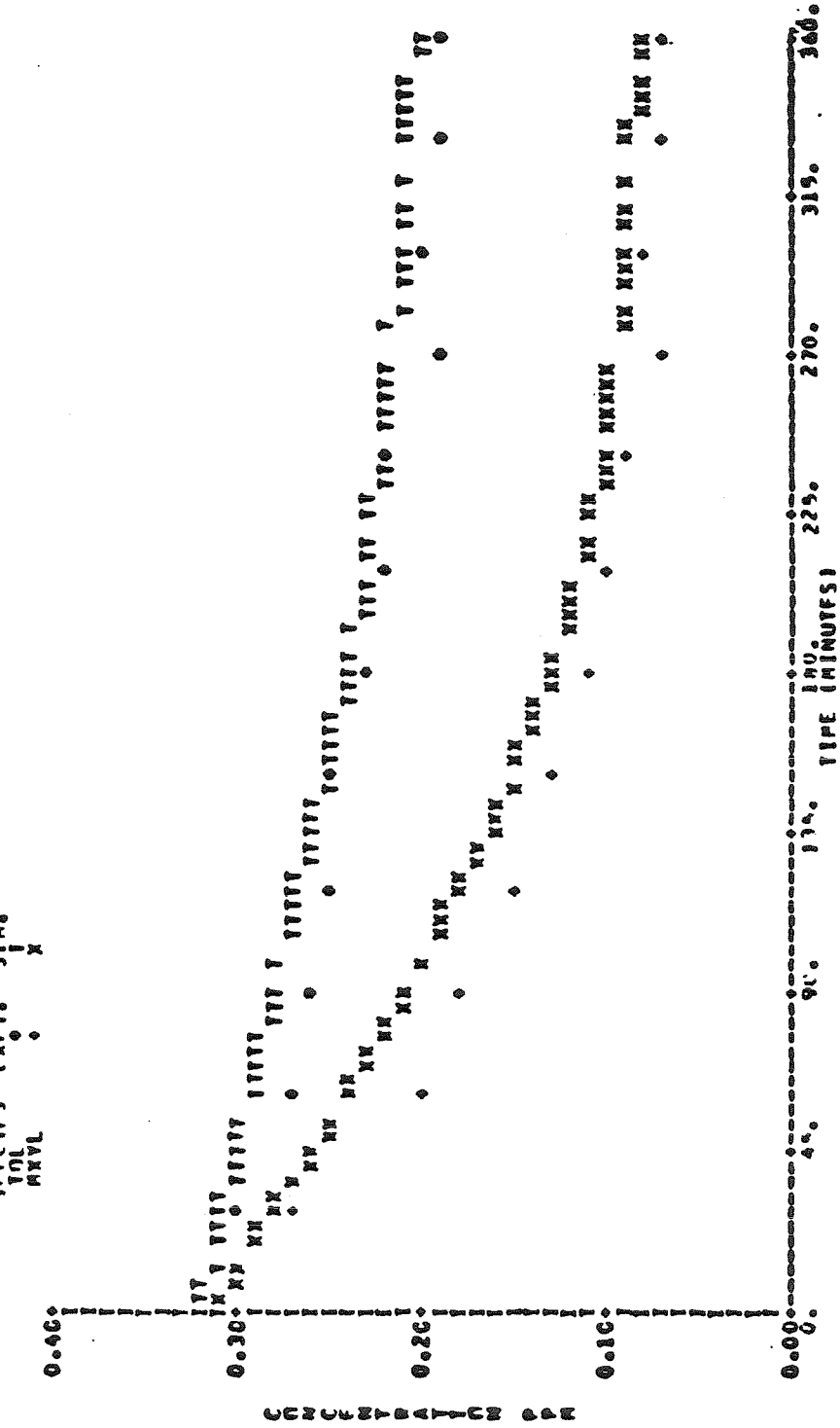

Figure A.8.e. Comparison of Concentration-Time Profiles Predicted by the Explicit Mechanism with Experimental Data from SAPRC Experiment EC-245.

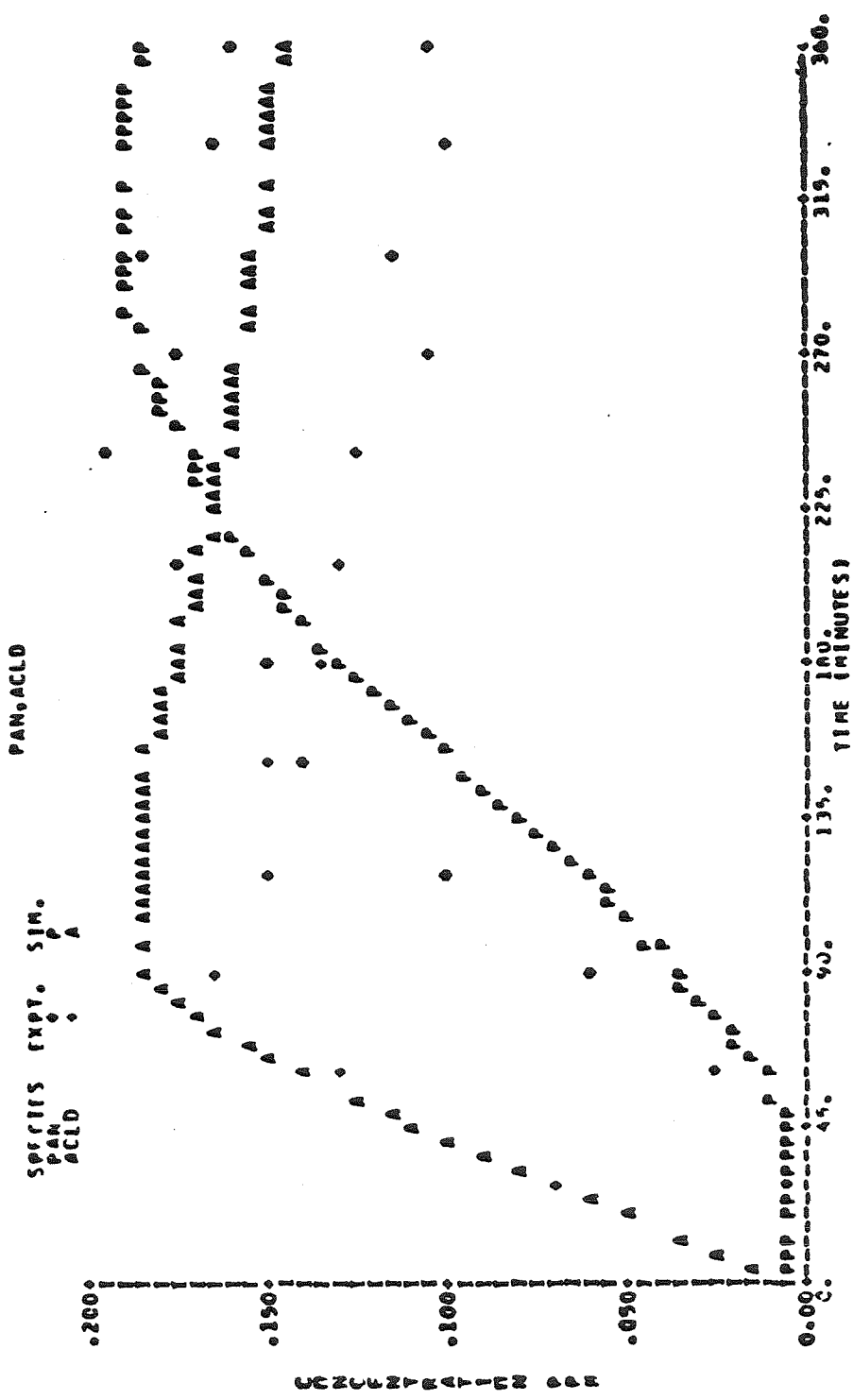

Figure A.8.f. Comparison of Concentration-Time Profiles Predicted by the Explicit Mechanism with Experimental Data from SAPRC Experiment EC-245.

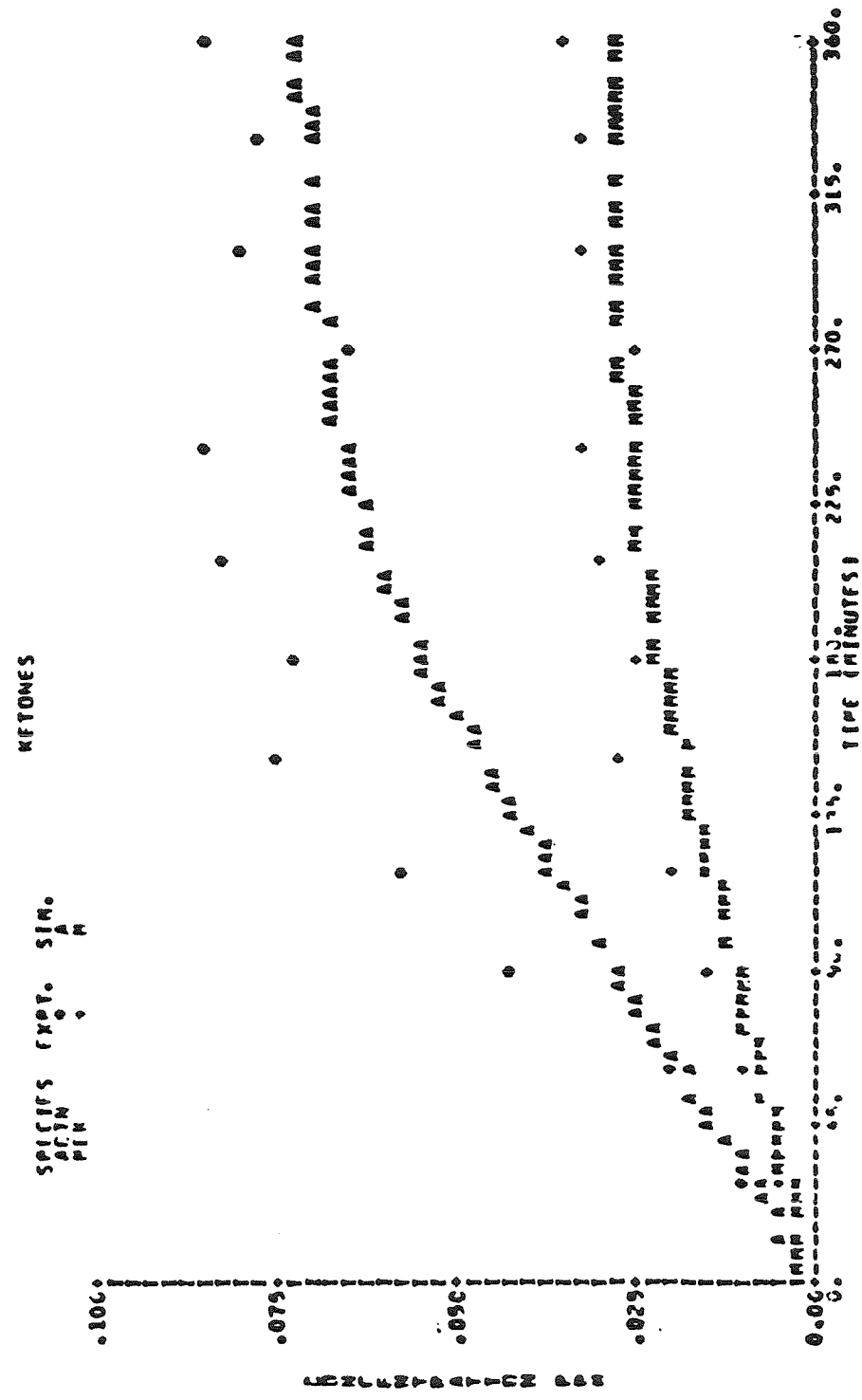

Figure A.8.g. Comparison of Concentration-Time Profiles Predicted by the Explicit Mechanism with Experimental Data from SAPRC Experiment EC-245.

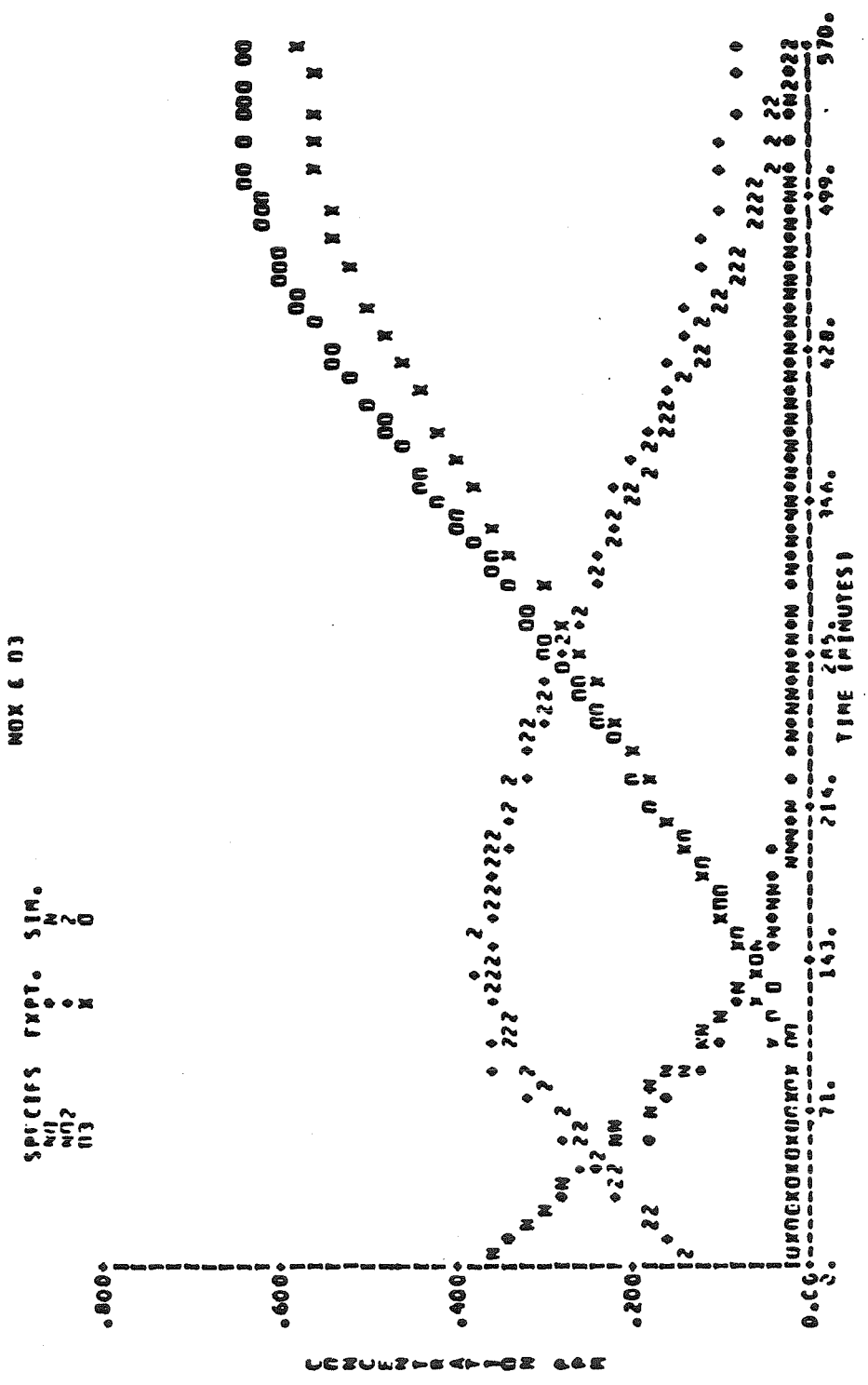

Figure A.9.a. Comparison of Concentration-Time Profiles Predicted by the Explicit Mechanism with Experimental Data from SAPRC Experiment EC-246.

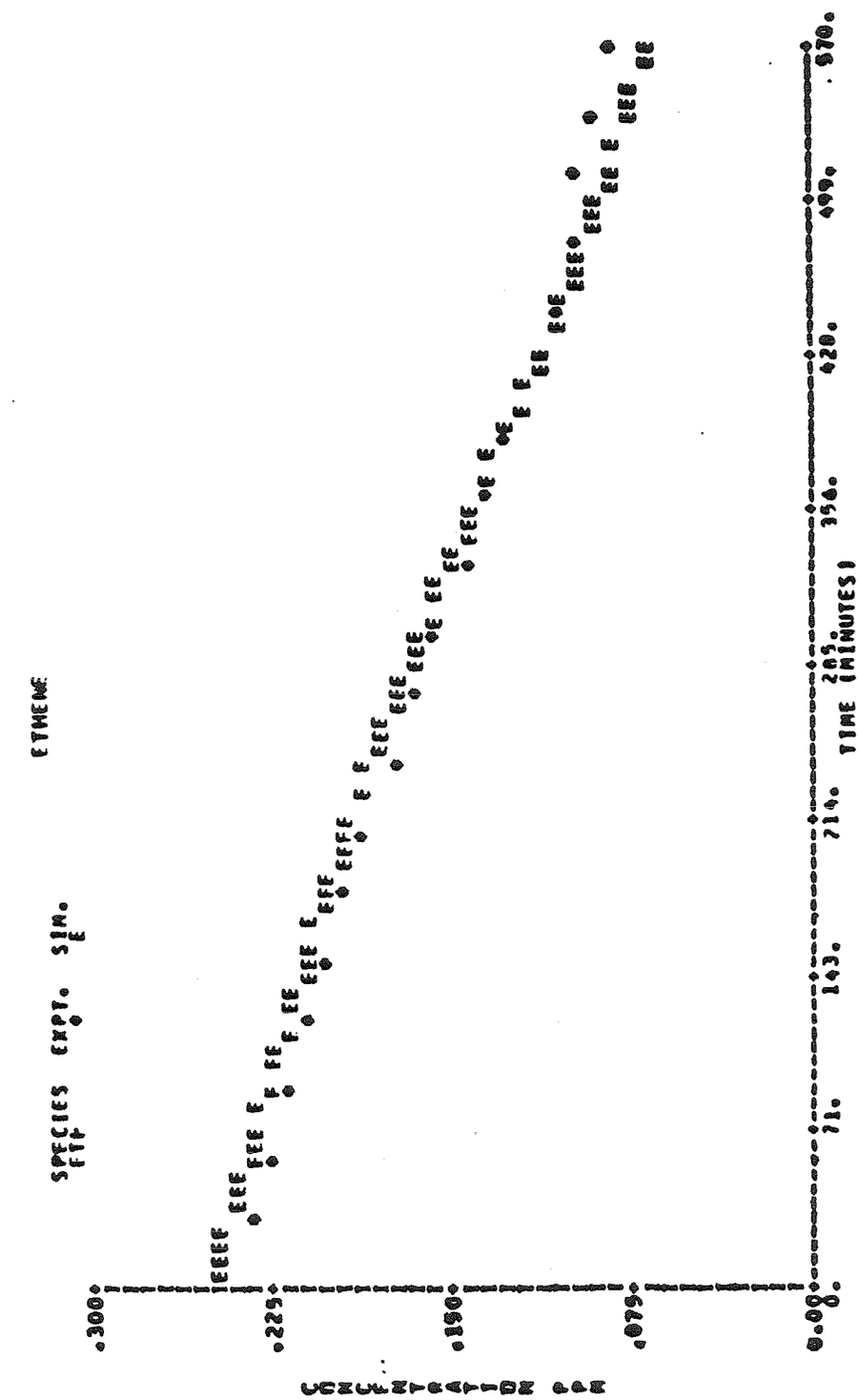

Figure A.9.b. Comparison of Concentration-Time Profiles Predicted by the Explicit Mechanism with Experimental Data from SAPRC Experiment EC-246.

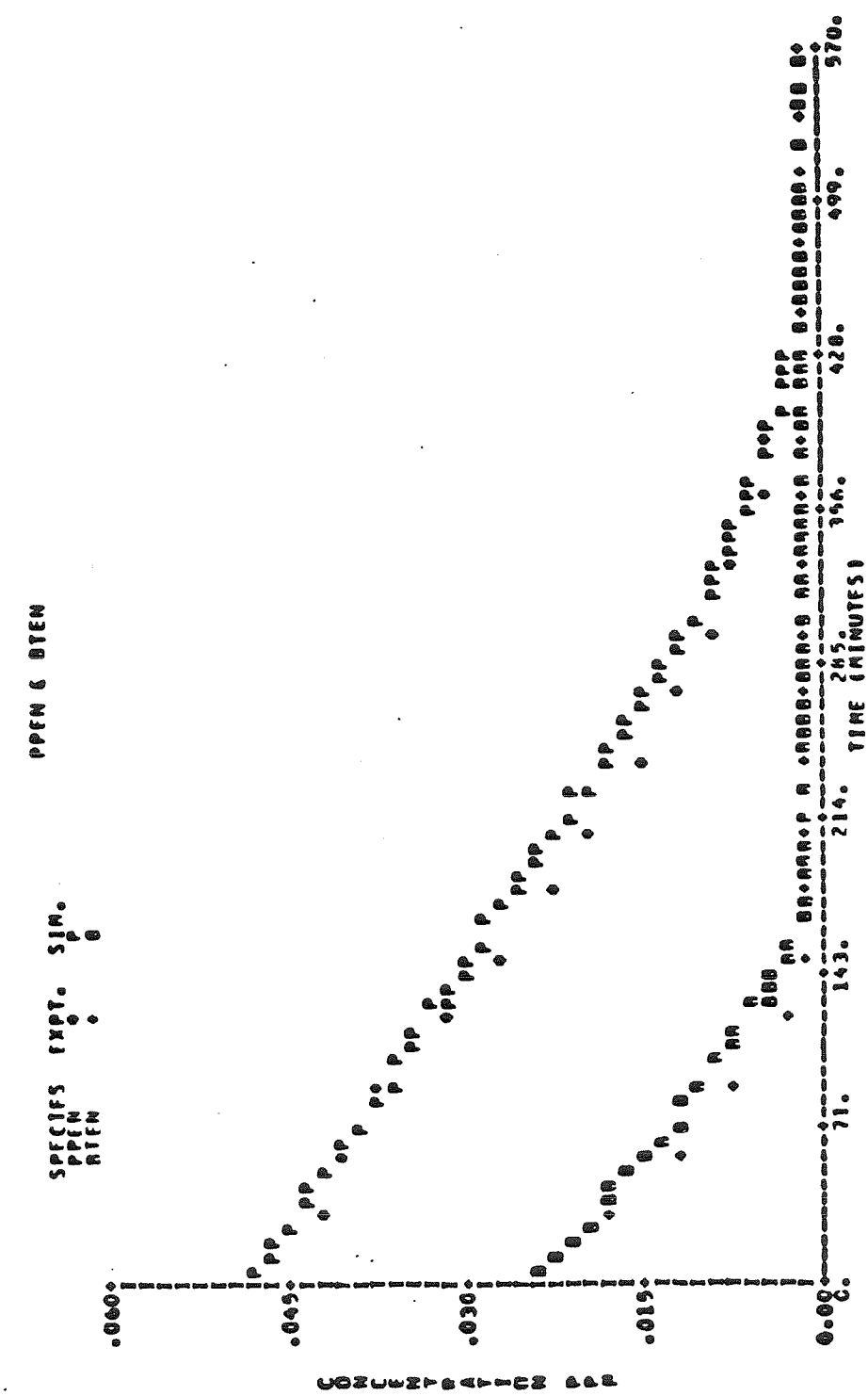

Figure A.9.c. Comparison of Concentration-Time Profiles Predicted by the Explicit Mechanism with Experimental Data from SAPRC Experiment EC-246.

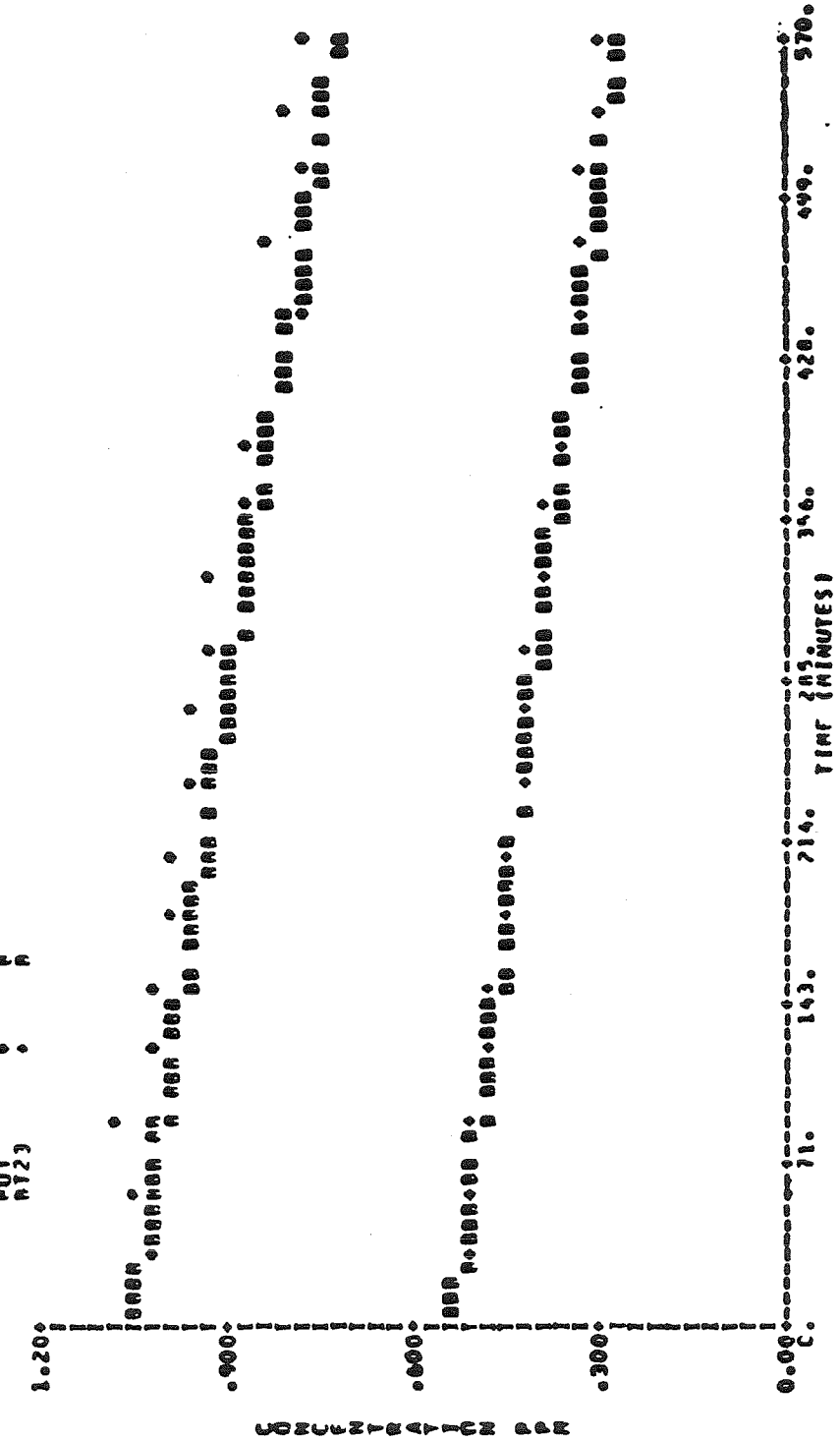

Figure A.9.d. Comparison of Concentration-Time Profiles Predicted by the Explicit Mechanism with Experimental Data from SAPRC Experiment EC-246.

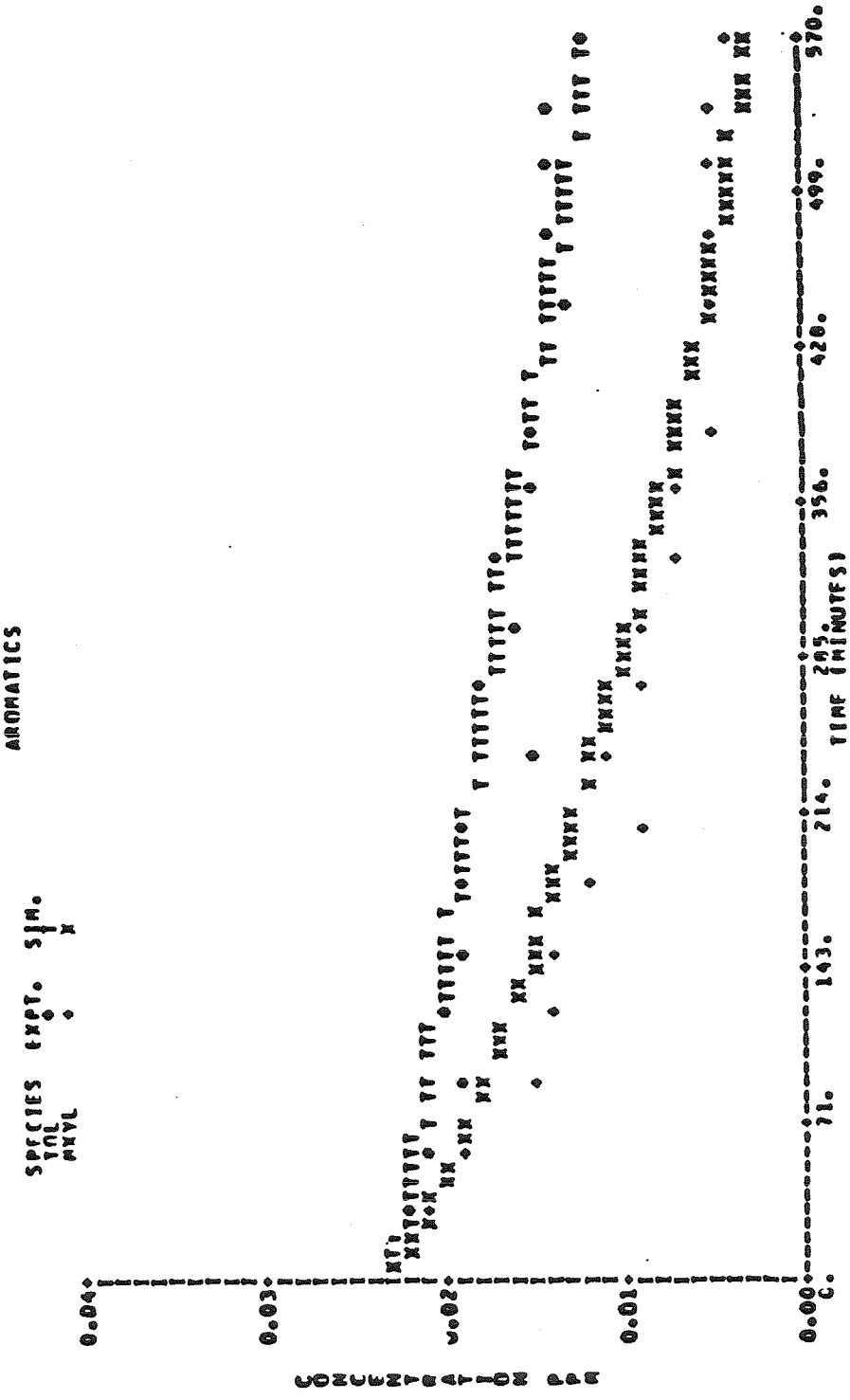

Figure A.9.e. Comparison of Concentration-Time Profiles Predicted by the Explicit Mechanism with Experimental Data from SAPRC Experiment EC-246.

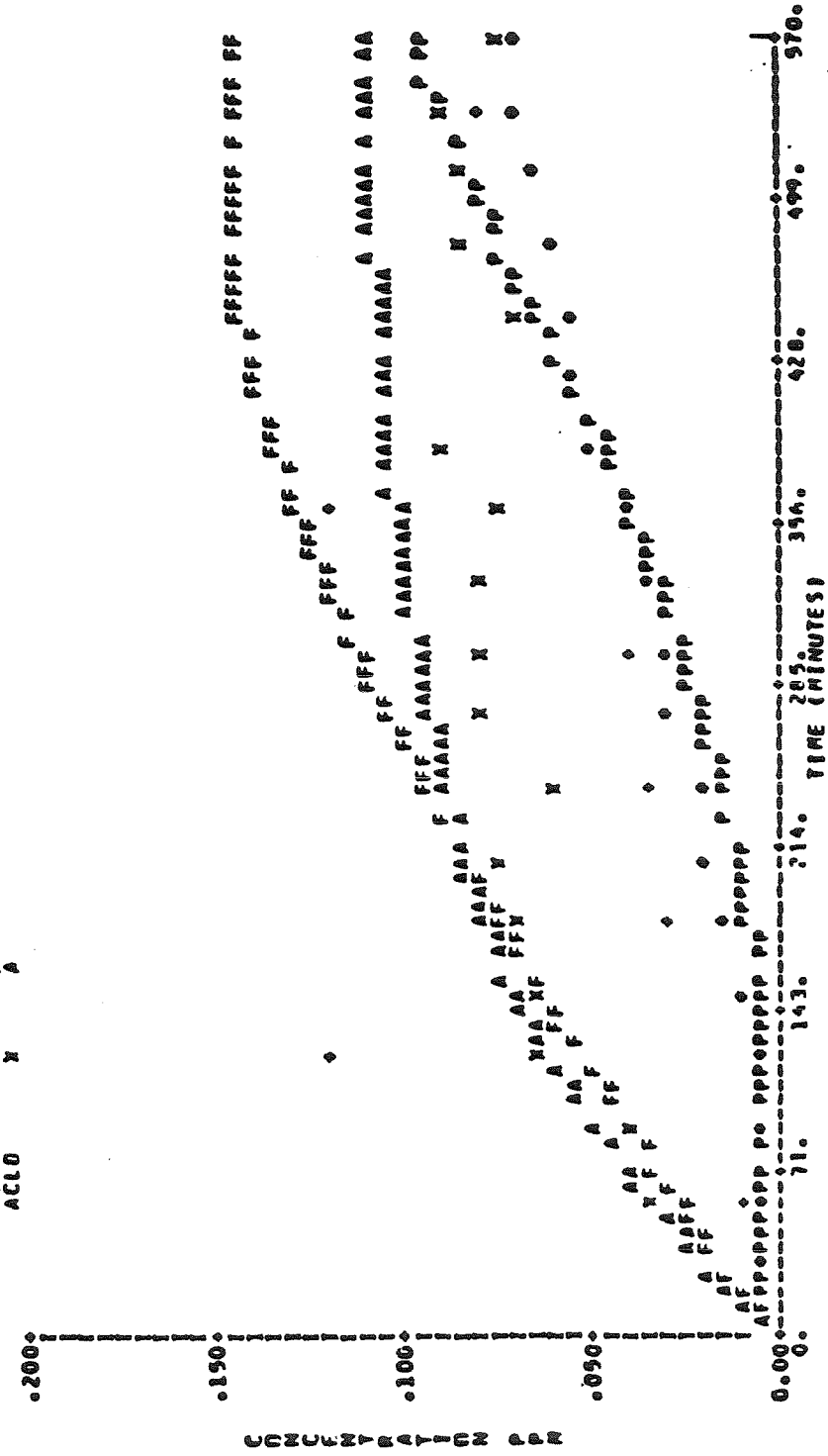

Figure A.9.f. Comparison of Concentration-Time Profiles Predicted by the Explicit Mechanism with Experimental Data from SAPRC Experiment EC-246.

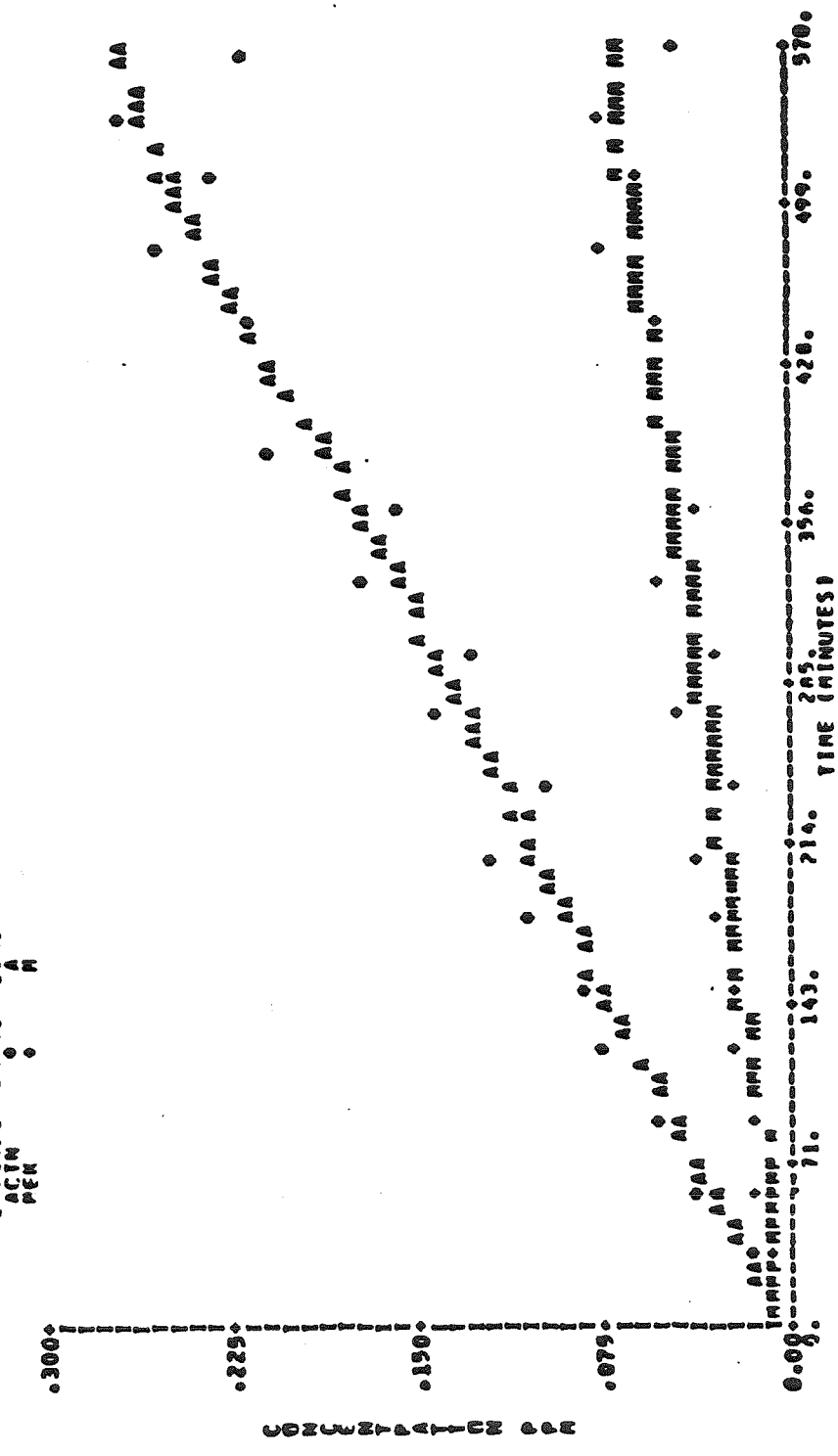

Figure A.9.g. Comparison of Concentration-Time Profiles Predicted by the Explicit Mechanism with Experimental Data from SAPRC Experiment EC-246.

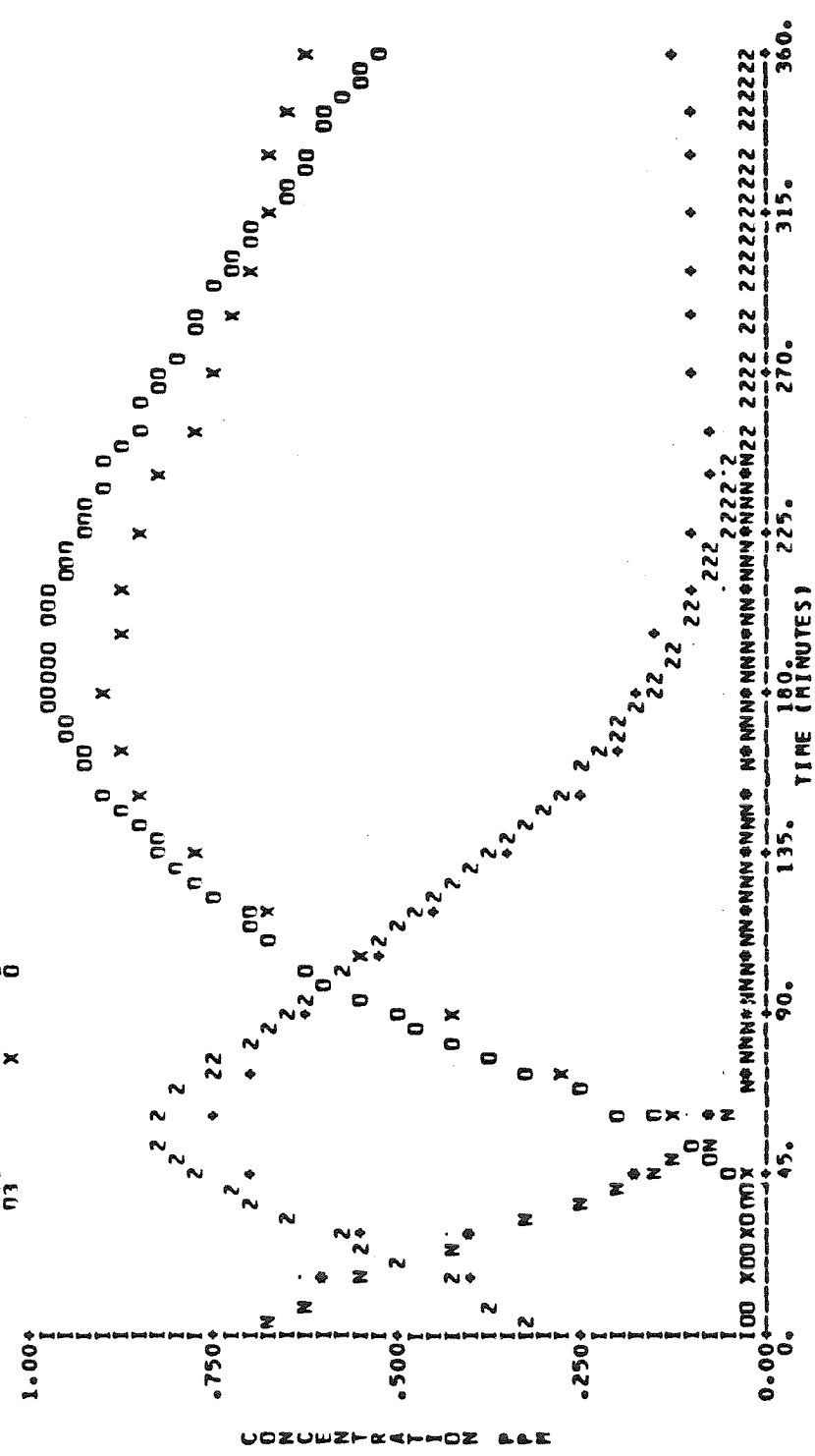

Figure A.10.a. Comparison of Concentration-Time Profiles Predicted by the SUR2 Mechanism with Experimental Data from SAPRC Experiment EC-245.

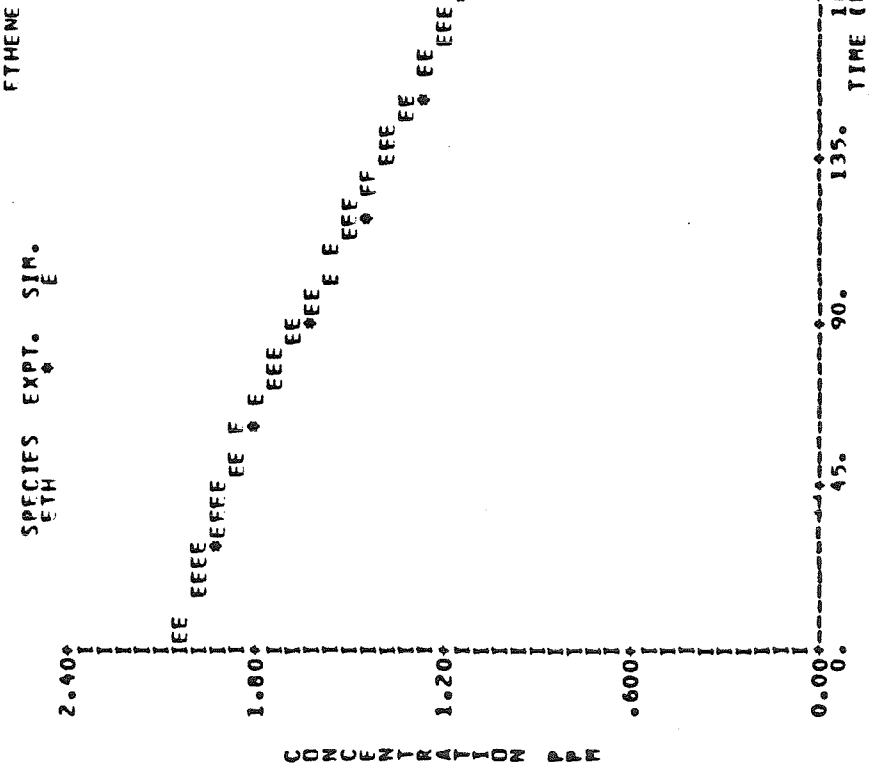

Figure A.10.b. Comparison of Concentration-Time Profiles Predicted by the SUR2 Mechanism with Experimental Data from SAPRC Experiment EC-245.

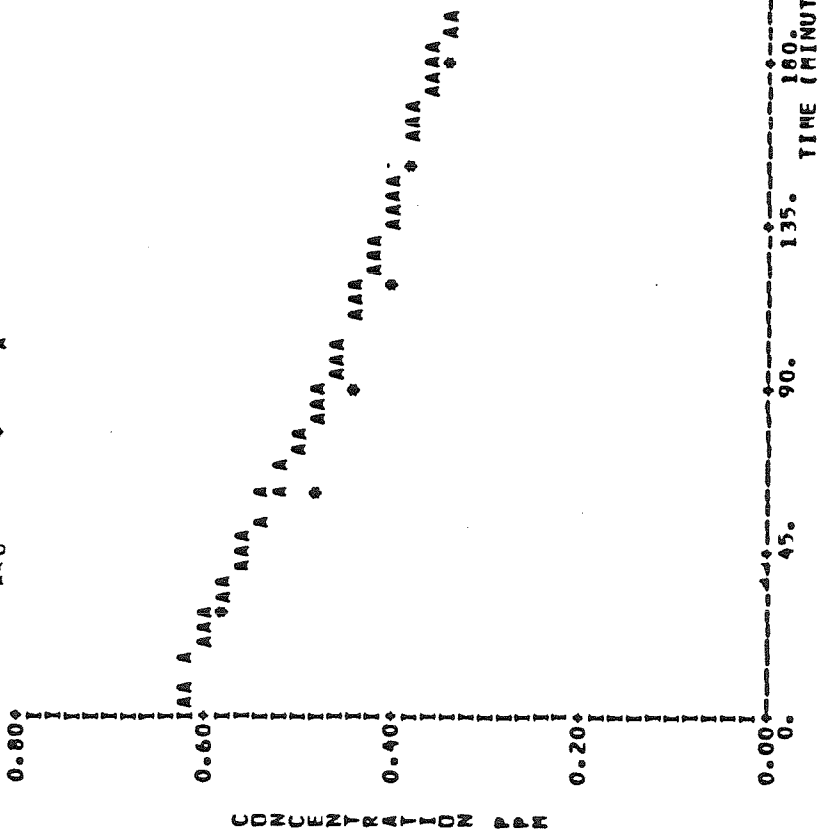

Figure A.10.c. Comparison of Concentration-Time Profiles Predicted by the SUR2 Mechanism with Experimental Data from SAPRC Experiment EC-245.

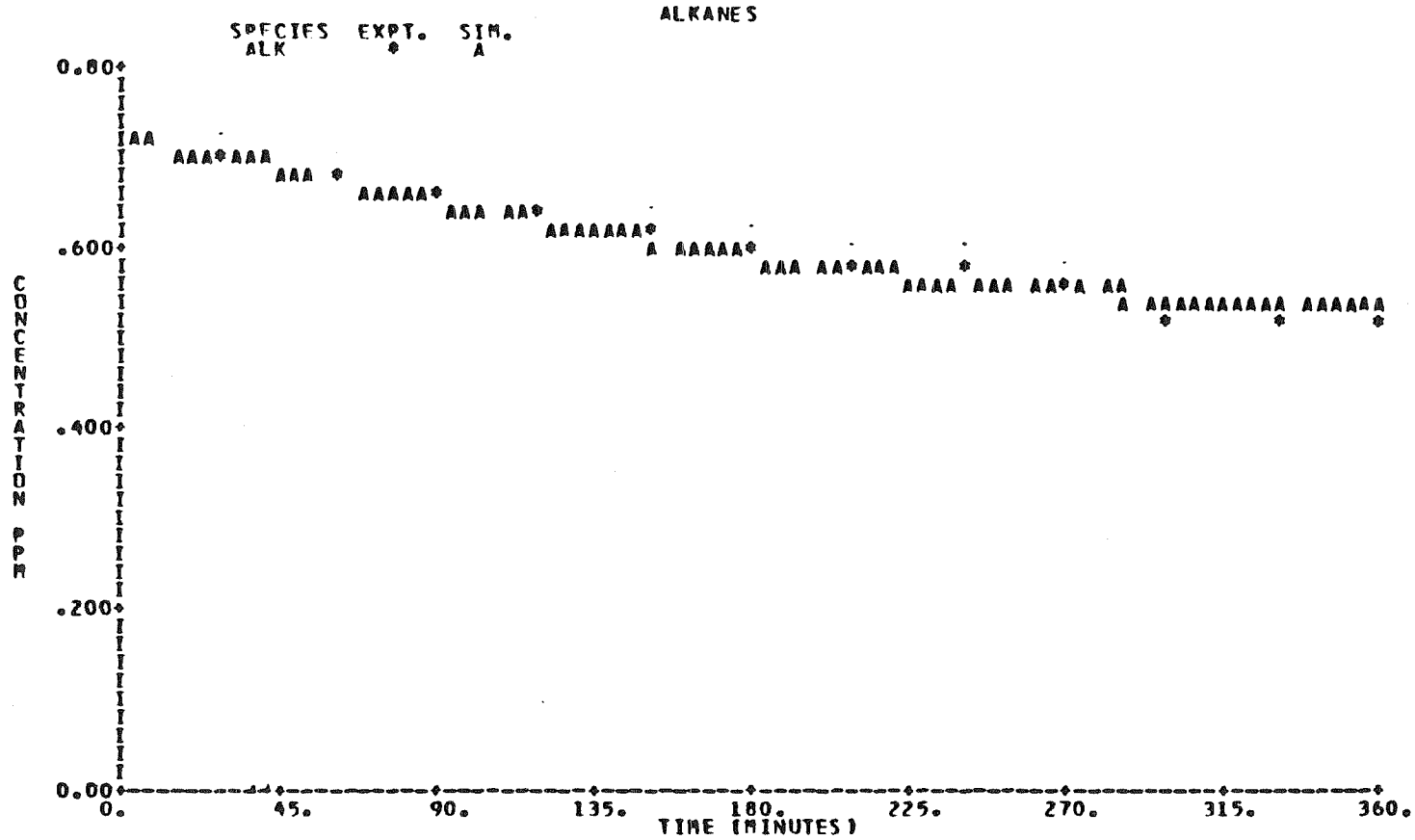

Figure A.10.d. Comparison of Concentration-Time Profiles Predicted by the SUR2 Mechanism with Experimental Data from SAPRC Experiment EC-245.

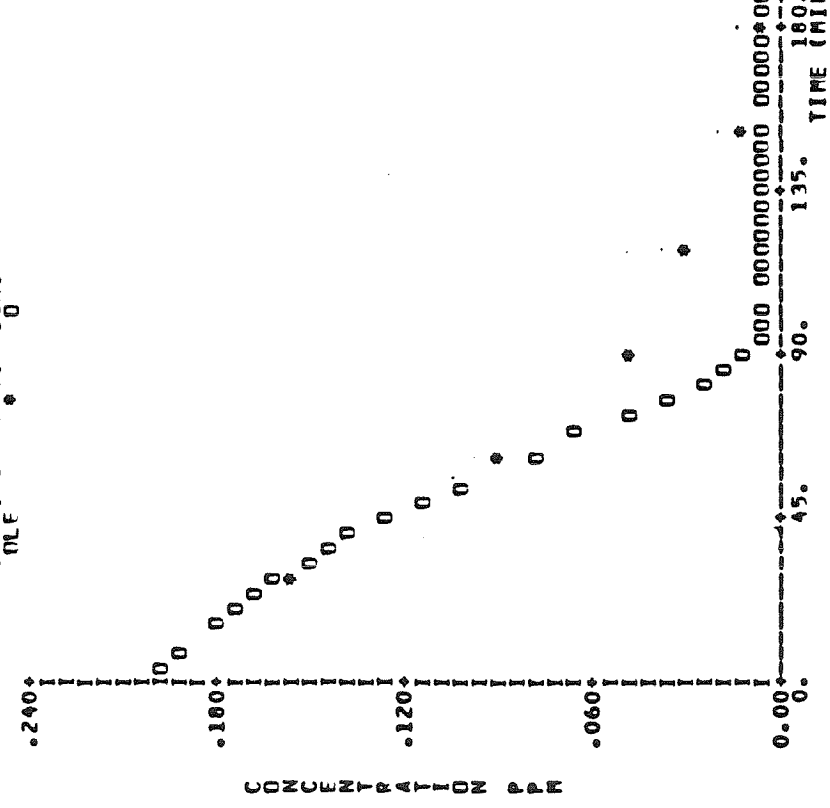

Figure A.10.e. Comparison of Concentration-Time Profiles Predicted by the SUR2 Mechanism with Experimental Data from SAPRC Experiment EC-245.

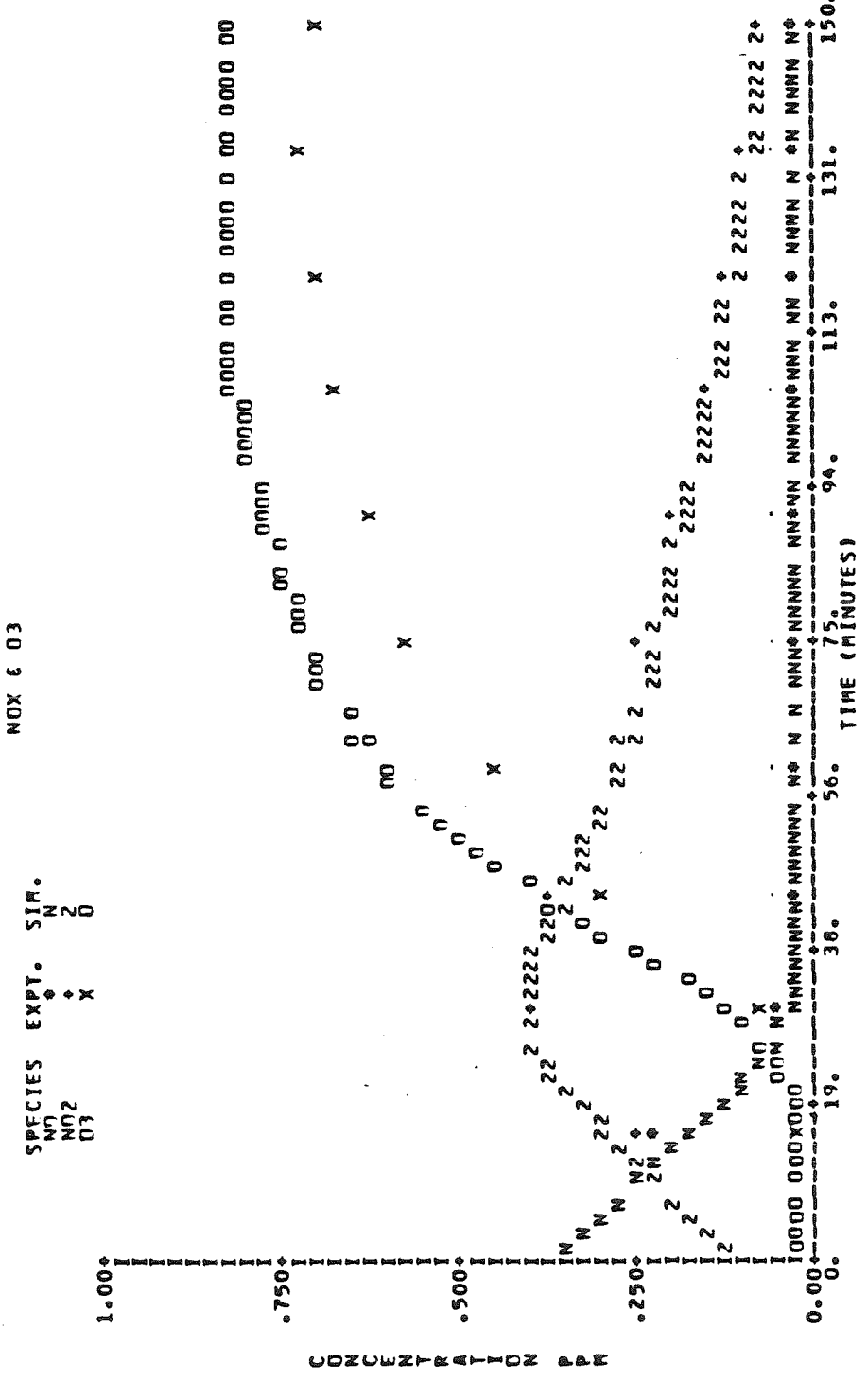

Figure A.11.a. Comparison of Concentration-Time Profiles Predicted by the SUR2 Mechanism with Experimental Data from SAPRC Experiment EC-243.

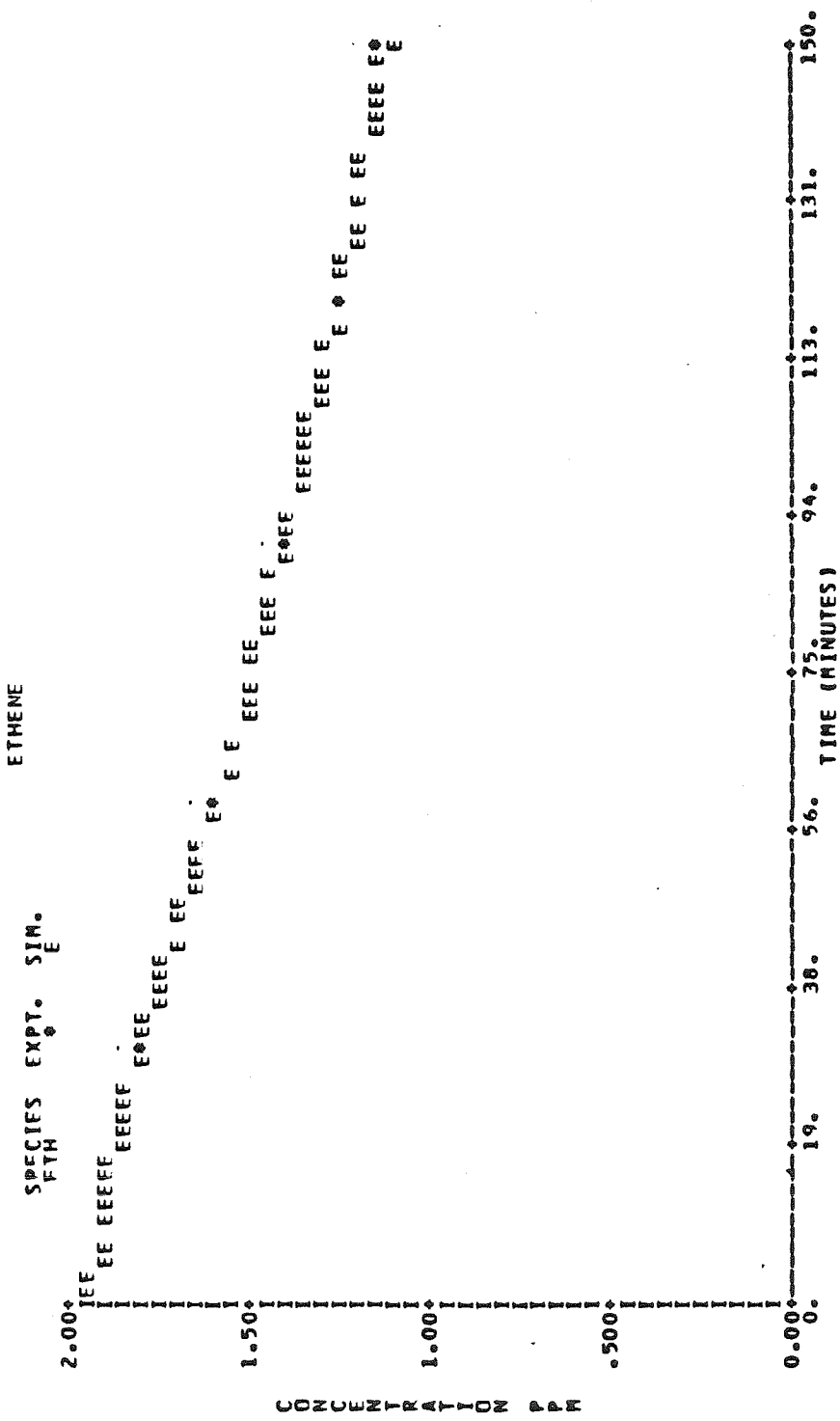

Figure A.11.b Comparison of Concentration-Time Profiles Predicted by the SUR2 Mechanism with Experimental Data from SAPRC Experiment EC-243.

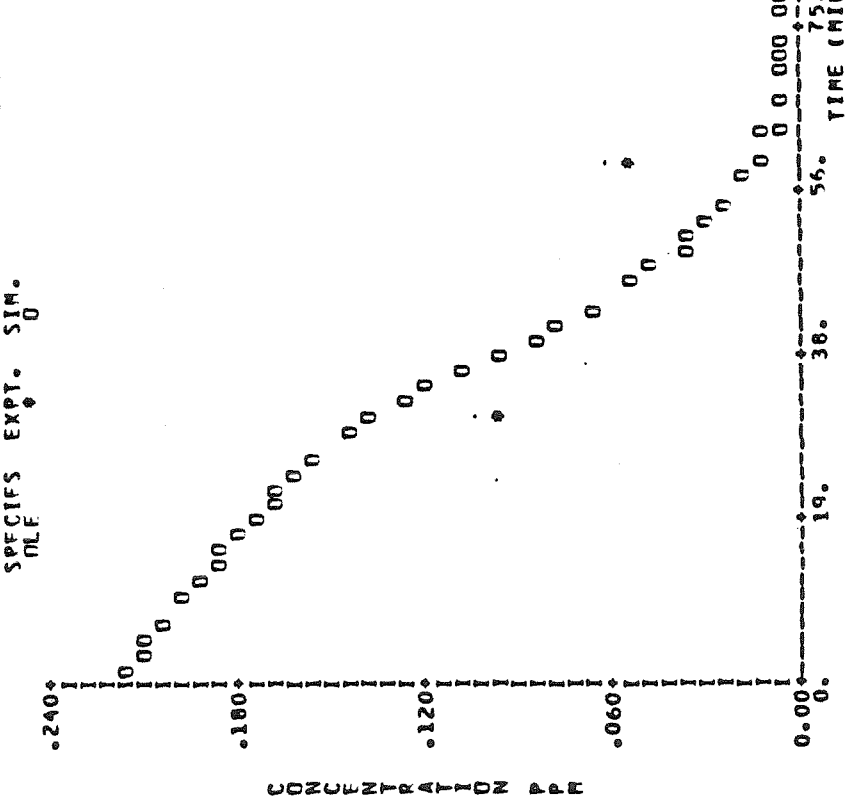

Figure A.11.c. Comparison of Concentration-Time Profiles Predicted by the SUR2 Mechanism with Experimental Data from SAPRC Experiment EC-243.

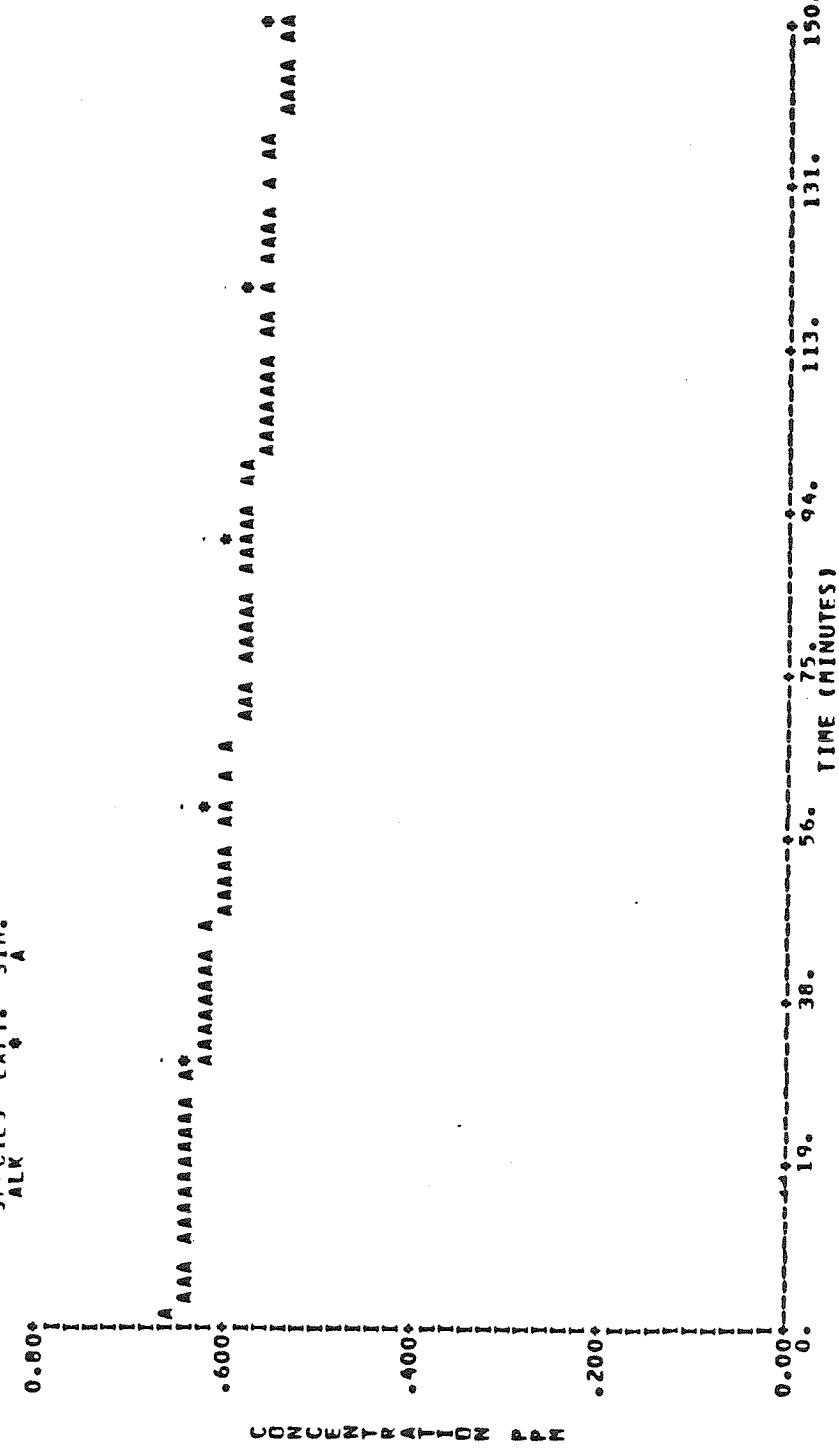

Figure A.11.d. Comparison of Concentration-Time Profiles Predicted by the SUR2 Mechanism with Experimental Data from SAPRC Experiment EC-243.

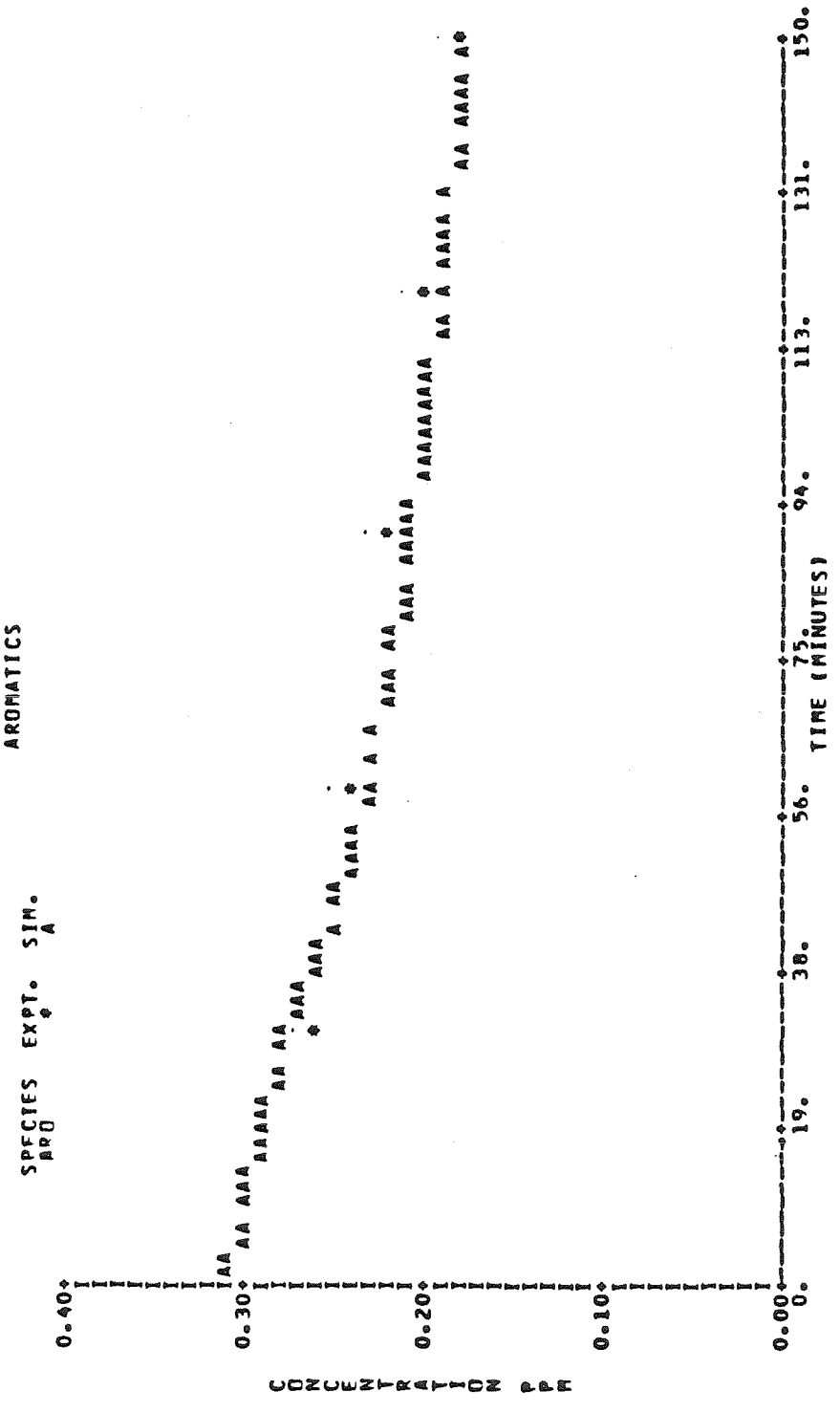

Figure A.11.e. Comparison of Concentration-Time Profiles Predicted by the SUR2 Mechanism with Experimental Data from SAPRC Experiment EC-243.

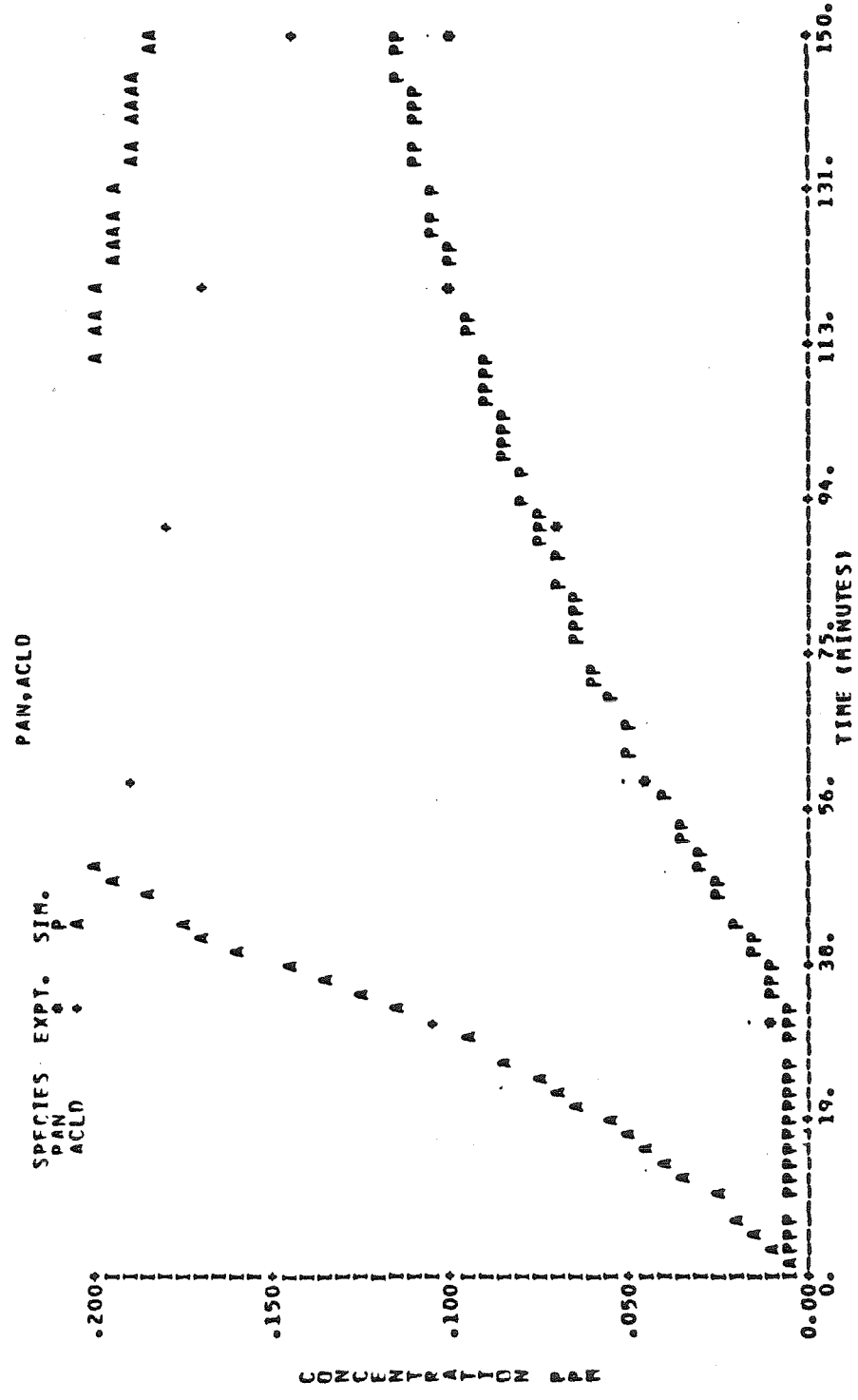

Figure A.11.f. Comparison of Concentration-Time Profiles Predicted by the SUR2 Mechanism with Experimental Data from SAPRC Experiment EC-243.

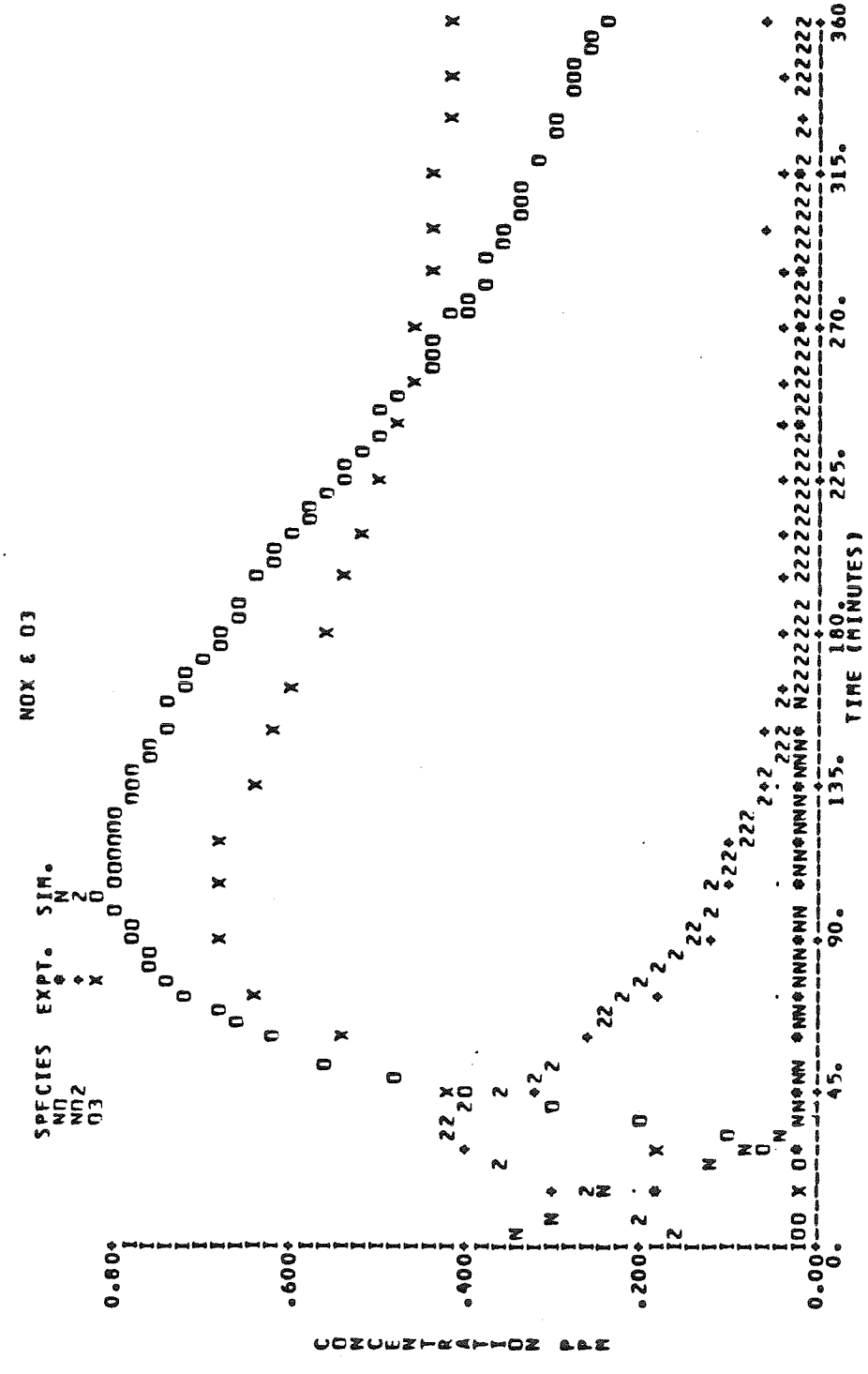

Figure A.12.a. Comparison of Concentration-Time Profiles Predicted by the SUR2 Mechanism with Experimental Data from SAPRC Experiment EC-242.

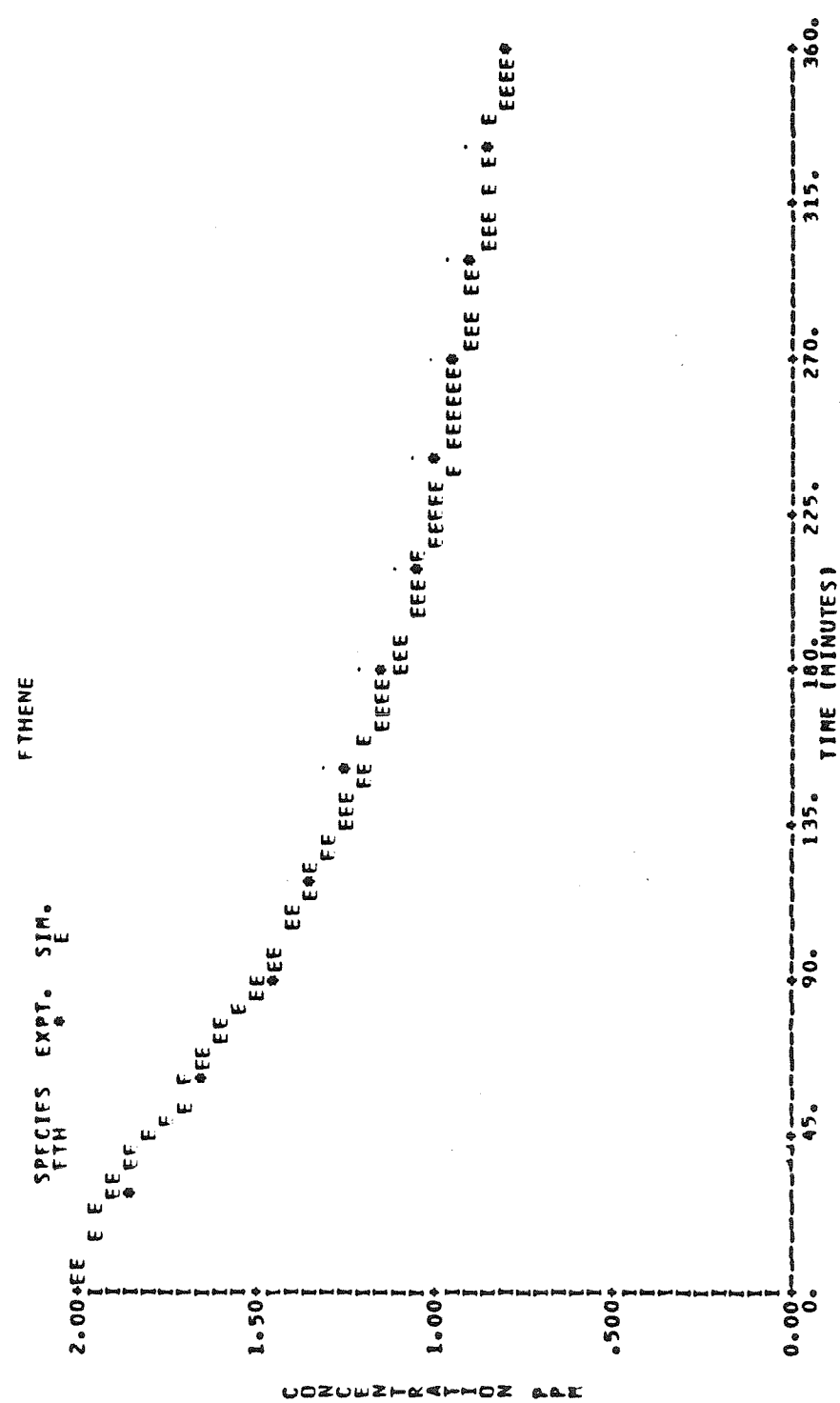

Figure A.12.b. Comparison of Concentration-Time Profiles Predicted by the SUR2 Mechanism with Experimental Data from SAPRC Experiment EC-242.

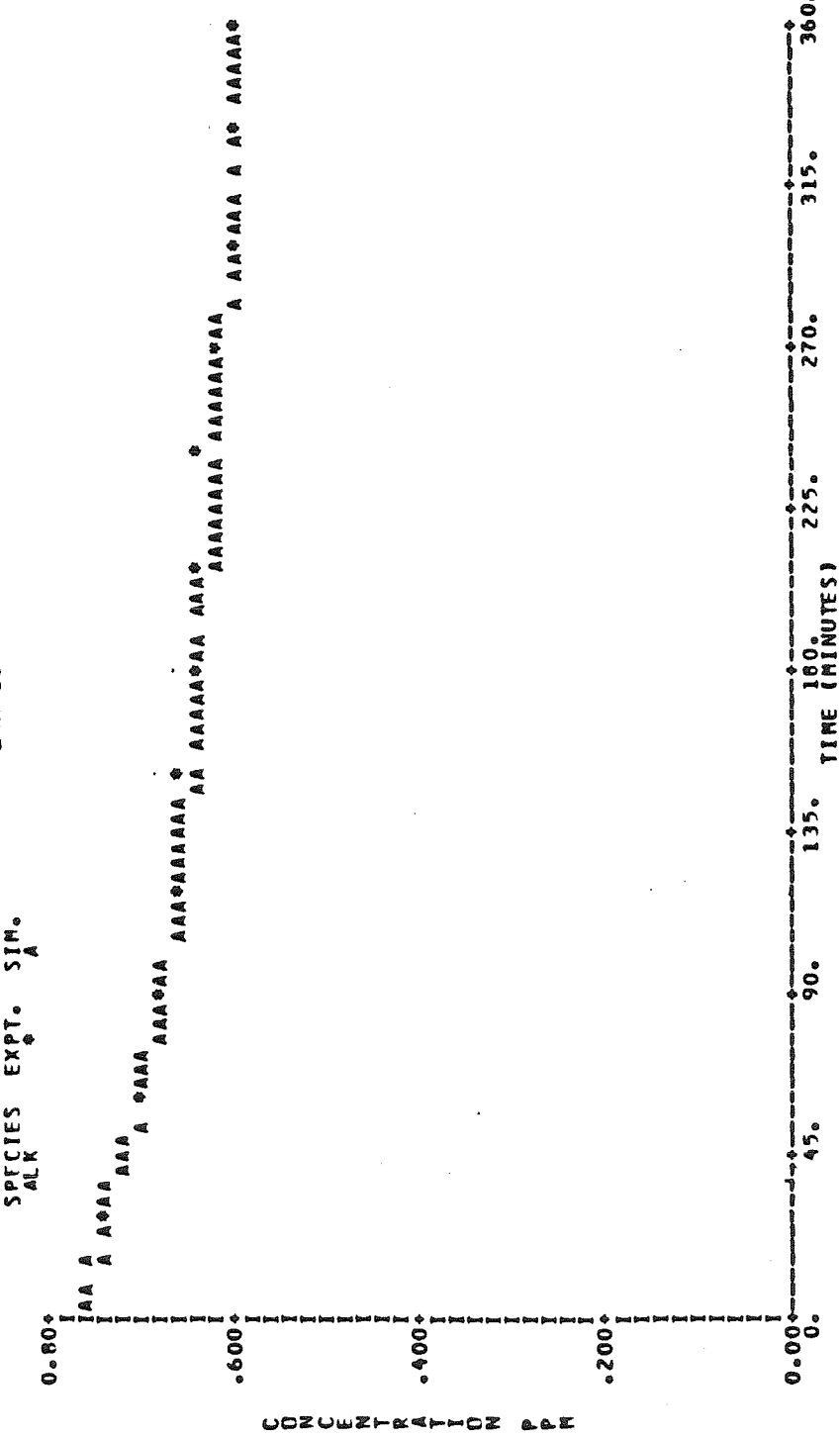

Figure A.12.c. Comparison of Concentration-Time Profiles Predicted by the SUR2 Mechanism with Experimental Data from SAPRC Experiment EC-242.

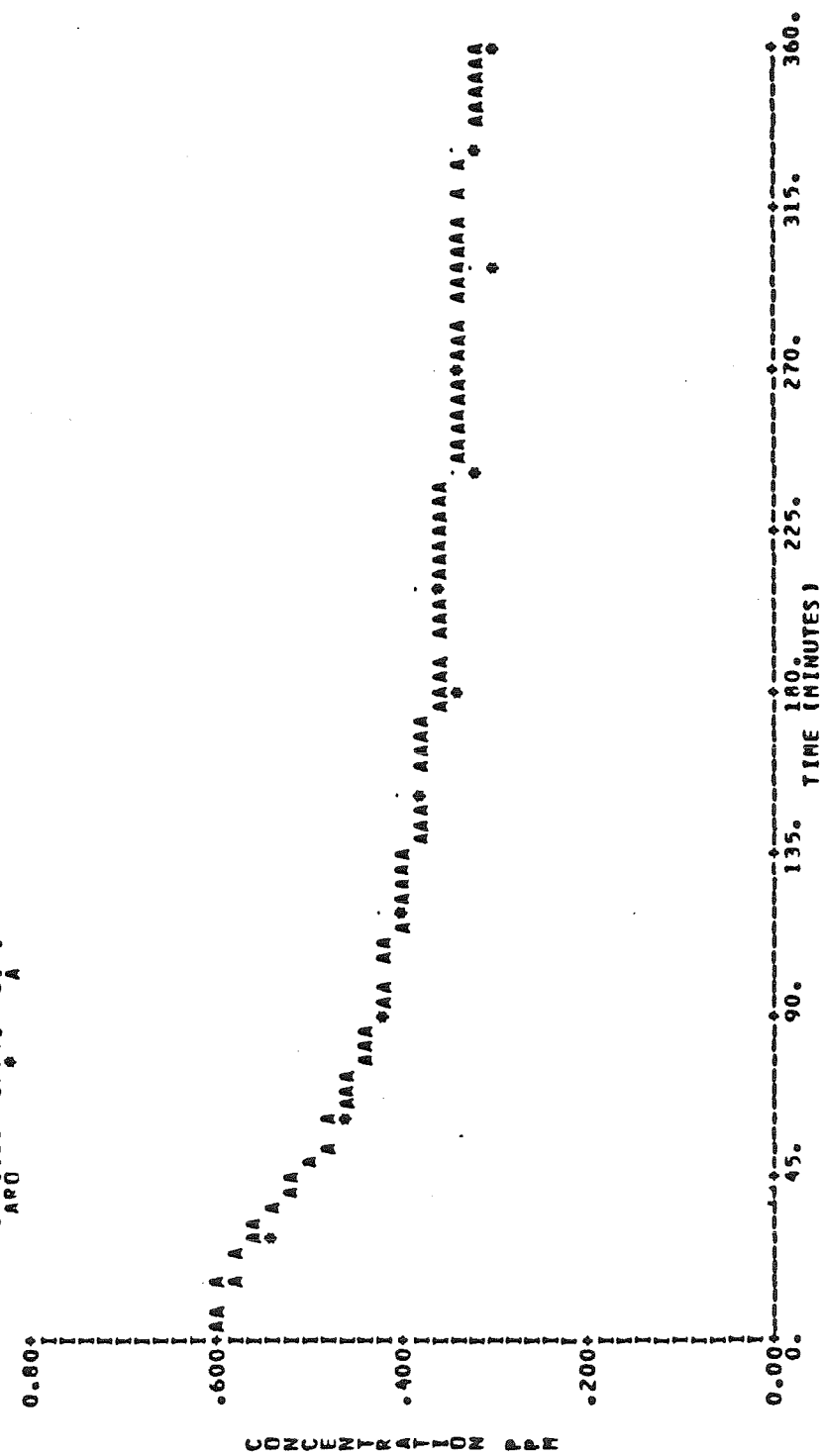

Figure A.12.d. Comparison of Concentration-Time Profiles Predicted by the SUR2 Mechanism with Experimental Data from SAPRC Experiment EC-242.

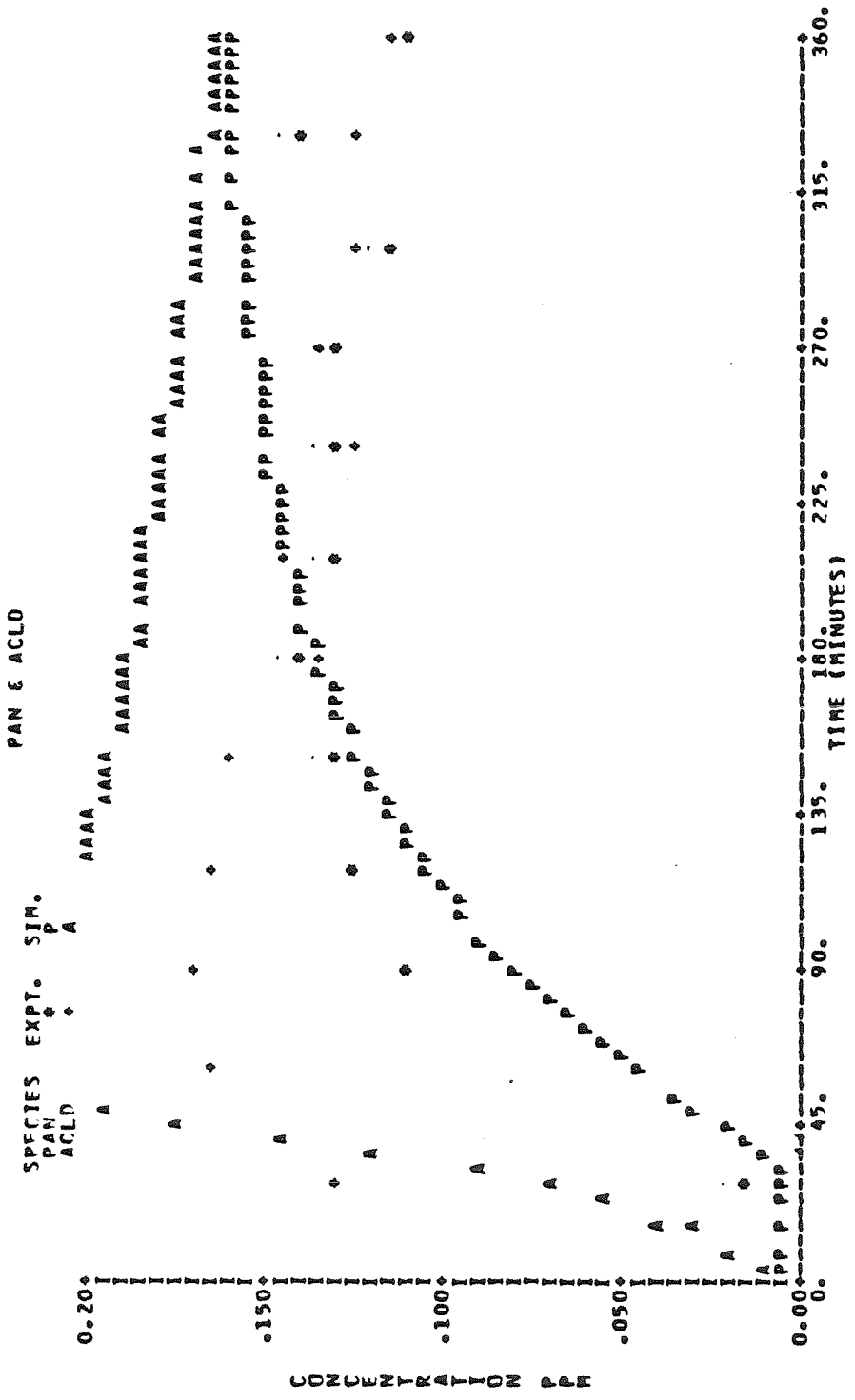

Figure A.12.e. Comparison of Concentration-Time Profiles Predicted by the SUR2 Mechanism with Experimental Data from SAPRC Experiment EC-242.

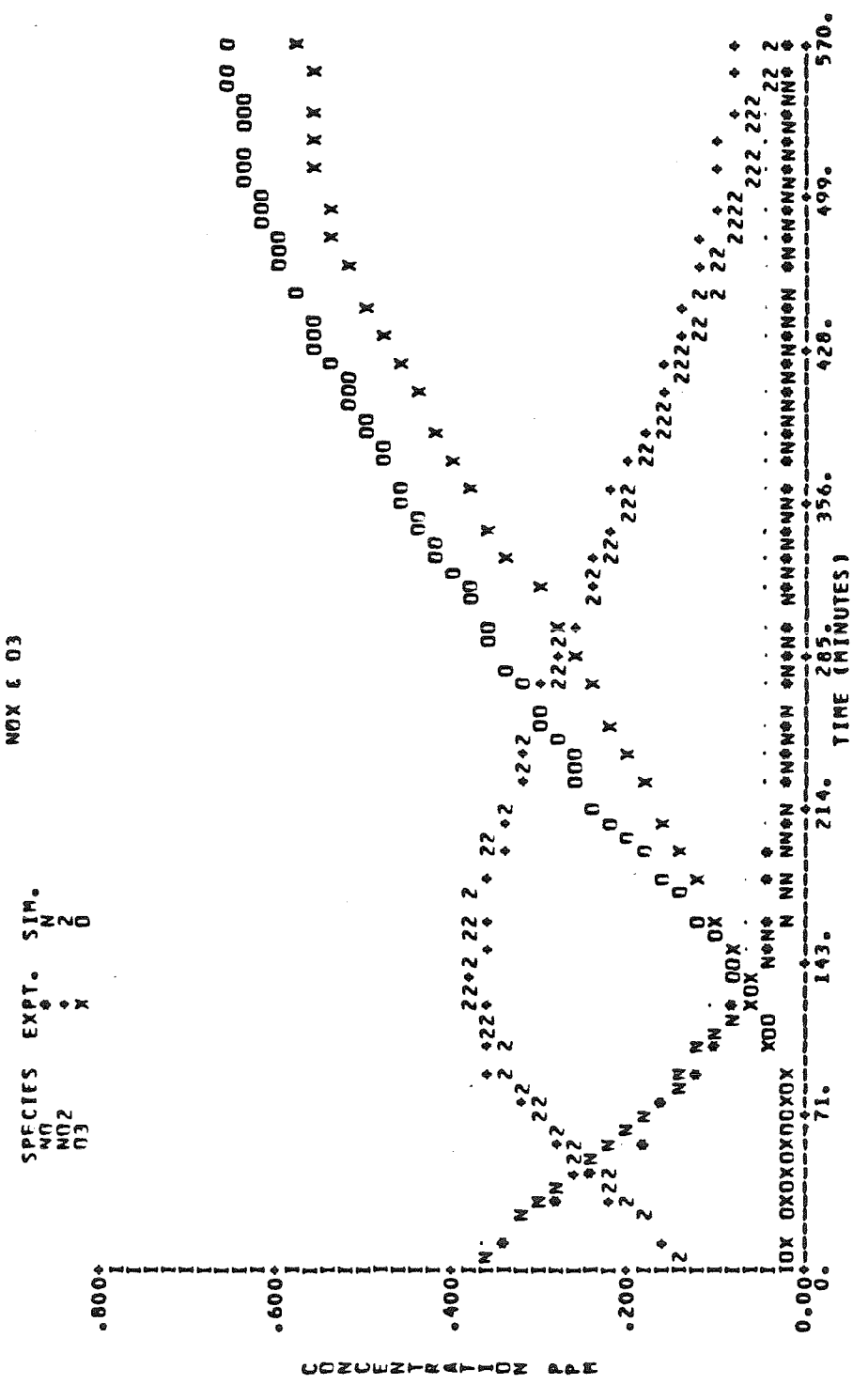

Figure A.13.a. Comparison of Concentration-Time Profiles Predicted by the SUR2 Mechanism with Experimental Data from SAPRC Experiment EC-246.

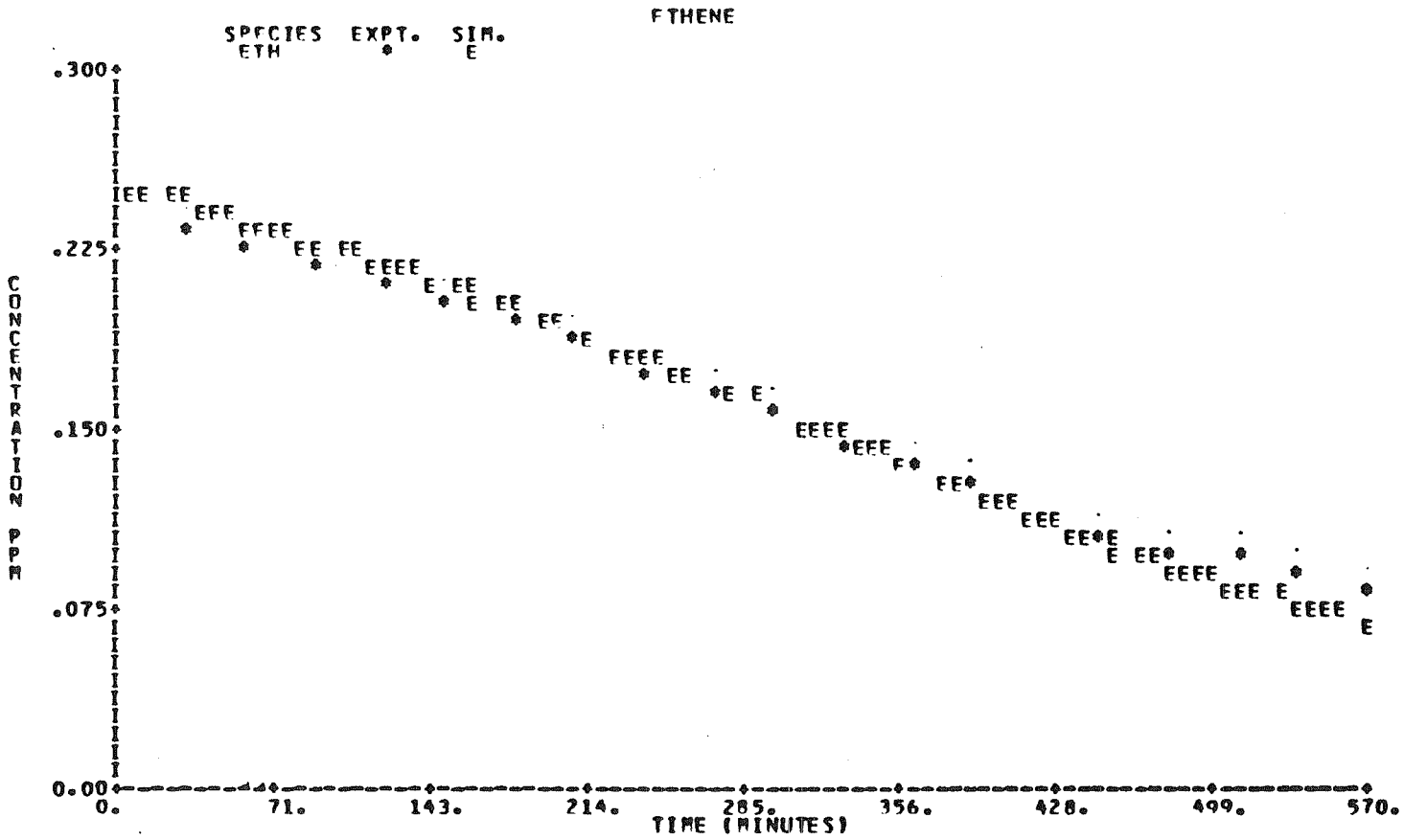

Figure A.13.b. Comparison of Concentration-Time Profiles Predicted by the SUR2 Mechanism with Experimental Data from SAPRC Experiment EC-246.

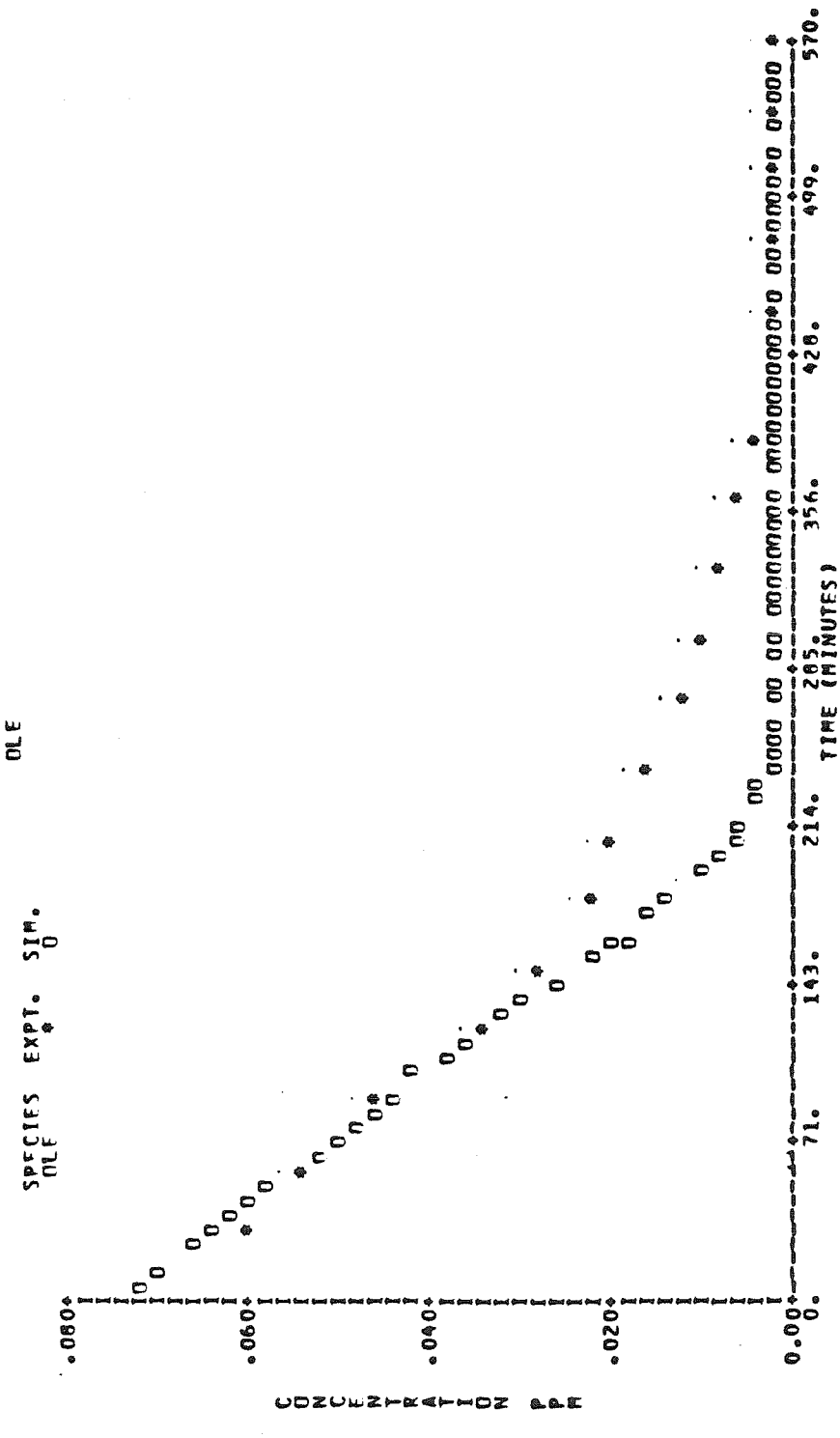

Figure A.13.c. Comparison of Concentration-Time Profiles Predicted by the SUR2 Mechanism with Experimental Data from SAPRC Experiment EC-246.

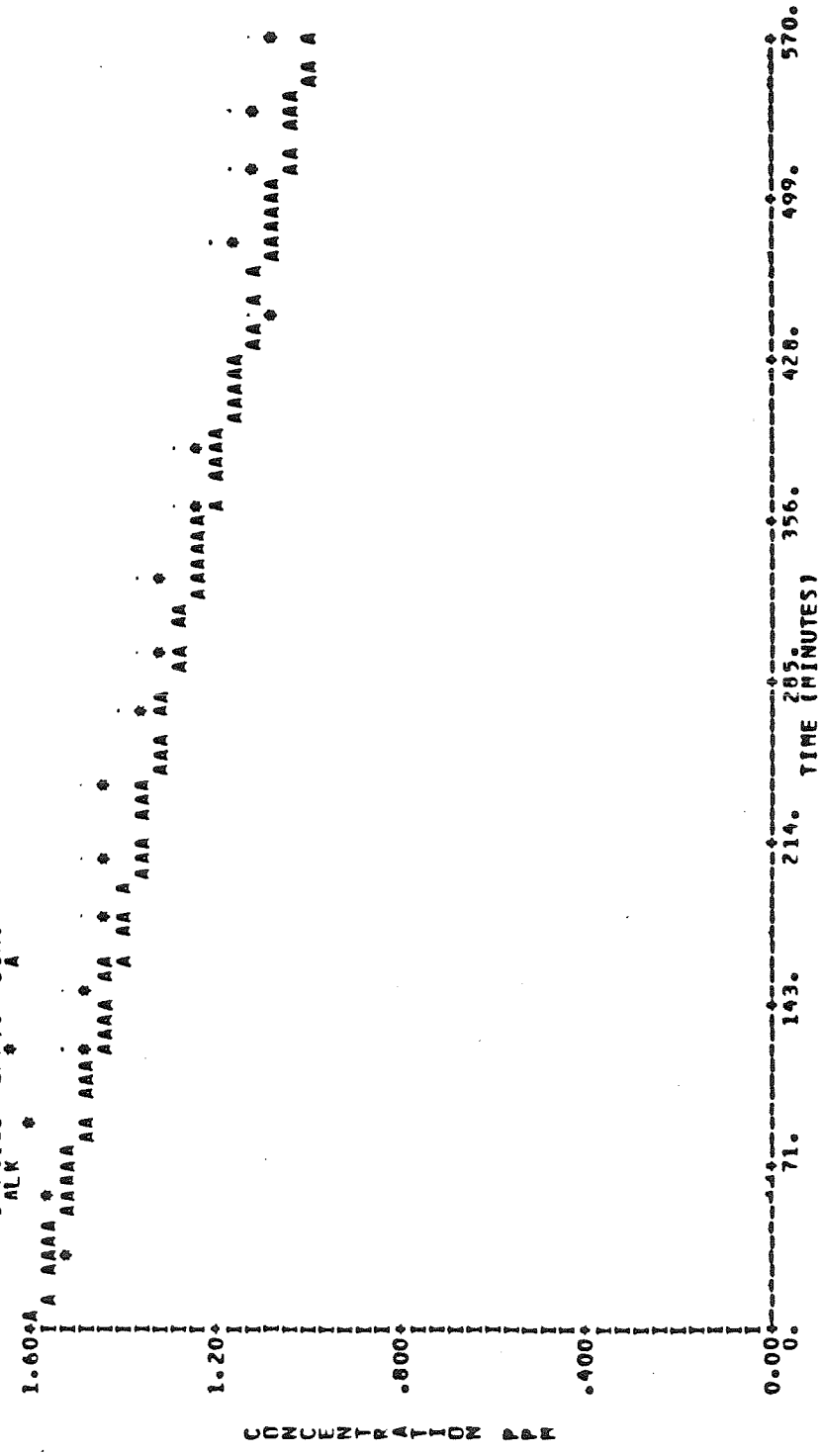

Figure A.13.d. Comparison of Concentration-Time Profiles Predicted by the SUR2 Mechanism with Experimental Data from SAPRC Experiment EC-246.

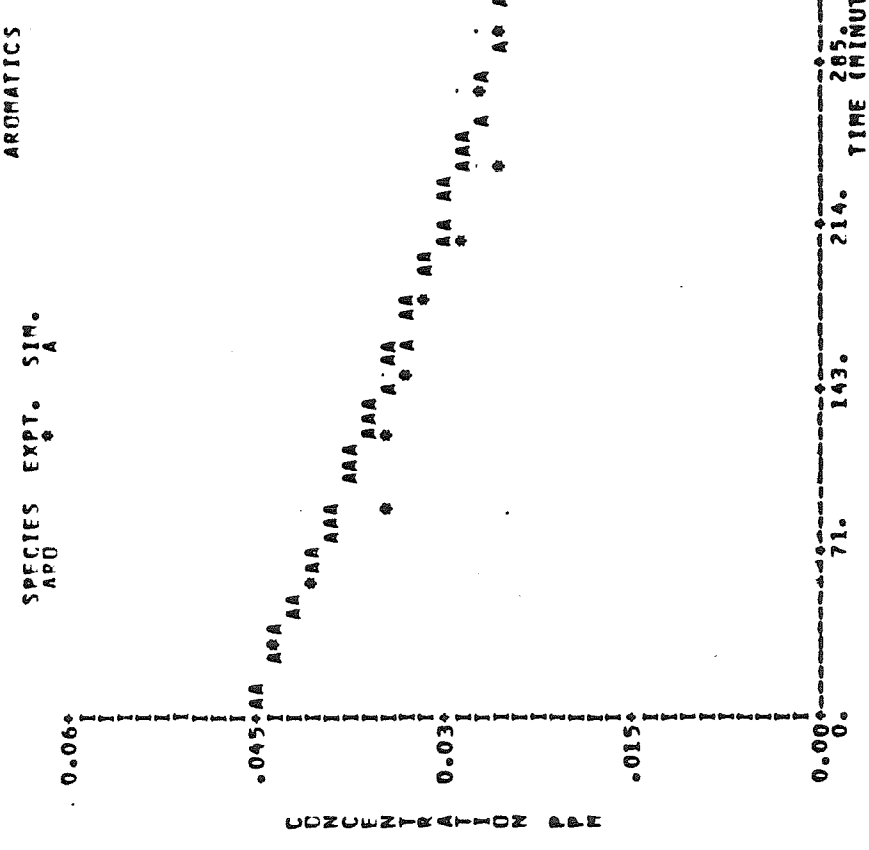

Figure A.13.e. Comparison of Concentration-Time Profiles Predicted by the SUR2 Mechanism with Experimental Data from SAPRC Experiment EC-246.

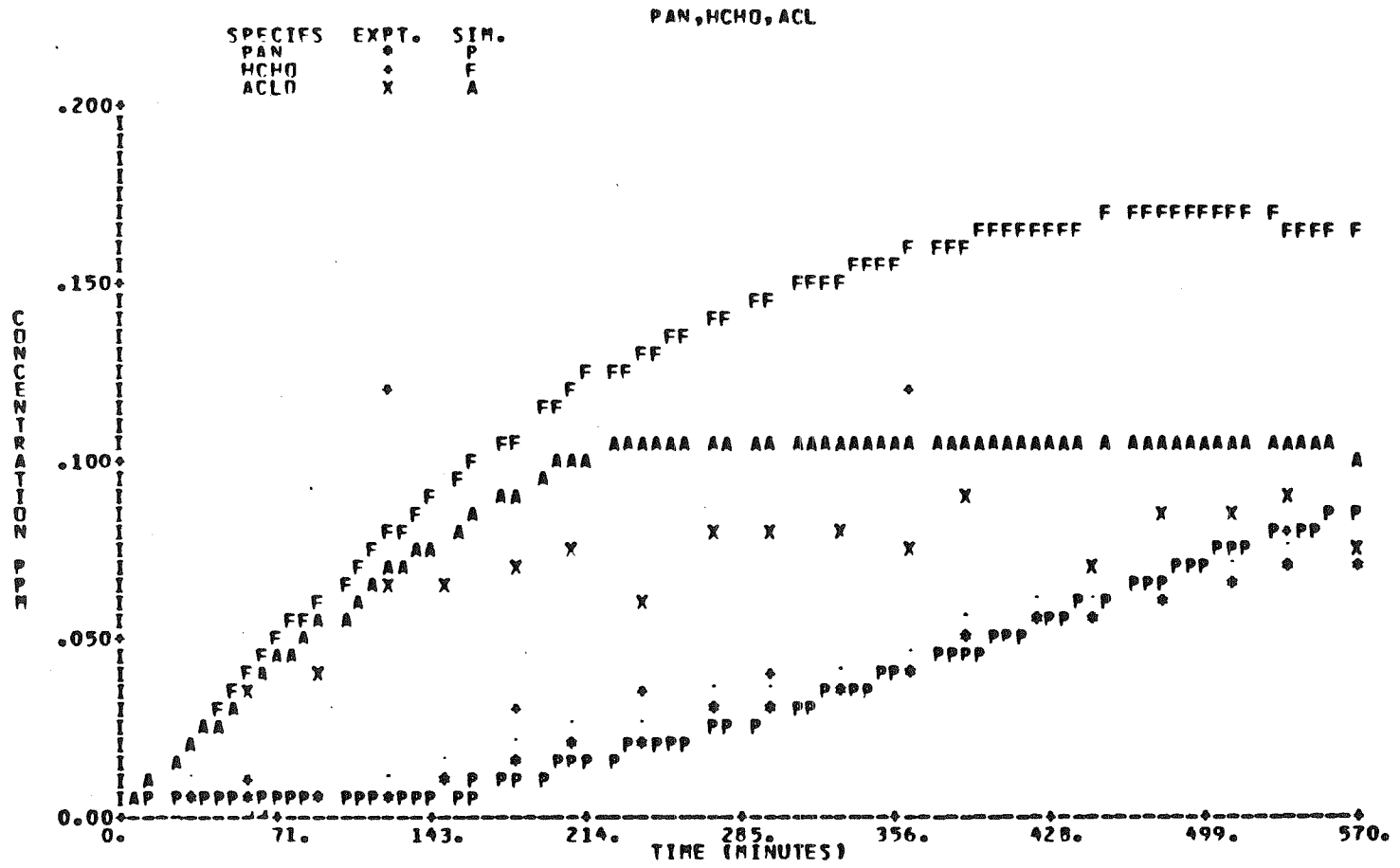

Figure A.13.f. Comparison of Concentration-Time Profiles Predicted by the SUR2 Mechanism with Experimental Data from SAPRC Experiment EC-246.

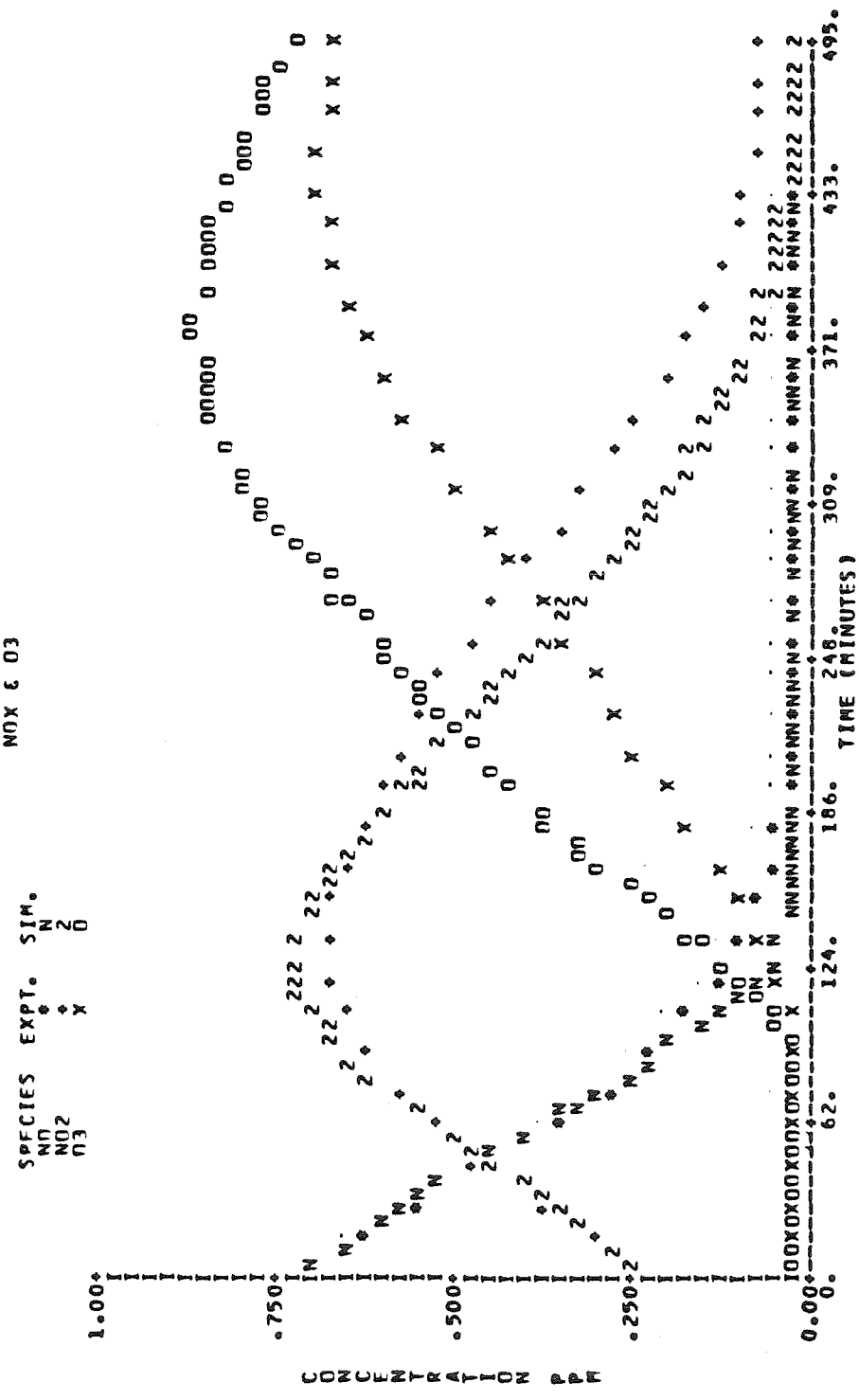

Figure A.14.a. Comparison of Concentration-Time Profiles Predicted by the SUR2 Mechanism with Experimental Data from SAPRC Experiment EC-238.

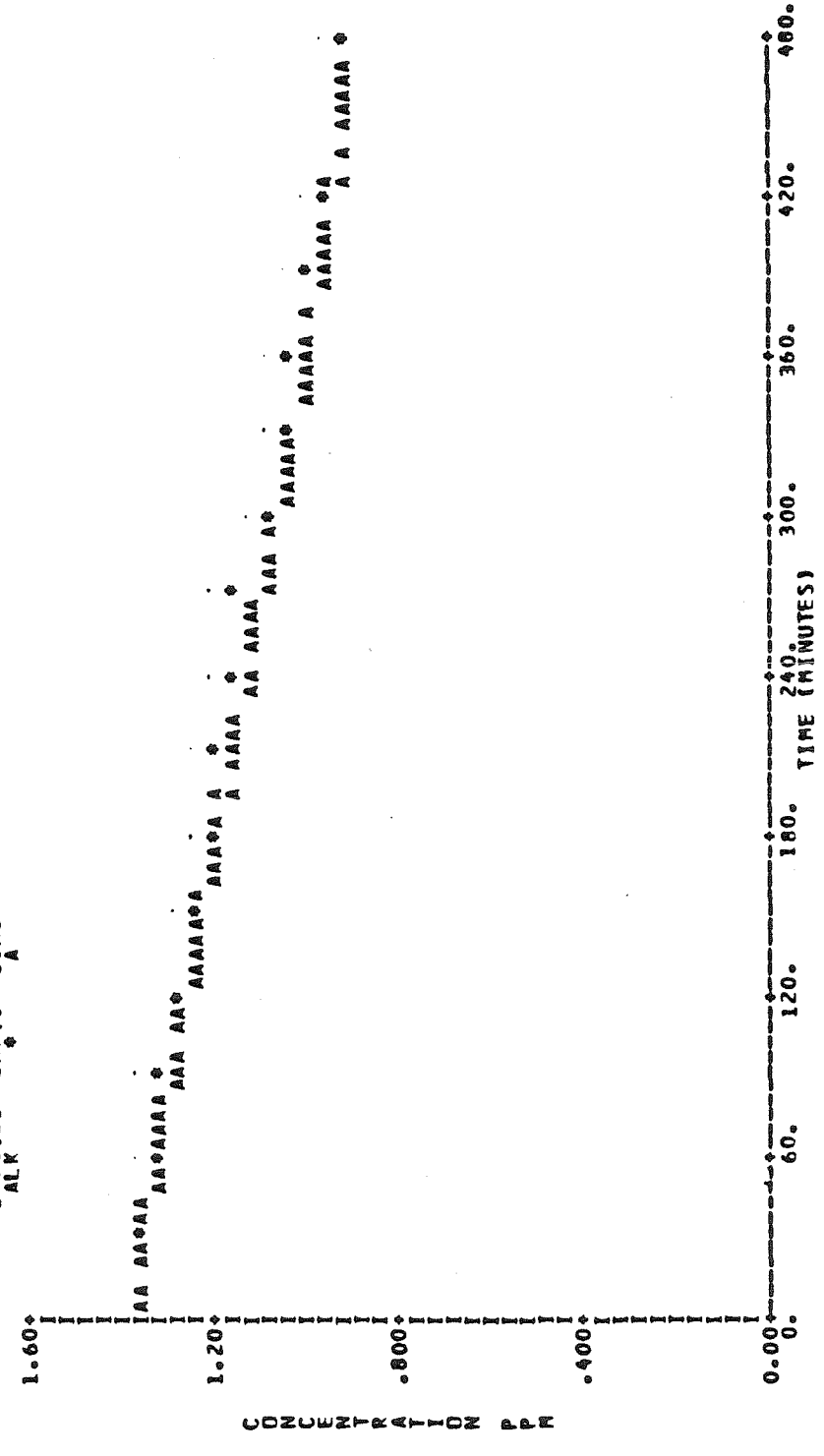

Figure A.14.b. Comparison of Concentration-Time Profiles Predicted by the SUR2 Mechanism with Experimental Data from SAPRC Experiment EC-238.

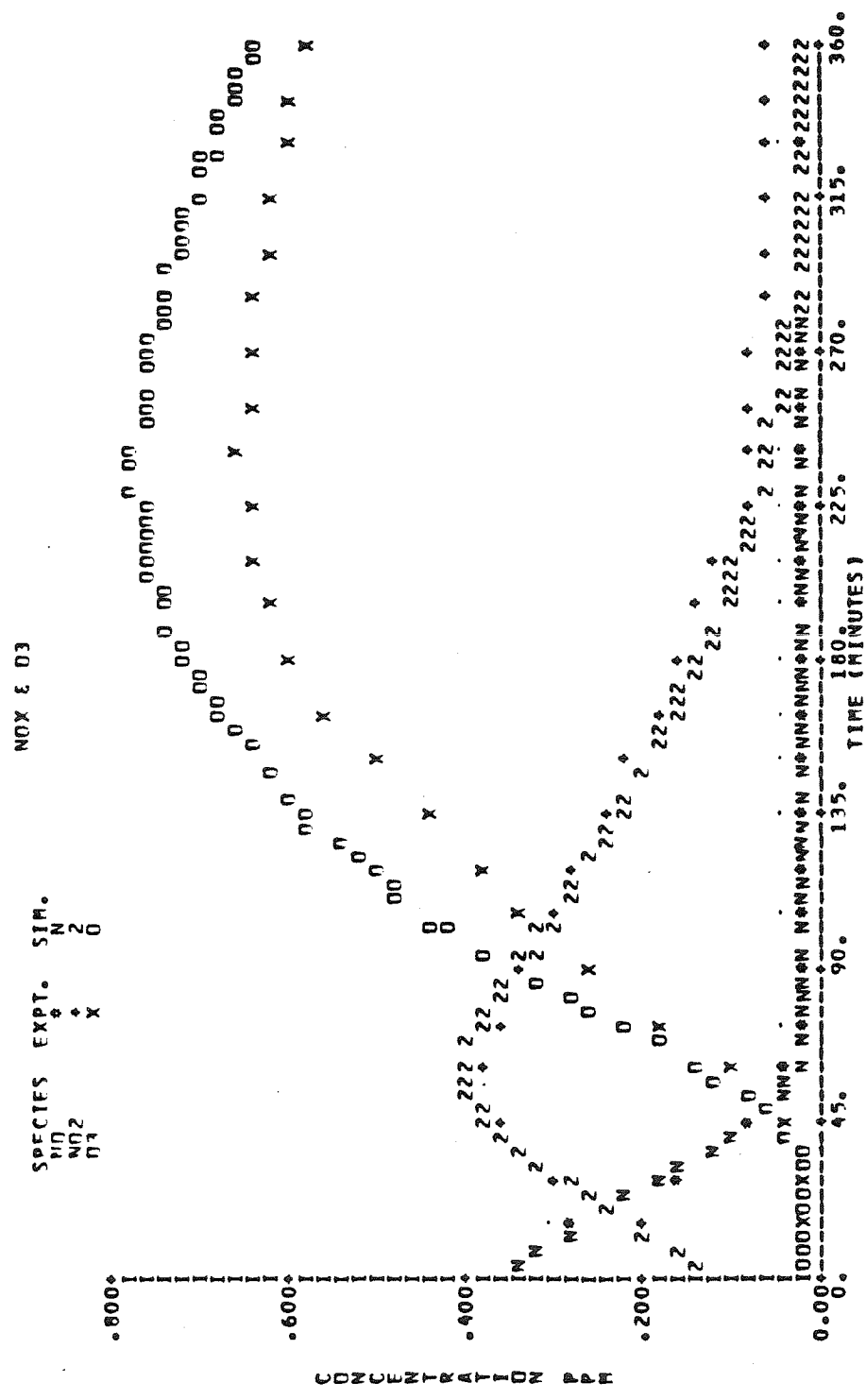

Figure A.15.a. Comparison of Concentration-Time Profiles Predicted by the SUR2 Mechanism with Experimental Data from SAPRC Experiment EC-237.

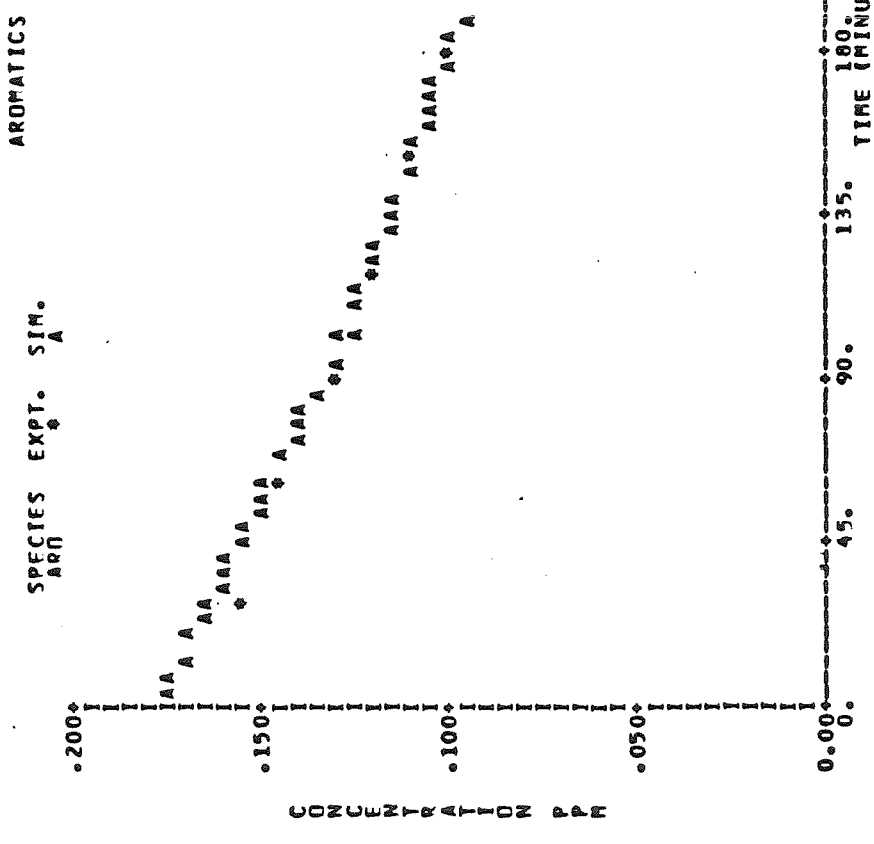

Figure A.15.b. Comparison of Concentration-Time Profiles Predicted by the SUR2 Mechanism with Experimental Data from SAPRC Experiment EC-237.

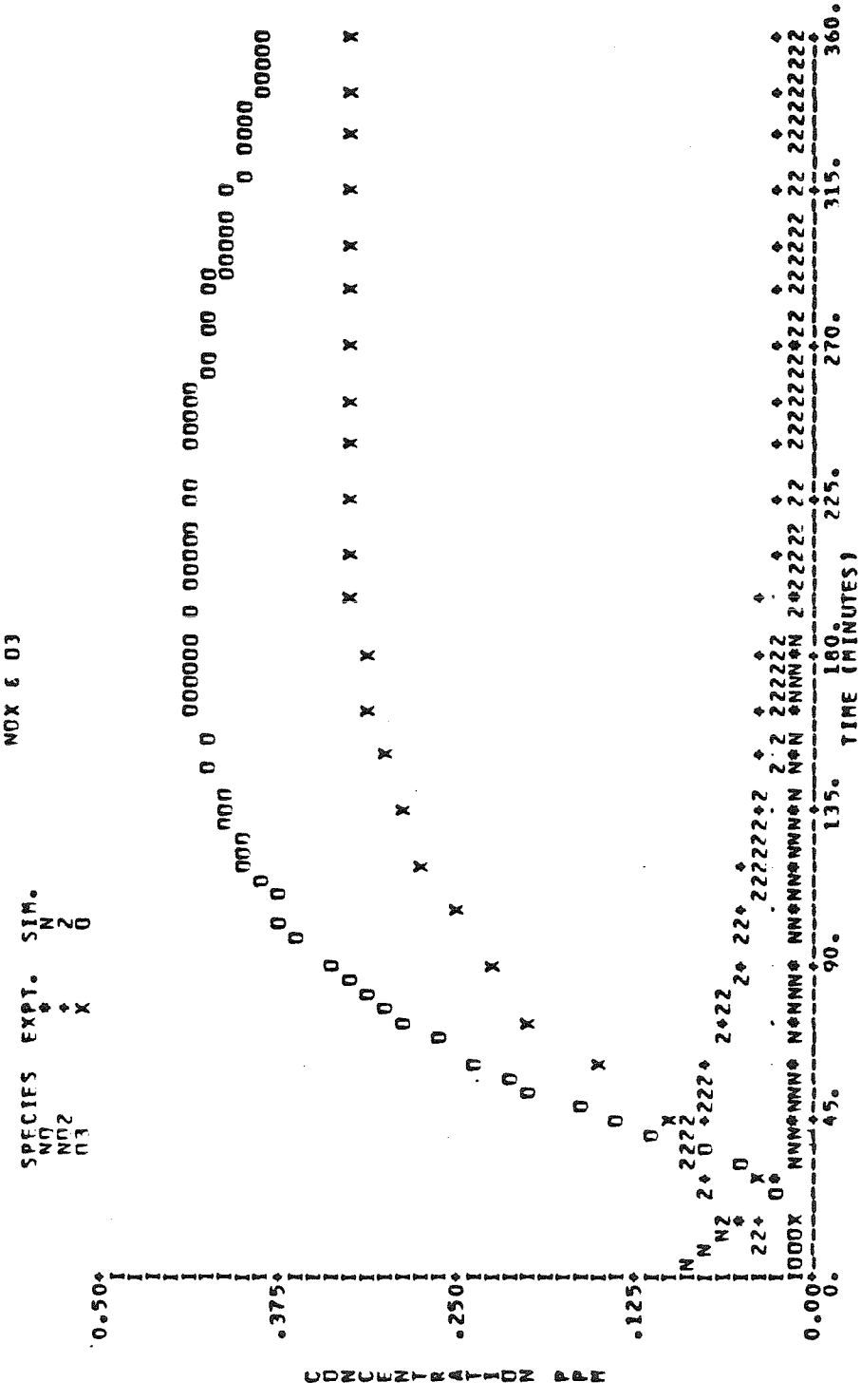

Figure A.16.a. Comparison of Concentration-Time Profiles Predicted by the SUR2 Mechanism with Experimental Data from SAPRC Experiment EC-233.

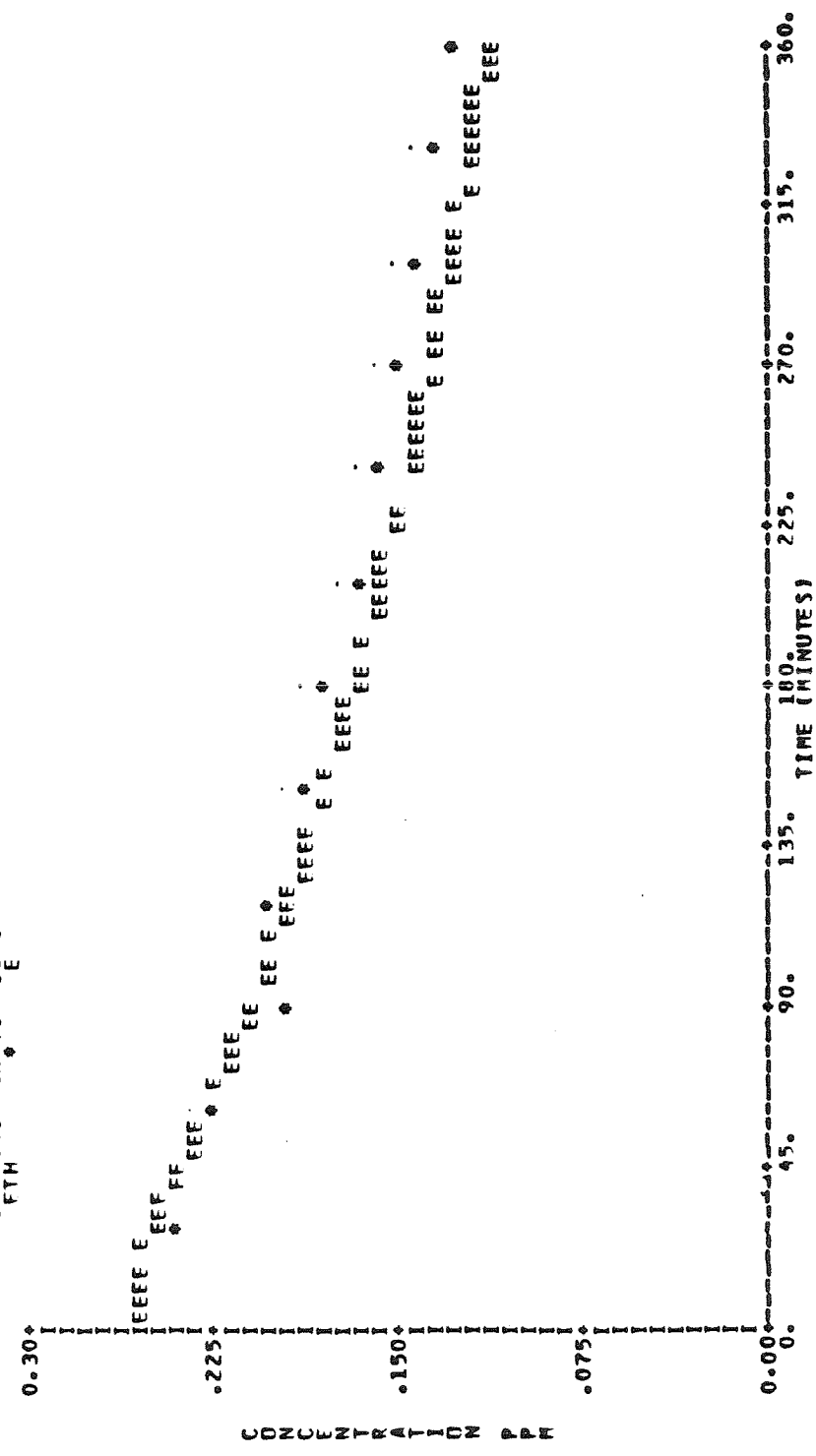

Figure A.16.b. Comparison of Concentration-Time Profiles Predicted by the SUR2 Mechanism with Experimental Data from SAPRC Experiment EC-233.

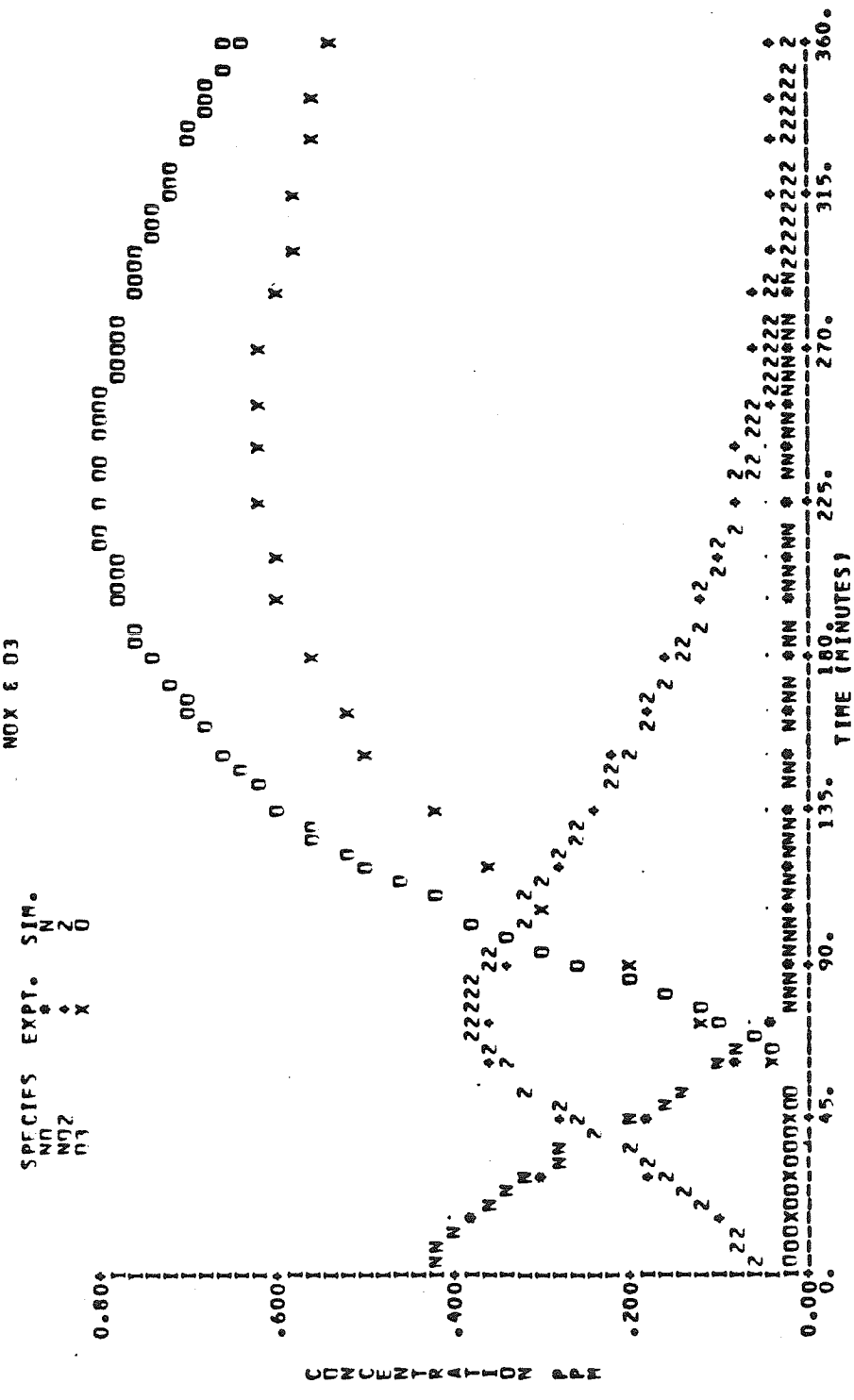

Figure A.17.a. Comparison of Concentration-Time Profiles Predicted by the SUR2 Mechanism with Experimental Data from SAPRC Experiment EC-231.

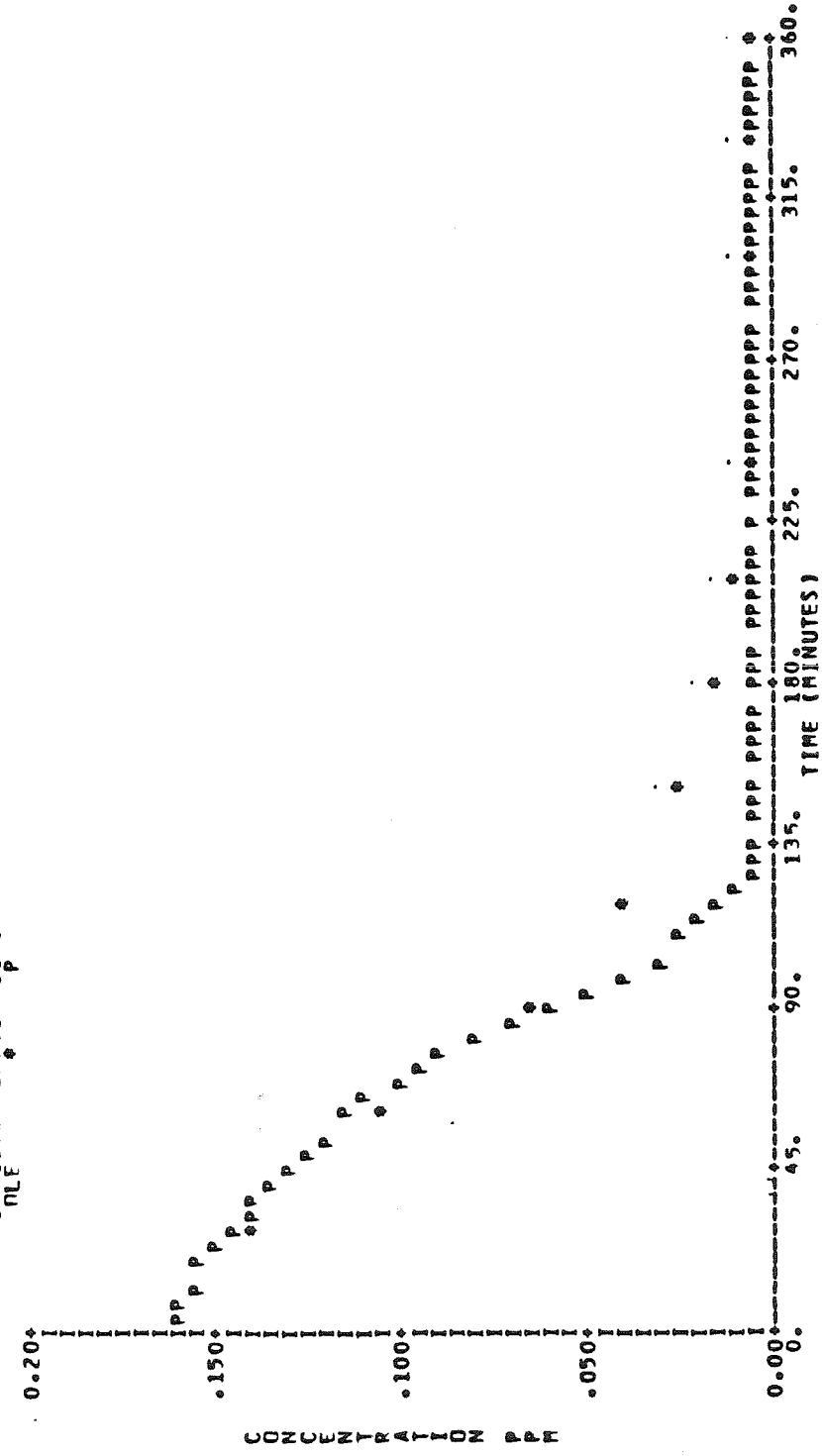

Figure A.17.b. Comparison of Concentration-Time Profiles Predicted by the SUR2 Mechanism with Experimental Data from SAPRC Experiment EC-231.

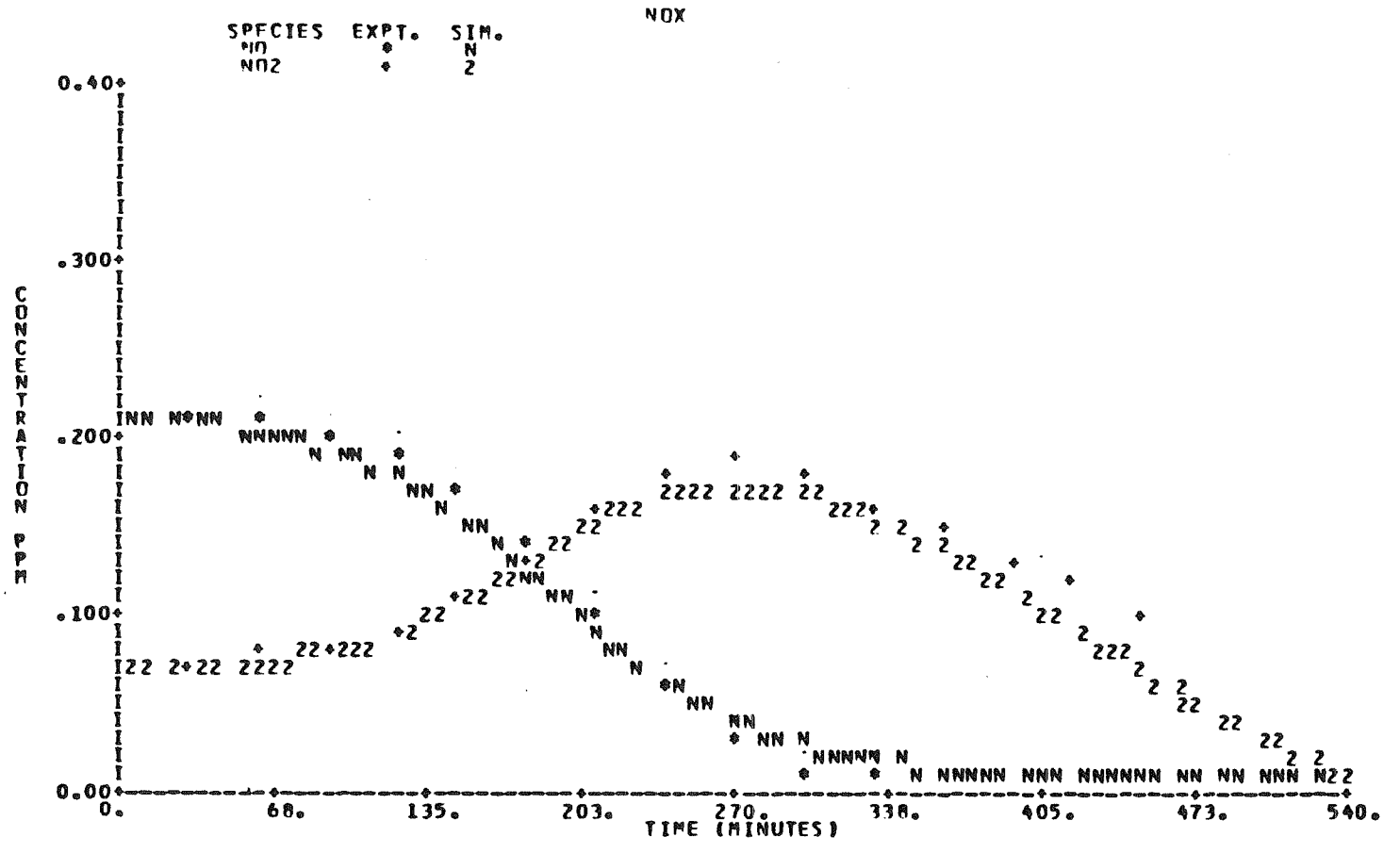

Figure A.18.a. Comparison of Concentration-Time Profiles Predicted by the SUR2 Mechanism with Experimental Data from the Blue Side of the UNC Experiment of July 8, 1982.

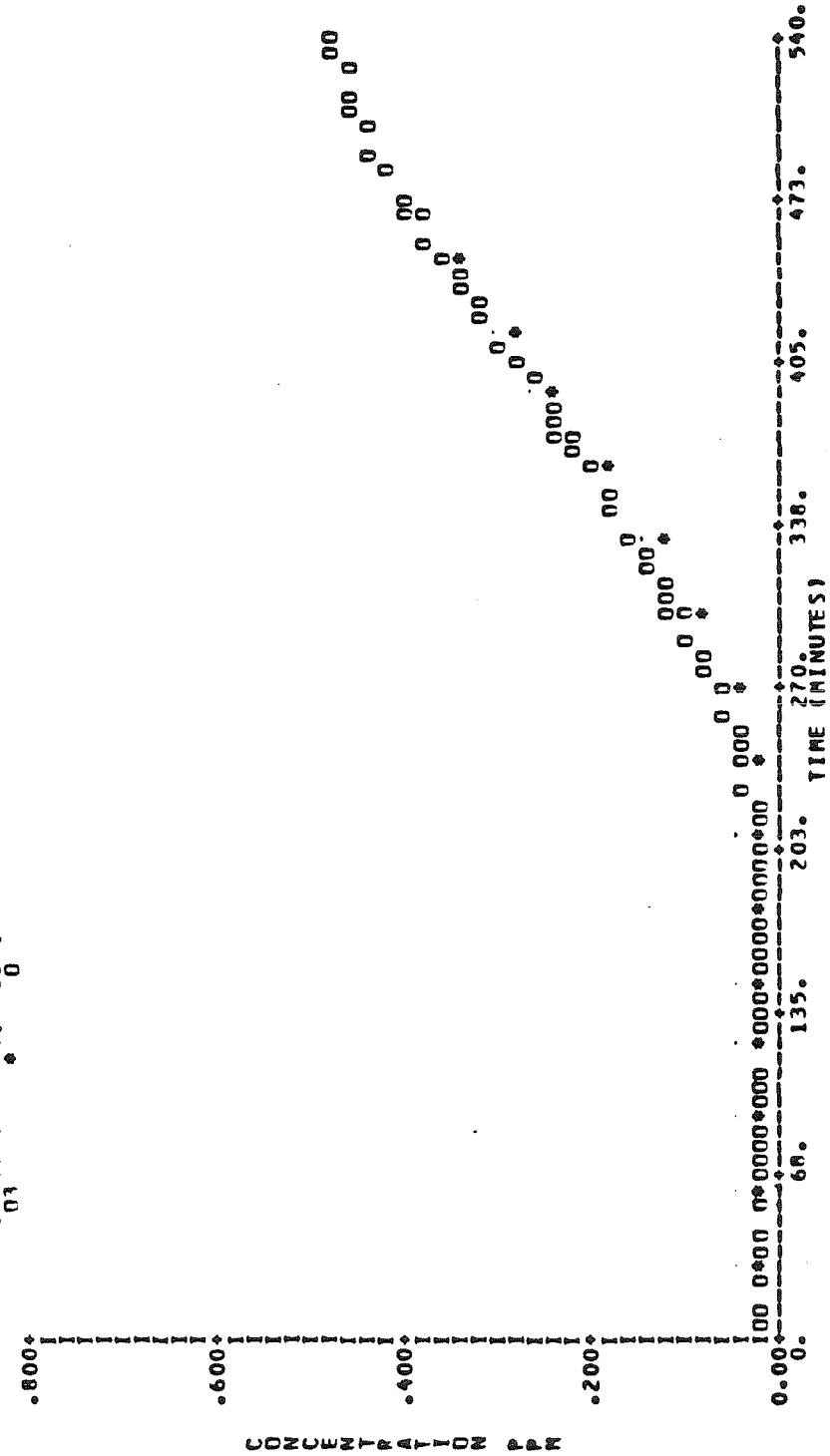

Figure A.18.b. Comparison of Concentration-Time Profiles Predicted by the SUR2 Mechanism with Experimental Data from the Blue Side of the UNC Experiment of July 8, 1982.

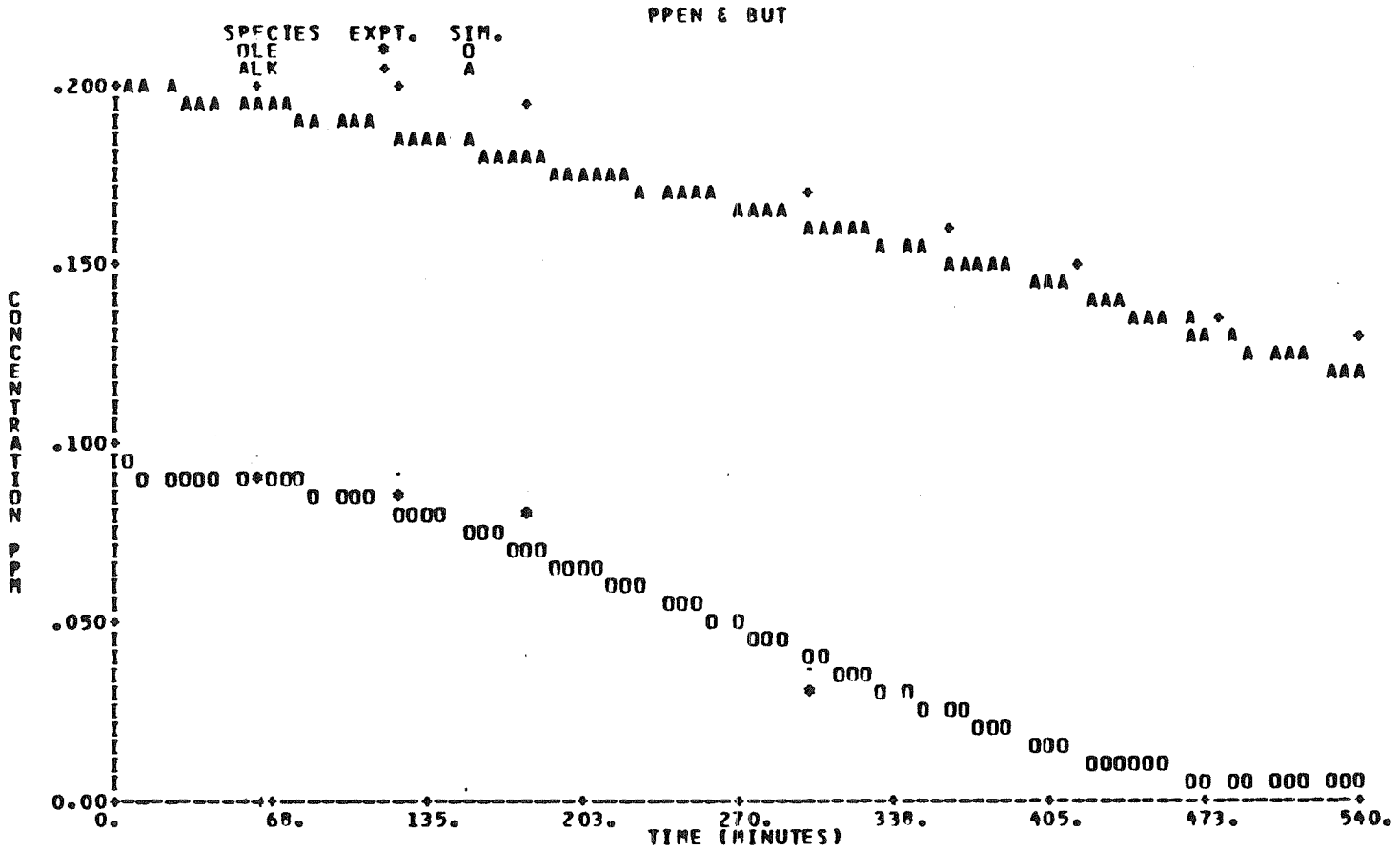

Figure A.18.c. Comparison of Concentration-Time Profiles Predicted by the SUR2 Mechanism with Experimental Data from the Blue Side of the UNC Experiment of July 8, 1982.

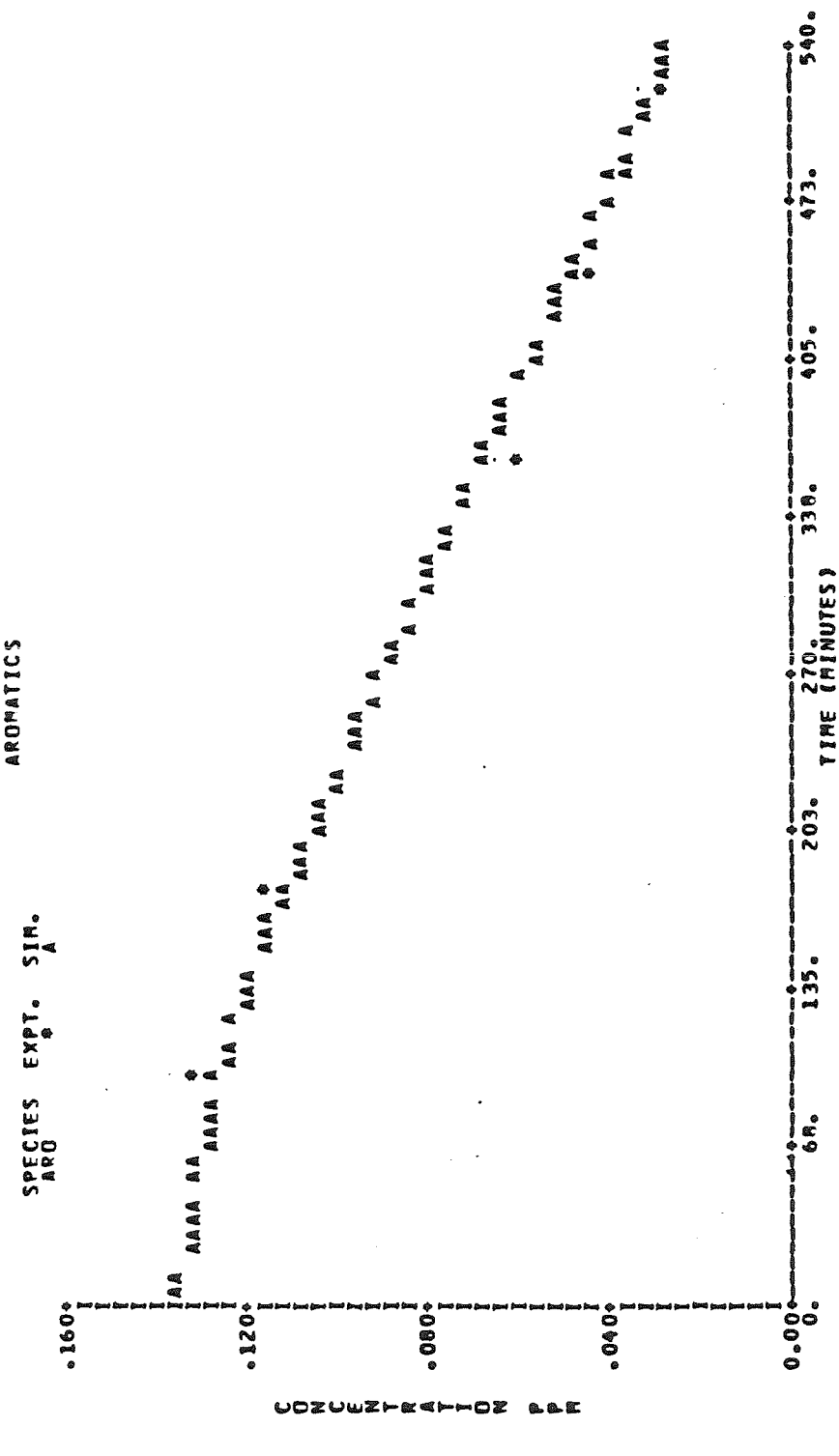

Figure A.18.d. Comparison of Concentration-Time Profiles Predicted by the SUR2 Mechanism with Experimental Data from the Blue Side of the UNC Experiment of July 8, 1982.

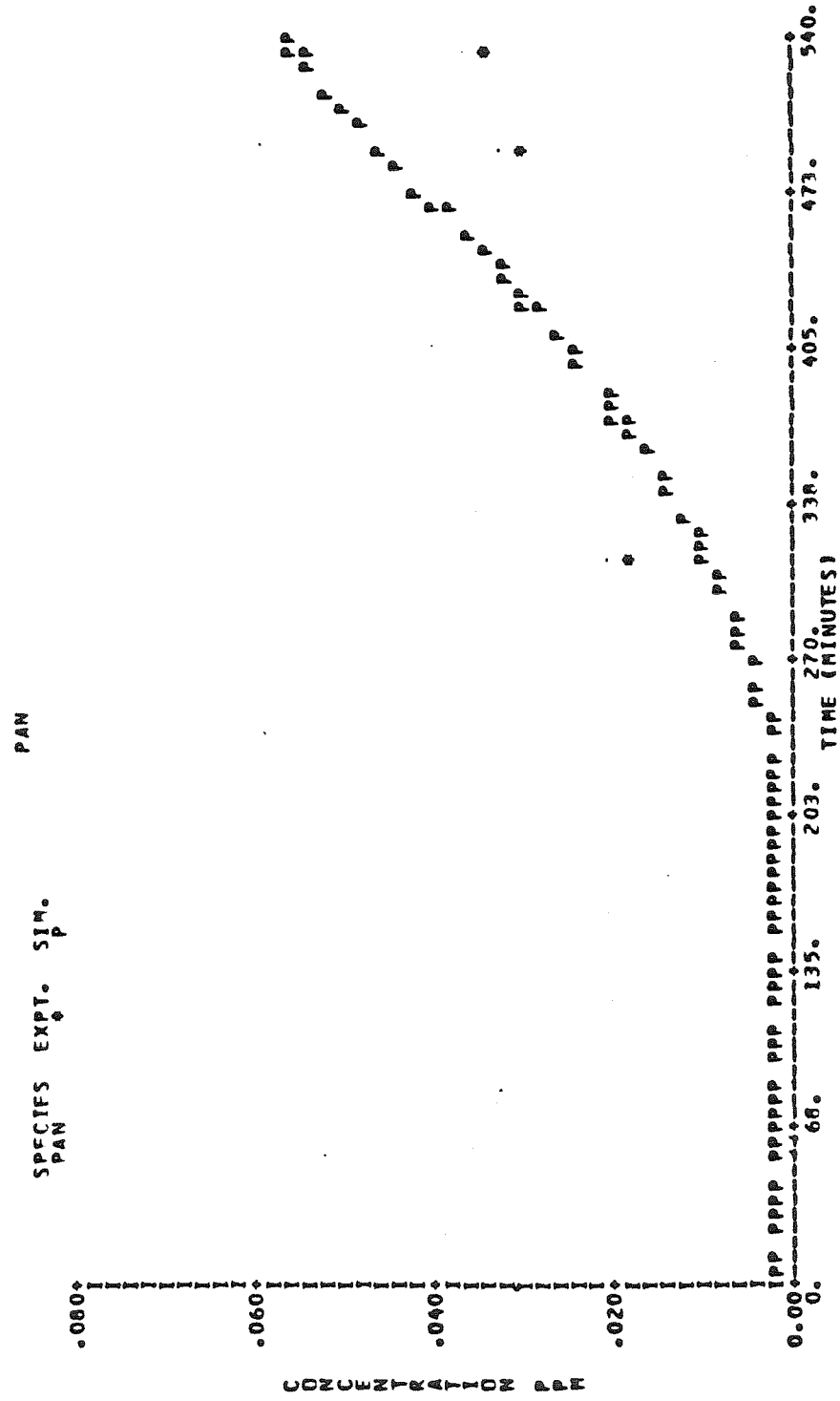

Figure A.18.e. Comparison of Concentration-Time Profiles Predicted by the SUR2 Mechanism with Experimental Data from the Blue Side of the UNC Experiment of July 8, 1982.

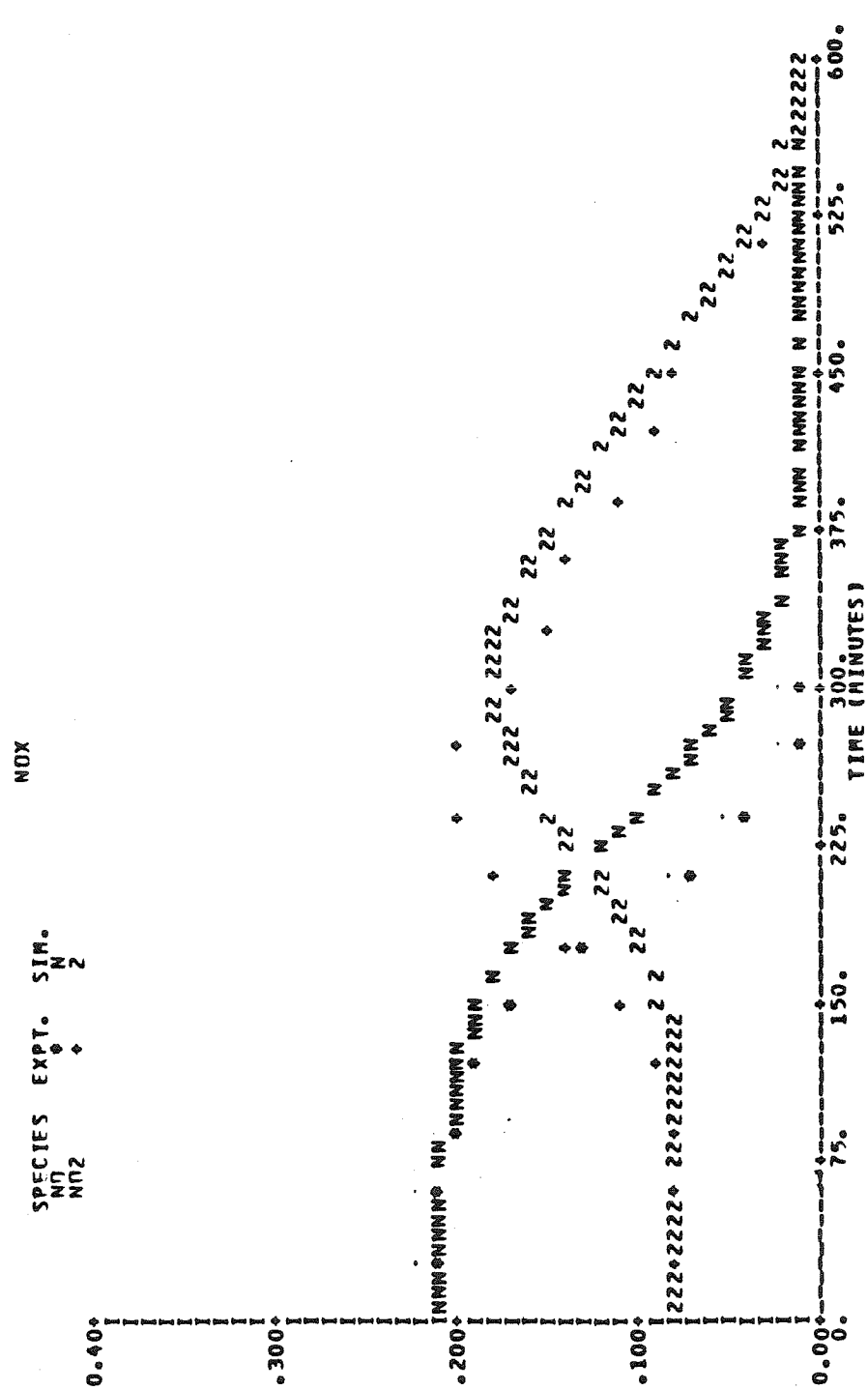

Figure A.19.a. Comparison of Concentration-Time Profiles Predicted by the SUR2 Mechanism with Experimental Data from the Red Side of the UNC Experiment of July 8, 1982.

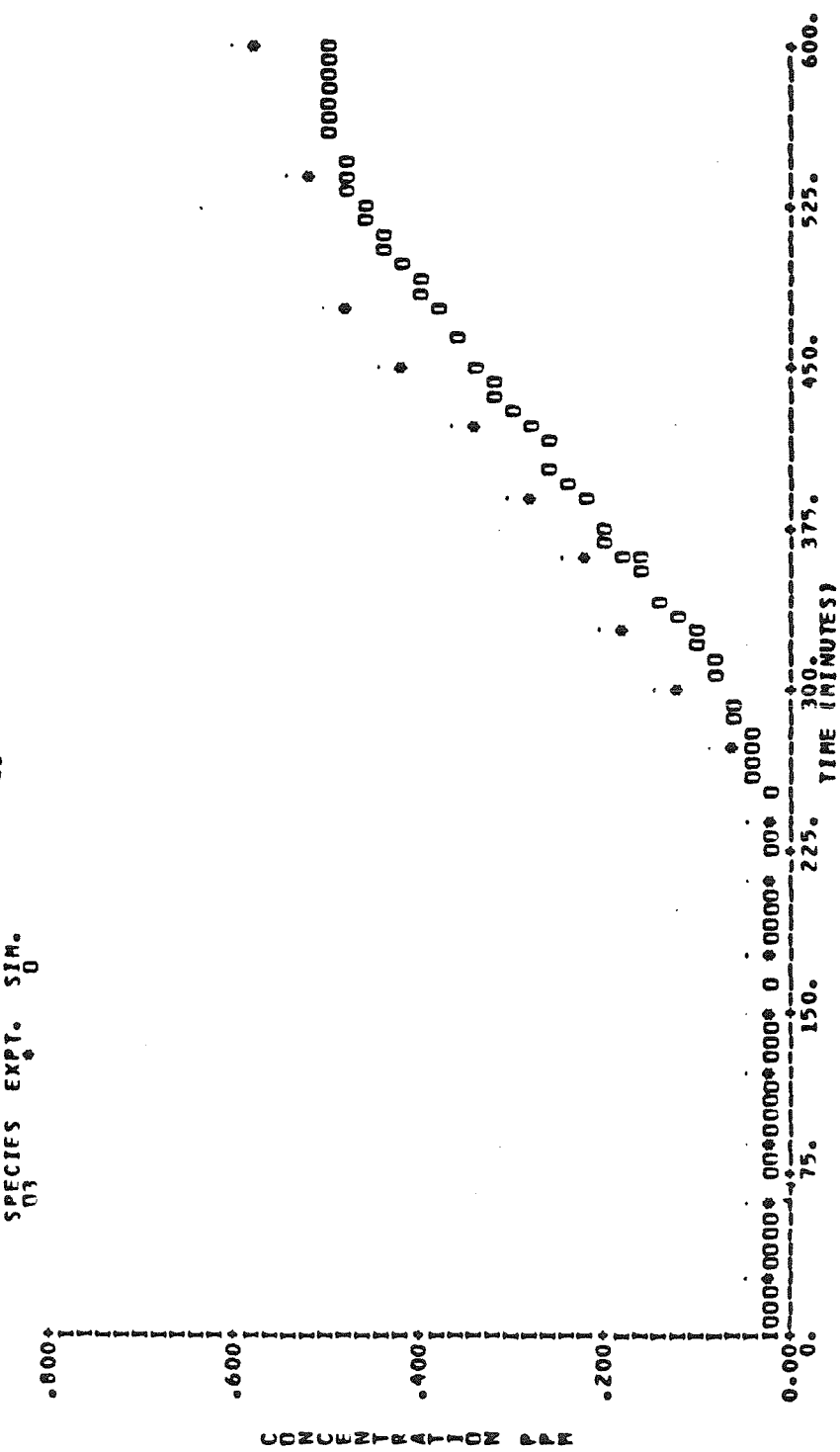

Figure A.19.b. Comparison of Concentration-Time Profiles Predicted by the SUR2 Mechanism with Experimental Data from the Red Side of the UNC Experiment of July 8, 1982.

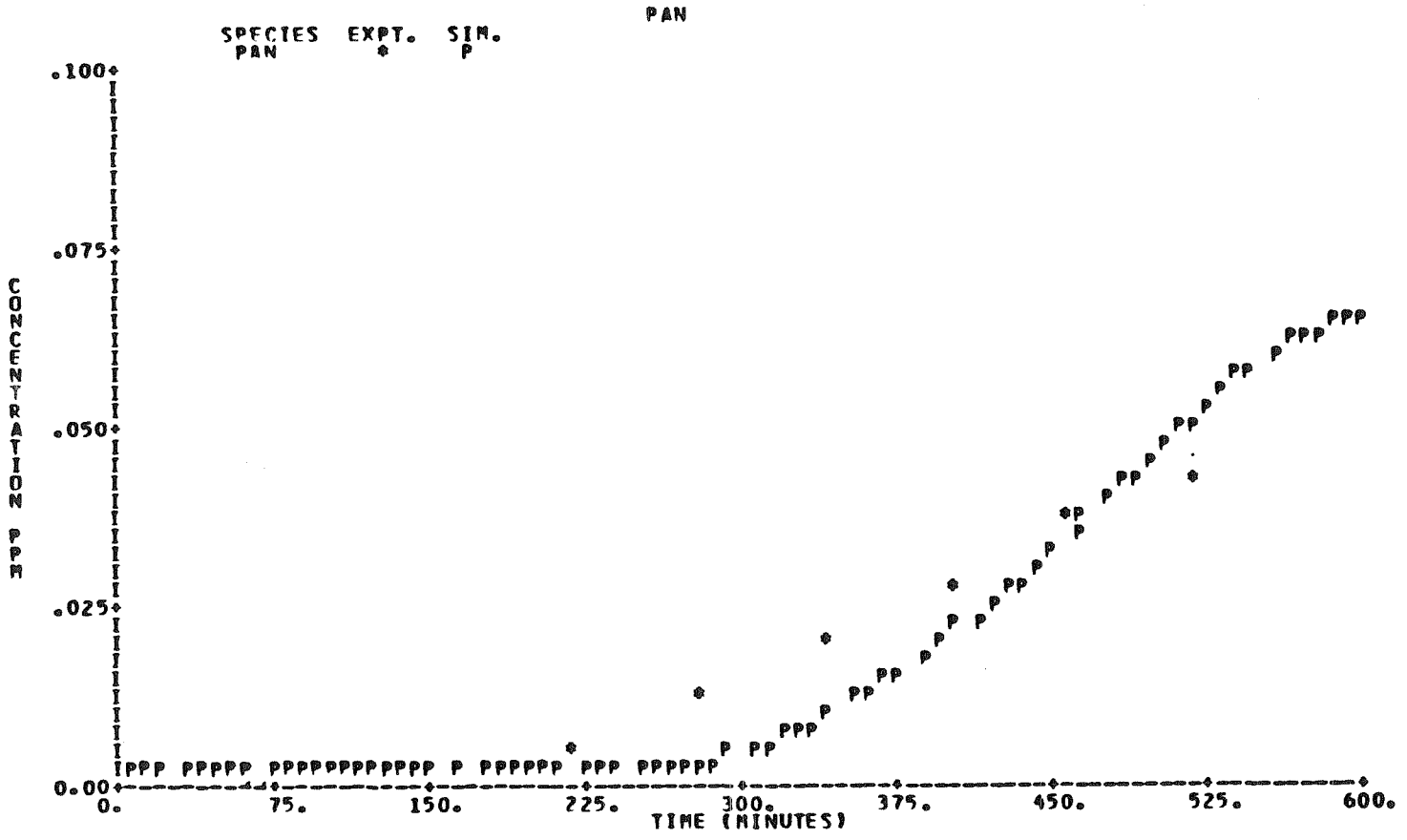

Figure A.19.c. Comparison of Concentration-Time Profiles Predicted by the SUR2 Mechanism with Experimental Data from the Red Side of the UNC Experiment of July 8, 1982.

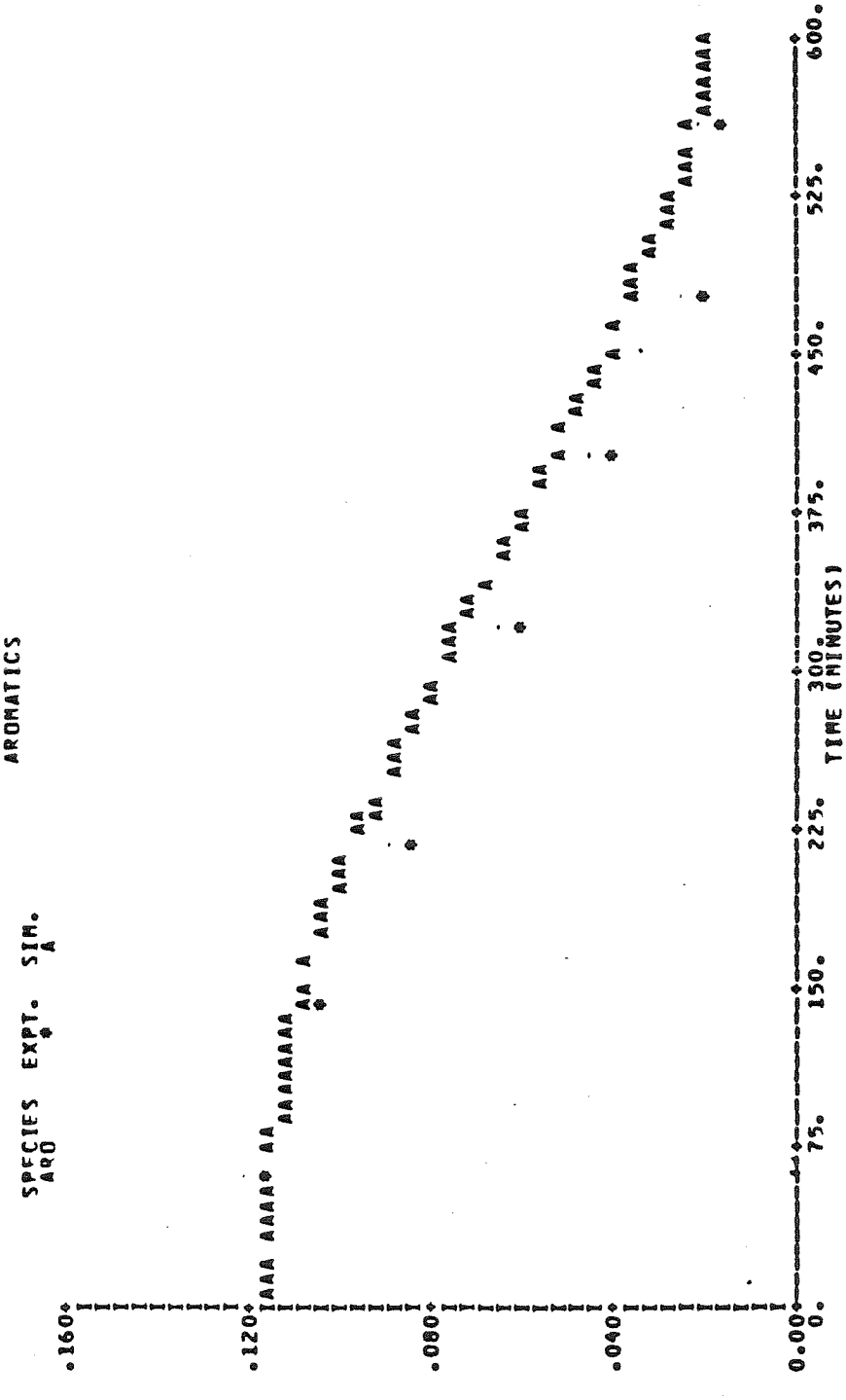

Figure A.19.d. Comparison of Concentration-Time Profiles Predicted by the SUR2 Mechanism with Experimental Data from the Red Side of the UNC Experiment of July 8, 1982.

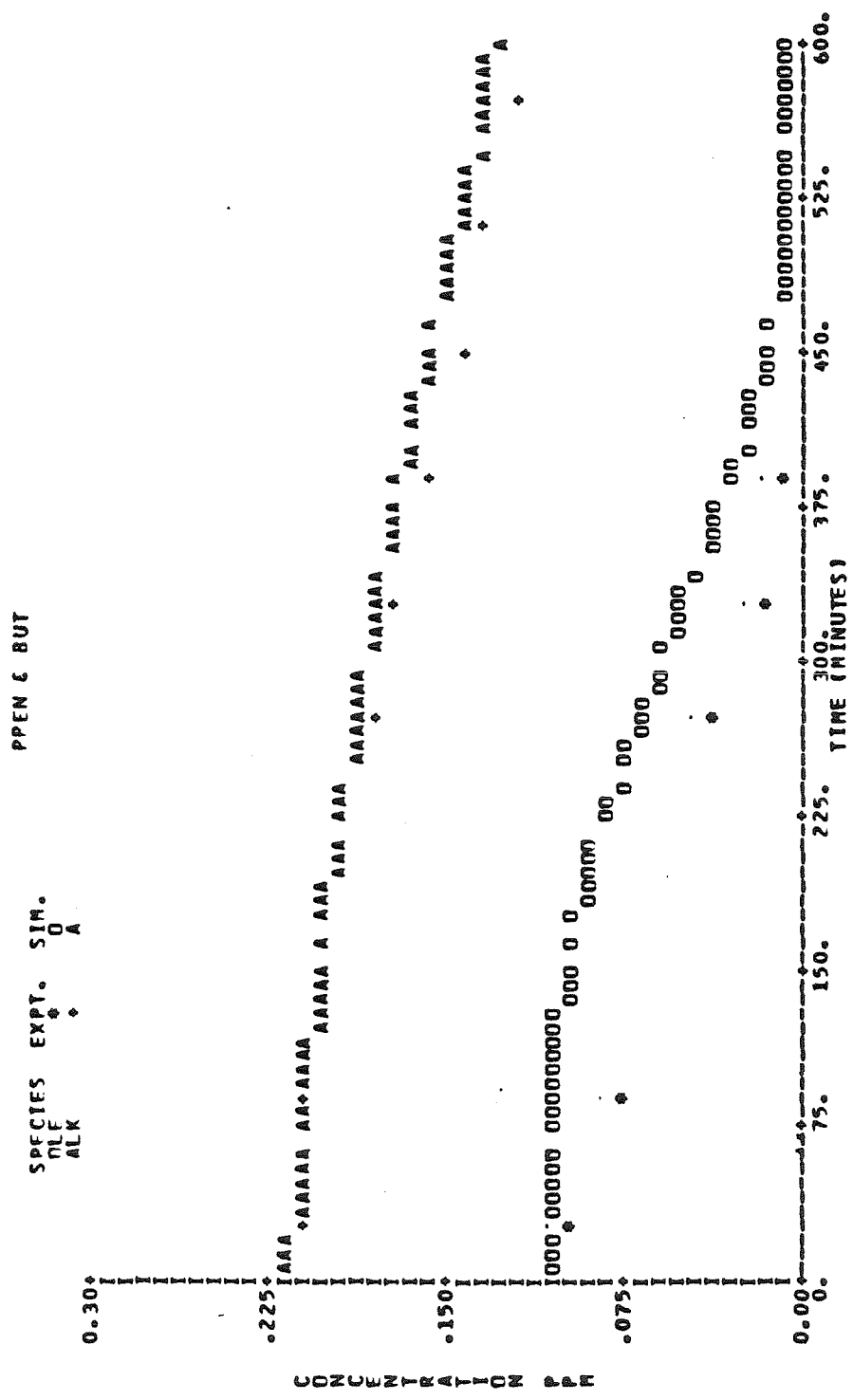

Figure A.19.e. Comparison of Concentration-Time Profiles Predicted by the SUR2 Mechanism with Experimental Data from the Red Side of the UNC Experiment of July 8, 1982.

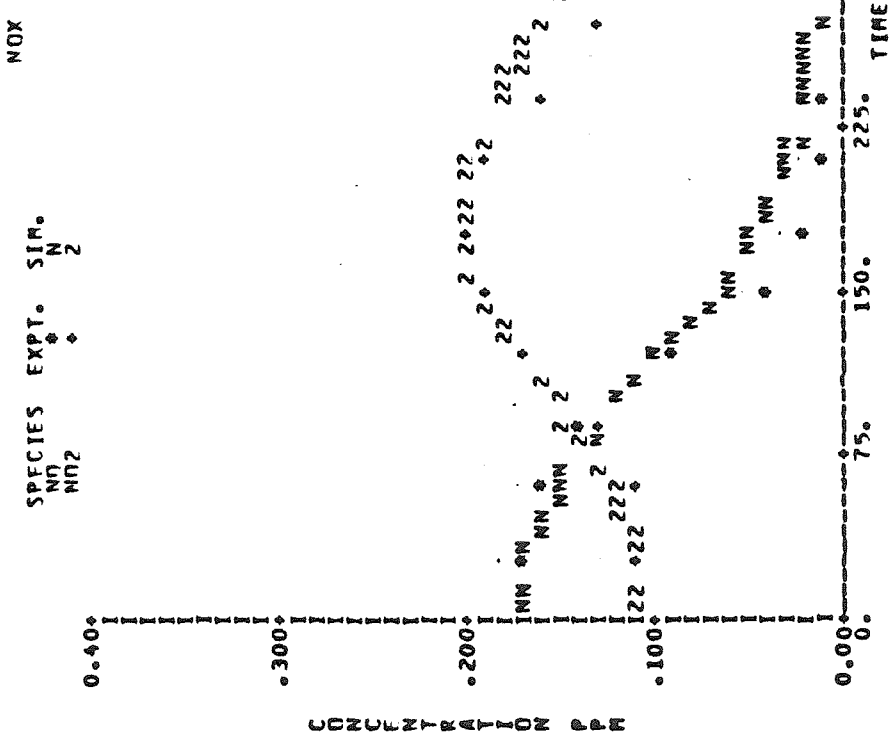

Figure A.20.a. Comparison of Concentration-Time Profiles Predicted by the SUR2 Mechanism with Experimental Data from the Red Side of the UNC Experiment of October 14, 1981.

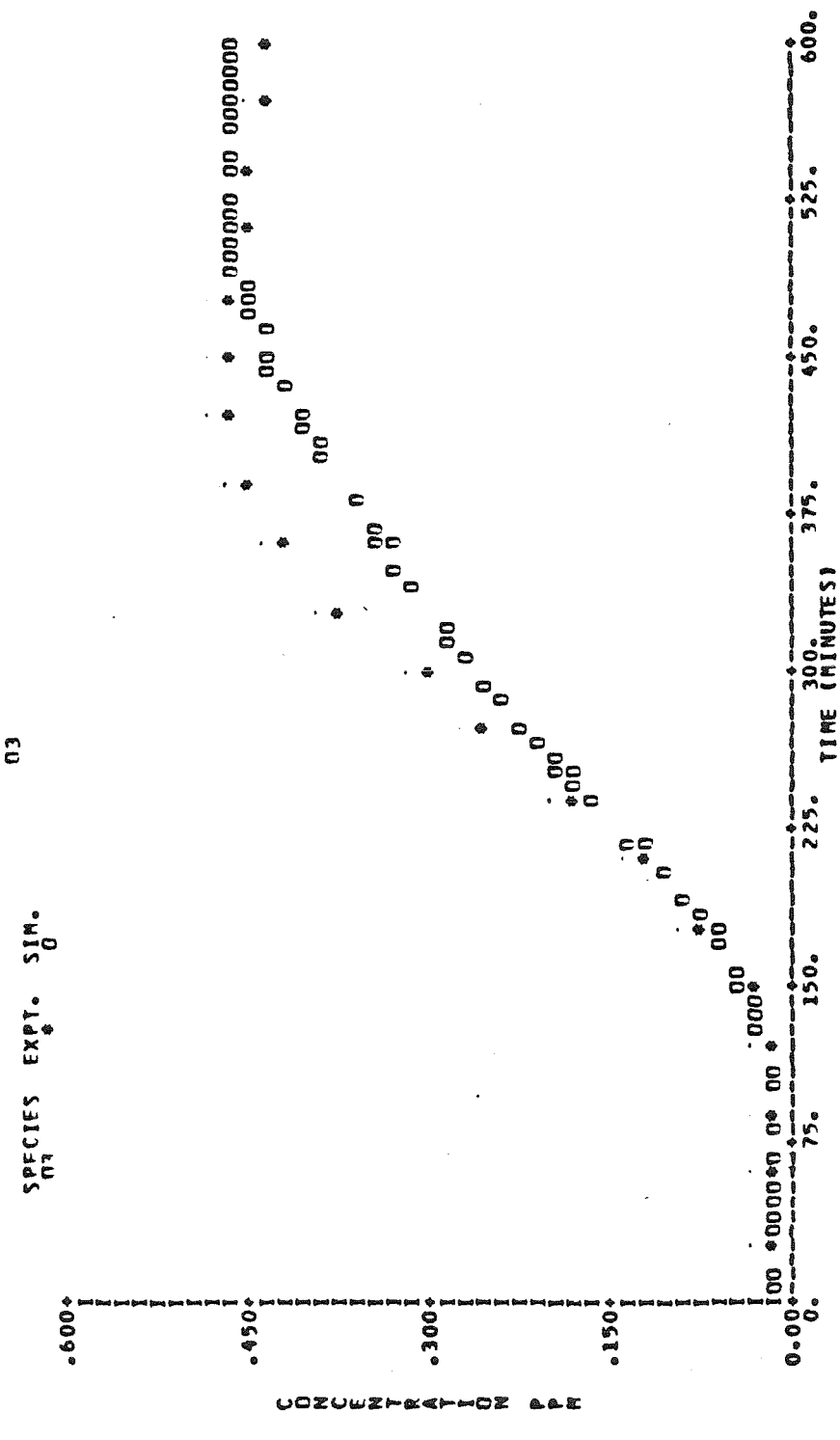

Figure A.20.b. Comparison of Concentration-Time Profiles Predicted by the SUR2 Mechanism with Experimental Data from the Red Side of the UNC Experiment of October 14, 1981.

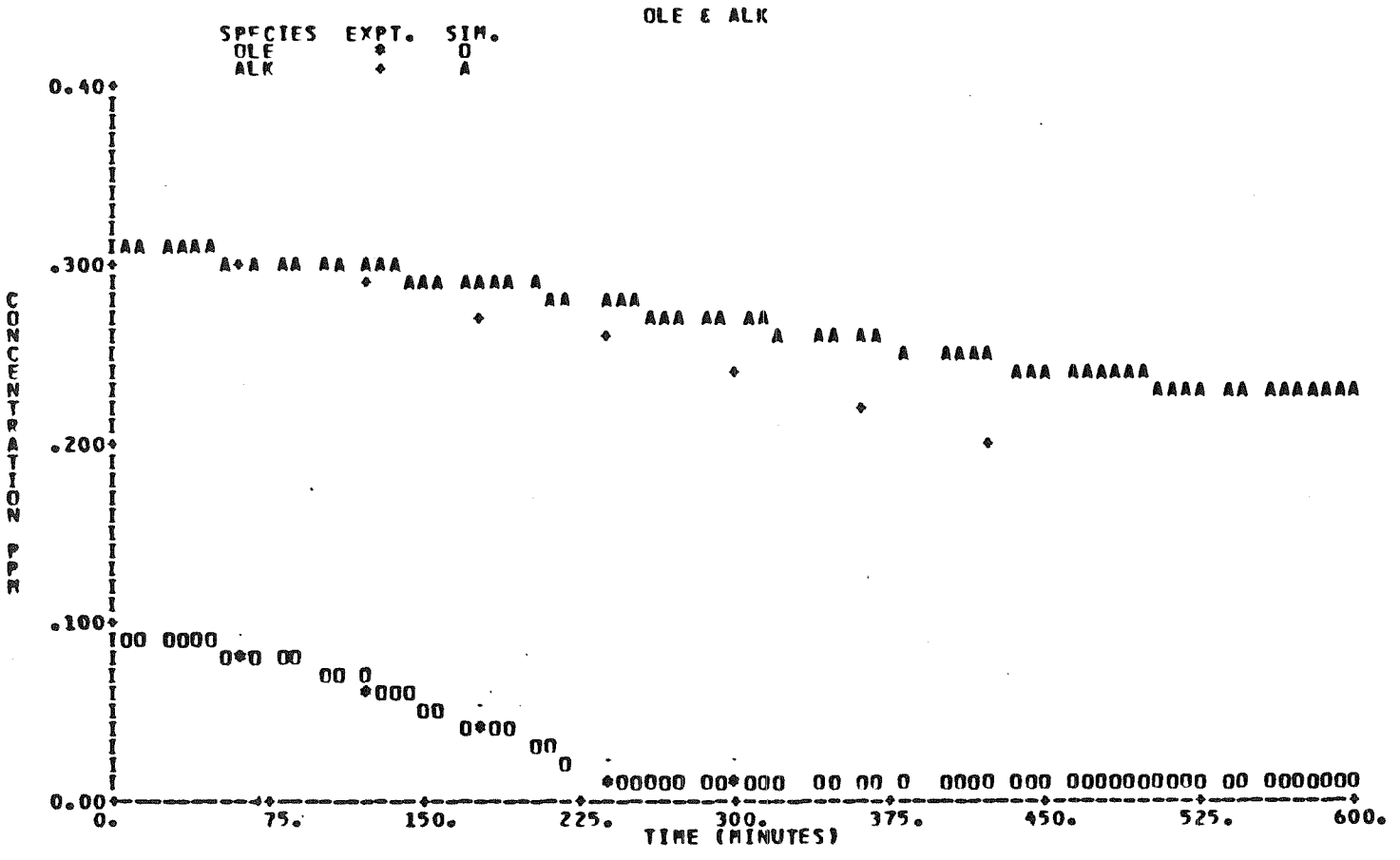

Figure A.20.c. Comparison of Concentration-Time Profiles Predicted by the SUR2 Mechanism with Experimental Data from the Red Side of the UNC Experiment of October 14, 1981.

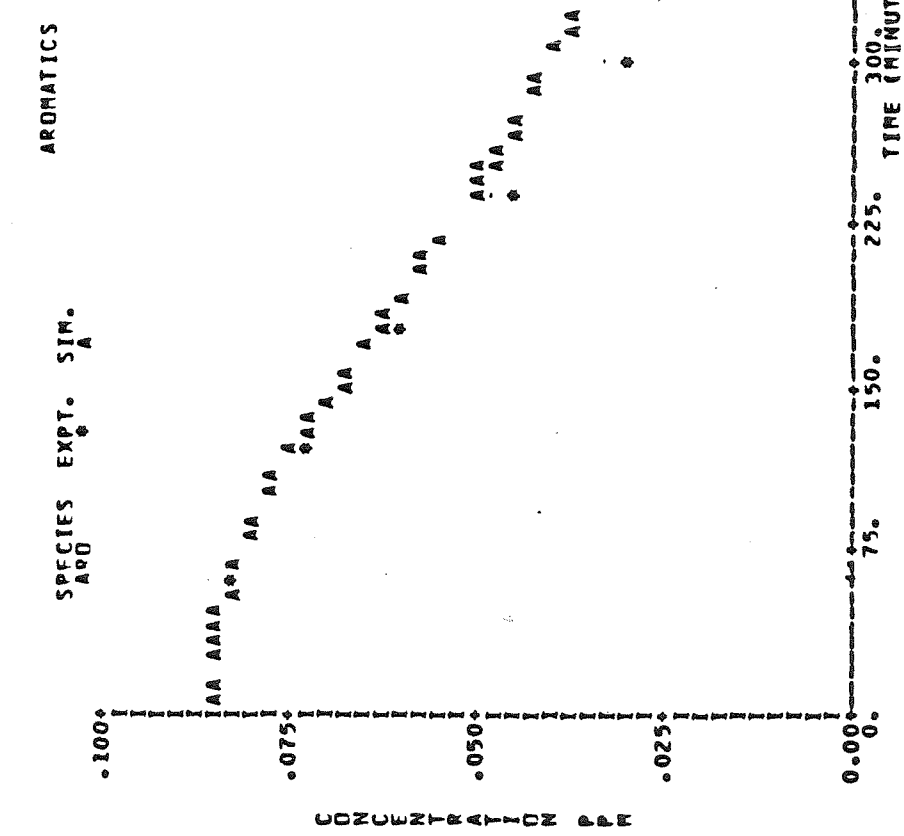

Figure A.20.d. Comparison of Concentration-Time Profiles Predicted by the SUR2 Mechanism with Experimental Data from the Red Side of the UNC Experiment of October 14, 1981.

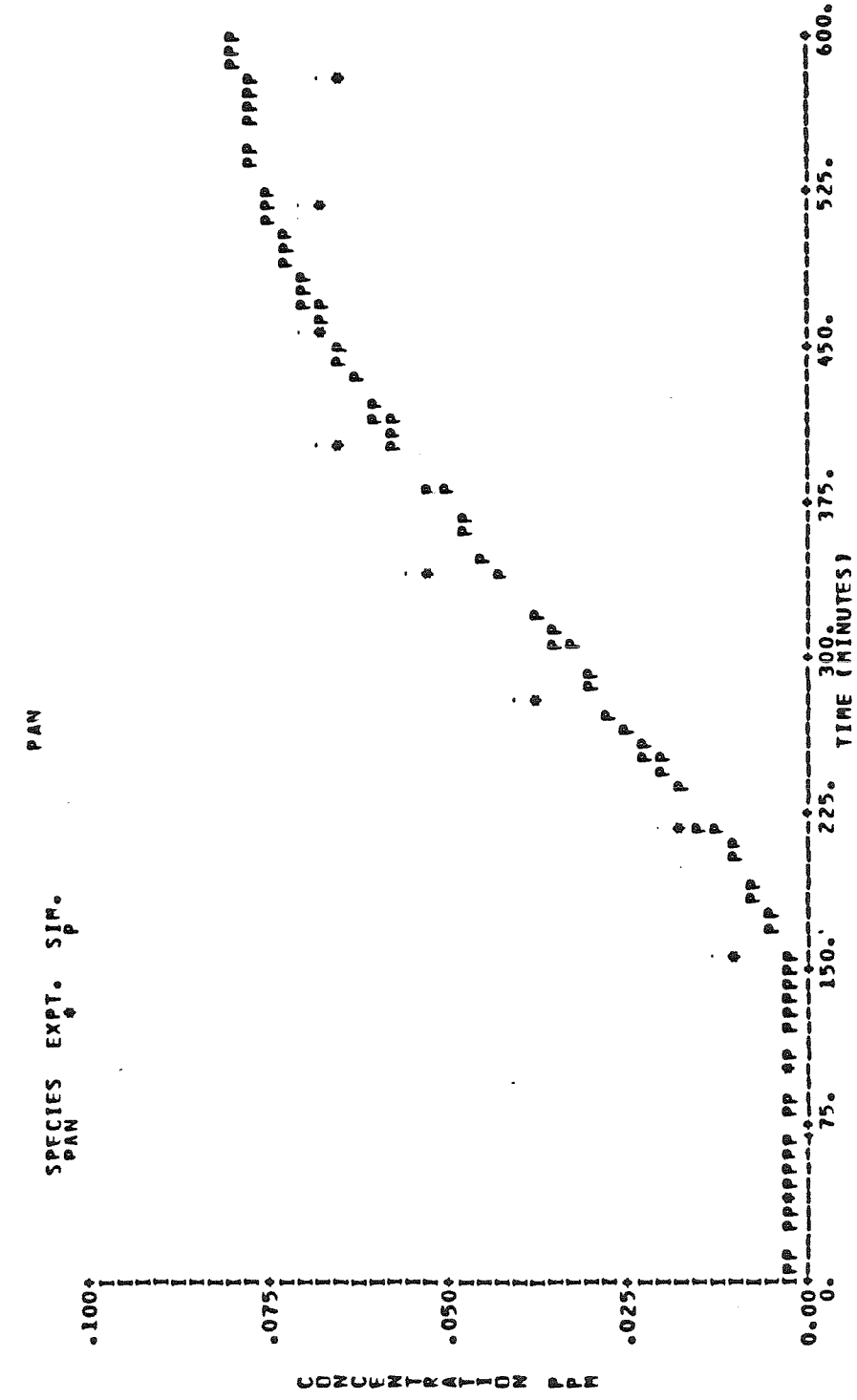

Figure A.20.e. Comparison of Concentration-Time Profiles Predicted by the SUR2 Mechanism with Experimental Data from the Red Side of the UNC Experiment of October 14, 1981.

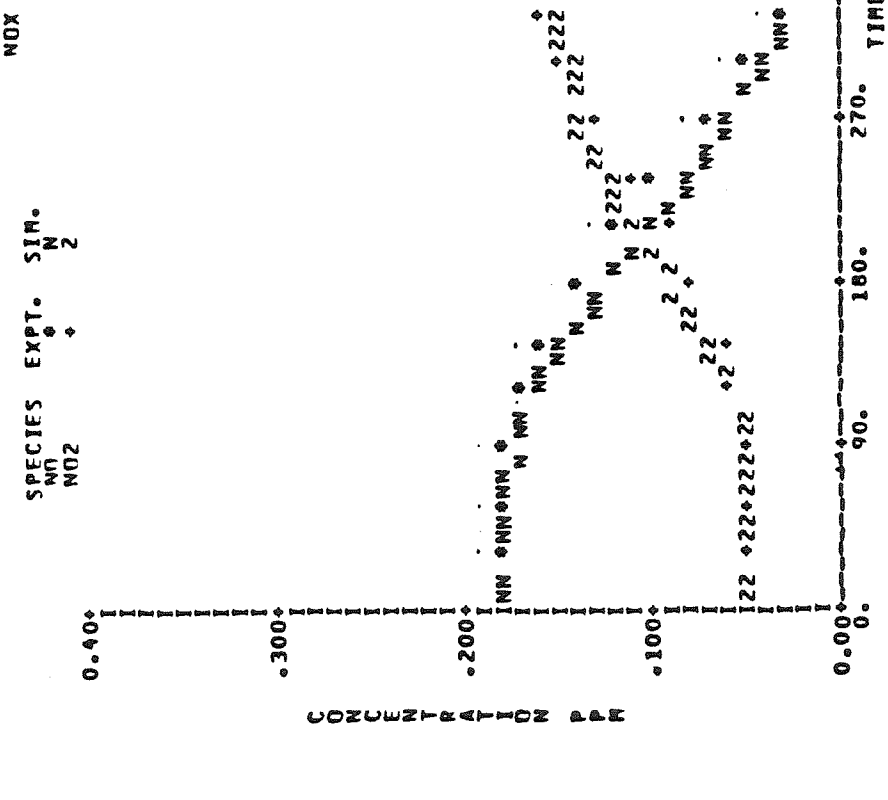

Figure A.21.a. Comparison of Concentration-Time Profiles Predicted by the SUR2 Mechanism with Experimental Data from the Red Side of the UNC Experiment of August 26, 1981.

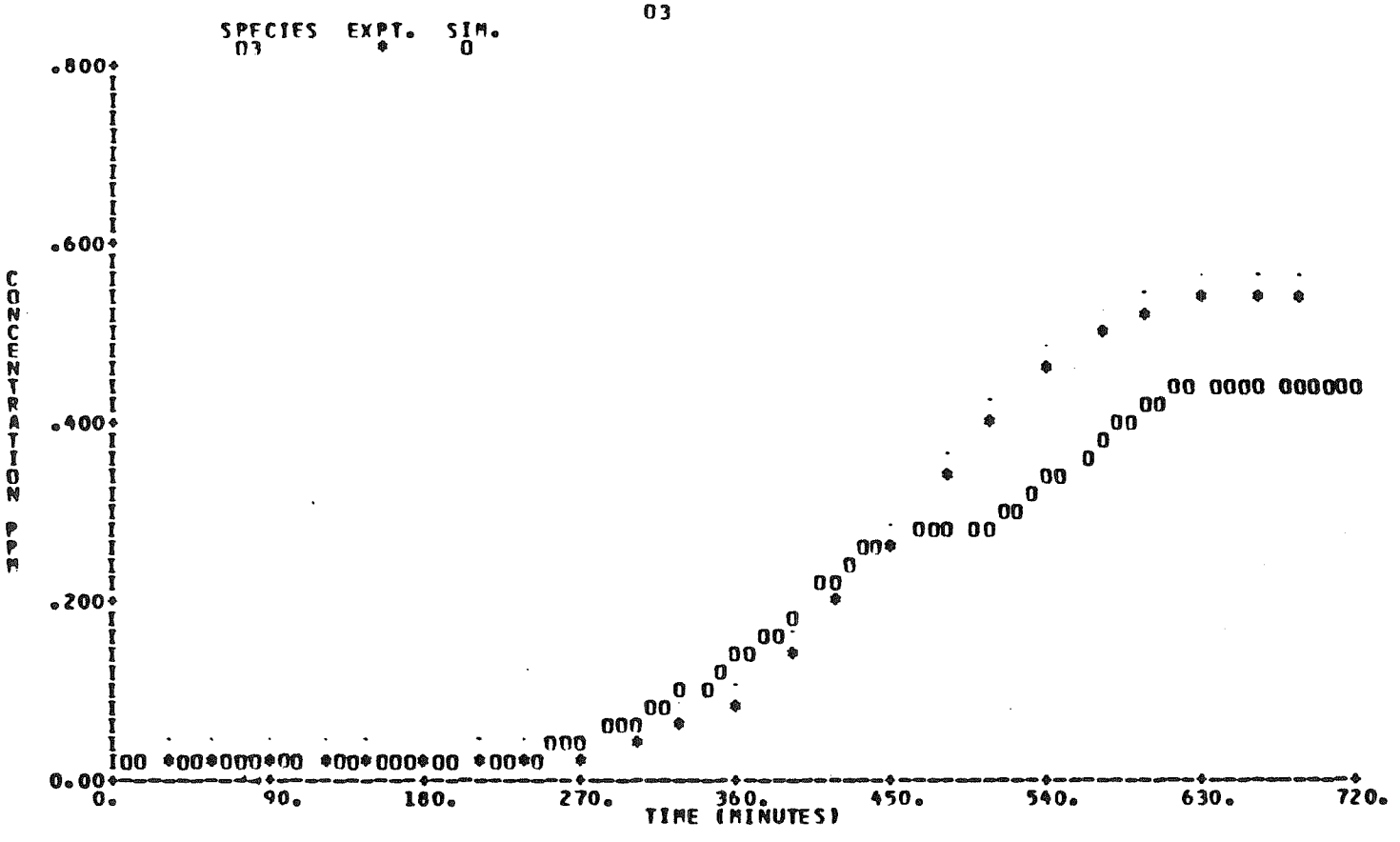

Figure A.21.b. Comparison of Concentration-Time Profiles Predicted by the SUR2 Mechanism with Experimental Data from the Red Side of the UNC Experiment of August 26, 1981.

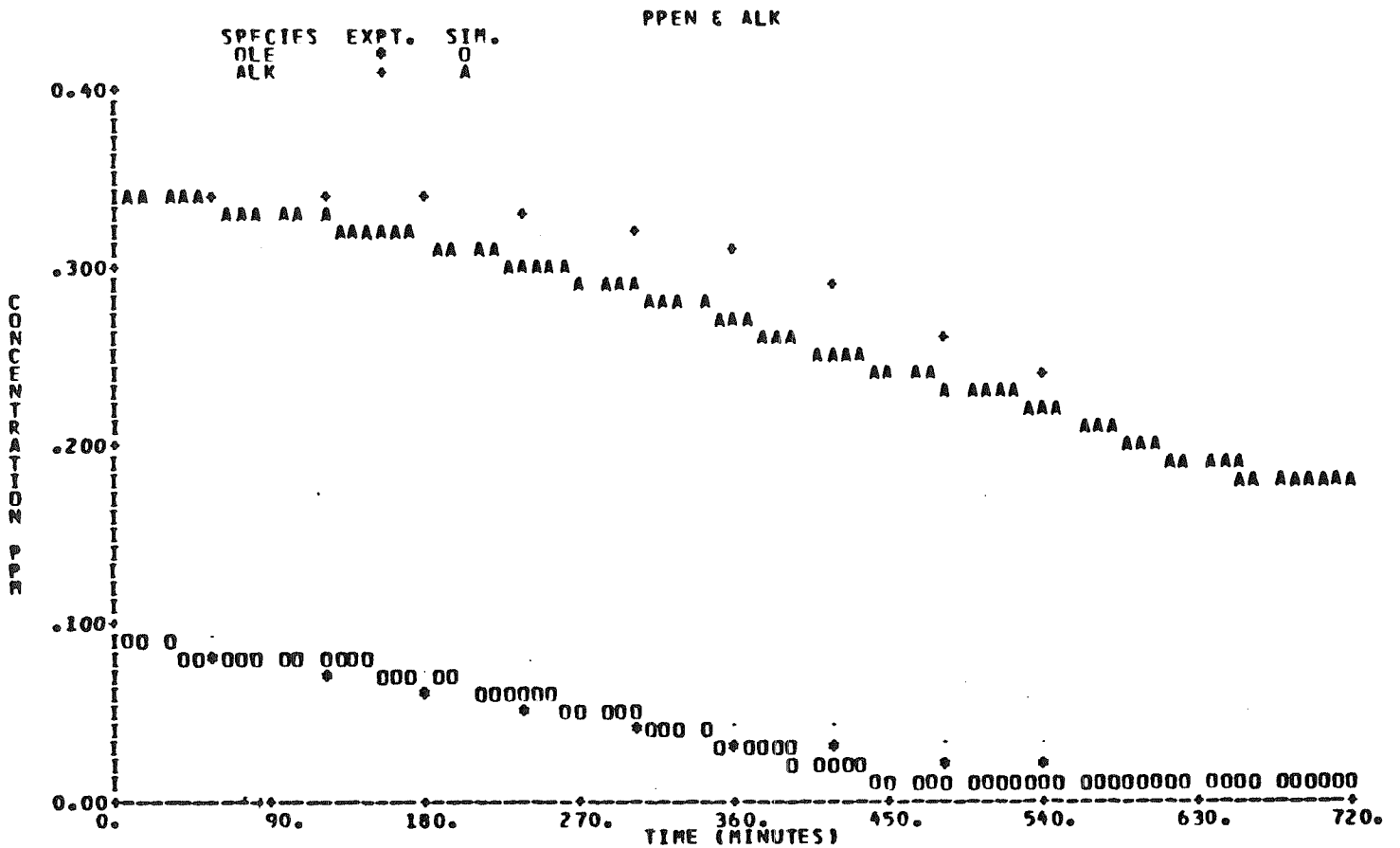

Figure A.21.c. Comparison of Concentration-Time Profiles Predicted by the SUR2 Mechanism with Experimental Data from the Red Side of the UNC Experiment of August 26, 1981.

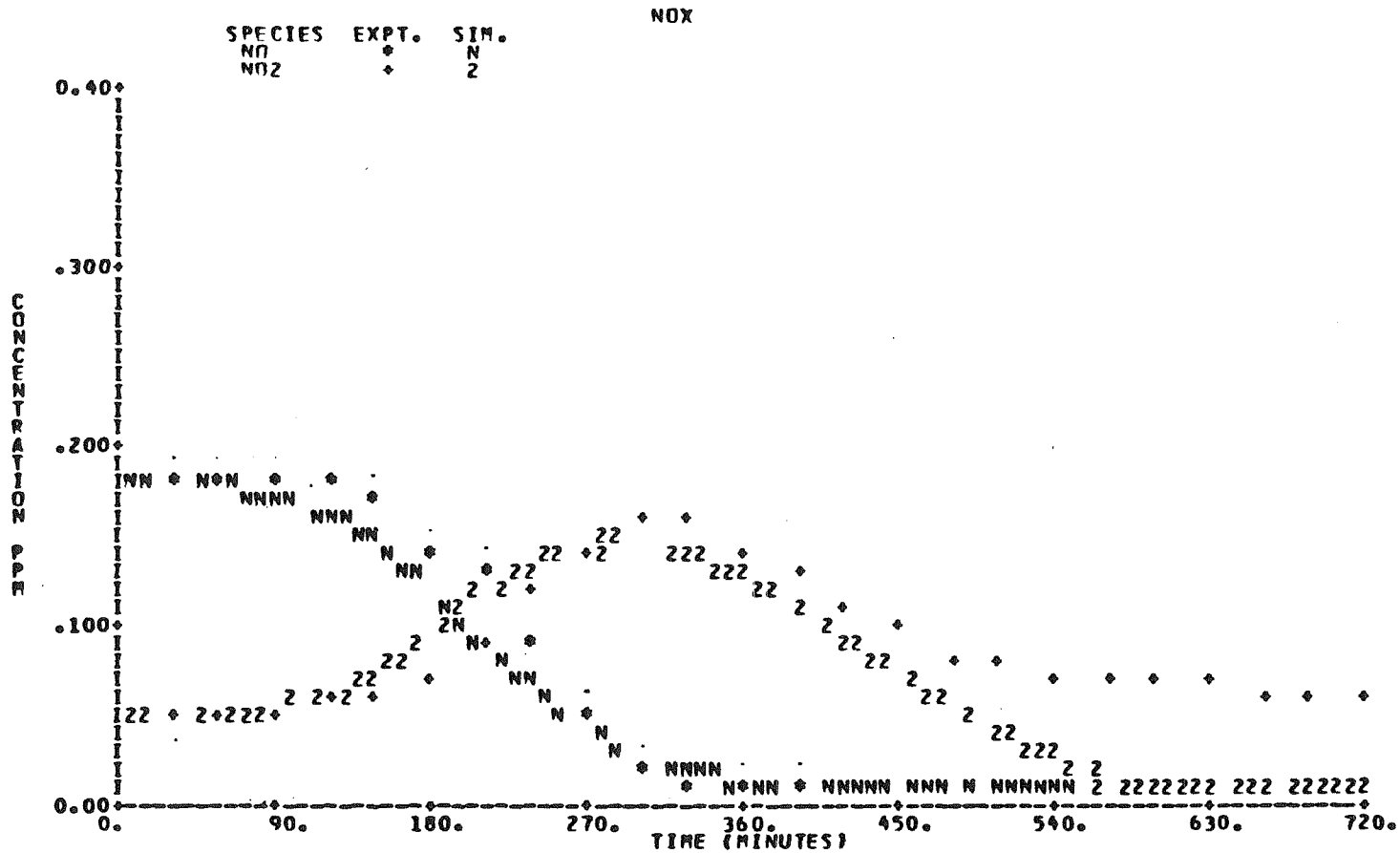

Figure A.22.a. Comparison of Concentration-Time Profiles Predicted by the SUR2 Mechanism with Experimental Data from the Blue Side of the UNC Experiment of August 26, 1981.

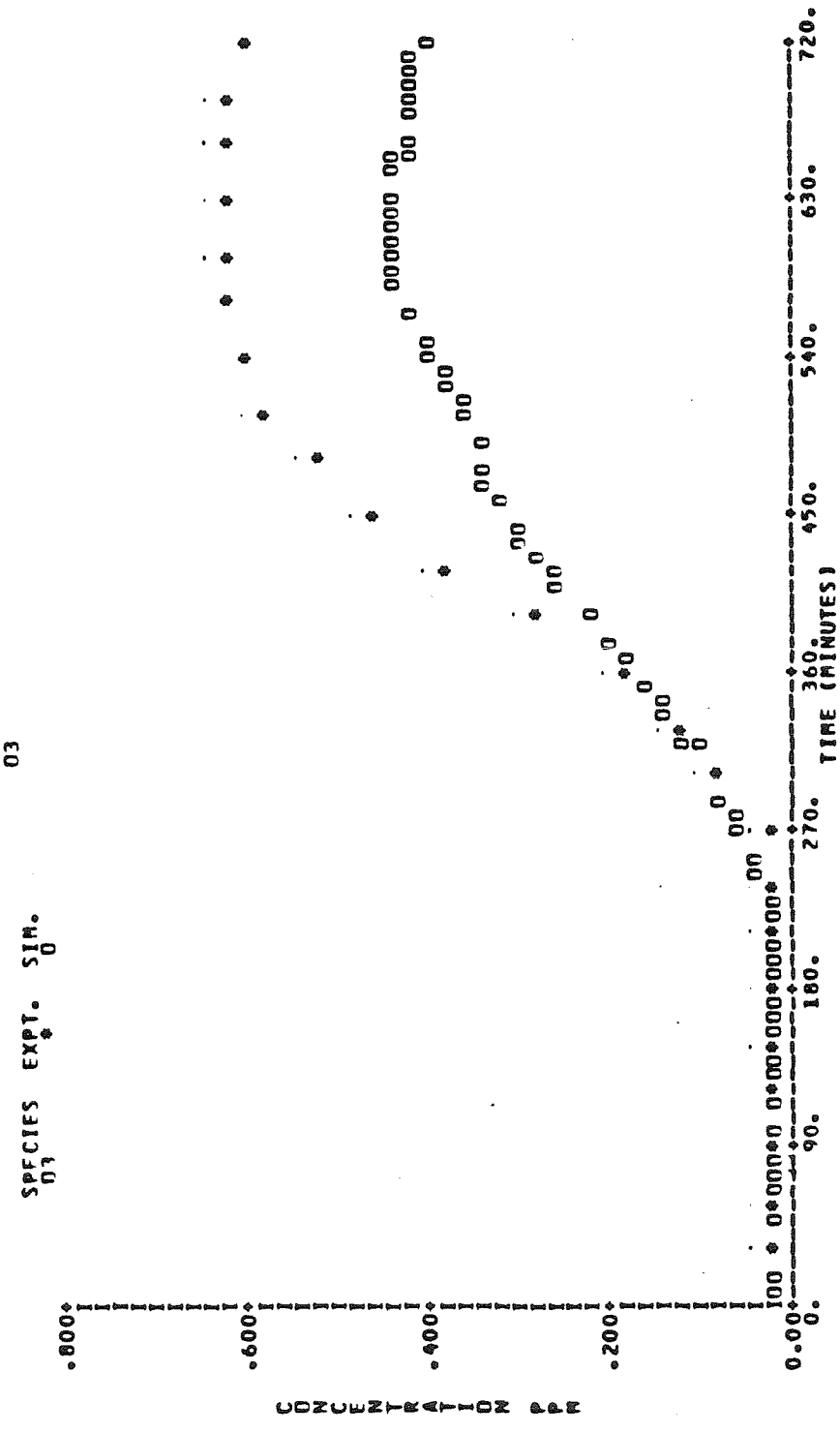

Figure A.22.b. Comparison of Concentration-Time Profiles Predicted by the SUR2 Mechanism with Experimental Data from the Blue Side of the UNC Experiment of August 26, 1981.

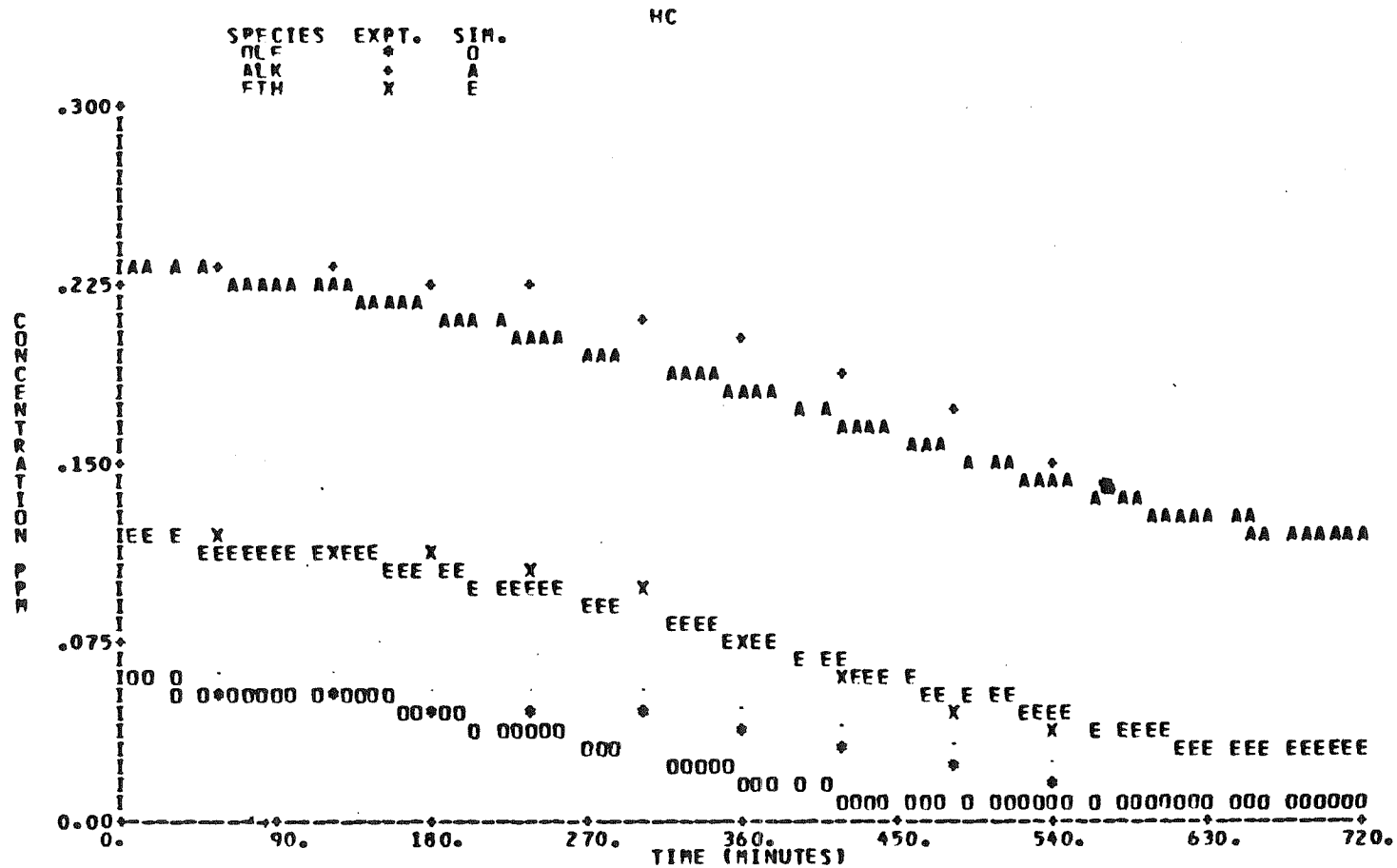

Figure A.22.c. Comparison of Concentration-Time Profiles Predicted by the SUR2 Mechanism with Experimental Data from the Blue Side of the UNC Experiment of August 26, 1981.

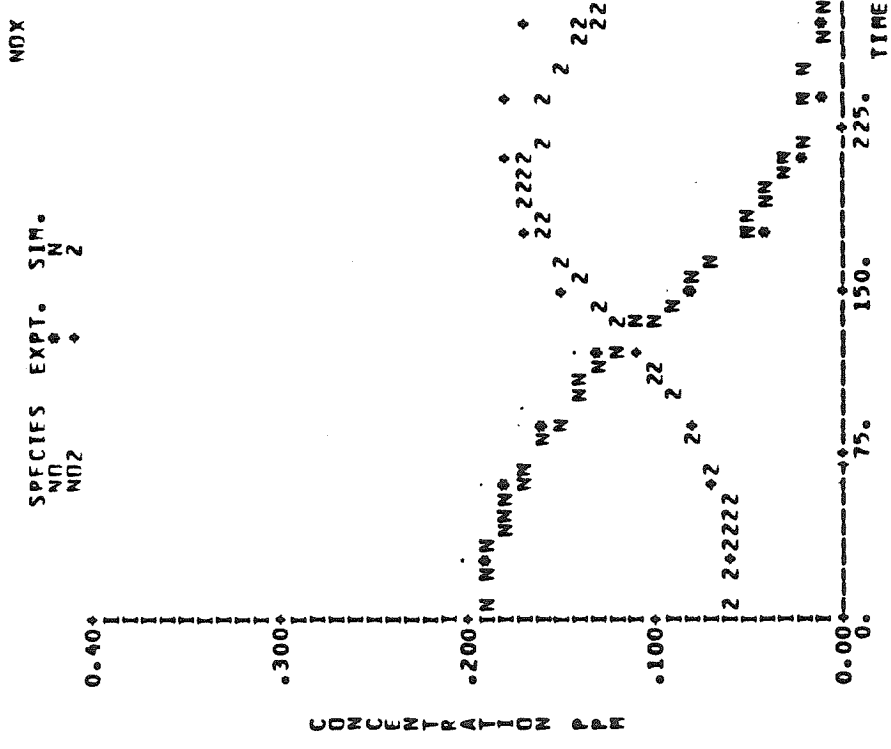

Figure A.23.a. Comparison of Concentration-Time Profiles Predicted by the SUR2 Mechanism with Experimental Data from the Red Side of the UNC Experiment of September 2, 1981.

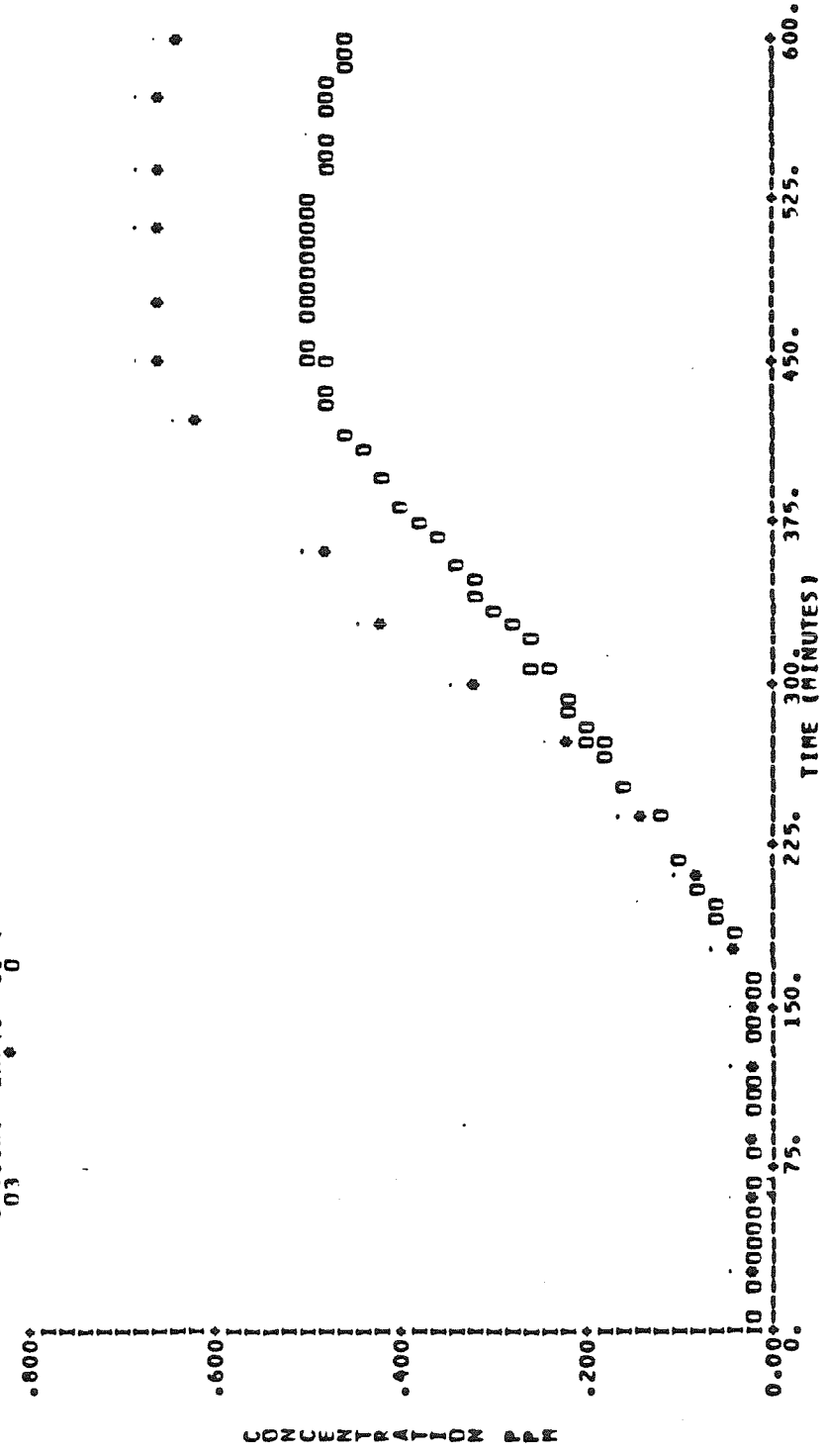

Figure A.23.b. Comparison of Concentration-Time Profiles Predicted by the SUR2 Mechanism with Experimental Data from the Red Side of the UNC Experiment of September 2, 1981.

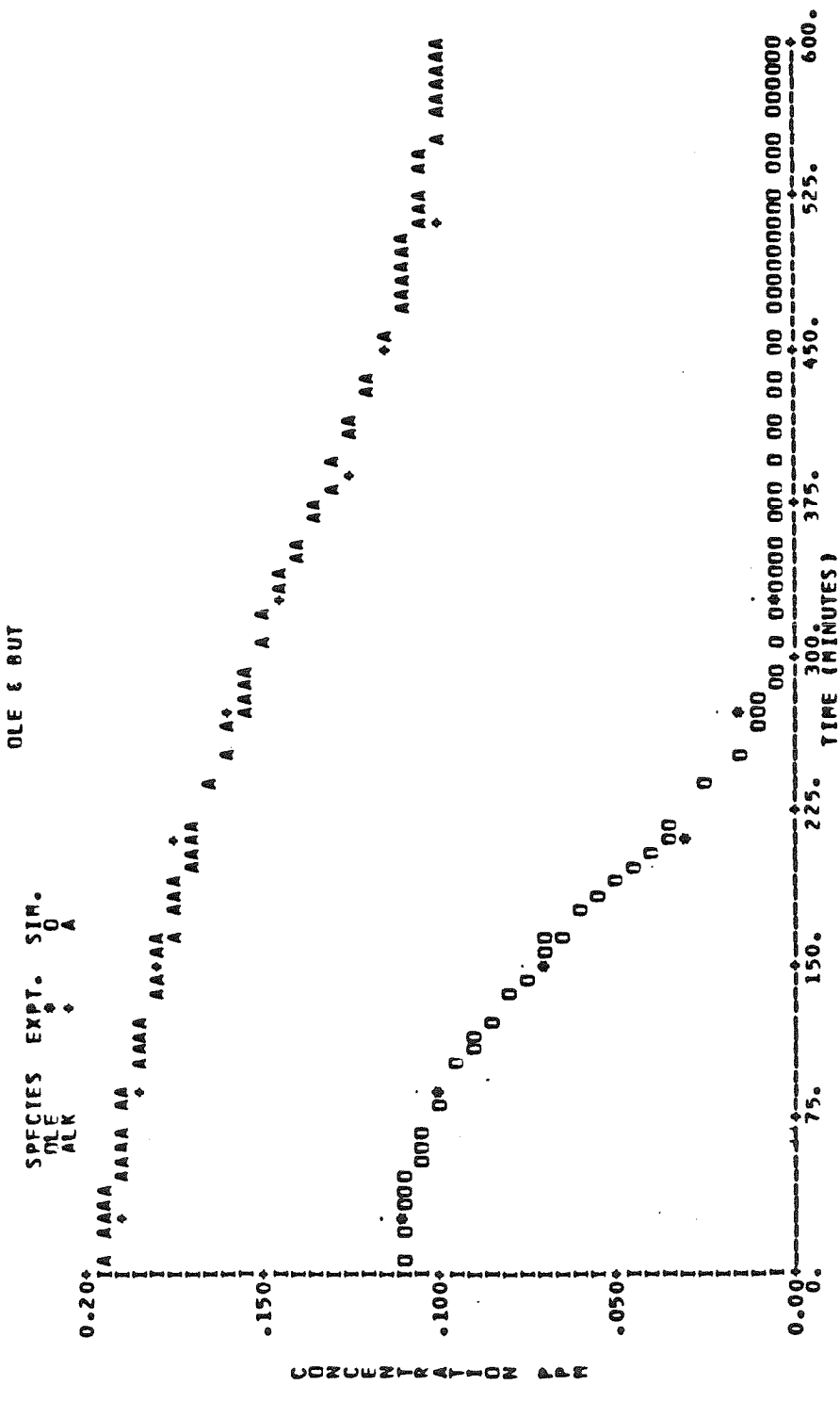

Figure A.23.c. Comparison of Concentration-Time Profiles Predicted by the SUR2 Mechanism with Experimental Data from the Red Side of the UNC Experiment of September 2, 1981.

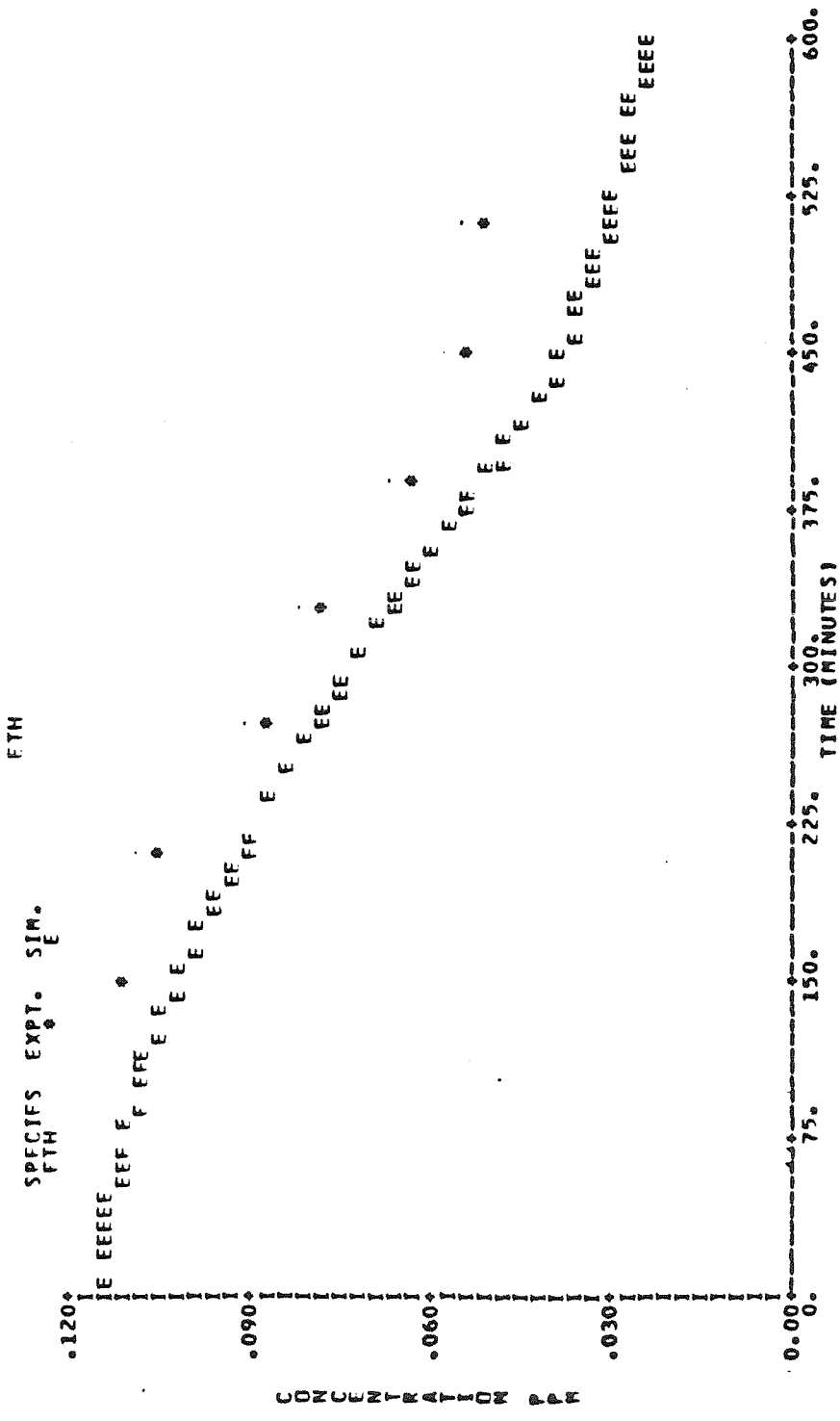

Figure A.23.d. Comparison of Concentration-Time Profiles Predicted by the SUR2 Mechanism with Experimental Data from the Red Side of the UNC Experiment of September 2, 1981.

CHAPTER 8

Recommendations for Future Research

RECOMMENDATIONS FOR FUTURE RESEARCH

A section summarizing the conclusions and recommendations for future work pertaining to each segment of this thesis can be found at the end of chapters 2 through 7. Instead of repeating that material in this chapter, we list here only what are possibly the most urgent research efforts needed in the fields of atmospheric aromatic chemistry and the analysis of chemical reaction mechanisms for photochemical smog.

It is clear that protocols for measuring the di-carbonyl products arising from cleavage of the aromatic ring should be developed before further smog chamber experiments with aromatic hydrocarbons are performed. Without the ability to measure these compounds, the data available from a typical smog chamber experiment are not sufficient to establish a definitive reaction mechanism for the aromatics. This is very evident from the results presented in Chapter 3. Once analytical methods are developed to measure these species, chamber experiments with toluene, the xylenes, benzene, methyl glyoxal, and the other important di-carbonyls can be carried out to determine the yields and subsequent fates of the di-carbonyl species.

With regard to condensed kinetic mechanisms for photochemical smog, the crucial need concerns the atmospheric application of the mechanisms. A detailed analysis of the behavior of the SUR2 mechanism needs to be carried out. This study should focus on comparisons of the emission control requirements predicted by the SUR2 and other existing mechanisms. The effects of hydrocarbons aloft, dilution, aldehydes aloft, and using different lumping categories for initial conditions on the predictions of the SUR2 mechanism need to be studied.

Some of the major differences between the existing lumped mechanisms arise because of different assumptions concerning the magnitude of chamber derived

sources of free radicals. Because this issue continues to be so controversial, it is appropriate to conclude this section with a comment on these radical sources. It is now clear that:

(1) Chamber derived radical sources are present in every existing smog chamber.

(2) The magnitude of these radical sources varies substantially from chamber to chamber.

(3) The fundamental mechanism leading to these radical sources is complex, making it very unlikely that a non-empirical description of the radical formation processes will be formulated in the near future.

With these facts in mind, it is apparent that we must for the time being learn to cope with these troublesome radical sources. This can best be accomplished if each chamber is characterized with regard to these wall radical sources before each series of experiments, and whenever a new chamber is employed. This can be achieved with a few simple CO-NO_x-air irradiations, such as those described in Chapter 3. These experiments are very simple to perform, require only a few readily available instruments, require only 2-3 hours of irradiation, and, based on the experiments performed at Caltech, give very reproducible results under a variety of initial conditions.

APPENDIX

INSTRUMENTATION

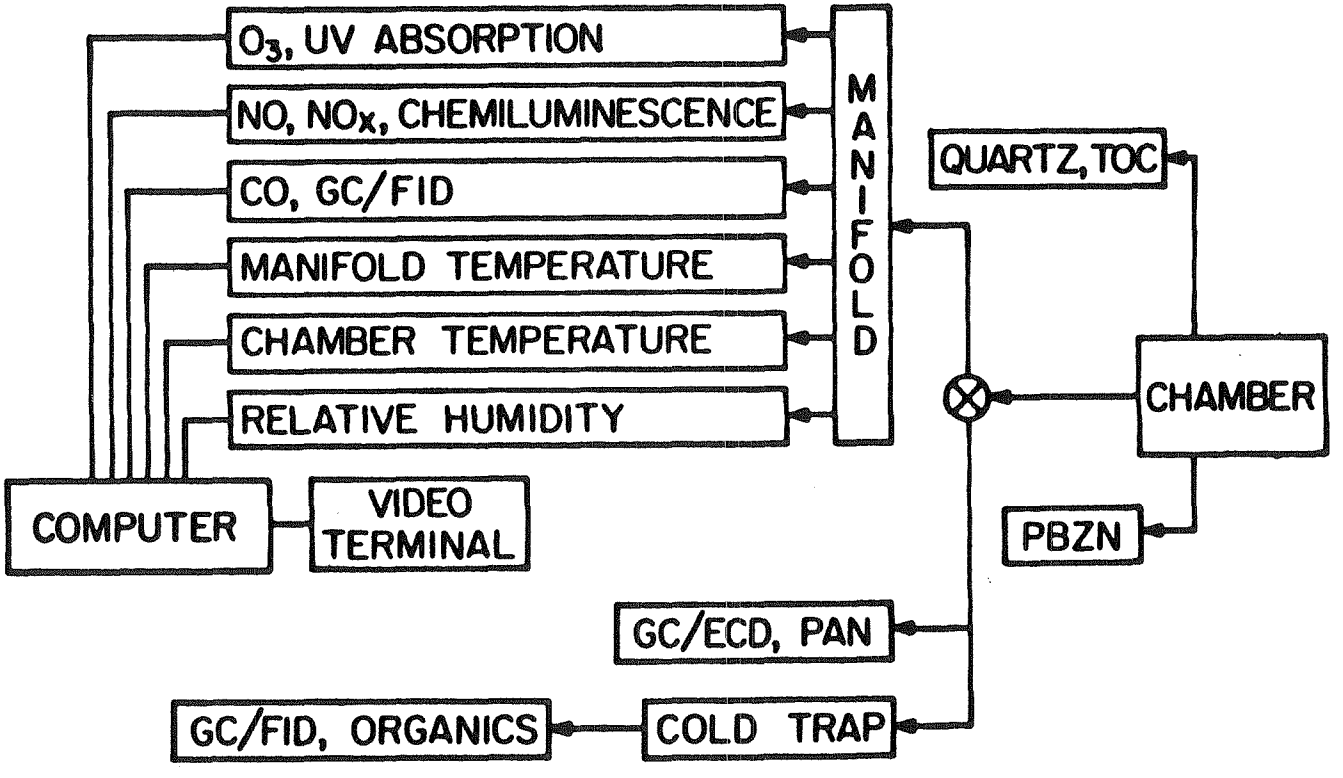

Summary of Instrumentation and Chemical Analyses Used in Outdoor Smog Chamber Irradiations.

Carbon balances for toluene-NO_x Irradiations

Experiment Number	Reacted Toluene (ppbC)	Recovered Carbon (ppbC)					Percent Carbon Recovered
		CO	benzaldehyde	o-cresol	PAN	Aerosol[1]	
TOLR22	4900	830	120	20	60	35	22%
TOLR23	980	420	40	0	15	13	50%
TOLR24	4200	1020	100	10	5	69	29%
TOLR25	3900	600	125	20	90	154	25%
TOLR26	2300	420	60	12	80	50	27%

[1]This is the amount of aerosol measured. The actual amount of aerosol formed may be considerably higher due to losses to the chamber walls and sample lines.

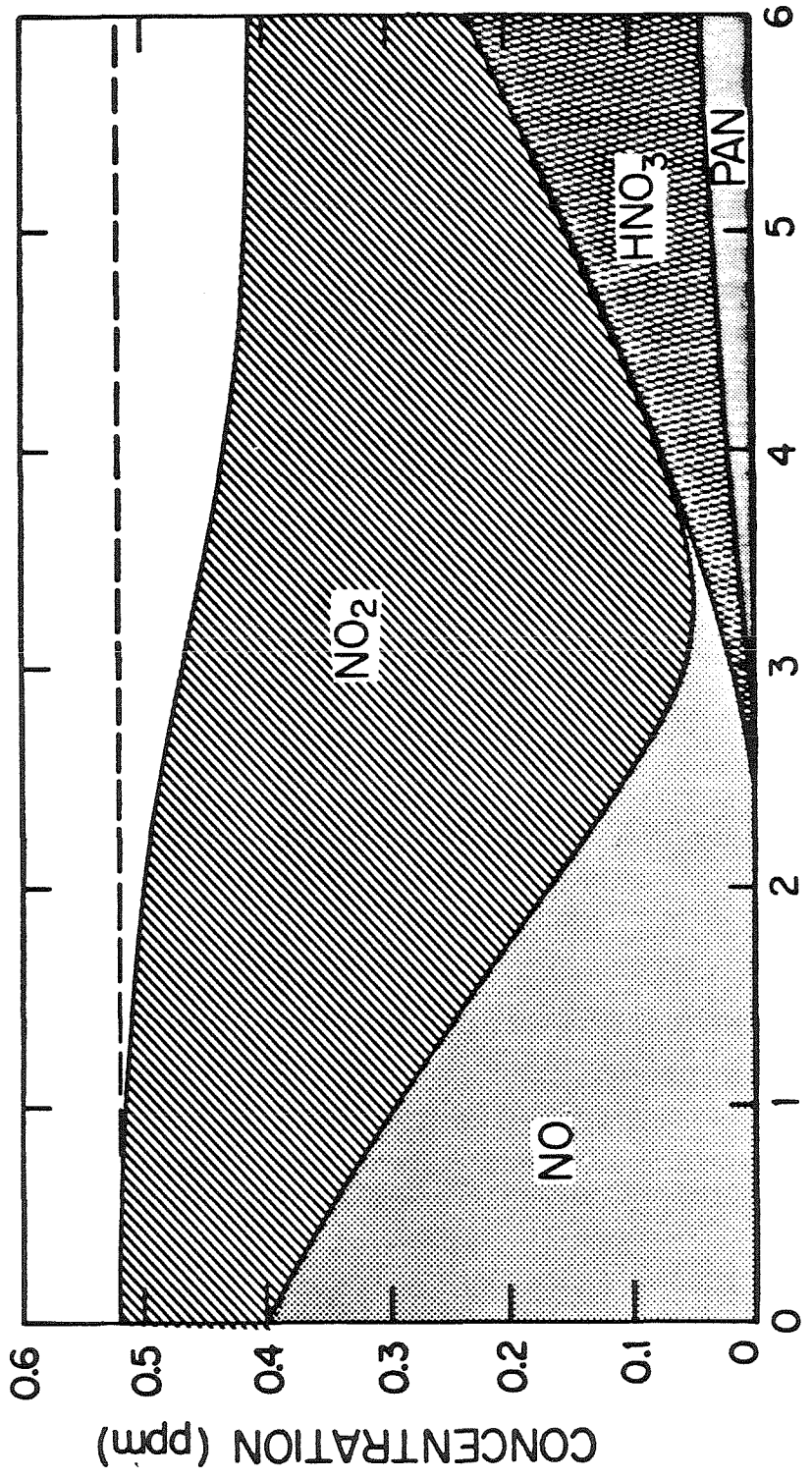

Concentration-Time Profiles of Nitrogen Compounds for Outdoor Smog Chamber Experiment TOLR26.

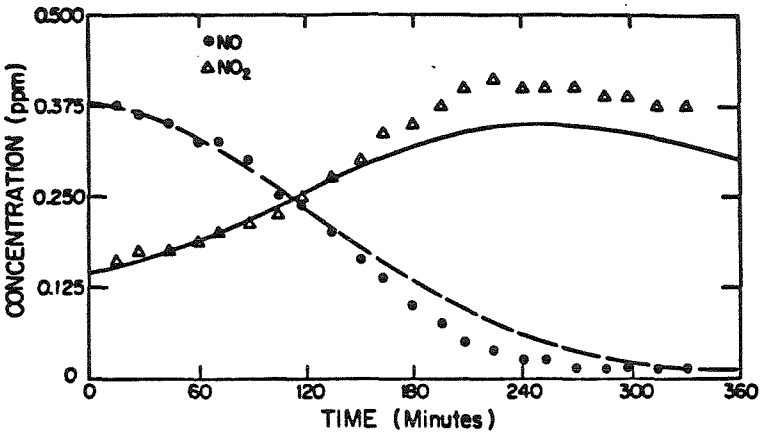

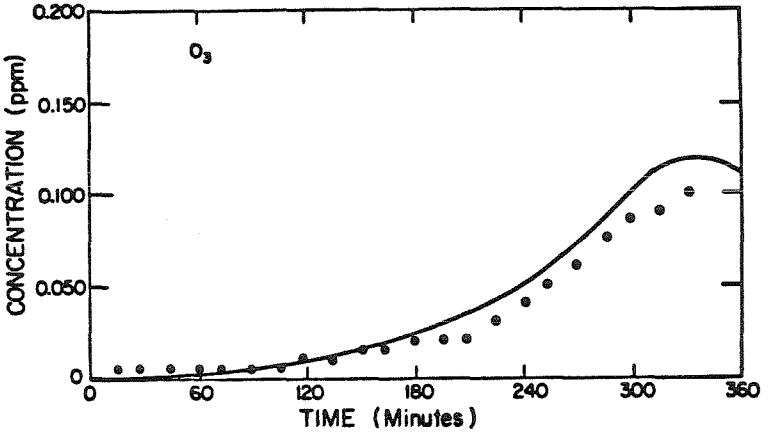

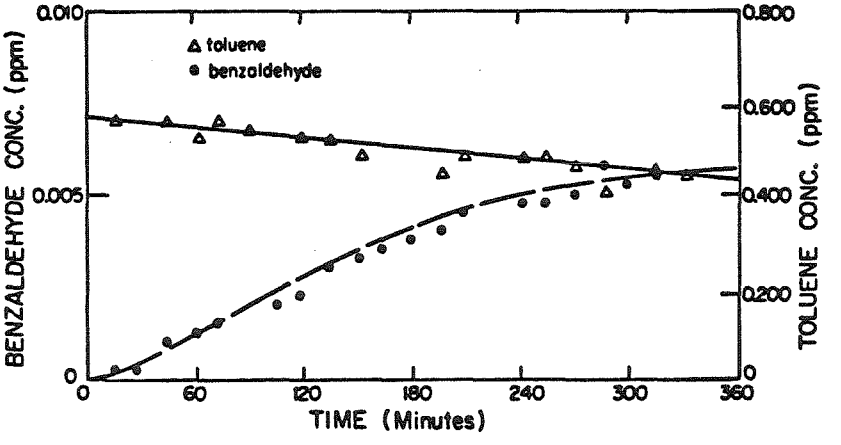

Observed and Predicted Concentration-Time Profiles for Toluene-NO_x Experiment TOLR23.